**Title**
Evaluation of dose rate and uncertainty of fuel debris in a canister for the safe retrieval of damaged nuclear fuel



**Author**
LEE, KYOUNGJIN

**Publication Date**
2021

Peer reviewed|Thesis/dissertation

# Evaluation of dose rate and uncertainty of fuel debris in a canister for the safe retrieval of damaged nuclear fuel

by

Kyoungjin Lee

A dissertation submitted in partial satisfaction of the
requirements for the degree of
Doctor of Philosophy
in
Engineering – Nuclear Engineering
in the
Graduate Division
of the
University of California, Berkeley

Committee in charge:

Professor Massimiliano Fratoni, Chair
Professor Jasmina Vujic
Professor Paul Grigas

Summer 2021

Evaluation of dose rate and uncertainty of fuel debris in a canister for the safe retrieval of damaged nuclear fuel

Abstract

Evaluation of dose rate and uncertainty of fuel debris in a canister for the safe retrieval of damaged nuclear fuel

by

Kyoungjin Lee

Doctor of Philosophy in Engineering - Nuclear Engineering

University of California, Berkeley

Professor Massimiliano Fratoni, Chair

Damaged fuel from core melting accidents like Three Mile Island and Fukushima Daiichi need to be retrieved and disposed. Retrieval of damaged fuel is considerably more complex than for standard fuel as fuel is relocated and deformed during the accident. Two major aspects need to be considered when planning damaged fuel retrieval: prevent to create conditions in which criticality could be achieved and protect workers and equipment from radiation. In the case of the Fukushima Daiichi Power Plant, damaged fuel cannot be covered with water, making retrieval operations more complex as water provides radiation shielding. This work provides an assessment of the radiation emissions from the Fukushima Daiichi damaged fuel necessary to determine shielding requirements.

In an initial scoping study, the photon and neutron dose rate of the fuel debris in a canister was evaluated in several parameters including canister designs, source term, geometry of fuel debris. This study provided the basis for the development of methods for the evaluation of the dose rate and uncertainty. The fuel debris was modeled by using random sampling on the size and distribution of fuel debris in a canister. The model uses the Monte Carlo method and performs random sampling on the geometry of the fuel debris to estimate the average dose rate and its standard deviation. SCALE and MCNP codes were used for neutron and photon transport calculations, and a Python code was developed to generate samples and to manage calculations for the evaluation. The Python code efficiently manages calculations of dose rate and flux by applying multiprocessing and parallel computing. The output data was evaluated by basic statistics, and a method which converts the output data into a cumulative format is proposed for the data fitting and the regression analysis of nonlinear data. The model provided variability and uncertainty of the radiation dose rate and flux in detail. However, this method is time consuming and computationally expensive, therefore, an analytical method is developed to approximately evaluate the flux and uncertainty in relatively short time.

The uncertainty of dose rate was evaluated as the standard deviation and the relative range of estimated dose rates. The uncertainty depends on the size of fuel debris, and uncertainty of a canister with larger debris is larger. The standard deviation can be larger than 30% of the average dose rate, and the relative range can be larger than 90% of the average dose rate depending on the condition of fuel debris. The uncertainty increases when canisters are contained in a transport cask which has several canisters in it. The average dose rate also depends on the size of debris, and a canister with larger debris has a

smaller dose rate. The distribution of fuel debris in a canister also affects the dose rate and uncertainty.

Variability of the dose rate and uncertainty by changes in the location of the detector was also evaluated. The maximum dose rate was estimated at the vertical center of a canister at 1 m from the surface of a canister which is loosely packed with fuel debris. In case of a canister with the close packed fuel debris, the maximum dose rate was estimated at the vertical center of the pile of debris which is not same as the vertical center of a canister. The uncertainty also depends on the vertical location of the detector, and the uncertainty can be minimized when the dose rate is estimated at the vertical center of the debris pile. The dose rate and uncertainty are variable when they are estimated near a canister, therefore, the dose rate and uncertainty of fuel debris can be characterized in more detail when they are estimated near a canister, and this can be applied for the characterization of the fuel debris.

Modified designs which can reduce the uncertainty of dose rate were evaluated. The uncertainty can be reduced by dividing the inner space of a canister by using inner containers or partitions which restrict the distribution of fuel debris in the canister. In case of the horizontal division, size of fuel debris can be restricted depending on the number of partitions used for the design. More partitions restrict the size, and uncertainty can be reduced since uncertainty of smaller debris is smaller. Vertical division does not restrict the size and it only restricts the vertical distribution of fuel debris. Even if the horizontal division can minimize the uncertainty when many partitions are installed in a canister, the vertical division of the inner space is more efficient than horizontal division in reduction of the uncertainty.

Evaluated results in this dissertation can help the safe retrieval of fuel debris in Fukushima Daiichi nuclear power plant. Models and methods developed in this dissertation can be used for the characterization of damaged nuclear fuel which can be made by an accident in the future. They also can be applied to develop methods to manage spent fuel of advanced nuclear reactors such as the fuel of pebble bed reactors.

**List of Figures**

**List of Tables**

# Acknowledgments

I would like to express my greatest gratitude to Professor Massimiliano Fratoni, my advisor and dissertation committee chair, for his professional advice and inspiring mentorship. I sincerely appreciate his encouragement and support during my study at UC Berkeley. When I first arrived to Berkeley, everything was difficult and unfamiliar. However, I was able to quickly get accustomed to this great university because my advisor encouraged me with positive words and feedback. When I was wandering around looking for my research topic, he gave me clear guidance and helped me to be prepared for the research. This dissertation would not have been possible without his guidance and advice. I appreciate the help I received from Professors Jasmina Vujic, Per Peterson, Paul Grigas, who taught me essential knowledge for my research.

I would like to thank Milos Ivo Atz, Alex Salazar, Seung Min Woo, Xudong Liu, who have been great mentors. I also would like to thank my research colleagues Jun Shi, Lorenzo Vergari, Pedro Junior Vicente Valdez who helped and encouraged me. Thank you to Franziska Schmidt who helped and advised me. I also thank Dajie Sun, Mitch Negus, Chris Keckler, Christopher Poresky, William Mason, Saad Kenany, Joey Kabel who helped me and encouraged me. I also would like to thank all graduate students in the UC Berkeley Department of Nuclear Engineering. I was very happy to study with great students in the UC Berkeley Department of Nuclear Engineering. I appreciate all the help that I received from the Department of Nuclear Engineering. In particular, I would like to thank Kirsten Wimple Hall for all the help and kindness.

Lastly, I owe endless thanks to my family for their unconditional love and support, they are the reason and meaning of my life. I am grateful to my wife for her patience, support, and encouragement. I also thank to my lovely sons who are always energetic and positive.

# Chapter 1. Introduction

## 1.1 Introductory Remarks

The Fukushima and the Three Mile Island (TMI) nuclear accidents are typical core melting accidents. In the case of TMI Unit 2 reactor (TMI-2), nuclear fuel melted and some of it fell to the bottom of the reactor pressure vessel (RPV). However, there were many intact fuels at the top of the RPV and leakage of radioactive materials was prevented by the safety system of TMI-2. On the other hand, the accident of Fukushima Daiichi nuclear power plant (1FNPP) was more serious than the TMI-2 and it severely damaged its nuclear fuel. Most of the fuel melted and fell to the bottom of the RPV. Moreover, the molten fuel melted through the RPV and fell to the bottom of the primary containment vessel (PCV). The molten fuels have mixed with sea water which has been poured to stabilize the nuclear reactor, and part of molten fuel has been mixed with concrete and chemically reacted. In addition to this, part of radioactive isotopes leaked due to hydrogen explosions, and it made the condition of damaged fuel more complicated. Therefore, the condition of the damaged nuclear fuel in 1FNPP is uncertain and its diversity is expected.

A severe nuclear accident makes the condition of the damaged nuclear fuel uncertain, and it makes the retrieval of damaged fuel difficult. Evaluation of nuclear radiation is important for the safety of workers, and properly estimated data helps management of the damaged nuclear fuel. However, precision of estimated data is limited by variability and errors in estimation of the nuclear radiation, and the estimated data can be different from the measurement results. Dose rate of damaged fuel can be different depending on the sampled location in a reactor because of the variability in condition of the damaged fuel. Measurement errors due to the estimation methodology also reduce the accuracy. Therefore, nuclear radiation from damaged fuels needs to be evaluated with proper assumptions for various possible conditions of damaged nuclear fuel. At the beginning of this study, radiation dose rate of fuel debris has been estimated as a function of various parameters, and sensitivity of dose rate due to changes in parameters has been evaluated. After the preliminary study, models and methods for the sensitivity and uncertainty analysis of the radiation dose rate for fuel debris have been developed based on understandings from the preliminary study results, and then its applications in the management of damaged nuclear fuel have been proposed.

## 1.2 Literature review

### 1.2.1 Damaged nuclear fuel of 1FNPP

After the 1FNPP accident, TEPCO (Tokyo Electric Power Company) investigated the inside of damaged nuclear reactors [1]. However, part of the investigation was not successful and information on the condition of damaged nuclear fuel in reactors is still not accurate enough. Even if all information has not been acquired, information about what is inside of 1FNPP Unit 2 reactor is comparatively well known due to several investigations and TEPCO is going to start the retrieval of damaged nuclear fuel of Unit 2 reactor in 2022. However, information on damaged fuel is still not accurate enough to start the work on a large scale. Therefore, the retrieval work will be carried out on a small scale at the

beginning of the fuel retrieval and then is going to be expanded to large scale based on information obtained from the work in Unit 2 [2].

The condition of spent fuel depends a lot on the burnup history of the nuclear reactor, and fuel with high burnup has complicated isotope composition. Burnup of fuel is not uniform, and spent fuel has different burnup by its location in the reactor core. Fuel of 1FNPP has been used from 113 days up to 5 years until the date of accident, and it has a diverse burnup history depending on fuel groups. It has various isotopes including fission products and actinides. Moreover, radioactive fission products decay to daughter isotopes and non-radioactive isotopes are also being converted by activation. Therefore, the damaged nuclear fuel of 1FNPP already was in very complicated and diverse isotope composition at the date of the accident.

The 1FNPP accident made the isotope composition of the nuclear fuel more complicated. Nuclear fuel of 1FNPP melted while overheated by the failure of the cooling system. Temperature of fuel increased higher than 3,138 ℃ and $UO_2$ fuel pellets were able to completely melt [3]. This temperature was high enough to melt structural components including fuel assembly and control rod, and molten structural components were mixed with molten fuel. Moreover, molten fuel damaged the bottom of RPV and it fell to the bottom of PCV. After fall to the bottom of PCV, the damaged fuel was solidified and relocated by the sea water which was used to stabilize the nuclear reactor. Chemical reaction and coalescence with concrete at the bottom of PCV also changed the damaged fuel to complicate mixture, and it made the estimation of the condition of fuel to be difficult.

### 1.2.2 Characteristics of damaged nuclear fuel

Characteristics of the 1FNPP fuel debris is not confirmed yet and there is uncertainty in the condition of fuel debris. Sampling of the resolidified fuel debris of 1FNPP was not enough to reveal the entire condition of the fuel debris, and available information on the resolidified fuel is limited. Therefore, the uncertain condition of fuel debris needs to be inferred from the limited information and previous studies on damaged nuclear fuels. As a reference for the estimation on the condition of the resolidified nuclear fuel, previous studies on the fuel debris of TMI-2 accident are referenced in this chapter. The accident process of TMI-2 was not the same as that of the 1FNPP accident, and it had only partial core melt whereas 1FNPP reactors suffered full meltdowns. Nuclear fuels of TMI-2 was mixed with materials in the reactor core by the partial melt of the core, but this was limited to materials at the RPV because it had not melted through the bottom of the RPV. On the other hand, nuclear fuels in case of 1FNPP meltdown were mixed with more materials including concrete. However, the core melting process of TMI-2 is still worthy to be reviewed for the understanding of the fuel debris of 1FNPP despite all the differences between these two accidents.

TMI-2 nuclear reactor was damaged by the partial melt of reactor core which resulted from the failure of the cooling system. TMI-2 nuclear reactor was overheated by the heat from radioactive decay and exothermic oxidation of the fuel cladding after failures of the reactor cooling system. The abnormal high temperature damaged fuel assemblies and it melted part of the reactor core. The molten fuel had mixed with other molten materials and flowed down. Part of the molten fuel fell to the bottom of RPV, and it also formed a large mass of molten materials at the center of the reactor core. The molten materials at the core were surrounded by hard crust, and part of the molten hard crust fell to the bottom of RPV. Temperatures of all regions at the core reached to 2,800K ~ 3,100K while the partial melt of reactor core, excepting for some regions at the top and the bottom of fuel assemblies [4]. This core melting process resulted in a diverse condition of damaged nuclear fuels at the RPV of the TMI-2 nuclear reactor.

The condition of the damaged TMI-2 fuel can be categorized into five types based on its location in the RPV : intact fuel rods, loose debris, hard crust, consolidated fuel, and lower plenum debris. Fuel rods of the TMI-2 reactor were severely damaged by the accident, and the center of fuel assemblies were molten to form fuel debris at the bottom of RPV. Temperature at the reactor core increased above 3,100K and many fuel rods were not able to maintain their full length. Only two fuel rods maintained 90 % of their full length after the partial core melt [5]. Temperature of the center of the reactor core increased above 3,100K while the core was melting, but the peak temperature at the top of the upper spacer grids stayed at 1,500K ~ 1,700K. The top of the fuel assembly remained in intact condition because of this relatively lower temperature. The other end of the damaged fuel rod immersed in the molten fuel at the core which was liquid mixture of fuel and other materials including cladding, control rod, structural materials. The liquid mixture flowed into the damaged end of fuel rods and it migrated upward to the spring region of the control rods. This molten mixture resolidified and remained at the inside of the upper plenum of the damaged fuel assembly. Therefore, the upper part of the damaged fuel assembly had a mixture of fuel and other materials whereas its cladding was almost in intact condition. At the bottom of the intact upper parts of fuel rods, fuel debris beds were formed by the loosen fuel pellets and other materials which were loosened from the top of damaged fuel assemblies. The debris bed was formed with fractured fuel pellets, control rod spacers, end fittings, and resolidified materials which were a mixture of fuel with other materials. These materials were heterogeneously deposited at the debris bed, but well mixed with each other. Small particles at the debris bed were ceramic $(U,Zr)O_2$ phases and a few pure $UO_2$ particles which were formed at the temperature at 2,700K and 3,100K each. Almost 90 % of these particles were between 1 ~ 5 mm in their maximum dimension. Temperatures of the debris bed were maintained below 2,000K while the partial core melted but it temperature increased to high levels for a short time, and this resulted in the differences in the phase of small particles. Resolidified materials in bulk size at the debris bed were also compositions of uranium, zirconium and oxygen. However, resolidified materials at the debris bed contained less amount of control materials than damaged fuels at other locations of the RPV. It contained smaller amount of control materials including silver, indium, cadmium. Content of materials from cladding and structural materials were also smaller than damaged fuels at other locations. At the center of the reactor core, the consolidated region was located by wrapped with hard crust. The consolidated region was formed by materials which were previously molten at 2,700K ~ 3,100K, and then it consolidated and

resolidified at the central region of the reactor core. The damaged fuel at this region was in a solid loaf which is 3 m in its maximum diameter and 1.5 m in maximum thickness. Bulk of damaged fuel at the consolidated region was a mixture of ceramic and metallic phase, and it contained metals from cladding and control materials. It also contained materials from structural materials in the reactor core. This central previously molten material was wrapped with a hard crust. The hard crust can be classified into three types : upper crust, peripheral crust, lower crust. The upper crust is the damaged fuel at the top of the central consolidated region, and it contains ceramic and metallic phase fuels. It also had other materials in metallic phases which are formed by the melting of control and structural materials at the high temperature of 2,700K. Peripheral crust is the damaged fuel which wrapped the side of the central consolidated region. It had zirconium rich metallic fuels and intact fuel pellets. The lower crust is at the bottom of the central consolidated region, and its principal contents were a mixture of structural and control materials. The lower crust has relatively smaller amount of $UO_2$ than other regions, and it is in a form of small inclusions at the metallic phase of other materials. The lower plenum debris is the damaged fuel at the bottom of the RPV. Its maximum depth and diameter were 1m and 4m each. It consists of fuel debris in forms of large rock and granular particles. The lower plenum debris contained previously molten ceramic $(U, Zr)O_2$ which are very porous. Debris of the lower plenum were formed at the high temperature of 2,800K ~ 3,100K, and non-uniformly distributed at the bottom of RPV due to the redistribution by the hydraulic forces of cooling water.

Material compositions of TMI-2 debris consisted of fuels in ceramic phases which are $(U, Zr)O_2$ or $(Zr, U)O_2$, and mixture of materials in metallic phases. The metallic materials consisted of $UO_2$ and elements from the control rod and other core materials. The debris in loose debris bed were in ceramic phase in $(U, Zr)O_2$ and $UO_2$, and fractured fuel pellets were also deposited at the loose debris bed. The central consolidated region was in a metallic phase mixture of structural, control materials and fuels. The upper hard crust was in ceramic and metallic phase which contains Fe-Ni, Ag-In-U, Ni-Sn. The peripheral crust was in a metallic phase which has Fe-Zn-Ni-Cr, Ag-In, Zr-Ni-In. Lower crust was in the metallic phase with Zr-Fe-Ni-Cr, Ag-In, Zr-Ni-In. Lower plenum debris were previously molten ceramics with $(U, Zr)O_2$. These are conditions of majorities at each region, and other materials were also contained at the damaged fuel of each region in metallic or ceramic phases.

Fuel debris of TMI-2 had diverse porosity and density because of the various phases and solidified conditions of the damaged nuclear fuel. Density of fuel debris at the lower plenum has been sampled and investigated by Idaho National Laboratory, and densities of samples from the bulk lower head debris were from 6.9 $g/cm^3$ to 9.4 $g/cm^3$ [6]. The sample at the northwest from the center of the bulk debris was composed of fine particulate debris with the density of 6.9 $g/cm^3$. The density of debris at the northeast was from 7.6 $g/cm^3$ to 9.29 $g/cm^3$, and its porosity was from 5.7% to 31.7%. The density of debris at the southeast was from 7.45 $g/cm^3$ to 9.4 $g/cm^3$, and its porosity was from 17.3% to 27.0%. The density of debris at the southwest was from 8.3 to 8.6, and its porosity was from 7.6% to 20.5%.

Part of fuel debris in RPV of 1FNPP reactors may have characteristics similar with debris of TMI-2 even though many fuels fell to the bottom of the PCV. Debris at the RPV may have characteristics in the five types of damaged fuel like TMI-2 reactors. Some debris at the upper part of RPV may be in ceramic phases with some of less damaged fuel assemblies, and a bulk damaged fuel mixture with other materials may be below. Even if the amount of fuel at these two regions can be very different from that of TMI-2, major characteristics of fuel debris will be similar. Fuel debris in diverse conditions may be located at the below of the bulk mixture like TMI-2, these debris also may have characteristics similar to TMI-2. However, many fuel debris of 1FNPP reactors had fallen to the bottom of PCV, and they were relocated by the sea water which has been used for the stabilization of the damaged reactors. This difference might have made the condition of fuel debris more complicated than the debris of TMI-2.

### 1.2.3 Damaged nuclear fuels in a canister

Estimated amounts of fuel debris in canisters of TMI-2 is reviewed for the understanding on the retrieved spent nuclear fuel from the damaged nuclear reactor. After the TMI-1 nuclear accident, 139 MT of damaged nuclear fuels were retrieved from the TMI-2 nuclear reactor, and 342 canisters were used to contain the retrieved fuel [7]. Among these canisters, 268 canisters are used for large debris or damaged fuel assemblies, and 12 canisters are used for debris in small particles. Remaining 62 of canisters are used to contain very fine particles which are smaller than 850 $\mu m$. The amount of special nuclear materials (SNM) at each canister has been estimated by Lassahn of Idaho national laboratory [5]. Lassahn used data on weigh of core material in each canister (payload) for the estimation. Data sheet on the length of retrieved fuel assemblies and number of certain structural components also used for the estimation. However, these data had large uncertainty in its details, and the estimation was done by many guesses and approximations.

Estimated amount of SNM in each canister was very diverse because damaged fuels were in various conditions. Payload of each canister was diverse, and the estimated amount of SNM was also a lot different by canisters depending on types of the retrieved damaged fuel. Some canisters had fuel assembly only, and such canisters had been estimated to have SNM in the amount of the retrieved fuel assembly. Some canisters were almost empty and had a little amount of SNM. Canisters with many debris had diverse amounts of SNM which are different from the amount of SNM in a fuel assembly. More details and data on the estimated amount of TMI-2 fuel debris are in Appendix A.1.

Damaged nuclear fuels of 1FNPP may be in more complicated and diverse conditions. Their shapes and size, physical and chemical characteristics may be more diverse than TMI-2 fuels. This diversity will affect the possible amount of fuel debris contained in each canister like TMI-2, and characteristics of the nuclear radiation and the criticality safety of fuel debris will be affected by this variability.

### 1.2.4 Uncertainty of damaged nuclear fuel condition

Condition of severely damaged nuclear fuel is uncertain and difficult to characterize. Intact spent nuclear fuel also has complicated characteristics depending on how were they used in a nuclear reactor. Long time of irradiation changes physical and chemical characteristics of the nuclear fuel. A spent fuel has less density and more porosity than a fresh fuel by the grain growth and re-crystallization. Fuel pellets crack and swell by the precipitation and release of fission products after being used. Spent fuel has many isotopes which are made by the fission and decay, and this changes the isotope composition and chemical properties of the fuel. These changes depend a lot on the burnup, and fuel assemblies have different burnup histories by fuel groups. Fuel pellets in a fuel assembly also have different burnup depending on their position within the fuel assembly. The nature of nuclear fuel makes the feature of spent fuels to be more complicated. However, the possible uncertainty of an intact spent fuel is smaller than that of a damaged nuclear fuel, and it does not pose a big problem to safe management. Criticality and nuclear radiation safety of intact spent nuclear fuels can be properly managed based on sufficient information. On the other hand, the condition of the severely damaged nuclear fuel is very complicated, and information for their safe handling is not enough unlike the intact fuel. A core melting accident damages and melts fuel cladding, and it releases fuel pellets from fuel assemblies. Released fuel pellets are also melting and mixing with other materials, and these change physical and chemical properties of the fuel. Other events such as hydrogen explosion and release of radioactive isotopes makes the condition of the damaged fuel more uncertain. Solidification of molten fuel in different conditions makes damaged nuclear fuel have diverse physical and chemical properties. Moreover, it is difficult to monitor the condition of fuel when an accident is in progress, and investigation after the accident is also very difficult because of the strong radioactivity from the damaged nuclear fuel. These difficulties make the condition of damaged nuclear fuels more uncertain. In the case of the TMI-2 nuclear reactor, fuel debris had been retrieved and investigated after the nuclear accident. However, details on the properties of fuel debris in canisters still have uncertainties. Estimated weight of fuel debris in each TMI-2 canister is uncertain because it had been estimated by guesses and approximations with limited information. Details on the size and shape of fuel debris, and their precise amount are uncertain. Thus, the condition of damaged nuclear fuel is uncertain, and its characteristics need to be estimated with limited information. In addition to this, verification of the estimated data also has uncertainty due to the possible measurement error. Model used for the estimation also has uncertainty depending on the analytical tool used for the calculation. Therefore, uncertainties of damaged nuclear fuel need to be properly categorized and estimated for the reasonable evaluation on the characteristics of fuel debris.

According to a general classification of uncertainties, the uncertainty associated with the damaged nuclear fuel can be classified as parametric and structural uncertainty. Parametric uncertainty comes from the model input which depends on the condition of damaged nuclear fuel. Structural uncertainty comes from the model itself such as inadequacy and error of the model. Parametric uncertainty can be classified as the random and non-random uncertainty. Random uncertainty comes from randomness of a parameter such as size and distribution of damaged fuel in a storage container. Intact nuclear fuels are made by certain standards even though their geometry can be slightly differ depending on its manufacturer,

and their geometry is almost the same when they are contained in storage containers. On the other hand, the geometry of severely damaged nuclear fuel is diverse and uncertain, and damaged fuels in each container are in different distributions and conditions. Therefore, the uncertainty of the geometry of the damaged fuel in each container can be considered as a random uncertainty. Non-random uncertainty can be considered as variability rather than uncertainty. As an example, burnup is an important variable which affects a lot on the nuclear radiation. Non-random uncertainty can be classified as information uncertainty and inherent uncertainty. Information uncertainty comes from incomplete information on a parameter. Detectors and measurement instruments can have errors and measurement with errors can result in uncertainty. Information can be incomplete because of inaccurate measurement or not enough data. It is difficult to precisely identify the condition of the fuel in a severely damaged nuclear reactor because of the large amount of radiation and decay heats from its fuel interrupts use of measurement instruments. Inherent uncertainty or variability comes from variability of the condition of spent nuclear fuel. Variability of burnup of spent fuel by its location in RPV is a good example of inherent variability. Structural uncertainty can be classified in model uncertainty and model error. Model uncertainty or variability comes from assumptions or input parameters of the model. As an example, the result of estimation on dose rate can be differ by assumptions on the design of the fuel container. Model error comes from defects of the model or numerical error of tools used for the model. As an example, estimated data from Monte Carlo simulation inevitably has numerical error or uncertainty. Uncertainty and variability evaluated in this dissertation are classified based on this category and tabulated in Table 1.1.

**Table 1.1 Classification of uncertainty and variability**

<table>
<tr><td rowspan="3">Parametric uncertainty</td><td colspan="2">Random</td><td>1. Shape of debris (Sphere, Non-sphere)<br>2. Size of debris<br>3. Distribution of debris in a canister</td></tr>
<tr><td rowspan="2">Non-random</td><td>Information</td><td>1. Release of isotope</td></tr>
<tr><td>Inherent</td><td>1. Height of detector<br>2. Distance from a canister<br>3. Burnup</td></tr>
<tr><td rowspan="2">Structural uncertainty</td><td colspan="2">Model uncertainty</td><td>1. Simplified design<br>a. Canister (Fuel, Knockout, Filter)<br>b. Transfer cask<br>c. Transport cask<br>2. Shielding materials</td></tr>
<tr><td colspan="2">Model error</td><td>1. SCALE error<br>2. Error of the analytical model<br>- Point source approximation<br>- Linear path from a source to a detector<br>- Self-attenuation<br>- Particle self-shielding</td></tr>
</table>

### 1.2.5 Criticality safety and radiation dose rate of fuel debris

There are a few precedents on nuclear accidents which severely damaged nuclear fuels, and almost all research papers are on Three Mile Island unit 2 (TMI-2) and Fukushima Daiichi nuclear power plant (1FNPP) accident. Hiroki et al (2016) [8] and Maria et al (2019) did analysis of criticality safety of fuel debris in damaged nuclear reactors [9]. Hiroki T. conservatively calculated the multiplication factor of debris dust which can be generated while drilling and cutting fuel debris bed. In his model, the debris bed has been assumed to be a sphere with a drill hole and debris dusts are randomly distributed in a cylindrical space above the hole. Fuel debris dust is assumed to be spheres in the same size which are smaller than 1mm. The multiplication factor has been calculated by using MVP 2.0 neutron transport Monte Carlo code with JENDL-4.0. Hiroki proposed to install a debris dust guide at the open end of the drill hole to reduce the multiplication factor. The possibility of this method has been verified by comparing the multiplication factor of debris dust in a distribution of concave cylinder (debris dust with dust guide) and in a distribution of cylinder (debris dust without dust guide). On the other hand, Maria calculated the effective multiplication factor of fuel debris in stationary condition by assuming regularly distributed debris particles which is Face Centered Cubic (FCC) structure. The geometry of the fuel debris bed has been simplified to a spherical arrangement of fuel particles for conservative estimation. All fuel particles were spheres in the same size which are regularly distributed (FCC) in a spherical fuel debris bed. Maria F. L. have evaluated the criticality safety of fuel debris bed for 6 parameters which are particle size (mm), porosity, debris size (cm), fuel composition, (wt%) amount of concrete (vol %), water boration (ppm). MCNP has been used for the model, and the effective multiplication factor has been calculated. After the study on criticality safety, Maria F. L. proposed to build a comprehensive database as a benchmark data for the criticality safety of 1F fuel debris retrieval.

In 2019, Eka S. R. et al calculated radiation dose rate of fuel debris in 1F nuclear reactor by assuming fuel debris as a uniform mixture of fuel and other materials [10]. PHITS (Particle and Heavy Ion Transport code System, JAEA) code which is similar to MCNP has been used for this study. Fuel debris has been assumed to be a uniform mixture of isotopes which has been generated by burnup of the 1F nuclear reactor. Isotope release after the 1F accident also has been considered for the calculation of the photon and neutron source term. As a result of the calculation, the characteristics of photon and neutron flux have been evaluated for photon and neutron source isotopes. Eka et al confirmed that the major neutron sources of fuel debris are the spontaneous fission of $^{244}$Cm and neutron induced fission reaction of fissile materials in fuel debris. They also confirmed that the subcritical multiplication factor affects the induced fission reaction in fuel debris. They also proposed that the 2.2 MeV photons can be a potential marker to identify the fuel debris in 1F PCV.

Study of the criticality safety of fuel debris in a canister was done by Xudong Liu in 2016 [11]. Liu assumed hexagonal close packed (HCP) fuel particle lattice for the analysis of the fuel debris in a canister and evaluated the variability of the neutron multiplication factor by changes in the particle diameter and pitch distance. JAEA also estimated criticality safety of fuel debris in a canister in 2016 [12]. However, JAEA assumed a uniform mixture of fuel and other materials for their model unlike the model of Xudong Liu.

### 1.3 Scope of the dissertation

Even if there were many research projects on severe nuclear accidents, most of them were focused on the environmental impact of the accident, and variability of the nuclear radiation by the uncertain condition of damaged nuclear fuel was not a major concern. Radiation from intact fuel is easy to estimate and many computer codes can provide precise estimation in a short time. However, radiation from severely damaged nuclear fuel is very different from that of the intact fuel, and its evaluation is not a simple task. Error or variability by the uncertain condition of damaged fuel may not be a big problem for conventional radiation shielding because it can be supplemented by adding more shielding materials. On the other hand, such an error is not neglectable when the estimated result is used for the characterization of damaged nuclear fuel. As an example, the error and uncertainty may impact an analysis when high energy photons from a damaged nuclear fuel are evaluated to identify unknown conditions of the fuel debris [10]. As another example, error and uncertainty of dose rate may not be ignorable when optimizing a design or the use of radiation monitoring devices. Quantification of error and uncertainty also can be important when the estimated result is used to deal with social issues such as public concern and anxiety on the nuclear waste management. Moreover, even if the use of the quantified uncertainty is limited to special cases, having the estimated data is better than having nothing.

This dissertation aims to develop a model to evaluate the variability and uncertainty of the radiation from damaged nuclear fuel. The evaluation is focused on the parametric uncertainty, and the random uncertainty is the main topic. This dissertation mainly deals with 1FNPP related topics and safe retrieval of fuel debris. However, it is not intended to be used for 1FNPP only but also for the potential nuclear accident in the future. Models developed in this dissertation estimate radiation dose rate of damaged nuclear fuel and evaluate its uncertainty. Methodology to save time for the evaluation is also proposed as an additional topic.

This dissertation consists of three parts. At first, variability of radiation dose rate is evaluated for major variables which affect the dose rate. After this preliminary study, a model is developed to estimate the uncertainty of dose rate by uncertain condition of fuel debris in a canister. The model uses Monte Carlo method for sampling, and dose rates are calculated by SCALE and Python code. An analytical method is developed to save time for the evaluation and compared with the result from SCALE. In the last part, several topics are discussed by applying the analytical method, and methods to reduce the uncertainty are evaluated.

Use of the estimated data in this dissertation may be limited to some cases of 1FNPP. However, the model and methods used for the estimation can be used for the potential nuclear accident in the future. Moreover, methods used for the estimation of uncertainty can be applied for other topics which are not limited to fuel debris.

# Chapter 2. Description of Model and Preliminary Analysis

## 2.1 Introductions

This chapter focuses on the development of a model which is the basis of studies in this dissertation. At the beginning of this chapter, preparations of essential data and assumptions for the preliminary study are explained. As a preliminary study, variability of radiation dose rate has been evaluated for several parameters including burnup, isotope composition, and geometry of fuel debris. Radiation shielding and benchmark study on TMI-2 and 1FNPP are also discussed as preliminary studies.

Typical designs of a canister which contains retrieved damaged nuclear fuel are proposed at the model, and then dose rate of each type of canister are calculated as a preliminary study. Shielding effect of water is evaluated to compare the attenuation of radiation in air and water. This has been studied because even if 1FNPP Unit 2 will not be filled with water and the retrieval work will be commenced in air, part of works on other reactors can be conducted in water. Burnup is an important variable which affects the source term of damaged nuclear fuel. Therefore, the effect of burnup on the change of source term and radiation dose rate has been studied. The effect of burnup on the multiplication factor is also evaluated to understand the neutron transport in damaged fuel. Variability of dose rate by changes in the radioactive isotope composition is also studied because part of volatiles and noble gases have been released from the nuclear reactor after the 1FNPP accident. Variability of dose rate by geometry of fuel debris and design factors of canister are also studied. As a last step of the preliminary study, radiation shielding performance has been evaluated for several materials. After parametric studies, results from these have been used to develop an advanced model and methods at Chapter 3.

## 2.2 Model development

### 2.2.1 Background and Assumptions

Fuel debris of a damaged nuclear reactor has various shapes, and a lot of them are asymmetric. However, the shape of fuel debris is simplified to sphere in this dissertation, and non-spherical debris are modeled by using random close packing. The random close packing is made by random sampling on diameter and distribution of spheres in a canister (Figure 2.1). This random packing is used in Chapter 3, and details on the method of sampling is discussed in that chapter. In the preliminary study, the size of the sphere is assumed to be the same for all debris, and diameter is decided depending on the purpose of each topic as a variable. Density of fuel debris from damaged nuclear reactors is diverse according to the literature review in the previous chapter. However, density of fuel debris is assumed to be the same for all fuel debris at this model except for some parametric studies. The density is decided to 9.6 g/cm$^3$ by assuming that the initial loading of $UO_2$ is well mixed with control and structural materials in a 1FNPP nuclear reactor. The initial loading and composition of materials are decided based on a JAEA report on the estimated fuel composition of 1FNPP nuclear reactors [13]. Composition of fuel debris is decided based on the estimated source term of 1FNPP debris by using the ORIGEN module of SCALE. Details on the source term are discussed in the next section.

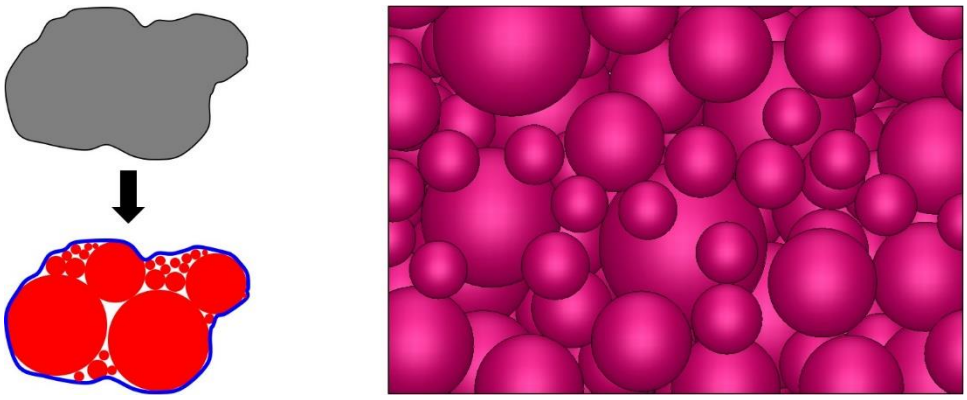

**Figure 2.1 Modeling of non-spherical debris by the random close packing.** The non-spherical debris is expressed by the assembly of spheres (left). The figure on the right is an example of the random close packing.

It is assumed that fuel debris are retrieved and contained in a canister 10 years after a nuclear accident. Inside of a canister is filled with fuel debris and dry air, and outside of the canister is also assumed to have dry air excepting for some parametric studies. Nuclear radiation less attenuates in air than water, so this assumption prevents underestimation of the radiation dose rate. Moreover, according to the 1FNPP fuel debris retrieval plan of TEPCO [2], retrieval work is going to be commenced in Unit 2 reactor and its fuel debris will be retrieved exposed to air. The dry air is replaced with a mixture of gases for some preliminary study because gases such as argon, nitrogen and helium can be filled in a canister as a cover gas. In the case of the TMI-2 canister, such gases are also used for the removal of water from the canister. The dry air inside and outside of a canister is also replaced with water when calculating the effective multiplication factor. The water is also assumed as a medium when the attenuation of nuclear radiation in water is evaluated. Canister design has been decided by referencing designs of TMI-2 canisters and then it has been compared with the design of 1FNPP canisters. Details on the canister design is discussed in section 2.2.3.

SCALE and MCNP are used for the calculation of dose rate, but SCALE is used as a major code for almost all topics in this dissertation. Primary usage of MNCP was to certify the reliability of SCALE output and double check errors. MEVRIC module of SCALE uses Consistent Adjoint Driven Important Sampling (CADIS) methodology, which uses importance map and biased sources [14]. CADIS of SCALE save time for the calculation of dose rate, but its results can be a little bit different from results of MCNP. The difference of cross section data of SCALE and MCNP also can make some differences in their outputs. However, the difference is acceptable, and it does not significantly affect to the result of estimation. Details of the comparison between the calculation by SCALE and MCNP is discussed in Appendix A.2. Dose rate is calculated by point tally or region tally for almost all topics. The location of estimation or the detector location is decided based on the purpose of each topics. For the parametric study on the variability of dose rate by the change of the detector location, dose rate near a canister is estimated at multiple points

located from the center of a canister to 1 m. Dose rate far from a canister is estimated by assuming the locations from the center to 10 m. The point detector placed 1m from the surface of a canister instead of the center depending on the purpose of topic. In case of the region tally used for the preliminary study, multiple cylindrical regions are assumed, and dose rates are regionally averaged at each cylindrical region (Figure 2.2). The thickness of each region is assumed to10 cm and height of region is assumed to be same with the height of a canister.

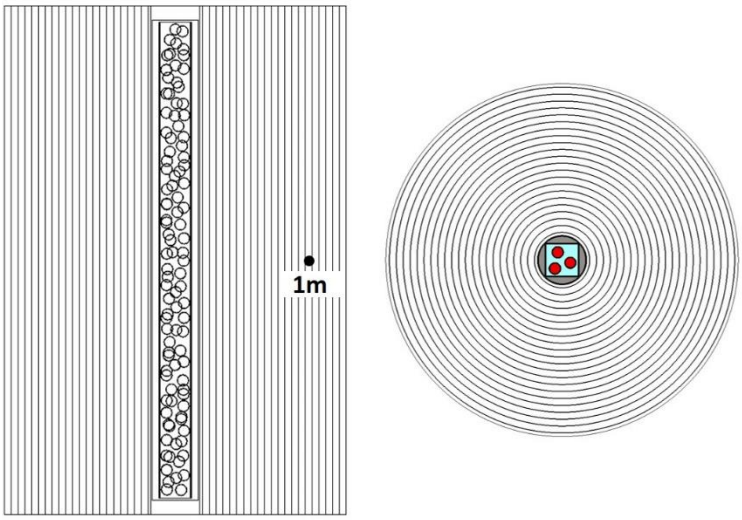


**Figure 2.2 Cross sectional view of cylindrical regions.** Cylindrical regions surround a canister containing fuel debris (red spheres). Detail on the canister design is in section 2.2.3.

### 2.2.2 Preparation of source term

Source term is the type and amount of radioactive material that is produced and released from a nuclear reactor following a severe nuclear accident. The source term of 1FNPP is used as the basis for the estimation of dose rate in this dissertation. The source term has been calculated by using the ORIGEN module of SCALE, and its result is compared with the estimated source term of JAEA. JAEA already estimated the fuel composition of 1FNPP nuclear reactors in 2012, and their report has details on the photon radiation intensities both by materials and energy groups [13]. However, in case of the neutron radiation intensity, the report does not have its intensities by energy groups. Therefore, the source term of 1FNPP has been calculated again to get more details of the radiation intensity. Essential parameters including initial loading and burnup of fuel has been assumed based on data of the JAEA report. According to the JAEA report, mass of $^{235}U$ and $^{238}U$ in 1 MT of fuel is assumed to be 37 kg and 963 kg each. Mass of other materials and more details are in Table 2.1. The mass per a core and an assembly are calculated based on parameters of 1FNPP Unit 1 which has 400 fuel assemblies in its core with 3.7 wt% of $^{235}U$ enrichment.

**Table 2.1 Initial mass of fuel and cladding materials**

| Components | Mass per tHM (g) | Mass per a core (g) | Mass per an assembly (g) |
|---|---|---|---|
| $^{235}U$ | 37,000 | 2,553,000 | 6,382.5 |
| $^{238}U$ | 963,000 | 66,447,000 | 166,117.5 |
| O | 134,538 | 9,283,122 | 23,207.81 |
| Cr | 204 | 14,076 | 35.19 |
| Fe | 530 | 36,570 | 91.43 |
| Ni | 102 | 7,038 | 17.6 |
| Zr | 200,118 | 13,808,142 | 34,520.36 |
| Sn | 2,977 | 205,413 | 513.53 |
| Total | 1,338,469 | 92,354,361 | 230,885.9 |

Photon energy structure of the JAEA report is in 18 groups which is a predetermined group of ORIGEN 2.0 [15]. However, the energy group of this dissertation is divided into more groups for more precise analysis. Energy group structure for photons has been assumed from $1.0 \times 10^3$ eV to $2.0 \times 10^7$ eV and it has been divided into 101 logarithmically spaced bins. Neutron energy has been also divided into 101 bins and its energy ranged from $1.0 \times 10^{-4}$ eV to $1.0 \times 10^8$ eV. Dates of irradiation and specific power of each fuel group is decided based on the burnup history of 1FNPP Unit 1 in JAEA report (Table 2.2) [13]. 1FNPP Unit 1 has 6 fuel groups and fuel assemblies of all groups is 9 x 9 sequence except for the group 4 which is 8 x 8 sequence. 1FNPP Unit 2 and Unit 3 have different burnup history and fuel groups, and details on their burnup history are in Appendix A.3. Decay of isotopes is calculated up to 10 years after the date of accident.

**Table 2.2 Burnup history of 1FNPP Unit 1 [13]**

| Dates of Irradiation | Specific power (MW / tHM) | | | | | |
|---|---|---|---|---|---|---|
| | Group 1 | Group 2 | Group 3 | Group 4 | Group 5 | Group 6 |
| 189 | 27.69 | 24.76 | 21.47 | 18.08 | 15.05 | 12.21 |
| 341 | | 30.93 | 26.11 | 21.34 | 17.66 | 14.16 |
| 349 | | | 32.29 | 25.69 | 21.13 | 16.75 |
| 445 | | | | 30.69 | 25.11 | 19.73 |
| 346 | | | | | 29.09 | 22.7 |
| 413 | | | | | | 25.55 |
| Burnup (MW / tHM) | 5,234 | 15,228 | 21,231 | 33,315 | 37,479 | 40,172 |
| number of fuel assembly | 64 | 64 | 80 | 68 | 64 | 60 |
| Fuel assembly sequence | 9 x 9 | 9 x 9 | 9 x 9 | 8 x 8 | 9 x 9 | 9 x 9 |

Figure 2.3 presents the energy distribution of photon and neutron radiation 10 year from the date of accident which is calculated by the ORIGEN module of SCALE. Photon and neutron intensities are calculated for all damaged fuel in a reactor core which is 69 tons for 1FNPP Unit 1. Peak photon intensity is at the energy bins from 647 keV to 713 keV which includes the γ decay energy of $^{137}$Cs and $^{134}$Cs. Photon intensity in energy range from 10 keV to 500 keV decreases by the increase of energy except for some peaks. Distribution of neutron energy is biased to high energy and its peak is at the energy bins from 1.36 MeV to 2.17 MeV.

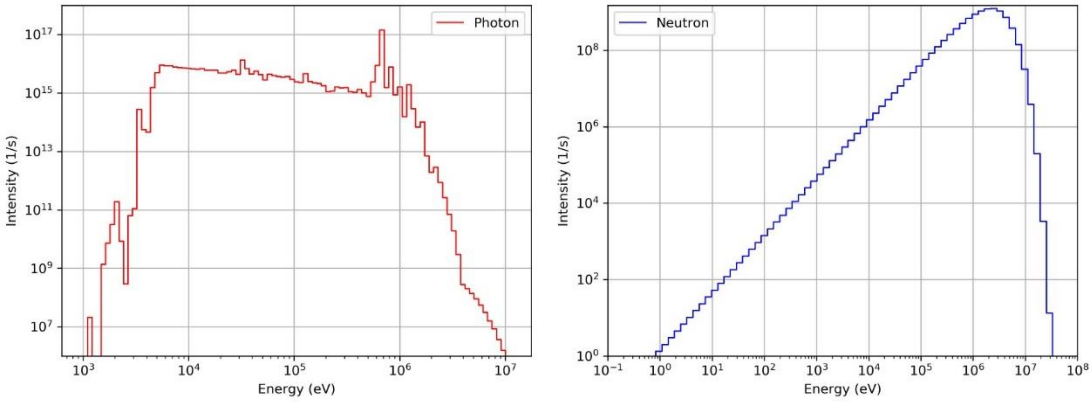


**Figure 2.3 Energy distribution of photons (left) and neutrons (right).** Y-axis of the graph is the radiation intensity per a reactor core. X-axis is the energy of 101 groups.

The photon energy distribution data is from the JAEA report and it has been divided into 18 energy groups. Neutron energy distribution is not in the report and it classified neutron intensities not by energy but by types of materials. In this dissertation, the photon energy spectrum, which has been estimated by the ORIGEN module of SCALE, has been converted from 101 energy bins to 18 energy bins to compare with the JAEA data (Figure 2.4). There are some differences between SCALE output and JAEA data when photon energy is smaller than 400 keV because SCALE calculated the photon energy spectrum in more detail with 101 energy bins. Values of 101 bins are converted to 18 bins by averaging values for each 18 bins and this resulted in the difference of data. Use of different energy libraries also affected the results. JAEA data has been calculated by using ORIGEN 2.0 with JENDL nuclear data library. On the other hand, the ORIGEN module of SCALE uses the ENDF/B-VII.1 nuclear data library. Even if there are some differences, this does not significantly affect the estimation of dose rate from fuel debris in a canister. Moreover, the difference can be ignored when this data is used for the evaluation of shielding performance because low energy photons are easy to be shielded. More details on the comparison of the calculation of dose rate by using SCALE output and JAEA data is explained in the Appendix A.4.

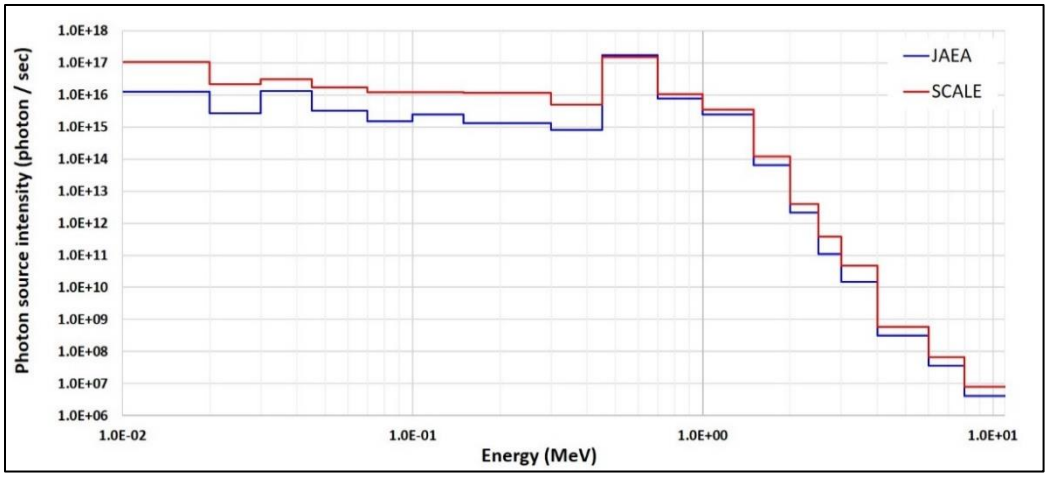


**Figure 2.4 Photon energy distribution from ORIGEN module of SCALE and ORIGEN 2.0 of JAEA.** Red line is data from SCALE which has been converted from 101 bin to 18 bin, and the blue line is data in the JAEA report. The time for estimation of the photon source intensity is 10 years after the nuclear accident.

Total source strength ($S$) from all damaged fuel in a reactor core is calculated by summing radiation intensities ($I_i$) for all energy ranges, and then the source strength of fuel debris in a canister is calculated by multiplying this by the fraction of fuel debris of a canister per total mass of fuel in a core.

$$S = \sum_i I_i \times \left(\frac{m_{canister}}{M_{core}}\right)$$

Mass of retrieved fuel debris can vary depending on the canister because the physical condition of debris is diverse. However, it is assumed that the mass is controlled, and the mass of retrieved fuel debris in each canister ($m_{canister}$) is maintained at 230.9 kg excepting for some parametric studies. The mass of fuel debris in a canister is decided to be similar with the mass of a fuel assembly by referencing the JAEA report [13], and the 230.9 kg of mass is calculated by dividing the sum of the mass of all components ($m_i$) in a reactor core by the total number of fuel assembly ($N$) in a reactor core.

$$m_{canister} = \frac{\sum_i m_i}{N}$$

Even if several variations of fuel assemblies were used for 1FNPP and their mass are different depending on manufacturers, the weight is calculated by considering the total weight of materials in the reactor core first.

### 2.2.3 Design of canisters

Designs of TMI-2 canister are referenced for the development of models in this dissertation [16]. There are three types of canisters which have been used for the retrieval of fuel debris from TMI-2 nuclear reactor, and their designs were referenced by JAEA for the development of 1FNPP canisters. According to a JAEA report, 1FNPP canister will be shorter and its maximum capacity is also smaller than TMI-2 canister [12]. Even if this design is more suitable for practical use in 1FNPP, it is considered only for the comparison with TMI-2 design because more details on TMI-2 design is available whereas details on the 1FNPP canister is not released yet. A design with three small containers in a canister is referenced in Chapter 4 to be compared with TMI-2 design, and a modified design which is shorter but has larger diameter than the TMI-2 canister is also evaluated in Appendix A.5.

TMI-2 fuel debris has been retrieved by using three types of canisters : 'Fuel canister', 'Knockout canister', 'Filter canister'. Fuel canister is designed to contain damaged fuels in large sizes, from the size of a fuel pellet to the size of an intact fuel assembly. Fuel debris are grabbed by mechanical arms or collected in a basket, and then are put into the fuel canister. Knockout canister and Filter canister are designed to be used with a hydraulic vacuum system which collects small particles. Damaged fuels in the form of fine particles are inhaled by the vacuum system and then pass the knockout canister first. The knockout canister captures large particles and passes small particles. Filter canister has filter modules which can filter fine particles, and it collects fine particles.

Details of TMI-2 designs such as bolts and drain connector are ignored and simplified design is used to develop a model. Fuel canister consists of inner space for fuel debris, inner shell with neutron absorber and shroud, concrete filler, outer shell. Details on the design of upper closure and bottom of the canister are simplified to thick disk by simplifying the original design of TMI-2 canister. The overall height of the original design of TMI-2 is 380.365 cm but this height includes components of upper heads including drain connectors which are ignored for simplification. Therefore, the height of the fuel canister in this model is 367 cm. The outer diameter of the canister is 35.6 cm and the wall thickness of the outer shell is 6.4 mm. Cross sectional shape of inner space to contain debris is square and its dimension is 23.2 cm × 23.2 cm and height is 350 cm. The thickness of the upper head and bottom of the canister is 10.2 cm. Boral plates are placed with a steel inner shell to surround the spaces for fuel debris, and space between the inner shell and outer shell is filled with concrete filler. Schematic cross section of the fuel canister is in Figure 2.5. Shape of fuel debris are assumed to be spheres, and geometrical distribution of fuel debris in a canister is in a random or a certain packing structure depending on the purpose of each topic in this dissertation. Number of debris spheres in a fuel canister is also decided depending on each topic. It has been calculated to meet the assumed weight of fuel debris in a canister for all topics except for some preliminary study which assumed it to be 100. Even if some topics assumed the size of fuel debris in a canister to be the same for all debris, fuel debris of most topics does not have the same size and is randomly sampled. The medium that fills the space between debris is decided depending on topics, and it is assumed to be a mixture of non-fuel materials with air and water for some topics whereas most topics assume it to be air or water. Material of the outer shell and inner shell is

assumed to be SS304L stainless steel. Details on the material composition of each component are in Appendix A.6.

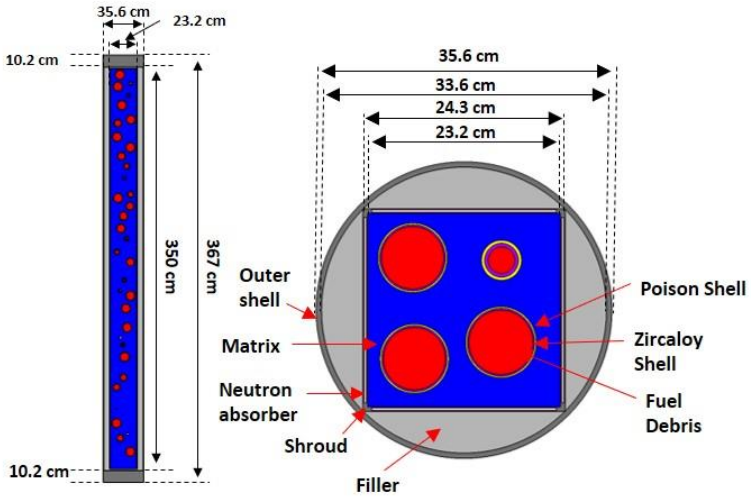


**Figure 2.5 Schematic cross section of fuel canister.** Red spheres in the canister are fuel debris. Debris spheres in this example are covered with thin films of zircaloy and boron, but this is assumed only on a few topics. Blue colored space is the medium between debris spheres, and this is filled with air or water, or it is assumed to be a mixture of non-fuel materials for some topics. Light grey colored spaces are filled with concrete filler. Dark grey colored spaces are filled with SS304L stainless steel.

The knockout canister consists of a filter screen, five tubes with poison rods, and an outer shell. Inlet pipes and support spiders of the original design are ignored for the simplification. Inner space of the knockout canister is filled with small debris particles, but this is assumed to be a uniform mixture of fuel. The fuel mixture consists of spent fuel, control materials, structural materials, water, and argon. Details of its composition is in Appendix A.6. Five tubes with poison rods are filled with boron carbide ($B_4C$). Outer shell is SS304L stainless steel. The overall height is assumed to be the same as the fuel canister, but its inner space is larger because the thickness of the bottom is different (Figure 2.6).

The filter canister consists of 17 filter modules and a central tube with neutron absorber, a drainage tube, 6 tie rods, outer shell (Figure 2.6). Fuel debris in the filter canister is a very fine particle which is in micrometer scale, and it is contained in the filter module and inner space between pipes and outer shell, and it also can remain in the drainage tube. Therefore, these three components are assumed as a mixture of fuel and non-fuel materials. Material composition of these components are different and details of it are in Appendix A.6. The tie rod is SS304L, and it provides structural integrity to the canister. The overall outer dimension is the same as the knockout canister, but the dimension of inner spaces is different.

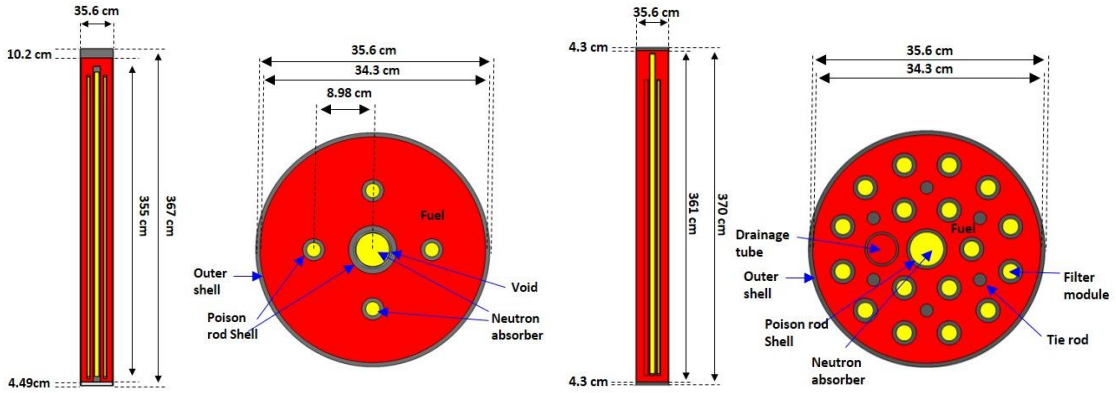


**Figure 2.6 Schematic cross sections of knockout (left) and filter (right) canister.** Red colored spaces are filled with a mixture of fuel and non-fuel materials. Yellow colored spaces are filled with neutron poison. Grey colored spaces are SS304L stainless steel.

## 2.3. Preliminary study

### 2.3.1 Variability of dose rate by changes in canister design

#### 2.3.1.1 Comparison of dose rate for 3 types of canisters

Dose rate of three types of canisters have been evaluated based on assumptions in the previous section. Mass of fuel in a canister is maintained at 230.9 kg for these three types of canisters, and shape of fuel debris is modified depending on types of canisters. The fuel canister has randomly distributed 100 spherical debris in a mixture of non-fuel materials. Debris of the fuel canister is a mixture of major actinides and isotopes in a spent nuclear fuel. The non-fuel material is a mixture of some steel, argon gas and water. The argon gas is assumed as a cover gas in a canister, and steel is added as a non-fuel debris. Amount of water in the non-fuel mixture is decided to be 10 % of the inner volume of the fuel canister, and the argon gas is 25 % in volume percent. The amount of steel is decided by subtracting the volume of fuel debris and other two non-fuel materials (water and argon) from the inner volume of the fuel canister. It is assumed that these three non-fuel materials are well mixed, and the non-fuel matrix filled the space between fuel debris. Density of the non-fuel matrix is 4.7 g/cm$^3$ whereas the density of the fuel debris is 9.6 g/cm$^3$. The fuel debris in this canister is coated with thin films of boral and zircaloy, and thickness of the layer is 0.2 cm each. All of these are assumed for the modeling of a canister which has fuel debris and non-fuel debris. On the other hand, knockout and filter canister have mixtures of fuel and non-fuel materials which are in red color at the Figure 2.6. Density of the fuel matrix is 5.4 g/cm$^3$, and the amounts of other materials are calculated in the same way as the fuel canister.

Canisters are placed in dry air and the dose rate of each canister has been calculated by using region tally from the surface of a canister up to 125 cm. Point tally also has been used to compare its values with results of the region tally. Detector location of the point tally is horizontally 100 cm from the center of a canister. Uncertainty by the Monte Carlo simulation of SCALE is maintained to less than 0.005 which is 0.5% of the calculated value.

This uncertainty is the standard deviation divided by the output response of SCALE, and this can be reduced by increasing batches to be used in the Monte Carlo simulation. The uncertainty also can be reduced by increasing the number of particles used for a batch.

In case of photon radiation, the highest dose rate is estimated from the knockout canister, and the filter canister is the next (Figure 2.7). Photon dose rate of the fuel canister is smaller than the other two. Regionally averaged photon dose rate at 100 cm from the center of a fuel canister is 56.7 rem/hr (567 mSv/hr). Dose rate of the knockout and the filter canister are 246.8 rem/hr (2,468 mSv/hr) and 227.6 rem/hr (2,276 mSv/hr) each. Dose rate at the point horizontally 100 cm from the fuel canister is 62.9 rem/hr (629 mSv/hr), the knockout and the filter canister are 281.6 rem/hr (2,816 mSv/hr) and 256.1 rem/hr (2,561 mSv/hr) each. This difference is due to the geometry of fuel debris and shielding materials in each canister. Photon sources of the knockout and the filter canister are in the form of tiny particles, and these particles are replaced by the fuel matrix in this model. Therefore, photon sources of the knockout and the filter canister are uniformly distributed in the overall inner space of each canister. On the other hand, photon sources of the fuel canister are concentrated in 100 of debris spheres, and these spheres are randomly distributed in the canister. These differences in the geometry of photon sources made differences in the path length from sources to a detector, and it resulted in the difference of the photon dose rate. Differences in their density also affected the dose rate, and photon radiation is more attenuated while passing the debris sphere with density of 9.6 g/cm$^3$ than the fuel matrix with density of 5.4 g/cm$^3$. The fuel canister has concrete filler, and space between debris is filled with a mixture of non-fuel materials whereas other two types of canisters do not have these. These differences in shielding materials are another reason that the fuel canister has a lower dose rate than other canisters.

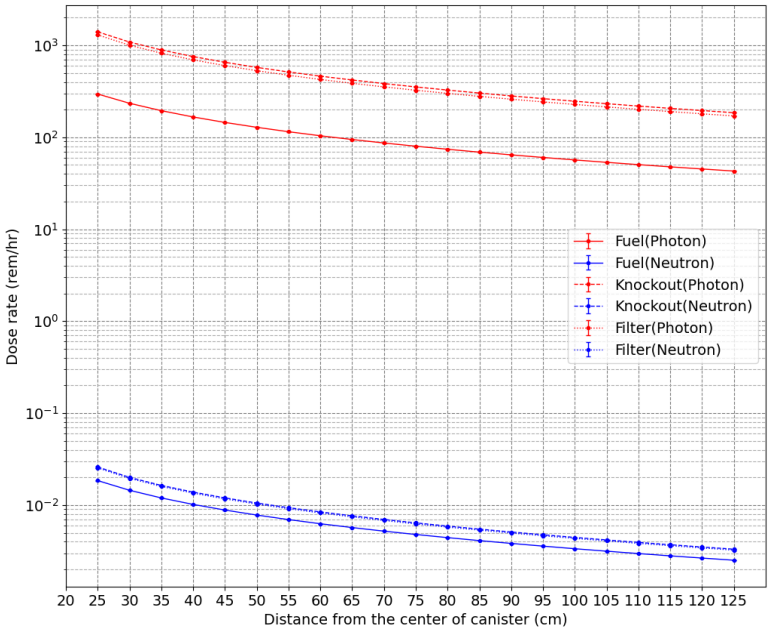


**Figure 2.7 Comparison of three types of canisters.** Red lines are the photon dose rates, and blue lines are the neutron dose rates from each type of canister.

In the case of neutron radiation, the knockout canister has the highest dose rate, but it is very similar with the dose rate of the filter canister (Figure 2.7). Dose rate of the fuel canister is smaller than others like as it is for photon dose rate. Regionally averaged neutron dose rate at 100 cm from the center of a fuel canister is 3.35 mrem/hr (33.5 μSv/hr). Dose rate of knockout and filter canister are 4.49 mrem/hr (44.9 μSv/hr) and 4.34 rem/hr (43.4 μSv/hr) each. Differences in geometry of fuel debris and shielding material of canister affected the difference of neutron dose rate like it did for photons, but the difference is smaller than that of photons. Differences in geometry of shielding material are less affected to the neutron dose rate than it is to the photon dose rate because the mean free path of neutrons in the shielding materials is larger than the mean free path of photon. Even if knockout canisters have 4 more neutron poison rods than filter canisters have, it has not significantly affected the difference in dose rate. More details on the estimated dose rate are in Appendix A.7.

Photon and neutron dose rates decrease a lot by changes in the distance from the debris, and the dose rate at 10 m is around 1% of the dose rate at 0.5 m (Figure 2.8). Neutron dose rate is smaller than 2 mrem/hr (20 μSv/hr) for all three types of canisters when the distance is larger than 2 m from the center of a canister. On the other hand, Photon dose rate at 10 m is larger than 1 rem/hr (10 μSv/hr) for all types of canisters.

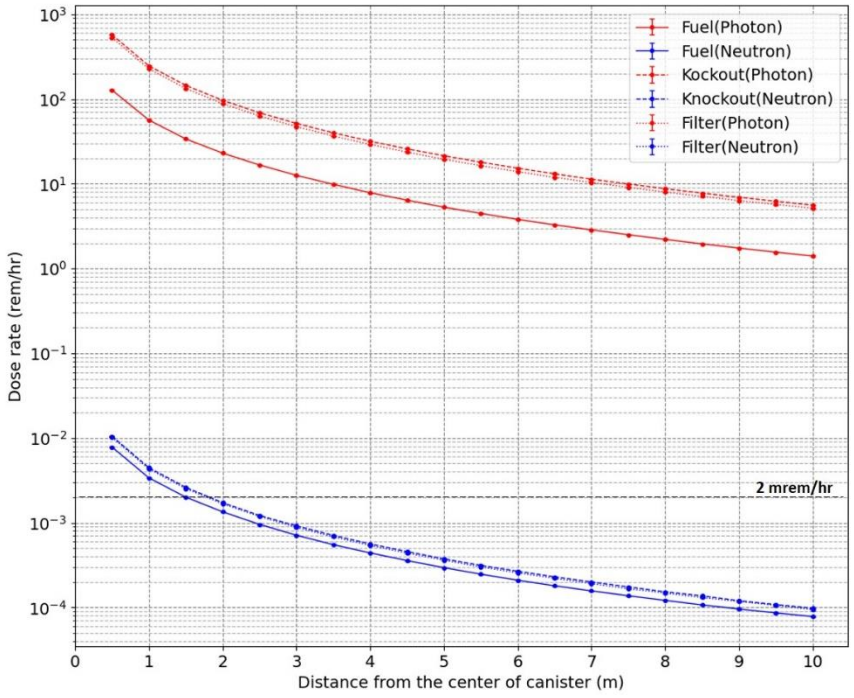


**Figure 2.8 Comparison of three types of canisters for the distance up to 10m from the center of a canister.** Red lines are photon dose rates and blue lines are neutron dose rates from each type of canister.

### 2.3.1.2 Comparison of dose rate of a canister in air and water

Radiation dose rate in dry air and in water is compared to evaluate the shielding effect of the medium which is surrounding a fuel canister. Water is a good shielding material, and nuclear radiation attenuates a lot when it is passing through water. At 100 cm from the center of a fuel canister, photon dose rate in water is 0.58 rem/hr (5.8 mSv/hr) which is around 0.01 times of the dose rate in dry air (Figure 2.9). This is because of the density ($\rho$) of water is much larger than the density of dry air. Mass attenuation coefficient ($\mu/\rho$) of water is not much different from dry air. However, the density of water is almost $10^3$ times larger than the density of dry air. Therefore, after the mass attenuation coefficient has been multiplied by density, attenuation coefficient ($\mu$) of water is much larger than that of dry air.

Neutron dose rate of a fuel canister is steeply decreased when it is in water. At 100 cm from the center of a fuel canister, it is 0.012 $\mu$rem/hr ($1.2\times 10^{-4}$ μSv/hr) which is less than $10^{-4}$ times of the dose rate in dry air. This value is much smaller than the U.S. NRC regulatory dose limit which is 2mrem/hr (20 μSv/hr) for individual members of the public, and neutron dose rate at 100 cm from a canister is ignorable when a canister is immersed in water. Results of the calculation of dose rate in water for knockout canister and filter canister are in Appendix A.7. Dose rate of other types of canisters are larger than that of the fuel canister, but they also decrease a lot by changes in the distance like the fuel canister does.

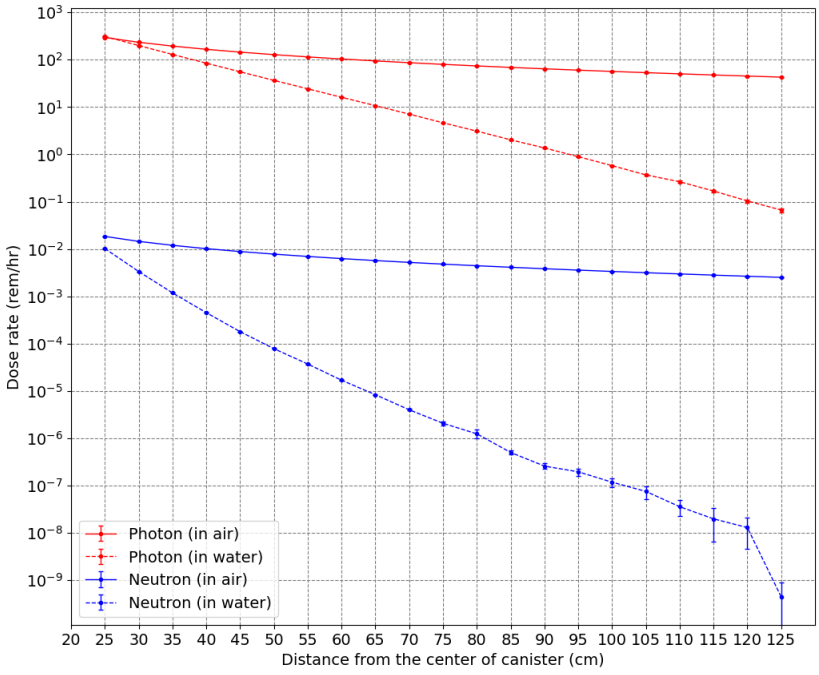


**Figure 2.9 Comparison of radiation dose rate of a fuel canister when it is in dry air (left) and water (right).** Red lines are the photon dose rates and blue lines are the neutron dose rate.

### 2.3.1.3 Variability of dose rate by changes in shielding materials

Shielding materials used in TMI-2 canisters are not the same for the three types of canisters, and this affected the differences in their radiation dose rate. More steel plates were used for the fuel canister than others, and the fuel canister has boral plates whereas other canisters have $B_4C$ rods. Moreover, the fuel canister has concrete filler between its inner steel plates and outer shell. These differences in the use of shielding material affected the smaller dose rate of the fuel canister. At this section, attenuation of radiation in typical shielding materials is evaluated by adding more shielding layers at the outer shell of a fuel canister. The thickness of the layer is adjusted, and dose rate is calculated at 100 cm from the center of the canister for different shielding materials including $B_4C$, Boral, Steel (SS304L), Lead, Tungsten-boron carbide (W-$B_4C$), Tungsten. Boral and boron carbide ($B_4C$) are neutron poisons which are commonly used for criticality safety. Radiations are attenuated while passing these poisons by absorption, but they are not efficient to be used for photon shielding. Photon radiation does not decrease below 10 rem/hr (100 mSv/hr) even 12 cm of poison materials are used (Figure 2.10). Steel, lead, tungsten are metallic materials which are commonly used for radiation shielding. Steel is the major structural material of a canister, and it can shield a considerable amount of photon radiation, but it is poor in neutron shielding. Lead is better than steel in photon shielding, but it is not good in neutron shielding. Tungsten is better in photon shielding than other materials, but it is less efficient than $B_4C$ in neutron shielding (Figure 2.11). The W-$B_4C$ compound is good for both photon and neutron shielding.

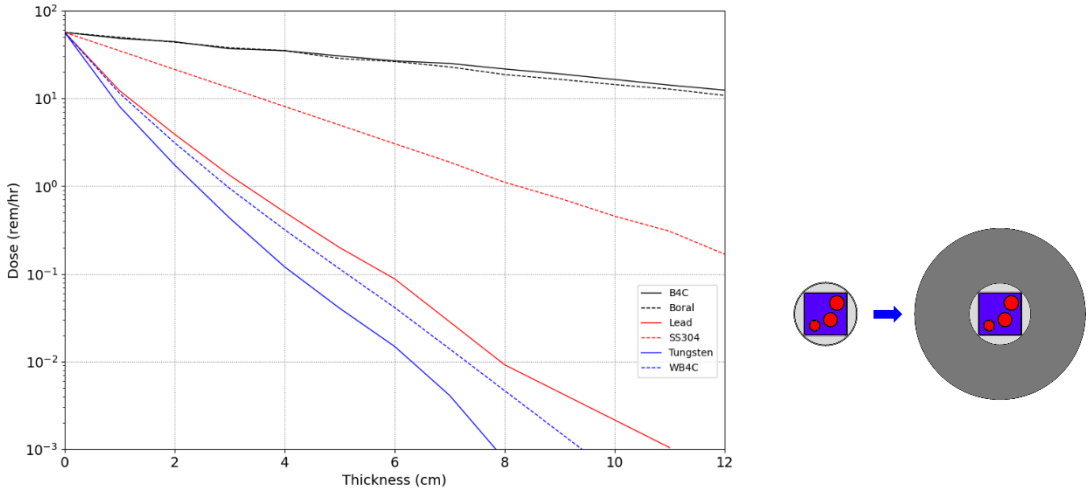


**Figure 2.10 Variability of photon dose rate by changes in thickness** of shielding materials which are added at outer shell of a fuel canister. The added shielding material is surrounded the outer shell of a canister like the figure at right.

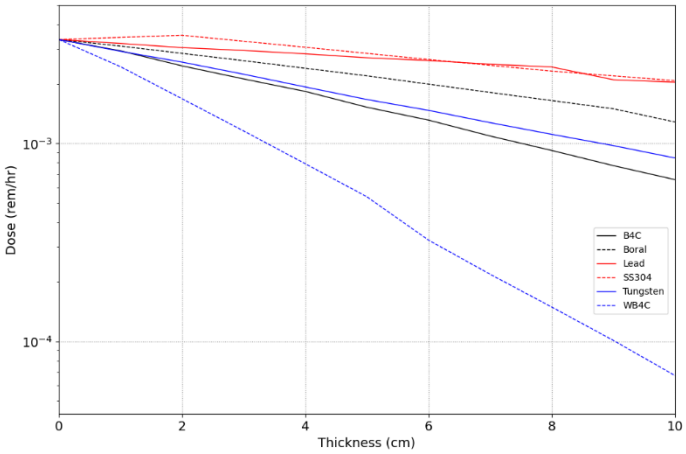


**Figure 2.11 Variability of neutron dose rate by changes in thickness** of shielding materials which are added at outer shell of a fuel canister.

Radiation dose rate is very sensitive to changes in thickness of shielding material, and the radiation can be shielded by adding larger amounts of materials to meet the safety requirements. However, the total mass of a canister increases by using more materials, and the use of more shielding material is limited by its weight. Moreover, good shielding metals such as tungsten have high density and can make a canister too heavy to handle. Therefore, a shielding material needs to be used with other materials rather than alone. Use of composite like W-$B_4C$ or alloy is a typical method to use shielding materials together. Use of multilayer shielding materials is also commonly used to enhance the shielding performance. More example on the use of composite are in Appendix A.8.

Use of multilayer is a good method to enhance the shielding efficiency, but materials need to be used in proper order to improve shielding performance. Especially gamma rays from neutron capture reaction $(n, \gamma)$ can reduce the shielding efficiency if layers are used in improper order. As an example, when $B_4C$ layer is used with tungsten layer, use of tungsten first and surrounding it with $B_4C$ layer is inappropriate because the neutron-capture gamma ray of tungsten isotopes reduces the shielding efficiency. $B_4C$ needs to be used inside and tungsten needs to surround $B_4C$ to enhance the efficiency (Figure 2.12).

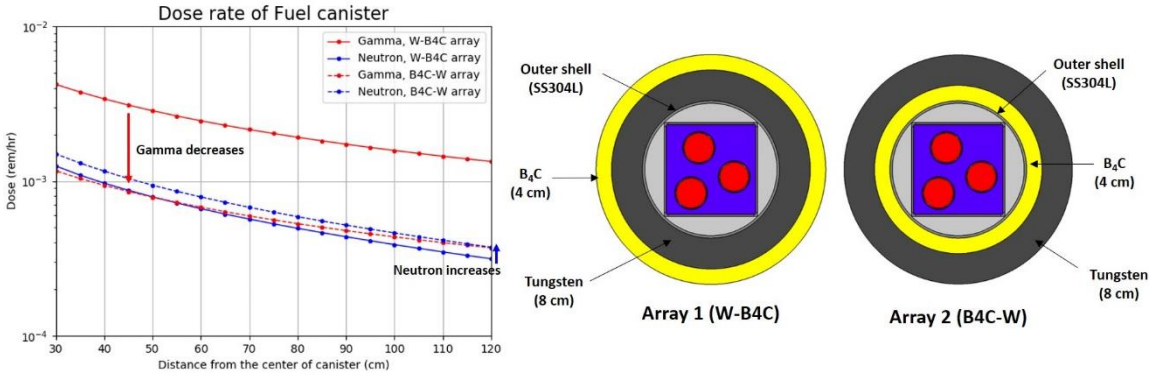


**Figure 2.12 Comparison of dose rate** between tungsten-$B_4C$ array and $B_4C$ -tungsten array.

### 2.3.2. Variability of dose rate by source term

#### 2.3.2.1 Comparison of dose rate between fuel debris of TMI-2 and 1FNPP

Burnup significantly affects the estimated radiation dose rate by impacting the source term which is the types and amounts of radioactive materials of the fuel debris. As a benchmark study, the photon dose rate of a canister and its source term are compared for burnup of TMI-2 and 1FNPP. TMI-2 reactor started its initial operation in December 1978 and a nuclear accident happened in March 1979. Therefore, the average burnup of TMI-2 fuel was only 3.18 GWd/MTU which is much lower than typical burnup of spent nuclear fuel. On the other hand, 1FNPP reactors were commissioned in March 1971, and a nuclear accident happened in March 2011. Fuels of 1FNPP have a long burnup history and its average burnup is up to 25.8 GWd/MTU. All fuel groups of 1FNPP have higher burnup than TMI-2 excepting for a fuel group in 1FNPP Unit 2 (Figure 2.13). Due to the large difference in burnup, the dose rate of 1FNPP fuel debris is more than 3 times larger than the dose rate of TMI-2 fuel debris (Figure 2.14).

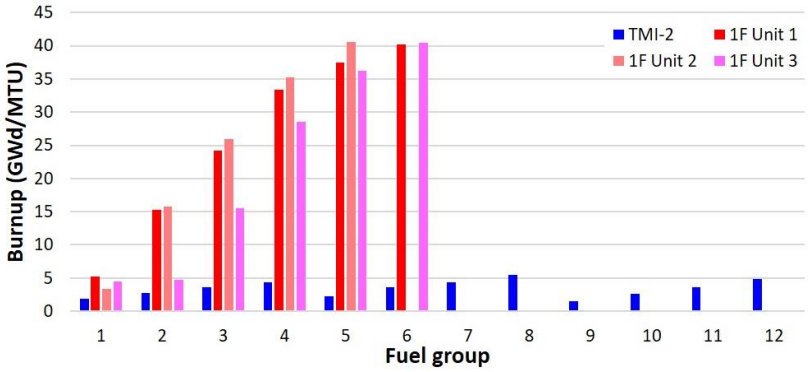


**Figure 2.13 Burnup history of TMI-2 and 1FNPP nuclear reactors.**

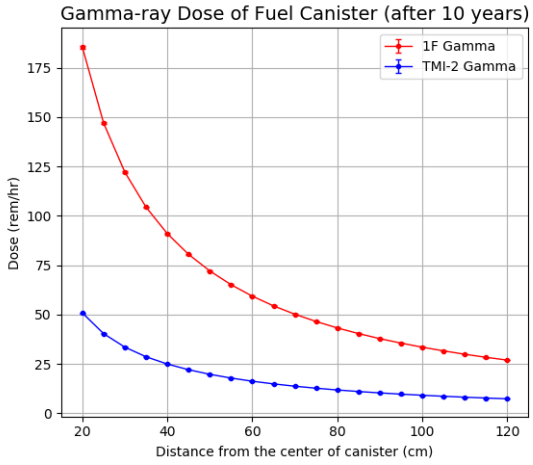


**Figure 2.14 Comparison of photon dose rate between fuel debris of TMI-2 and 1FNPP.** Amount of fuel debris in a fuel canister is assumed to be the same. Assumptions for the analysis are the same with other topics of this chapter.

### 2.3.2.2 Variability of dose rate due to changes in burnup

Burnup is a very important factor in the evaluation of dose rate because it affects the variability of radiation source term. Different fuel groups have different burnup, and this makes spent fuels to have diverse isotope compositions. Moreover, the burnup of spent fuel is diverse depending on the location of fuels in a reactor core. Severe nuclear accidents make this worse by mixing and relocating damaged fuels by melting the reactor core. Therefore, radioactivity of fuel debris can be diverse, and this affects the uncertainty of the evaluated dose rate. At this section, variability of dose rate by changes of burnup is calculated by using SCALE to estimate the magnitude of the variability. Dose rates are calculated based on assumptions of the model for the fuel canister, and only burnup has been changed as a variable.

Radiation intensity of fresh fuel increases by increasing burnup because the fuel has more fission products and actinides. Therefore, fuel debris with more burnup has higher radiation dose rate (Figure 2.15). Neutron dose rate steeply increases compared to the photon dose rate by the increasing burnup. It can be increased to $10^3$ time by the increase of 50 GWd/MTU in burnup whereas photon dose rate increases to 10 times of the initial value. According to the result of calculation by using ORIGEN module of SCALE, total neutron source strength, which is the sum of neutron intensity for overall energy, increases more than $10^3$ times of its initial value by increasing burnup from 10 GWd/MTU to 60 GWd/MTU. On the other hand, the photon dose rate increases less than 10 times of its original value by the increasing burnup.

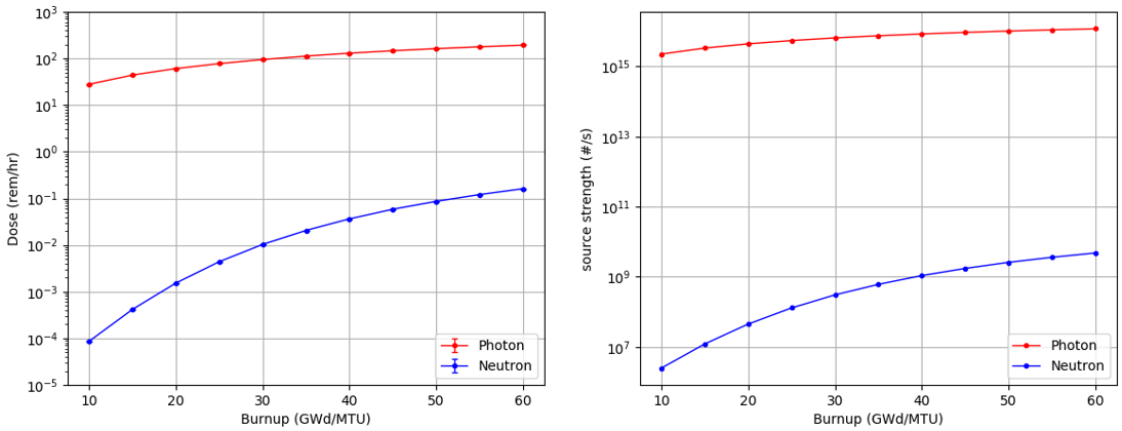


**Figure 2.15 Variability of the radiation dose rate due to the change of burnup.** Graph at left is the change of photon (red) and neutron (blue) dose rate as a function of burnup. Graph at right is the change of source strength as a function of burnup. Dose rate has been estimated 1m from the center of a canister and its surrounding medium is air.

Spent nuclear fuel gets more neutron sources by the increasing burnup (Figure 2.16). Actinides which are made by neutron capture reactions and decaying of converted isotopes are major neutron sources in spent nuclear fuel. Amounts of actinides in a fuel steeply

increases by the increasing of burnup excepting for $^{239}$Pu. $^{239}$Pu production and consumption reach an equilibrium when burnup is larger than 20 GWd/MTU, so $^{239}$Pu concentration in a fuel maintains a similar amount. Curium is a major photon source in a spent fuel and it affects the change of dose rate by increasing burnup. Especially, steep increase of $^{244}$Cm concentration affected the change of neutron dose rate.

According to the result of calculation by using SCALE, fission products are major photon sources of spent nuclear fuel (Figure 2.16). The amount of photons from cesium is the most, and the amount of photons from plutonium and other fission products are less than photons from cesium. Therefore, variability of photon dose rate by burnup depends a lot on the concentration of cesium in a spent fuel.

The density of fuel debris also affects the change in dose rate. However, the density of fuel debris is not sensitive to the change of burnup. In case of intact spent fuel, change of isotope concentration does not significantly affect the variability of density, but growth of voids and crack by burnup affect the change of density. In case of fuel debris, variability of dose rate by burnup is due to the change in intensity of radiation source rather than the change in density of fuel debris. Major actinides and cladding materials consist of more than 93 % of the fuel debris, and concentration of these materials decides the density of fuel debris. Cladding materials are not affected by changes in burnup and maintain almost the same amount (Figure 2.17). Isotopes of uranium and plutonium are sensitive to changes in burnup excepting for $^{238}$U. $^{238}$U is the most abundant isotope in fuel debris but it is not affected by changes in burnup and maintains almost the same amount. Even if change in burnup reduces some amounts of sensitive materials, it does not change the density of fuel debris because of $^{238}$U and cladding materials are not sensitive to changes in burnup. Therefore, variability of dose rate by burnup depends more on the change of source term rather than on the change of density.

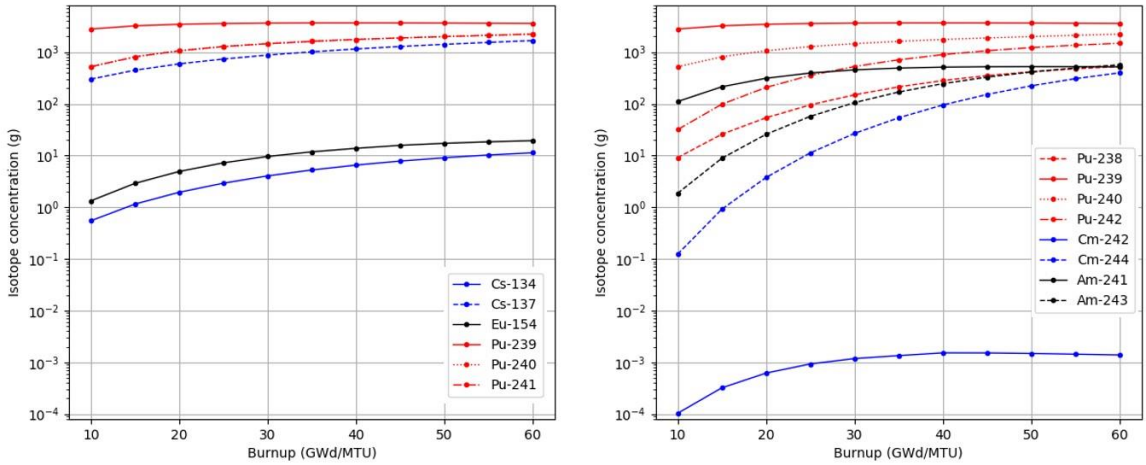


**Figure 2.16 Change of the isotope concentration** of major photon sources as a function of burnup (left) and change of the isotope concentration of major neutron sources as a function of burnup (right). The amount of fuel (debris) has been assumed to be 1MT.

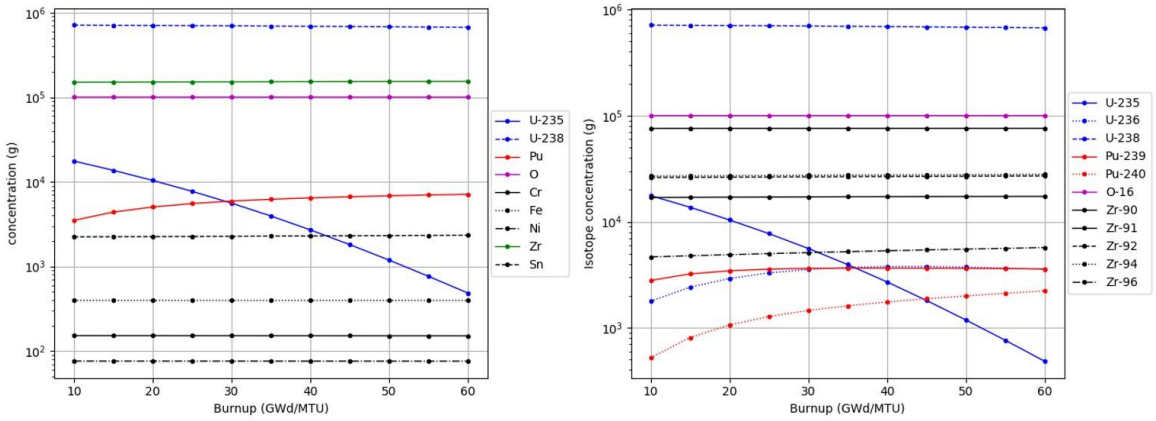


**Figure 2.17 Change of the concentration of major elements** which constitute fuel and cladding (left) and concentration of major isotopes which accounts for more than 93% of fuel debris in weight (right)

### 2.3.2.3 Variability of multiplication factor by changes in burnup

Even though we focus on the evaluation of dose rate, criticality safety cannot be ignored, and its safety requirements need to be satisfied. Moreover, estimation of multiplication factor helps understanding the characteristics of the neutron radiation from fuel debris. Therefore, variability of the effective multiplication factor by burnup has been evaluated by using the KENO module of SCALE. A fuel canister is placed in water instead of air for the evaluation, and space between fuel debris is also replaced from air to water for the conservative analysis. Other assumptions are the same with the model explained in section 2.2.1. Effective multiplication factor ($K_{eff}$) of fuel debris is decreased by increasing burnup. $K_{eff}$ is 0.46 at 10 GWd/MTU of burnup whereas it is 0.28 at 60 GWd/MTU. Sensitivity of $K_{eff}$ by changes in burnup is due to the changes in $^{235}U$. Even if amount of other fissile isotopes is increasing by burnup, it does not affect a lot on the variability of $K_{eff}$ (Figure 2.18).

Variability of the isotope concentration by changes in burnup is evaluated for neutron absorbers which are important in criticality safety (Figure 2.19). Concentrations of absorbers are increasing by burnup excepting for $^{149}Sm$. $^{149}Sm$ which has been produced by the decay of $^{149}Nd$, has a large neutron cross section and its removal by neutron absorptions surpasses its production at high burnup. Variability of concentration of actinides by changes in burnup also evaluated (Figure 2.19). Concentrations of actinides are increase by increasing of burnup excepting for $^{235}U$ and $^{238}U$. $^{238}U$ maintains almost same amount for change in burnup. Even if concentrations of neutron absorbers are sensitive in change of burnup, variability of $k_{eff}$ by burnup relies almost exclusively on the amounts of fissile isotopes.

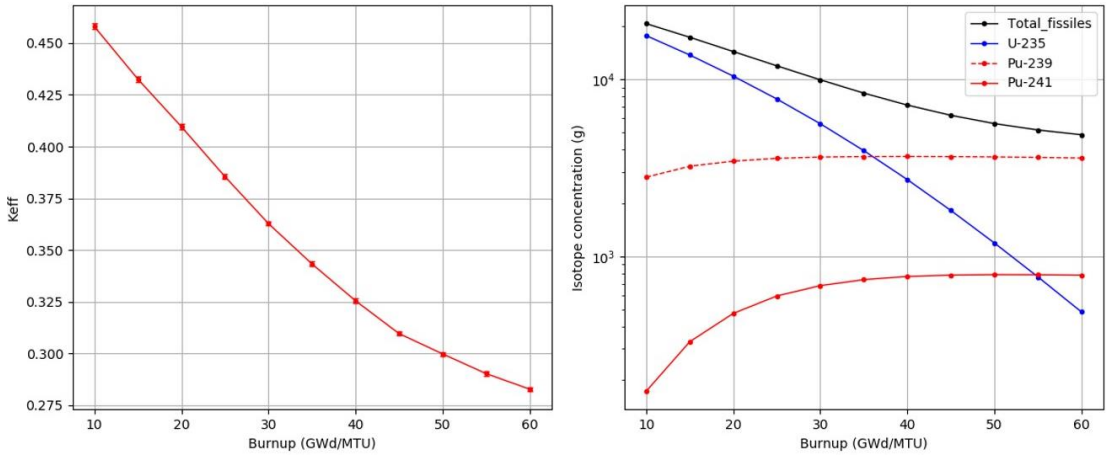


**Figure 2.18 Variability of the effective multiplication factor by changes in burnup**. Change of the effective multiplication factor of fuel debris in a canister as a function of burnup (left). Change of the concentration of major fissile isotopes (right). The surrounding medium is water, and space between debris is also filled with water.

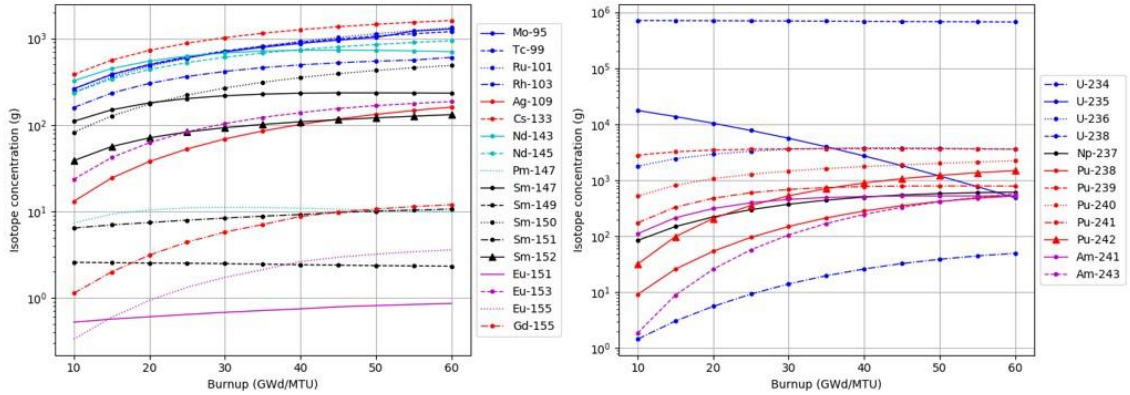


**Figure 2.19 Variability of the isotope concentration by changes in burnup.** Change of the concentration of important fission products (left) and actinides (right) in 1MT of fuel debris as a function of burnup.

### 2.3.2.4. Variability of dose rate due to the release of noble gases and volatiles

According to the IAEA report on the 1FNPP nuclear accident, there were some isotope releases after the accident [3]. This may have changed the composition of fuel debris which will affect the nuclear radiation from the damaged fuel. However, the amount of isotope release is still unclear even after several investigations on the condition of damaged fuel in 1FNPP reactors. Variability of radiation dose rate by the isotope release has been evaluated in this section for major volatiles. Noble gases and some non-volatile elements also included at this evaluation because some of them also might have been released by the accident.

Photon and neutron dose rates have been calculated for fuel debris with less amounts of certain elements which are released by the nuclear accident. An element released by an accident is assumed based on a JAEA repot [3]. As a first step of the evaluation, source terms and composition of debris are calculated by using the ORIGEN module of SCALE. The initial source term at the time of the accident is calculated by using burnup history of 1FNPP, and then the initial source term is used to calculate the source term after 10 years from the accident. The source term at the time of the accident affects the source term after 10 years from the accident by the decay of radioactive isotopes, and loss of a certain element by the accident changes the source term after 10 years. Each source term for the loss of each element is calculated by using the ORIGN module of SCALE, and SCALE input for the estimation of dose rate is made based on the changed source term (Figure 2.20).

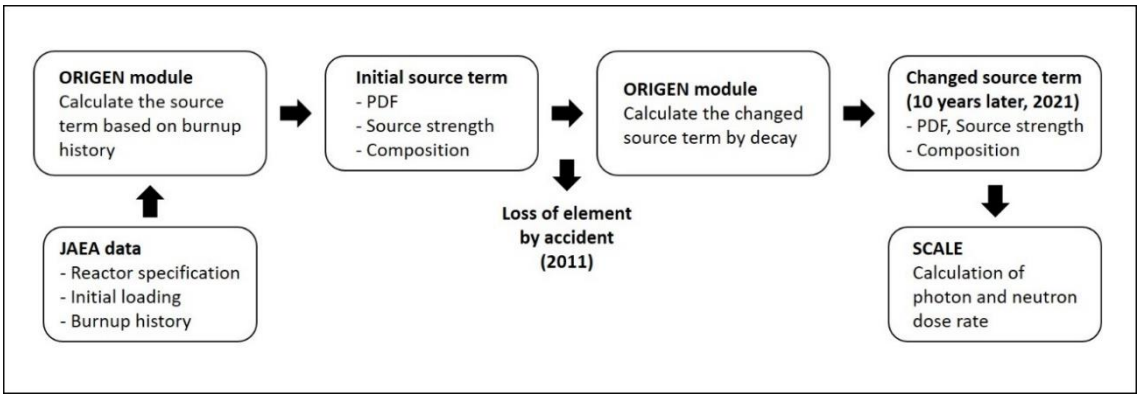


**Figure 2.20 Model for the evaluation on the variability of dose rate by the release of volatiles.**

Changes in photon and neutron dose rate are visualized in Figure 2.21. Photon dose rate shows considerable changes when cesium is released, and it is reduced up to 23 % of its initial value. The photon dose rate is 54.9 rem/hr (549 mSv/hr) if there is no release, and it is 12.5 rem/hr (125 mSv/hr) if 90 % of cesium is released by an accident. Cesium is a major photon emitter which affects a lot on the photon dose rate of fuel debris. The change of cesium concentration changes the photon intensity from fuel debris especially for the photon energy of around 5 keV and 0.5 MeV. The release of strontium also affects changes in dose rate, but not as large as cesium. The photon dose rate reduces to 48.9 rem/hr (489 mSv/hr) by 90% of strontium release. Strontium affects the overall photon intensity from a debris for the photon energy 1 keV ~ 1 MeV. The photon dose rate is reduced by the loss of zirconium, but the reason for this reduction is different from cesium. This reduction is due to the increase in the density of fuel debris by increases in the relative content of heavy metals in fuel debris by the loss of zirconium. Photon generated from a fuel debris is attenuated not only while passing shielding materials but also while transmitting through the fuel debris itself, and density of fuel debris affects the attenuation. On the other hand, the photon dose rate increases by the loss of uranium because the density of fuel debris decreases by the loss. However, this can be ignored because a few Uranium and Zirconium might have been released by the accident. Changes of photon dose rate by the loss of other elements is negligible.

In the case of neutrons, the concentration of Curium affected a lot in the change of dose rate by changing the neutron intensities from fuel debris for high energy neutrons. Neutron dose rate which is 3.4 mrem/hr (34 µSv/hr) reduces to 0.46 mrem/hr (4.6 µSv/hr) if 90 % curium is released. Loss of plutonium also affects the neutron dose rate, but not as large as curium. The release of other elements makes only a few changes in the neutron dose rate even after 90% of release. More details are in Appendix A.10.

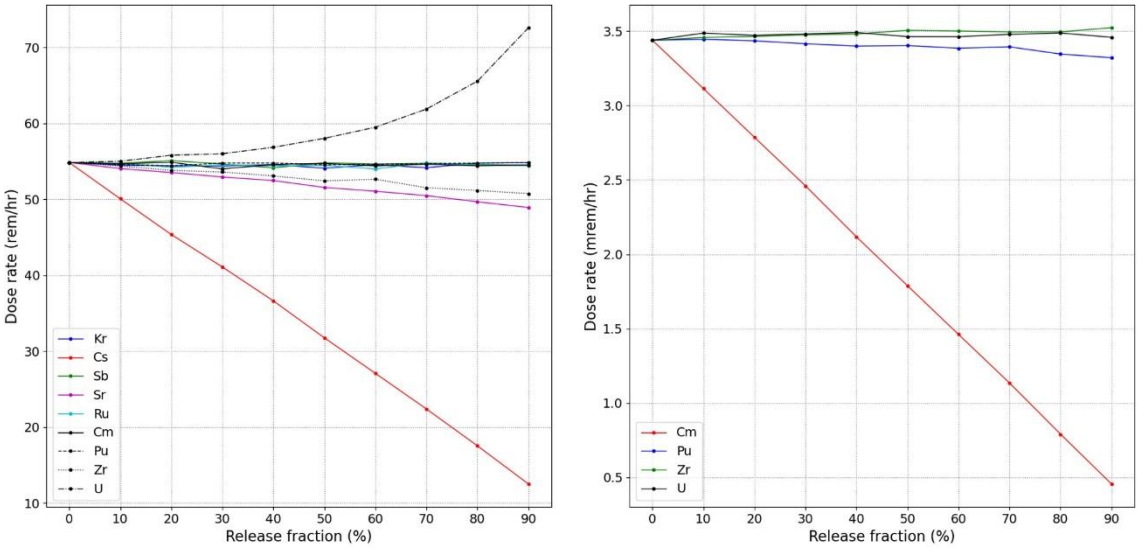


**Figure 2.21 Changes in photon (left) and neutron (right) dose rate by the loss of element.**

According to the report of F. Zeggar and H. Berkoune (2013), around 80 % of Cesium has been released from the reactor core by the 1FNPP nuclear accident [17]. Their estimation on the released amounts of volatiles is at the table 2.3. Release of Strontium and Curium were estimated to be 10 % and 0.3 % each. Source term has been calculated based on the estimated release of volatiles, and dose rate of a fuel canister is estimated by SCALE. The estimated photon and neutron dose rates have been compared with dose rates for fuel debris without loss of element (Figure 2.22). Photon dose rate is sensitive to changes of volatile concentration, and it decreases a lot after the release of volatiles. On the other hand, neutron dose rate is not sensitive to changes, and fuel debris maintains almost similar neutron dose rate after the release of volatiles.

**Table 2.3 Release of volatiles by the 1FNPP nuclear accident (F. Zeggar at el [17])**

| Release fraction | 90 % | 80 % | 15 % | 10% | 3 % | 0.3 % |
|---|---|---|---|---|---|---|
| Elements | Kr, Xe, I | Cs, Rb | Sb, Te | Sr, Ba | Ru, Mo, Rh, Tc | Cm, Pu, Am, Ce, La, Nb, Nd, Np, Pr, Y, Zr |

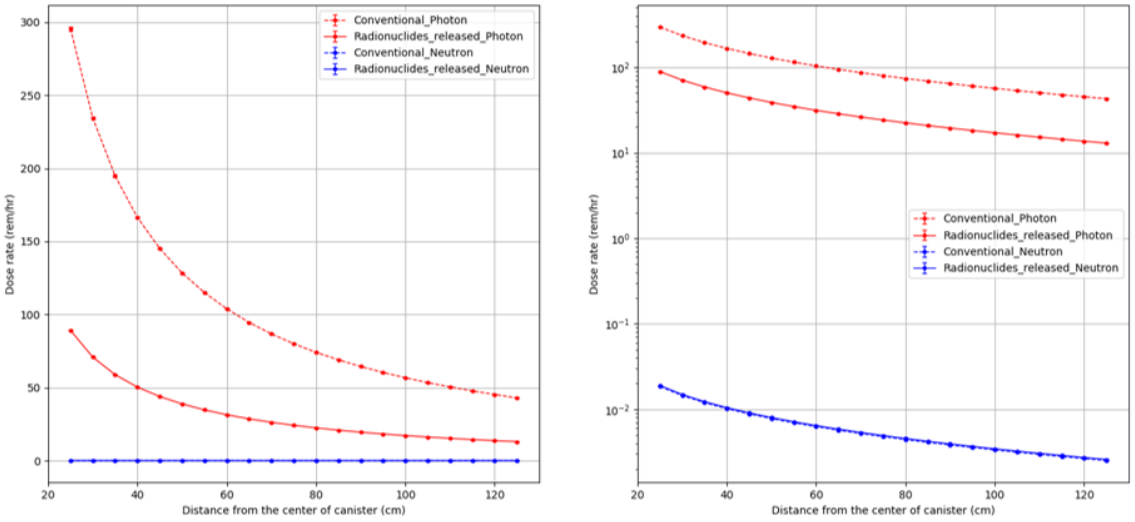


**Figure 2.22 Dose rate before and after the release of volatiles.** Y-axis of the graph at right is in log scale. Two graphs are plotted with the same data, and the only difference is the scale of Y-axis.

### 2.3.3 Variability of dose rate by the geometry of fuel debris

#### 2.3.3.1 Size of debris

Size of debris affects its packing structure, and it changes possible amounts of debris in a canister. As the first step of study, the photon dose rate has been estimated for a canister filled with fuel debris at a height of 150 cm. Shape of fuel debris is sphere, and debris in a canister are the same size. Mass of fuel debris in a canister is not maintained to be the same, and fuel debris of the same radius are packed in the body centered cubic (BCC) structure. The photon dose rate of fuel debris is calculated at 100 cm from the center of a fuel canister, and the diameter of debris is changed from 1 cm to 10 cm. According to the estimation, dose rate non-linearly decreases by increases in the size of debris (Figure 2.23). Porosity of debris piles in a canister increases by changes in the size of debris, and this is the major reason for the decrease of dose rate. The self-attenuation of photons in fuel debris also affects the decrease because photons are more attenuated in large debris. The non-linearity of some diameter is because the boundary of the debris pile is restricted by the inner space of fuel debris. The pitch distance of fuel debris depends on the size of debris when its boundary is restricted, and it affects the non-linear changes. Differences in the increases of porosity by changes in the size are also affects the non-linearity.

As the second topic, piles of fuel debris in the same mass but with different sizes are compared. A canister has fine particles uniformly distributed in a canister, and this is modeled by assuming a uniform mixture of the fuel debris. Another canister has fuel debris with a diameter of 6 cm, and debris are packed in a BCC structure. Photon dose rates of these are compared at Figure 2.24. There are differences between these two, and the canister with fine particles has a larger dose rate. This is because their porosity is different,

and the total path lengths of radiation which are attenuated in voids between fuel debris are not the same. Self-attenuation also somewhat contributed to the difference.

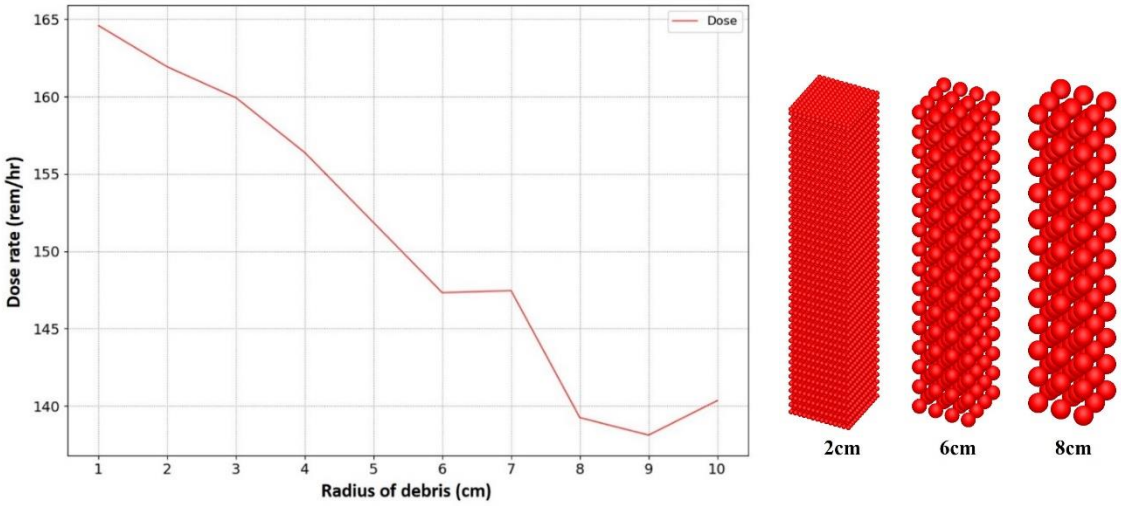


**Figure 2.23 Dose rate by changes in the diameter of fuel debris.** The maximum height of debris pile in a canister is maintained to 150 cm from the bottom to the top, and the mass of debris is not the same for each sample. Figures at the right visualizes the array of fuel debris for the diameter 2cm, 6cm, 8cm.

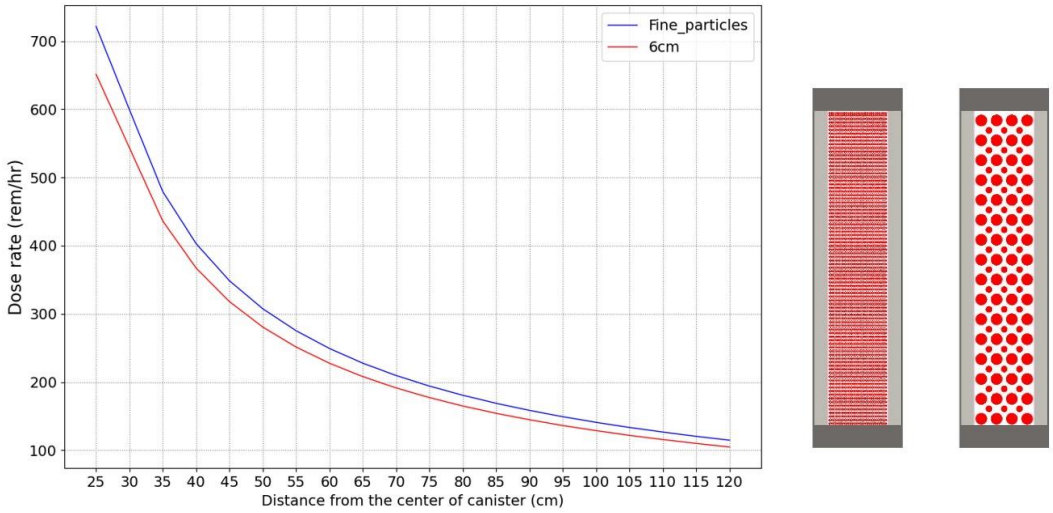


**Figure 2.24 Comparison of photon dose rate between debris in fine particles and 6 cm in diameter.** Mass of fuel debris in a canister is same (490 kg). Fuel debris are uniformly distributed in a canister, and the overall volume of the pile of fuel debris is the same. 6 cm of fuel debris are modeled to a BCC array of spheres, and fine particles are modeled to a uniform mixture of particles.

Difference of dose rate between a solid loaf of damaged fuel and fuel debris with a diameter of 1 cm is compared in Figure 2.25. Fuel debris is in a BCC array, and the shape of the loaf of solid fuel is the same as the inner space of a fuel canister. Dose rate has been calculated by using region tally, and it also calculated by using point tally to double check. According to the result of the calculation, the photon and neutron dose rates of these fuels are different, even though their mass is the same. Fuel debris are radiation sources in the canister, and radiations from debris in different volumes have different path lengths from sources to a detector. Therefore, the differences in total path length affected the differences in the dose rate. Difference in porosity and self-attenuation of radiation in fuel debris also affected the differences in the dose rate.

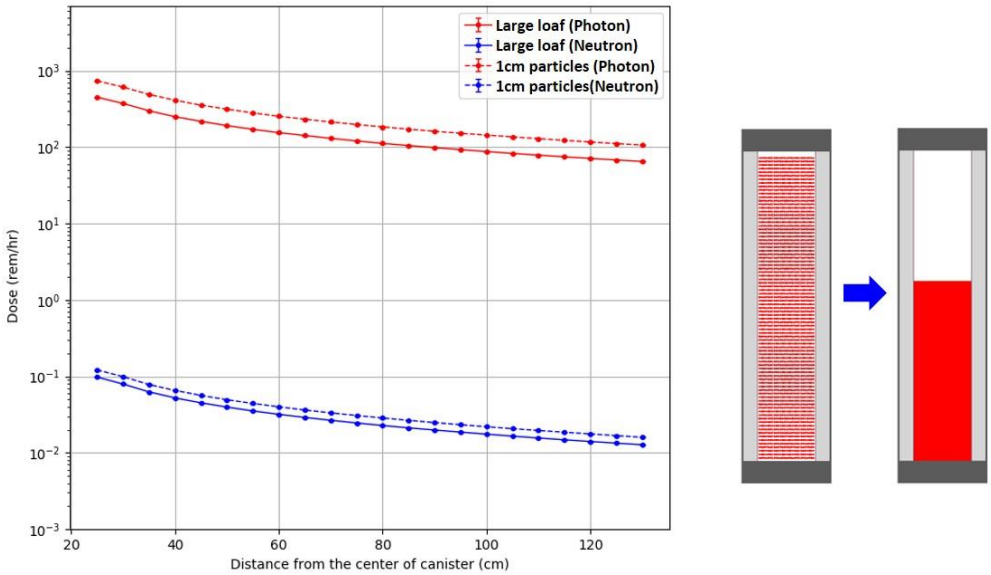


**Figure 2.25. Comparison of the radiation dose rate between fuel debris with diameter of 1 cm and a solid loaf of damaged fuel.**

At Figure 2.26, dose rate of fuel debris in a fuel canister has been evaluated for different diameters. Mass of debris in a canister is assumed to be 230.9 kg for all canisters, and fuel debris are closely packed at the center of each canister. Diameters of fuel debris in a canister are the same, and this has been modified from 4 cm to 20 cm as a variable. Piles of fuel debris are located at the vertical center of a canister. This assumption may not be physically reasonable because fuel debris will be packed from the bottom to the top. However, this has been assumed for the purpose to minimize the variability of dose rate by the design factors of a canister. The packing structure of debris is not the same for all diameters, and the pile of debris has a certain packing structure because its packing space is restricted by the inner space of a canister. Especially fuel debris cannot have a complete set of packing structures such as FCC or BCC when the diameter of debris is larger than 14 cm because of the spatial restriction. Pitch distance is the distance between fuel debris, and this is also not the same for all sample groups. Closely packed particles in a free space have larger pitch distance when they are in larger diameter. However, in case of fuel debris in a canister, debris with larger diameter does not necessarily have larger pitch distance

because of the differences in their packing structure. Changes in length from the bottom to the top of the debris pile is also variable depending on the diameter. In case of the closely packed fuel debris in a free space, the length increases by the increase of the diameter if debris piles are in the same packing structure. However, the closely packed fuel debris in a canister has different packing structure depending on the diameter, and the length from the bottom to the top of the debris pile is also different. Therefore, the dose rate of the close packed fuel debris non-linearly changes by changes in the diameter of fuel debris. Dose rate almost linearly decreases when the diameter is between 4 cm and 6cm, and then it has a non-linear section when the diameter is between 6 cm and 14 cm. Dose rate almost linearly decreases for the diameter between 14 cm and 17 cm, and then slope of the graph has been changed for the debris with the diameter larger than 17 cm. This non-linearity is due to the differences in packing structure of fuel debris.

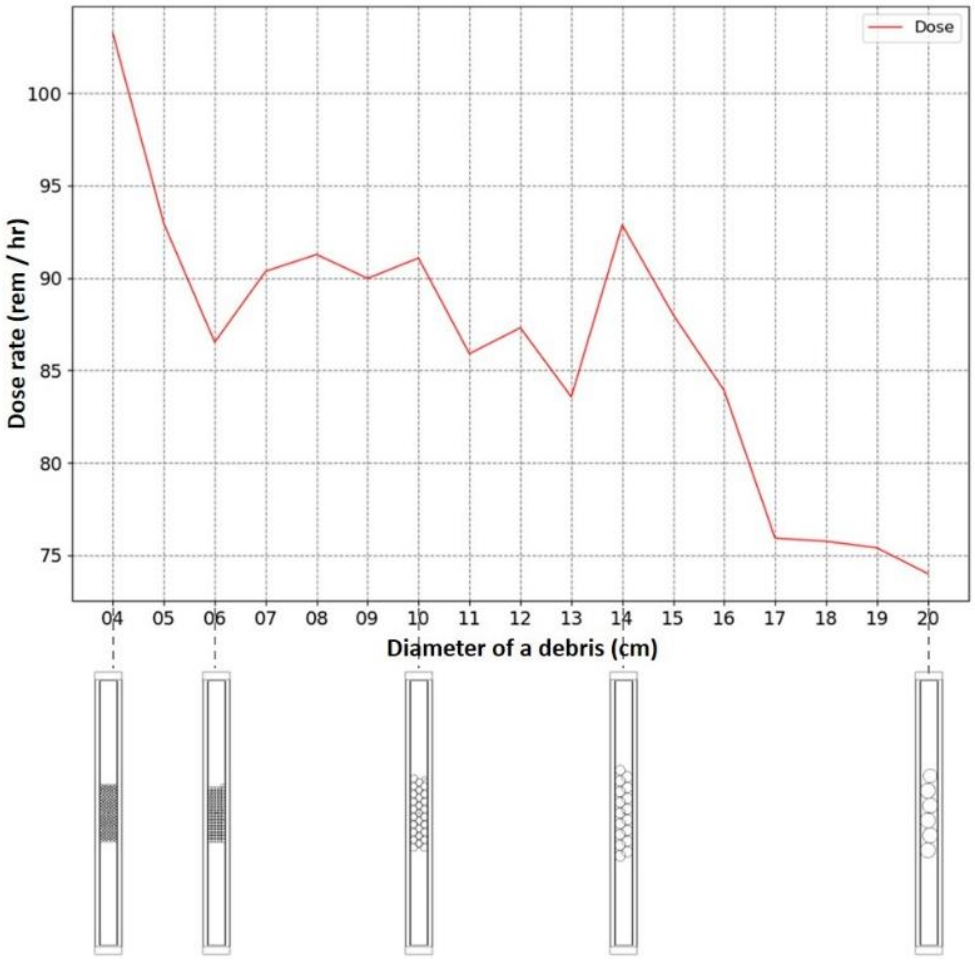


**Figure 2.26. Variability of dose rate by changes in diameter.** Figures below the graph are the cross-sectional view of fuel canisters for the diameter of 4 cm, 6 cm, 10 cm, 14 cm, 20cm.

### 2.3.3.2 Distribution of fuel debris in a canister

Dose rate of fuel debris has been evaluated for two different geometries which are close packing and loose packing. For these two types of packing, mass of fuel debris is assumed to be the same (230.9 kg). Size of debris and total numbers of debris in a canister are also assumed to be the same. Other assumptions are decided based on the model assumed in section 2.2. In case of the loose packing, fuel debris are randomly distributed in a fuel canister. On the other hand, for the close packing, fuel debris are closely packed in FCC structure. Dose rate has been estimated from the surface of a canister up to 10 m.

Near a canister, the radiation dose rate of the close packed fuel debris is larger than the dose rate of the loose packed debris (Figure 2.27). Photon dose rate of the close packed debris is 91.6 rem/hr (916 mSv/hr) whereas the photon dose rate of the loose packed debris is 56.7 rem/hr (567 mSv/hr) at 100 cm from the center of a canister. This difference decreases as the distance from the center of a canister increases. At a distance over 3 m from the center of a canister, the difference in dose rate can be ignored. However, the dose rate of the close packed debris is smaller than the dose rate of the loose packed debris at 10 m from the center of a canister. Photon dose rate of the close packed debris is 1.3 rem/hr (13 mSv/hr) whereas the loose packed debris is 1.4 rem/hr (14 mSv/hr). This reversal of superiority is due to two factors which are the vertical distribution of fuel debris and the attenuation of radiation at fuel debris. Near to a canister, dose rate is affected a lot by the geometric distribution of fuel debris in a canister. Especially, differences in vertical distribution makes differences in total path length from sources to a detector (or a region for tally). At a distance far from a canister, relative differences in total path length are decreased and it can be ignored. On the other hand, differences in the attenuation of radiation at fuel debris is not affected by changes in distance from a canister to a detector. Radiation can be more attenuated when fuel debris are closely packed because radiation passes more debris than it passes loosely packed debris. Therefore, the dose rate of the close loose packed debris is larger than the dose rate of the loose packed debris near a canister whereas it is smaller at far from a canister.

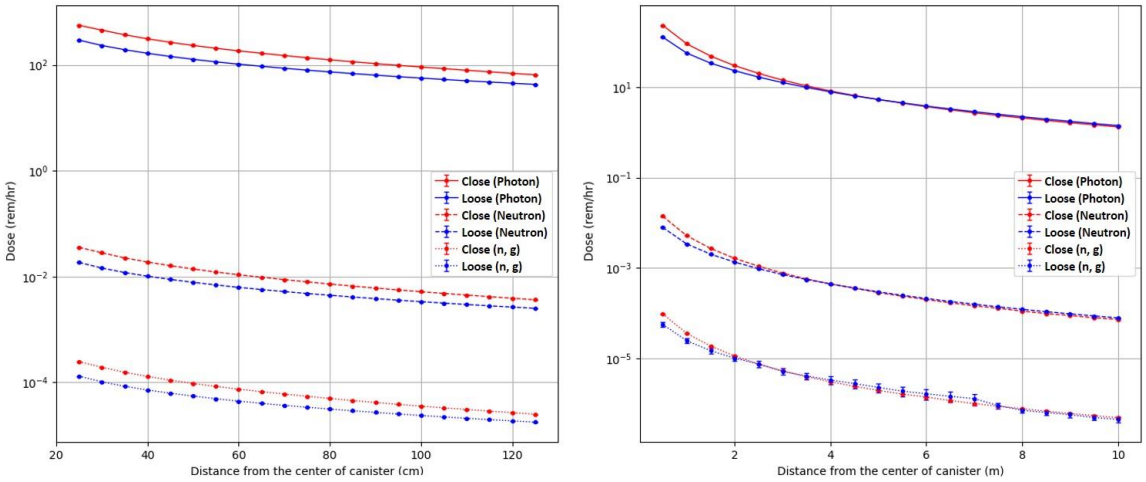


**Figure 2.27. Comparison of radiation dose rate between close packed debris and loose packed debris.**

## 2.4. Summary and discussion

A model for the evaluation of dose rate for fuel debris was developed in this chapter. The model assumed that 10 years have passed from the time of an accident and retrieved fuel debris are contained in a canister. Even if shapes of actual fuel debris are diverse, debris of this model is assumed to be spheres. For the modeling of non-spherical debris, close packing of spheres in random size was proposed. Source term of fuel debris was calculated based on data with burnup record of 1FNPP, and TMI-2 data was also used for comparison. SCALE code was used for the estimation of dose rate, and its ORIGEN module was used for the calculation of source term. MCNP code was also used, but it was used only to double check the estimated dose rate by SCALE code. After the development of a model, variability of dose rate by changes in several parameters was evaluated as a preliminary study.

Variability of dose rate is evaluated for three factors which are canister design, source term, and geometry of fuel debris. Material used for the design of a canister affect the estimated dose rate, and it accounts for the dose rate of the fuel canister which is lower than other two types. Steel is a good shielding material and adding more steel can enhance the shielding performance of a canister. Use of boron in a form of $B_4C$ or Boral is helpful in neutron shielding but it needs to be used with other shielding materials because of its poor shielding performance for photons. Medium surrounding a canister is also affects the dose rate, and nuclear radiation is easy to be shielded by immersing a canister in water. Variability of dose rate by the changes in source term is much larger than the variability by design factors. Burnup changes the source term a lot, and fuel debris with higher burnup has a higher dose rate. Release of radioactive isotopes by a nuclear accident also affects the source term by changing the composition of radioactive isotopes in fuel debris. The loss of radioactive material at the time of accident changes the source term 10 years after the accident, and fuel debris with loss has lower dose rate than fuel debris without loss. Variability of dose rate by the changes in geometry of fuel debris is smaller than the variability by the source term. However, it also affects the dose rate like the canister design does. Fuel debris in larger size has a smaller dose rate than debris in smaller size when they are contained in a canister with the same total weight. Limited inner space of a canister works as a restriction in the location of fuel debris, and fuel debris with different diameter cannot have the same packing structure for all diameters. The differences in the packing structure and the distribution of debris in a canister affect the path length from radiation sources to detectors, and it affects the dose rate.

Variability of dose rate by several factors has been evaluated in this chapter. Variability of dose rate by changes in source term is larger than other factors. However, geometry of fuel debris also affects the estimated dose rate, and further studies are going to be done in the next chapter.

# Chapter 3. Development of Methodology

## 3.1 Introductions

Variability of the radiation dose rate by changes in major variables are evaluated in the previous chapter. Design of a canister is the basis of the evaluation, and elements in canister design affect the dose rate of fuel debris. Elements in design can be considered as control variables, and their details can be defined before the evaluation. On the other hand, geometry of fuel debris is an uncertain variable, and it makes the estimated dose rate uncertain. Fuel debris varies in shape and size, and the retrieval process including cutting and drilling makes the geometry more diverse. Moreover, the geometry of fuel debris can easily change while a canister is in transport or storage unless debris are tightly held by canister fillers. Therefore, this chapter focuses on the uncertainty of dose rate by the geometry of fuel debris, and a model is developed to quantify the uncertainty.

The model of Chapter 2 is updated in this chapter to evaluate the fuel debris with uncertain geometry, and the geometry is expressed by random sampling on the size and distribution of fuel debris in a canister. The conceptual design of the fuel canister and the source term of fuel debris in Chapter 2 are used for the model of this chapter. Shape of debris is sphere, but non-spherical shape is also approximately expressed by closely packing fuel debris in random size. A Python code is made for the random sampling and data processing for the evaluation. The code generates input files for SCALE, and it efficiently manages output data by applying the multiprocessing and the parallel computing methods. After the evaluation on the uncertainty, an analytical model is developed to save time for the evaluation. The numerical method with SCALE code takes a very long time for the uncertainty quantification even though a parallel computing method is used. The analytical code is developed for approximate evaluation of the uncertainty, and its results are compared with the results from the numerical method with SCALE.

Radiation dose rate and its uncertainty are evaluated for photons and neutrons from fuel debris. The dose rate is estimated at a point which is a point detector. The random arrangement of fuel debris in a canister is classified to the loose packing and the close packing. The uncertainty of dose rate is evaluated by calculating the standard deviation of output data, and the coefficient of variation and the percent relative range are calculated for the quantification of uncertainty. The sensitivity of dose rate by changes in variables is evaluated in sensitivity coefficient. Functions on the average dose rate and the standard deviation are derived by data fitting, and a method converting data to cumulative values is proposed for the data fitting.

## 3.2 Sensitivity analysis of random variables by Monte Carlo method

### 3.2.1. Background and assumptions

Geometry of fuel debris is an uncertain and random variable which affects the reliability of the estimated radiation dose rate. Condition of fuel debris in 1FNPP is still uncertain even if approximate locations of damaged fuels were identified by several investigations. Shape and size, details of the location in each reactor are still uncertain, and more information is required. Tokyo Electric Power Company (TEPCO) is going to start the retrieval of fuel debris in 1FNPP unit 2 next year, and it will reduce the uncertainty a lot. However, even if we can identify the geometry of fuel debris in a reactor, their geometry at a canister is another matter. Identified information of fuel debris in a reactor does not remove the randomness of geometry, and it makes another uncertainty after fuel debris are contained in a canister. The simplified model in the previous chapter estimated the variability of dose rate without considering such uncertainty. Therefore, the previous model of chapter 2 is updated at this chapter to quantify the uncertainty of dose rate which is due to the randomness of the geometry and the limited information.

Assumptions including the canister design and payload of a canister are same with the model of the preliminary study. It is assumed that fuel debris are contained in a fuel canister after 10 years from the date of accident. Dimension of the fuel canister and material used for its components are same with that of the previous model. Outside of the canister is filled with dry air, and space between debris is also filled with dry air instead of the non-fuel matrix which is used in the previous chapter. The dry air inside and outside of a canister is replaced with water only when calculating the effective multiplication factor. Mass of fuel debris in a canister is assumed to 230.9 kg per canister, and source term is calculated based on the 1FNPP data on burnup and reactor specification. The isotope release by the 1FNPP accident is considered for the calculation of source term, and the released amount is decided based on the estimated data by F. Zeggar at el which is at the table 2.3 [17]. The location of the detector is assumed to be 1m horizontally from the center of a canister. Dose rates are calculated at a point detector or averaged in a region. For the estimation of dose rate by the changes in vertical location of detectors, the region at horizontally 1m from the center of a canister is vertically divided into multiple regions. Fuel debris is assumed to be a sphere like the previous mode, and non-spherical geometry of fuel debris are replaced to randomly sampled spheres in their size and location. A debris sphere is a uniform mixture of fuel and non-fuel materials, and it does not have any thin film on its surface which is assumed at the preliminary study. This is assumed for the purpose to focus on the uncertainty by the geometry of fuel debris in a canister.

Sensitivity of photon and neutron dose rate by changes in size and distribution of fuel debris in a canister has been evaluated by direct sampling method. SCALE has been used for the calculation of dose rate and Monte Carlo sampling has been used for the direct sampling of random variables which are size and distribution of fuel debris in a canister. SCALE has a module for sensitivity and uncertainty analysis to quantify physical parameters for safety analysis and design. TSUNAMI is the module of SCALE for the sensitivity and uncertainty analysis. TSUNAMI can quantify uncertainty of dose rate for variables such as isotope composition of fuel debris, design factor of a canister (thickness of wall, size of components). However, the TSUNAMI module is not appropriate for this

model which has a lot of debris with random size and random location. This is because it needs a lot of random sampling for the analysis which is more than simple perturbation of variables. Therefore, a python code has been made for the random sampling of these variables, and SCALE has been used only for the calculation of dose rate.

### 3.2.2 Model for the sampling

#### 3.2.2.1 Random sampling

Packing of fuel debris in a canister has been sampled in two configurations which are the random loose packing and the random close packing (Figure 3.1). In case of the loose packing geometry, locations of fuel debris in a canister are randomly sampled, and debris does not necessarily contact each other. On the other hand, fuel debris in the close packing geometry are contacted with other debris to maintain static equilibrium. The packing structure of this close packing geometry is not uniform, and debris are randomly placed in a form of perturbed close packing. The close packing is physically more reasonable configuration for the modeling of the damaged fuel debris than the loose packing because dense and heavy debris are placed in a space filled with dry air. However, the loose packing also can be used for the modeling of fuel debris in a canister because the debris is not a perfect sphere but can be in any shape which may make many pore spaces when contained in a canister. Damaged fuel debris are in various shapes and sizes, and this results in the randomness of geometry. Piles of fuel debris with pebble-like debris can have more closely packed geometry while piles of debris with large loaves of rods and rocks can have more loosely packed geometry. Packing of fuel debris can be loosened when a canister has some debris which are coalesced with concrete. Structural materials of PCV and other materials such as mud and dirt also can loosen the packing of fuel debris by taking up spaces between debris. These mud and dirt are easily contained with debris unless removed from the surface of fuel debris by the cleansing process. Therefore, radiation dose rate of fuel debris in a canister needs to be evaluated not only for the close packed geometry but also for the loose packed configuration.

Loose packed geometries of fuel debris are made by random sampling on diameter and location for each fuel debris in a canister. Diameter and location of fuel debris are assumed to be random variables of the model, and the inner space of a canister has been used as a constraint. Other parameters including total mass (230.9 kg) and isotope composition are assumed to be constants and maintained to be the same for all sampled canisters. Number of debris in a canister is a dependent variable and it has been calculated based on the sampled diameter of fuel debris and the total mass of debris in a canister. There can be more than 1,000 particles for small debris and less than 10 for large debris. The variance of the diameter is limited to 2 cm for each sampling group and the minimum radius of each sample group is ranged from 1 cm to 9 cm for 17 sampling groups. Location of debris is randomly sampled by using the Random module of Python and their locations are maintained not to be overlapped with each other. In case of the close packed geometry, space for the random sampling of location has been used as an additional constraint. The space for the sampling is limited to small at the beginning of the sampling process, then it has been gradually increased by filling a canister with fuel debris. At the beginning of the sampling process, the limited space for the random sampling is defined to be 2 times of the

diameter in z direction and same with the inner space of a canister in other direction. After a random sampling of the location, the location has been checked to avoid overlapping with other debris. If the location overlaps with others, a location has been randomly sampled again and this process is repeated until find a location which does not overlap with others. The number of trials for finding a location is limited to 100 times, and the space for the location is expanded in z direction to two times the diameter of the debris. The space is increased until find an appropriate location by repeating the process (Figure 3.2). A canister is filled with 230.9 kg of fuel debris by repeating this process, and debris in a canister were able to have perturbed close contact.

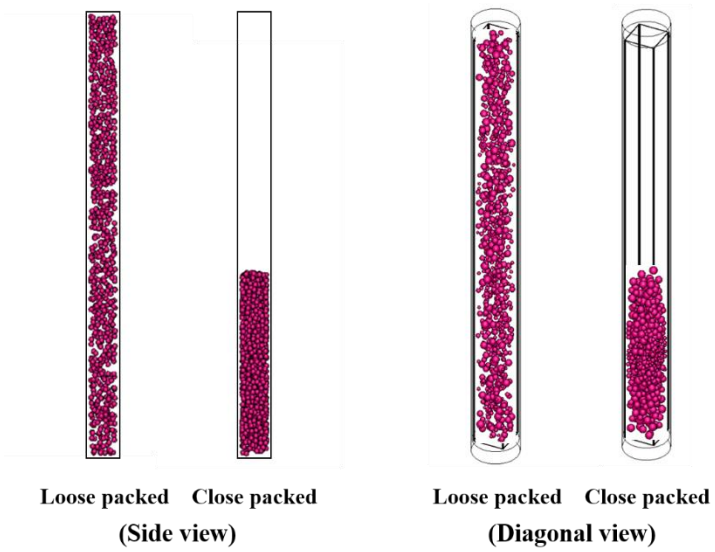


**Figure 3.1 Cross sectional view of fuel debris in fuel canisters.** Close packed and loose packed debris are randomly placed in canisters. Figure at left is the side view, and at right is the diagonal view.

Each sampling group performed the random sampling process to fill 1,000 canisters, and SCALE calculation also has been performed 1,000 times per a group for 17 groups. Therefore, SCALE calculated 1,7000 times each for the loose packed and the close packed debris which is a total of 34,000 times. Thus, SCALE performs its entire process for the estimation of dose rate for 34,000 times with 34,000 inputs and the same number of outputs. A Python code was made to control and manage output data for all processes. Python performs random sampling and generates SCALE inputs, and it controls SCALE code to run inputs. The code also maintains the optimized performance of computing nodes until the end of all processes. The Python code generates plots and tables based on the outputs from 3,4000 times of SCALE operation at the end of the process. This model with the Monte Carlo method is not efficient, and it takes a very long time to get a result. Therefore, a multiprocessing method and a parallel computing method were implemented to the Python code to enhance the efficiency of the model. SAVIO high performance computing system of UC Berkeley was used for running the Python code and SCALE code. 24 nodes

of SAVIO which have 20 cores per node were used for this study, and it saved time for the analysis a lot. Personal desktop computers also have been used for some topics with small computational works by making a personal cloud. 10 of desktop computers which have 4 ~ 12 CPU cores were connected to make a cloud, and the Python code controlled these computers by using parallel computing methods. Even if this small cloud system is less efficient than SAVIO nodes, it has been used as an auxiliary system, and it saves time for analysis.

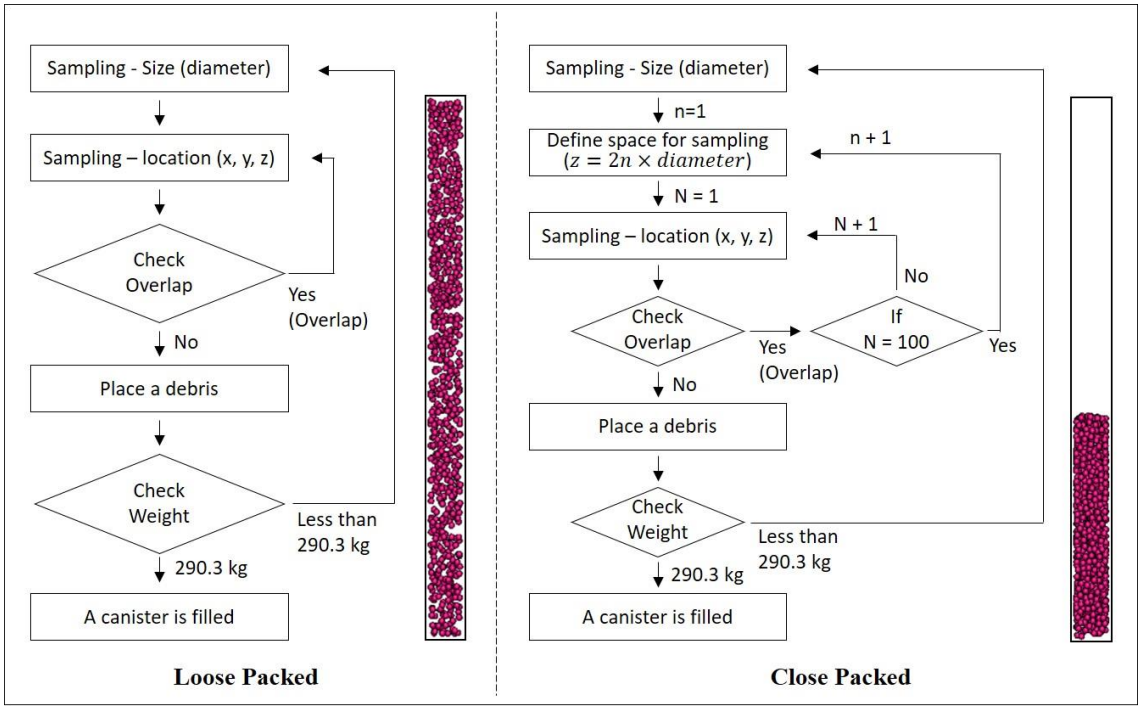


**Figure 3.2 Sampling process for loose packed (left) and close packed (right) fuel debris in a canister.** Size and geometric distribution of fuel debris are randomly sampled by using a random module of Python which is pseudo-random numbers.

### 3.2.2.2. Methods used for the multiprocessing

The Central Processing Unit (CPU) with the latest design has enhanced multiprocessing capability, and it allows more concurrent computations in a unit. Use of 8 core CPU for a personal computer is common these days, and 64 core CPU is also available. Having more cores in a CPU allows more concurrent computation in a single unit. Therefore, optimized use of multicore CPU is important for the efficiency of computational work. SCALE code is used in this dissertation as a major nuclear code for the calculation of radiation dose rate. However, SCALE is not optimized to use the multiprocessing capability of the latest multicore CPU. SCALE uses only part of the cores while computing, and its CPU usage is less than 20% for 8 core CPUs. This results in waste of time and expenses by unoptimized computational works. Therefore, it is recommended to modify the SCALE code to be

optimized for the use of the latest multi-core CPU. However, permission on the use of source code is required for the modification of SCALE, and SCALE code is used as it is for this dissertation. Instead of the modification of SCALE, a Python code was made which concurrently ran multiple SCALE works. The model of this dissertation uses Monte Carlo method, and SCALE needs to run many input files to get a result. The Python code controls SCALE code to run multiple inputs at the same time. The number of multiple works at a time is decided based on the capability of CPU and work loads of SCALE inputs. As an example, a node of the SAVIO high performance computing system has 20 cores, and SCALE uses a little CPU when it is running a single input file. On the other hand, CPU usage of a SAVIO node is around 75 % when 15 SCALE inputs are running at the same time by using the Python code.

The Python code has been developed based on the flowchart at the Figure 3.3. As a first step of the process, SCALE inputs are generated from the Python code which is based on the model of figure 3.2. The Python code did random sampling for the location and size of fuel debris, and sampled data is used for generating SCALE input files with total number of N. The Python code start to run SCALE code after the random sampling, and SCALE receives order from the Python code for running works. Number of works (n) at a time is decided based on the number of CPU core and workloads of the SCALE input file. In the case of 8 core CPUs, CPU usage for 10 works (n = 10) is around 75 %. 75 % CPU usage is 15 works for 12 core CPU, and it is more than 15 works for 20 core CPU. However, the number of works (n) can differ by workload of SCALE input, and CPU usage can be larger than these examples when SCALE needs to do a more complicated calculation which needs more work. Number of works can be increased by using 100 % of CPU capability. However, maintaining 100 % CPU usage for a long time results in the temperature increase of the CPU, and it slows down the clock speed of the CPU. Multiprocessing with 100 % of CPU usage is not efficient, and it can damage the CPU cooler by overload. The Python code gives order to SCALE with 5 seconds of interval between each work. This time delay is given for the efficiency in use of system memory RAM (Random Access Memory). Memory usage of SCALE code can be larger than 16 GB for a work when SCALE uses Consistent Adjoint Driven Importance Sampling (CADIS) method. However, SCALE does not use a lot of memory for the entire process, and the peak of memory usage is maintained for a short time. The peak memory usage is only several seconds, but it can be longer than a couple of minutes depending on the workload and performance of the hardware. In case of 15 multiprocessing with a 12 core CPU, memory usage can be larger than 240 GB at the peak time if all works are started at the same time without the time delay. The 5 seconds of time delay prevents the large memory usage, and it enhances the efficiency of multiprocessing. After the start of work by SCALE, SCALE generates status messages, and the Python code monitors the SCALE work by reading the message. The Python code moves the SCALE input file and its outputs to the Error directory if there are errors at the status message from SCALE. After error files are moved to the Error directory, the code gives a new work order to SCALE. If there are no error messages from SCALE, the code checks if the work is completed. If the work is not completed, the code waits for 30 seconds, and it reads status messages again after 30 seconds. If the work is completed, the Python code checks if there are remaining works. If there is remaining work, the code gives a new work order to SCALE. The Python code generates plots and tables after the completion of all SCALE works.

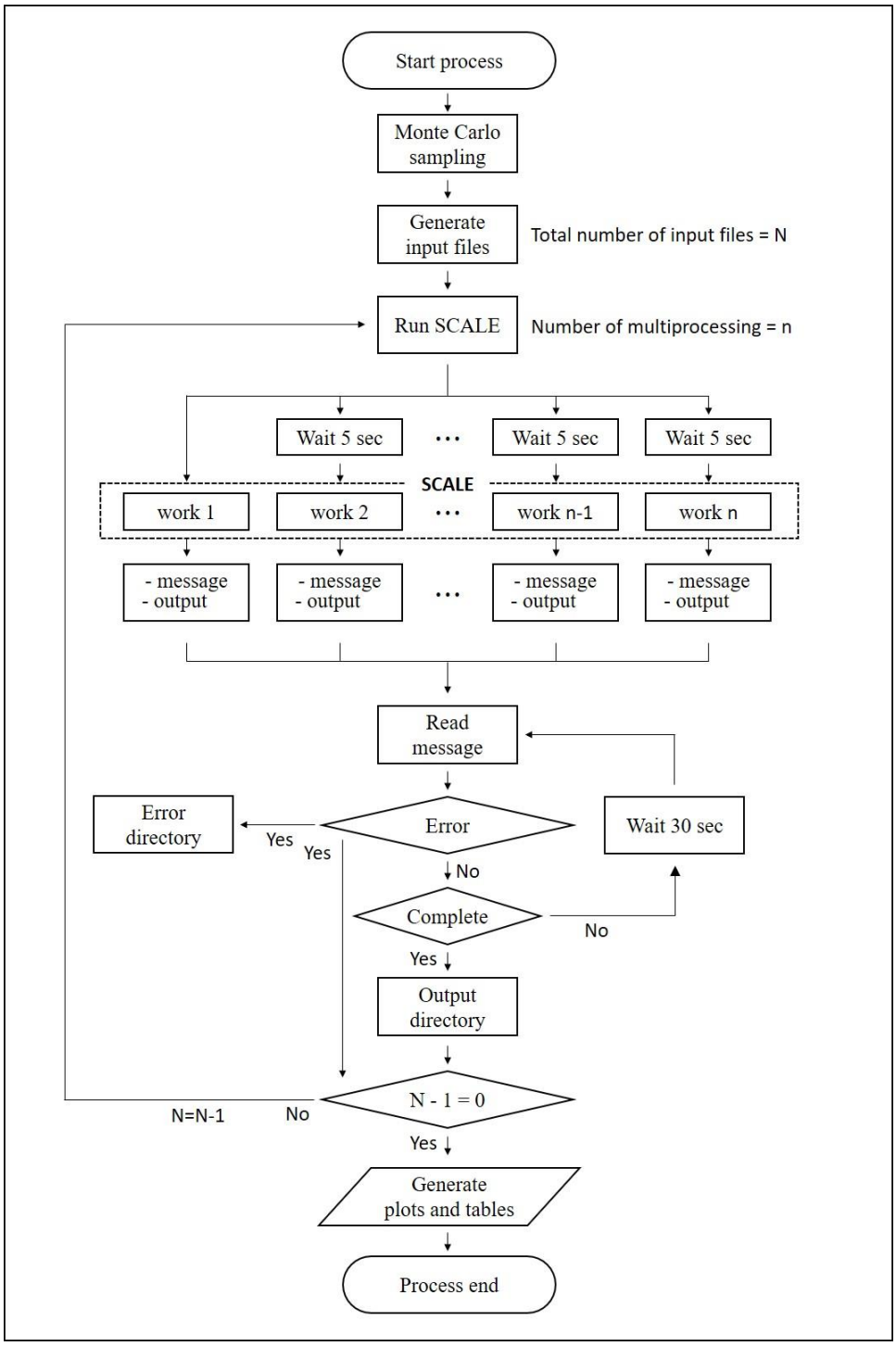


**Figure 3.3 Flowchart of multiprocessing for SCALE work.**

Even if the SAVIO high performance computing system is used for a major part of the calculation, a personal cloud is also used as an auxiliary system. The personal cloud system has been made by using 10 of the personal desktop computers, and a parallel computing method in the form of task parallelism is used for the concurrent computation. A Python code has been made for the task parallelism which focuses on distributing tasks to 10 of computers. Among 10 computers, 2 computers have 12 core CPUs, and 3 computers have 8 core CPUs. A computer with 6 core CPU is also used and other 4 computers have 4 core CPU. These computers were connected to a network switcher, and they formed a cloud by using the Python code. All computers use the Python code which is based on the flow chart at figure 3.3 for the multiprocessing of SCALE works, and a Python code is added for reporting their work status to a server. The computer with 6 core CPU is used as a server, and other computers are used as nodes. However, the computer with 6 core CPU also did computational work as a node while controlling other computers. The computer with 6 core CPU allocated work to other computers and monitored their work status by reading status messages from other computers. This personal system works like a computer with a 70 core CPU by forming a cloud. Even if its performance cannot be compared with the SAVIO high performance computing system, it is comparable with 2 nodes of SAVIO.

### 3.2.3. Results of the analysis

Sensitivity analysis by using direct sampling with Monte Carlo method is not efficient and it takes a very long time to get a result from a lot of calculations. It can take more than a month to get a complete set of output data which are photon dose rate, neutron dose rate and effective multiplication factor. Especially, calculation of the neutron dose rate to get the standard deviation takes more time than the other two. However, this inefficient process is still worthwhile because its result helps to characterize fuel debris. Moreover, results from the process are necessary to develop analytical models and theories for the uncertainty quantification of the radiation dose rate.

#### 3.2.3.1. Variability of dose rate by changes in distribution of fuel debris

As an uncertain variable, the distribution of radiation sources in a canister affects the dose rate at a detector, and fuel debris is the major source of the radiation. At this section, dose rate from fuel debris in a canister has been estimated for 1,000 samples based on the updated model. However, random sampling for the radius of debris is excluded from the model, and it is assumed to be the same for all fuel debris. The radius of each debris sphere is calculated to 3.86 cm based on the total weight and number of debris which are 230.9 kg and 100 spheres. A point detector is located horizontally 1 m from the center of a fuel canister, and other assumptions including source term and composition of shielding material are based on the updated model (Figure 3.4). Photon and neutron dose rates are estimated at the point detector by using the MAVRIC module of SCALE for 1,000 canisters, which is total number of samples.

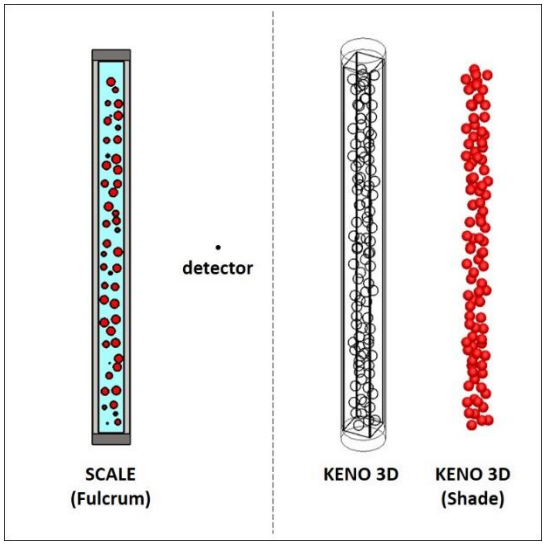


**Figure 3.4 the cross-sectional view and 3D view of fuel debris in a canister.** The figure at the left is the cross-sectional view of fuel debris in a canister which has been drawn by the Fulcrum user interface of SCALE. Red colored spheres are fuel debris. Diameter of fuel debris looks different because they are a cross sectional view of fuel debris which can be seen at the plane of the cross-section. Light gray colored material is the concrete filler of a canister, and dark gray colored material is the stainless steel of the canister. The figure at the right has been drawn by the user interface of the KENO 3D module of SCALE. The wireframe image is the diagonal view of the canister, and the red colored spheres at its right side is the shaded image of fuel debris in a canister.

The range of photon dose rate is 12.9 rem/hr (129 mSv/hr) which is the difference between the maximum and minimum value of the dose rate (Figure 3.5). This informs that a measured value of photon dose rate can be different up to 86.7 % of other measurements by the geometric distribution of fuel debris in a canister. Average photon dose rate is 20.85 rem/hr (208.5 mSv/hr) and its standard deviation is 1.85 rem/hr (18.5 mSv/hr) which is around 8 % of the average value. The range of neutron dose rate is 1.2 mrem/hr (12 μSv/hr), and a measured value of neutron dose rate can be different up to 34 % of other measurements. Average neutron dose rate is 4.09 mrem/hr (40.9 μSv/hr), and its standard deviation is 0.16 mrem/hr (1.6 μSv/hr) which is around 4 % of the average value.

Geometric distribution of fuel debris in a canister for the maximum and minimum neutron dose rates are the same for the maximum and minimum of photon dose rate. Estimation of neutron dose rate takes more time than the estimation of photon dose rate when it has been calculated by using SCALE. Therefore, it can be better to estimate the photon dose rate first before the estimation of neutron dose rate when evaluating the maximum and minimum of dose rate for fuel debris in the same size. For fuel debris in the same size, calculation of neutron dose rate by using the geometric distribution of fuel debris which has maximum and minimum photon dose rate can provide the maximum and minimum values of neutron dose rate, and this can save time for the calculation.

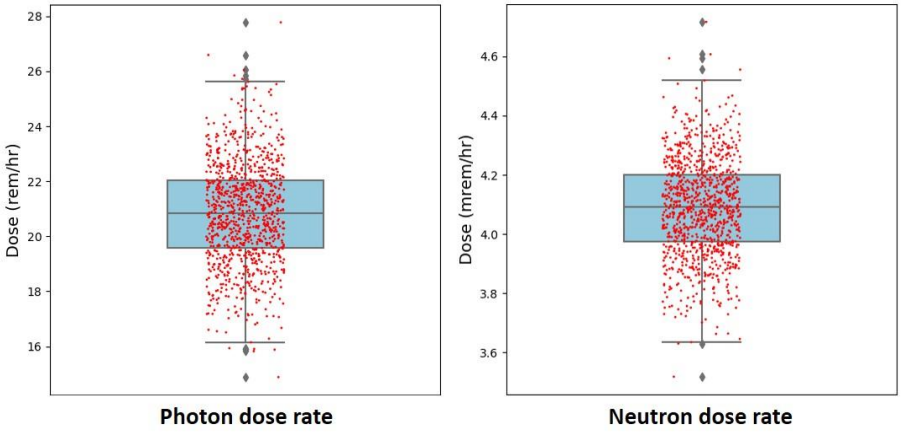


**Figure 3.5 Box plot of photon and neutron dose rate.** Red dots are the dose rates which are calculated by using MEVRIC module of SCALE. Therefore, each box plot has 1,000 red dots. The height of the box is the interquartile range. The lowest line of the box is the 25th percentile (Q1), and the line at the top of box is the 75th percentile (Q3). The height of the box is the interquartile range (IQR), and the horizontal line in a box is the median value of dose rate (Q2). The horizontal line at the lowest end of the vertical line is the minimum which is Q1 – 1.5 * IQR. The horizontal line at the top of the vertical line is the maximum which is Q3 + 1.5 * IQR. Gray dots outside of the maximum and minimum are outliers. Outliers are larger than the maximum or smaller than the minimum, and the difference between the maximum outlier and the minimum outlier is the largest value of possible variability in the measurement of dose rate.

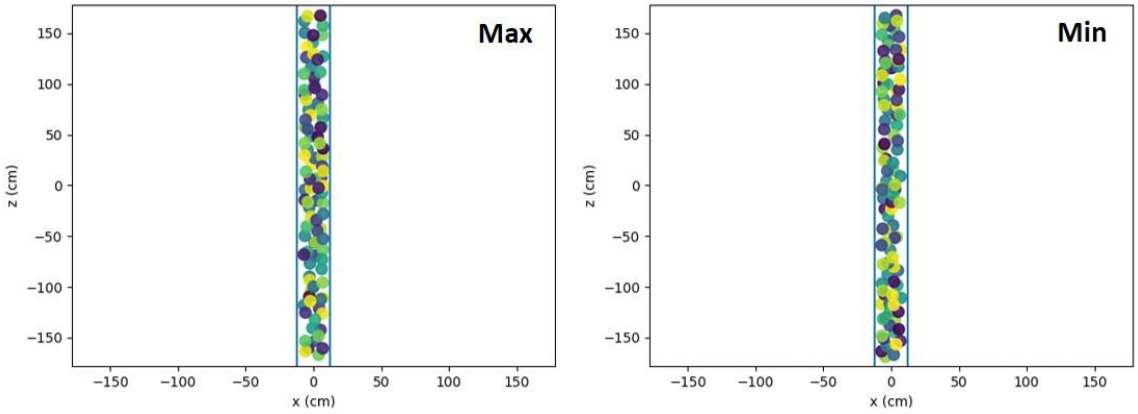


**Figure 3.6 Distribution of fuel debris in a canister.** The plot at left is the distribution of fuel debris for the maximum dose rate, and at right is that for the minimum. X-axis of the graph is the horizontal location of fuel debris in x direction. Y-axis of the graph is the vertical location of fuel debris in z-direction. Colors of fuel debris are decided by the horizontal location in y-direction. A debris with brighter color is located at +y direction, and dark colored debris is located at -y direction.

A canister has the maximum dose rate at a detector when more fuel debris are located at the center of the canister because the detector is placed at 1m from the center of a canister (Figure 3.6). On the other hand, a canister has the minimum dose rate when more fuel debris are located at the top and the bottom of a canister. Radius of fuel debris of this model is assumed to be 3.86 cm, and a few fuel debris are located at each path of radiation from a fuel debris to a detector. Therefore, screening and attenuation of nuclear radiation from debris by other debris has not significantly affected the variability of the dose rate. Difference in total path length affected more on the variability of dose rate in this case.

The criticality safety is not the main subject of this chapter, but it is also evaluated because fuel debris need to maintain subcritical condition for the use of source term. The source term of the model needs to be changed if the debris is not in a subcritical condition. Variability of geometric distribution of fuel debris also affects the criticality safety, and effective multiplication factor depends on the geometric distribution. Dry air of the model is replaced to water for the estimation of the effective multiplication factor ($k_{eff}$), and then SCALE calculated $k_{eff}$ for 1,000 samples. The range of $k_{eff}$ is 0.05, and $k_{eff}$ can differ up to 21% by the geometric distribution of fuel debris (Figure 3.7). Average value of $k_{eff}$ is 0.43 and its standard deviation is 0.008. Geometric distribution of fuel debris does not affect a lot on the variability of $k_{eff}$, and the debris maintains subcritical condition for all canisters. This small differences in $k_{eff}$ for fuel debris in different geometric distribution can affect the criticality safety when fuel debris are in free spaces with larger total weight. However, the total amount of fuel debris is restricted to 230.9 kg in this model, and available spaces for the geometric distribution of fuel debris are also restricted by the inner space of the canister. The radius of fuel debris is also assumed to be 3.86 cm in this model. Therefore, the fuel debris maintains subcritical conditions at these assumptions and restrictions.

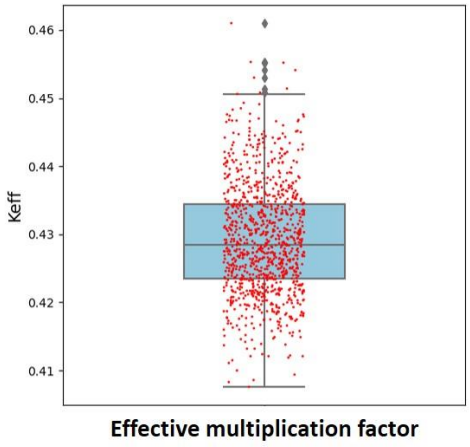


**Figure 3.7 Effective multiplication factor of fuel debris in a canister.** Red dots are the effective multiplication factors which are calculated by the KENO module of SCALE.

### 3.2.3.2. Variability of the dose rate by changes in the radius of debris

In the previous section, the radius of fuel debris and the total number of fuel debris in a canister has been considered as constants, and the standard deviation of dose rate was estimated only for the changes in the distribution of debris in a canister. At this section, the size and the total number of debris is considered as variables, and variability of dose rate by changes in the size is evaluated. The number of fuel debris in a canister is a dependent variable, and it is calculated based on the radius of debris and the total weight of debris which is 230.9 kg per canister. The diameter of debris is the same for each sample group, and it increases for 0.5 cm by the changes in the group. Other assumptions are the same with the model of this chapter.

Photon dose rate of fuel debris decreases by the change of the radius of debris. Figure 3.8 is a graph which displays box plots of each sample group. Red dots on box plots are estimated photon dose rates which are calculated by SCALE. Value for each red dot has been calculated by running SCALE, and a total of 17,000 times of calculation were performed for 17,000 input files. The median value of photon dose rate which is the center of each box plot decreases by changes in the radius. The average photon dose rate is 93.2 rem/hr (932 mSv/hr) for the radius of 2.0 cm, and it decreases to 40.0 rem/hr (400 mSv/hr) for the radius of 9.0 cm. Deviation of data increases by increases in radius. The standard deviation of photon dose rate is 1.29 rem/hr (12.9 mSv/hr) for the radius of 2.0 cm, and it increases to 4.7 rem/hr (47 mSv/hr) for the radius of 9.0 cm. These values are 1.4 % and 11.8 % of the average dose rate for 2.0 cm and 9.0 cm of radius. Range of dose rate is 11.1 rem/hr (111 mSv/hr) and 28.7 rem/hr (287 mSv/hr) for the radius of 2.0 cm and 9.0 cm which are 11.9 % and 71.8 % of the average dose rate for each.

Neutron dose rate also decreases by the change of the radius, but its relative change is smaller than that of photon dose rate (Figure 3.9). The average neutron dose rate is 6.86 mrem/hr (68.6 μSv/hr) for the radius of 2.0 cm, and it is 6.27 mrem/hr (62.7 μSv/hr) for the radius of 9.0 cm. Therefore, the relative changes in neutron dose rate from the radius of 2.0 cm to 9.0 cm is 8.6 % of the dose rate of the radius of 2.0 cm whereas the relative changes in photon dose rate is 57.1 %. Deviation of data increases by the increases of radius like the photon dose rate does. The standard deviation of neutron dose rate is 0.07 mrem/hr (0.7 μSv/hr) for the radius of 2.0 cm, and it is 0.68 mrem/hr for the radius of 9.0 cm. These two deviations are 1.1 % and 10.8 % of the average dose rate for 2.0 cm and 9.0 cm. Range of dose rate is 0.46 mrem/hr (4.6 μSv/hr) and 4.19 mrem/hr (41.9 μSv/hr) for the radius of 2.0 cm and 9.0 cm which are 6.7 % and 66.8 % of the average dose rate for each.

As indicated in figure 3.8 and figure 3.9, estimated photon and neutron dose rate from fuel debris are smaller for larger debris. Variability of neutron dose rate by changes in the radius is smaller than the variability of photon dose rate. Thus, the photon dose rate is more sensitive for changes in the radius than the neutron dose rate. Uncertainty or error of data is evaluated as the standard deviation and the percent relative range, and they are larger for larger fuel debris. Uncertainty of the neutron dose rate is smaller than that of the photon dose rate, but the difference between these two is not significant.

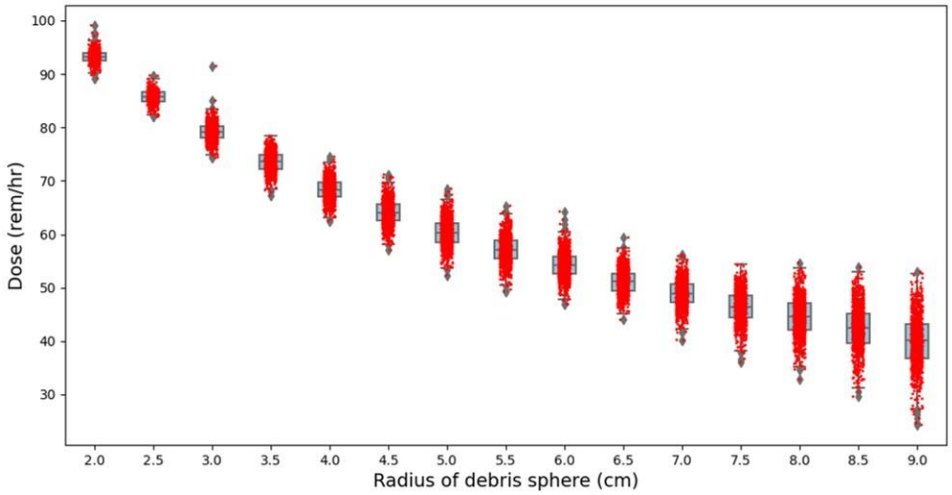


**Figure 3.8 Photon dose rate of fuel debris in a fuel canister.** Photon dose rates estimated by SCALE are plotted as red dots on box plots. Fuel debris in a sample group has the same radius. X- axis is the radius debris which is assumed for each sample group, and Y-axis is the dose rate in rem/hr.

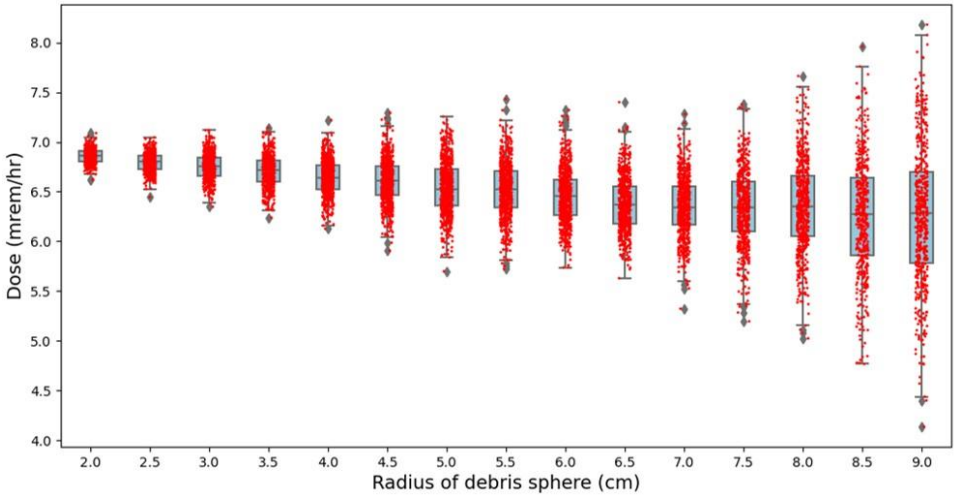


**Figure 3.9 Neutron dose rate of fuel debris in a fuel canister.** Neutron dose rates estimated by SCALE are plotted as red dots on box plots.

### 3.2.3.3. Fuel debris in random size and distribution

In the previous section, the radius of fuel debris was the same for each sample group, and the radius of each group was increased by 0.5 cm. Radius of fuel debris is assumed to be a random variable at this section, and its range at each sample group is assumed to be 2 cm. Thus, differences between the maximum and minimum radius in a group is 2 cm. The median radius of each sample group is increased by 0.5 cm like assumed at the previous section. After assuming these random variables, variability of dose rate is evaluated for the loose packing and the close packing of fuel debris in a canister.

Dose rate of fuel debris in a canister decreases by increases in the minimum radius of debris (minimum of the randomly sampled radius of fuel debris). Figure 3.10 is the box plot of photon dose rate for the loose packed fuel debris in a canister. Red dots at the graph are values of dose rate calculated by using SCALE. 17 groups of dose rates are plotted with box plots and each group has 1,000 values of dose rate which are calculated by SCALE for 1,000 times. Total number of red dots at the figure is 17,000 which are from 17,000 SCALE outputs. Photon dose rate of fuel debris decreases to more than 50% of the values in the sample group with the radius of 1cm by the increasing of the radius from 1cm to 9cm. The range of dose rate data at each sample group increases by increases in the minimum radius of debris. The graph in Figure 3.10 is very similar to the graph in Figure 3.8. However, deviation of data is larger for the fuel debris with random radius than the debris with constant radius.

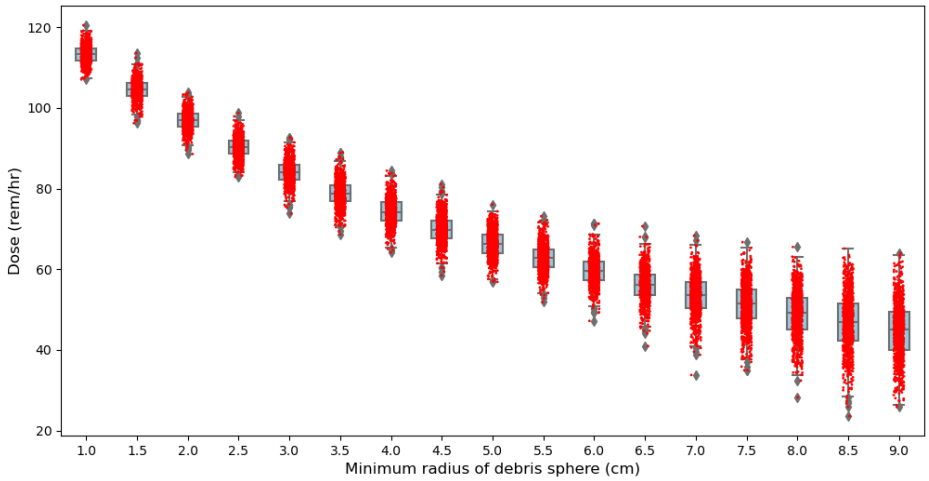


**Figure 3.10 Box plot of photon dose rate for loose packed fuel debris in a fuel canister.** Photon dose rates estimated by SCALE are plotted as red dots on box plots.

In case of the close packed fuel debris in a canister, photon dose rate does not decrease by the increase of the radius (Figure 3.11). The dose rate increases by changes in the radius for the radius less than 5.5 cm. The dose rate decreases by the increase of radius for the radius larger than 5.5 cm. This inconsistent change is made because the point detector is

not located at the center of the pile of debris but is located at the center of a canister. The maximum height of the debris pile is changed by changes in the radius, and it causes the differences in the path length from debris to the point detector (Figure 3.12).

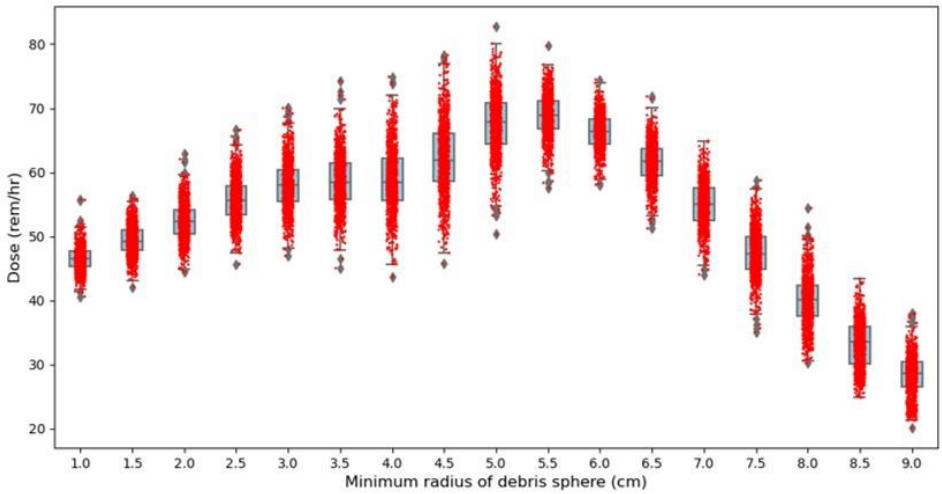


**Figure 3.11 Box plot of photon dose rate for close packed fuel debris in a canister.**

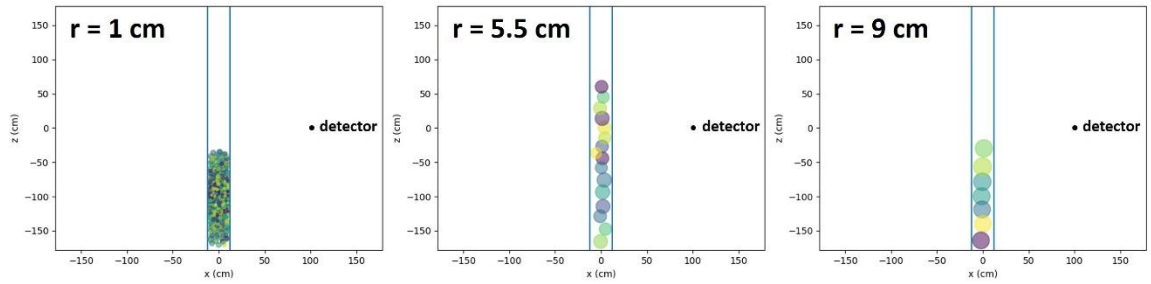


**Figure 3.12 Distribution of fuel debris in a canister.** Color of the sphere is decided by the location of debris in the Y-axis. Dark color and bright colors are opposite locations from the center in Y-axis. These graphs display the distribution of debris in each canister for the maximum dose rate in their group. The graph at left is for the radius of 1 cm, at the center and right are for the radius of 5.5 cm and 9 cm.

Dose rate at the center of debris is not the same with the dose rate at the center of a canister. For the estimation of dose rate at the center of the pile of fuel debris, the pile of debris is moved to the center of a canister instead of to adjust the location of the point detector. Fuel debris will not stay at the center of a canister in actual situations, but this is assumed for the simplicity of the model. Photon reflection at the bottom of a canister is ignored by this adjustment, but this does not affect the result of evaluation. Photon dose rate is estimated for the pile of debris which is relocated to the center of a canister based

on this assumption. In case of this, dose rates are decreased by increases in the radius, but amounts of decrease in dose rate by the increase of radius from 1 cm to 9 cm is less than the decreased amount of loose packed debris. Slope of decrease is also different from the graph of loose packed debris (Figure 3.13). Dose rates of each fuel group are decreased by increases in the radius from 1cm to 6cm, then the increase of radius changes the dose rate only a little amount for the minimum radius larger than 6 cm. Range of dose rate which is the difference between maximum and minimum dose rate at each sample group does not gradually increase unlike the loose packed debris, and it has its maximum at the radius of 5.5cm.

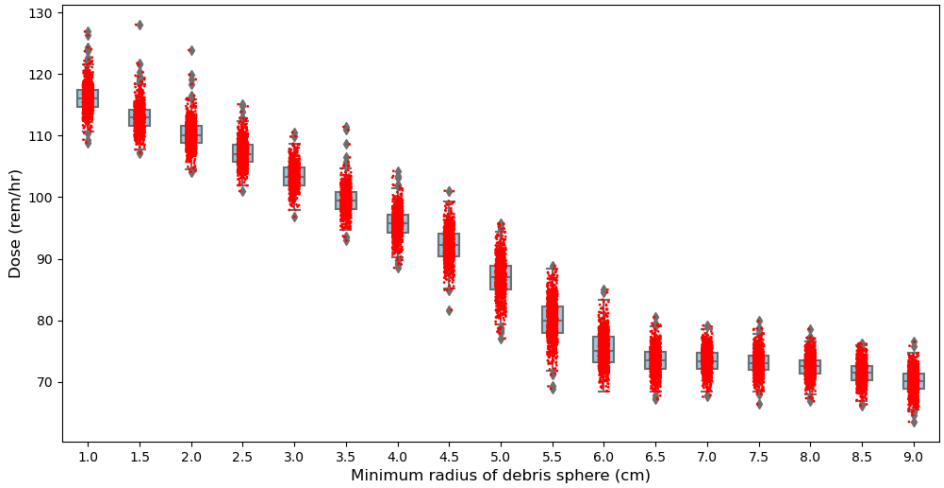


**Figure 3.13 Box plot of photon dose rate for close packed fuel debris in a fuel canister.**

The average photon dose rate of each sample group has been calculated for the loose packed and the close packed debris. $\mu_i$ is the average photon dose rate of $ith$ sample group, and $D_k$ is the photon dose rate calculated for a sample. $N_i$ is the total number of sample in $ith$ group which is 1,000 for each.

$$\mu_i = \frac{\sum_{k=1}^{N_i} D_k}{N_i}$$

The average photon dose rate of the close packed and the loose packed fuel debris in a fuel canister are compared in Figure 3.14. The average dose rate of the loose packed fuel debris exponentially decreases by changes in the minimum radius of debris in each sample group, and it is easy to be fitted to an exponential function. It decreases from 113.3 rem/hr (1,133 mSv/hr) to 44.75 rem/hr (447.5 mSv/hr) by the change of radius from 1cm to 9cm. The average dose rate of close packed debris is also decreased by changes in the minimum radius of sample groups, but the amount of decrease from 1cm to 9cm is less than the amount of change in loose packed debris. Graph on the dose rate of close packed debris has a saddle point at the minimum diameter of 6.5 cm, and non-linear regression analysis is required to fit the data to a function.

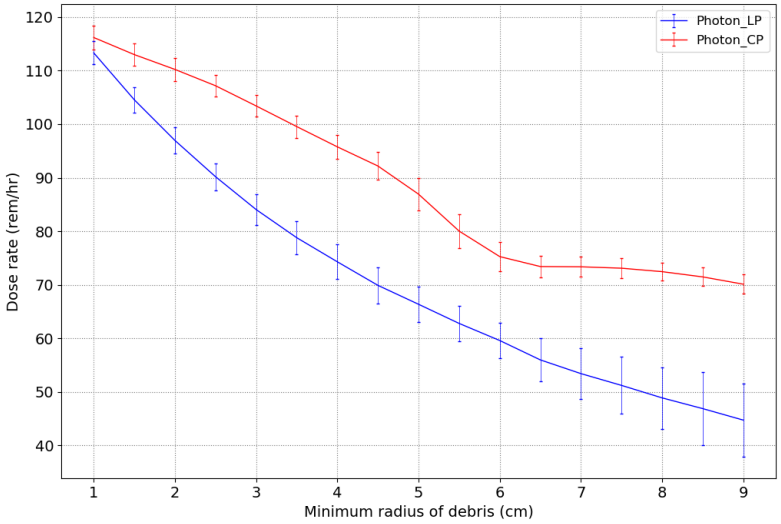


**Figure 3.14 Comparison of the average photon dose rate between the loose packed and the close packed fuel debris.** Dose rates on the graph are average values of sample groups which are grouped by the minimum radius of debris. The error bar on the graph visualizes the standard deviation of average dose rates.

Standard deviation is calculated for each sample group.

$$\sigma_i = \sqrt{\left(\frac{\sum_{k=1}^{N_i} D_k^2}{N_i}\right) - \mu_i^2}$$

$\sigma_i$ is the standard deviation of $ith$ sample group. Standard deviations of the average dose rate are compared at Figure 3.15 for the loose and the close packed debris. Standard deviation of the loose packed debris nonlinearly increases by changes in the minimum radius, and it is decreased a little at the radius of 9 cm. The standard deviation increases up to 6.84 rem/hr (68.4 mSv/hr) which is around 15 % of the average dose rate at the radius of 9 cm. Standard deviation of the close packed debris does not continue to decrease by changes in radius and it has a concave point at the radius of 5.5cm.

The coefficient of variation is calculated by dividing the standard deviation by the average photon dose rate, and it has been visualized at the figure 3.16.

$$CV = \frac{\sigma_i}{\mu_i} \times 100$$

A sample of photon dose rate in a group can have value larger than the standard deviation, and some of values may deviate from the standard deviation. Therefore, the relative percent range is also calculated for each sample group.

$$\%\, range = \frac{Max\ D_i - Min\ D_i}{\mu_i} \times 100$$

The relative percent range of dose rates in each sample group has been displayed at Figure 3.16. The relative percent range can be up to 88.6 % of the average dose rate for the loose packed debris whereas it is less than 24 % of the average dose rate for the close packed debris. These values of percent range are 41.5 rem/hr (415 mSv/hr) and 20 rem/hr (200 mSv/hr) for each.

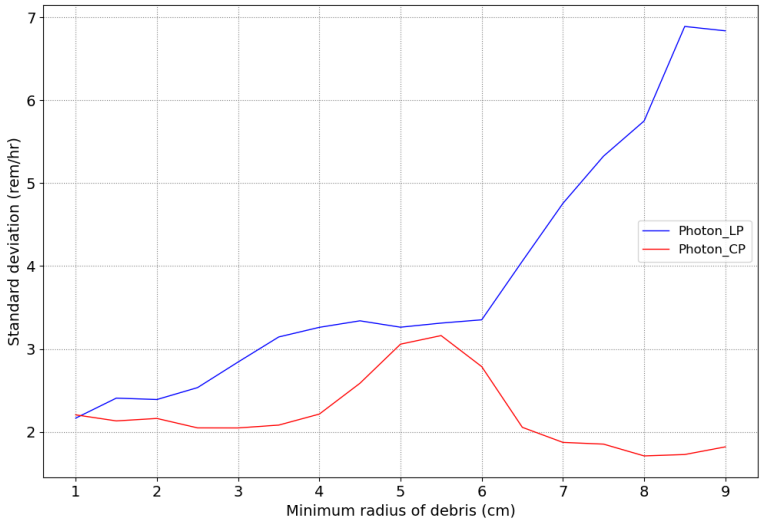


**Figure 3.15 Comparison of the standard deviation between loose packed and close packed debris in a canister.**

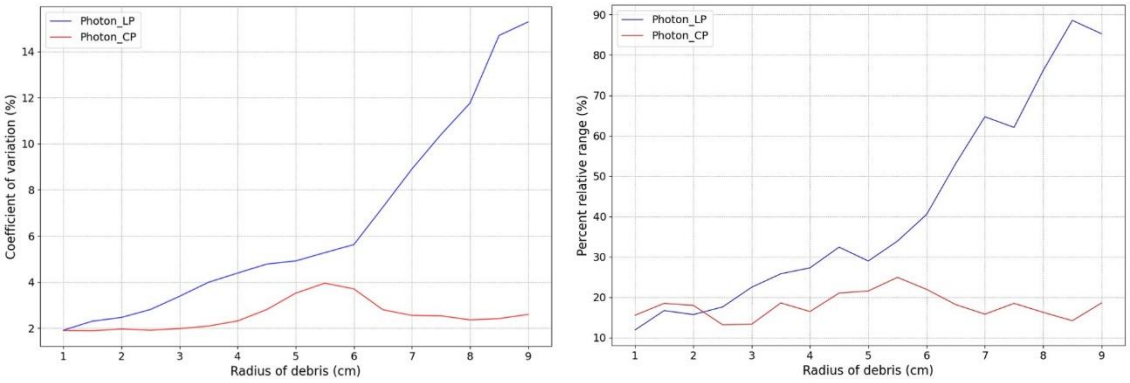


**Figure 3.16 Comparison of the coefficient of variation (left) and the percent relative range (right) between loose packed and close packed debris.**

The sensitivity coefficient is a means to describe the relative changes by an uncertain variable, and it is commonly calculated with the perturbation theory in reactor physics. The concept of sensitivity coefficient is used to describe the sensitivity of dose rate by changes in the radius of fuel debris. The sensitivity coefficient is defined as,

$$S_i = \frac{\delta\mu_i / \mu_i}{\delta r_{min,i} / r_{min,i}}$$

$S_i$is the sensitivity coefficient of a sample group $i$, and $r_{min,i}$ is the minimum radius of the sample group. $\delta\mu_i$ is the relative change of the average dose rate, and $\delta r_{min,i}$ is the relative change of the minimum radius of the sample group $i$. The relative change of dose rate $\delta\mu_i$ is calculated by approximation as,

$$\delta\mu_i = \frac{\mu_{i+1} - \mu_i}{\mu_i} \times 100$$

and $\delta r_{min,i}$ is calculated the same way as $\delta\mu_i$

$$\delta r_{min,i} = \frac{r_{min,i+1} - r_{min,i}}{r_{min,i}} \times 100$$

The sensitivity coefficient of the close packed fuel debris and the loose packed fuel debris are calculated by these, and its results are compared in Figure 3.17. The photon dose rate of the loose packed fuel debris is more sensitive by changes in the radius of debris than the close packed debris. However, the photon dose rate of the close packed fuel debris is very sensitive when the $r_{min}$ is 5 cm ~ 5.5 cm.

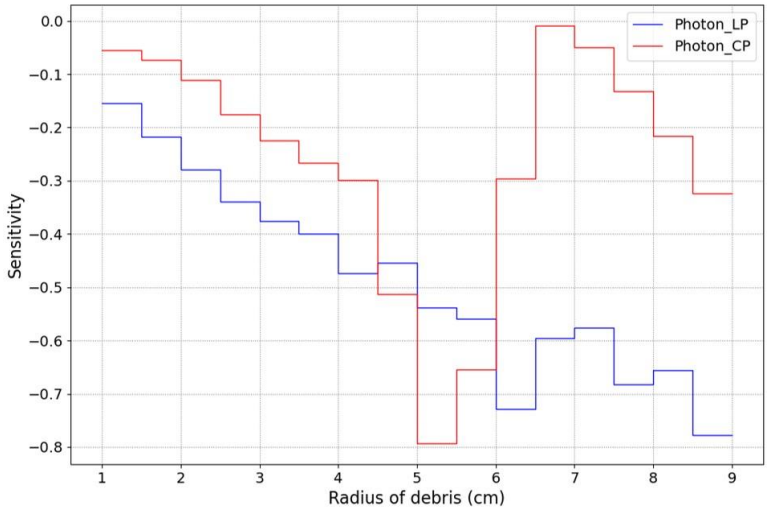


**Figure 3.17 Comparison of the sensitivity coefficient between the loose packed and the close packed debris.**

Neutron dose rate of the loose packed fuel debris is visualized in Figure 3.18. The neutron dose rate of fuel debris with random size is similar to that of fuel debris with constant size (Figure 3.9), but it is a little bit smaller. Neutron dose rate of the close packed fuel debris with random size is calculated for the fuel debris relocated to the vertical center of a canister like it did for the photon dose rate, and its results are visualized in Figure 3.19. Neutron dose rate of the close packed fuel debris decreases by increases in the minimum radius of each sample group when the minimum radius is smaller than 6.0 cm. However, it increases by the increase of the radius when the minimum radius of the sample group is larger than 6.0 cm.

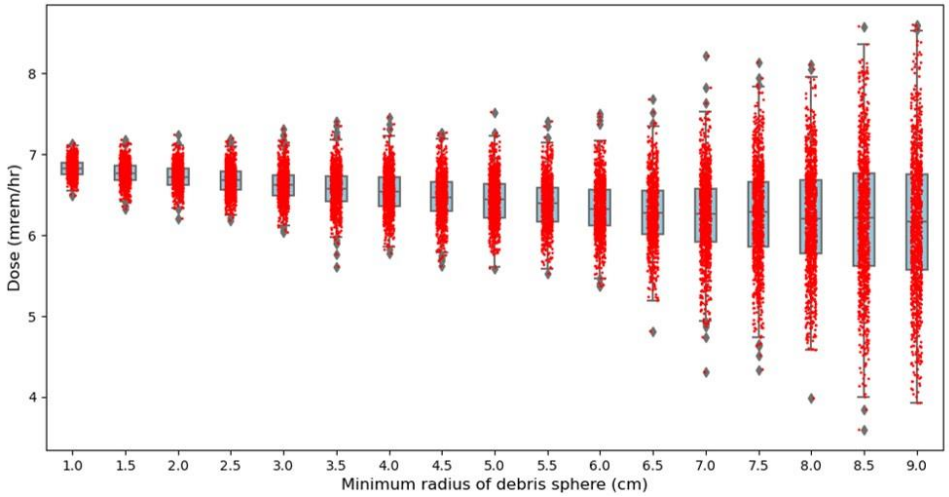


**Figure 3.18 Box plot of neutron dose rate for the loose packed fuel debris in a fuel canister.**

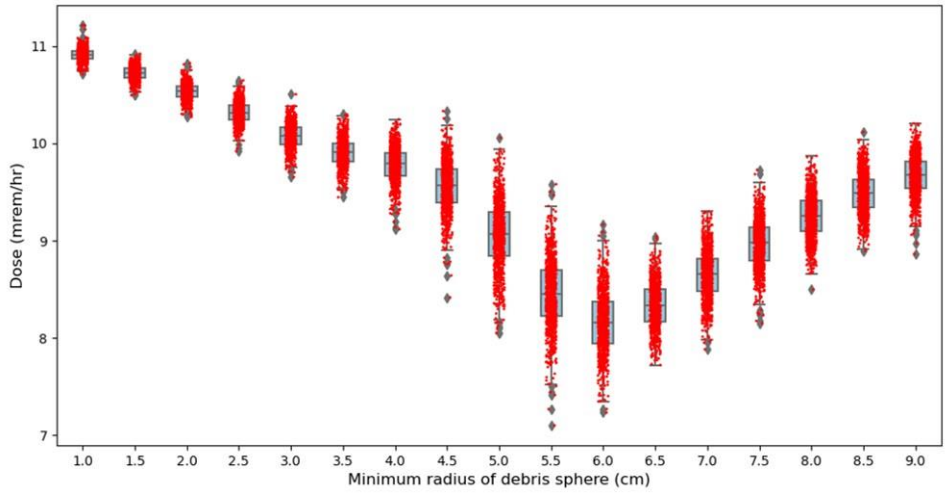


**Figure 3.19 Box plot of neutron dose rate for the close packed fuel debris in a fuel canister.**

The average neutron dose rate is compared in Figure 3.20. Neutron dose rate of the loose packed debris is almost linearly decreased by changes in the minimum radius whereas the dose rate of the close paced debris does not continue to be decreased. Decreased amount of dose rate is less than 1 mrem for the loose packed debris whereas the amount can be up to 2.8 mrem for the close packed debris. The graph of close packed debris has a convex point at the minimum radius of 6cm, and then the average dose rate increases by changes in the radius.

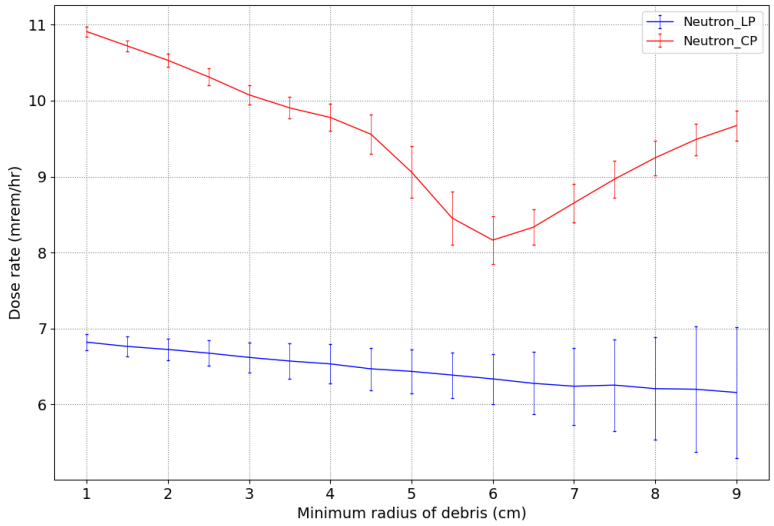


**Figure 3.20 Comparison of neutron dose rate between the loose packed and the close paced debris.** Dose rates on the graph are average values of sample groups which are grouped by the minimum radius of debris. The error bar on the graph visualizes the standard deviation of average dose rates.

Standard deviation of the neutron dose rate is calculated in the same way as that of photon dose rate, and the standard deviation is compared for the loose packed debris and the close packed debris in Figure 3.21. The standard deviation of the loose packed debris increases by changes in the minimum radius of debris like the standard deviation of photon dose rate does. The standard deviation of the close packed debris has a concave point at the radius of 5.5cm. The loose packed fuel debris has larger standard deviation than the close packed fuel debris excepting for 4.5 cm ~ 6 cm of $r_{min}$.

The coefficient of variation (CV) of neutron dose rate is similar with that of photon dose rate. CV increases by changes in $r_{min}$ for the loose packed fuel debris like that of the photon dose rate does. CV of the close packed fuel debris has a local maximum like CV of the photon dose rate does. CV of the loose packed fuel debris is larger than that of the close packed debris for all $r_{min}$ (Figure 3.22). This is because the standard deviation of the loose packed debris is divided by the average neutron dose rate which is smaller than that of the close packed debris. The relative percent range of neutron dose rate is also calculated in the same way as that of the photon dose rate, and its results are compared for the loose packed and the close packed fuel debris (Figure 3.22). This is also similar with that of

photon dose rate even though there are some differences in details. The percent relative range of the loose packed fuel debris is larger than that of the close packed fuel debris for all $r_{min}$ like the coefficient of variation does. The percent relative range of the close packed fuel debris has a local maximum at $r_{min} = 5.5\ cm$ like CV of the close packed debris does.

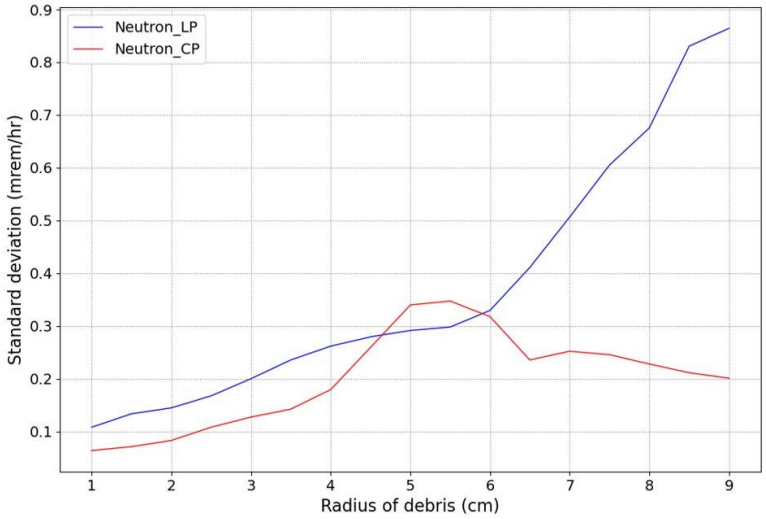


**Figure 3.21 Comparison of the standard deviation between the loose packed and the close packed debris in a canister.**

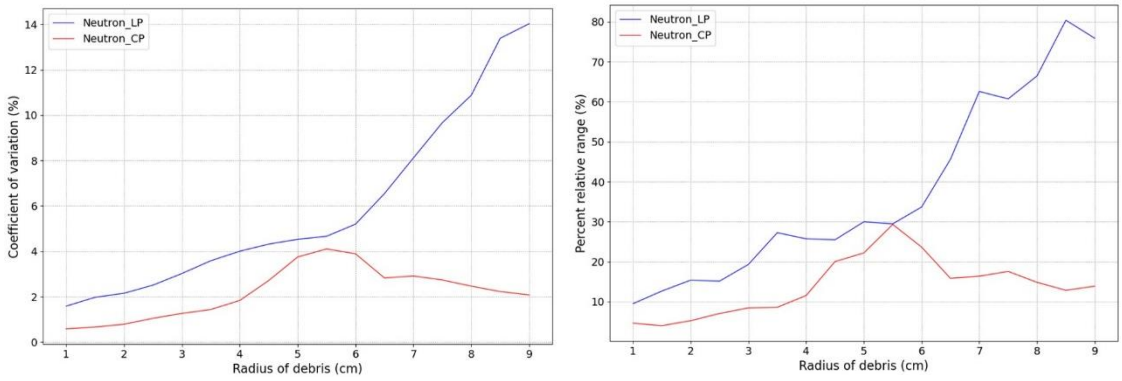


**Figure 3.22 Comparison of the coefficient of variation (left) and the percent relative range (right) between the loose packed and the close packed fuel debris in a canister**

The sensitivity coefficient is calculated, and its results are shown in Figure 3.23. The sensitivity coefficient of the loose packed fuel debris maintains 0.1 ~ - 0.1. On the other hand, the coefficient of the close packed fuel debris has a minimum of -0.67 at $r_{min} = 5\ cm$ and a maximum of 0.51 at $r_{min} = 7\ cm$. This difference explains that the average neutron dose rate of the close packed fuel debris changes a lot by changes in $r_{min}$ whereas

that of the loose packed debris has smaller changes. Thus, the neutron dose rate is more sensitive by changes in $r_{min}$ when fuel debris is closely packed than the other cases.

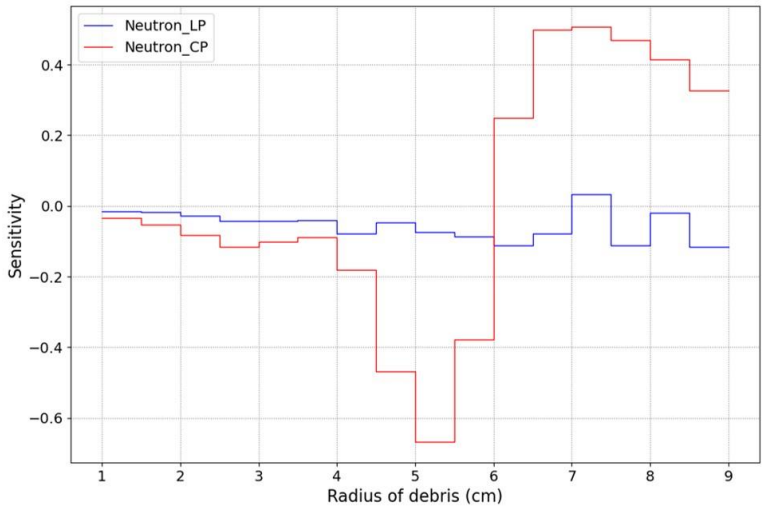


**Figure 3.23 Comparison of the sensitivity coefficient between the loose packed and the close packed fuel debris in a canister**

### 3.2.4 Data fitting to cumulative distribution function

Estimated dose rate values on graphs in the previous section are stochastic and nonlinear, and some graphs have noncontinuous points. Regression analysis of these types of data is not easy, and fitting of these data to a simple function is difficult. Therefore, estimated data in the previous section is converted to cumulative values for the simplification.

Distribution of values on dose rate at each sample group has been accumulated, and cumulative average dose rate has been calculated. Average dose rate of $i$th sample group is

$$\mu_i = \frac{\sum_{k=1}^{N_i} D_k}{N_i}$$

$D_k$ is a value of dose rate, and $N_i$ is the total number of values at a sample group. 1,000 of SCALE output data is at a sample group, so $N_i$ is 1,000 based on the assumption at the previous section. Standard deviation of $i$th sample group is

$$\sigma_i = \sqrt{\left(\frac{\sum_{k=1}^{N_i} D_k^2}{N_i}\right) - \mu_i^2}$$

The cumulative average dose rate of $j$th sample group is

$$\mu_j = \sum_{i=1}^{j}\sum_{k=1}^{N_i} D_{k,i} \Big/ \sum_{i=1}^{j} N_i \tag{3.1}$$

The cumulative standard deviation of $j$th sample group is

$$\sigma_j = \sqrt{\left(\sum_{i=1}^{j}\sum_{k=1}^{N_i} D_{k,i}^2 \Big/ \sum_{i=1}^{j} N_i\right) - \mu_j^2} \tag{3.2}$$

The cumulative average dose can be restored to the average dose rate of $i$th sample group by using a function below.

$$\mu_i = \frac{N_j\mu_j - N_{j-1}\mu_{j-1}}{N_i} \tag{3.3}$$

$$N_j = \sum_{i=1}^{j} N_i \tag{3.4}$$

The cumulative standard deviation can be restored to the standard deviation of $i$th sample group by using a function below.

$$\sigma_i = \sqrt{\frac{N_j\left(\sigma_j^2 + \mu_j^2\right) - N_{j-1}\left(\sigma_{j-1}^2 + \mu_{j-1}^2\right)}{N_i} - \mu_i^2} \tag{3.5}$$

Distribution of average dose rate and its standard deviation have been converted to the cumulative distribution by function 3.1 and 3.2, and the converted distribution is displayed at Figure 3.24 and 3.25.

The cumulative average photon dose rate of the loose packed fuel debris exponentially decreases by changes of the minimum radius of debris at each sample group, and it can be fitted to a function below.

$$D = A_d(C + e^{-br}) \tag{3.6}$$

$A_d$, $b$, C, are coefficients which affect to the photon dose rate $D$. Estimated values of these constants are at Table 3.1. The cumulative average photon dose rate of the close packed debris decreases in the shape of reflected S by increases in the radius, and it can be fitted to the function below.

$$D = -A_d\left[exp\left(-e^{(b-r)/d}\right) - C\right] \tag{3.7}$$

$A_d$, $b$, C, d are coefficients which affect to the photon dose rate $D$. Estimated values of these constants are in Table 3.1.

Cumulative standard deviation of the average dose rate increases by changes in the minimum radius (Figure 3.25). Standard deviation of the loose packed debris is fitted to the function at below

$$\sigma_D = A_\sigma(\gamma - e^{-\beta r}) \tag{3.8}$$

$A_\sigma$, $\beta$, $\gamma$, are coefficients which affect to the standard deviation $\sigma_D$. Estimated values of these constants are in Table 3.1. The standard deviation of the close packed debris is fitted to the function below.

$$\sigma_D = -A_\sigma[exp(-e^{(r-\beta)/\varepsilon}) - \gamma] \tag{3.9}$$

$A_\sigma$, $\beta$, $\gamma$, $\varepsilon$ are coefficients which affect to the standard deviation $\sigma_D$. Estimated values of these constants are in Table 3.1. Total and uncollided flux of fuel debris tend to follow functions 3.6 and 3.7, and they have same coefficient excepting for the coefficient $A_d$ which decides the amplitude of the plot (Figure 3.26). Standard deviation of the total and uncollided flux tend to follow functions 3.8 and 3.9, and they also have same coefficient excepting for the coefficient $A_\sigma$ which decide the amplitude of the plot (Figure 3.27).

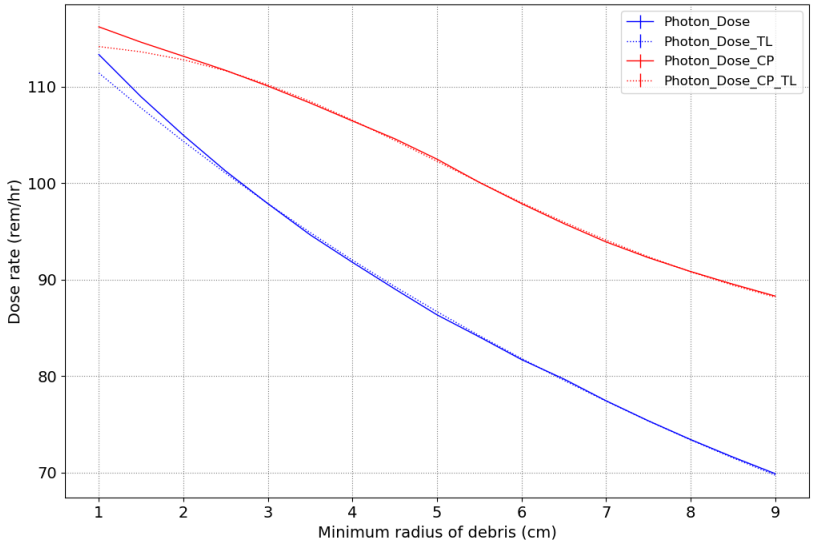


**Figure 3.24 Cumulative average photon dose rate of the close packed fuel debris and the loose packed fuel debris.** Red and blue lines are the dose rate of the close packed and the loose packed debris. Dashed lines are trend lines which are fitted to functions.

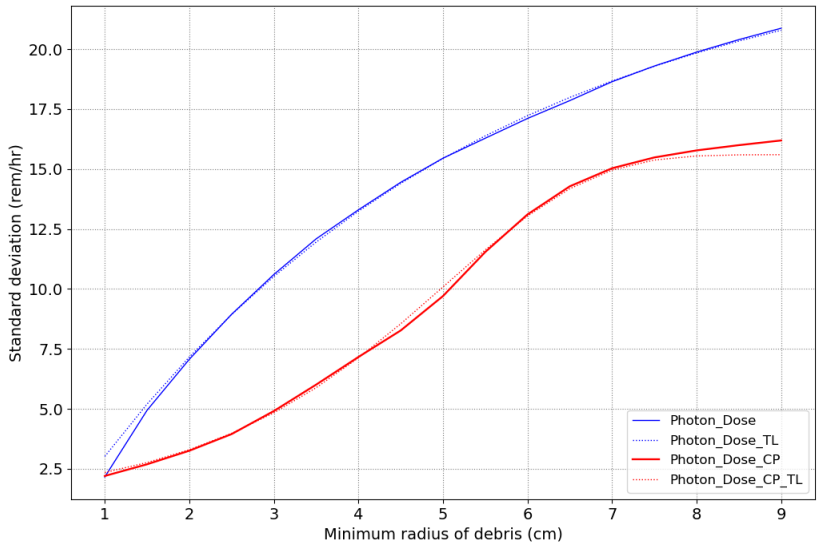


**Figure 3.25 Cumulative standard deviation of photon dose rate.** Red and blue lines are the cumulative standard deviation of the close packed and the loose packed debris. Dashed lines are trend lines which are fitted to functions.

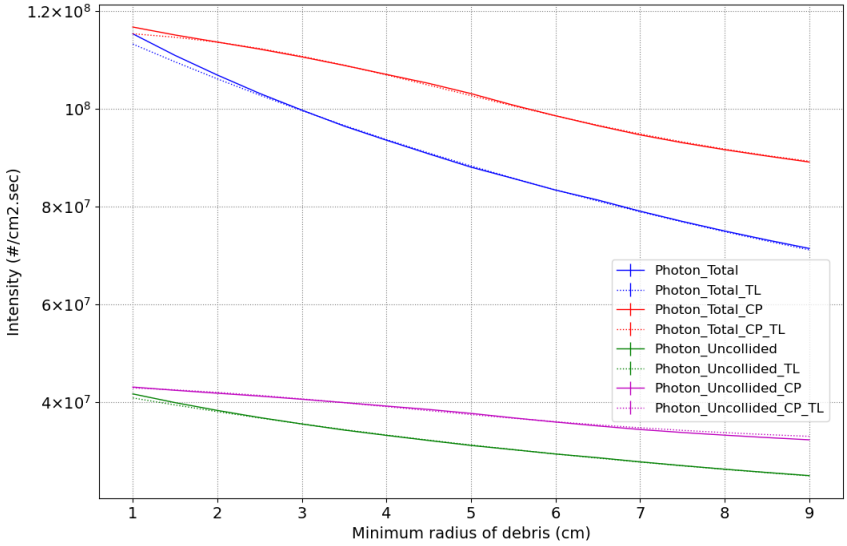


**Figure 3.26 Cumulative total and uncollided flux of the close packed and the loose packed fuel debris.** Red and purple lines are the total and uncollided flux of the close packed fuel debris. Blue and green lines are the total and uncollided flux of the loose packed fuel debris. Dashed lines are trend lines of each flux.

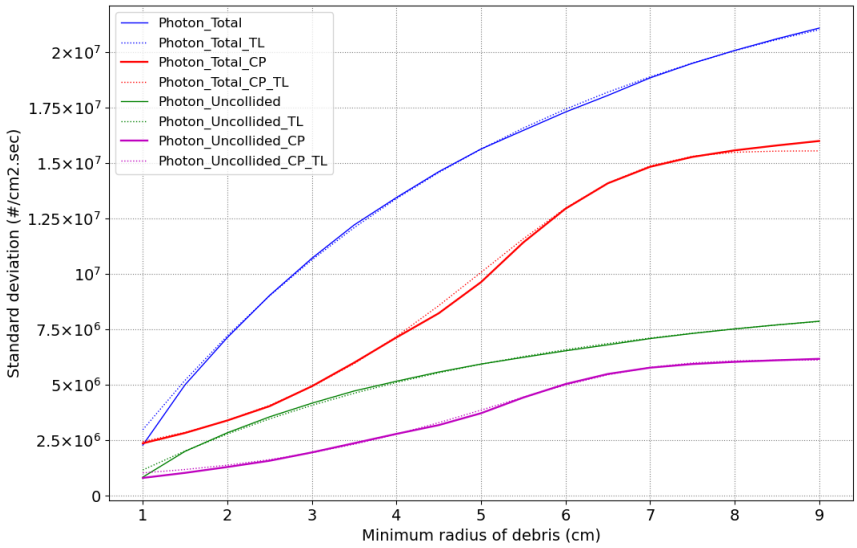


**Figure 3.27 Cumulative standard deviation of photon total flux and uncollided flux.** Red and purple lines are the cumulative standard deviation for the total and the uncollided flux of the close packed fuel debris. Blue and green lines are the cumulative standard deviation for the total and the uncollided flux of the loose packed fuel debris. Dashed lines are trend lines of the standard deviation.

**Table 3.1 Estimated coefficients for photon dose rate**

| Coefficient | | Loose Packed | Close Packed |
|---|---|---|---|
| Dose | $A_d$ | 86.3 | 34.1 |
| | b | 0.094 | 4.9 |
| | C | 0.381 | 2.95 |
| Total flux | $A_\phi$ | $8.79 \times 10^7$ | $3.43 \times 10^7$ |
| | b | 0.094 | 4.9 |
| | C | 0.381 | 2.95 |
| Uncollided flux | $A_\phi$ | $3.11 \times 10^7$ | $1.26 \times 10^7$ |
| | b | 0.105 | 5.1 |
| | C | 0.411 | 2.73 |
| d | | - | 3.36 |
| Dose | $A_\sigma$ | 26.9 | 14.56 |
| Total flux | | $2.64 \times 10^7$ | $1.44 \times 10^7$ |
| Uncollided flux | | $9.75 \times 10^6$ | $5.58 \times 10^6$ |
| $\beta$ | | 0.22 | 5.1 |
| $\gamma$ | | 0.9 | 1.7 |
| $\varepsilon$ | | - | 1.07 |

After fitting data on the photon dose rate to function 3.6 and 3.7, cumulative neutron dose rate has been calculated by using these functions. Values from functions are compared with the cumulative average neutron dose rate which has been estimated by SCALE (Figure 3.28). The estimated dose rate by the function 3.6 is well matched with the cumulative average neutron dose rate of the loose packed debris. The dose rate of the close packed debris is also similar with the function 3.7, but the function is not matched with the SCALE data when the minimum radius of debris is larger than 5.5cm. Total and uncollided flux also can be fitted to the function, but the total flux calculated by function 3.7 is not matched with the data from SCALE for the close packed debris with the minimum radius larger than 5.5cm (Figure 3.29).

Cumulative standard deviation of the neutron dose rate is also calculated by function 3.8 and 3.9, but discordance between values from functions and SCALE data is much larger than the discordance in the cumulative average dose rate. In case of the loose packed debris, the discordance can be decreased by modifying function 3.8 to the function at below.

$$\sigma_D = A_\sigma(\gamma + e^{\beta r}) \tag{3.10}$$

Calculated values by function 3.10 are compared with the SCALE data in Figure 3.30. Total flux and the uncollided flux are also fitted to function 3.9 and 3.10, but there are discordance between the calculated values and SCALE data (Figure 3.31). Coefficients of functions for the data fitting of the standard deviation is at the table 3.2.

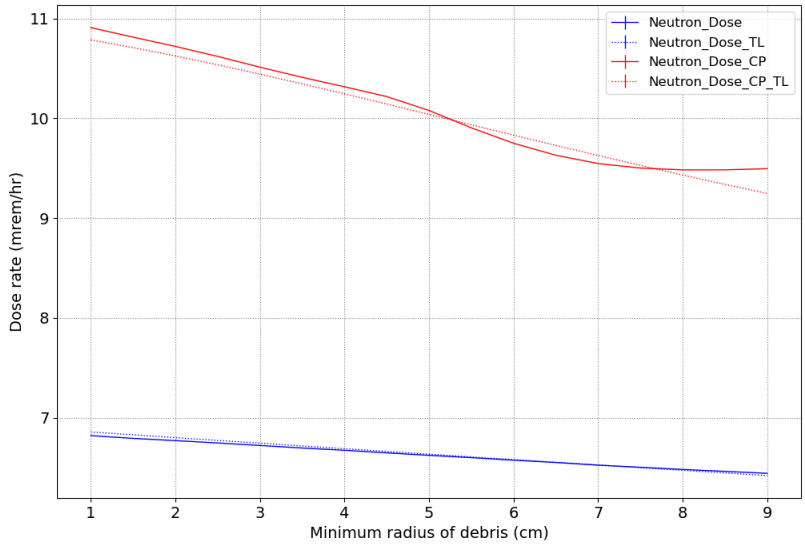


**Figure 3.28 Cumulative average neutron dose rate of the close packed fuel debris and the loose packed fuel debris.** Red and blue lines are the dose rate of the close packed and the loose packed debris. Dashed lines are trend lines of dose rate which are calculated by the function 3.6 and 3.7.

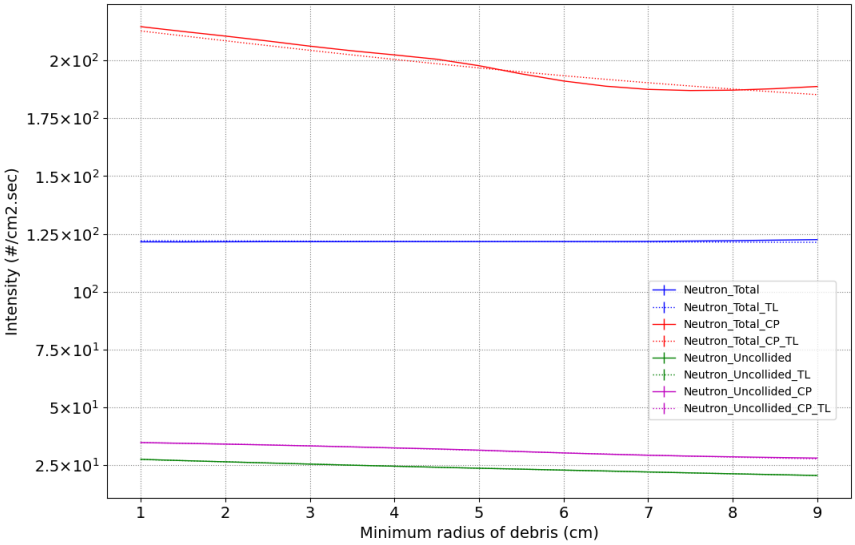


**Figure 3.29 Cumulative total and uncollided neutron flux of the close packed and the loose packed fuel debris.** Red and purple lines are the total and the uncollided flux of the close packed debris. Blue and green lines are the total and the uncollided flux of the loose packed debris. Dashed lines are trend lines.

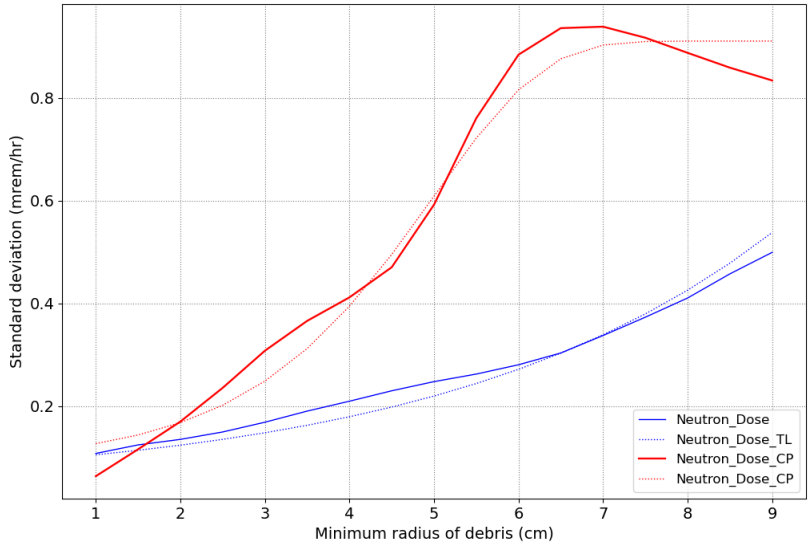


**Figure 3.30 Cumulative standard deviation of neutron dose rate.** Red and blue lines are the standard deviation of the close packed and the loose packed debris. Dashed lines are trend lines of the standard deviation.

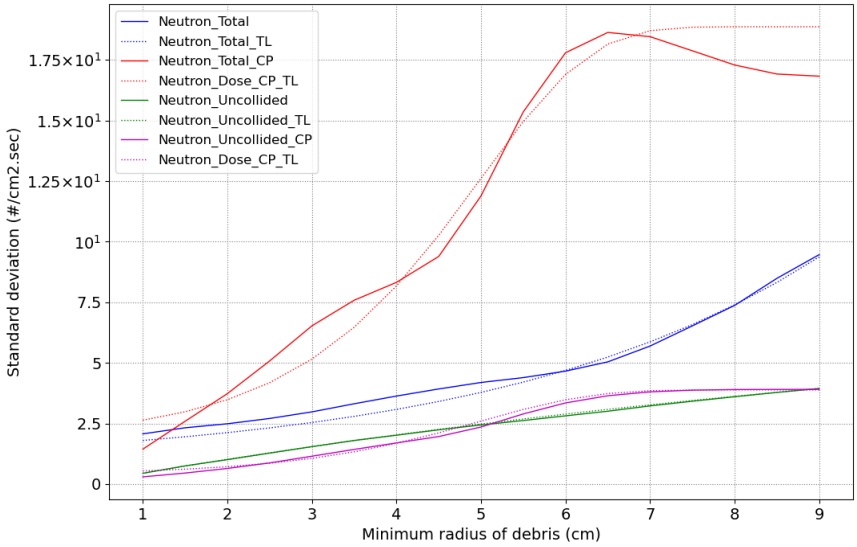


**Figure 3.31 Cumulative standard deviation of neutron total flux and uncollided flux.** Red and purple lines are the standard deviation for the total and the uncollided flux of the close packed debris. Blue and green lines are the standard deviation for the total and the uncollided flux of the loose packed debris. Dashed lines are trend lines of the standard deviation.

**Table 3.2 Estimated coefficients for neutron dose rate**

| Coefficient | | Loose Packed | Close Packed |
|---|---|---|---|
| Dose | $A_d$ | 0.006 | 0.003 |
| | b | 0.008 | 5.3 |
| | C | 0.044 | 5.94 |
| Total flux | $A_\phi$ | 121.7 | 65.9 |
| | b | $2.3 \times 10^{-4}$ | 1.73 |
| | C | $4.8 \times 10^{-3}$ | 6.19 |
| Uncollided flux | $A_\phi$ | 23.68 | 10.5 |
| | b | 0.045 | 4.99 |
| | C | 0.2 | 3.85 |
| d | | - | 3.34 |
| Dose | $A_\sigma$ | $4.95 \times 10^{-5}$ | $8.2 \times 10^{-4}$ |
| Total flux | | 0.838 | 0.017 |
| Uncollided flux | | 0.008 | 0.0035 |
| $\beta$ | | 0.26 | 5.0 |
| $\gamma$ | | 0.84 | 1.3 |
| $\varepsilon$ | | - | 1.11 |

## 3.3 Analytical solution of the photon flux

### 3.3.1. Background and assumptions

Uncertainty of the radiation dose rate was evaluated at the previous section by using SCALE and a Python code. The Python code did the random sampling on size and distribution of the fuel debris in a canister, and SCALE calculated the radiation dose rate for each sample. The Python code used the multiprocessing and the parallel computing methods to enhance efficiency of the evaluation because the calculation by using SCALE takes a long time to get a result. Even though several methods were used to enhance the efficiency, it still takes a long time for the evaluation of uncertainty since a lot of samples needed to be calculated. Therefore, a method is proposed at this section which uses a simplified model for the evaluation of dose rate and its uncertainty. The simplified model analytically calculates the photon flux from fuel debris by using simplified functions on the radiation transport in shielding materials. After the calculation, results from the simplified model have been compared with the estimation of SCALE. The simplified method cannot provide precise evaluation, and it gets approximate values only. However, its results can save time for the sensitivity analysis and the uncertainty quantification by providing brief information on the nuclear radiation.

The simplified model analytically calculates photon flux by using formulas on the attenuation of radiation. Scattering and build up factor are ignored, and the path of photon transport is simplified to a straight line from a source to a detector. Photon sources are approximated to point sources which are at the center of each debris. The space between debris in a canister is filled with air and the medium outside of a canister is also air. The attenuation of photons commonly is described by the Beer-Lambert law ($I = I_0 e^{-\mu x}$), and the law was applied as the basis of the derivation of equations for the analytical method. Attenuation coefficients are averaged and grouped to 101 groups, and photon flux of each group has been calculated. Flux of all energy groups summed to get the total value of flux. Photon attenuation data of the National Institute of Standards and Technology (NIST) has been referenced for the attenuation coefficients [18]. Assumptions including the source term and the specifications of canister are same with the model of the previous section.

### 3.3.2. Simplified model

For a debris, the flux at a detector is defined as below

$$\phi(\ell_d) = \frac{S}{4\pi {\ell_d}^2} e^{-\mu \ell_d} \tag{3.11}$$

Path length from a source to a detector $(\ell_d)$, Radius of a debris $(r)$ for the self-attenuation, sum of chord lengths of debris in a path $(\ell_c)$ for the particle self-shielding are defined as in Figure 3.32. $S$ is the source strength and $\mu$ is the photon attenuation coefficient which is

$$\mu = \rho \sum_i \mu_{m,i} c_i$$

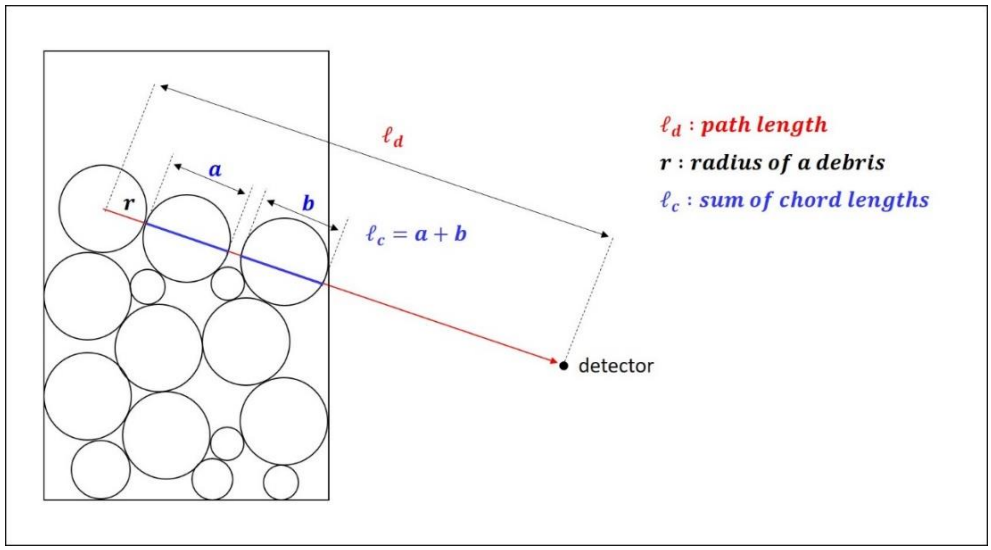


**Figure 3.32 Path and chord length from a debris to a detector**. The red line is the path length ($\ell_d$) and the blue lines are the chord length ($\ell_c$).

The formula by the point source approximation can make errors because a photon source is not a point, but sources are uniformly or randomly distributed in a fuel debris. Errors from this can be supplemented to a degree by using theories on the self-attenuation of radiation. Nuclear radiation can be attenuated not only by materials which are surrounding a source but also by the source material itself. Some articles named this as self-shielding or self-attenuation. However, the expression of self-shielding can be confused with the self-shielding of fuel pellets despite needing to be distinguished. Therefore, the attenuation of radiation in a fuel debris will be called as the self-attenuation in this section. Many researchers developed methods for the calculation of the self-attenuation coefficient. J.R Francois (1973) has calculated the coefficient for a spherical radioactive source [19] and J. K. Dickens (1971) has calculated it for a cylindrical sample [20]. E. Trucco (1964) [21] and K.A.A. Gamage et al (2011) also calculated the coefficient by using methods which are similar with other researchers [22].

Gamage et al calculated the attenuation coefficient by integrating the attenuated radiation intensities in unit shells for overall volume of a sphere [22]. Radioactive materials with a large absorption cross section serve as absorbers at the same time they are emitting nuclear radiation as source materials. This self-attenuation modifies the source term from $S_0 = \sum_i \lambda_i N_i b_i$ to the modified form $S = \sum_i \lambda_i N_i b_i F_i$. $F_i$ is the self-attenuation factor of the isotope $i$ and $b_i$ is the branching ratio. In case of a point source, the radiation intensity after being attenuated by an absorber is $I = I_0 e^{-\mu x}$. $\mu$ is the attenuation coefficient which is $\mu = \mu_m \rho$ and $\rho$ is the density of absorber. This can be rewritten as $\mu = \rho \sum_i \mu_{m,i} c_i$ for an absorber which contains several isotopes. In the case of a spherical radiation source, the volume of the sphere can be calculated by considering the sphere as a group of thin circular layers. If the thickness of each layer is very thin, attenuation of radiations which are generated at a layer can be ignored at the layer and it can be assumed that radiations are

attenuated only while transmitting through other layers. The volume element of this sphere is

$$\mathrm{dv} = \frac{4}{3}\pi[(x+dx)^3 - x^3]$$

which can be simplified to $\mathrm{dv} = 4\pi x^2 dx$. The attenuated radiation intensity of this volume element is $\mathrm{dI} = (4\pi x^2 dx)\rho\,\gamma e^{-\mu(r-x)}$. $\gamma$ is the source strength per a unit mass and $r$ is the radius of a sphere. After integrating this for overall volume of a sphere, the radiation intensity can be calculated as

$$\mathrm{I}(r) = \frac{4\pi\rho\gamma}{\mu^3}[r^2\mu^2 - 2r\mu + 2 - 2e^{-\mu r}]$$

The attenuation coefficient is the radiation transmission through a source material which is a sphere.

$f = I/I_0$ and $I_0 = \frac{4\pi r^3}{3}\rho\gamma$

The attenuation coefficient of a spherical radiation source is

$$f(r) = \frac{3}{r^3\mu^3}[r^2\mu^2 - 2r\mu + 2 - 2e^{-\mu r}] \qquad (3.12)$$

Radiation transmission from a spherical source through a homogeneous media is $\mathrm{T} = f(r)\,e^{-\mu x}$. For a spherical source with the source strength $I_0$, radiation after being attenuated by a homogeneous media is $\mathrm{I} = f(r)\,I_0 e^{-\mu x}$.

After adding function 3.12, function 3.11 is modified to

$$\phi(\ell_d) = \frac{S}{4\pi{\ell_d}^2} f e^{-\mu\ell_d} \qquad (3.13)$$

If assume that N debris are in a fuel canister, flux of a debris can be rewritten as

$$\phi_{ij} = \frac{\phi_{ij}^0}{4\pi\ell_i^2}\, f_{ij} e^{-\mu_j\ell_i} \qquad (3.14)$$

$i = 1, 2, 3, \cdots, N$ ($N$ : Total number of debris in a canister)

$j = 1, 2, 3, \cdots, n$ ($n$ : Total number of energy groups)

$\ell_i$ : Path length from a debris to a detector

For path which has $m$ of sections which are different medium or debris,

$$\mu_j\ell_i = \sum_k \mu_{jk}\ell_{ik}$$

$k = 1, 2, 3, \cdots, m$ ($m$ : Total number of sections in a path)

Flux at a detector has been calculated by sum $\phi_{ij}$ for all $i$ and $j$

$$\phi = \sum_{i}^{N}\sum_{j}^{n} \frac{\phi_{ij}^{0}}{4\pi\ell_i^2} f_{ij} e^{-\Sigma_j \ell_i} \tag{3.15}$$

$$\phi_{ij}^{0} = \frac{\rho V_i}{m_{tot}} S_j = \frac{\rho V_i}{m_{tot}} \left(\frac{4\pi r_i^3}{3}\right) = \frac{4\pi\rho r_i^3 S_j}{3m_{tot}}$$

$m_{tot}$ : $Total\ mass\ of\ debris\ in\ a\ canister$

$S_j$ : Number of radiation from debris in a canister for an energy bin $'j'$

$\rho$ : $Density\ of\ fuel\ debris$

$$\phi = \sum_{i}^{N}\sum_{j}^{n} \frac{1}{4\pi\ell_i^2} \frac{4\pi\rho r_i^3 S_j}{3m_{tot}} f_{ij} e^{-\Sigma_j \ell_i} = \frac{\rho}{3m_{tot}} \sum_{i}^{N}\sum_{j}^{n} \frac{r_i^3 S_j}{\ell_i^2} f_{ij} e^{-\Sigma_j \ell_i}$$

The flux at a detector is defined as below.

$$\phi = \frac{\rho}{3m_{tot}} \sum_{i}^{N}\sum_{j}^{n} f_{ij} \frac{r_i^3 S_j}{\ell_i^2} e^{-\Sigma_j \ell_i} \tag{3.16}$$

The Python code made for functions of this model is designed to use the multiprocessing method. The Python code does many calculations including the calculation of path length from sources to detectors, attenuation of radiation in materials for 101 energy groups. For the multiprocessing of this Python code, three options were considered. The first option is the use of the multiprocessing module of Python. The module is easy to use but it is not convenient to control CPU usage. Second option is serial processing of each task, and multiprocessing its subtask (Figure 3.33). The task is a calculation of flux for a canister, and the subtask is a calculation of the attenuated radiation from a debris to a detector. The second option divides the subtasks into the number of processing based on the capability of the CPU, and it saves time by multiprocessing these subtasks. This option is efficient when the code needs to compute a large matrix which takes a long time. However, the CPU can be overloaded by this method when the matrix calculation takes a short time because the CPU usage can repeatedly increase and decrease dramatically. This is similar to the possibility of damage to a vehicle if quick start and rapid braking are repeated. As an example, calculation of photon flux which takes 5 hours can be reduced to 1 hour by using the second option of multiprocessing. However, CPU usage repeats up and down for 1 hour while calculating dose rates for 17,000 canisters, and the CPU cooler starts to be damaged. As another option, tasks can be divided into the number of multiprocessing, and perform serial processing of subprocesses for each task (Figure 3.34). This method is similar to the method used for the multiprocessing of SCALE works. This method is more efficient than the first method which uses a multiprocessing module, because the CPU usage can be

optimized. This method takes similar time with the second method for the entire process, but this gives less stress to the CPU than the second method. Therefore, the third method has been used for the Python code for efficiency and stability.

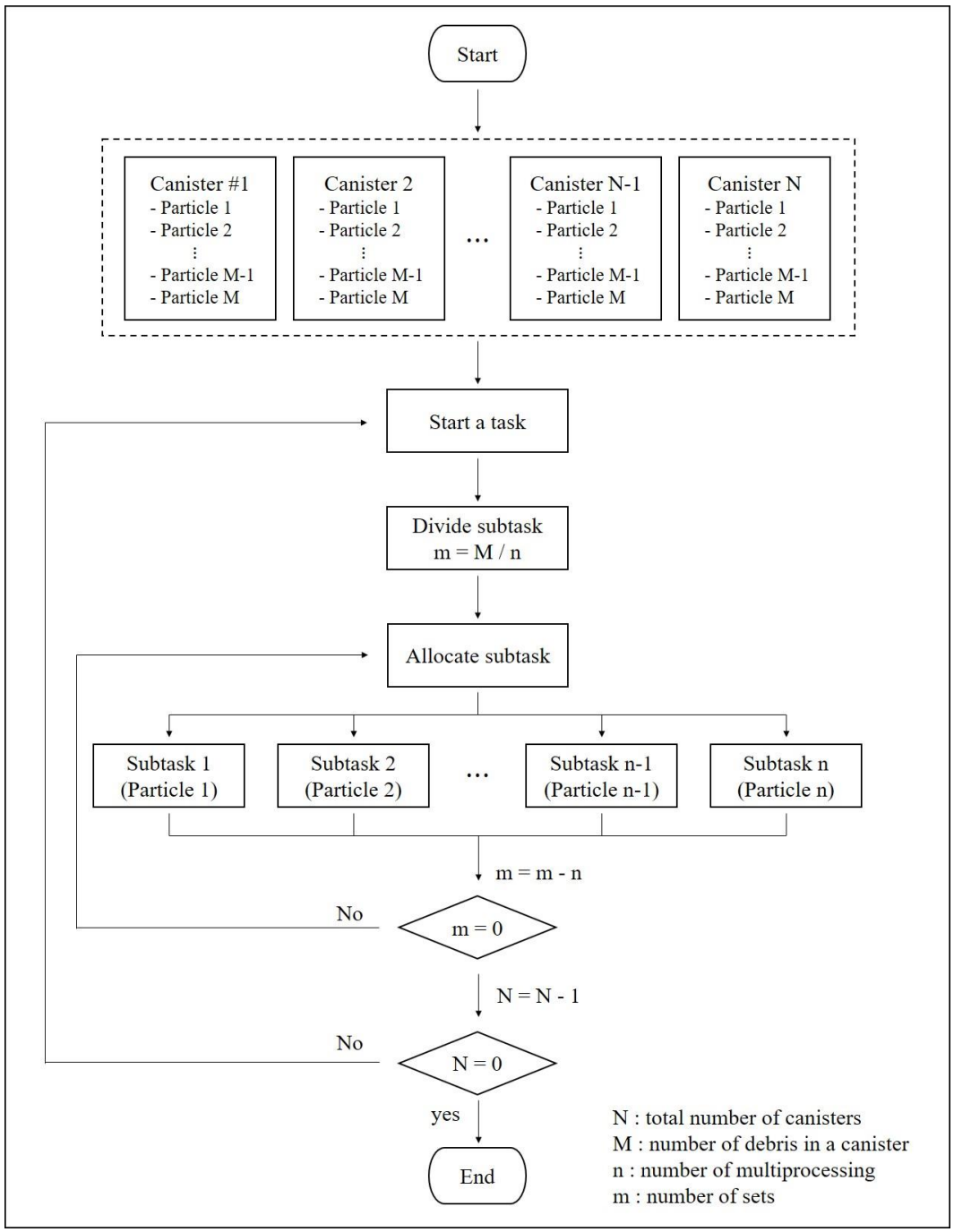


**Figure 3.33 Flowchart of multiprocessing for the option 2.**

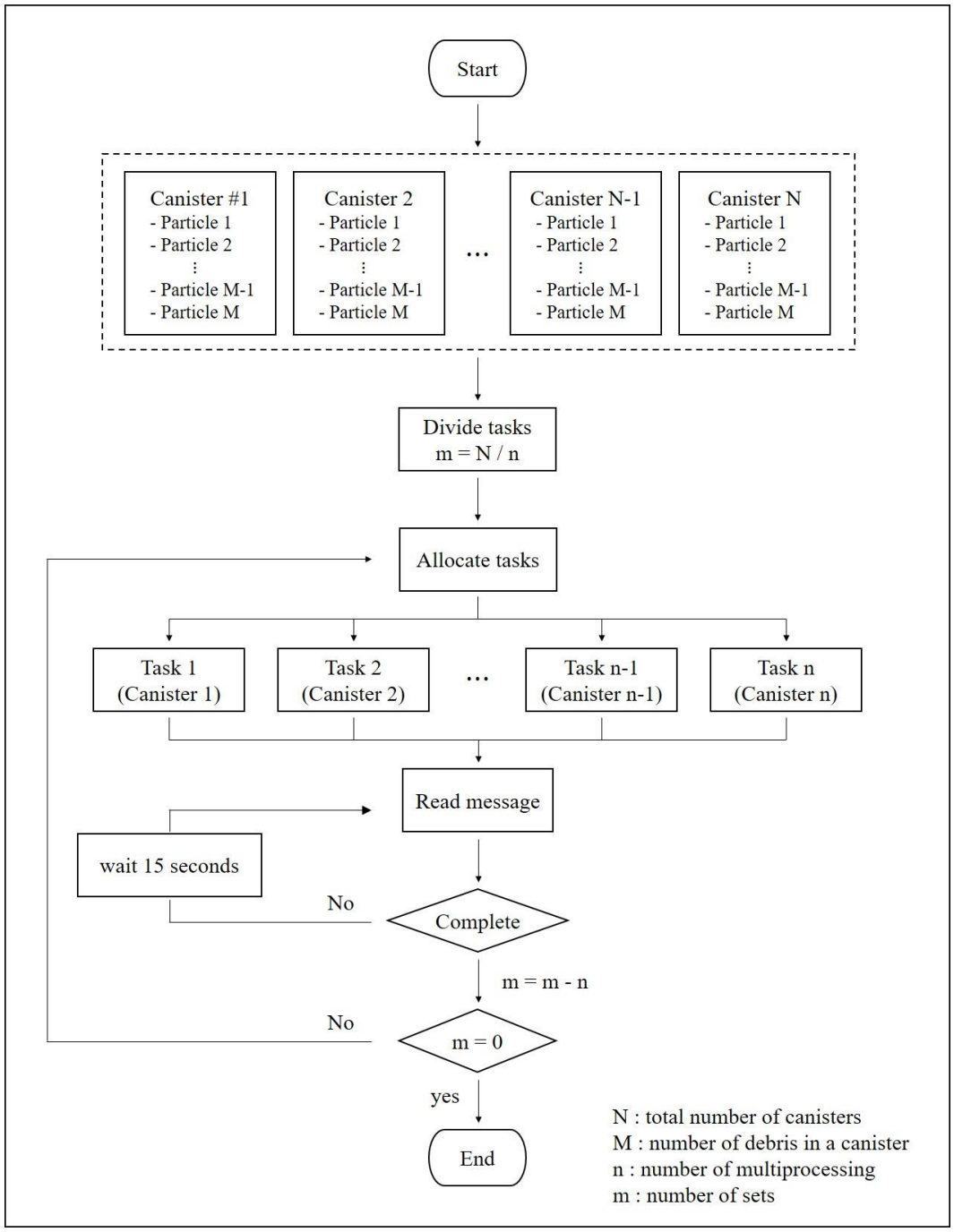


**Figure 3.34 Flowchart of the multiprocessing for the option 3.**

The photon flux from debris to a detector is calculated for the loose packed debris in a fuel canister. Diameters of debris are randomly sampled, and the same amounts of debris (230.9 kg) are filled in a canister for 1,000 times per sample group. Flux of these canisters are calculated for 1,000 times (1,7000 times total) and then the average flux is estimated. According to the result of the analytical calculation, the intensity of photon flux increases

by increases in the size of debris when the minimum radius of the debris sphere is less than 2 cm. However, this increase is the error which is made by approximations assumed for this model. For debris with the minimum radius larger than 2 cm, the intensity of flux decreases by increases in the size of debris. This result is compared with the calculation of SCALE in Figure 3.35. For debris with the minimum radius smaller than 2 cm, differences of the average photon flux between the simplified model and the estimation of SCALE are larger than $5 \times 10^7$ photons/cm$^2$sec which is 45 % of the estimation of SCALE. The difference between two models decreases by increases in the minimum radius of debris.

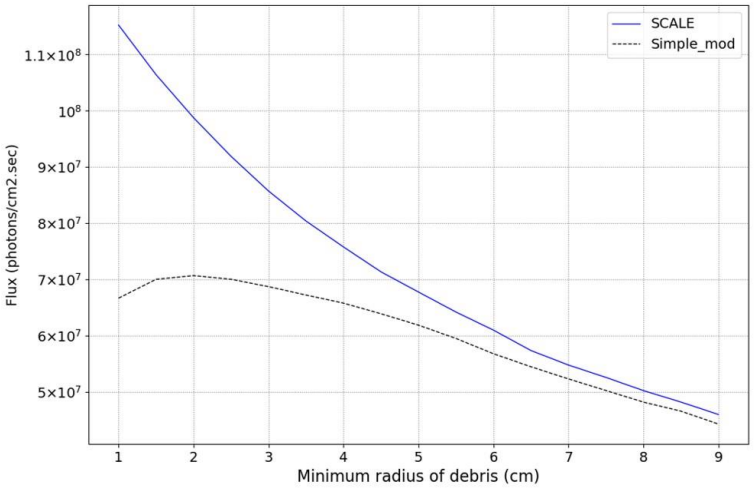


**Figure 3.35 Comparison of the photon flux from fuel debris in a canister** between the result from the simplified model (dashed dark line) and the result from SCALE (blue line).

### 3.3.3. Modified model on the radiation attenuation in small debris

A model developed by Shmakov is referenced to reduce error of the simplified model [22]. The model of Shmakov describes the neutron transmission through a mixture of particles and matrix material. Shmakov divided a matrix containing particles of equal size and shape into multiple layers. The particle distribution in a layer is assumed to be independent from the distribution in other layers, and the thickness of a layer is assumed small enough. The thickness of a layer L is assumed to be the same as the diameter of a particle. Shmakov derived the effective macroscopic cross section of a mixed material based on these assumptions, and the effective macroscopic cross section is defined as

$$\bar{\Sigma} = \Sigma_m - \frac{1}{L} ln \left[ 1 - q + q \int exp(-\Delta\Sigma t) p(t) dt \right] \qquad (3.17)$$

$\Sigma_m$ is the total macroscopic cross section of the matrix material and $L$ is the thickness of a layer. $p(t)$ is the probability density function of the chord length. $\Delta\Sigma$ is defined as $\Delta\Sigma = \Sigma_a - \Sigma_m$. $\Sigma_a$ is the macroscopic cross section of a particle. $q$ is the probability of interaction of the incident flux with a particle in the layer L.

$$q = \frac{\alpha L S_0}{V_0} = \frac{\alpha L}{\bar{t}} \tag{3.18}$$

$\alpha$ is the volume fraction of particles and $S_0$ is the projection area of a particle on a plane. $V_0$ is the volume of a particle. $\bar{t}$ is a mean chord or mean length of interception of the radiation in a particle.

In case of the cubic particle of edge $h$ which is $h = L$, $\bar{\Sigma}$ is defined as

$$\bar{\Sigma} = \Sigma_m - \frac{1}{h} ln[1 - \alpha + \alpha\, exp(-h\Delta\Sigma)]$$

In case of the spherical particle of diameter $D$ which is $D = L$, $\bar{\Sigma}$ is defined as

$$\bar{\Sigma} = \Sigma_m - \frac{1}{D} ln\left[1 - \frac{3\alpha}{2}\left(1 - J(-D\Delta\Sigma)\right)\right] \tag{3.19}$$

where $$J(-D\Delta\Sigma) = \frac{2}{(D\Delta\Sigma)^2}[1 - (1 + D\Delta\Sigma)exp(-D\Delta\Sigma)]$$

Photon flux of fuel debris is estimated by applying the effective macroscopic cross section defined as the function 3.19, and its result is compared with the estimated photon flux by SCALE (Figure 3.36). The estimated photon flux by the Shmakov model does not match with the estimated flux by SCALE for the minimum radius smaller than 4 cm. However, estimation by the Shmakov model is better than the estimation by the simple model for the radius larger than 4 cm. The Shmakov model is also better in the estimation of uncertainty than the simple model. The estimated standard deviation by the Shmakov model is compared with the estimations of other models in Figure 3.37. The coefficient of variation is also compared with results from other methods in Figure 3.37.

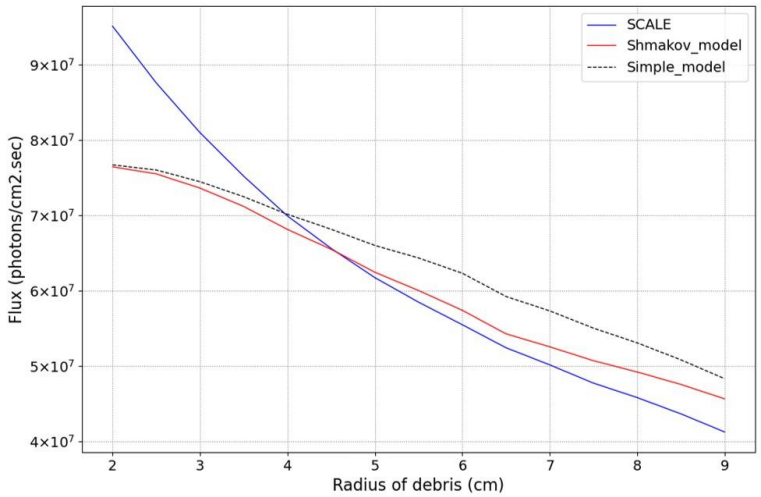


**Figure 3.36 Comparison of the photon flux.** The blue line is the estimated average photon flux by SCALE, and the dashed dark like is the estimation by the simple model. The red line is the estimation by the Shmakov model.

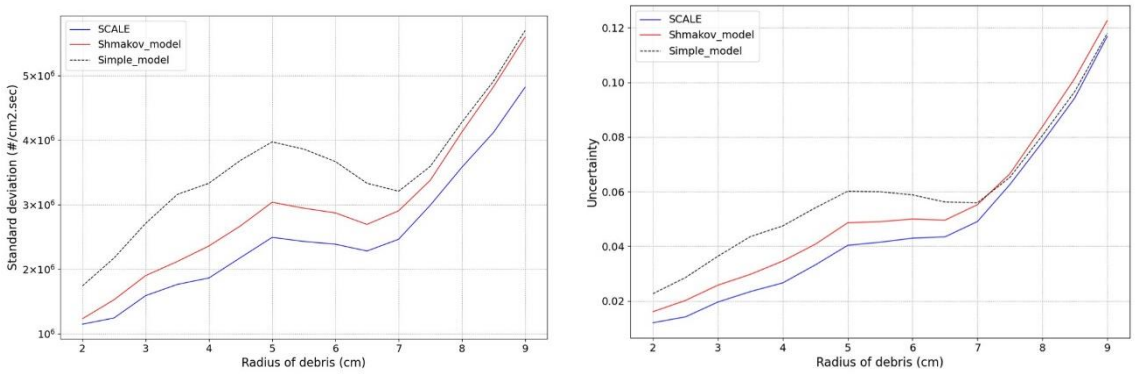


**Figure 3.37 Comparison of the standard deviation (left) and the coefficient of variation (right).** The coefficient of variation is calculated by dividing the standard of deviation by the average photon flux. The coefficient of variation is visualized in ratio instead of the percentage in this graph.

Shamakov's model has assumed that the size of a particle is the same as the thickness of a layer L, and the size of the particle is the same for all particles. This resulted in discordance between the model and measurement, and T. Yamamoto supplemented the Shmakov's model to be used for a medium which contains several particles in different sizes [23].

The thickness of layer L can be larger than the radius of a particle ($L \geq max(D_k)$). Yamamoto et al derived the effective macroscopic cross section as

$$\bar{\Sigma} = \Sigma_m - \frac{1}{L} ln \left[ 1 - \sum_k q_k + \sum_k q_k J(-\Delta\Sigma_k,\ D_k) \right] \tag{3.20}$$

where $$q_k = \frac{3\alpha_k L}{2(D_k)}, \quad \Delta\Sigma_k = \Sigma_{a,k} - \Sigma_m$$

$J(-\Delta\Sigma_k,\ D_k)$ can be calculated by using $J(x, y)$ which is defined as

$$J(x,y) = \frac{2}{y^2}\left[\frac{1}{x^2} + \left(\frac{y}{x} - \frac{1}{x^2}\right) \exp(xy)\right] \tag{3.21}$$

For the use of the Shmakov model and the modified model of Yamamoto, diameter of fuel debris is classified into 11 groups and it has been applied to the modified Shmakov model.

$$D_k = \{ D_1,\ D_2,\ D_3, \cdots,\ D_{11} \}$$

Total attenuation coefficient of debris which is same with total macroscopic cross section is defined as

$$\Delta\Sigma_k = \Sigma_{a,k} - \Sigma_m$$

$\Sigma_a$ : Total macroscopic cross section of the debris

$\Sigma_m$ : Total macroscopic cross section of the matrix material

The effective attenuation coefficient of the modified model of Yamamoto et al is

$$\bar{\Sigma} = \Sigma_m - \frac{1}{L} ln \left[ 1 - \sum_k q_k + \sum_k q_k J(-\Delta\Sigma_k,\ D_k) \right] \tag{3.22}$$

where $$J(-\Delta\Sigma_k,\ D_k) = \frac{2}{D_k^2}\left[ \frac{1}{(\Delta\Sigma_k)^2} - \left( \frac{D_k}{\Delta\Sigma_k} + \frac{1}{(\Delta\Sigma_k)^2} \right) e^{-\Delta\Sigma_k D_k} \right] \tag{3.23}$$

and $$q_k = \frac{3\alpha_k L}{2\ D_k} \tag{3.24}$$

After the effective attenuation coefficient has been calculated by using the modified model, flux was calculated for all energy range. Flux of a point source is defined for a group as

$$\phi_{ij} = \frac{\phi_{ij}^0}{4\pi \ell_i^2}\ e^{-\Sigma_j \ell_i} \tag{3.25}$$

$i = 1, 2, 3, \cdots, N$ ($N$ : Total number of debris in a canister)

$j = 1, 2, 3, \cdots, n$ ($n$ : Total number of energy groups in PDF)

$\ell_i$ : $Path\ length\ from\ a\ debris\ to\ a\ detector$

Flux at a detector has been calculated by sum $\phi_{ij}$ for all $i$ and $j$

$$\phi = \sum_i^N \sum_j^n \frac{\phi_{ij}^0}{4\pi \ell_i^2} e^{-\Sigma_j \ell_i} \tag{3.26}$$

$$\phi_{ij}^0 = \frac{\rho V_i}{m_{tot}} S_j = \frac{\rho V_i}{m_{tot}} \left( \frac{4\pi r_i^3}{3} \right) = \frac{4\pi \rho r_i^3 S_j}{3 m_{tot}}$$

$m_{tot}$ : Total mass of debris in a canister

$S_j$ : Number of radiation from debris in a canister for an energy bin $'j'$

$\rho$ : Density of fuel debris

$$\phi = \sum_i^N \sum_j^n \frac{1}{4\pi \ell_i^2} \frac{4\pi \rho r_i^3 S_j}{3 m_{tot}} e^{-\Sigma_j \ell_i} = \frac{\rho}{3 m_{tot}} \sum_i^N \sum_j^n \frac{r_i^3 S_j}{\ell_i^2} e^{-\Sigma_j \ell_i}$$

Adding self-attenuation coefficient

$$f_{ij} = \frac{3}{r_i^3 \Sigma_j^3} \left[ r_i^2 \Sigma_j^2 - 2 r_i \Sigma_j + 2 - 2 e^{-\Sigma_j r_i} \right] \tag{3.27}$$

$$\phi = \frac{\rho}{3 m_{tot}} \sum_i^N \sum_j^n f_{ij} \frac{r_i^3 S_j}{\ell_i^2} e^{-\Sigma_j \ell_i} \tag{3.28}$$

Photon flux of the loose packed fuel debris in random size is calculated by using functions of the modified model, and it is compared with data from SCALE (Figure 3.38). The estimated photon flux by the modified model is not well matched with the results from SCALE for small debris likewise other models. However, estimation of the modified model is better than others, and it is the most similar with the estimation of SCALE. The difference between the estimated average photon flux by SCALE and by the simple model is larger than 40% of the flux of SCALE for small debris. The Shmakov model also does not properly estimate the average photon flux because it is designed to be used for particles of the same size. On the other hand, the difference between the estimated average photon flux by SCALE and by the modified Shmakov model is smaller than 15 % for small debris. The standard deviation estimated by the modified model is similar with the estimation of SCALE (Figure 3.39). The coefficient of variation is compared in Figure 3.39. The estimation by the modified model matches well with the estimation of SCALE, and its results are better than other models.

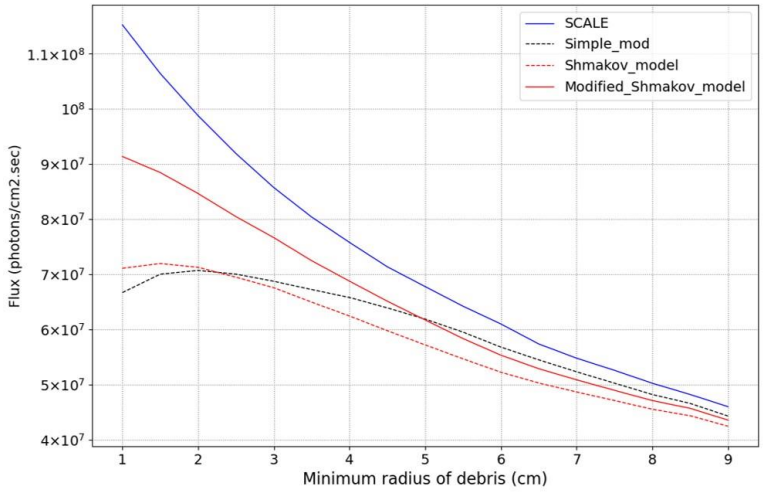


**Figure 3.38 Comparison of the photon flux for fuel debris of random size.**

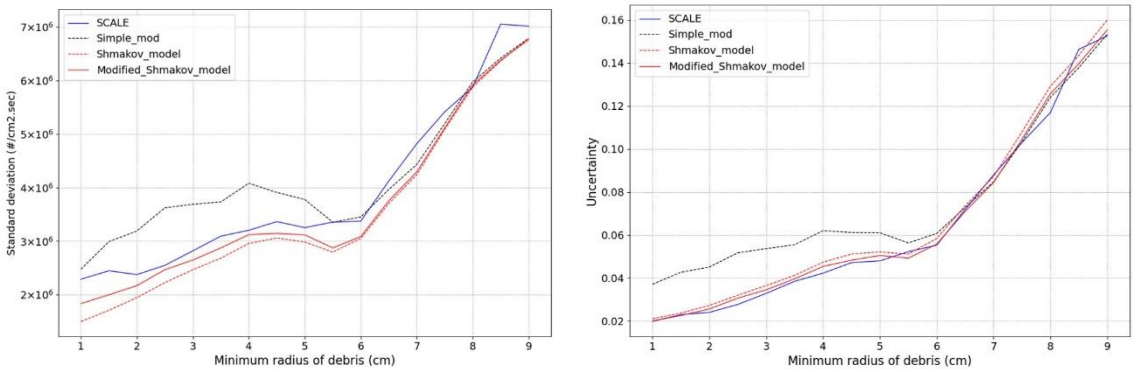


**Figure 3.39 Comparison of the standard deviation (left) and the coefficient of variation (right).** The coefficient of variation is visualized in ratio instead of the percentage in this graph.

### 3.4 Summary and discussion

The model in the previous chapter has been updated and the uncertainty of radiation dose rate was evaluated by using the updated model in this chapter. The model did the random sampling to simulate the uncertain condition of fuel debris, and it estimates the radiation dose rate of the randomly distributed fuel debris in a canister. Photon and neutron dose rate of fuel debris depends on size and distribution of the fuel debris in a canister, and their uncertainty also varies by changes in these two factors. Photon and neutron dose rates vary by changes in size of the fuel debris, and the photon dose rate is more sensitive in the change than the neutron dose rate. Both dose rates are more sensitive in the size of fuel debris when the fuel debris are loosely arranged than when they are closely packed in a canister. Uncertainty of the radiation dose rate is estimated as the coefficient of variation which is calculated by dividing the standard deviation by the average dose rate. The uncertainty also depends on the size of fuel debris like the radiation dose rate does, and the uncertainty of photon dose rate is more sensitive in the change of size than the uncertainty of neutron dose rate. In most cases, the maximum uncertainty is less than 35 % of the average dose rate, and the uncertainty of debris smaller than 1 cm is ignorable. However, the range of data is much larger than this, and single estimation of dose rate can be very different from the average value.

The estimated data by the model is not linear and it is not easy to be fitted to simple functions. Therefore, an idea which transforms the original data to a cumulative form is proposed for the data fitting. The estimated average dose rate and its standard deviation have been transformed to cumulative values by functions 3.1 ~ 3.4. The transformed data on the average photon dose rate has been well fitted to the exponential functions 3.6 and 3.7. The transformed standard deviation also fitted to functions 3.8 and 3.9. On the other hand, data of the neutron dose rate and its standard deviation are more irregularly varied by changes in size of the fuel debris, and it is difficult to be fitted to a simple function even after the transformation.

The estimation of dose rate and its standard deviation for large sample groups takes a long time when SCALE code is used. Therefore, several methods are proposed which use Python code for the multiprocessing of the random sampling and the calculation of dose rate. However, performance improvement by these methods is limited, and it still takes a long time. Therefore, a model is proposed based on theories on the attenuation of nuclear radiation in a medium with particles. Photon and neutron radiation generated in a fuel debris can be attenuated while escaping from the debris itself by the self-attenuation effect. The radiation also can be attenuated while transmitting through other fuel debris by the particle self-shielding effect. The proposed model was developed based on these two with some assumptions. The model assumed that all radiation comes from at the center of each fuel debris, and the radiation at the surface of each debris is calculated based on the theories on the self-attenuation. The scattering of radiation is ignored, and the attenuation of radiation has been calculated by the Lambart-Beer law. This simplified model was not well matched with the data from SCALE especially when the size of fuel debris is small. Therefore, the model is updated by considering the particle self-shielding effect by fuel debris. Models of Shamkov and Yamamoto on the effective attenuation coefficient are referenced for the update of the model with some modifications. The model is updated by modifying the attenuation coefficient of the medium with fuel debris, and the photon flux

is calculated for the comparison with SCALE. Estimates by the updated model are better than estimations by the simple model. However, the model did not properly estimate the photon flux and its uncertainty for small debris. This error is made because the Shmakov model assumes the size of fuel debris to be the same. The effective attenuation coefficient is modified by the model of Yamamoto. Yamamoto expanded the Shamakov model on the effective attenuation coefficient to the media containing several particles with different sizes. In the case of the model developed in this dissertation, size of the fuel debris is not the same for all debris because they were randomly sampled. Therefore, the radius of fuel debris in each sample group has been grouped to 11 groups, and then the method of Yamamoto is used for the calculation of the effective attenuation coefficient for each group. The updated model better estimated the photon flux and its uncertainty than other models, and it provided estimations similar with SCALE. There are still discrepancies between data from the updated model and data from SCALE because the model does not perform the random walk of particles. Errors of the updated model can be reduced by applying more detailed theories on the radiation transport. However, it has not been considered at this time because the purpose of this simplified model is to save time for the evaluation. Although estimations of this simplified model are not the same as data from SCALE, this model is still worth using in that it can provide brief estimation in a short time.

The radiation flux and dose rate of fuel debris depend on the size and distribution of fuel debris in a canister, and this can be explained by Equation 3.27 and 3.28.

$$\phi = \frac{\rho}{3m_{tot}} \sum_{i}^{N} \sum_{j}^{n} f_{ij} \frac{r_i^3 S_j}{\ell_i^2} e^{-\Sigma_j \ell_i} \tag{3.28}$$

$$f_{ij} = \frac{3}{r_i^3 \Sigma_j^3} \left[ r_i^2 \Sigma_j^2 - 2 r_i \Sigma_j + 2 - 2 e^{-\Sigma_j r_i} \right] \tag{3.27}$$

$i = 1, 2, 3, \cdots, N$ ($N$ : Total number of debris in a canister)

$j = 1, 2, 3, \cdots, n$ ($n$ : Total number of energy groups in PDF)

The flux decreases by increases in the size of fuel debris, and this is due to changes in three factors including the self-attenuation coefficient, the effective attenuation coefficient, the distribution of fuel debris. The self-attenuation coefficient $f_i$ in Equation 3.27 inversely proportional to the radius of fuel debris $r_i$, and it decreases by increasing in the radius. Therefore, larger debris has smaller $f_i$, and the flux of larger debris is smaller. The self-attenuation of radiation is the attenuation of the radiation in a debris which is the radiation is generated. On the other hand, changes in the effective attenuation coefficient by the particle self-shielding is the attenuation of the radiation by other debris which are not the debris the radiation is generated. The attenuation coefficient or the macroscopic cross section of radiation in the medium with particles is calculated by applying the equation of Shmakov and Yamamoto, and it is calculated as the effective attenuation coefficient by Equation 3.22 ~ 3.24.

$$\bar{\Sigma} = \Sigma_m - \frac{1}{L} ln \left[ 1 - \sum_{k} q_i + \sum_{k} q_i J(-\Delta\Sigma_k,\ D_k) \right] \tag{3.22}$$

where $$J(-\Delta\Sigma_k,\ D_k) = \frac{2}{D_k^2}\left[\frac{1}{(\Delta\Sigma_k)^2} - \left(\frac{D_k}{\Delta\Sigma_k} + \frac{1}{(\Delta\Sigma_k)^2}\right) e^{-\Delta\Sigma_k D_k}\right] \quad (3.23)$$

and $$q_k = \frac{3\alpha_k L}{2\ D_k} \quad (3.24)$$

All debris has different diameter $D_k$, and this cannot be used for these equations. Therefore, the diameter $D_k$ is lumped into 11 groups.

$$D_k = \{ D_1,\ D_2,\ D_3, \cdots,\ D_{11}\}$$

The size of fuel debris affects to Equation 3.22 by changes in the diameter $D_k$, and the effective attenuation coefficient decreases by increases in the size of fuel debris. Therefore, radiation is less attenuated while transmitting through fuel debris in large size. Moreover, changes in the size of fuel debris changes the distribution of fuel debris, and distribution of fuel debris affects the effective attenuation coefficient. $\alpha_k$ is the volume fraction of the debris with $D_k$, and the effective attenuation coefficient with larger $\alpha_k$ is larger. In other words, distribution of fuel debris with larger $\alpha_k$ is more dense, and more radiation can be attenuated by the dense debris. Size of fuel debris affects the distribution of fuel debris when the debris is contained in a canister. The inner space of the canister constraints the available packing structures, and the distribution of fuel debris changes by changes in the size of debris. The volume fraction of fuel debris is not uniform when the fuel debris is randomly packed in a canister, and it can be different depending on the location inside the canister. Therefore, changes in the size of fuel debris changes $\alpha_k$ and the effective attenuation coefficient. Thus, if the effective attenuation coefficient is considered without considering other factors, the flux can be proportional to the radius of debris. Changes in the distribution of fuel debris changes the path length $\ell_i$ from debris to a detector, and the flux from debris decreases by increases in the path length. The height of a debris pile depends on the size of debris, and differences in the height affects the path length. Therefore, changes in the size of debris changes the height of the debris pile and the path length, and it changes the flux from fuel debris.

A model using SCALE for the calculation of dose rate has been developed at this chapter and the uncertainty of dose rate was estimated by using the model. Some exponential functions and coefficients on the dose rate and its standard deviation is derived based on the estimated data. Method which can save time for the estimation has been proposed, and a model with a simplified function was developed. Although these methods and models have some errors for small debris, they can enhance the efficiencies in the evaluation of uncertainty.

# Chapter 4. Application of Methodology

## 4.1 Introductions

The model developed in Chapter 3 simulated the uncertain condition of fuel debris by random sampling on the size and the distribution of fuel debris in a canister, and SCALE was used for the estimation of photon and neutron dose rate. After the evaluation of dose rate by using the model, a function and a model were developed based on theoretical models of the self-attenuation and the effective attenuation coefficient. This chapter focuses on the application of the model for the evaluation of nuclear radiation and its uncertainty.

The radiation dose rate and its uncertainty were estimated for a point detector in the previous chapter, and vertical location of the detector was assumed at the center of a canister or the pile of debris. However, estimated dose rate and its uncertainty depends on the vertical location of the detector, and their variability by changes in the location need to be estimated for reliable estimation. The variability of photon and neutron dose rate by changes in height of a detector is evaluated by using the model developed in Chapter 3. SCALE has been used for the estimation of dose rate, and the region tally was applied for vertically allocated meshes for the calculation. Results from the model are visualized as density plots and line plots for the evaluation. The uncertainty is evaluated by analyzing the output data from SCALE, and its sensitivity by changes in the height of the detector is evaluated as the density map on the sensitivity index. After the evaluation of dose rate by SCALE, the photon flux and its uncertainty are evaluated by using three analytical methods. These are evaluated to verify the reliability of the modified Shamkov model. Results from three models were compared with the estimation of SCALE. After verifying the reliability of the modified Shmakov model, the variability of the photon flux by changes in the horizontal location of the detector is evaluated by using the model.

Even if the uncertainty of the estimated data less affects the evaluation of shielding performance, it is important when the data is used for the characterization of fuel debris. The coefficient of variation of dose rate can be larger than 30 % depending on the condition of fuel debris, and data with large deviation is less reliable to be used for the characterization. Therefore, methods to reduce the uncertainty need to be developed. As examples of the method to reduce uncertainty, two modified designs of canisters are evaluated in this chapter. A design has small containers in a canister, and fuel debris are put into the small containers first, then small containers are put into the fuel canister. Another design has partitions which horizontally divide the inner space of a canister, and fuel debris are put into each space almost in a row. TEPCO plans to use the design with small containers, and the design with inner partition is also under development by US engineers.

Fuel canisters need to be moved to a storage facility after the retrieval of fuel debris, and casks are used for the temporary shielding and transportation of canisters. Nuclear radiation from fuel debris in a canister attenuates after transmitting through shielding materials of a cask, and nuclear radiation from a cask has uncertainty which is not same with that of a canister. Therefore, photon flux and uncertainty are estimated for a fuel canister in a temporary shielding cask and fuel canisters in a transport cask.

## 4.2. Uncertainty of dose rate by the vertical location of detector

### 4.2.1. Evaluation of the photon dose rate by SCALE

The point detector is replaced with vertically arranged regions, and radiation dose rate and its uncertainty are evaluated by region tally. Size and distribution of fuel debris in a canister are sampled based on the model of Chapter 3, and SCALE is used for the estimation of dose rate. A cylindrical region surrounding a canister is assumed for the estimation, and the region is vertically divided into 25 regions (Figure 4.1). Height of each small region is 20 cm, and the total height of 25 regions is 500 cm. The inner surface of the cylinder is 1 m from the surface of the canister, and its thickness is 10 cm.

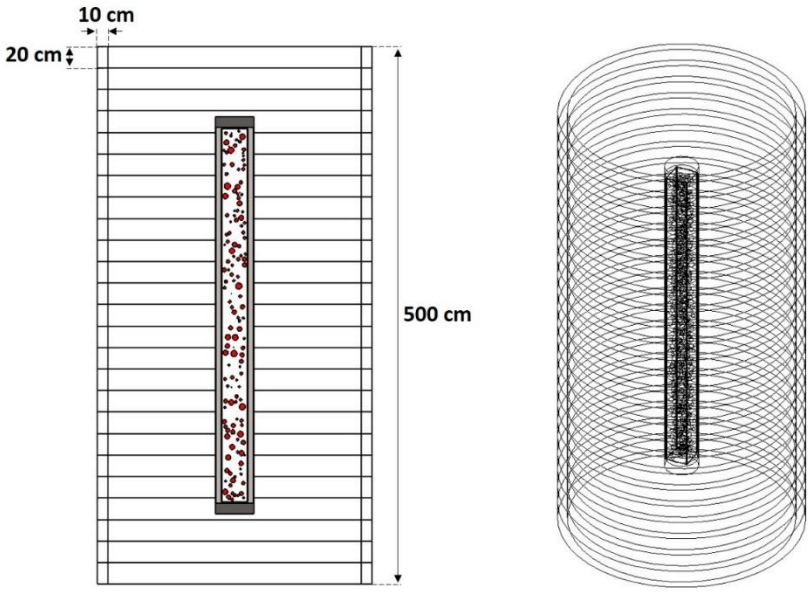


**Figure 4.1 Side view and diagonal view of regions for the estimation of dose rate.**

Photon dose rates are calculated for 25 regions by SCALE, and estimated results are visualized as the density plot. The line plot is also used to visualize details on the estimated values. Figure 4.2 visualizes the estimated photon dose rate for the loose packed fuel debris in a canister. The region at the center is designated to 0 at the Z-axis of the density plot, and regions at the top and bottom are designated to 240 and -240 each. X-axis of the density plot is the minimum radius of debris at each sample group. According to the density plot in Figure 4.2, the photon dose rate decreases as the vertical location of the detector moves away from the center (z = 0) of a canister, and the local maximum of each sample group decreases by increases in the minimum radius. Local maximums of the photon dose rate are at the vertical center of a canister, and the global maximum is at the minimum radius of 1 cm ($r_{min} = 1$ cm). Total path length from fuel debris to a region for the estimation is shortest when the region is at the vertical center of a canister (z = 0), and each sample group has the maximum dose rate at z=0 since the radiation is less attenuated.

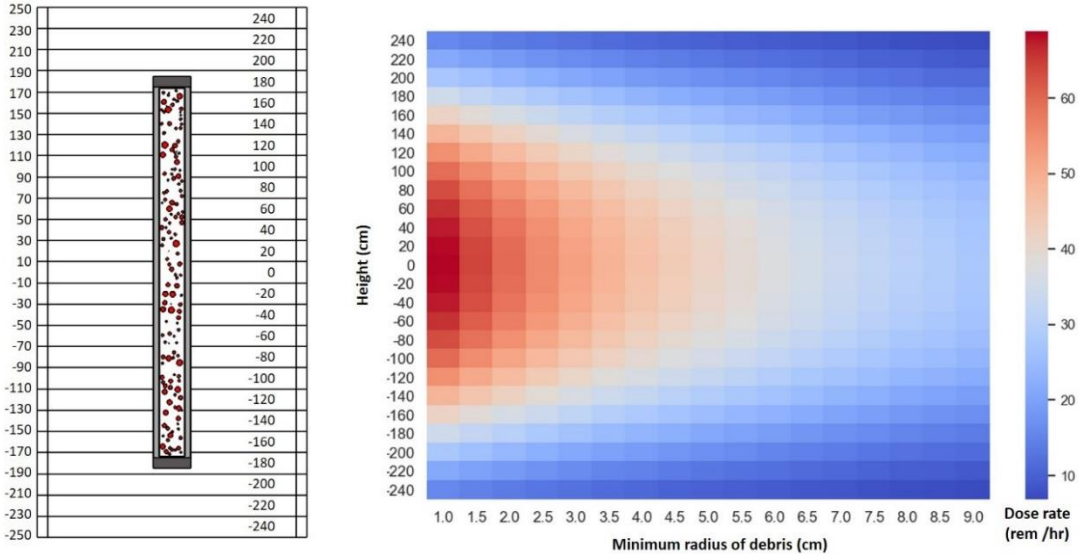


**Figure 4.2 Density plot of the average photon dose rate for the loose packed fuel debris in a canister**

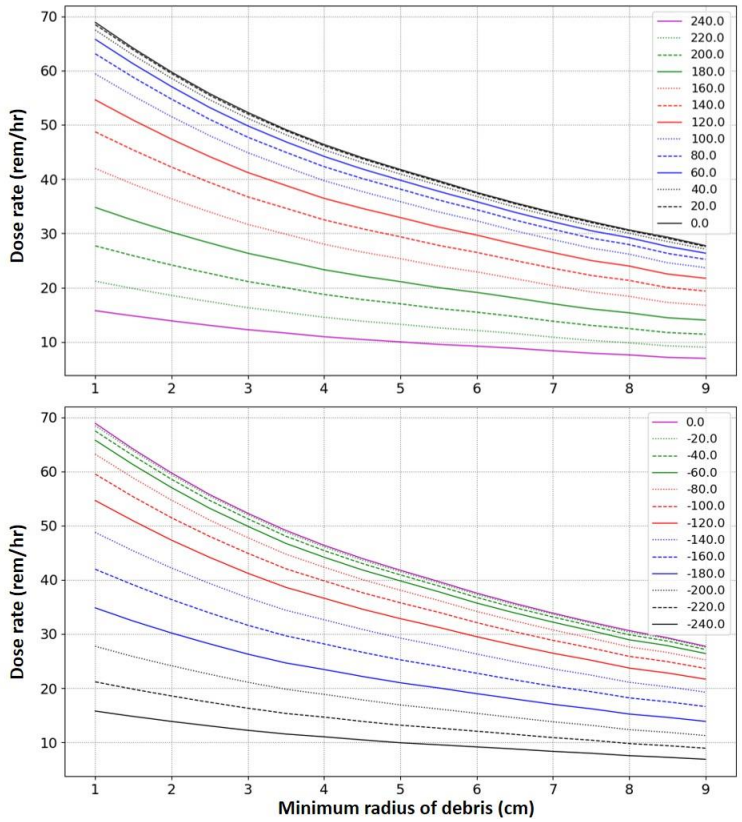


**Figure 4.3 Line plots of the average photon dose rate for the loose packed fuel debris in a canister**

Details of the estimated dose rate is visualized by line plots in Figure 4.3. The photon dose rate at the vertical center (z = 0) is 68.9 rem/hr (689 mSv/hr) for the minimum radius of 1 cm ($r_{min} = 1$ cm), and it decrease to 27.7 rem/hr (277 mSv/hr) for $r_{min}$ = 9 cm which is 59.8 % of the dose rate at $r_{min}$ = 1 cm. On the other hand, the photon dose rate at the top (z = 240 cm) or the bottom (z = -240 cm) is 15.7 rem/hr (157 mSv/hr) for $r_{min}$ = 1 cm whereas it is 7 rem/hr (70 mSv/hr) for $r_{min}$ = 9 cm which is around 55.4 % of the dose rate at $r_{min}$ = 1 cm. Even if there are some differences in the relative changes of dose rate between z = 0 and z = 240 cm (or -240 cm), it is not a lot when $r_{min}$ = 9 cm. This can be explained with Equation 3.28. Even if the location far from the vertical center of a canister has longer path length $\ell_i$, the photon flux less affected by changes in the path length $\ell_i$ when the radius of debris $r_i$ is large. The sensitivity of photon dose rate by changes in the minimum radius is visualized in Figure 4.4. The photon dose rate is more sensitive by changes in the radius if the radius is larger. For small debris, the sensitivity is similar by changes in the vertical location of detectors. On the other hand, large debris has different sensitivity by the vertical location of the detector.

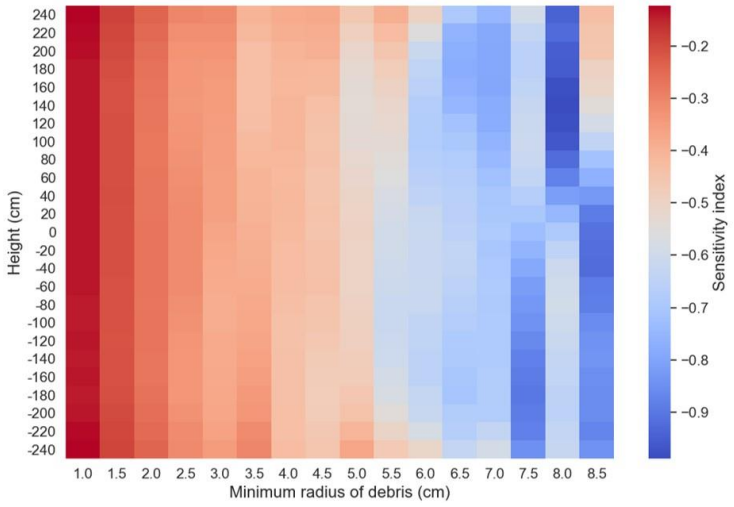


**Figure 4.4 Density plot on the sensitivity of the photon dose rate by changes in the minimum radius of debris.**

The coefficient of variation (CV) is calculated for the photon dose rate of the loose packed fuel debris, and it is visualized in Figure 4.5. CV increases by increases in the minimum radius of debris, and CV is negligible for small debris. There are almost no changes by change in the vertical location of the detector when the size of debris is small. On the other hand, CV is sensitive to changes in the vertical location when the size of debris is large. The maximum CV is 29.3 % of the average dose rate, and the density plot has two global maximums at the top (z = 240 cm) and the bottom (z = -240 cm) with $r_{min}$ = 9 cm. Details of CV are visualized by line plots in Figure 4.6. The percent relative range (PRR) is much larger than CV, and its global maximum is larger than 160 % of the average dose rate. These mean that even though the standard deviation of dose rate is smaller than 30 % of the average dose rate, a measurement can be very different from the average dose rate depending on the location of the detector. The density plot of PRR is in Appendix D.

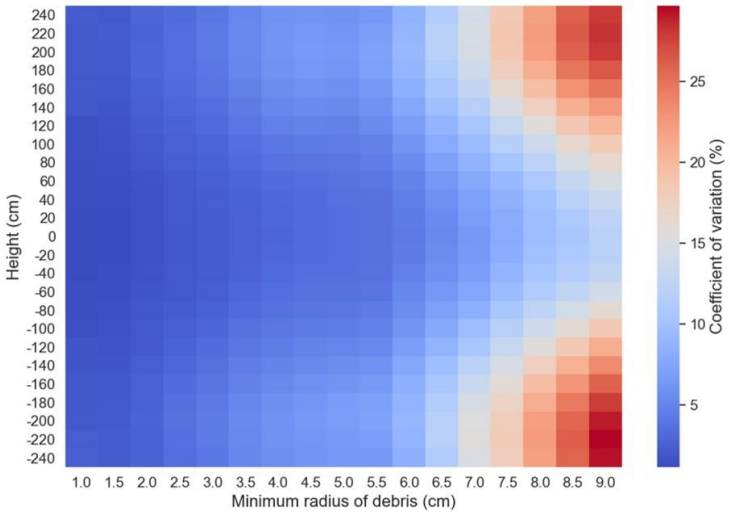


**Figure 4.5 Density plot of the coefficient of variation of the photon dose rate of the loose packed fuel debris in a canister**

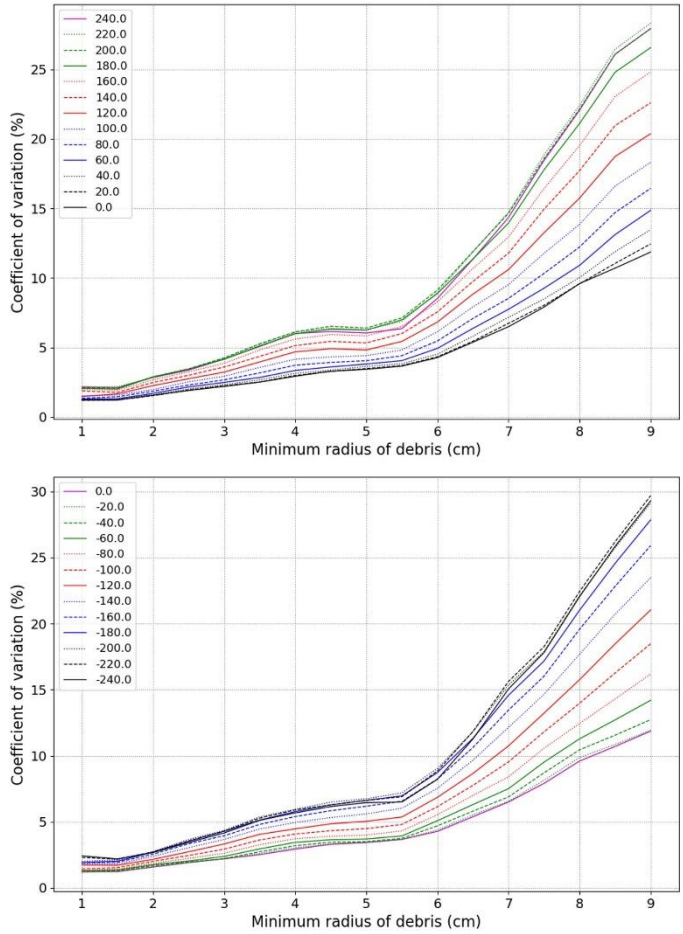


**Figure 4.6 Line plots of the coefficient of variation of the photon dose rate of the loose packed fuel debris in a canister**

In case of the close packed fuel debris in a canister, local maximums of the dose rate are not at the vertical center (z = 0) of a canister, and they are biased to the bottom (Figure 4.7). Fuel debris has not fully filled a canister and piled from the bottom to upward, and this made the average dose rate to be biased. The global maximum is -100 cm from the vertical center of a canister with $r_{min}$ = 1 cm, but vertical locations of local maximums are different depending on $r_{min}$. The vertical location of local maximums increases by changes in $r_{min}$ for $r_{min}$ smaller than 6 cm, and it decreases by the increase of $r_{min}$ for $r_{min}$ larger than 6 cm. This is because the height of the debris pile depends on the radius of debris, and each sample group has a different height of the debris pile (Figure 4.8). Fuel debris has its maximum dose rate at the vertical center of the pile of debris when it is measured at 100 cm from the surface of the canister. In case of the close packed fuel debris, the vertical center of the pile of debris is different depending on the size of fuel debris in each sample group. Therefore, the location of maximums in the density plot is different depending on the size of the fuel debris.

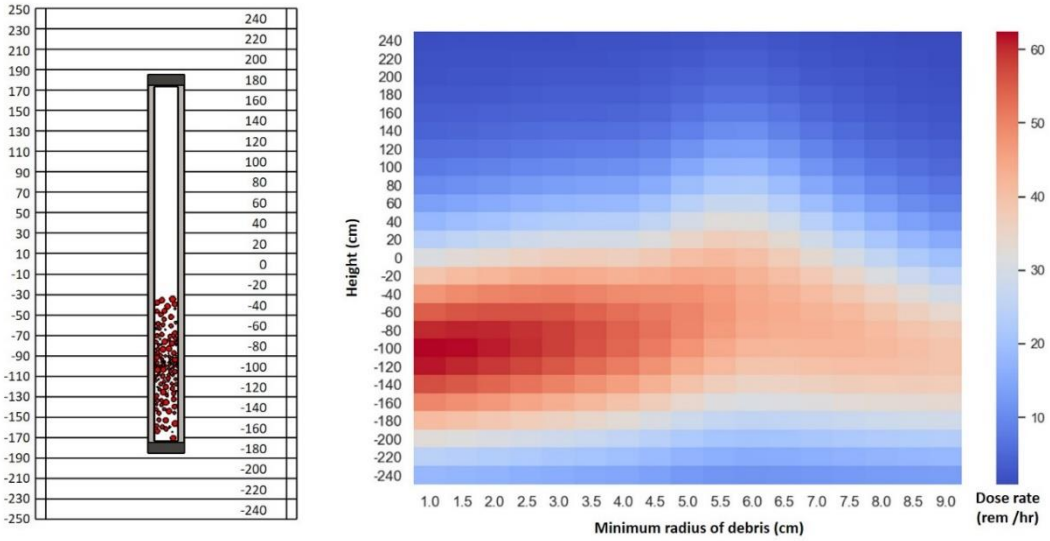


**Figure 4.7 Density plot of the average photon dose rate for the close packed fuel debris in a canister**

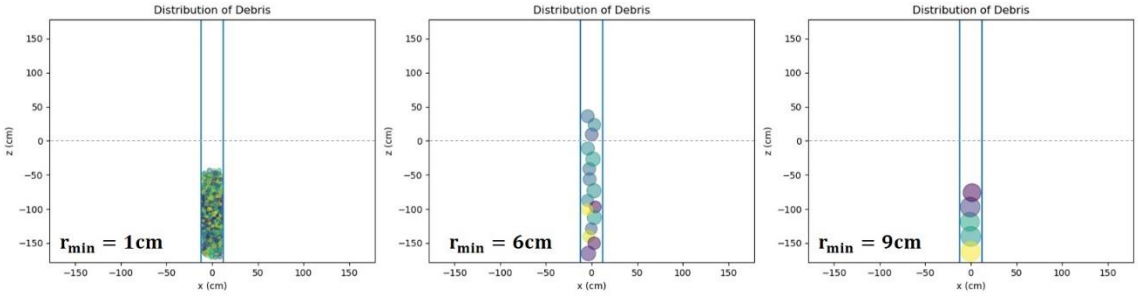


**Figure 4.8. Side view of the close packed fuel debris in a canister.** Colors are the location of fuel debris in y-direction.

Details of the estimated dose rate is visualized by line plots in Figure 4.9. The average photon dose rate has a maximum at $r_{min}$ = 5.5 cm or 6 cm when the height of the detector is higher than -40 cm (z = -40 cm), and it has a minimum like a saddle point when the height is lower than -40 cm. Overall dose rate increases by increases in the height when the height is smaller than -100 cm, and then it decreases by changes in the height for the height larger than -60 cm. For the height between -100 cm ~ -60 cm, changes in the average dose rate depend on the size of debris, and it decreases by increase of the height for $r_{min}$ = 1 cm whereas it increases for $r_{min}$ = 6 cm. The density plot and the line plot of the close packed fuel debris are more complicated than that of the loose packed fuel debris, and the density plot on the sensitivity index of the close packed fuel debris is also very different from that of the loose packed fuel. The density plot on the sensitivity index of the close packed fuel debris is visualized in Figure 4.10. Overall values of the sensitivity index are larger than that of the loose packed fuel debris which means the dose rate of the close packed fuel debris is more sensitive by changes in size of fuel debris. The photon dose rate is less sensitive by changes in $r_{min}$ when $r_{min}$ is smaller than 3 cm, and the sensitivity indexes are similar for all heights from the bottom to the top. On the other hand, the average photon dose rate is more sensitive by changes in $r_{min}$ when $r_{min}$ is larger than 3 cm and the height is higher than zero (z = 0).

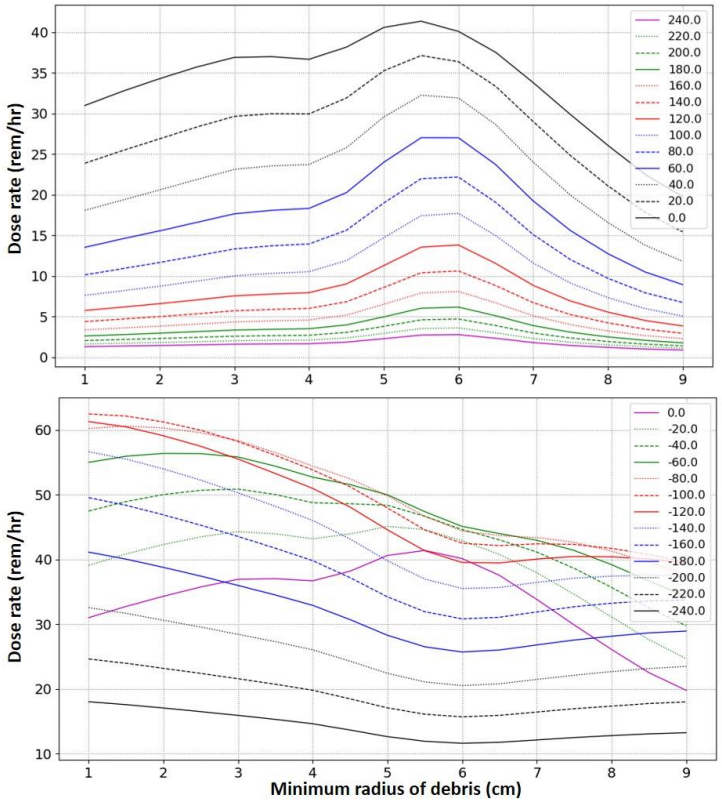


**Figure 4.9 Line plots of the average photon dose rate for the close packed fuel debris in a canister**

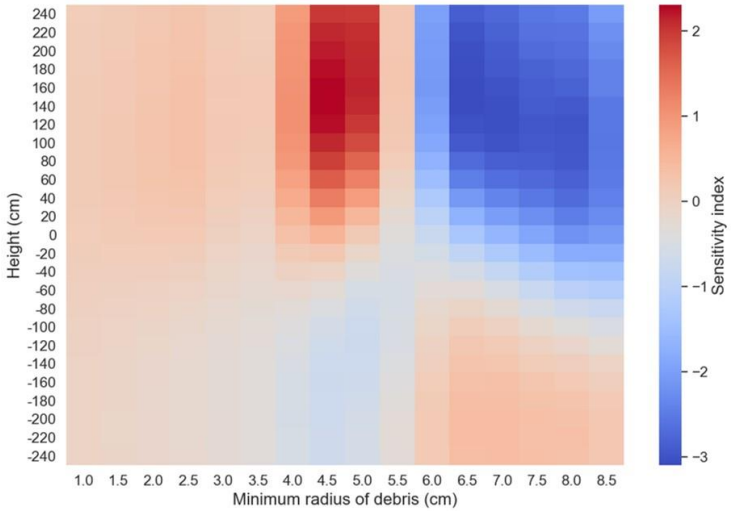


**Figure 4.10 Density plot on the sensitivity of the photon dose rate by changes in the minimum radius of debris for close packed fuel debris.**

The coefficient of variation of the close packed fuel debris is smaller than that of the loose packed fuel debris, and its global maximum is 16.9 %. Thus, the maximum of the standard of deviation is 16.9% of the average dose rate. CV of the close packed fuel debris is biased, and it has its global maximum at 140 cm from the vertical center of a canister (z = 140 cm) with $r_{min} = 5$ cm (Figure 4.11). Detail of CV is visualized by line plots in Figure 4.12. The line plot of CV is more complicated than that of the loose packed fuel debris, and it has several local maximums or minimums depending on the size of fuel debris. The percent relative range is much larger than CV, and its maximum is 139 %. The density plot of PRR is in Appendix D.

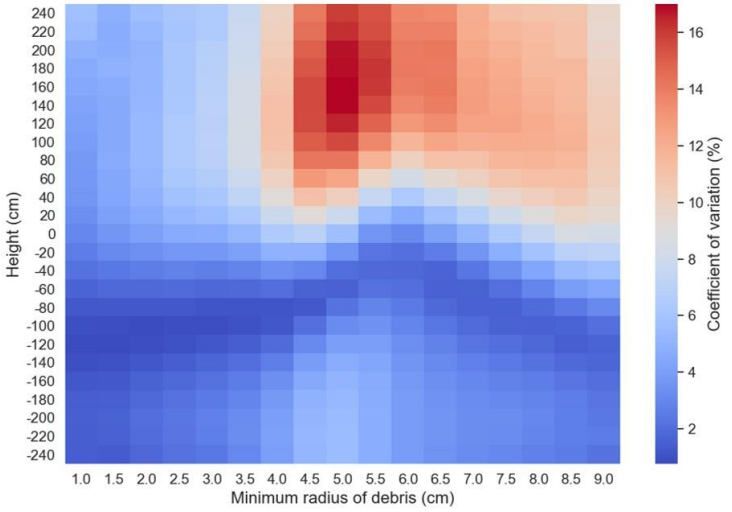


**Figure 4.11 Density plot of the coefficient of variation of photon dose rate for the close packed fuel debris in a canister**

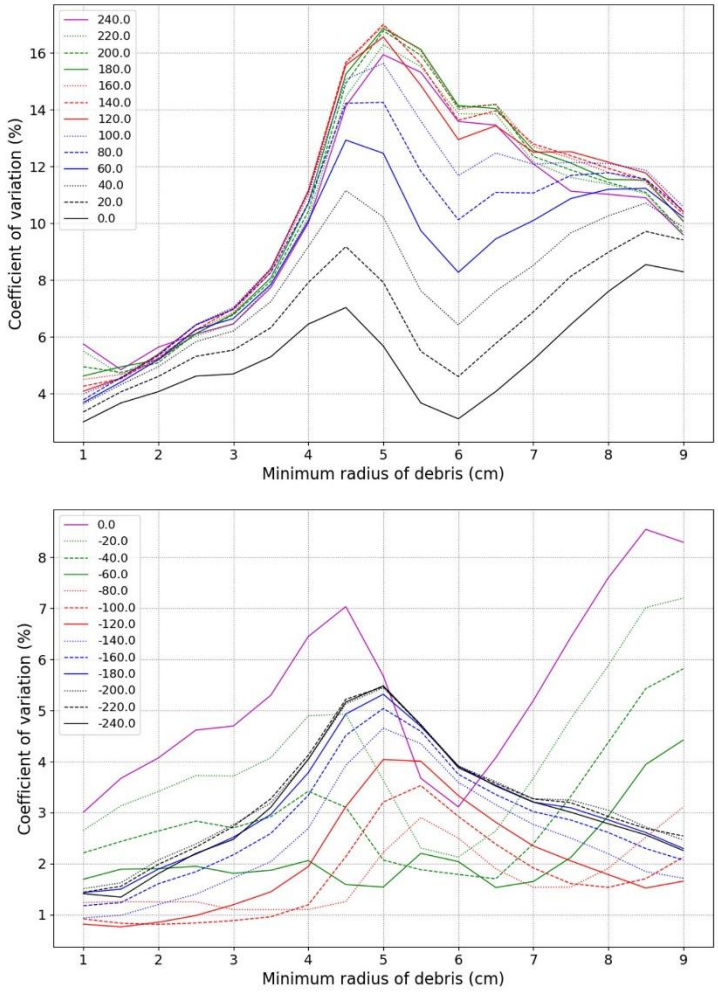


**Figure 4.12 Line plots of the uncertainty of photon dose rate for the close packed fuel debris in a canister**

### 4.2.2. Evaluation of the neutron dose rate by SCALE

The average neutron dose rate is evaluated for the loose packed fuel debris in a canister and visualized in Figure 4.13. The average neutron dose rate dose not decreases a lot by changes in the minimum radius of debris in each sample group, and their change by changes in the height of the detector are similar for all $r_{min}$. Local maximums of the dose rate are at the vertical center of a canister (z = 0), and the global maximum is at z = 0 and $r_{min}$ = 1cm. In case of the close packed fuel debris, local maximums are biased like the photon dose rate. However, the density plot has two maximums at $r_{min}$ = 1 cm and $r_{min}$ = 9 cm, and has a saddle point at $r_{min}$ = 6 cm. Details on the estimated dose rate are visualized as line plots in the Appendix D.

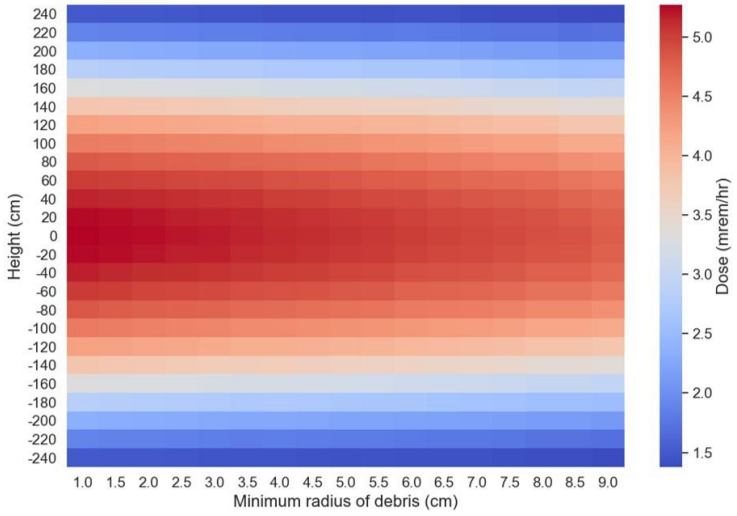


**Figure 4.13 Density plot of the average neutron dose rate for the loose packed fuel debris in a canister**

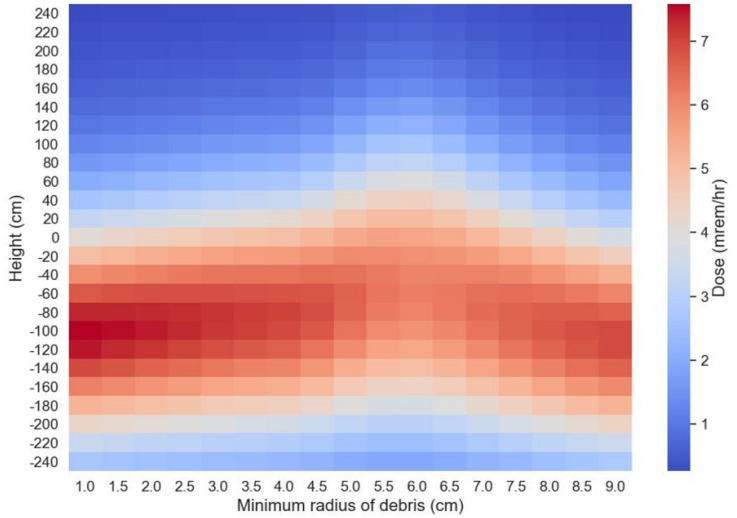


**Figure 4.14 Density plot of the average neutron dose rate for the close packed fuel debris in a canister**

The coefficient of variation is visualized for the loose packed and the close packed fuel debris in Figure 4.15 and 4.16 each. Patterns of these density plots are very similar with that of the photon dose rate even though their values are a little bit smaller. The density plot on the percent relative range and the sensitivity index are also very similar with that of the photon dose rate. These density plots are in Appendix D. The similarity between density plots of the neutron dose rate and the photon dose rate is due to the distribution of fuel debris in a canister is the major factor which makes the pattern of the graph. The difference in the photon attenuation coefficient and the macroscopic cross section of neutrons affects the dose rate, and it makes the average dose rate between photon and

neutron to be different. On the other hand, the uncertainty does not depend a lot on the difference in the attenuation coefficient between photon and neutron because the uncertainty is due to the size and distribution of fuel debris in a canister. Similarity in the sensitivity is the same reason.

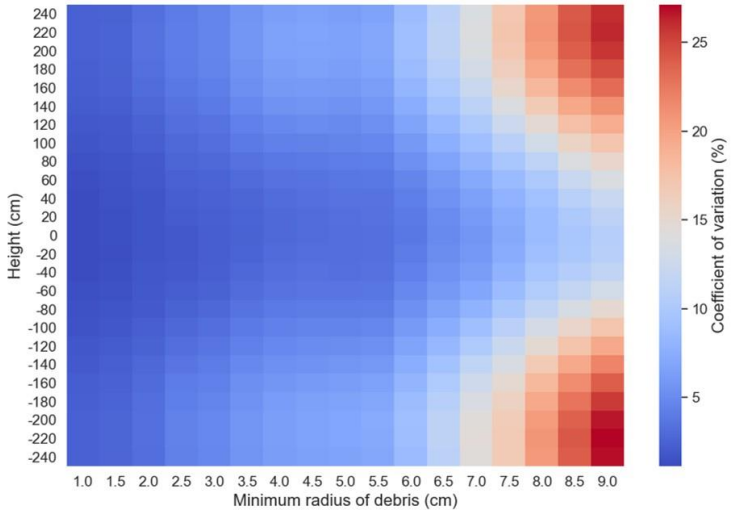


**Figure 4.15 Density plot of the coefficient of variation of the neutron dose rate of the loose packed fuel debris in a canister**

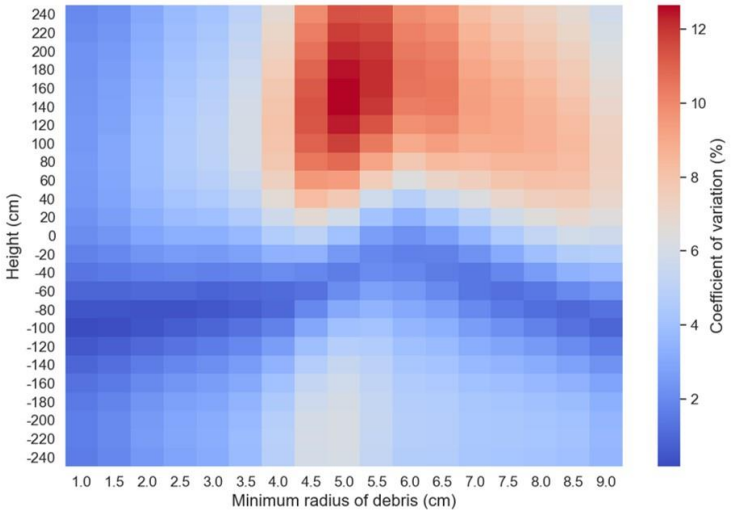


**Figure 4.16 Density plot of the coefficient of variation of the neutron dose rate of the close packed fuel debris in a canister**

### 4.2.3. Comparison of the estimation between SCALE and analytical models

Photon flux of the loose packed fuel debris in a canister has been calculated by using analytical models (the simple model, Shmakov model, the modified Shmakov model), and their results are compared with the estimation of SCALE (Figure 4.17). The estimated photon flux is visualized as a heat map to compare the magnitude of values. The simple model underestimates the attenuated photon flux, and the estimated global maximum of the simple model is not matched with the maximum of SCALE. Especially, there are a lot of differences between these two when the size of the fuel debris is small. The Shmakov model better estimates the photon dose rate than the simple model, but it cannot properly estimate that when the size of fuel debris is small. On the other hand, the modified Shmakov model gets better estimation on the photon flux than other two. Like other models, this model has some errors when the size of fuel debris is small, but the error is much smaller than other models. The modified Shmakov model has the global maximum at the vertical center of a canister with $r_{min} = 1$ cm like SCALE does whereas other two models have the maximum at different conditions. The uncertainty of the photon flux is also compared for these models (Figure 4.18). All three models overestimate the uncertainty, but the estimation by the modified Shmakov model is the most similar with the result of SCALE. The maximum coefficient of variation estimated by analytical models are around 35 % of the average photon flux whereas the maximum estimated by SCALE is around 30 %.

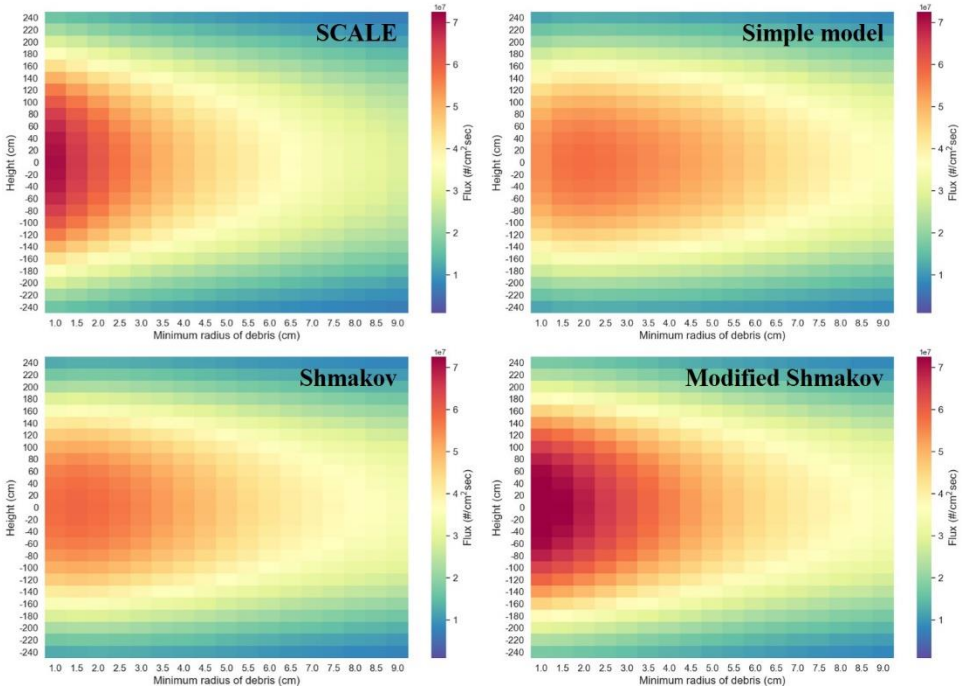


**Figure 4.17 Density plots of photon flux for the loose packed debris in a canister**

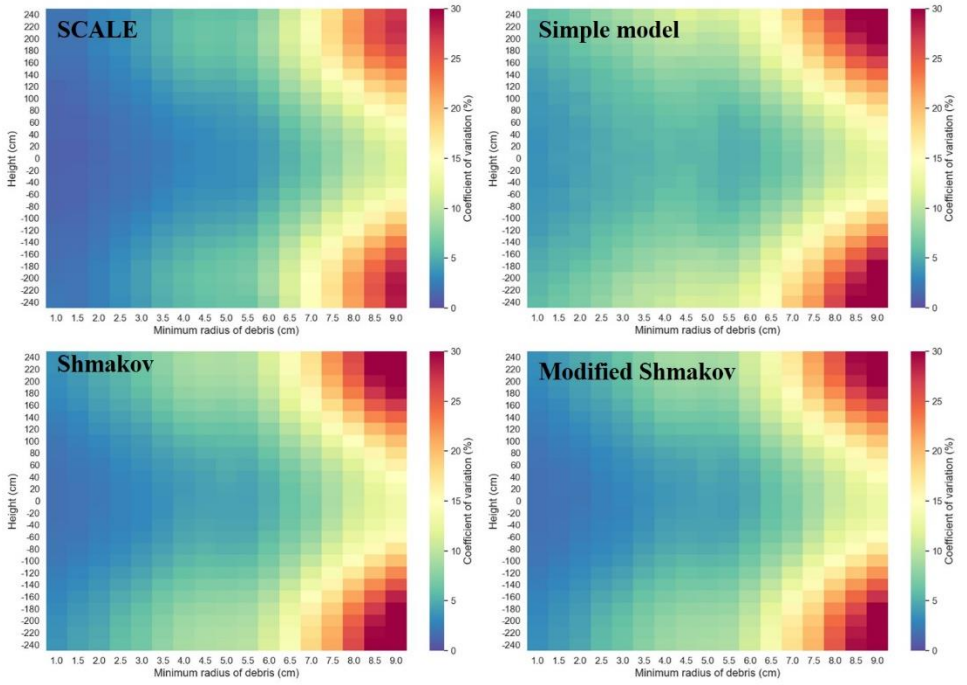


**Figure 4.18 Density plots of the coefficient of variation for the loose packed fuel debris in a canister**

Photon flux of the close packed fuel debris in a canister has been estimated by using analytical models, and their results are compared with the estimation of SCALE in Figure 4.19. Results from all of three models were not matched with the result from SCALE, and they overestimated the photon flux. The global maximum of the simple model is not same with the maximum of SCALE, and it is at -80 cm from the center of a canister with $r_{min}$ = 4.5 cm whereas the maximum of SCALE is at -100 cm from the center of a canister with $r_{min}$ = 1 cm. The global maximum of the Shmakov model and the modified Shmakov model are at -100 cm with $r_{min}$ = 2.5 cm and -100 cm with $r_{min}$ = 1.5 cm each. The estimated CV by the simple model is quite different from that of SCALE, and its maximum is around 35 % whereas the estimated maximum by SCALE is less than 17 %. The estimated uncertainty by the modified Shmakov model is the most similar with the estimation of SCALE (Figure 4.20). More details on the estimated data are in Appendix D.

Even if there are errors in the estimation of photon flux and its uncertainty, the modified Shmakov model can provide better estimation than other two models. The differences between the estimated values by SCALE and by the modified Shmakov model is not larger than the coefficient of variation of the estimation, and it can be supplemented by multiplying correction values. The modified model can estimate the condition for the global maximum of data which are the radius and vertical location for the maximum. Therefore, the modified model can be used for the approximate estimation of the photon flux and the evaluation of the uncertainty except for the fuel debris in very small size.

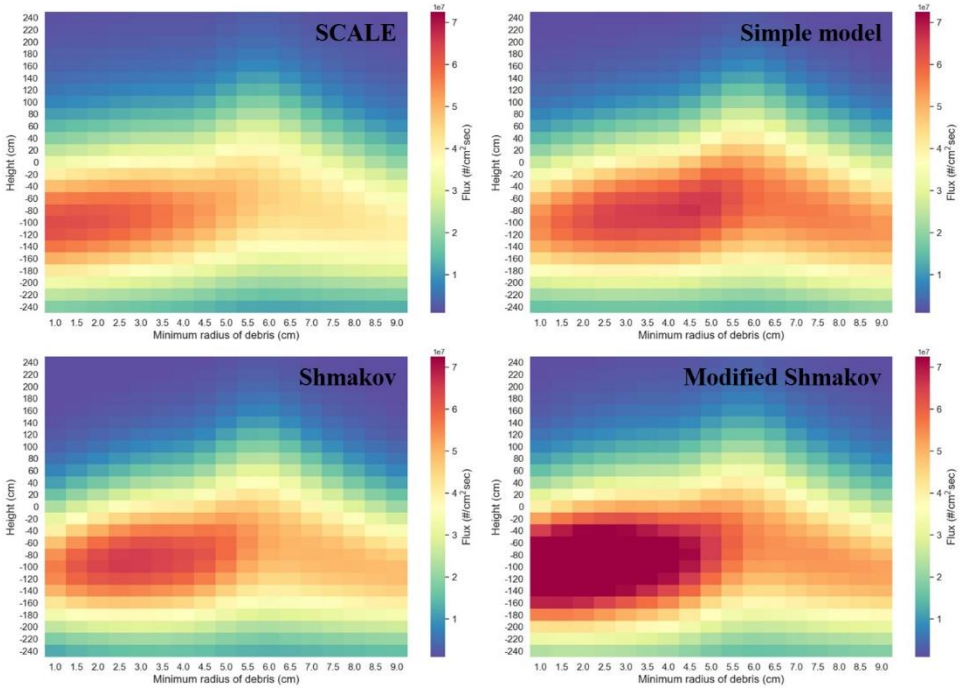


**Figure 4.19 Density plots of the photon flux for the close packed fuel debris in a canister**

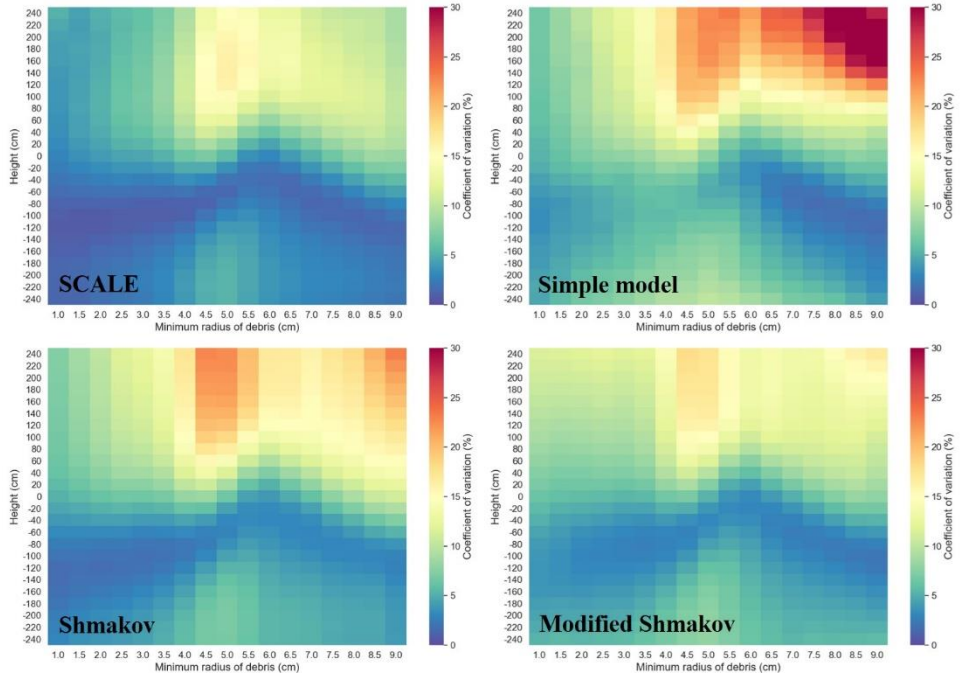


**Figure 4.20 Density plots of the coefficient of variation for the close packed fuel debris in a canister**

### 4.3 Sensitivity of the photon flux by change in the horizontal location of detector

Attenuation of photons from fuel debris depends on the distance from a canister to a detector, and it has been evaluated for a simplified example in Chapter 2. The differences in dose rates between the loose packed and the close packed fuel debris reduces by the changes in the distance from the canister to a detector according to the evaluation in Chapter 2. However, the preliminary estimation of Chapter 2 is performed only for a sample without any random sampling on size and distribution of the fuel debris. Therefore, sensitivity of the photon flux by changes in the distance is evaluated in this section by using the analytical model developed in Chapter 3. The minimum radius of debris is ranging from 1 cm to 9 cm, and 1,000 samples are random sampled for each sample group which are 17 groups in total, like other sections of this chapter. The vertical location of a point detector is assumed to be the vertical center of a fuel canister, and the distance from the surface of a canister to the point detector is between 1 m and 6 m.

The photon flux of the loose packed fuel debris decreases by changes in the distance from the surface of a canister to a point detector (Figure 4.21). In case of the loose packed fuel debris, the global maximum and the high intensity photon flux are biased to the sample group with small radius. On the other hand, the global maximum and the strong flux of the close packed fuel debris are less biased to the sample group with small debris than the loose packed fuel debris does.

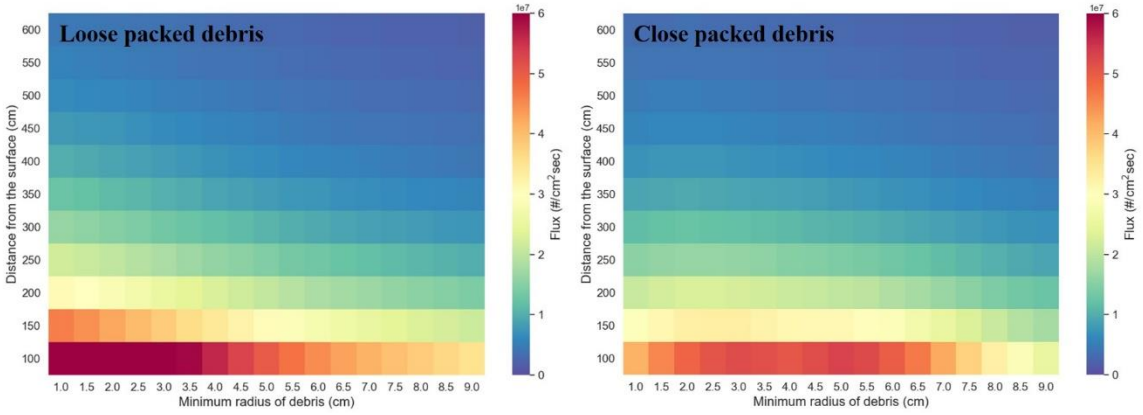


**Figure 4.21 Comparison of photon flux between the loose packed and the close packed fuel debris.**

The coefficient of variation is compared for the loose packed and the close packed fuel debris in Figure 4.22. CV of the loose packed fuel debris is large when the size of fuel debris is large, and it rapidly decreases by the changes in the distance from the surface to a detector. On the other hand, CV of the close packed fuel debris is less sensitive by changes in the distance than the loose packed fuel debris does. The percent relative range is around 5 times larger than CV, and it is more sensitive by changes in the distance when fuel debris is loosely packed (Figure 4.23).

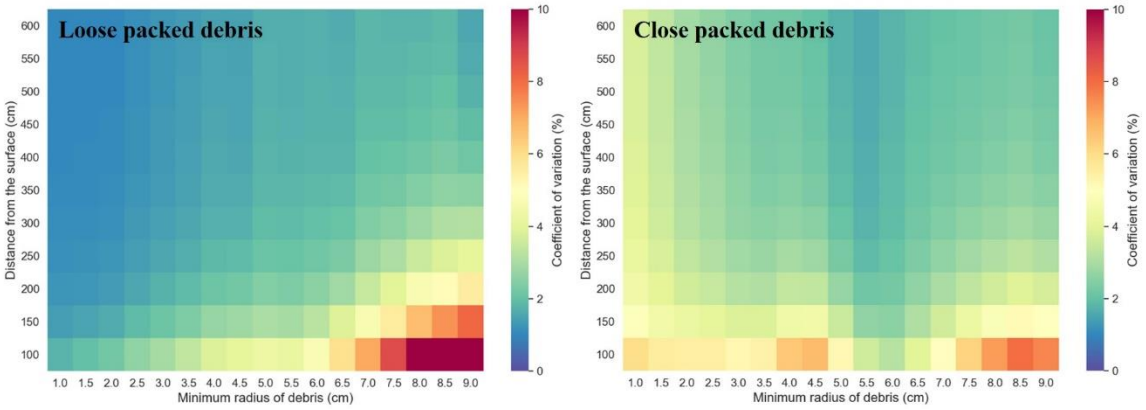


**Figure 4.22 Comparison of the coefficient of variation between the loose packed and the close packed fuel debris.**

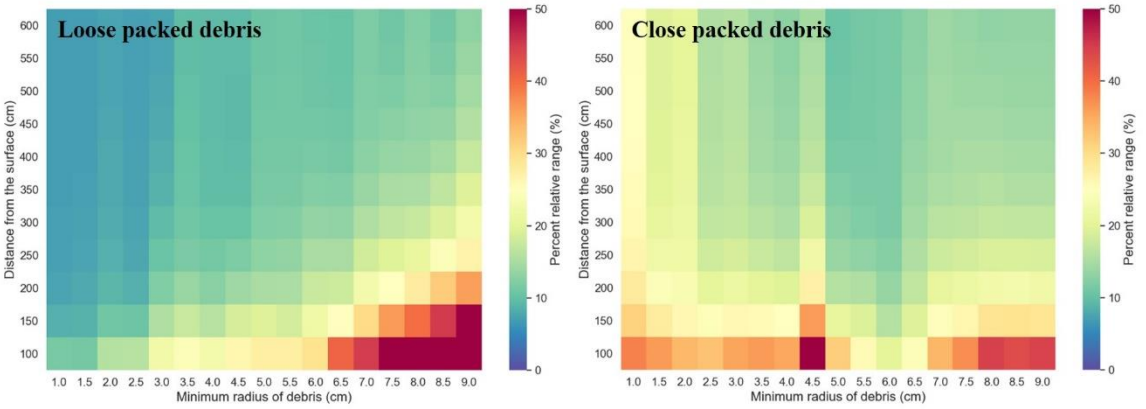


**Figure 4.23 Comparison of the percent relative range between the loose packed and the close packed fuel debris.**

The sensitivity of the photon flux by changes in $r_{min}$ and changes in the distance between a canister to a detector is estimated for the loose packed debris (Figure 4.24) and the close packed fuel debris (Figure 4.25). Limit of the distance is modified from 600 cm to 400 cm in these density plots for better resolution. The loose packed fuel debris is more sensitive by changes in the distance than the close packed fuel debris does. In case of the absolute value of sensitivity by changes in $r_{min}$, the close packed fuel debris is larger than the loose packed fuel debris. The absolute value of sensitivity by change in the distance increases by increasing the distance. In case of the close packed fuel debris, the maximum sensitivity index values are biased to the top and bottom of the density plot. The sensitivity index of the close packed fuel debris estimated for the detector location which is -100 cm from the center of a canister, and its density plots are visualized in Figure 4.26. The estimated sensitivity index with this modified height of detector has a global maximum at $r_{min} = 6\ cm$ and 100 cm from the surface of the canister.

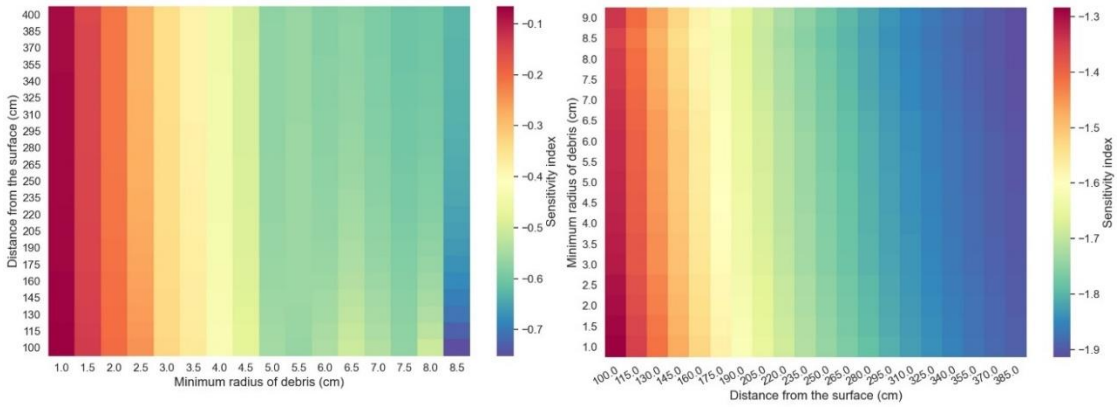


**Figure 4.24 Sensitivity of the photon flux** for changes in $r_{min}$ (left) and the distance from a canister to a detector (right) for the loose packed debris.

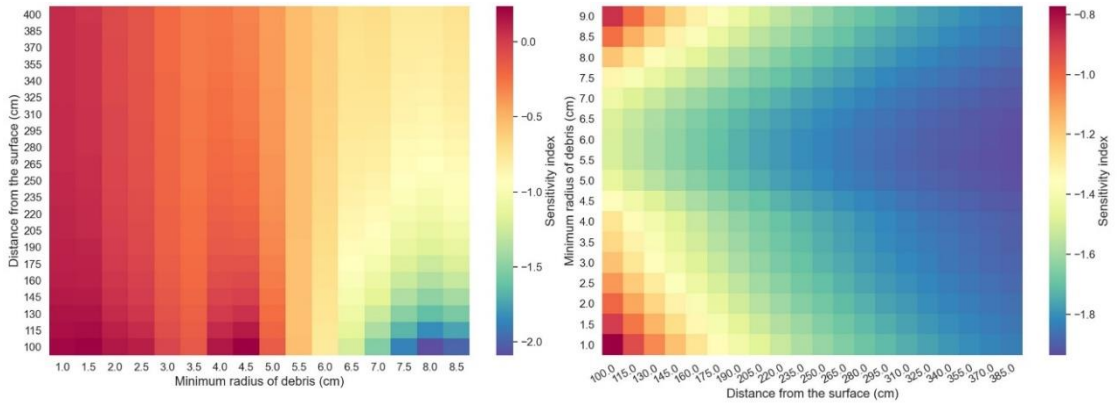


**Figure 4.25 Sensitivity of the photon flux** for changes in $r_{min}$ (left) and the distance from a canister to a detector (right) for the close packed debris.

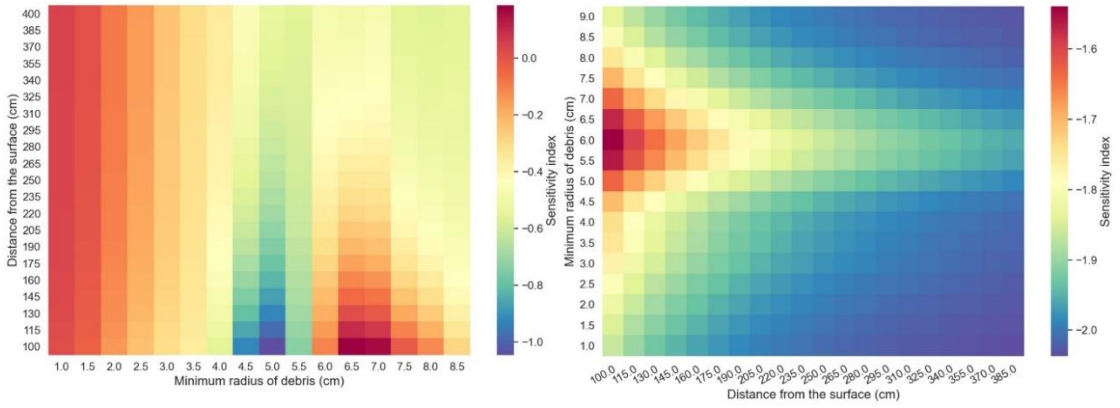


**Figure 4.26 Sensitivity of the photon flux** for changes in $r_{min}$ (left) and the distance from a canister to a detector (right) for the close packed debris. Vertical locations of detectors are -100 cm from the vertical center of a canister.

## 4.4 Modification of the design for the reduction of uncertainty

### 4.4.1 Vertical division of the inner space of canister

As a method to reduce the uncertainty of the estimated dose rate, distribution of fuel debris can be controlled by limiting the volume of debris pile. The vertical height of fuel debris affects the uncertainty, and it can be limited by modifying the dimension of the fuel canister. TEPCO Japan designed a small container which can be placed in a fuel canister with retrieved fuel debris, and the container can reduce the uncertainty by limiting the distribution of fuel debris. Details on the design are not released to the public but three or more of them will be placed in a fuel canister depending on their dimension [2]. Therefore, a simplified design of the canister with three small containers in it is evaluated at this section as an example of the method to reduce the uncertainty (Figure 4.27). Materials used and the wall thickness of the small canister can affect a lot to the evaluation. However, these are ignored for the simplification by assuming the thickness of the wall is almost zero. Therefore, changes of the estimated dose rate by the modified canister design only depend on the vertical division of fuel debris into three sectors. Inner space of a fuel canister is divided into 3 spaces, and the same amount of fuel debris are randomly placed at each division. Total amount of fuel debris in a canister is 230.9 kg which is the same as the model of Chapter 3, and this has been divided by three to put the same amounts of debris in each container. Other assumptions are the same with the model of Chapter 3. SCALE code is used for the calculation of dose rate, and the estimated photon dose rate of the original design and the modified design are compared for the loose packed and the close packed fuel debris.

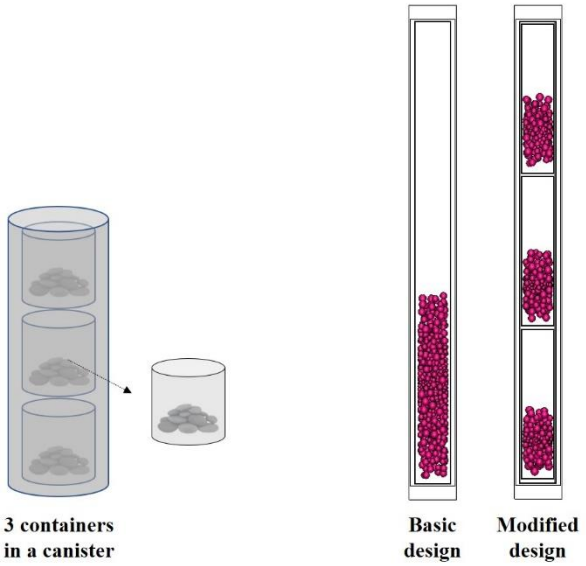


**Figure 4.27 Small containers in a fuel canister.** The figure at the left is the concept of the modified design which has three small containers in a fuel canister. The figure at the right is the side view of the fuel canister without small containers (left) and the fuel canister with three small containers (right). Red spheres are fuel debris.

Photon dose rate at 1m from the center of a canister is estimated, and its results are visualized in Figure 4.28. There are almost no differences in photon dose rate between two designs when fuel debris are loosely packed in each canister. In case of the close packed fuel debris, estimated dose rate of the modified design is larger than the other when $r_{min}$ is smaller than 4.5 cm or larger than 7.5 cm. However, these differences are made due to the center of a canister is not the same as the center of the debris pile. In case of the close packed fuel debris, the maximum dose rate estimated at the vertical center of a canister is a local maximum, and the global maximum can be estimated at the vertical center of a debris pile. Therefore, the photon dose rate estimated at the center of the debris pile is also visualized in Figure 4.28 for the comparison. The photon dose rate of the modified design is much smaller than the other when the dose rate of the original design is estimated at the center of the debris pile instead of the center of a canister. Thus, the maximum of the average photon dose rate of each sample group with close packed fuel debris is reduced by packing fuel debris in small containers. This reduction is due to the pile of fuel debris is vertically placed by the divided spaces of the modified design. Path lengths from fuel debris to a point detector is increased by spaces between divided debris piles, and photon dose rate is reduced by more attenuations.

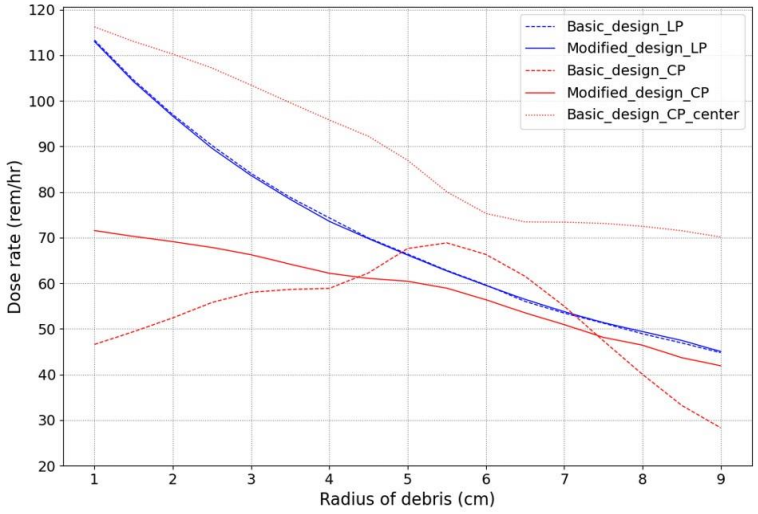


**Figure 4.28 Comparison of the photon dose rate.** The blue and red dashed lines are the photon dose rate of the basic design with the loose packed (blue) and the close packed (red) fuel debris. The Thick blue and red lines are the photon dose rate of the modified design with the loose packed (blue) and the close packed (red) fuel debris. The fine dashed red line is also the photon dose rate of the basic design with the close packed fuel debris, but it has been estimated at the vertical center of the debris pile instead of the vertical center of a canister.

Coefficient of variation (CV) of the photon dose rate is estimated, and its results are compared in Figure 4.29. In case of the loose packed fuel debris, the CV of the photon dose rate is reduced to half by using small containers in a canister. The maximum CV of the modified design is around 8 % of the average photon dose rate whereas the maximum CV of the original design is around 15 %. CV of the close packed fuel debris also can be reduced by using the modified design. However, the CV of the modified design can be larger than the CV of the basic design when it has been estimated at the vertical center of the debris pile instead of the vertical center of a canister.

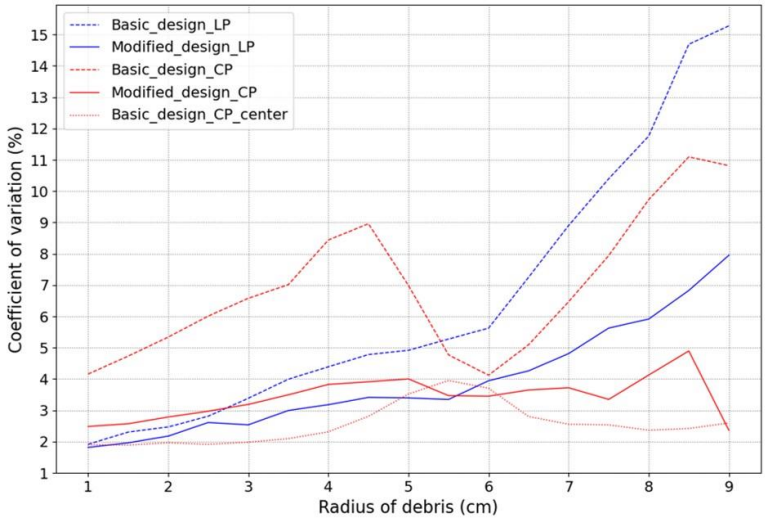


**Figure 4.29. Comparison of the coefficient of variation.** The blue and red dashed lines are CV of the basic design with the loose packed (blue) and the close packed (red) fuel debris. The Thick blue and red lines are CV of the modified design with the loose packed (blue) and the close packed (red) fuel debris. The fine dashed red line is CV of the close packed fuel debris which is estimated at the vertical center of the debris pile.

Even though CV in Figure 4.29 is less than 15 % of the average dose rate, the percent relative range (PRR) of the estimated data is much larger than this (Figure 4.30). In case of the loose packed fuel debris, PRR of photon dose rate can be larger than 80 % of the average dose rate for the basic design of canister, and PRR can be 40 % of the average dose rate for the modified design with three small containers. PRR of the close packed fuel debris is smaller than that of the loose packed fuel debris, and it also can be reduced by using the modified design. However, it depends on the vertical location of the detector like the coefficient of variation does, and PRR of the modified design can be larger than that of the basic design if it is estimated at the vertical center of the close packed pile of debris.

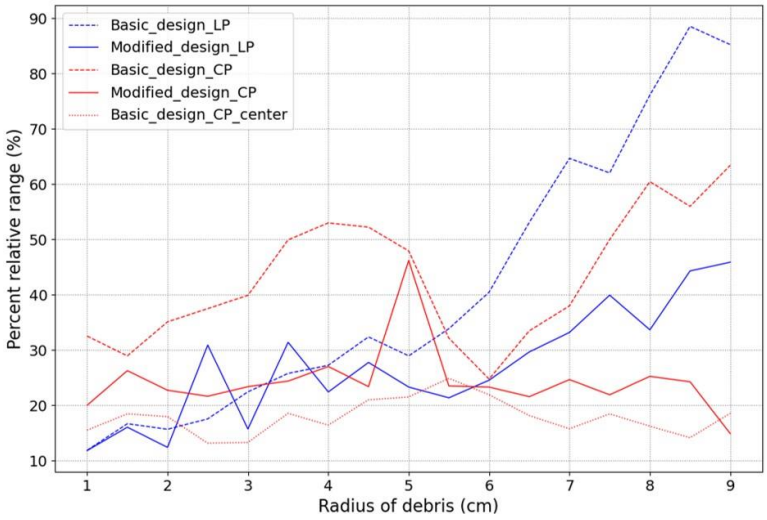


**Figure 4.30 Comparison of the percent relative range.** The range in this graph is the difference between the maximum and the minimum photon dose rate in each sample group. The blue and red dashed lines are PRR of basic design with the loose packed (blue) and the close packed (red) fuel debris. The Thick blue and red lines are PRR of the modified design with the loose packed (blue) and the close packed (red) fuel debris. The fine dashed red line is PRR of the close packed fuel debris which is estimated at the vertical center of the debris pile.

Photon dose rate of fuel debris depends on the vertical location (height) of the detector, and it has been evaluated for the basic design of fuel canister in Chapter 4.2. Therefore, the variability of photon dose rate by the height of the detector is evaluated for the modified design, and its result has been compared with the result of Chapter 4.2 (Figure 4.31). Two plots at the top of Figure 4.31 are the density plot of the basic design for the loose packed (left) and the close packed (right) debris, and two plots at the bottom of Figure 4.31 are plots of the modified design for the loose packed (left) and the close packed (right) debris. In case of the loose packed fuel debris, the density plot of the modified canister design with three small containers is very similar with the plot of the basic design. On the other hand, in case of the close packed fuel debris, the average photon dose rates in the density plot are less biased than the dose rate of the basic design, and its global maximum is smaller than that of the basic design. The global maximum of the modified design is 44 rem/hr (440 mSv/hr)whereas that of the basic design is 62.5 rem/hr (625 mSv/hr). Details on the estimated values of the photon dose rate is in Appendix D.

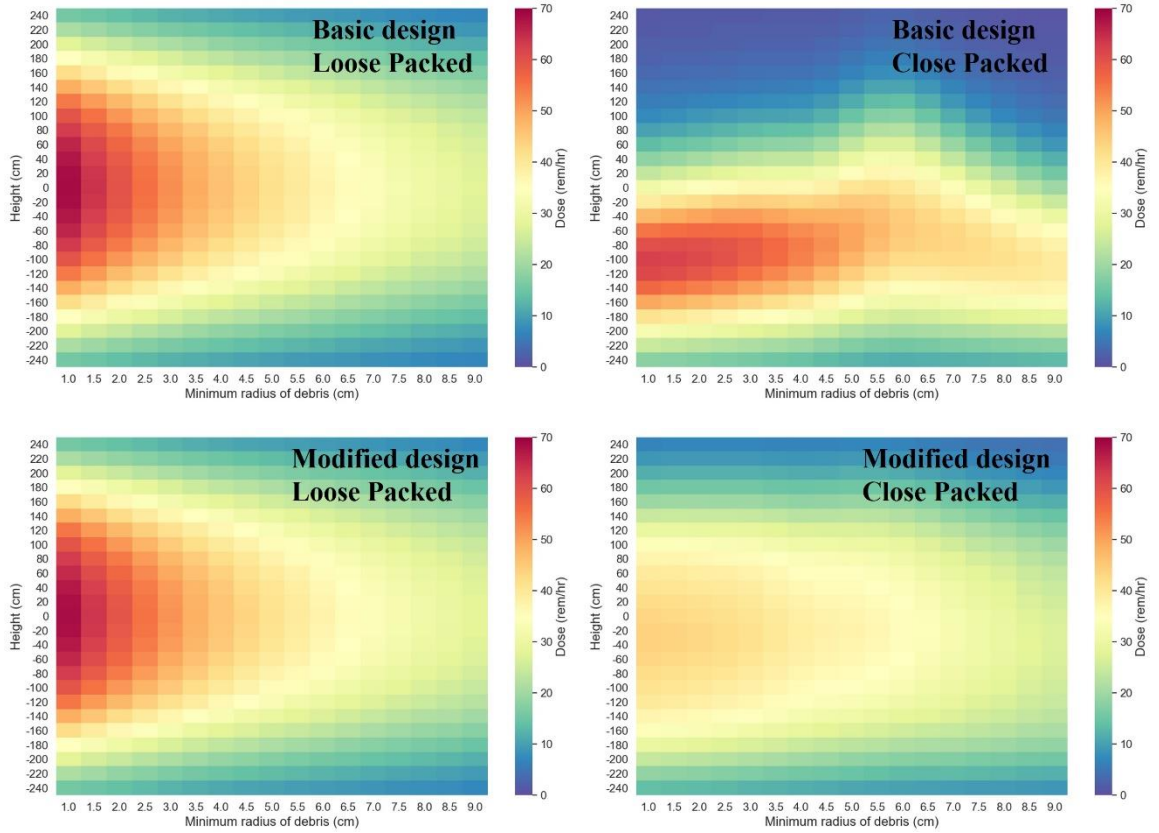


**Figure 4.31 Comparison of the photon dose rate.** The Y-axis of the density plot is the height of the region for the estimation from the vertical center of a canister. The X axis of the density plot is the minimum radius of fuel debris in each sample group. Color of the density plot is ranged from blue to red, and it visualizes the average dose rate.

The coefficient of variation of the photon dose rate is visualized in Figure 4.32 for the comparison between the basic design and the modified design. Two graphs at the top of Figure 4.32 are CV of the original design, and two graphs at the bottom are that of the modified design. CV is reduced by the modified design, and the modified design has a smaller global maximum than the basic design. The global maximum of CV is 12.7 % for the loose packed fuel debris in a canister with the modified design whereas the loose packed fuel debris in a canister with the basic design is 29.3 %. The global maximum of CV is only 8.22 for the close packed fuel debris with the modified design whereas that of the close packed fuel debris with the basic design is 15.9. In case of the CV of the modified design, the density plot has three local minimums. The three local minimums of the close packed fuel debris are biased, and the height of local minimums depends on the $r_{min}$ of fuel debris. More details on the estimated CV are in Appendix D.

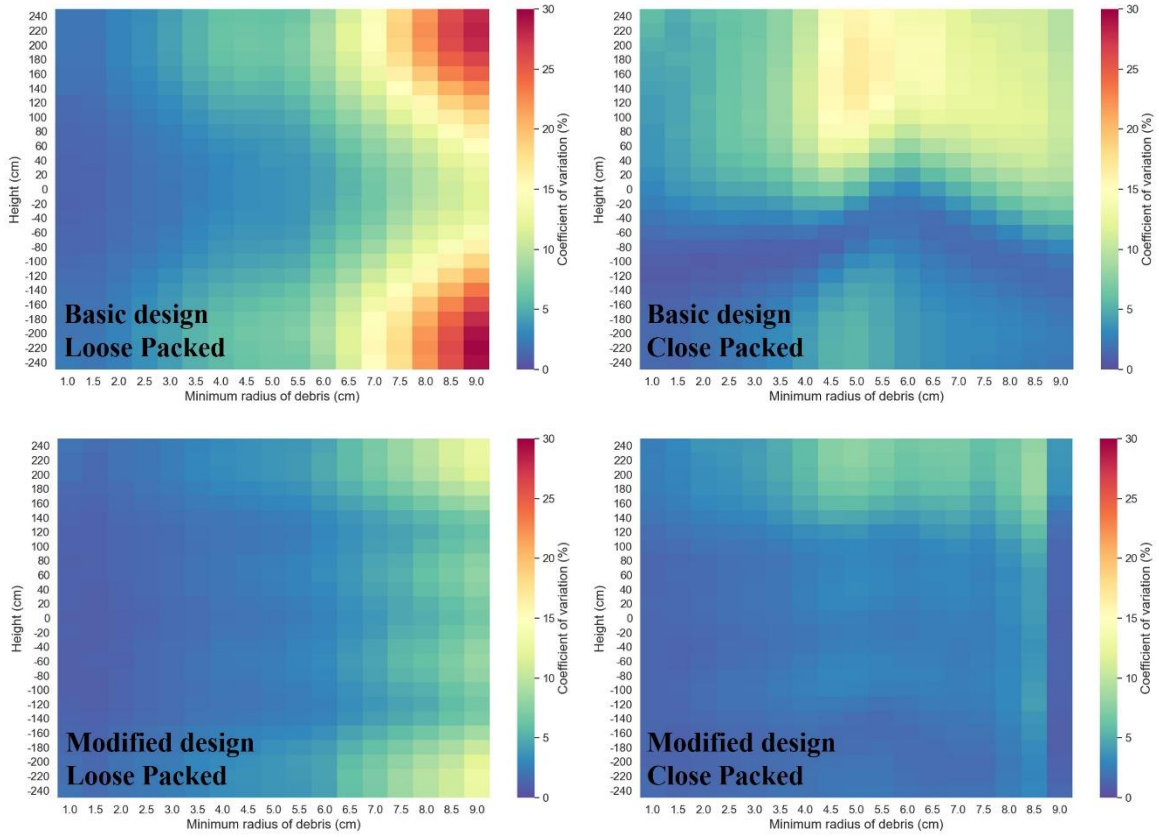


**Figure 4.32 Comparison of the coefficient of variation.** The X and Y axis of the density plot is same with the figure 4.31. The color visualizes the coefficient of variation.

### 4.4.2 Horizontal division of the inner space of canister

As another comparison of design, the inner space of a fuel canister is divided into 4 spaces by partitions. Wall thickness of partitions and its shielding effect are ignored to evaluate the effect of the spatial separation of inner space on the reduction of dose rate and uncertainty. The diameter of fuel debris is limited to smaller than 7cm by dividing the inner space of a canister, and fuel debris are loosely packed in each space. Photon dose rate of this modified design is estimated for a point detector which is located 1 m from the center of a canister. The vertical location of the point detector is at the center of a canister. Compared to the average dose rate of the basic design in which fuel debris are distributed in a space, the dose rate is decreased when the inner space of a canister is divided into 4 spaces because fuel debris are vertically dispersed in each space (Figure 4.33). The reduced dose rate by the canister with 4 partitions is smaller than the dose rate of a canister with three small containers for the $r_{min}$ larger than 2.5 cm. The average dose rate of the canister with 4 partitions is larger than the other two when the size of fuel debris is smaller than 2 cm.

The standard deviation of photon dose rate decreases when the inner space of a canister is divided into 4 for $r_{min}$ smaller than 2.5 cm (Figure 4.34). However, it is larger than other

two for $r_{min}$ larger than 3 cm. The coefficient of variation also can be reduced by the 4 partitions for $r_{min}$ smaller than 2.5 cm (Figure 4.35). The CV of the canister with three small containers is smaller than the other two.

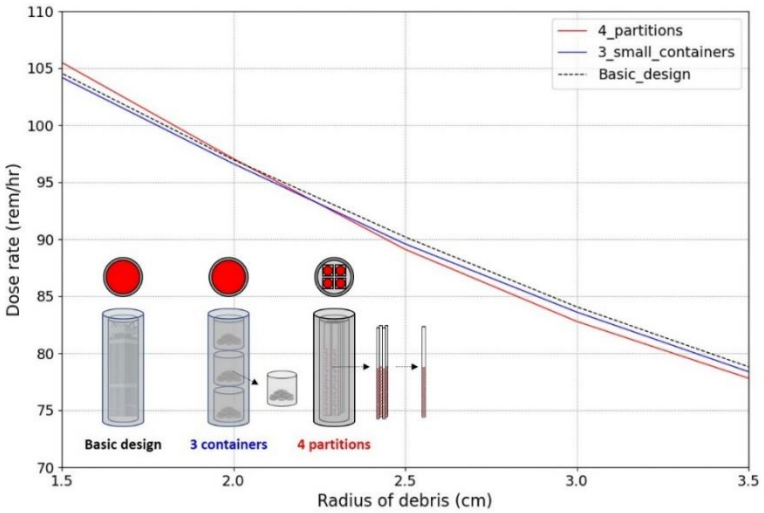


**Figure 4.33 Comparison of the average photon dose rate.** The dark dashed line is the dose rate of a canister without partition (The basic design) and the red line is the dose rate of a canister with 4 partitions. The blue line is the dose rate of a canister with 3 small containers.

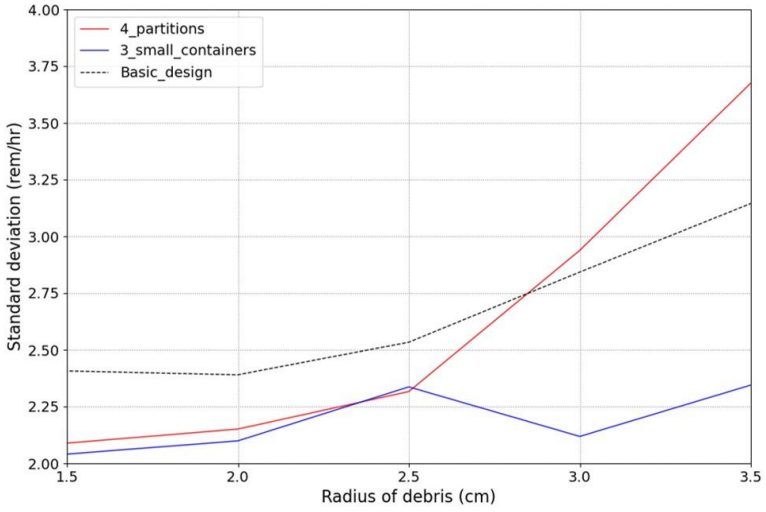


**Figure 4.34 Comparison of standard deviation.** The dark dashed line is the standard deviation of a canister without partition (Basic design of a fuel canister) and the red line is that of a canister with 4 partitions. The blue line is the standard deviation of a canister with 3 small containers in a canister.

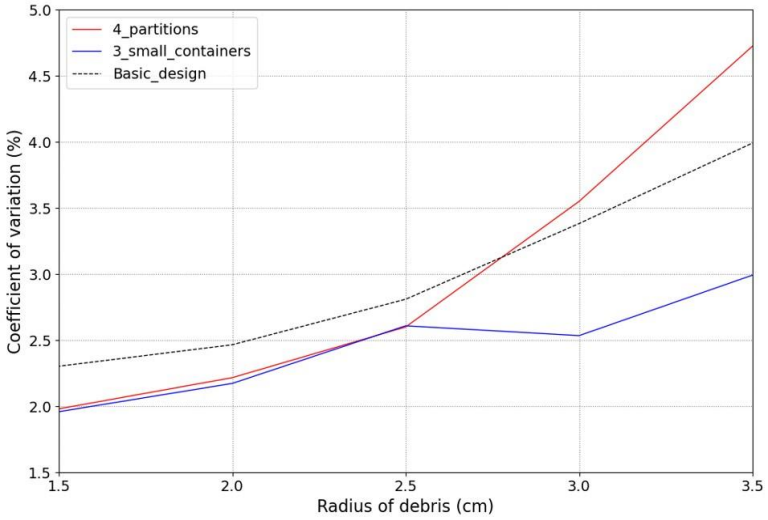


**Figure 4.35 Comparison of the coefficient of variation** between a canister with 4 partitions and a canister without partition. The dark dashed line is CV of a canister without partition and the red line is CV of a canister with 4 partitions. The blue line is the CV of a canister with 3 small containers in a canister.

## 4.5 Attenuation of photon radiation by the fuel transfer cask

Nuclear radiation from a fuel canister is much larger than the regulatory dose limits, and it needs to be shielded for the safety of workers. Therefore, casks which are used for the transport or the storage of canisters have thick outer shells with shielding materials to meet the regulatory dose limit. In addition to this, the fuel canister also needs to be shielded during temporary handling before placing it in a cask. In case of the defueling of TMI-2 reactor, a transfer cask has been used to transfer canisters from the spent fuel pool to transport casks. TEPCO also is considering the use of a transfer container as a temporary shielding tool while handling fuel canisters. According to the technical strategy plan of TEPCO, they plan to prepare an on-site transfer container to transfer fuel canisters from the reactor building to the on-site temporary storage facility [2]. At this section, the photon flux of a fuel canister in the transfer canister is estimated to evaluate changes in the uncertainty of dose rate by the transfer cask.

A transfer cask has a relatively thick wall with shielding materials for the sufficient attenuation of the nuclear radiation. Several options can be considered for the use of shielding materials, and it has been discussed in Chapter 2. As an example of the conceptual design of the transfer cask, a cylinder which is made with 15 cm thick SS304L is evaluated, and the photon flux at 1m from its surface is approximately estimated by using the modified Shmakov model. Vertically arranged 25 detectors are assumed for the estimation like the model of the chapter 4.2 (Figure 4.36).

The photon flux from fuel debris is attenuated a lot by transmitting through the 15 cm of SS304L (Figure 4.37). The photon flux is sensitive by changes in the size of debris and the vertical location of the detector even after being attenuated by the 15 cm of SS304L. Density plots of the photon flux for the loose packed debris and the close packed debris has patterns similar with the density plot of a canister without the transfer cask. The density plot of the loose packed debris has its global maximum at the vertical center with $r_{min} =$ 1.0 cm, but it is less sensitive to the change in the vertical location of the detector than the sensitivity of a canister without the transfer cask. The density plot of the close packed debris is biased to the lower height like the canister without the transfer cask, and it has a saddle point at $r_{min} = 6.0$ cm.

The coefficient of variation (CV) of the photon flux is visualized in plots of Figure 4.38. The CV of the photon flux is larger than the CV of a canister without the transfer cask. In case of the loose packed fuel debris, the maximum CV is larger than 70 % whereas it is less than 35 % for a canister without the transfer cask. CV of the close packed fuel debris is larger than 80 % which is larger than CV of the loose packed fuel debris. The location of the maximum in the density plot is similar with the location for a canister without the transfer cask. Thus, uncertainty in photon flux is increased even if the radiation safety is enhanced by the transfer cask. More details on the photon flux of a canister in the transfer cask is in Appendix G.

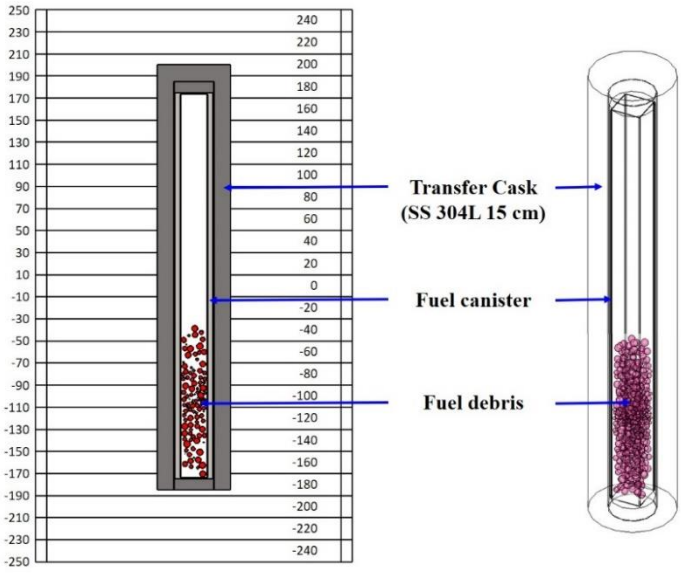


**Figure 4.36 Side view of the canister in a transfer cask**

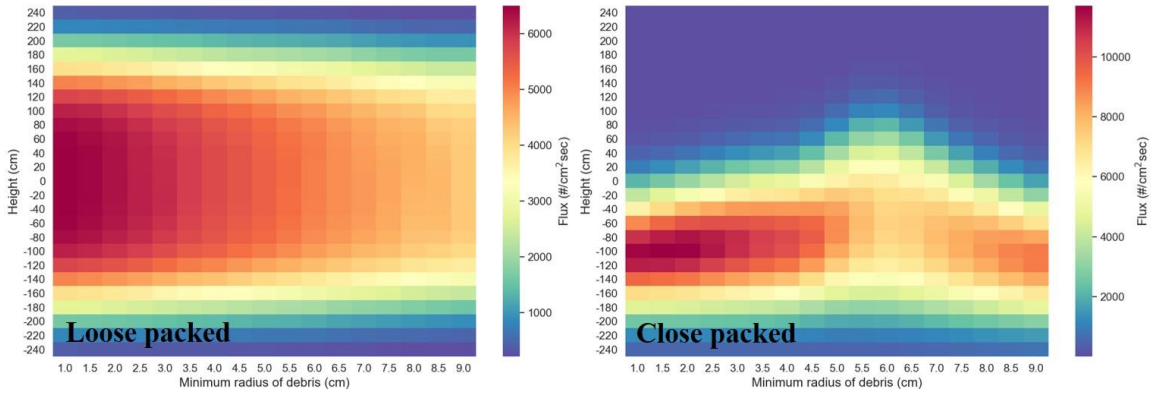


**Figure 4.37 Comparison of the photon flux** between the loose packed and the close packed fuel debris which are contained in a fuel canister in a transfer cask.

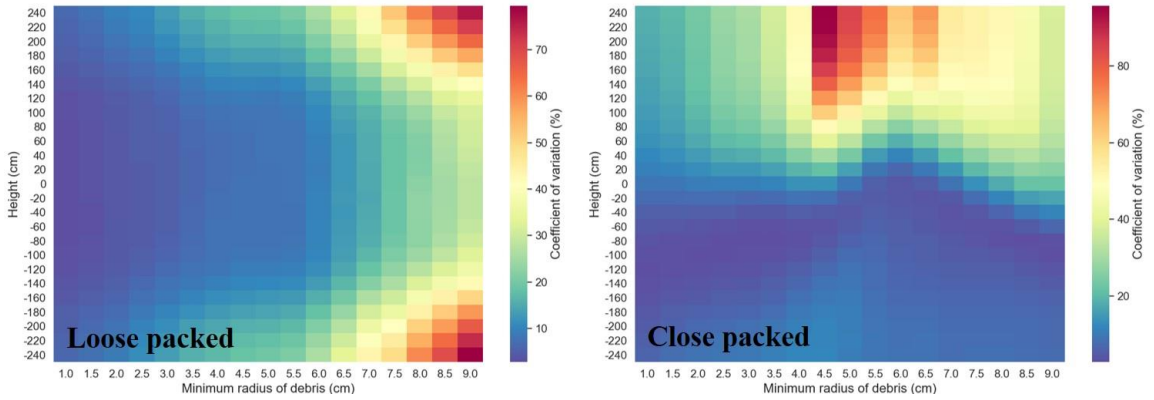


**Figure 4.38 Comparison of the coefficient of variation** between the loose packed and the close packed fuel debris which are contained in a fuel canister in a transfer cask.

## 4.6 Attenuation of the photon radiation by the transport cask

Photon flux of the fuel debris in a transport cask is estimated by using the modified Shmakov model. The simplified design of the transport cask is visualized in Figure 4.39. The cask has seven canisters, and each fuel canister has the same amount of fuel debris which is 230.9 kg. The cask has seven steel cylinders to contain fuel canisters, and fuel canisters are surrounded by SS304L shell and the concrete filler. Materials in dark color in Figure 4.39 are SS304L, and the light gray color is the concrete filler. Red spheres are fuel debris, and space between debris is filled with dry air. Outside of the cask is also filled with dry air, and photon flux is estimated for vertically divided regions. The photon flux is estimated for the loose packed and the close packed fuel debris like other models of this chapter.

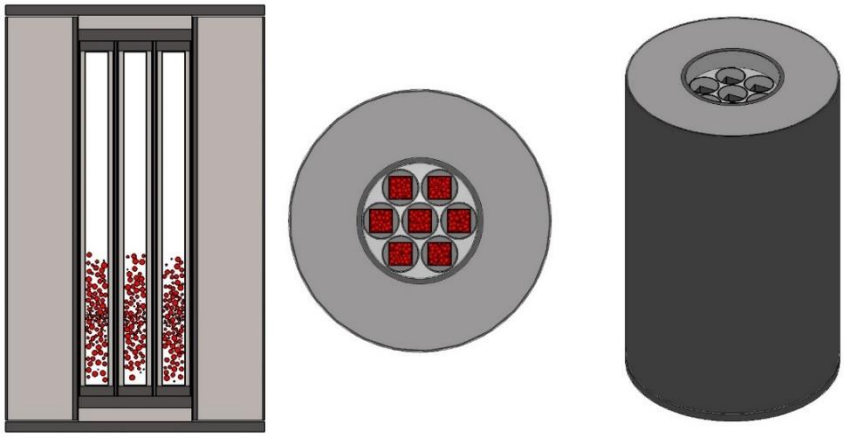

**Figure 4.39 Simplified design of the transport cask.** The figure at left is the side view, and the figure at the center is the cross-sectional view. The figure at right is the diagonal view of the cask. Plates at the top of the figure at right are removed to visualize the inside.

The estimated photon flux is visualized in Figure 4.40. The density plot at the left is for the photon flux of the loose packed fuel debris, and the plot at the right is for the photon flux of the close packed fuel debris. Y axis is the height of the estimated region, and X axis is the minimum radius of fuel debris in each sample group. The color spectrum from the blue to the red visualizes the estimated photon flux. These graphs are similar to the density plot of fuel debris in a fuel canister. The density plot of the loose packed fuel debris is symmetric, and its global maximum is at the vertical center of the cask like the density plot of a canister. The density plot of the close packed fuel debris is biased to the lower part of the cask, and its global maximum is at -100 cm from the vertical center of the cask. However, the photon flux is less sensitive by changes in $r_{min}$ than the fuel debris in a canister. Overall photon flux is much smaller than the photon flux from a canister because it has been attenuated by shielding materials of the transport cask.

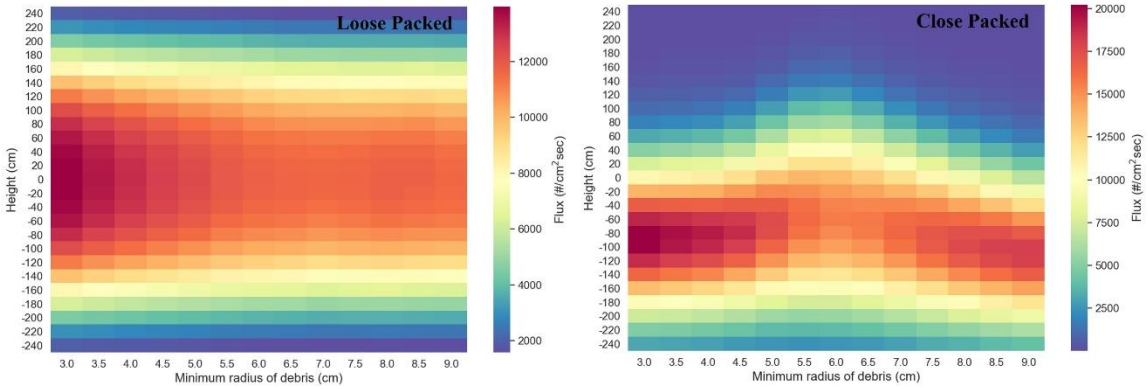


**Figure 4.40 Comparison of the photon flux** between the loose packed and the close packed fuel debris in seven canisters in a transport cask.

The density plot of the coefficient of variation is similar with that of a fuel canister (Figure 4.41). However, the CV of the transport cask is larger than that of a fuel canister. The global maximum of CV is 33.1 % of the average photon flux for the loose packed fuel debris, and the global maximum of the close packed fuel debris is larger than 35%. Thus, the estimated photon flux of the transport cask is more uncertain than that of a fuel canister. The global maximum is at the each end of the transport cask for the loose packed fuel debris, and it is at the top for the close packed fuel debris. Therefore, the estimated photon flux at the top of the transport cask with close packed fuel debris is very uncertain, and it can be different from the actual measurement.

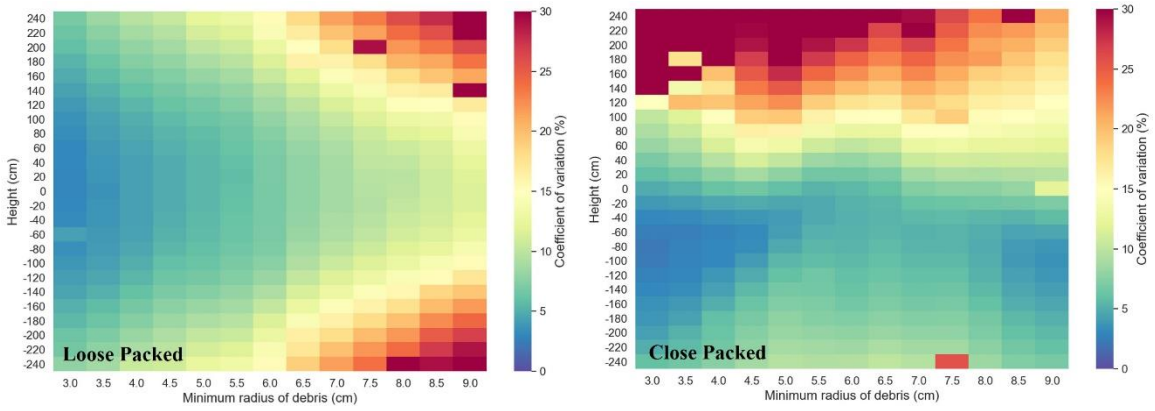


**Figure 4.41 Comparison of the coefficient of variation** between the loose packed (left) and the close packed (right) fuel debris in seven canisters in a transport cask.

The percent relative range of the transport cask is much larger than CV (Figure 4.42). The global maximum of the percent relative range is larger than 97 % of the average photon flux for the loose packed fuel debris, and it is larger than 160 % of the average photon flux for the close packed fuel debris.

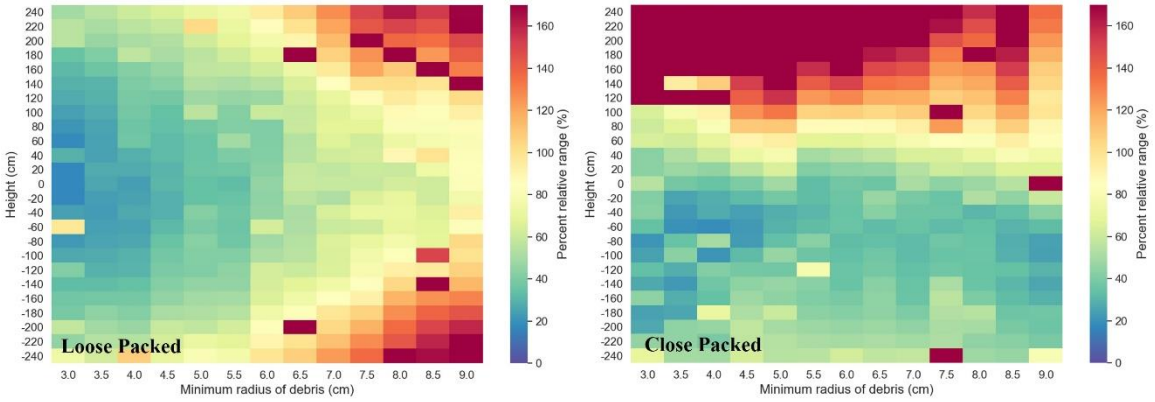


**Figure 4.42 Comparison of the percent relative range** between the loose packed (left) and the close packed (right) fuel debris in seven canisters in a transport cask.

## 4.7 Summary and discussion

The model developed in Chapter 3 was used for the evaluation of dose rate and flux in this chapter. At the beginning of this chapter, the model was used for the evaluation on the variability and sensitivity of the radiation dose rate by changes in the vertical location of the detector. After the evaluation, photon flux and its uncertainty were evaluated by using SCALE and analytical models, and their results were compared. These have been compared to verify the reliability of the modified Shmakov model, and then sensitivity of the photon flux by changes in the horizontal distance of the detector were evaluated by using the modified Shamkov model. After these evaluations, the photon flux and its uncertainty were evaluated for designs of the cask and the modified canister.

Variability and sensitivity of the radiation dose rate by changes in the vertical location of the detector were evaluated. Photon dose rate of the loose packed fuel debris decreases as the location of the detector moves away from the vertical center of a canister. The path length from fuel debris to the location of the detector increases by changes in the location from the vertical center, and the dose rate at the detector decreases since the dose rate is inversely proportional to the path length. Changes in the average dose rate are symmetrical up and down for the vertical center because loosely packed fuel debris are randomly distributed in the overall inner space of the canister. The maximum dose rate of each sample group is estimated when the height of the detector is zero (z = 0) which is the vertical center of a canister. The global maximum is estimated when the height of detector is zero (z = 0) and the minimum radius of sample group is 1 cm ($r_{min}$ = 1 cm). The average dose rate of the loose packed fuel debris decreases by increases in the size of debris for all vertical locations of the detector, and the width of the intense dose rate in the density plot decreases by increase of the size of debris. The density plot on the coefficient of variation has maximum at the top and the bottom of the graph, and the global maximum is at $r_{min}$ = 9 cm. In case of the close packed fuel debris, the maximum is biased downward from the vertical center of a canister, and the intense dose rate in the density plot is also biased. This is because the center of the canister is not the center of the closely packed fuel debris, and the vertical location of the maximum dose rate depends on the height of the pile of debris. The height of the close packed fuel debris depends on the size of debris, and it affects the path length from debris to detector. The changes in the path length changes the flux and dose rate, and the maximum of the average dose rate of the close packed fuel debris is biased to the downward with a unique pattern. The coefficient of variation is also biased, and its maximum is biased to upward of the density plot.

The neutron dose rate of the loose packed fuel debris is also symmetric like the photon dose rate, and the condition of its maximum is the same as that of photons. However, neutron dose rate does not decrease a lot by changes in size of debris, and the width of intense neutron dose rate in the density plot is very similar for all $r_{min}$. The neutron dose rate of the close packed fuel debris is biased downward like that of photons, but the pattern of its density plot is not the same as that of photons. The coefficient of variation of the neutron dose rate is a little bit smaller than that of photons, but patterns in the density plot are very similar. Thus, conditions for the maximum dose rate and its uncertainty are very similar with that of photons.

Sensitivity and uncertainty of dose rate is less affected by the size and distribution of fuel debris when it has been estimated far from a canister. The coefficient of variation of the estimated data is smaller than 5 % when the distance from the surface of the canister is further than 5 m. This is because the differences in path length by the distribution of fuel debris reduces to negligible when the distance is further enough. Variability of the estimated data is affected by the self-attenuation and the particle self-shielding at the long distance rather than the differences in path length. On the other hand, the distribution of fuel debris in a canister and the difference in path length by the distribution affects more on the variability of the estimated data when it has been estimated near a canister. Estimated data at a location close to a canister is more sensitive by changes in variables, and it has unique characteristics when it is visualized to a graph. Therefore, the error by uncertain size and distribution of fuel debris will be larger when dose rate or flux is estimated near a canister. Even if the expected error may not significantly affect the evaluation of shielding performance of a canister, but it may not be negligible when dose rate or flux is evaluated for the characterization of fuel debris. As an example of the practical use of the data estimated near a canister, the unknown size and distribution of fuel debris in a canister can be estimated by comparing the estimated data with the data measured near a canister. The error significantly affects this estimation, and it needs to be minimized to ensure a reliable estimation.

Two modified designs of canister are evaluated as examples to reduce the uncertainty of the estimated dose rate. The modified design with three small canisters helps to reduce the uncertainty of estimated data by limiting the distribution of fuel debris in small spaces. The modified design also helps to reduce the maximum dose rate measured near a canister by preventing concentration of fuel debris at a location. The modified design with four partitions has a smaller dose rate when the minimum radius of fuel debris in a sample group is larger than 2.5 cm. However, the design is less efficient than the design with three containers in reducing uncertainty.

Photon flux and uncertainty are evaluated for fuel debris in the transfer cask and the transport cask for the evaluation of their shielding performance and the understanding of changes in uncertainty. These two types of casks are efficient in photon shielding, and photons from fuel debris are attenuated a lot by these casks. However, the estimated data still has significant uncertainty, and its coefficient of variation is larger than that of a fuel canister. The coefficient of variation of the estimated data is larger for the transport cask than the transfer cask. This is because the transport cask has seven fuel canisters with fuel debris in uncertain size and distribution.

# Chapter 5. Conclusion and future works

## 5.1 Summary of results and conclusions

Nuclear radiation from damaged fuel debris was evaluated in this dissertation. The evaluation is focused on photon and neutron dose rate and their uncertainty which is caused by the uncertain conditions of the fuel debris. The uncertain condition of fuel debris was simulated by Monte Carlo method, and size and distribution of fuel debris in a canister were randomly sampled by the model developed at chapter 3. Randomly sampled variables were used for the inputs of SCALE, and dose rate and flux are estimated by SCALE and the analytical model developed at chapter 3. The uncertain condition of fuel debris which was simulated by the random sampling method caused deviations of the estimated dose rate, and the uncertainty of dose rate was evaluated by calculating the standard deviation of dose rate and the coefficient of variation. Sensitivity of dose rate or flux by changes in variables was evaluated by calculating the sensitivity index.

Factors which affect the uncertainty of nuclear radiation are categorized to three which are source term, physical condition of fuel debris, geometric condition of fuel debris in a canister. The source term is types and amounts of radioactive material in fuel debris, and it is the factor that has the greatest influence on variability of the estimated dose rate and flux. It has been calculated by the ORIGEN module of SCALE, and burnup history of 1FNPP was used for the calculation. Variability of the nuclear radiation by changes in the source term was evaluated for changes of the source term by burnup and isotope release. The burnup is the major factor which decides the source term, and neutron intensity from fuel debris is more sensitive by the change of burnup than photon intensity does. Fission products including cesium is the major source of photon whereas actinides including $^{244}Cm$ is the major neutron source according to the evaluation. A lot of noble gases and volatiles have been released after the 1FNPP accident, and it changed the material composition of fuel debris. The variability of source term by the isotope release was evaluated by the ORIGEN module of SCALE. The major isotopes which affect the estimation of dose rate were decided before the evaluation, and then source term was calculated by modifying weight percent of each isotope from 10 % to 100 %. SCALE calculated photon and neutron dose rate for each modification, and variability of dose rate by changes in amounts of isotopes by the release was evaluated. Photon dose rate is sensitive by changes of the amount of cesium and strontium isotopes, and neutron dose rate is sensitive by changes of the amount of curium isotopes. Physical condition of fuel debris is focused on the density of fuel debris and it has been decided by referencing reports of JAEA on the composition of damaged fuel in 1FNPP reactors. Fuel debris are in diverse density depending on the location of retrieved debris according to the TMI-2 reports. However, it has been assumed to be the same for fuel debris in a canister at this dissertation. Variability and uncertainty of the nuclear radiation by changes in the geometric condition in a canister is the major topic of this dissertation, and the geometric condition is focused on the size and distribution of fuel debris in a canister. The uncertain condition of fuel debris was simulated by the random sampling on the size and the distribution of fuel debris in a canister, and the uncertainty of dose rate was evaluated by the coefficient of variation of dose rate or flux. In addition to this, percent relative range was also calculated to show that possible error of measurement in dose rate can be larger than estimated coefficient of variation.

A model for the evaluation of the radiation dose rate has been developed at chapter 2 of this dissertation, and it was updated at chapter 3 for the evaluation of uncertainty. Conceptual designs of canisters were decided for the evaluation by referencing reports on TMI-2 and 1FNPP accident. Python based code was made for the random sampling of size and distribution of fuel debris in a canister, and the code converts the random sampled data to SCALE input scripts. Distribution or packing of fuel debris in a canister is categorized to two types which are the loose packed debris and the close packed debris, and dose rates of these two types of packing were compared. The loose packed fuel debris are randomly distributed in an inner space of the canister. The close packed fuel debris is also randomly placed in a canister, but debris are in contact with each other and have randomly placed voids. The shape of fuel debris was assumed to be a sphere, but non-spherical shapes were also approximately modeled by the close packing of fuel debris. The radiation dose rate of the loose packed fuel debris is almost continuously changed by changes in the size of fuel debris. On the other hand, the change of dose rate of close packed fuel debris is discontinuous by changes in variables. For the vertical locations of estimation or height of detectors, the dose rate of the loose packed fuel debris is symmetrical up and down with respect to the vertical center of a canister whereas that of the close packed fuel debris is biased to down. This lets us know that types of packing of fuel debris can be estimated by identifying the height of the detector for the maximum dose rate near a canister. The maximum of dose rate will be measured at near the vertical center of a canister if fuel debris are loosely packed, or it will be measured at the location biased to down if fuel debris are closely packed in a canister. The dose rate of the close packed fuel debris can be larger or lesser than that of the loose packed fuel debris depending on the height of the detector. Maximum dose rate of the close packed fuel debris also can be larger or smaller than that of the loose packed fuel debris depending on the condition of fuel debris. The dose rate of the close packed fuel debris can be larger than that of the loose packed fuel debris when it is estimated at a location horizontally close from the canister, and opposite each other at a location horizontally far from the canister. This variability is due to three factors which are path difference, self-attenuation of radiation in fuel debris, particle self-shielding effect. The path difference is the difference in path length of fuel debris, and the path length is the distance from the debris to the location of the detector. The path difference dominates near a canister whereas the other two affect more at far from a canister, and this causes the variability. However, maximum values of these two types are similar and their differences are not large.

Evaluation of dose rate and uncertainty takes a long time if SCALE is used for the calculation. Therefore, a model was proposed to analytically calculate the approximate value. The model was developed based on three factors which are path difference, self-attenuation, particle self-shielding, and it was used for the calculation of photon flux from fuel debris in a canister. The model does not use the method of random walk for the particle transport, and it approximately calculates attenuation of radiation in linear paths. Lambert-Beer law is the basis of the model, and all radiation is assumed to be generated from at the center of each fuel debris by applying the point source approximation. The exponential function of Lambert-Beer law is modified by the self-attenuation of nuclear radiation, and particle self-shielding of radiation in medium between fuel debris is reflected at the function by applying models of Shmakov and Yamamoto. The model of Shmakov and Yamamoto is modified by applying a method which divides radius of fuel debris in each

sample group into 11 groups, and then it is applied to calculate the effective attenuation coefficient. Even though the estimation of the model has errors when the size of fuel debris is small, its output was similar with the estimation of SCALE. Error and discordance of the estimated data is because the model is developed based on methods which have approximations.

Uncertainty of radiation dose rate is evaluated by the standard deviation and the coefficient of variation, and it is visualized as a line plot and a density map. The graph of uncertainty is discontinuous by changes in the size of fuel debris, and it is not easy to be fitted to a simple formula. Therefore, a method which converts data to cumulative values was proposed at chapter 3, and data was fitted to simple functions after conversion by the method. When doing data fitting, Monte Carlo method was used instead of an analytical calculation, and the coefficient of the function is automatically decided.

Sensitivity of photon flux by changes in the distance from a canister to a detector was evaluated for the loose packed and the close packed fuel debris in chapter 4. Sensitivity of the close packed fuel debris is larger than that of the loose packed fuel debris, and photon flux is more sensitive by changes in the distance when the distance is closer than 400 cm. The estimated sensitivity of photon flux was visualized as a density map, and its pattern is variable by changes in the size of fuel debris. Therefore, the estimated sensitivity of photon flux is good for the characterization of fuel debris, and its data can be applied for the estimation of the unknown condition of fuel debris in a canister.

Radiation dose rate and uncertainty of fuel debris in uncertain condition was evaluated in this dissertation. Topics of research and developed models in this dissertation were studied considering usage for the retrieval of fuel debris in 1FNPP. However, application of methods and output data of this research are not limited to 1FNPP, and they can be applied for possible nuclear accidents in the future. Methods proposed in this dissertation pursue to save time and computational expenses which are required for the Monte Carlo simulation. Especially, the analytical model of this dissertation can estimate the photon flux and uncertainty of fuel debris a lot faster than SCALE does. The methods of multiprocessing and parallel computing used in this dissertation can enhance the efficiency of evaluation. Estimated data and results of the data fitting can be utilized for the characterization of fuel debris in uncertain condition.

## 5.2 Recommendations for future works

The model developed in this dissertation assumed the shape of fuel debris to be a sphere. However, the shape of actual fuel debris is diverse and non-spherical. Even if the non-spherical shape of fuel debris is approximately simulated by applying the concept of close packing of spheres, there are differences between the approximated model and the real fuel debris. Therefore, the model needs to be supplemented by adding non-spherical debris with random sampling on their shapes for more realistic simulation.

Dose rate and uncertainty of fuel debris in a canister is the main topic of this dissertation, and its characteristics were understood by studies. However, characteristics of a single fuel canister are not the same as that of multiple canisters which are in a storage cell. Even if the photon flux from a transport cask with seven canisters was evaluated at chapter 4, estimation on the flux from many canisters in a storage cell is still required. As a future work, evaluation on the uncertainty for canisters in a storage cell is recommended. Visualization of the uncertainty in a form of density plot will be helpful for the management of the retrieved fuel debris.

SCALE is reliable and it uses advanced methods for more efficient calculation. However, SCALE does not efficiently use the capability of modern computing devices which have high performance CPU and RAM. Therefore, a python code was developed for the efficient use of the CPU and RAM by applying methods of multiprocessing and parallel computing. As a future work, an update on the SCALE code for efficient utilization of the modern computing devices is recommended. Implementing methods for the efficiency into its source code will be better than the use of the supplementary code.

Monte Carlo method was used for the data fitting instead of an analytical calculation at Chapter 3. The method is handy and automatically finds the coefficient of a function. However, it can take a long time when a data has many local optimums. Therefore, the method needs to be updated by applying optimization methods such as gradient descent.

**Bibliography**

[1] TEPCO, Technical Strategic Plan 2017 for Decommissioning of the Fukushima Daiichi Nuclear Power Station of Tokyo Electric Power Company Holdings, Inc., 2017, Nuclear damage compensation and decommissioning facilitation corporation, 2017

[2] TEPCO, Technical Strategic Plan 2020 for Decommissioning of the Fukushima Daiichi Nuclear Power Station of Tokyo Electric Power Company Holdings, Inc., Nuclear damage compensation and decommissioning facilitation corporation, 2020

[3] IAEA, The Fukushima Daiichi Accident technical volume 1 description and context of the accident, 2015

[4] Richard K. McCARDELL, et al., SUMMARY OF TMI-2 CORE SAMPLE EXAMINATIONS, 1990, Nuclear Engineering and Design 118 (1990) 441-449

[5] G. Lassahn, Uranium and Plutonium Content of TMI-2 Defueling Canisters, 1993, EG&G Internal technical report, September 1993.

[6] D.W. Akers et al., Examination of relocated fuel debris adjacent to the lower head of the TMI-2 reactor vessel, 1994, NUREG/CR-6195 TMI V(92)EG10 EGG-2732

[7] Historical summary of the three mile island unit 2 core debris transportation campaign, Idaho national engineering laboratory, DOE/ID-10400, 1993

[8] Hiroki Takezawa & Toru Obara, Passive measure for preventing recriticality of fuel debris dust for defueling at Fukushima Daiichi nuclear power station, 2016, Journal of Nuclear Science and Technology, 53:12, 1960-1967

[9] María Freiría López, Michael Buck and Jörg Starflinger, A CONSERVATIVE CRITICALITY ANALYSIS OF FUEL DEBRIS IN FUKUSHIMA, ERMSAR 2019, March 18-20, 2019

[10] Eka Sapta Riyana, Keisuke Okumura & Kenichi Terashima, Calculation of gamma and neutron emission characteristics emitted from fuel debris of Fukushima Daiichi Nuclear Power Station, Journal of Nuclear Science and Technology, 56:9-10, 922-931

[11] X. Liu, J. Ahn, and F. Hirano, “A Criticality Safety Study for the Disposal of Damaged Fuel Debris,” presented at the International High-Level Radioactive Waste Management Conference, Charleston, SC, USA, 2015.

[12] JAEA, JAEA report (燃料デブリの処理・処分に関する予察的調査), 2016, JAEA

[13] JAEA, Estimation of Fuel Compositions in Fukushima-Daiichi Nuclear Power Plant, 2012, JAEA

[14] B.T. Rearden, M.A. Jessee, Editors, SCALE Code System, ORNL/TM-2005/39 Version 6.2.2, 2017

[15] A. G. Croff, A User's Manual ORIGEN2 Computer Code, ORNL/TM-7175

[16] US. DOE, TMI Fuel Characteristics for Disposal Criticality Analysis, DOE/SNF/REP-084, 2003

[17] Study on volatile isotopes released during a nuclear accident applied to MTR reactor, F. Zeggar, H. Berkoune, Nuclear ractors and generation 4, 2013.

[18] M.J. Berger et al. NIST (National Institute of Standards and Technology) standard reference database 8 (XGAM), DOI : https://dx.doi.org/10.18434/T48G6X

[19] Francois, J.P., 1974. "On the calculation of the self-absorption in spherical radio-active sources", Nuclear Instruments and Methods 117, 153–156.

[20] J. K. DICKENS (1972), "Self-absorption of gamma rays produced in large cylindrical samples", nuclear instrument and methods 98 (I972) 451-454;

[20] ERNESTO TRUCCO (1964), "Self -absorption in spheres and cylinders of radioactive material", Bulletin of mathematical biophysics VOLUME 26, 1964

[21] K.A.A. Gamage, M. J. Joyce (2011), "An analytical approach to g-ray self-shielding effects for radioactive bodies encountered nuclear decommissioning scenarios", Applied Radiation and Isotopes 69 (2011) 1521–1532

[22] V. M. Shmakov, V. D. Lyutov, V. F. Dean, ''Effective cross section for calculations of criticality of dispersed media,'' Proc. PHYSOR 2000, Pittsburgh, PA, USA, May 7–11, 2000, (2000).

[23] Toshihiro Yamamoto, Yoshinori Miyoshi & Toshikazu Takeda (2006), "Extension of Effective Cross Section Calculation Method for Neutron Transport Calculations in Particle-dispersed Media, Journal of Nuclear Science and Technology", 43:1, 77-87

[24] Three mile accident of 1979 knowledge management digest recovery and cleanup, NUREG/KM-0001, Supplement 1, Office of nuclear regulatory research, 2016

# Appendix A Preliminary study

## A. 1 Estimated weight of materials in TMI-2 canisters

Gordon Lassahn of the Idaho National Engineering Laboratory has estimated the weight of materials in TMI-2 canisters based on limited data [1]. He used data on the payload of major materials contained at each canister, and data sheets on the number and length of fuel assemblies at each canister. Plots at this chapter are plotted based on the estimated data of Lassahn, and Python has been used for the visualization of data. Payload of materials at each canister includes fuel debris, fuel assemblies, structural components and other materials. Fuel assemblies at each canister are damaged by the partial core melting of TMI-2 reactor, and they have been cut during the retrieval process. Therefore, the length of fuel assemblies at each canister are uneven. Number of structural materials is also approximated because they were broken and melted out by the accident. Amount of fuel debris was also briefly estimated because of the limited information.

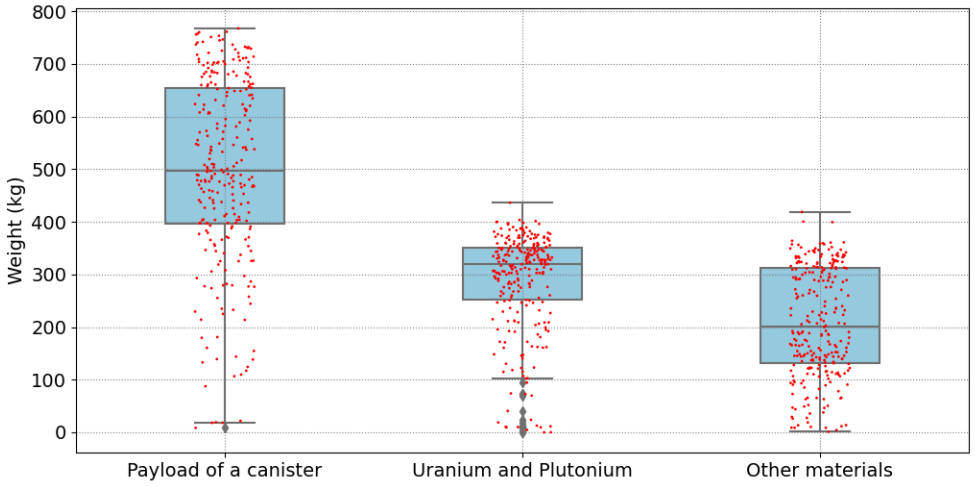


**Figure A.1 Box plot on the weight of payload and SNM in each canister of TMI-2 reactor.** This graph is the same as the graph at Figure 1.1 at Chapter 1.2.3. Data at this graph is on the payload of fuel canister only, and other two types of canisters are excluded. The box plot at left is on the payload, and at center is on the weight of uranium and plutonium at each canister, at right is on the weight of other materials at each canister. Red dots are the estimated amount at each canister. The height of the box is the interquartile range. The lowest line of the box is the 25th percentile (Q1), and the line at the top of the box is the 75th percentile (Q3). The height of the box is the interquartile range (IQR), and the horizontal line in a box is the median value of dose rate (Q2). The horizontal line at the lowest end of the vertical line is the minimum which is Q1 – 1.5 * IQR. The horizontal line at the top of the vertical line is the maximum which is Q3 + 1.5 * IQR. Gray dots outside of the maximum and minimum are outliers. Outliers are larger than the maximum or smaller than the minimum, and the difference between the maximum outlier and the minimum outlier is the largest value of possible variability in the measurement.

Payload of fuel canisters at the graph is widely scattered with the standard deviation of 175.4 kg (Figure A.1). The maximum payload is 767.5 kg, and the minimum is 8.6 kg. Average of the payload is 498.5 kg, and median value is 497.8 kg. Many canisters have 300 ~ 400 kg of uranium and plutonium, but the amount at other canisters is diverse. The maximum amount of special nuclear materials (SNM) at a canister is 436.4 kg and two canisters do not have SNM. Average of the weight of SNM is 288.4 kg, and the median is 320.3 kg. Standard deviation of the weight of SNM is 95.1 kg. Weight of other materials is also a lot scattered, and its standard deviation is 103.1 kg. The average weight of other materials is 210.2 kg, and the median is 201.5 kg. The maximum weight of other materials is 418.9 kg, and the minimum is 1.1 kg. The average weight percent of uranium in each canister is 52.3 %, and the standard deviation is 13.7 %. Weight percent of uranium and other material in each canister is plotted on the graph at Figure A.2. Weight percent of uranium at many canisters is 52.4 %, and this is visualized as concentrated red dots on the box plot. These biased and concentrated red dots are made because canisters for these red dots contain fuel debris only. Weight of SNM per weight of debris is assumed to be the same for all debris with 10% of uncertainty, and this assumption resulted in the biased data for fuel canisters with debris only. Weight of debris in each canister and their weight percent are at box plot of Figure A.3 and Figure A.4. Biased and concentrated red dots at these box plots are also because a lot of canisters have debris only or do not have debris. Weights of canisters which contain debris and fuel assemblies both are a lot scattered on box plots.

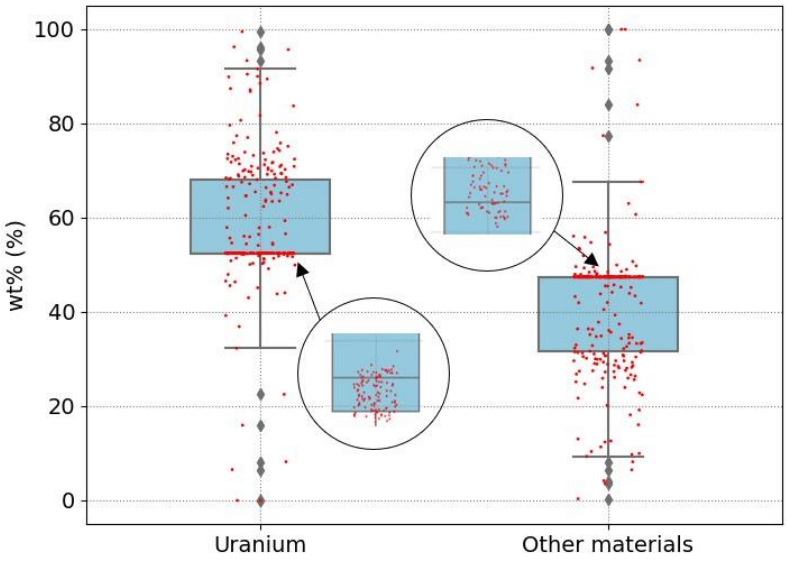


**Figure A.2 Weight percent of uranium and other materials in each canister.** Data of the biased and concentrated red dots are enlarged at two circles.

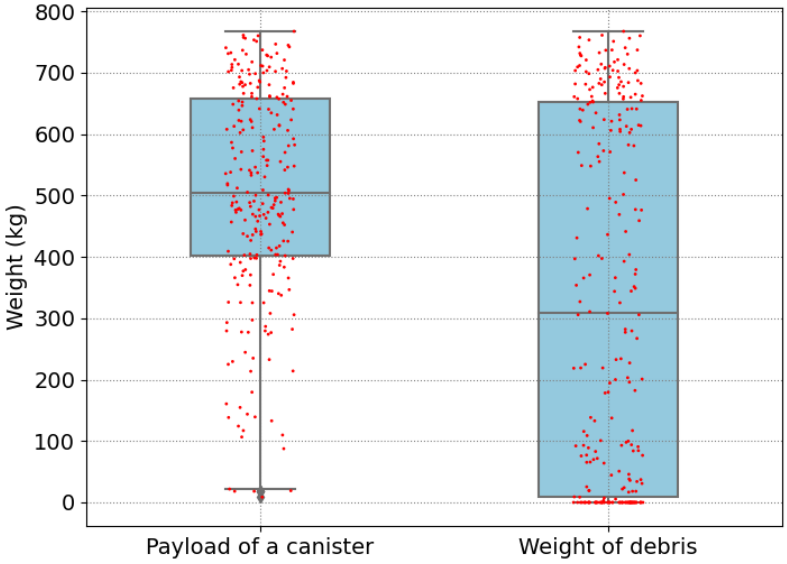


**Figure A.3 Weight of debris in each canister.** Box plot at the left is payload of a canister, and a the right is weight of debris.

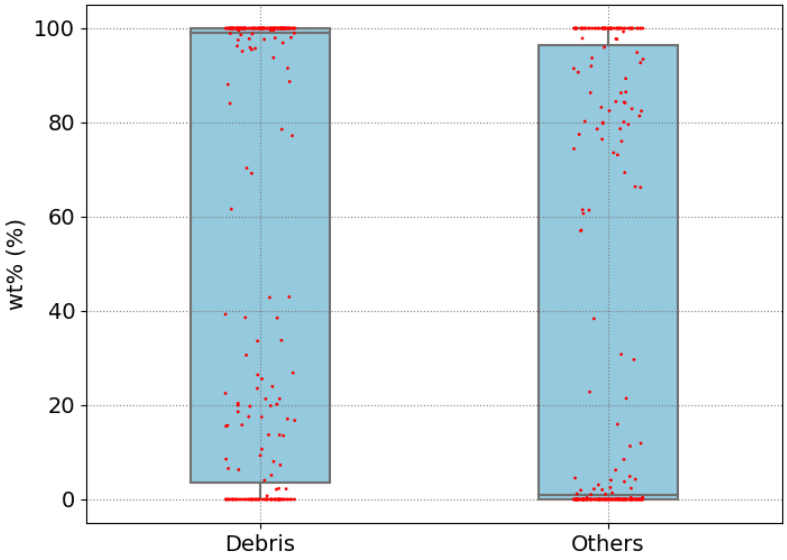


**Figure A.4 Weight percent of debris in each canister.** Box plot at left is the weight percent of debris in each canister, and at right is for others.

Weight of $^{235}$U in each canister is also a lot scattered on the box plot because it has been calculated based on the weight of uranium in each canister and assumed enrichment (Figure A.3). The maximum weight of $^{235}$U in a canister is 10.1 kg. The average weight of $^{235}$U is 6.4 kg, and the standard deviation is 2.19 kg. Weight of plutonium is much smaller than uranium, and the maximum weight is 0.94 kg. Average weight of the plutonium in a canister is 0.56 kg, and its standard deviation is 0.2 kg.

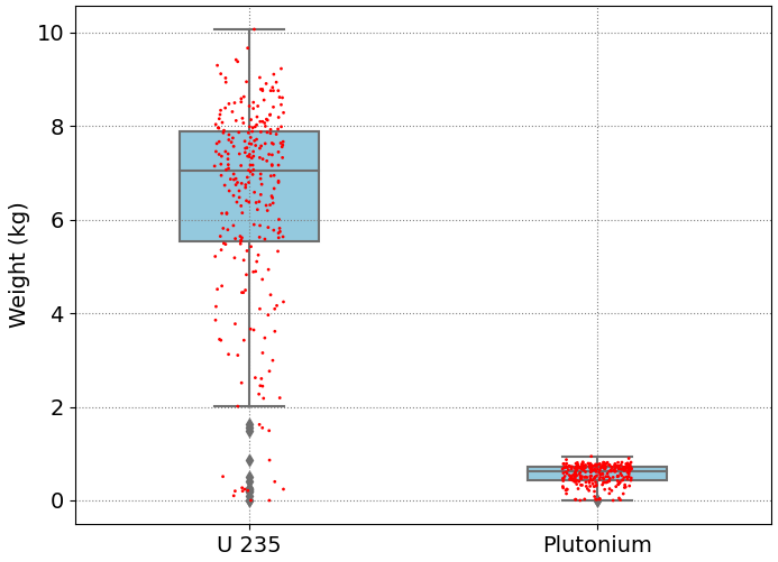


**Figure A.5 Weight of $^{235}$U and plutonium in a canister.** The box plot at left is on the weight of $^{235}$U, and plot at right is on the weight of plutonium.

Other two types of canisters have been used for the retrieval of TMI-2 fuel debris. One is the knockout canister which was used for fuel debris in the form of small particles. Another is the filter canister which were used for fuel debris in fine particles which are smaller than 850 $\mu m$. These canisters were used by connecting to the hydraulic vacuum systems which inhales particles into the two types of canisters. 62 of filter canisters and 12 of knockout canisters had been used for the retrieval of small particles. The maximum payload of a filter canister is 411 kg, and payload of 22 canisters are estimated to be zero (Figure A.6). The maximum weight of SNM at a filter canister is 216 kg. The maximum payload of knockout canister is 842 kg, and the maximum weight of SNM is 442.8 kg. The payload of a knockout canister is estimated to zero (Figure A.7).

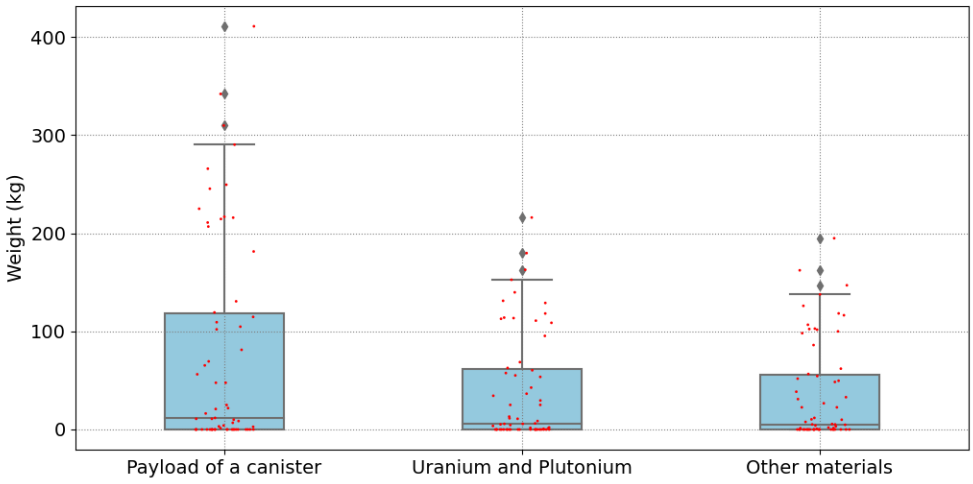


**Figure A.6 Box plot on the weight of payload and SNM in each filter canister of TMI-2 reactor.** Box plot on the left is for the payload of each canister, center is for the weight of uranium and plutonium, right is for the weight of other materials.

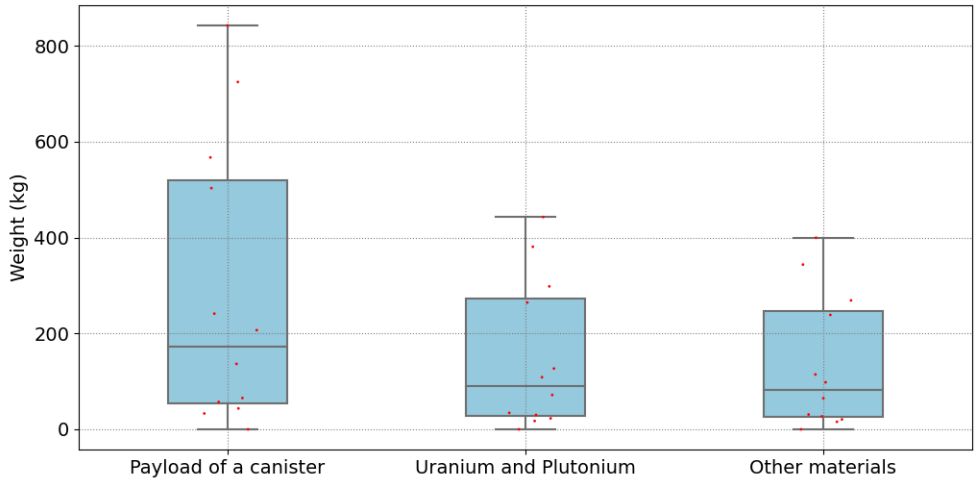


**Figure A.7 Box plot on the weight of payload and SNM in each knockout canister of TMI-2 reactor.** Box plot on the left is for the payload of each Knockout canister, center is for the weight of uranium and plutonium, right is for the weight of other materials.

## A. 2 Comparison of the estimated dose rate of SCALE and MCNP

Radiation dose rate of fuel debris in a fuel canister has been estimated by using MCMP and its results have been compared with the estimated dose rate by SCALE. Design of the fuel canister is the same with the basic design at chapter 2, and assumptions in chapter 2 have been used with some exceptions. At this comparison, isotope composition of fuel debris is simplified to $UO_2$, and inside of the fuel canister and outside of the canister is filled with dry air. Dose rate has been estimated from the surface of the fuel canister to 100m. Region tally has been used for the estimation by assuming 20 cylindrical regions, and dose rates are averaged at each region (Figure A.8).

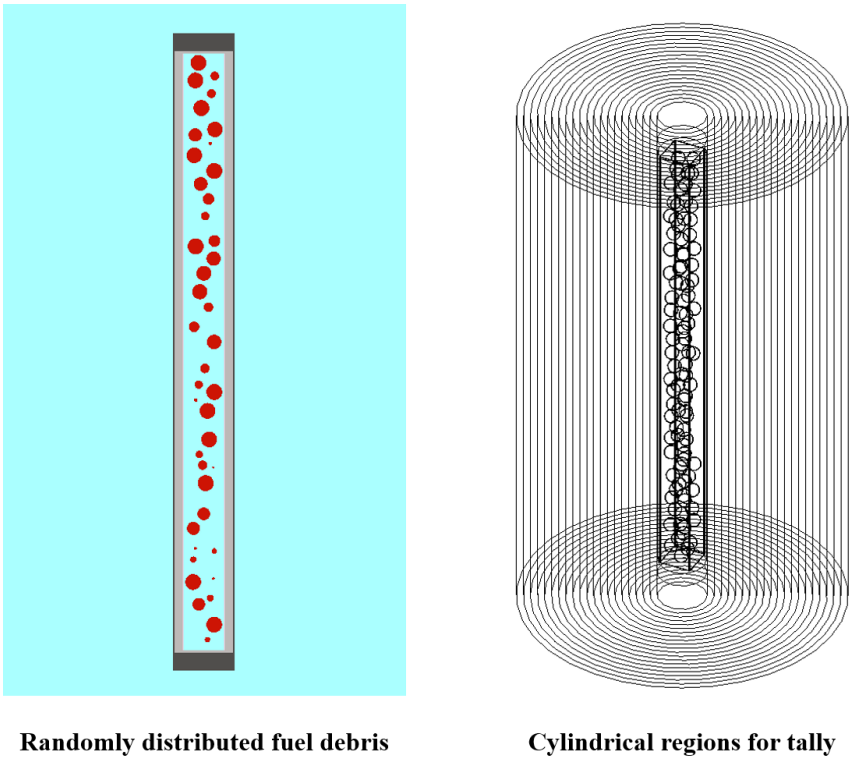


Figure A.8 Cross sectional view of the fuel debris in a canister. Figure at the left is a cross sectional view of the fuel canister with 100 debris spheres in it. Red spheres are fuel debris which are assumed to $UO_2$ spheres. Figure at the right is 20 cylindrical regions which has been used to calculate the average dose rate in each region.

Estimated neutron dose rate from the two codes is very similar, and SCALE neutron dose rate is 0.07% ~ 0.25 % higher than MCNP dose rate (Figure A.9). Photon dose rate is comparatively more different, and SCALE photon dose rate is 3.07 % ~ 4.97% lower than MCNP dose rate (Figure A.10).

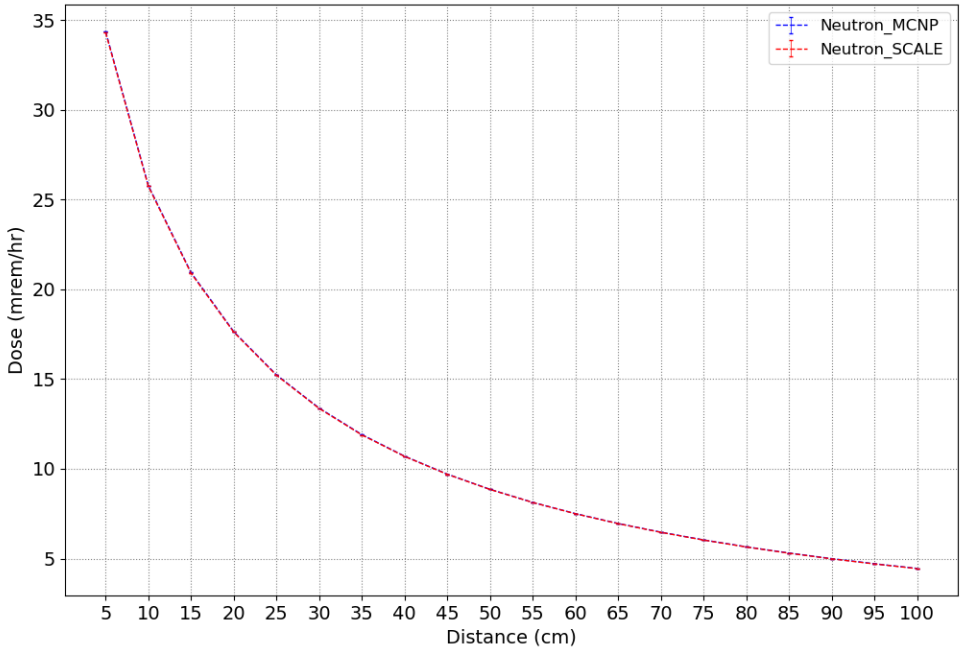


**Figure A.9 Comparison of neutron dose rate** between SCALE and MCNP. Blue line is the dose rate of MCNP and the red line is the dose rate of SCALE.

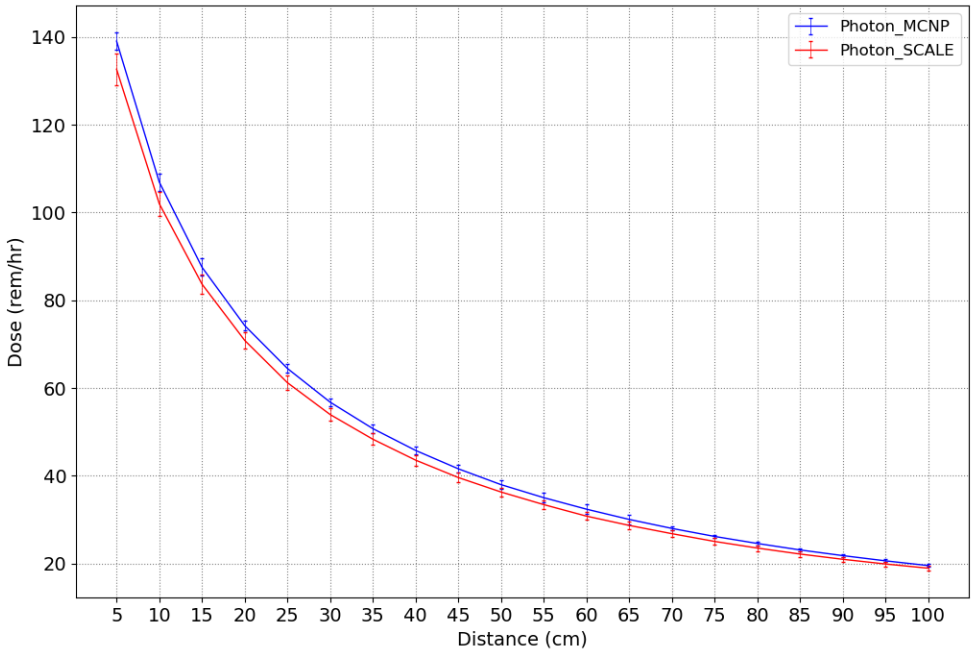


**Figure A.10 Comparison of photon dose rate** between SCALE and MCNP. Blue line is the dose rate of MCNP and the red line is the dose rate of SCALE.

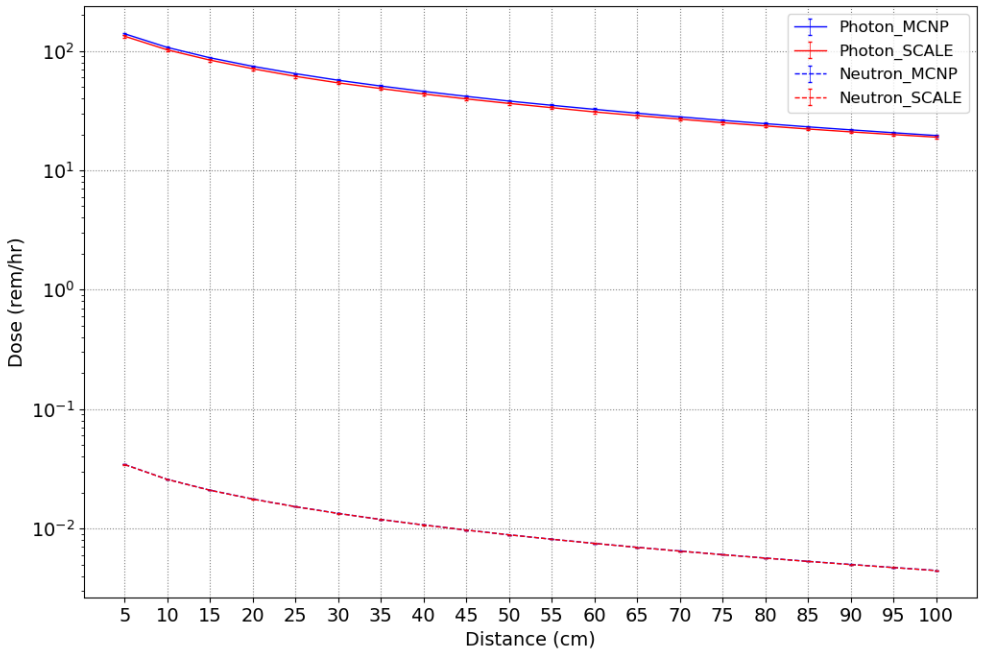


**Figure A.11 Comparison of dose rate between SCALE and MCNP.** Neutron and photon dose rates at figure A.9 and A.10 are plotted at a graph. Y-axis is the dose rate in log scale.

**Table A.1 Dose rates from fuel debris in a fuel canister**

| Distance (cm) | Photon dose rate | | | Neutron dose rate | | |
|---|---|---|---|---|---|---|
| | MCNP (rem/hr) | SCALE (rem/hr) | Difference (%) | MCNP (mrem/hr) | SCALE (mrem/hr) | Difference (%) |
| 5 | 139.0550±1.99 | 132.6400±3.63 | 4.61 | 34.3684±0.014 | 34.3257±0.038 | 0.12 |
| 10 | 106.9230±1.53 | 101.9900±2.78 | 4.61 | 25.7845±0.010 | 25.7443±0.028 | 0.16 |
| 15 | 87.5212±1.25 | 83.6745±2.28 | 4.40 | 20.9360±0.006 | 20.9021±0.022 | 0.16 |
| 20 | 74.2286±1.08 | 70.8491±1.93 | 4.55 | 17.6466±0.005 | 17.6170±0.019 | 0.17 |
| 25 | 64.4553±0.93 | 61.2152±1.67 | 5.03 | 15.2361±0.005 | 15.2135±0.016 | 0.15 |
| 30 | 56.7780±0.82 | 53.9582±1.47 | 4.97 | 13.3831±0.004 | 13.3625±0.014 | 0.15 |
| 35 | 50.7482±0.73 | 48.3314±1.32 | 4.76 | 11.9075±0.004 | 11.8881±0.013 | 0.16 |
| 40 | 45.7795±0.66 | 43.5709±1.19 | 4.82 | 10.7048±0.003 | 10.6929±0.011 | 0.11 |
| 45 | 41.5952±0.60 | 39.6027±1.08 | 4.79 | 9.7042±0.003 | 9.6959±0.010 | 0.09 |
| 50 | 37.9849±0.55 | 36.3046±1.00 | 4.42 | 8.8579±0.003 | 8.8513±0.009 | 0.07 |
| 55 | 35.0163±0.51 | 33.4330±0.92 | 4.52 | 8.1323±0.002 | 8.1266±0.009 | 0.07 |
| 60 | 32.3944±0.47 | 30.8074±0.85 | 4.90 | 7.5043±0.003 | 7.4983±0.008 | 0.08 |
| 65 | 30.0577±0.44 | 28.6942±0.80 | 4.54 | 6.9559±0.003 | 6.9478±0.008 | 0.12 |
| 70 | 28.0105±0.41 | 26.8100±0.75 | 4.29 | 6.4716±0.003 | 6.4631±0.007 | 0.13 |
| 75 | 26.1814±0.38 | 25.0429±0.70 | 4.35 | 6.0413±0.002 | 6.0322±0.007 | 0.15 |
| 80 | 24.5807±0.36 | 23.5322±0.66 | 4.27 | 5.6560±0.002 | 5.6472±0.006 | 0.16 |
| 85 | 23.1041±0.34 | 22.1653±0.62 | 4.06 | 5.3107±0.002 | 5.2995±0.006 | 0.21 |
| 90 | 21.8119±0.32 | 20.9729±0.59 | 3.85 | 4.9976±0.002 | 4.9864±0.005 | 0.22 |
| 95 | 20.6222±0.30 | 19.9027±0.56 | 3.49 | 4.7128±0.002 | 4.7030±0.005 | 0.21 |
| 100 | 19.5424±0.29 | 18.9418±0.53 | 3.07 | 4.4528±0.002 | 4.4417±0.005 | 0.25 |

## A. 3 Fuel group summary of TMI-2 and 1FNPP nuclear reactors

**Table A. 2 Initial loading and average burnup of 1FNPP nuclear reactors**

| Parameters | TMI-2 | 1F Unit1 | 1F Unit2 | 1F Unit3 |
|---|---|---|---|---|
| **Power (MWt)** | | 1380 | 2381 | 2381 |
| **U-235 enrichment (wt%)** | | 3.7 | 3.7 | 3.7 |
| **number of fuel assembly** | | 400 | 548 | 548 |
| **Initial loading of uranium (ton)** | | 69 | 94 | 94 |
| **Specific power (MW/tHM)** | | 20 | 25.3 | 25.3 |
| **Average burn up (GWd/tHM)** | 3.25 | 25.8 | 23.1 | 21.8 |

**Table A. 3 Fuel group summary of TMI-2**

| Fuel group | Number of fuel nodes | Initial Enrichment (wt%) | Initial Uranium (MT) | Average Burnup (MWd/MTU) | Minimum Burnup (MWd/MTU) | Maximum Burnup (MWd/MTU) |
|---|---|---|---|---|---|---|
| 1 | 72 | 1.98 | 4.7684 | 1863 | 1436 | 2240 |
| 2 | 68 | 1.98 | 4.5035 | 2746 | 2488 | 3158 |
| 3 | 152 | 1.98 | 10.067 | 3637 | 3190 | 4021 |
| 4 | 100 | 1.98 | 6.6228 | 4391 | 4087 | 4905 |
| 5 | 105 | 2.64 | 6.9540 | 2239 | 1647 | 2741 |
| 6 | 76 | 2.64 | 5.0334 | 3552 | 2810 | 3890 |
| 7 | 230 | 2.64 | 15.233 | 4315 | 3907 | 4952 |
| 8 | 16 | 2.64 | 1.0597 | 5465 | 5227 | 6213 |
| 9 | 136 | 2.96 | 9.0071 | 1548 | 910 | 2020 |
| 10 | 164 | 2.96 | 10.861 | 2644 | 2100 | 3143 |
| 11 | 76 | 2.96 | 5.0334 | 3554 | 3261 | 4192 |
| 12 | 44 | 2.96 | 2.9140 | 4878 | 4453 | 5572 |

**Table A. 4 Fuel group summary of 1F unit 1**

| | | Fuel group / Number of fuel assemblies | | | | | |
|---|---|---|---|---|---|---|---|
| | | 1 | 2 | 3 | 4 | 5 | 6 |
| | | 64 | 64 | 80 | 68 | 64 | 60 |
| Irradiation History (dates) | 189 | 27.69 | 24.76 | 21.47 | 18.08 | 15.05 | 12.21 |
| | 341 | | 30.93 | 26.11 | 21.34 | 17.66 | 14.16 |
| | 349 | | | 32.29 | 25.69 | 21.13 | 16.75 |
| | 445 | | | | 30.69 | 25.11 | 19.73 |
| | 346 | | | | | 29.09 | 22.70 |
| | 413 | | | | | | 25.55 |
| Burnup (MWd/MTU) | | 5,234 | 15,228 | 24,231 | 33,315 | 37,479 | 40,172 |

**Table A. 5 Fuel group summary of 1F unit 2**

| | | Fuel group / Number of fuel assemblies | | | | |
|---|---|---|---|---|---|---|
| | | 1 | 2 | 3 | 4 | 5 |
| | | 116 | 116 | 120 | 120 | 76 |
| Irradiation History (dates) | 113 | 29.34 | 27.19 | 25.00 | 22.77 | 20.95 |
| | 390 | | 32.68 | 29.09 | 25.26 | 22.60 |
| | 336 | | | 35.13 | 28.93 | 25.03 |
| | 400 | | | | 32.65 | 27.49 |
| | 333 | | | | | 29.95 |
| Burnup (MWd/MTU) | | 3,315 | 15,817 | 25,972 | 35,205 | 40,557 |

**Table A. 6 Fuel group summary of 1F unit 3**

| | | Fuel group / Number of fuel assemblies | | | | | |
|---|---|---|---|---|---|---|---|
| | | 1 (MOX) | 1 (UO2) | 2 | 3 | 4 | 5 |
| | | 32 | 116 | 112 | 140 | 112 | 36 |
| Irradiation History (dates) | 169 | 26.67 | 28.06 | 26.46 | 24.68 | 22.91 | 21.87 |
| | 339 | | | 32.53 | 28.20 | 24.58 | 22.60 |
| | 438 | | | | 33.71 | 27.18 | 23.73 |
| | 403 | | | | | 29.99 | 24.95 |
| | 334 | | | | | | 26.03 |
| Burnup (MWd/tHM) | | 4,507 | 4,742 | 15,497 | 28,497 | 36,196 | 40,499 |

## A. 4 Comparison of the estimated dose rate for SCALE and JAEA data

Photon dose rate has been estimated by using SCALE with photon source term from ORIGEN-ARP, and then it has been compared with the estimated dose rate which used photon source term of JAEA. JAEA estimated the source term of 1FNPP fuel debris by using ORIGEN 2.0 and JENDL nuclear data library. JAEA grouped photon energy in 18 groups which is predetermined by ORIGEN 2.0. On the other hand, we have used ORIGEN-ARP of SCALE with ENDF/B-VII.1, and photon energy has been grouped in 101 groups for better details in use of continuous energy (CE) library. This affected the estimated radiation dose rate, and there is a difference between output data from these two codes. The estimated dose rate by ORIGEN-ARP is larger than the estimation of ORIGEN 2.0 because of differences in use of data library and details in energy groups (Figure A.12). 101 energy groups from ORIGEN-ARP are averaged and fitted to 18 groups of JAEA data, and this resulted in differences in source term. Especially, there are comparatively large differences in low energy photons. The difference in low energy groups is the major cause of the discrepancy, and this can be reduced by ignoring low energy photons below 100 keV (Figure A.13).

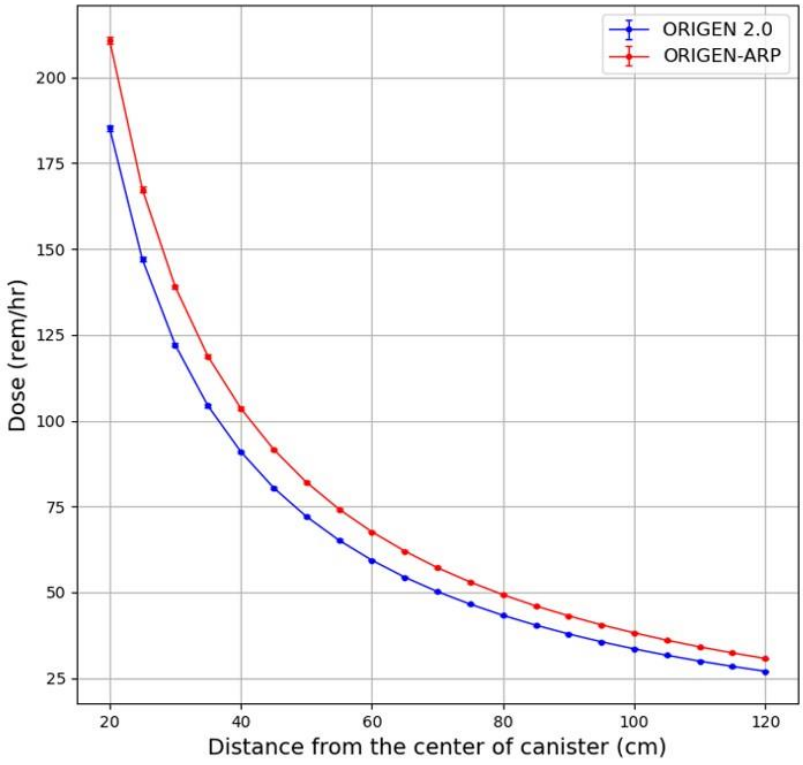


**Figure A.12 Comparison of photon dose rate** between output data by source term from ORIGEN-ARP and ORIGEN 2.0. Red line is the dose rate calculated with the ORIGEN-ARP module of SCALE. Blue line is the dose rate calculated with ORIGEN 2.0.

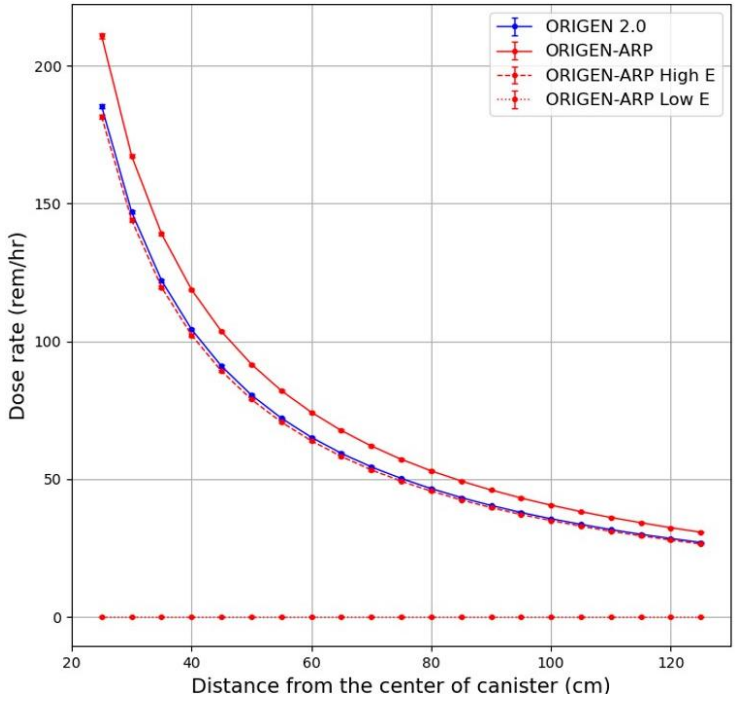


**Figure A.13 Comparison of photon dose rate.** Red thick dashed line is the dose rate of high energy photons, and the thin dashed line is the dose rate of low energy photons.

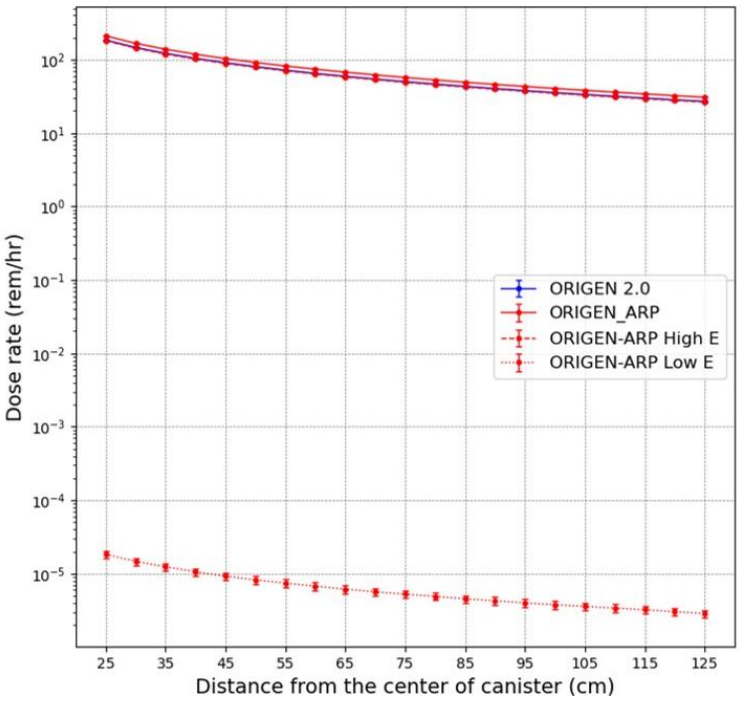


**Figure A.14 Comparison of photon dose rate.** The Y-axis of the figure A.13 is converted to log scale.

## A. 5 Modified conceptual designs of canisters (1FNPP data has been referenced)

### A. 5. 1 1F Ver.1 Fuel canister

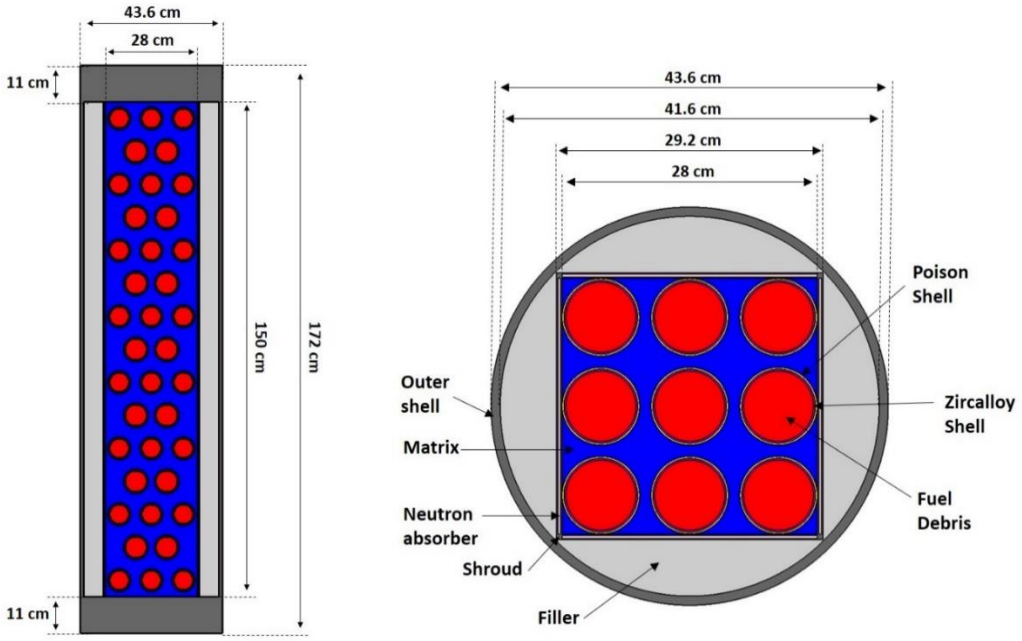


**Figure A. 15 The modified design of the fuel canister**

### A. 5. 2 Ver.1 Knockout canister

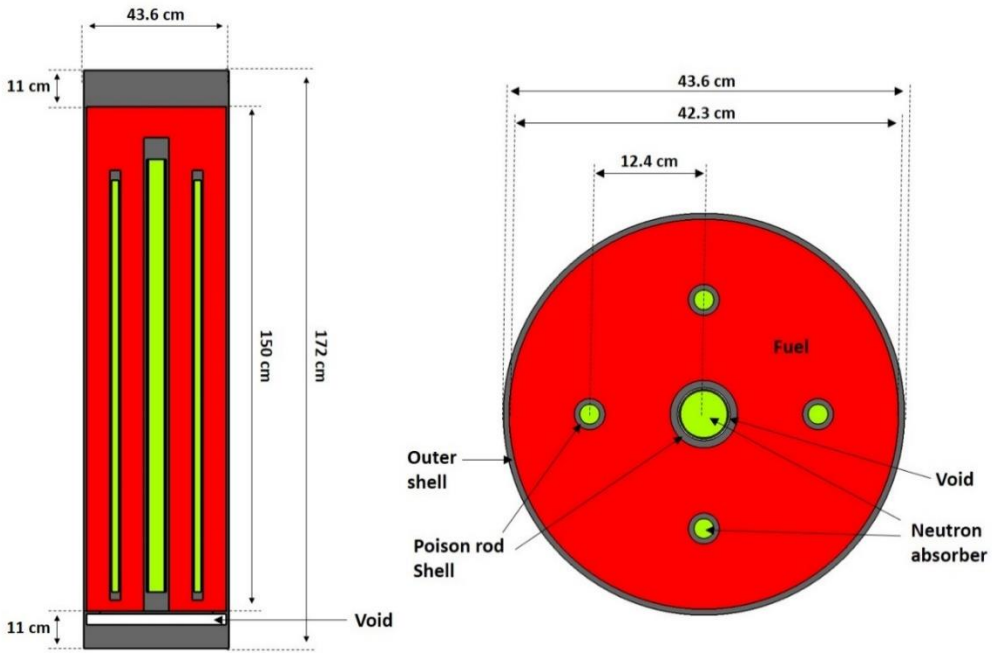


**Figure A. 16 The modified design of the Knockout canister**

## A. 5. 3 Ver.1 Filter canister

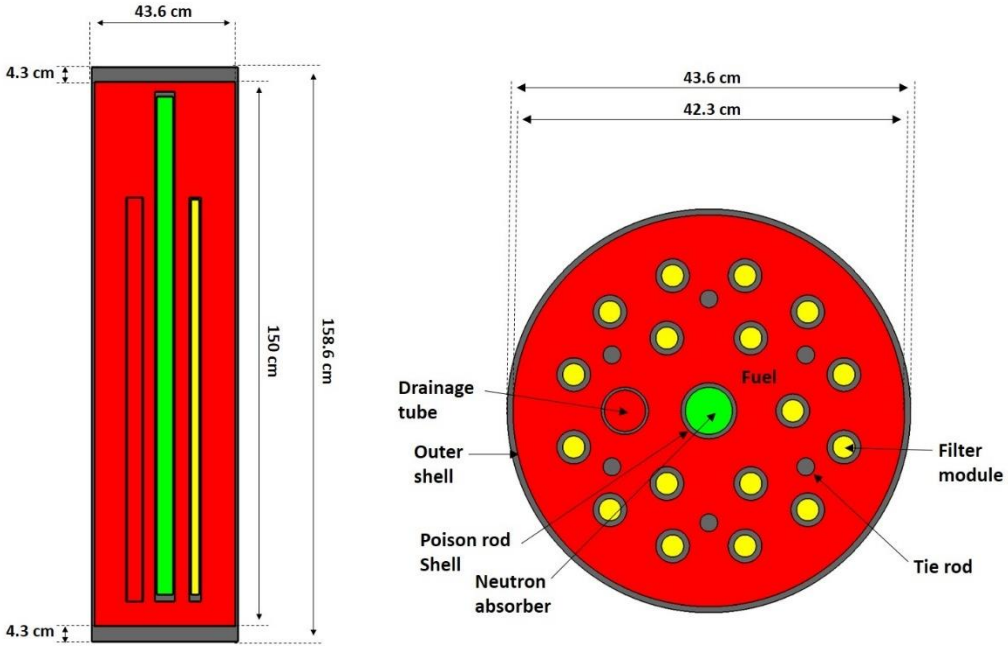


**Figure A. 17 The modified design of the Filter canister**

## A. 6 Materials used in the canister model

**Table A. 7 Material composition used for the canister design**

| Material name | Composition | Density [g / cm$^3$] | Canister |
|---|---|---|---|
| Fuel debris | Isotope concentrations from ORIGEN (Varies for burnup and initial condition) | 9.56 | All |
| Non-fuel matrix | 12% Water, 30% Ar, 58% SS304L [vol%] | 4.73 | Fuel |
| Fuel matrix | 8% Fuel debris, 10% Water, 25% Ar, 57% SS304L [vol%] | 5.43 | Knockout |
| Fuel matrix | 7.8 % Fuel debris, 10% Water, 25% Ar, 57.2% SS304L [vol%] | 5.42 | Filter |
| Filter module | 18.1% Fuel debris, 81.9% SS304L [vol%] | 8.45 | Filter |
| Boron carbide ($B_4C$) | 78% B, 22% C [vol%] | 2.52 | All |
| Boral | 65% Al, 27% B, 8% C [wt%] | 2.53 | Fuel |
| LICON | 54% O, 22.4% Al, 15.7% Ca, 6.9% Si, 1% Na [wt%] | 1.00 | Fuel |
| SS304L | 71% Fe, 19% Cr, 10% Ni [wt%] | 8.0 | All |
| Zircaloy | 97% Zr, 3% Sn [wt%] | 6.56 | Fuel |

**Table A. 8 Isotope composition of fuel debris (Major isotopes which are 98.8 wt%)**

| Isotopes | wt% | Isotopes | wt% | Isotopes | wt% |
|---|---|---|---|---|---|
| u-238 | 70.70 | pu-240 | 0.11 | mo-100 | 0.05 |
| o-16 | 10.02 | nd-144 | 0.08 | sn-118 | 0.05 |
| zr-90 | 7.59 | ba-138 | 0.08 | nd-143 | 0.05 |
| zr-94 | 2.72 | sn-120 | 0.07 | mo-98 | 0.05 |
| zr-92 | 2.63 | ce-140 | 0.07 | mo-97 | 0.05 |
| zr-91 | 1.70 | la-139 | 0.07 | tc-99 | 0.05 |
| u-235 | 1.18 | cs-133 | 0.07 | mo-95 | 0.05 |
| zr-96 | 0.49 | ce-142 | 0.07 | sn-116 | 0.03 |
| pu-239 | 0.32 | pr-141 | 0.07 | ru-104 | 0.03 |
| u-236 | 0.27 | cs-137 | 0.06 | y-89 | 0.03 |

Remaining 1.2 wt% are other fission products, actinides, activations

## A. 7 Estimated photon and neutron dose rate for three types of canisters

### A. 7. 1 Dose rate of canisters in air

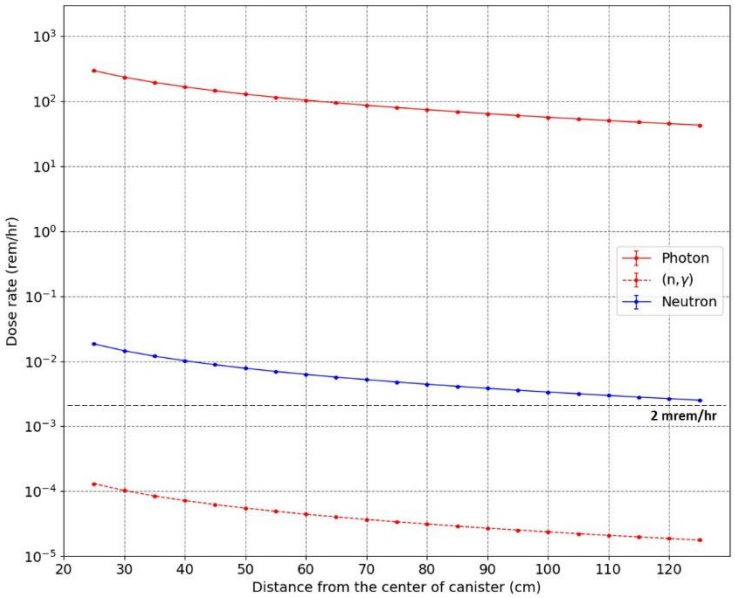


**Figure A. 18 Dose rate of TMI-2 fuel canister**

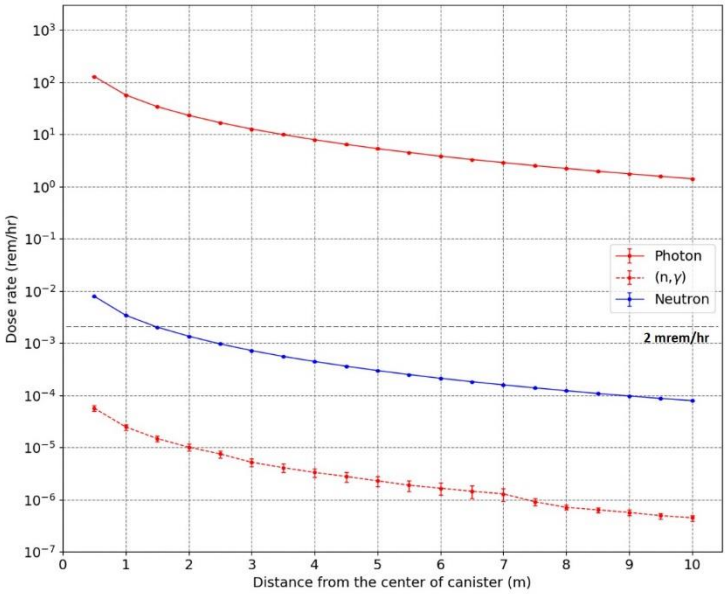


**Figure A. 19 Dose rate of TMI-2 fuel canister (up to 10m)**

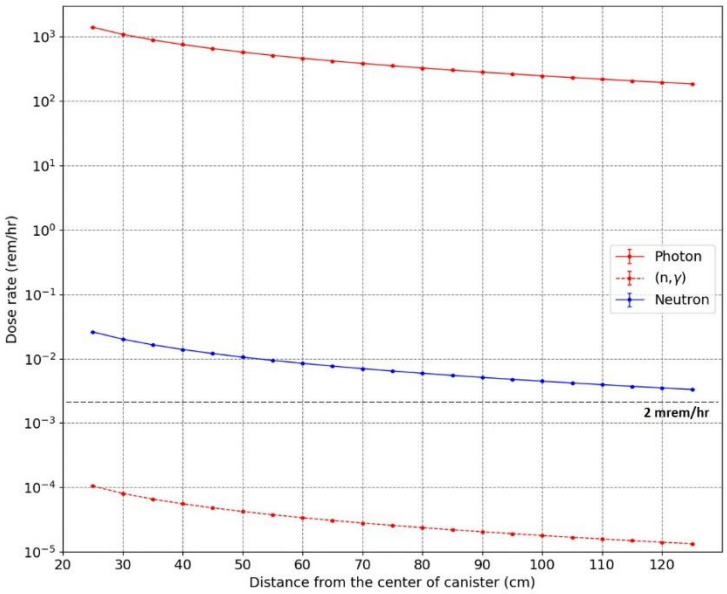


**Figure A. 20 Dose rate of TMI-2 Knockout canister**

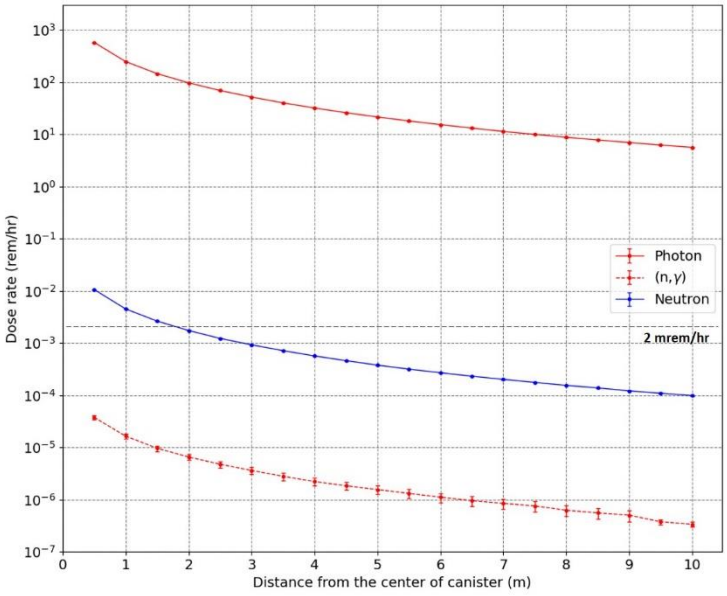


**Figure A. 21 Dose rate of TMI-2 Knockout canister (up to 10m)**

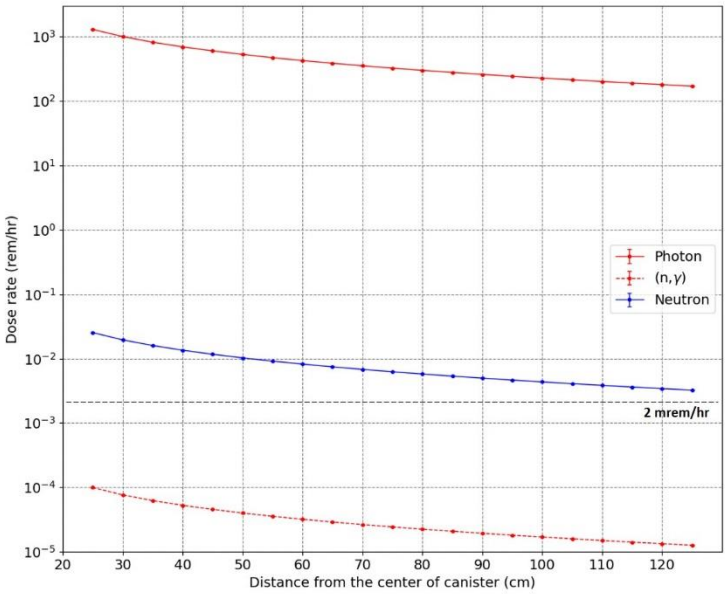


**Figure A. 22 Dose rate of TMI-2 Filter canister**

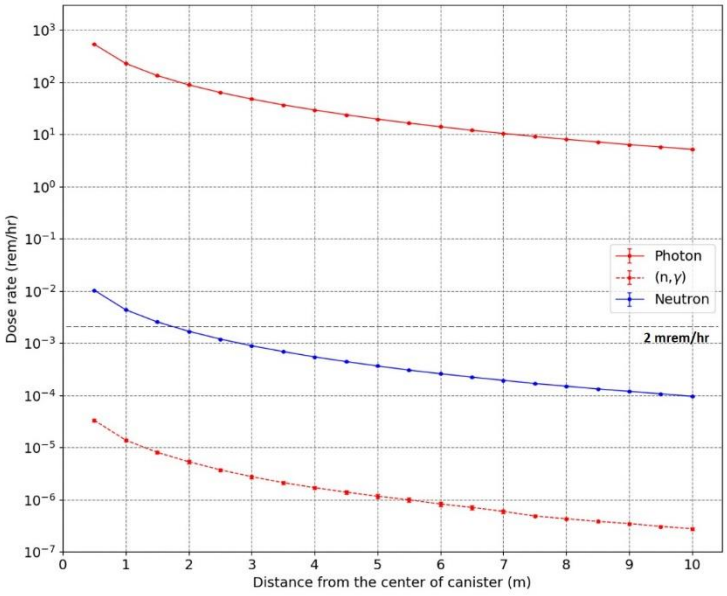


**Figure A. 23 Dose rate of TMI-2 Filter canister (up to 10m)**

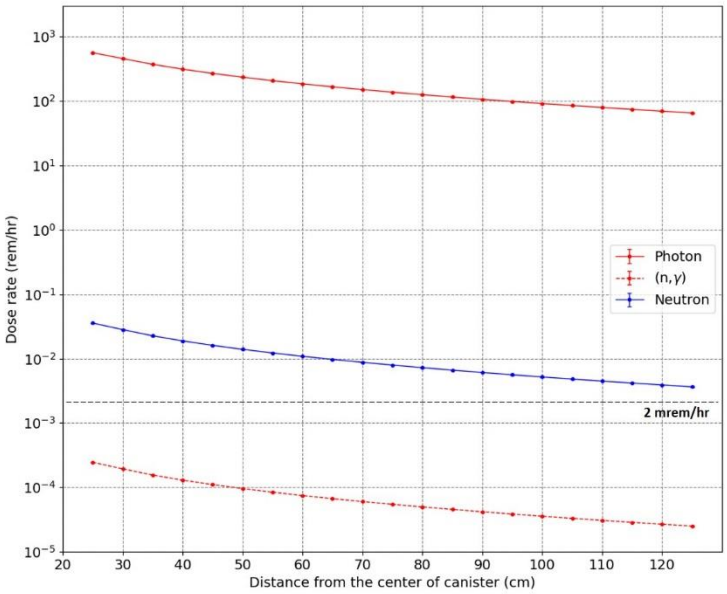


**Figure A. 24 Dose rate of the modified fuel canister**

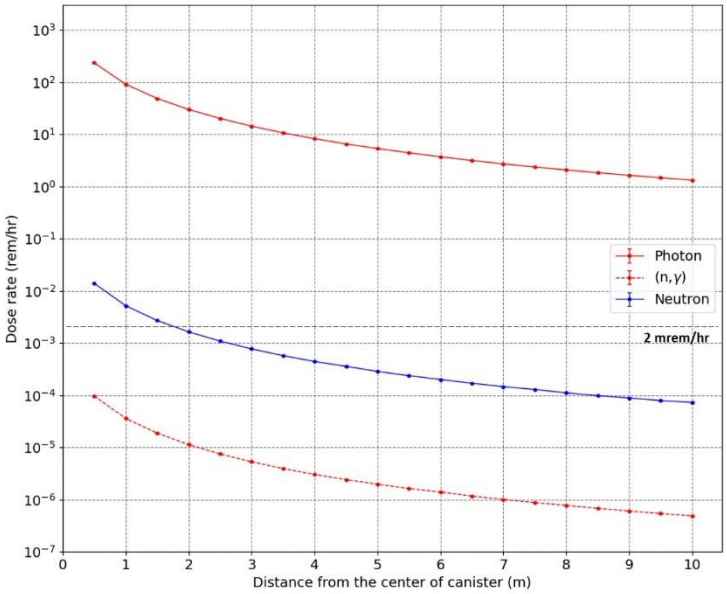


**Figure A. 25 Dose rate of the modified fuel canister (up to 10m)**

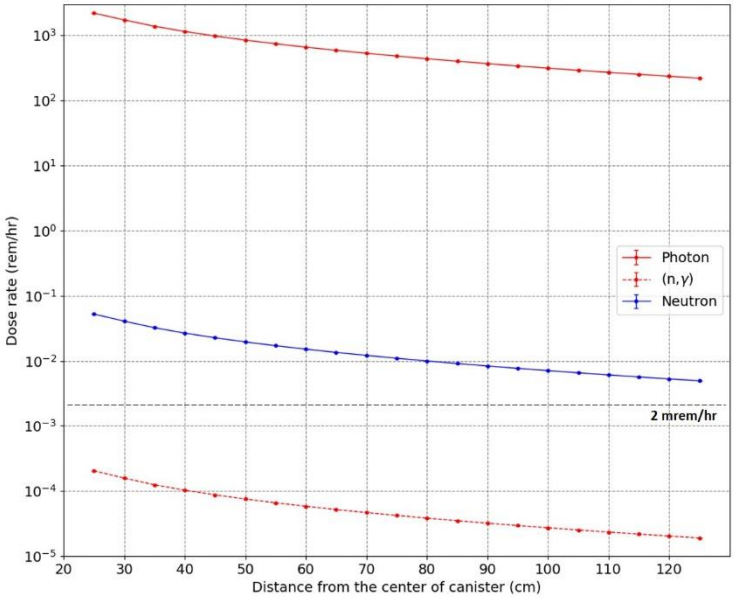


**Figure A. 26 Dose rate of the modified knockout canister**

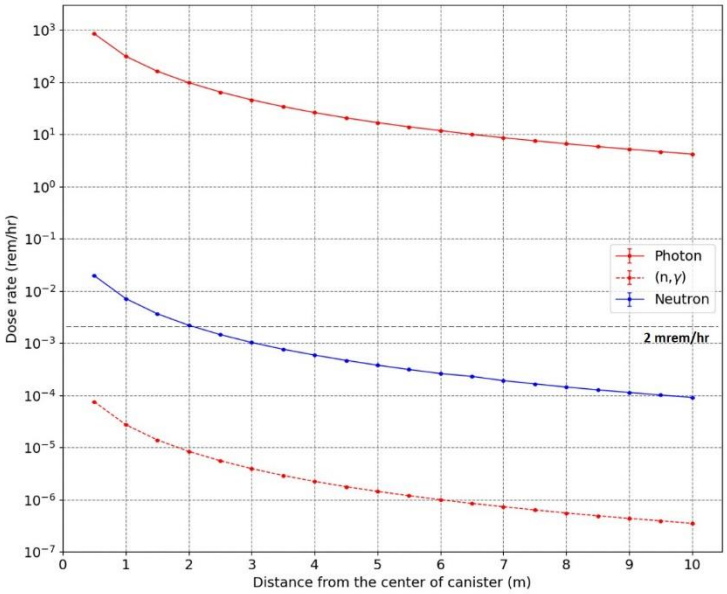


**Figure A. 27 Dose rate of the modified knockout canister (up to 10m)**

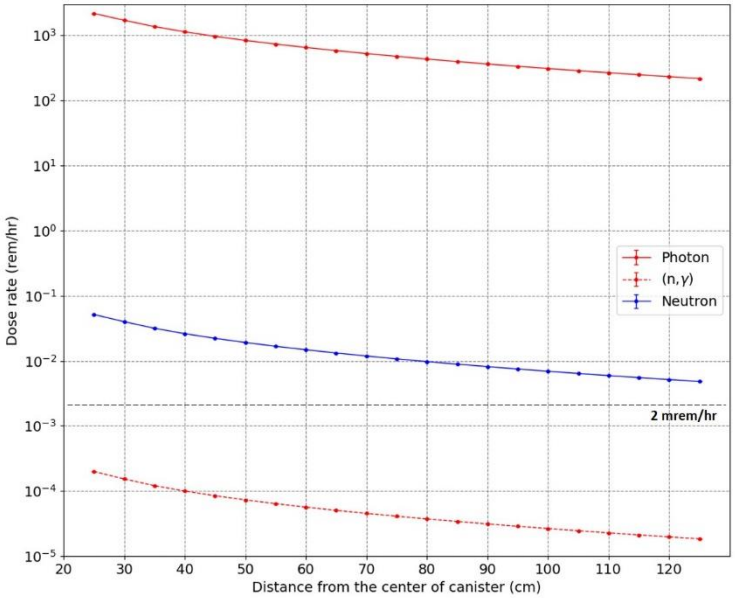


**Figure A. 28 Dose rate of the modified filter canister**

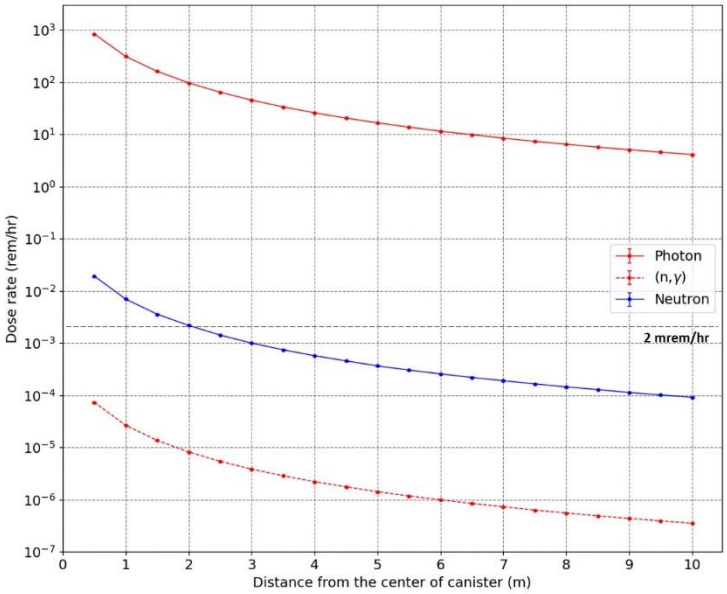


**Figure A. 29 Dose rate of the modified filter canister (up to 10m)**

## A. 7. 2 Dose rate of canisters in water

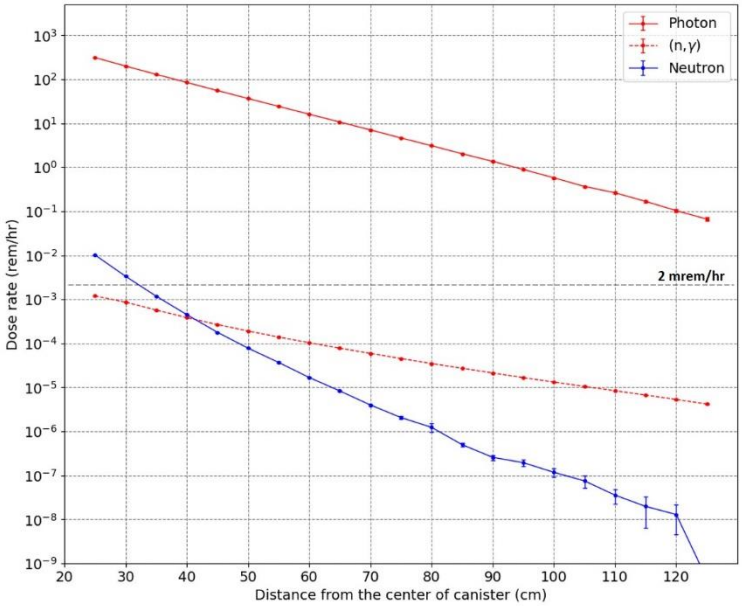


**Figure A. 30 Dose rate of TMI-2 fuel canister in water**

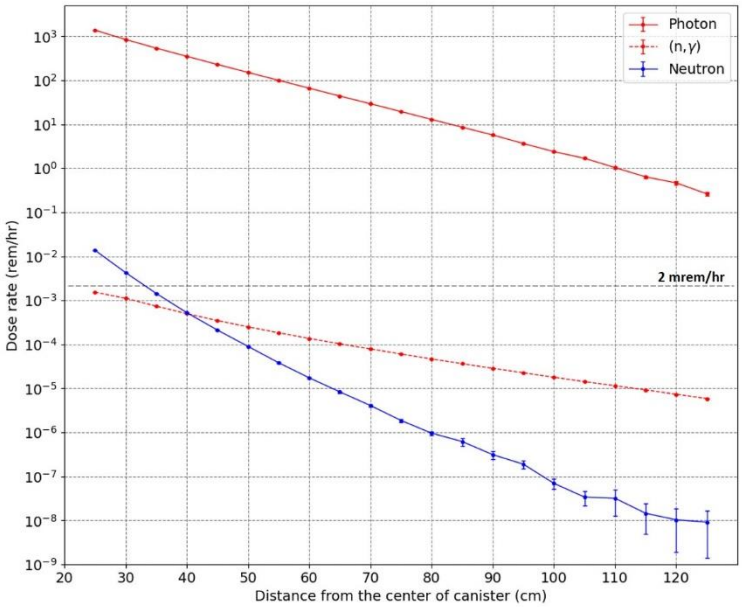


**Figure A. 31 Dose rate of TMI-2 knockout canister in water**

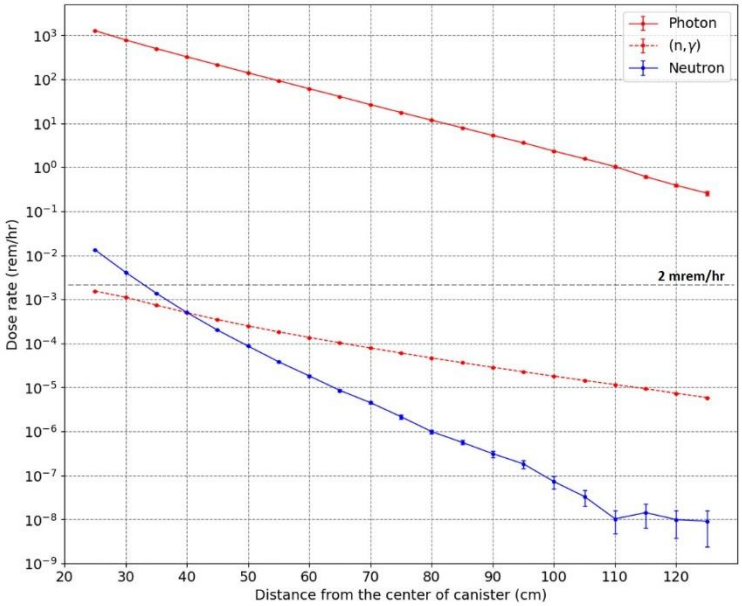


**Figure A. 32 Dose rate of TMI-2 filter canister in water**

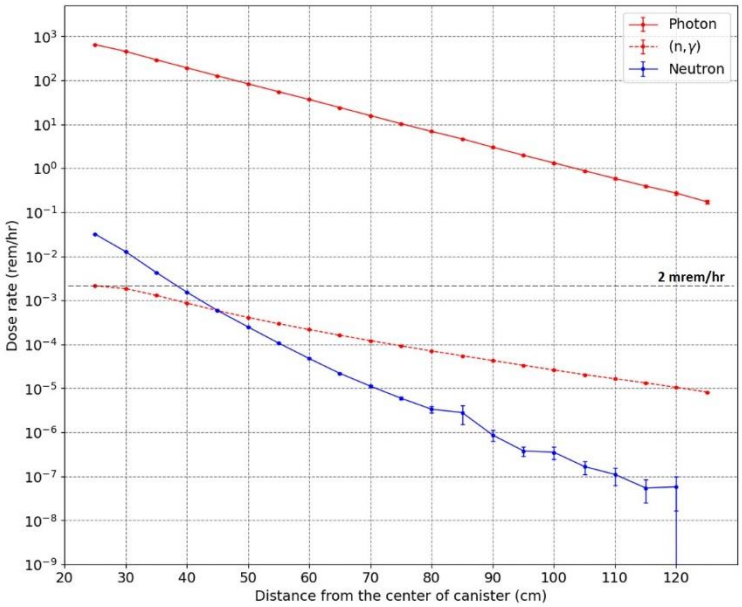


**Figure A. 33 Dose rate of the modified fuel canister in water**

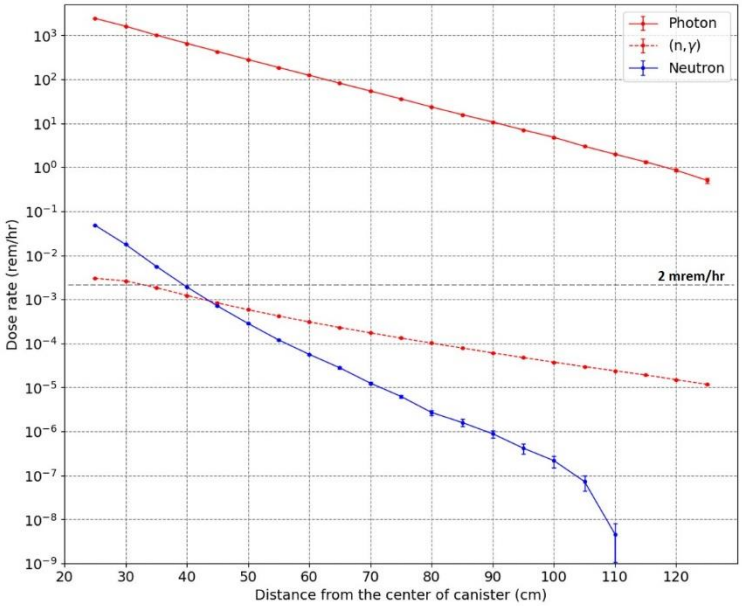


**Figure A. 34 Dose rate of the modified knockout canister in water**

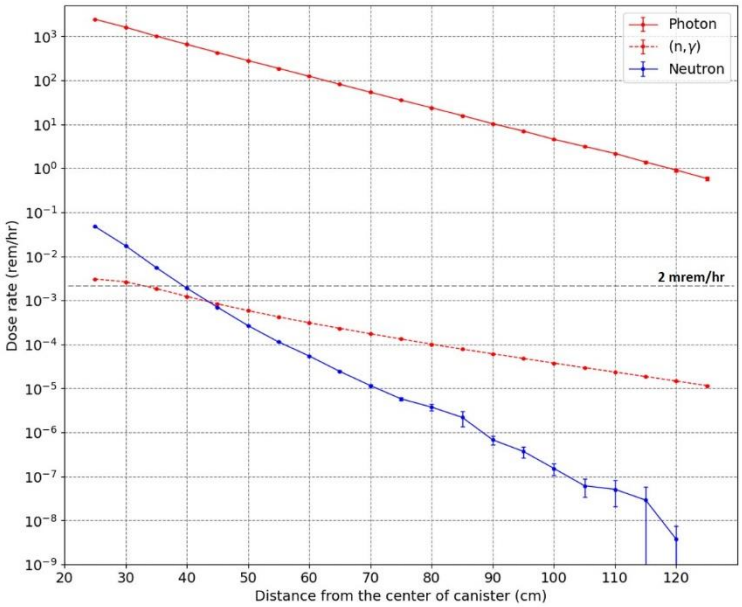


**Figure A. 35 Dose rate of the modified filter canister in water**

## A. 8 Neutron shielding performance of the epoxy-based resin

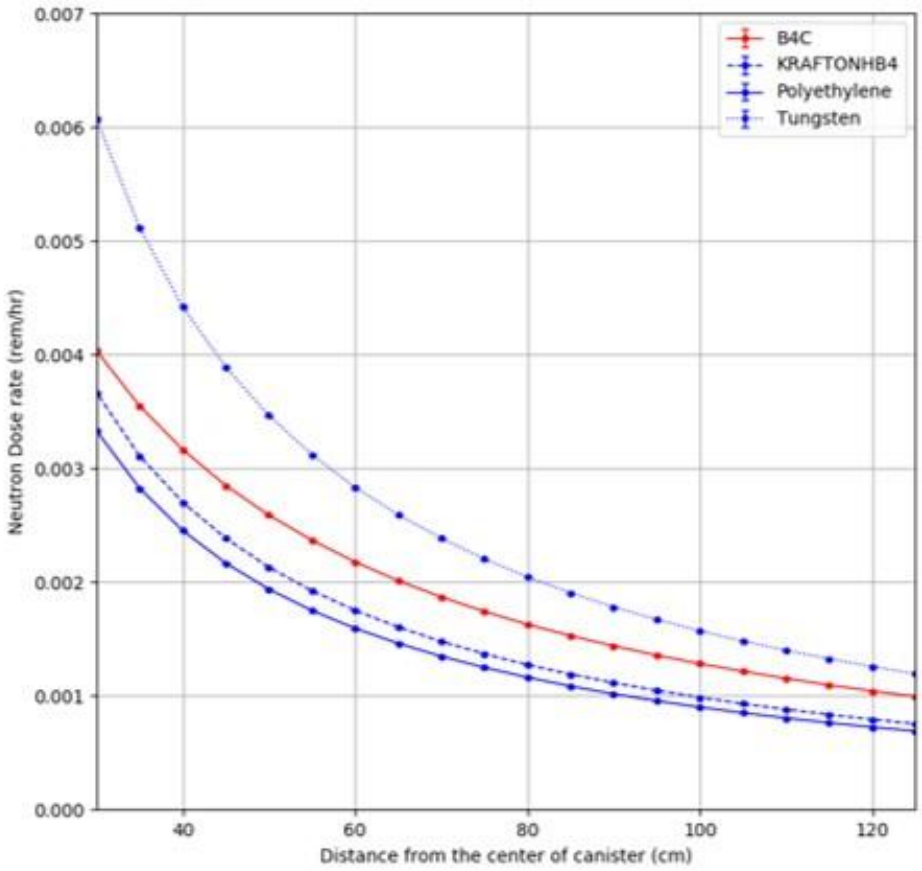


**Figure A. 36 Comparison of the neutron dose rate for advanced materials**

## A. 9 Sensitivity of dose rate by changes in burnup

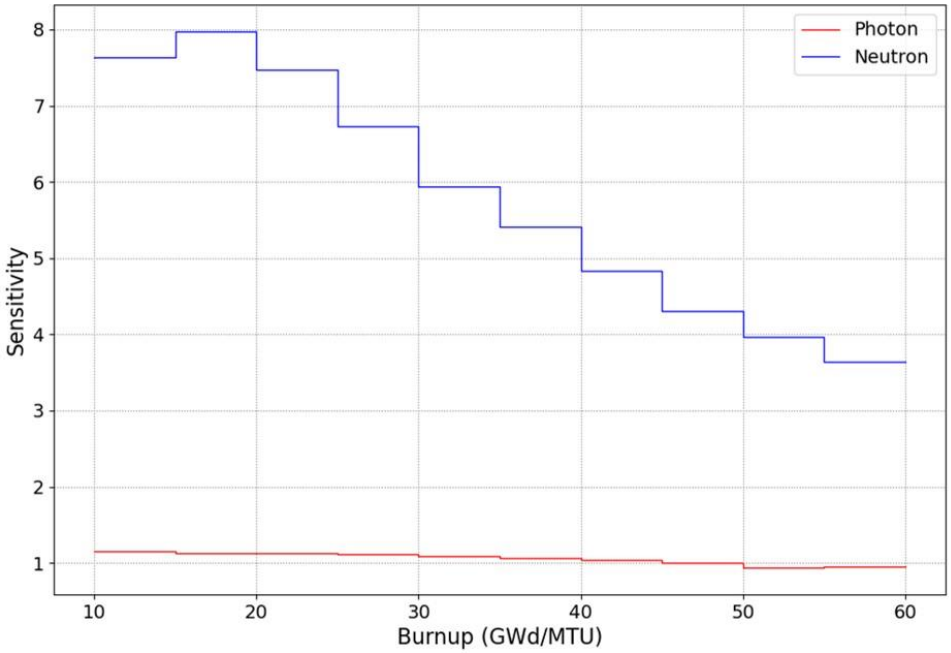


**Figure A. 37 Comparison of the sensitivity index by changes in burnup between photon and neutron dose rate**

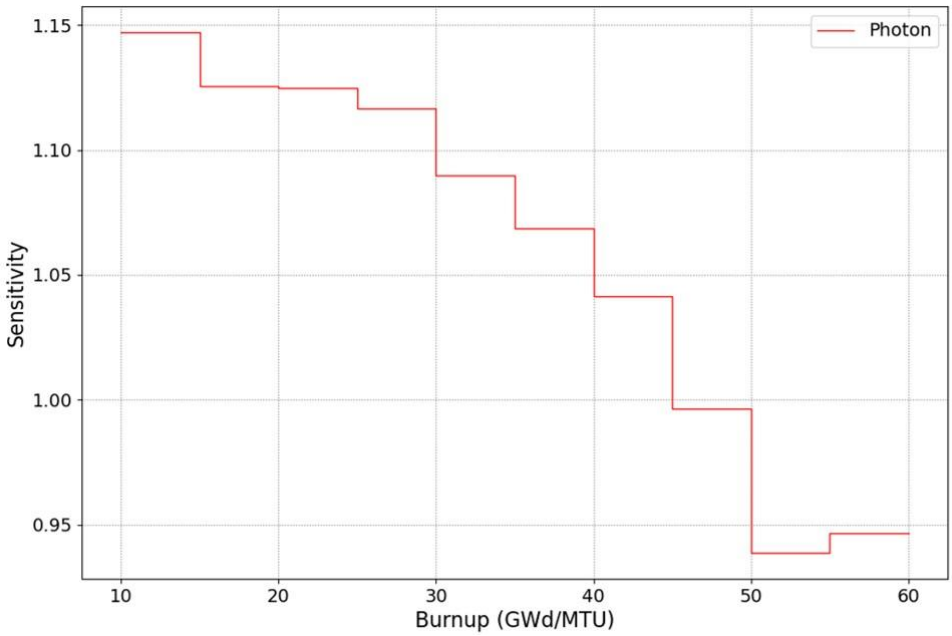


**Figure A. 38 Sensitivity index of the photon dose rate by changes in burnup**

## A. 10 Variability of dose rate by the release of element

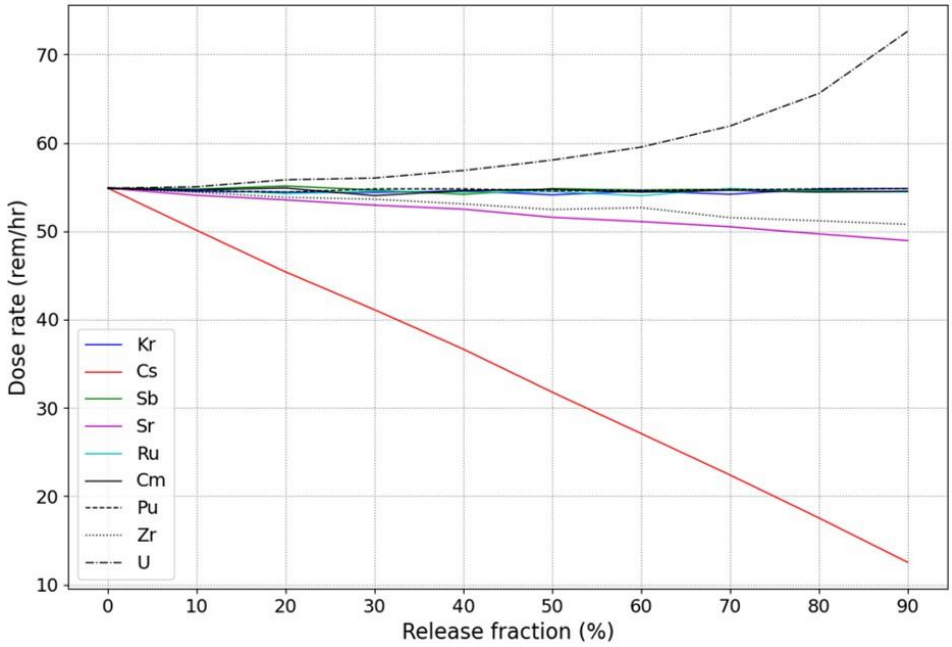


**Figure A. 39 Photon dose rate by changes in release fraction**

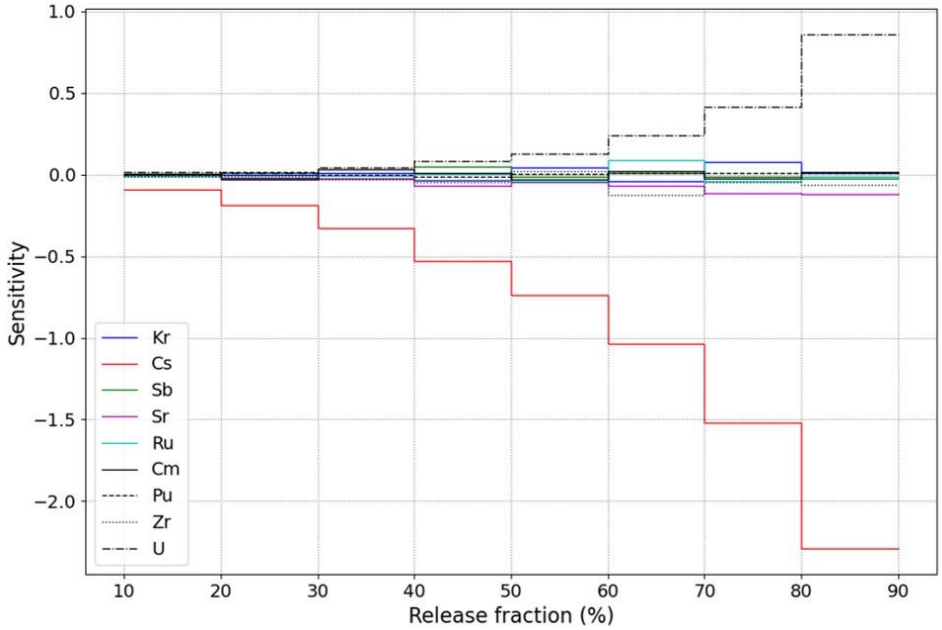


**Figure A. 40 Sensitivity of photon dose rate by changes in release fraction**

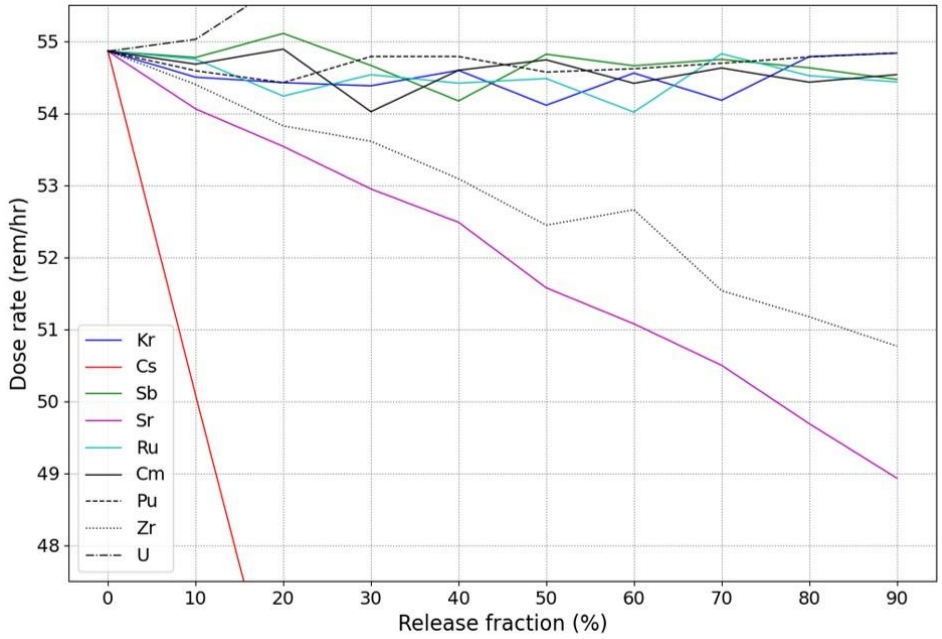


**Figure A. 41 Photon dose rate by changes in release fraction.** Y-axis are displayed from 47.5 rem/hr to 55.5 rem/hr.

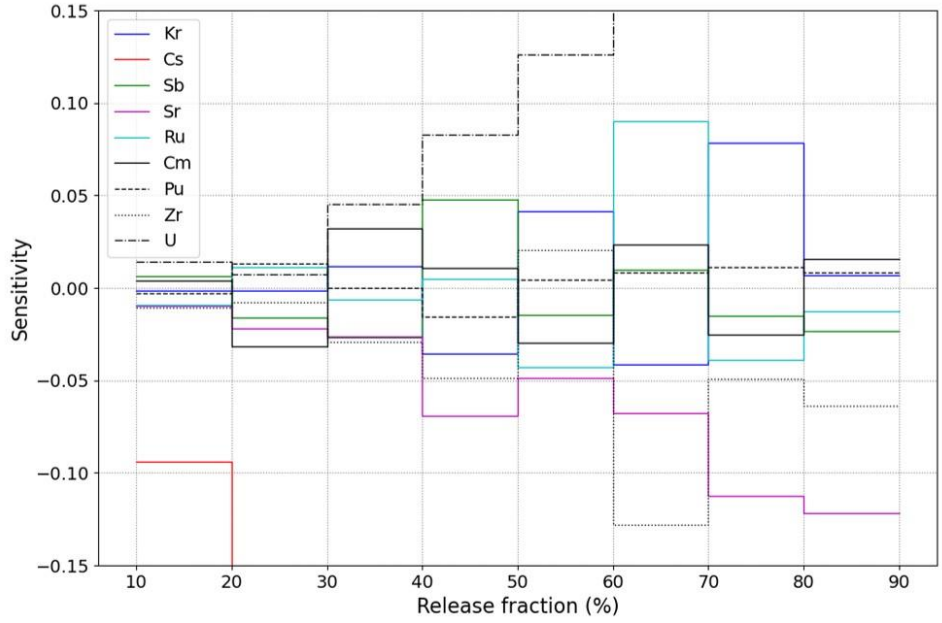


**Figure A. 42 Sensitivity of photon dose rate by changes in release fraction.** Y-axis are displayed from -0.15 to 0.15.

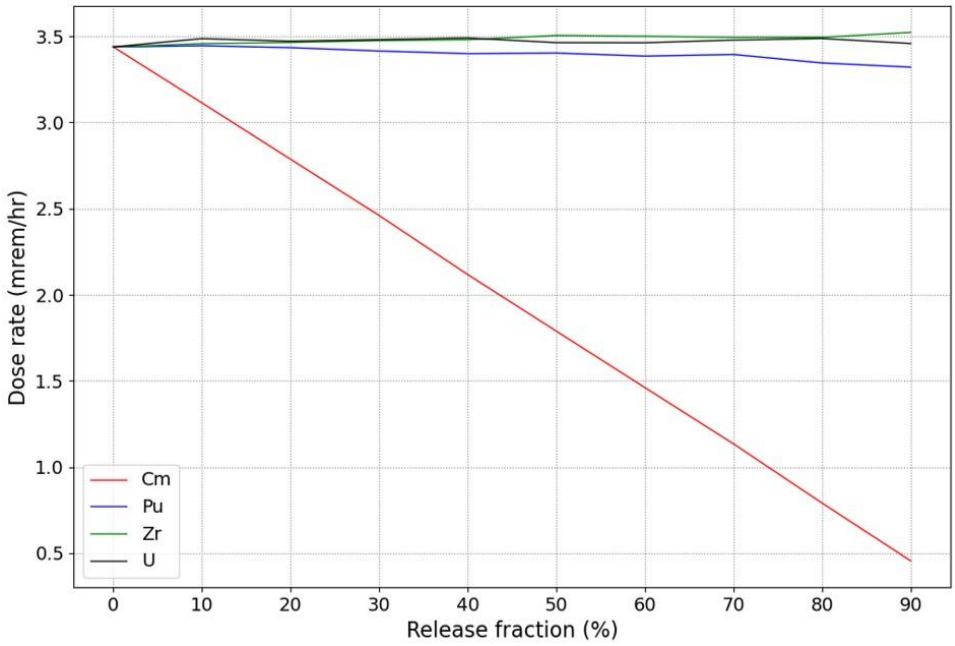


**Figure A. 43 Neutron dose rate by changes in release fraction**

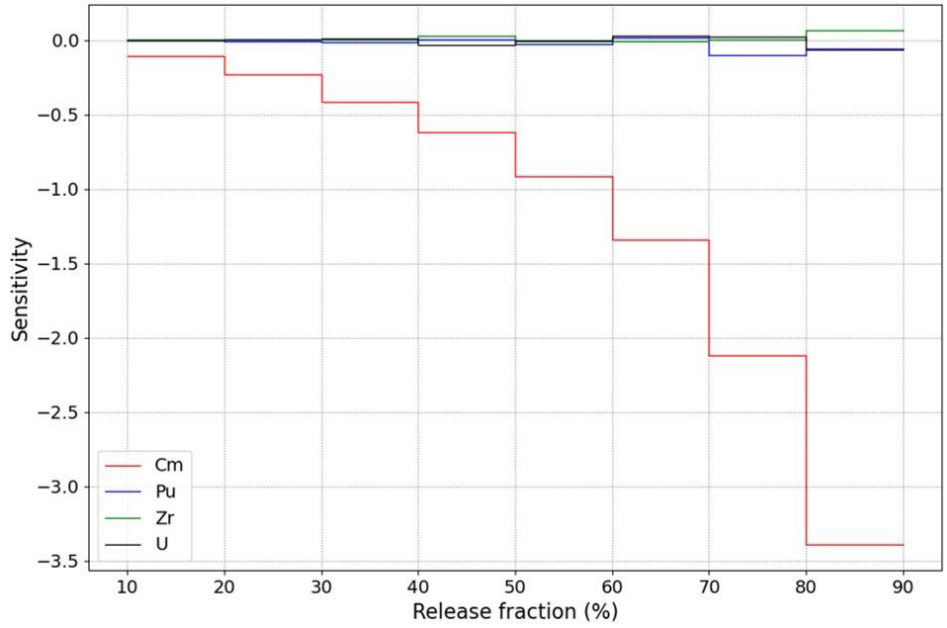


**Figure A. 44 Sensitivity of neutron dose rate by changes in release fraction**

**Table A.9 Estimated changes in dose rate by isotope release**

| Group | Element | Decay Mode of major isotopes | Half life of major isotopes | $\gamma$ energy release of major isotopes | Decrease of dose rate by 90% of release | |
|---|---|---|---|---|---|---|
| | | | | | Photon | Neutron |
| Noble gases | Krypton (Kr) | $\gamma,\ \beta^-$ | 10.7 y | 151 keV~ 840 keV | 0.05 | - |
| | Xenon (Xe) | $\beta^-$ | 2 ~ 5 d | 81 keV | - | - |
| Halogens | Iodine (I) | $\gamma,\ \beta^-$ | 6.57 h, 8 d | 159 ~ 364 keV | - | - |
| Alkali metals | Cesium (Cs) | $\gamma,\ \beta^-$ | 2.9 h, 30 y | 11 ~ 847 keV | 77.17 | - |
| | Rubidium (Rb) | $\beta^-$ | $4.9 \times 10^{10}$ y | 10 ~ 400 keV | - | - |
| Tellurium group | Antimony (Sb) | $\beta^-$ | 2.7 y | 35 ~ 670 keV | 0.71 | - |
| | Tellurium (Te) | $\beta^-$ | $10^{20}$ ~$10^{24}$y | - | - | - |
| Alkaline earth | Strontium (Sr) | $\gamma,\ \beta^-$ | 50 d ~ 28.74 y | 203 ~ 2,319 keV | 10.81 | - |
| | Barium (Ba) | - | stable | - | - | - |
| | Ruthenium (Ru) | $\gamma,\ \beta^-$ | 39 d ~ 374 d | 238.2 keV | 0.78 | - |
| | Mo, Rh, Tc | $\gamma,\ \beta^-$ | 6 h ~ 65 h | 90 ~ 778 keV | - | - |
| Rare earth | Curium (Cm) | $\alpha,\ SF$ | 160 d, 18.1 y | - | 0.59 | 86.75 |
| | Plutonium (Pu) | $\alpha,\ SF$ | 14 y ~ $10^7$ y | - | 0.04 | 3.41 |
| | Am, Ce, La, Nb, Nd, Np, Pr, Y | diverse | diverse | diverse | - | - |
| Fuel rods | Zirconium (Zr) | $\beta^-$ | $10^6$ ~$10^{19}$y | 10 ~ 70 keV | 7.47 | - 2.46 |
| | Uranium (U) | $\alpha,\ SF,\ \beta^-$ | $10^5$ ~$10^9$y | 10 ~ 12,000 keV | -32.4 | - 0.576 |

## Appendix B Photon and neutron dose rate at a point detector

This chapter has graphs which estimate dose rate and uncertainty at a point detector using the SCALE based model developed in Chapter 3. Photon and neutron dose rate are estimated at a point detector which is located at horizontally 1 m from the center of a canister and vertically center of the canister (Figure B. 1). The center of the debris pile is moved to the center of the canister for Appendix B.3 and B.5. This is moved to estimate dose rate at the vertical center of the debris pile instead of the center of the canister. Fuel debris are randomly distributed in the inner space of a canister in loose packing or close packing. Radius of debris are randomly sampled excepting for Appendix B.6 and B.7. Canisters of Appendix B.8 and B.9 have three small containers in their inner spaces each.

Graphs of each section are organized as follows : estimated dose rate, uncertainty, sensitivity, cumulative graphs, distribution of fuel debris in a canister. Graphs on the estimated dose rate consist of three graphs which are the box plot of the estimated dose rate, the average dose rate with error bars on the standard deviation, the average dose rate with error bars on the range. The box plot of the estimated dose rate has 17 boxes and red dots. Each box is the box plot of the estimated dose rate for a sample group, and each sample group has 1,000 red dots which are calculated dose rates by 1,000 times of SCALE works (1,000 SCALE outputs). The line plot of the average dose rate with the standard deviation visualizes the average dose rate, and vertical lines are error bars which visualizes the standard deviation. The line plot of the average dose rate with the range visualizes the average dose rate, and vertical lines are error bars which visualizes the range. The length of each error bar is the same as the range of each sample group, and each bar is drawn up and down half the range. The uncertainty consists of three plots which are the standard deviation, the coefficient of variation, the percent relative range. The line plot of the sensitivity visualizes the sensitivity index of the average dose rate by changes in the size of debris. The cumulative graph consists of the cumulative graph of the average dose rate and the cumulative graph of the standard deviation. Error bars of the line plot of the cumulative average dose rate visualizes the cumulative standard deviation. The distribution of fuel debris in a canister consists of 34 plots which are the distribution of fuel debris in a canister for the maximum and minimum dose rate of each sample group. Plots at the left are distributions for the minimum dose rate, plots at the right are distributions for the maximum dose rate.

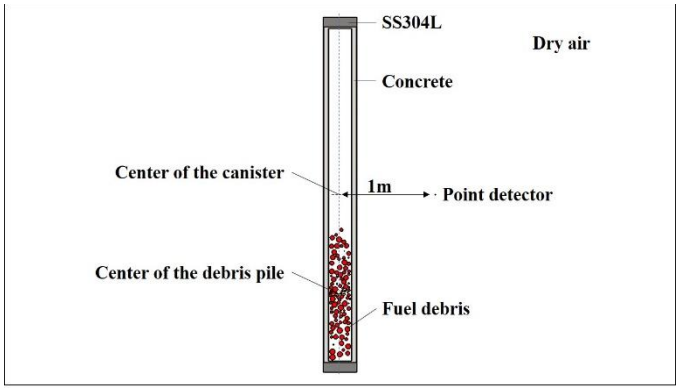


**Figure B. 1 Cross sectional view of the fuel debris in a canister**

**B. 1. Photon dose rate of the loose packed fuel debris in a canister**

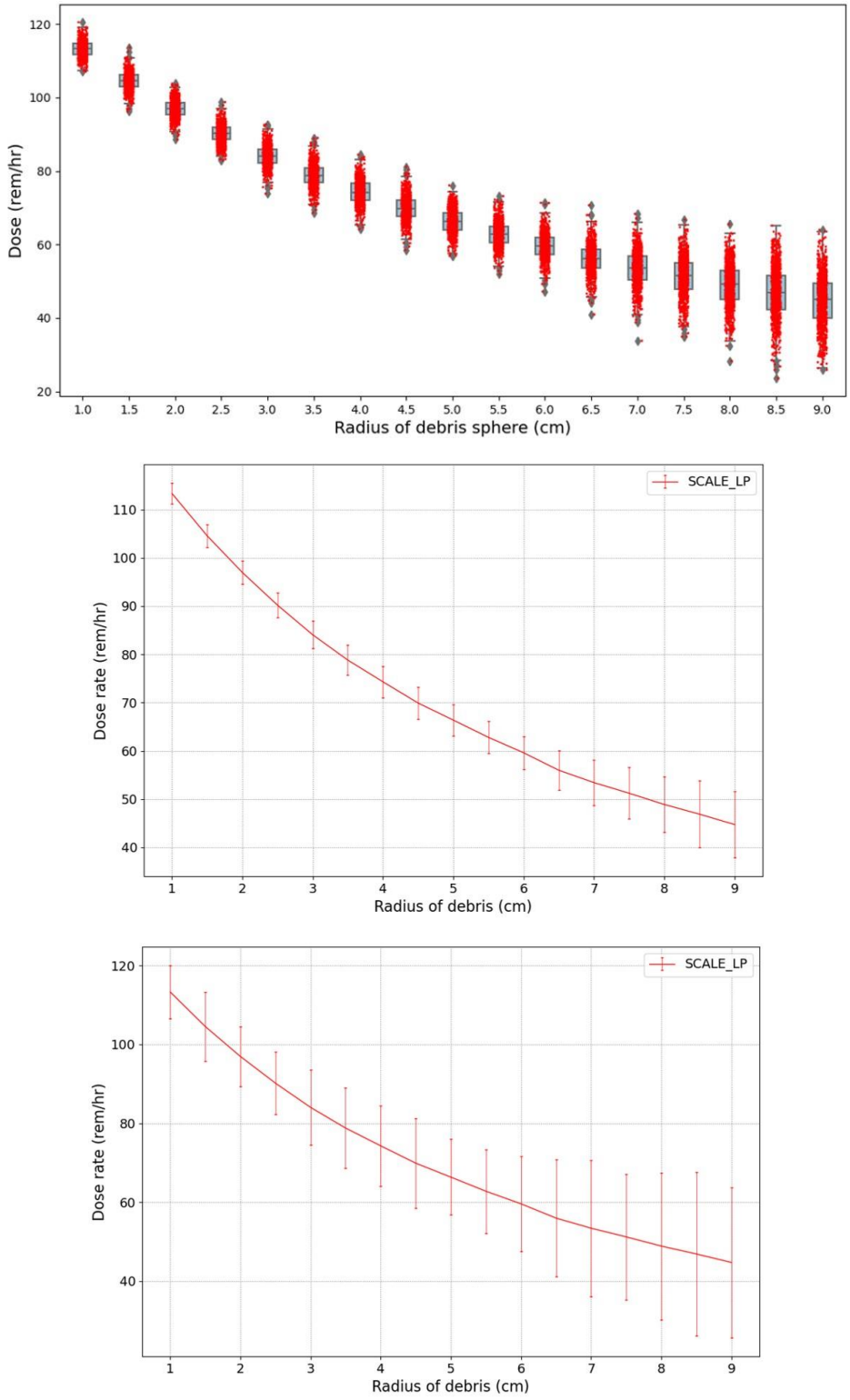


**Figure B. 2 Photon dose rate of the loose packed fuel debris.** The estimated dose rates (top), the average dose rate with the standard deviation (middle), the average dose rate with the range (bottom)

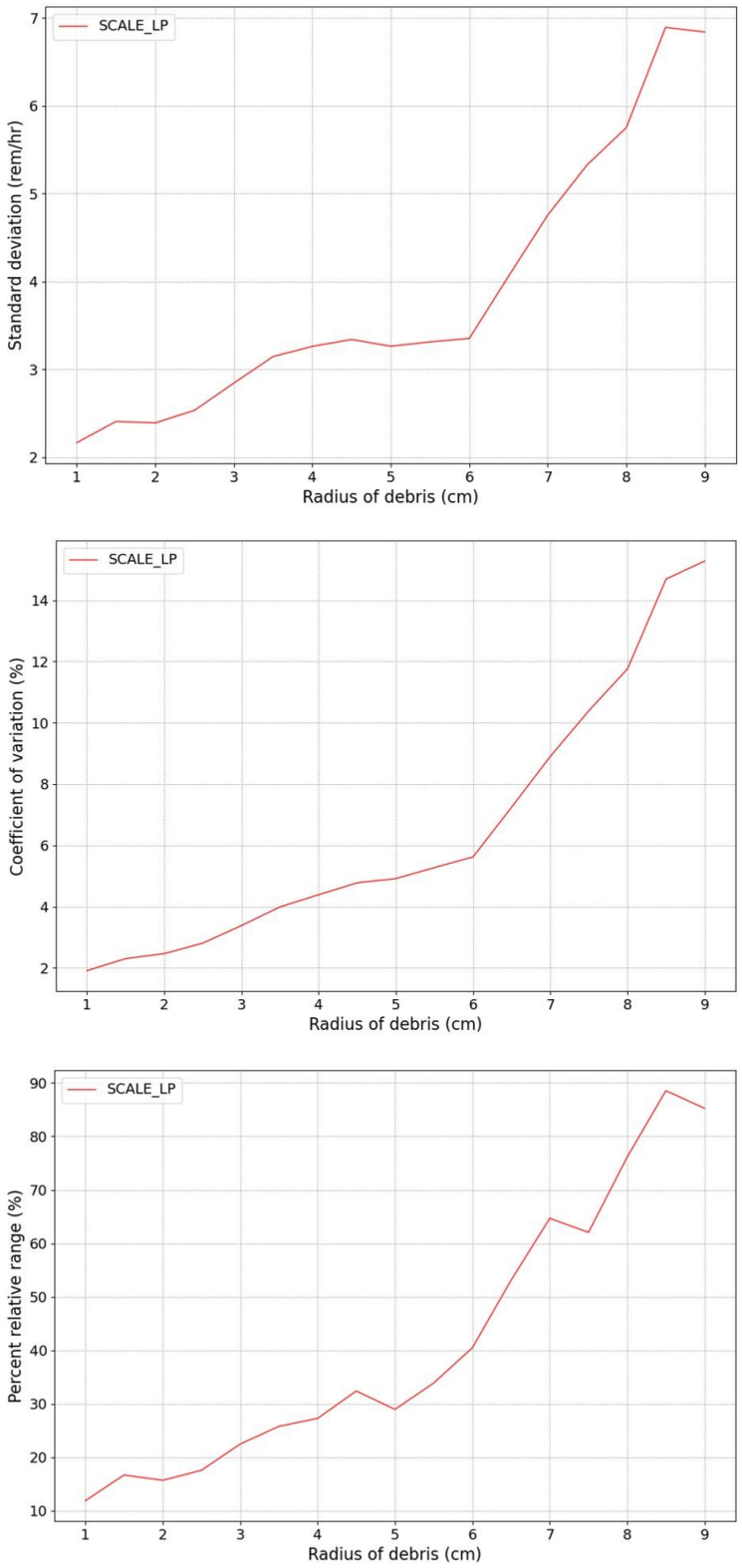


**Figure B. 3 Uncertainty of the loose packed fuel debris.** The standard deviation (top), the coefficient of variation (middle), the percent relative range (bottom)

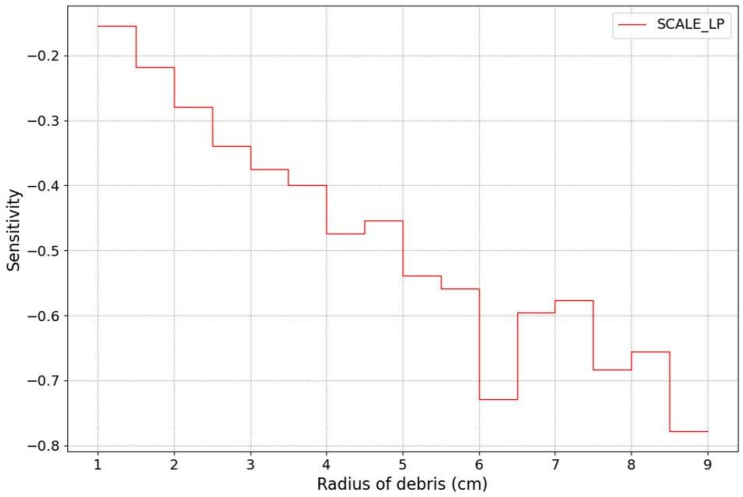


**Figure B. 4 Sensitivity index of the loose packed fuel debris.**

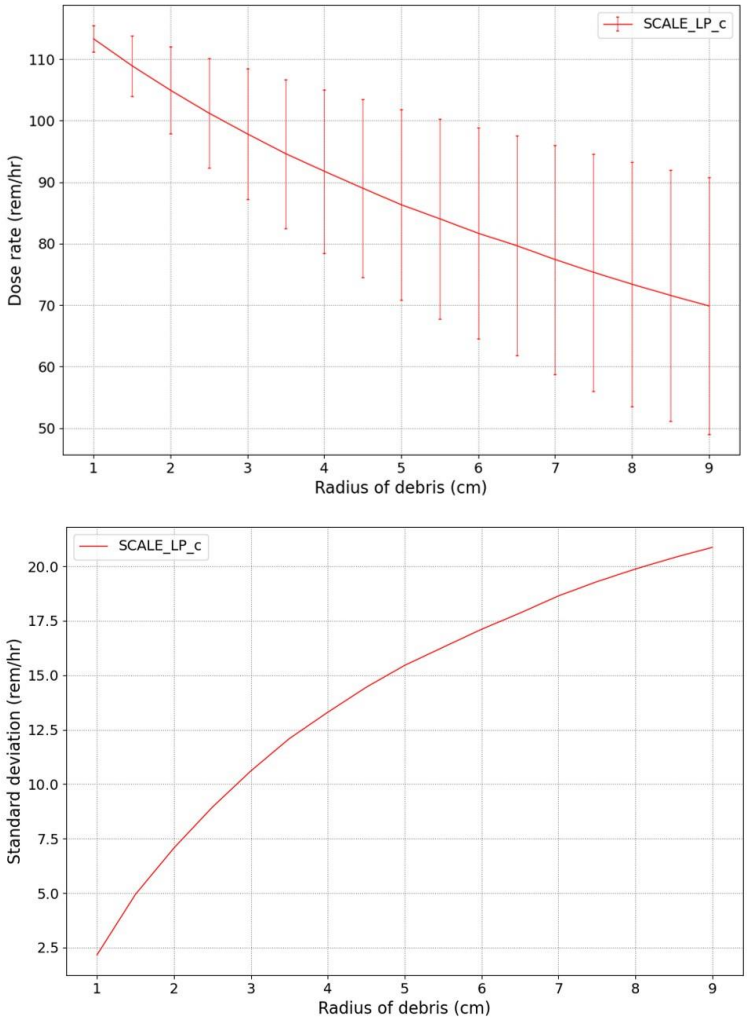


**Figure B. 5 Cumulative graphs.** The average dose rate (top), the standard deviation (bottom)

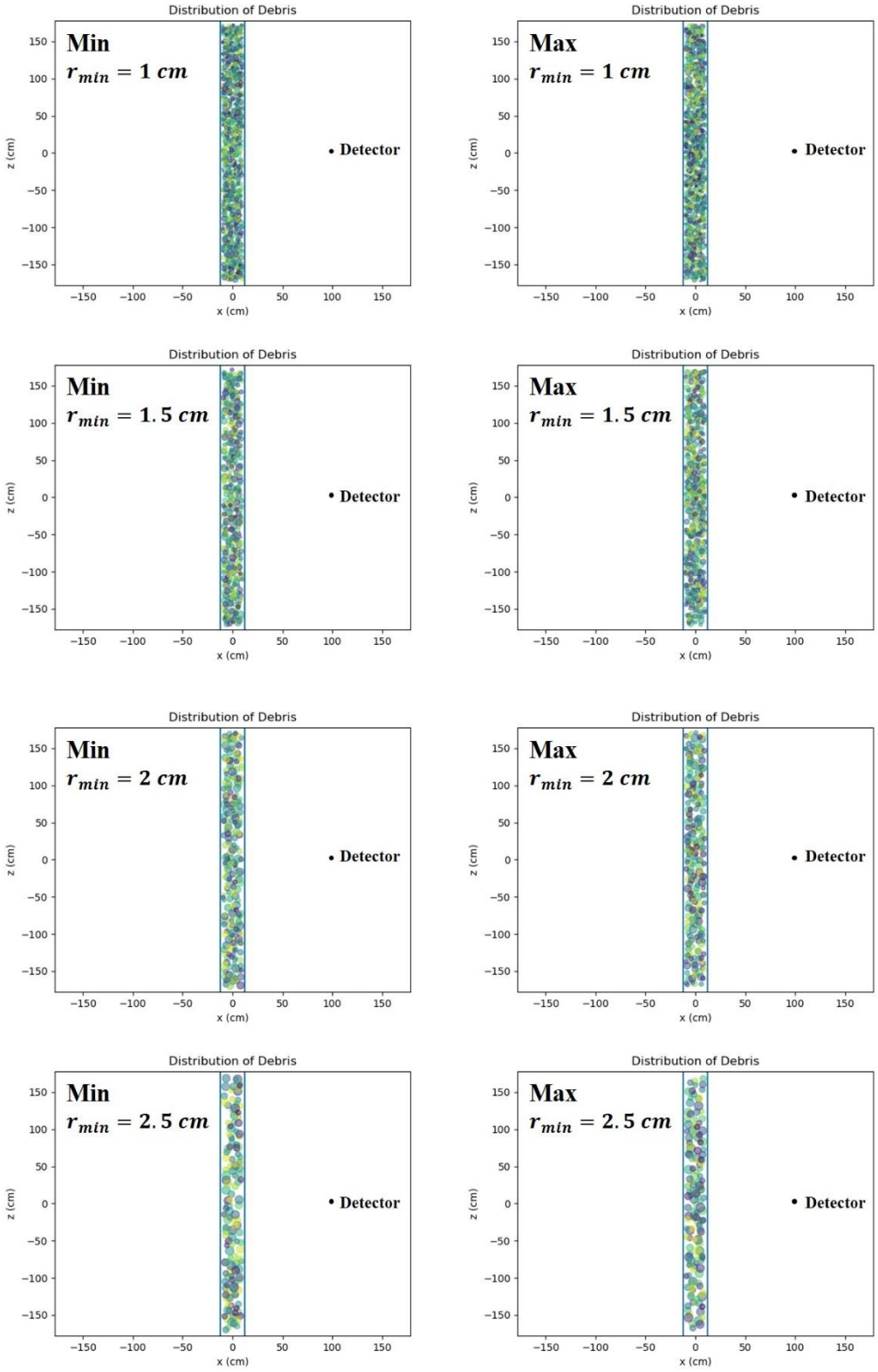


**Figure B. 6 Distribution of the loose packed fuel debris in a canister.**

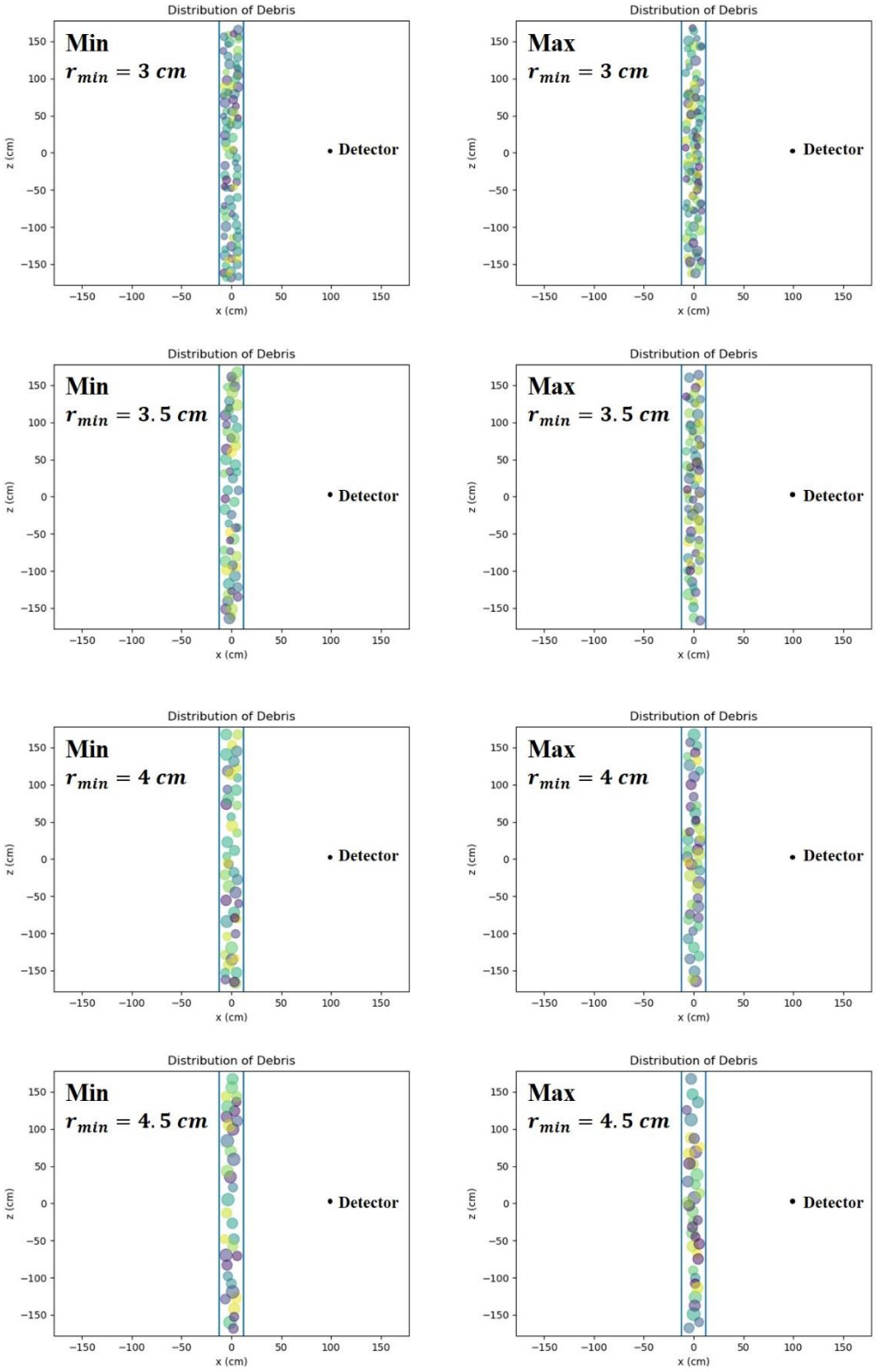


**Figure B. 7 Distribution of the loose packed fuel debris in a canister.**

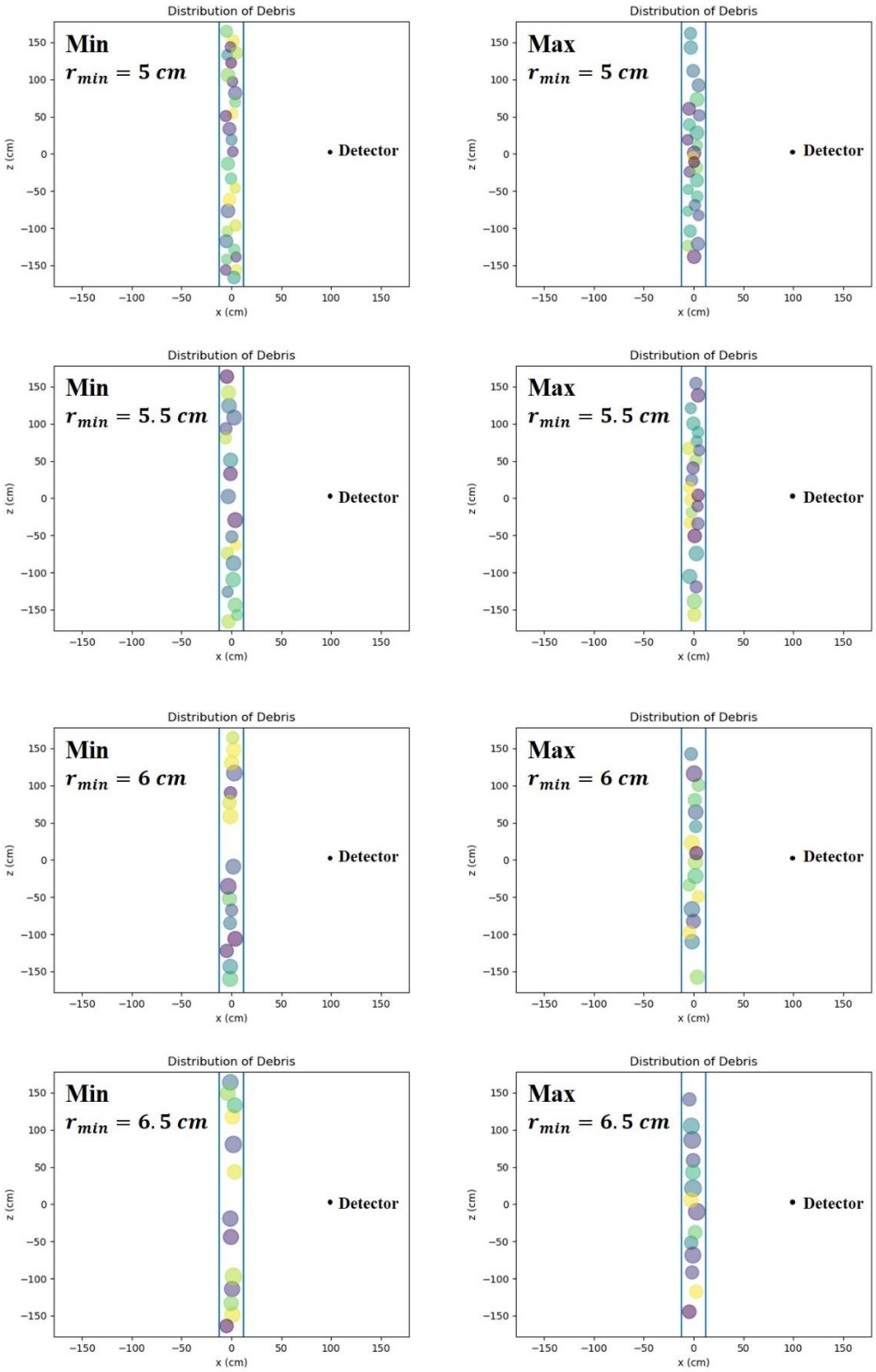


**Figure B. 8 Distribution of the loose packed fuel debris in a canister.**

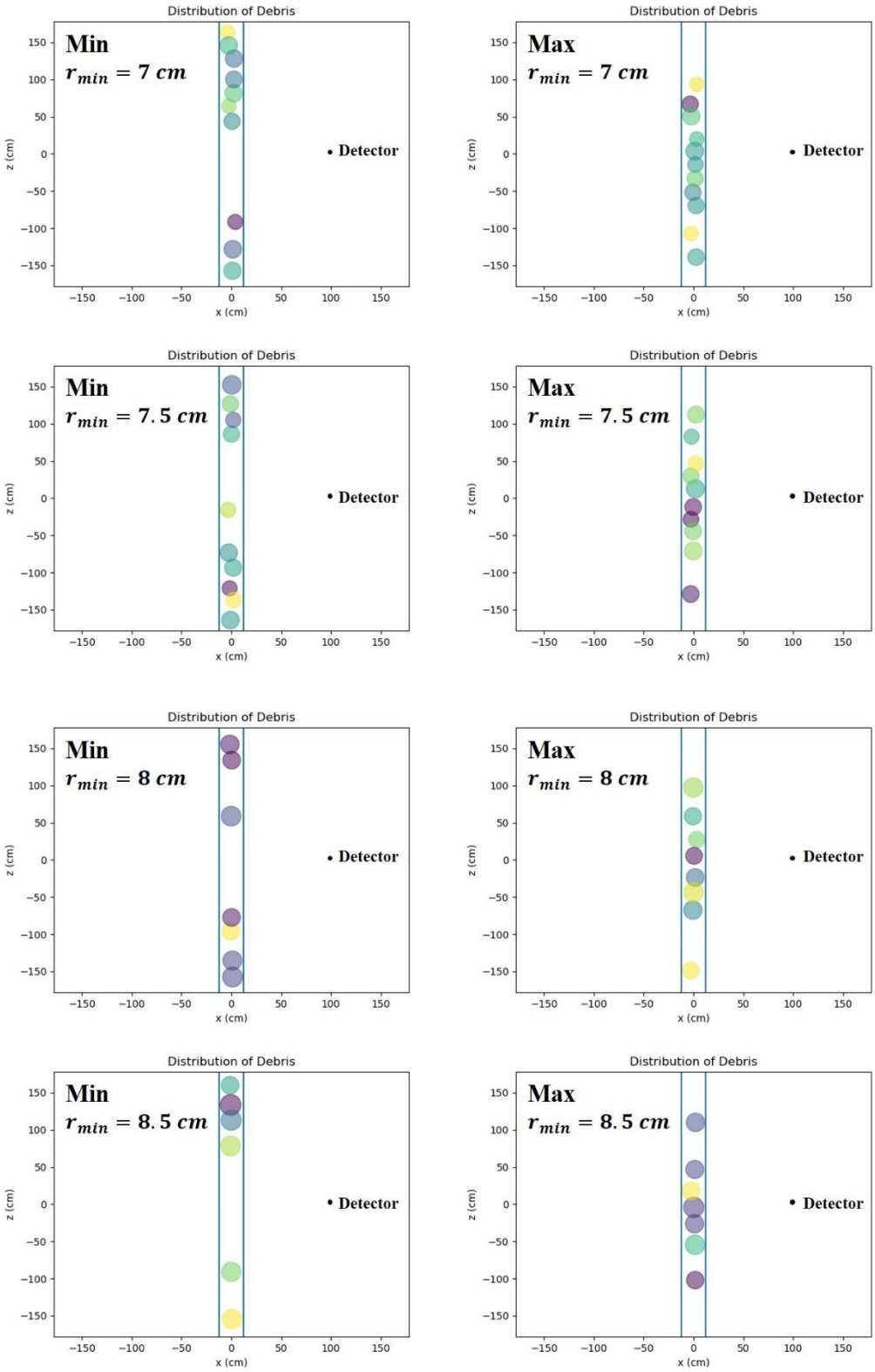


**Figure B. 9 Distribution of the loose packed fuel debris in a canister.**

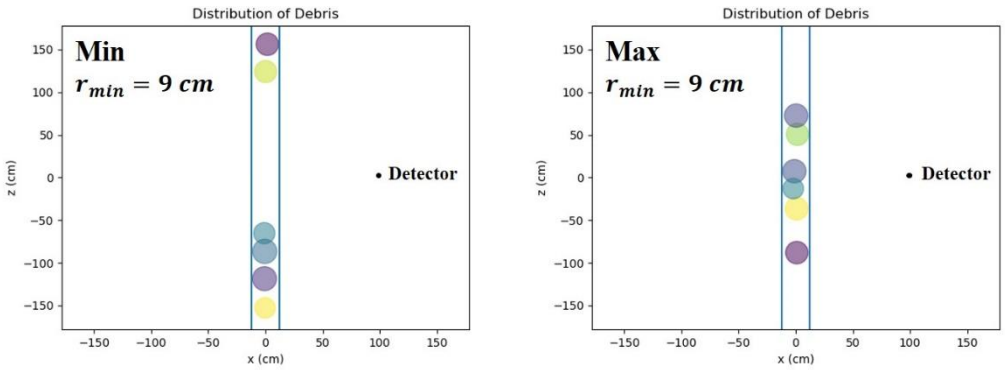


**Figure B. 10 Distribution of the loose packed fuel debris in a canister.**

Dose rate of loose packed fuel debris exponentially decreases by the increase of the minimum radius ($r_{min}$) of fuel debris. Average photon dose rate of each sample groups continuously decreases by the increase of $r_{min}$, and its graph has a smooth exponential curve (Figure B. 2). The average dose rate is 113.3 rem/hr for $r_{min}$ of 1 cm, then it decreases up to 44.8 rem/hr for the radius of 9 cm. Each sample group has 1,000 output values from SCALE, and deviations of output values are plotted as a scatter graph which is overlapped on a box plot. Dispersion of output values of each group increases by the increase of $r_{min}$, and its standard deviation also depends on the radius. However, the gradient of the standard deviation is discontinuous, and the graph of standard deviation is not smooth unlike the graph of the dose rate. The standard deviation is 2.17 rem/hr for the 1cm of $r_{min}$, and it increases up to 6.84 rem/hr for the 9cm of $r_{min}$. These values are 1.9 % and 15.3 % of the average dose rate for each $r_{min}$ (Figure B. 3). Even if the standard deviation of the dose rate is only 2.17 rem for the $r_{min}$ of 1cm, a sample at the sample group can has a value which is very different from the average. The range of the dose rate is much larger than the standard deviation, and the deviation of value is much larger than the standard deviation if outliers are included for the calculation of the range. The range of dose rate at a sample group is 13.5 rem/hr for $r_{min}$ of 1cm, and it increases up to 38.2 rem/hr for $r_{min}$ of 9 cm. Even if a canister to have the dose rate of outlier in a sample group is less possible than to have the average value, this value also needs to be considered for the reliable estimation on the radiation dose rate.

## B. 2. Photon dose rate of the close packed fuel debris in a canister

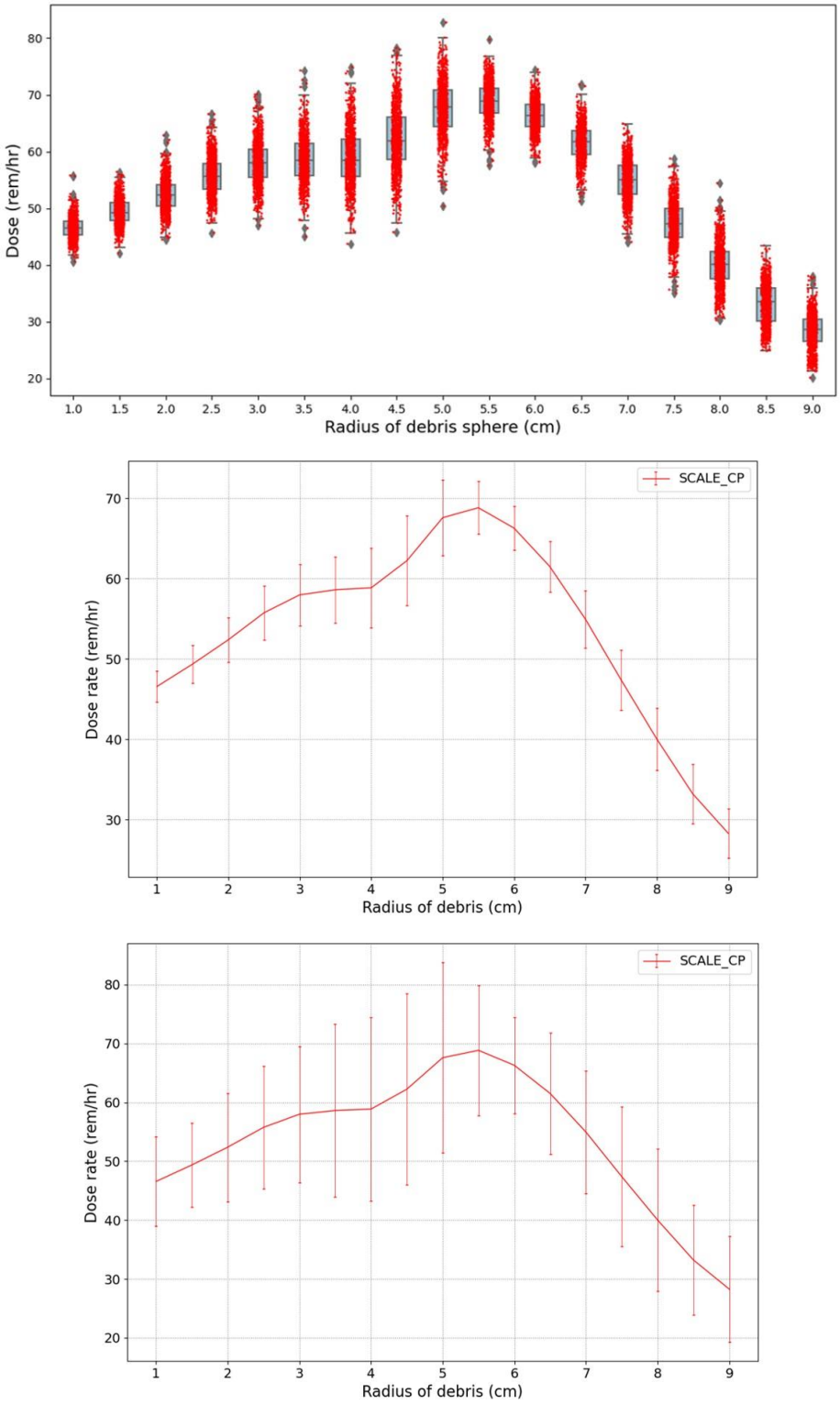


**Figure B. 11 Photon dose rate of the close packed fuel debris.** The estimated dose rates (top), the average dose rate with the standard deviation (middle), the average dose rate with the range (bottom)

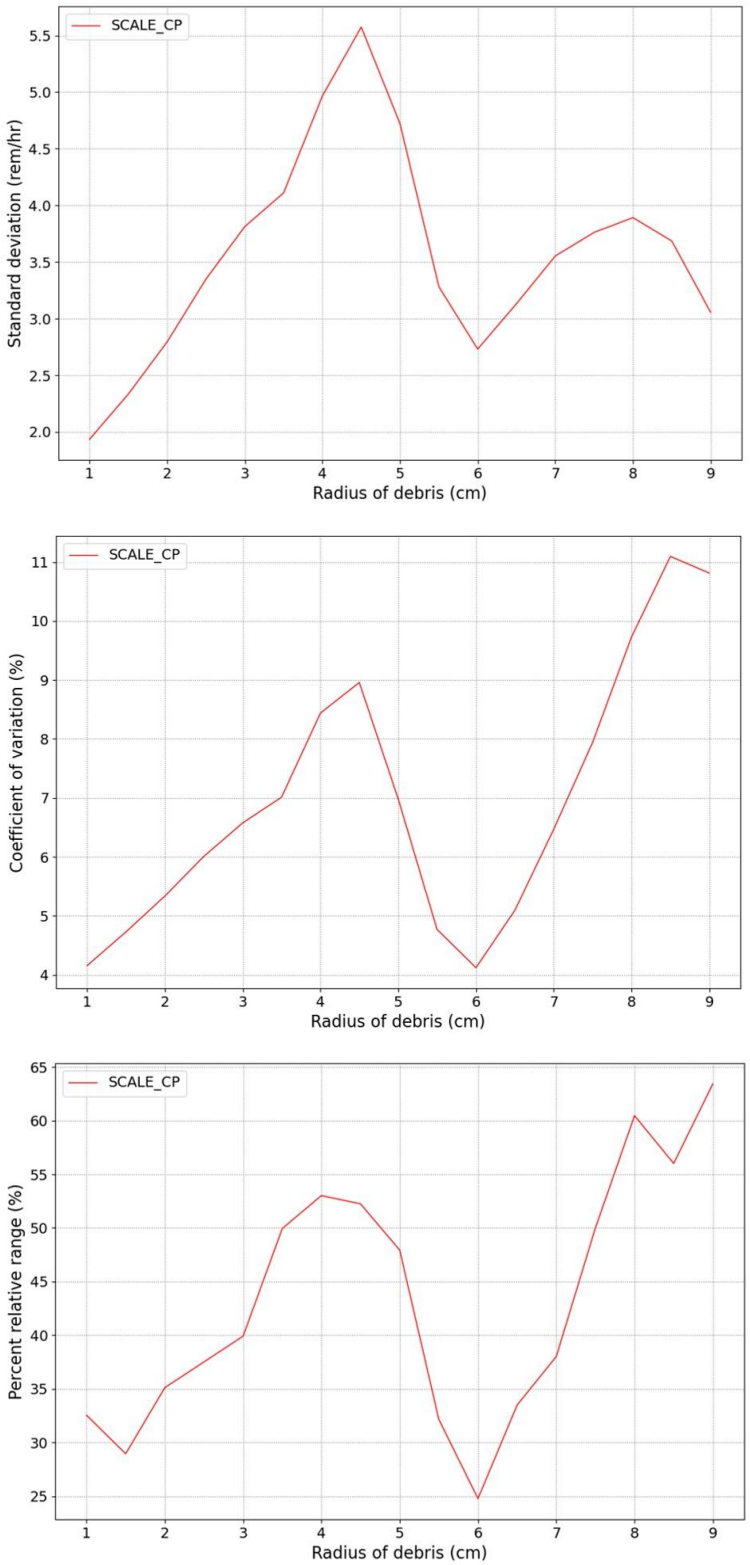


**Figure B. 12 Uncertainty of the close packed fuel debris.** The standard deviation (top), the coefficient of variation (middle), the percent relative range (bottom)

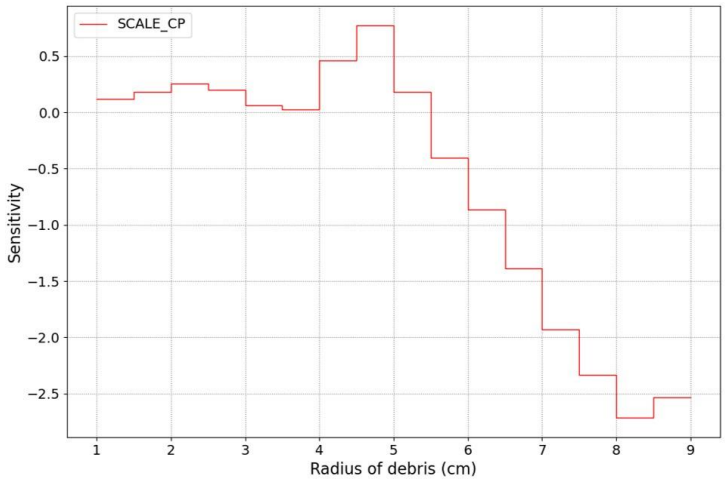


**Figure B. 13 Sensitivity index of the close packed fuel debris.**

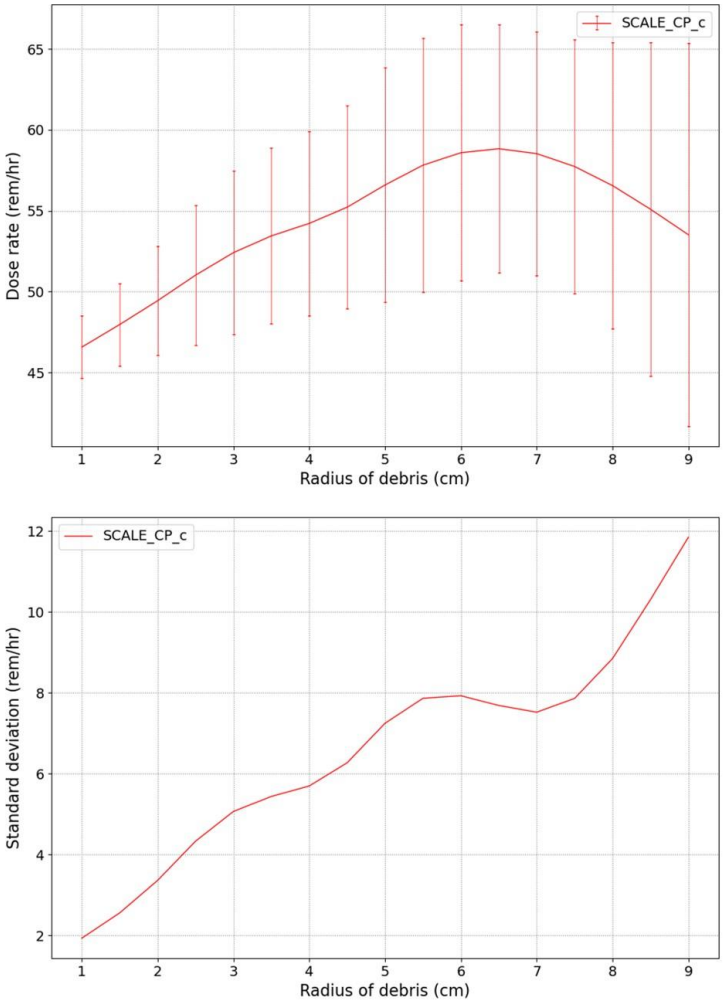


**Figure B. 14 Cumulative graphs.** The average dose rate (top), the standard deviation (bottom)

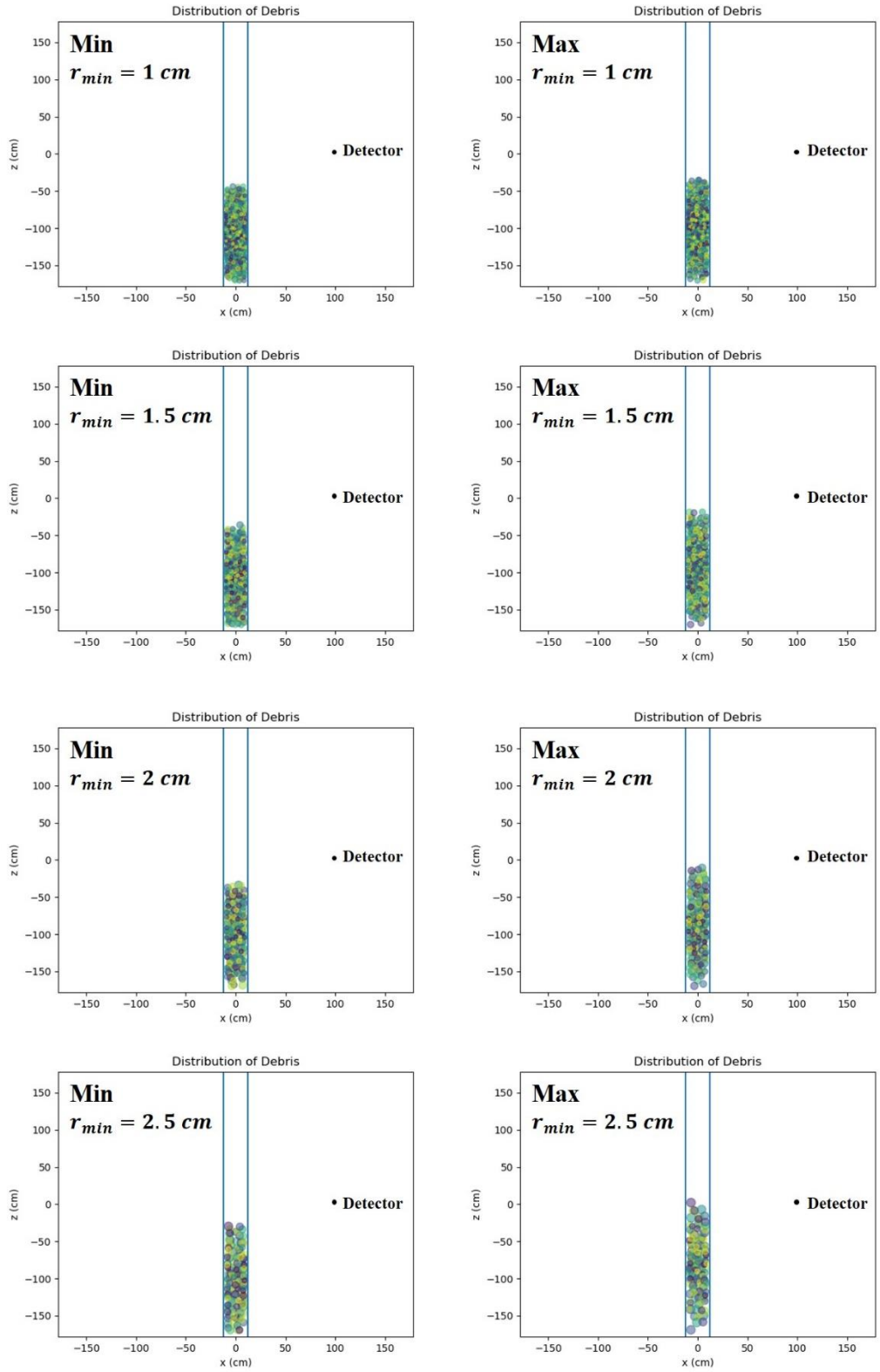


**Figure B. 15 Distribution of the close packed fuel debris in a canister.**

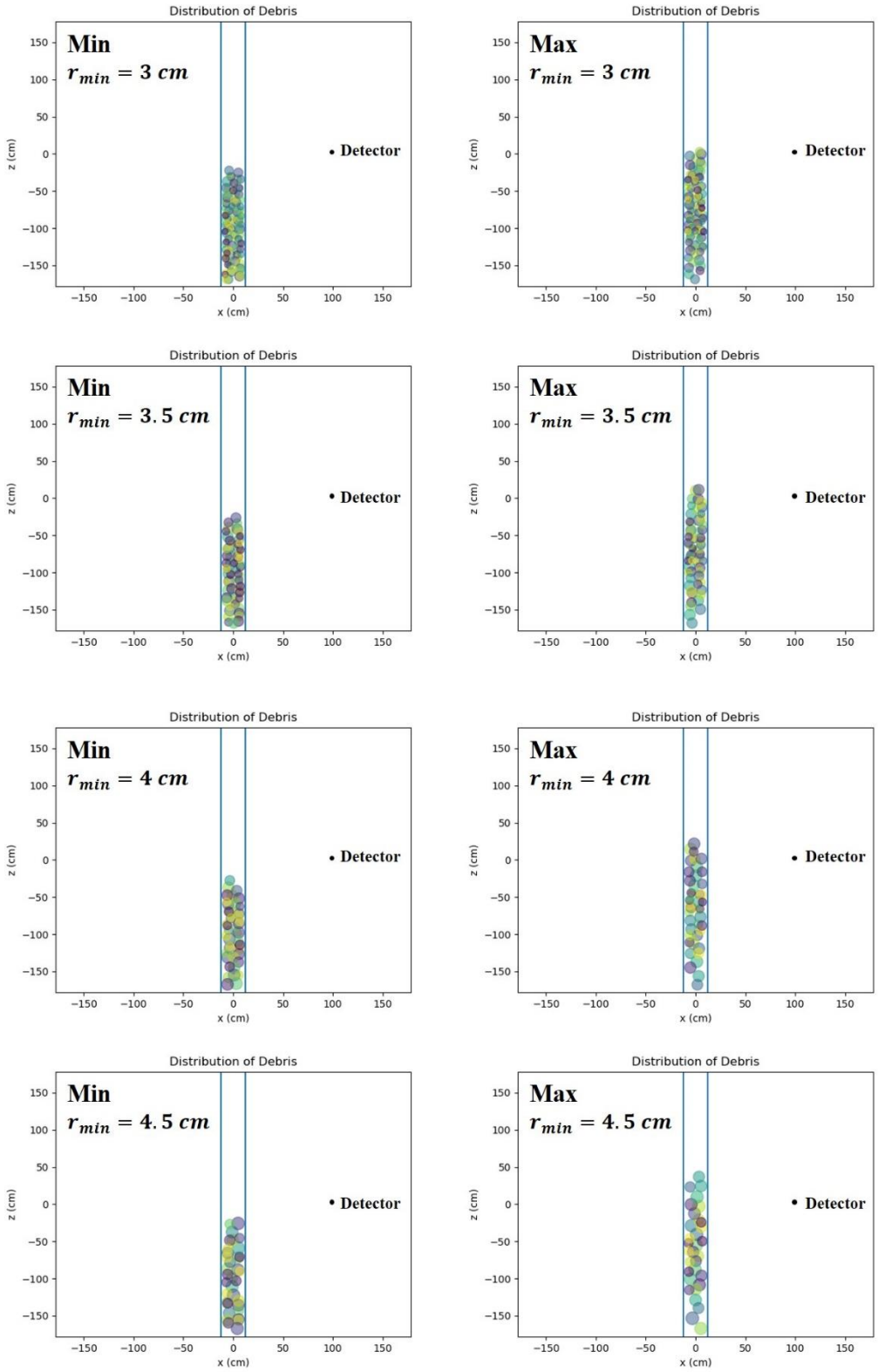


**Figure B. 16 Distribution of the close packed fuel debris in a canister.**

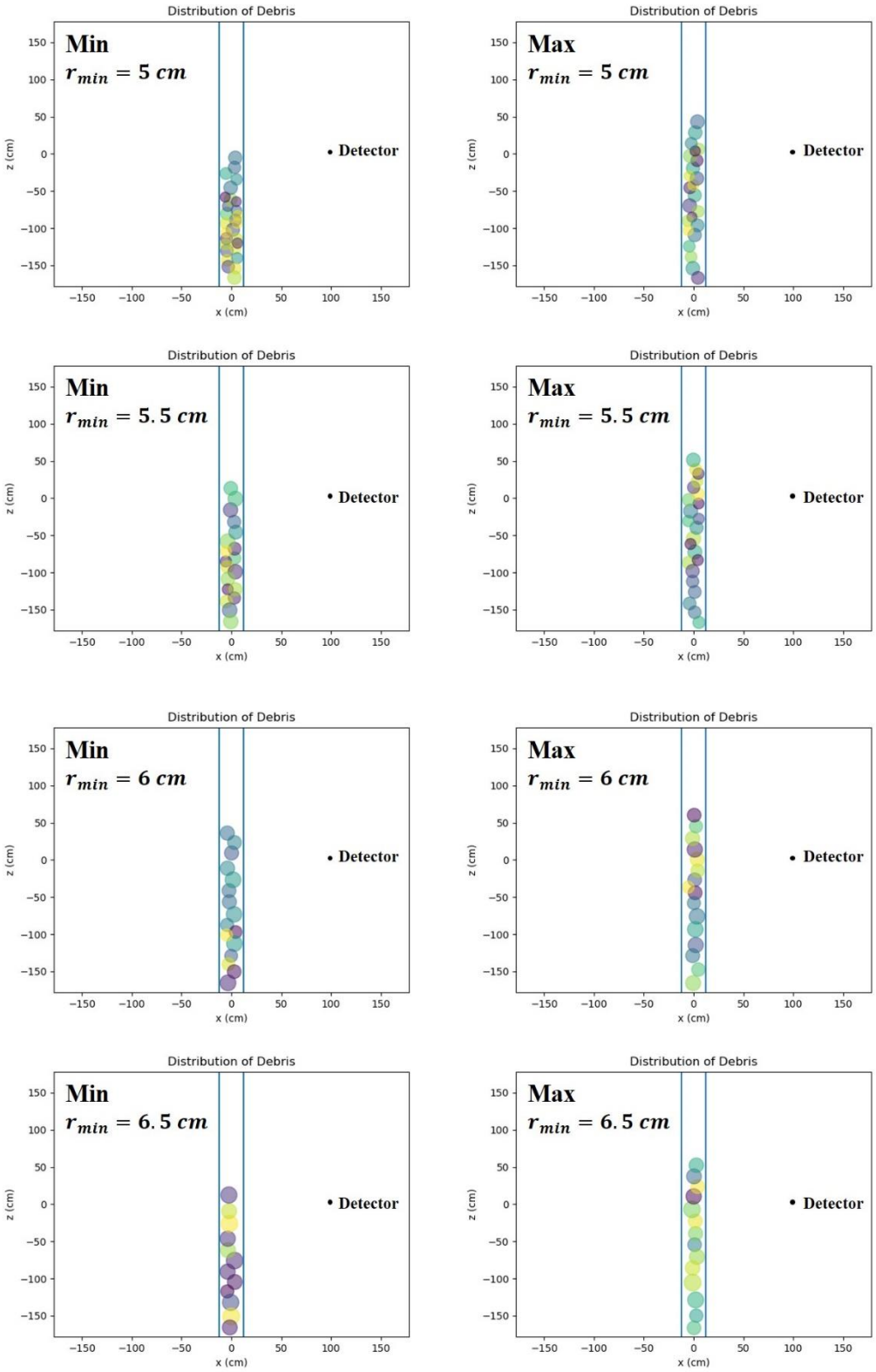


**Figure B. 17 Distribution of the close packed fuel debris in a canister.**

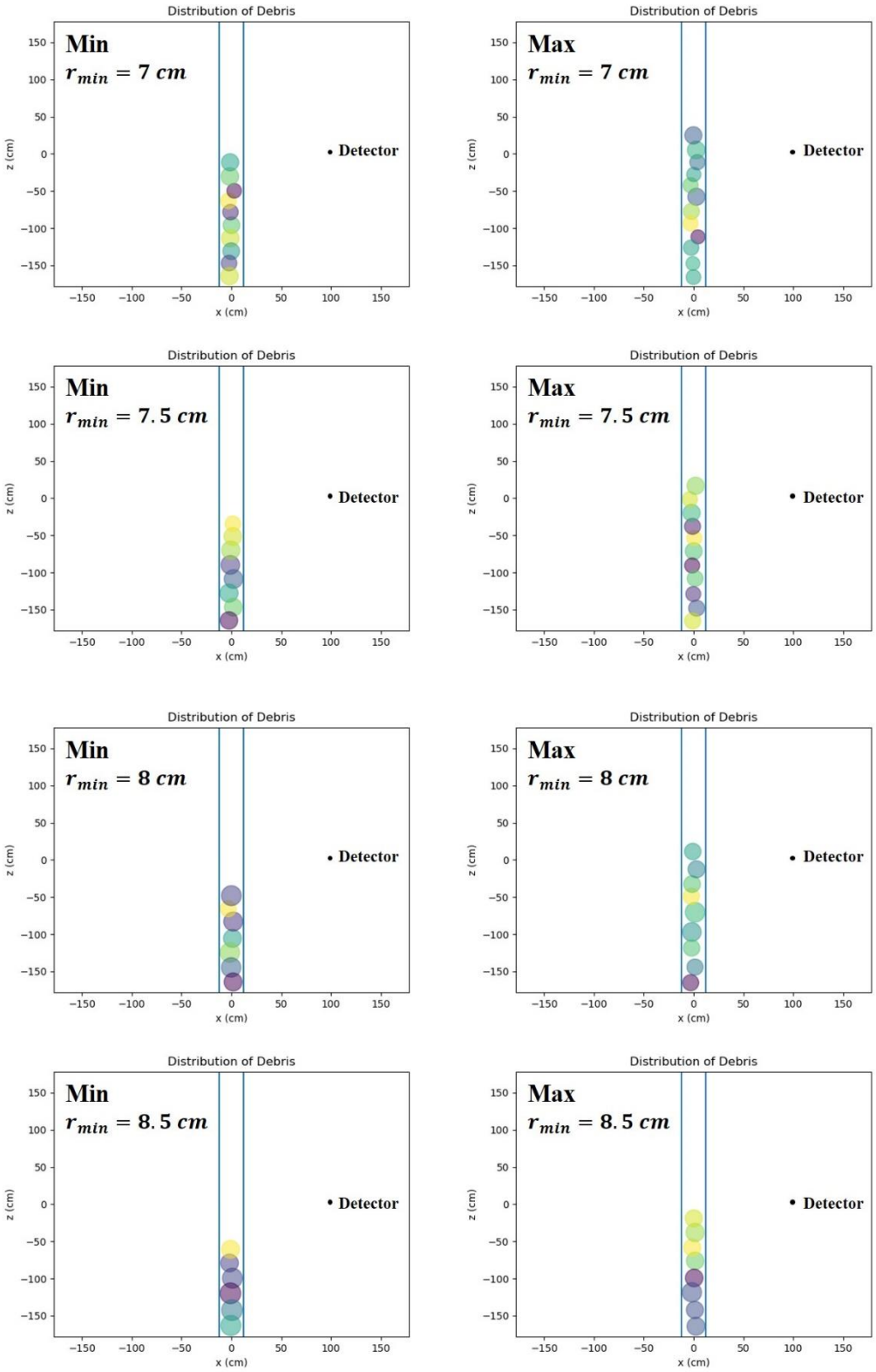


**Figure B. 18 Distribution of the close packed fuel debris in a canister.**

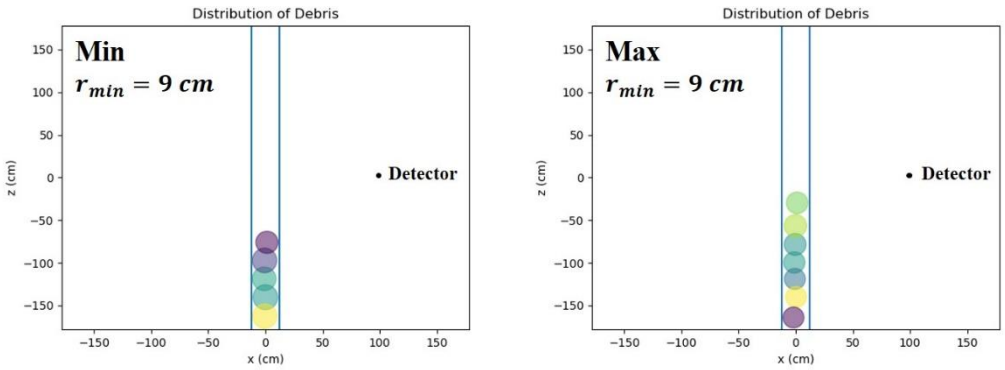


**Figure B. 19 Distribution of the close packed fuel debris in a canister.**

Compare to the continuous decreases in photon dose rate of the loose packed debris, dose rate of the close packed debris increases by increases in the minimum radius $r_{min}$ when $r_{min}$ is smaller than 5.5 cm. The dose rate decreases for $r_{min}$ which is larger than 5.5 cm. Therefore, graph of the average dose rate has its maximum point at 5.5 cm of $r_{min}$ (Figure B. 11). The average photon dose rate for $r_{min}$ of 5.5 cm is 68.84 rem/hr. Dispersion of data at the graph also does not continue to increase by the change of $r_{min}$ unlike the data of the loose packed debris. Graph of the standard deviation has two local maximum points at $r_{min}$ of 4.5 cm and 8 cm, and the absolute maximum of the graph is the point at $r_{min}$ of 4.5cm (Figure B. 12). The average dose rate at $r_{min}$ of 4.5 cm and 8 cm are 62.2 rem/hr and 40.0 rem/hr each, and the standard deviation for these points are 5.57 rem/hr and 3.89 rem/hr. Even if the value of standard deviation at $r_{min}$ of 4.5 cm is larger than the value at $r_{min}$ of 8 cm, the uncertainty which is calculated by dividing the standard deviation by the average dose rate at $r_{min}$ of 8 cm is larger than the uncertainty at $r_{min}$ of 4.5 cm. The maximum uncertainty is at $r_{min}$ of 8.5 cm, and it is 11.1% of the average dose rate. Graph of the range also has minimum and local maximums, and the absolute maximum value is 32.5 rem/hr at $r_{min}$ of 4.5 cm.

**B. 3. Photon dose rate of the close packed fuel debris in a canister (moved to center)**

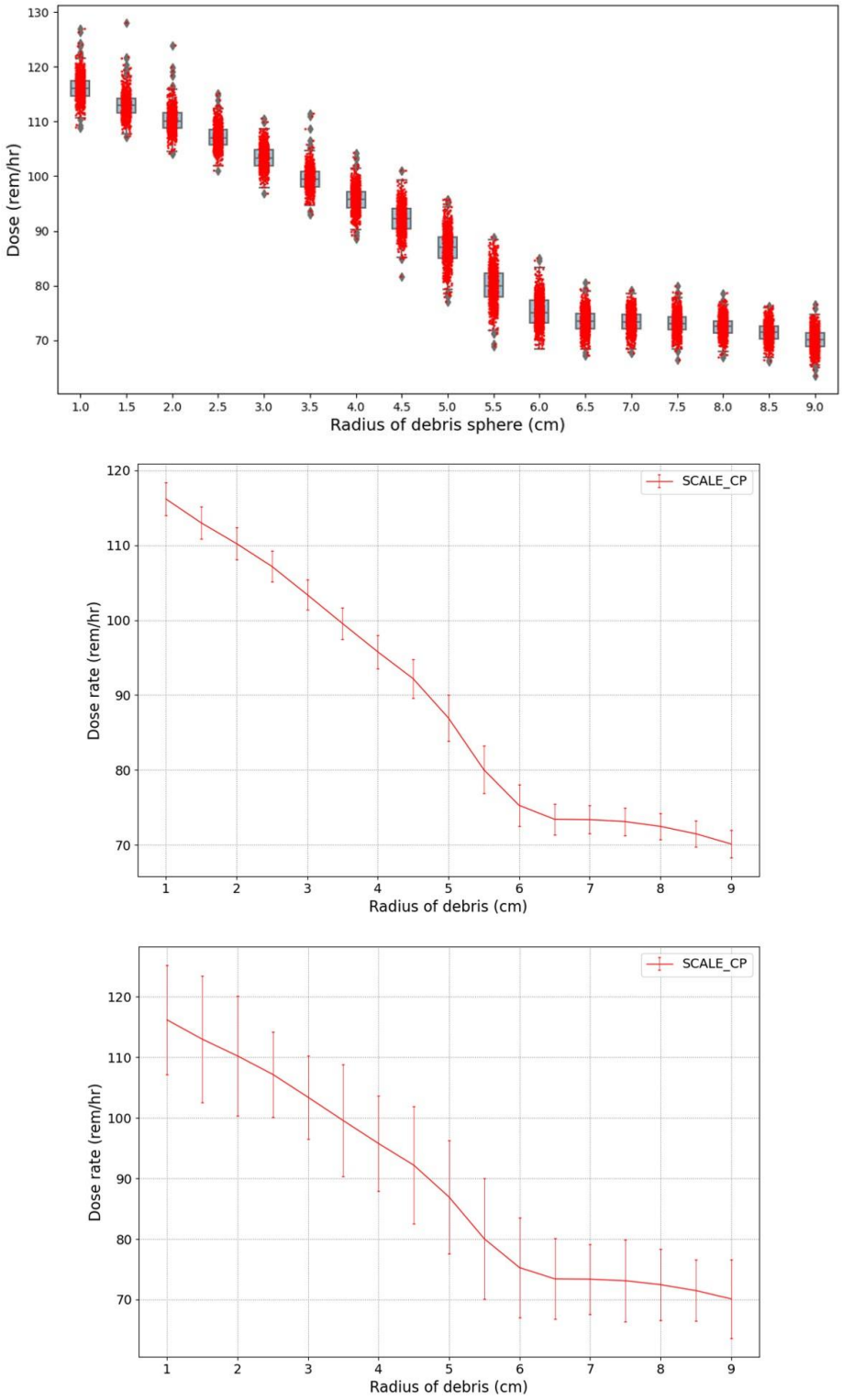


**Figure B. 20 Photon dose rate of the close packed fuel debris.** The estimated dose rates (top), the average dose rate with the standard deviation (middle), the average dose rate with the range (bottom)

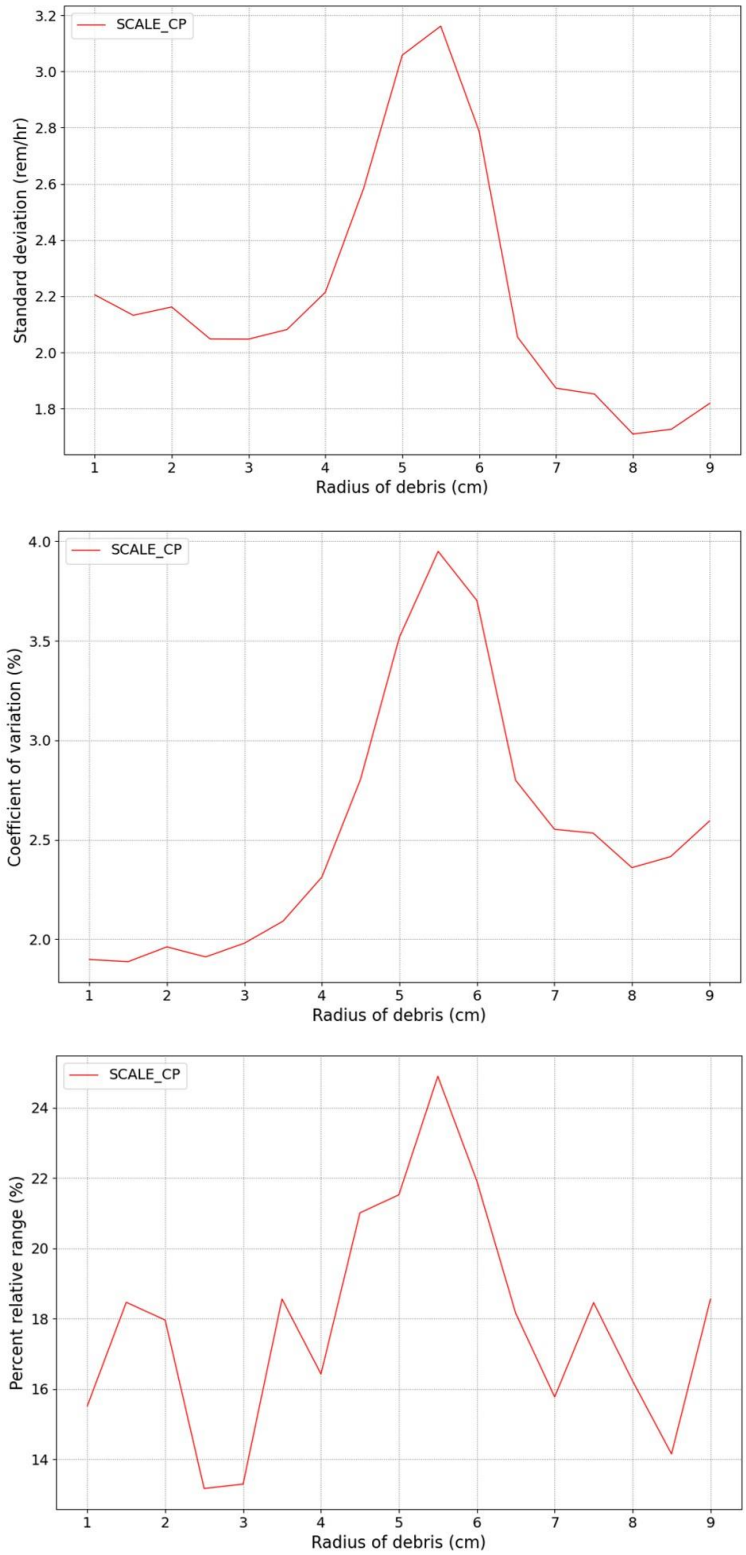


**Figure B. 21 Uncertainty of the close packed fuel debris.** The standard deviation (top), the coefficient of variation (middle), the percent relative range (bottom)

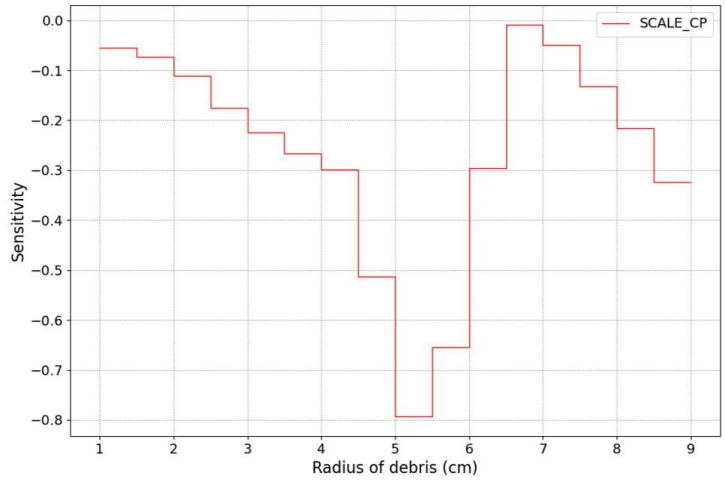


**Figure B. 22 Sensitivity index of the close packed fuel debris.**

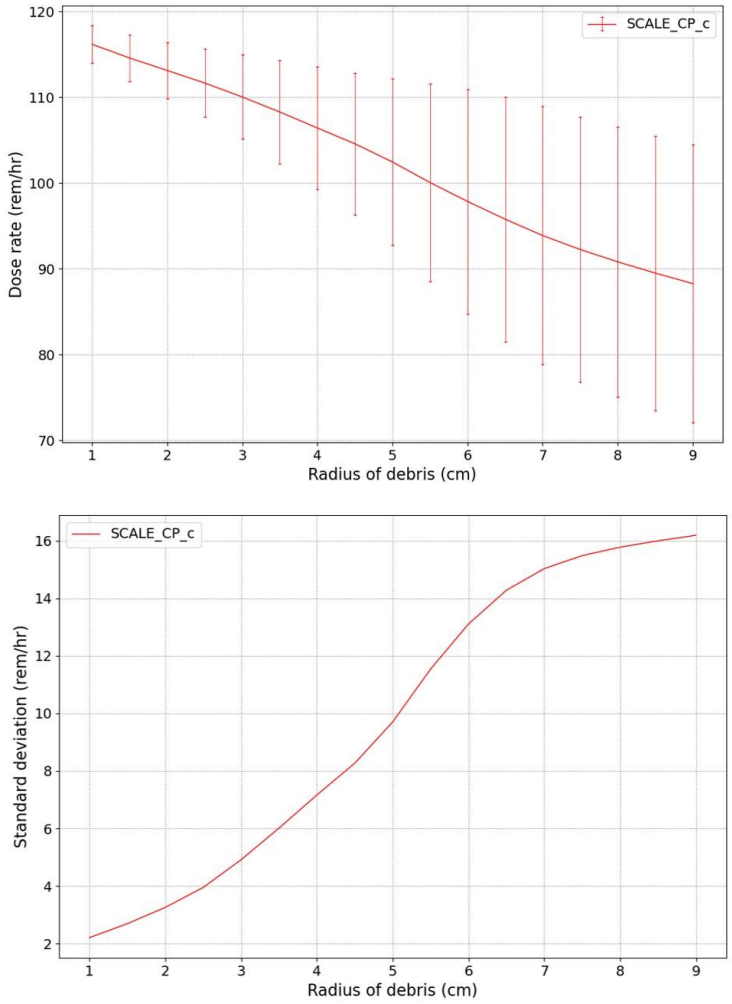


**Figure B. 23 Cumulative graphs.** The average dose rate (top), the standard deviation (bottom)

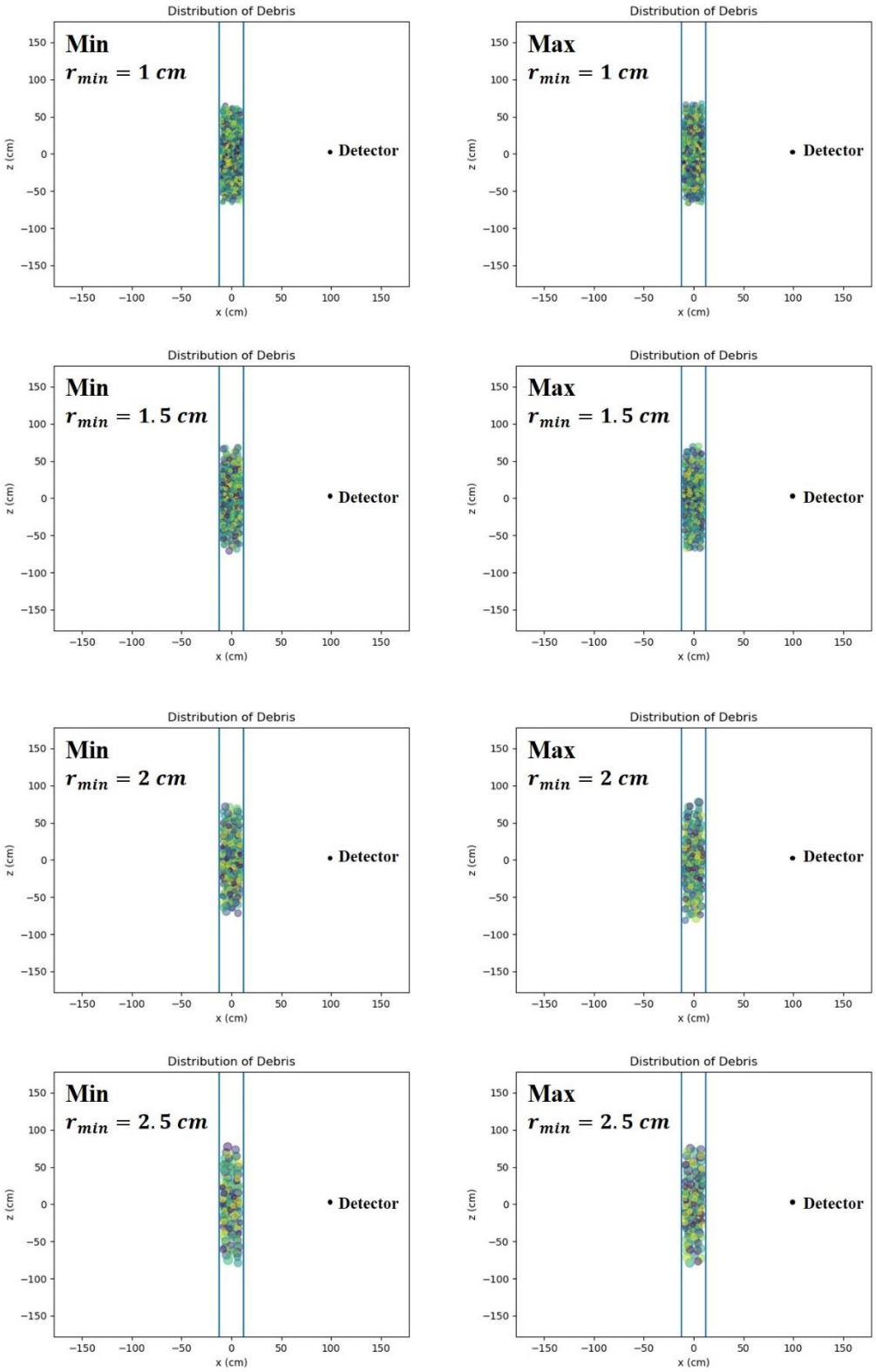


**Figure B. 24 Distribution of the close packed fuel debris in a canister.**

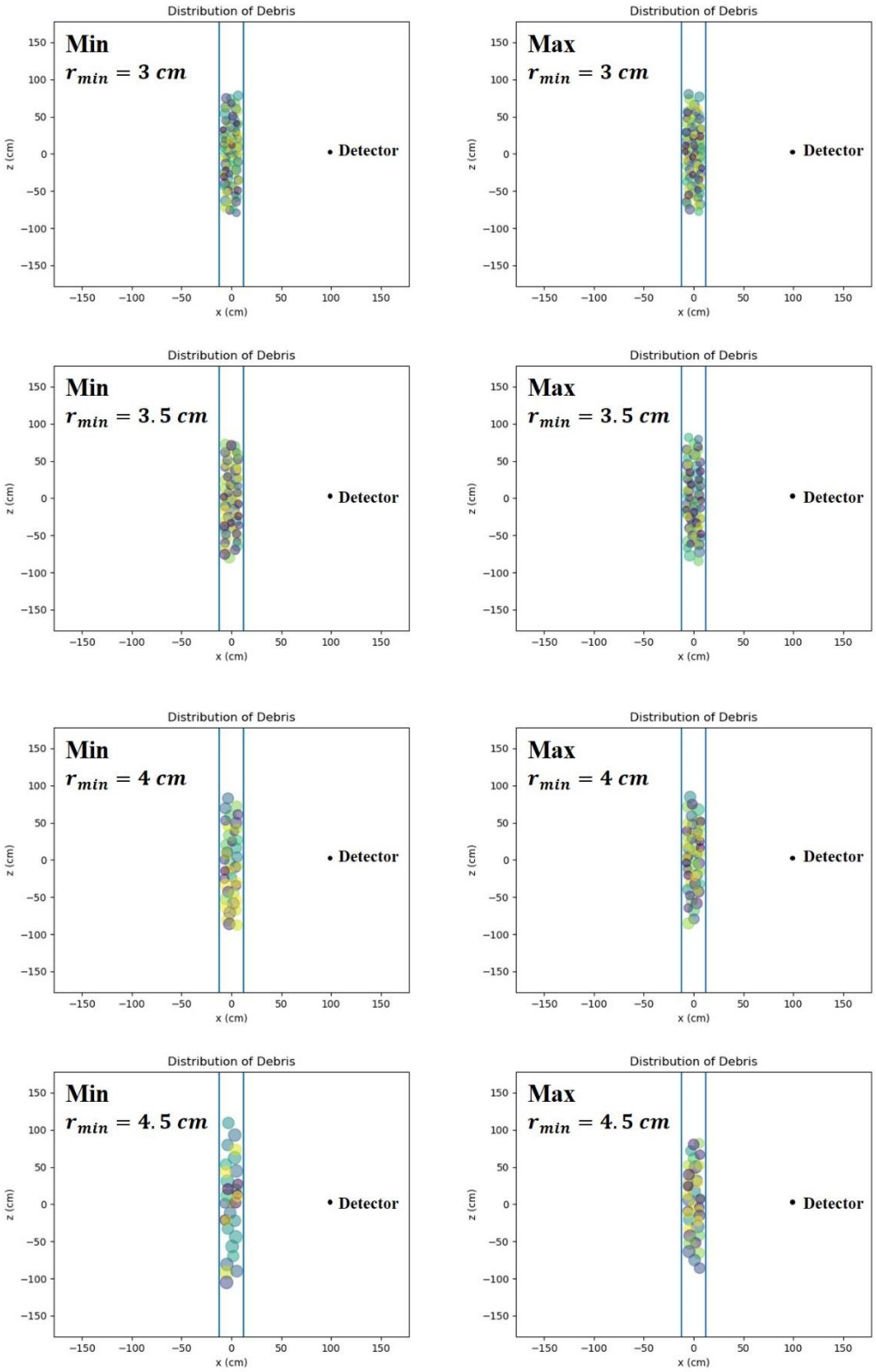


**Figure B. 25 Distribution of the close packed fuel debris in a canister.**

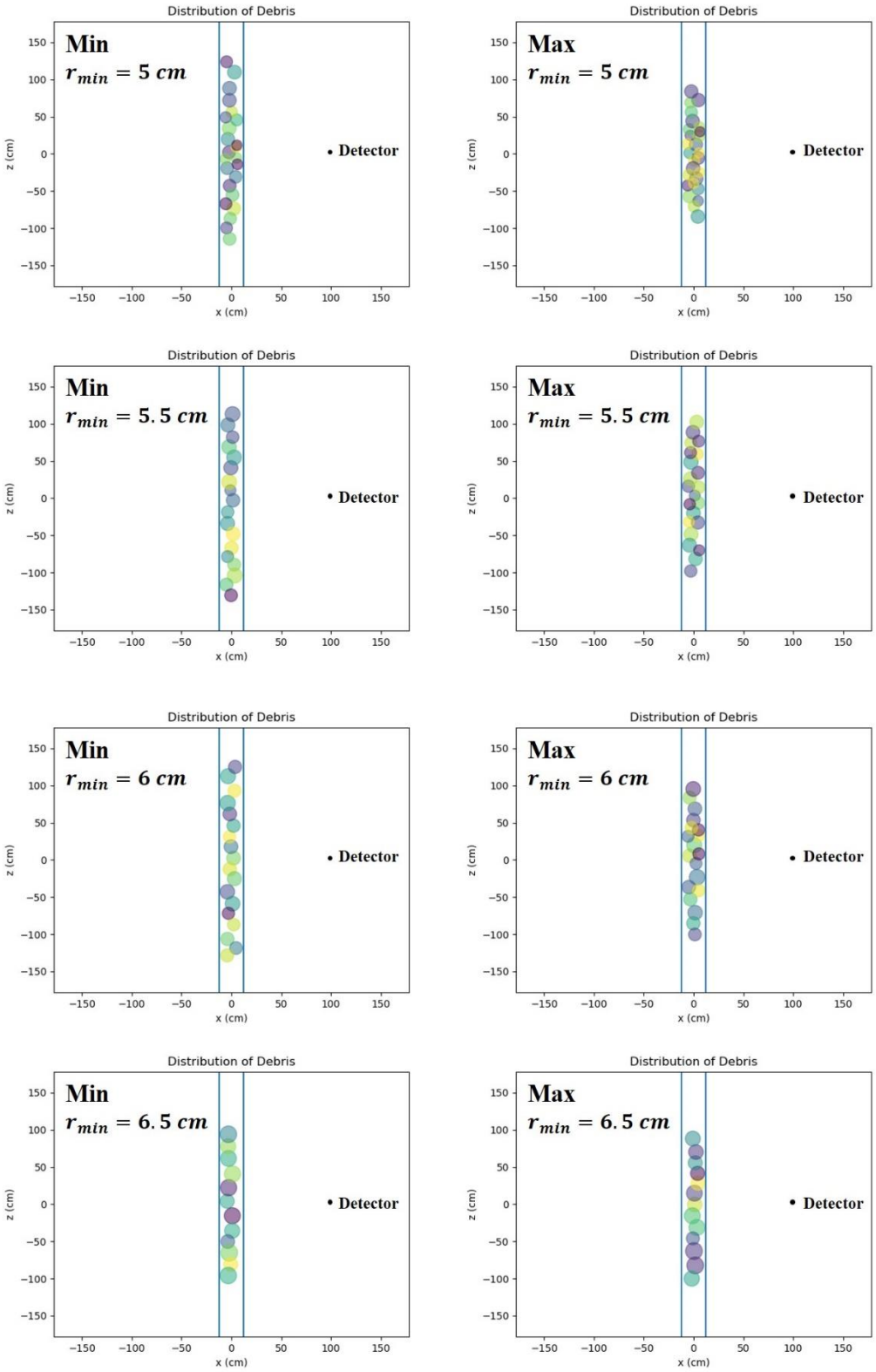


**Figure B. 26 Distribution of the close packed fuel debris in a canister.**

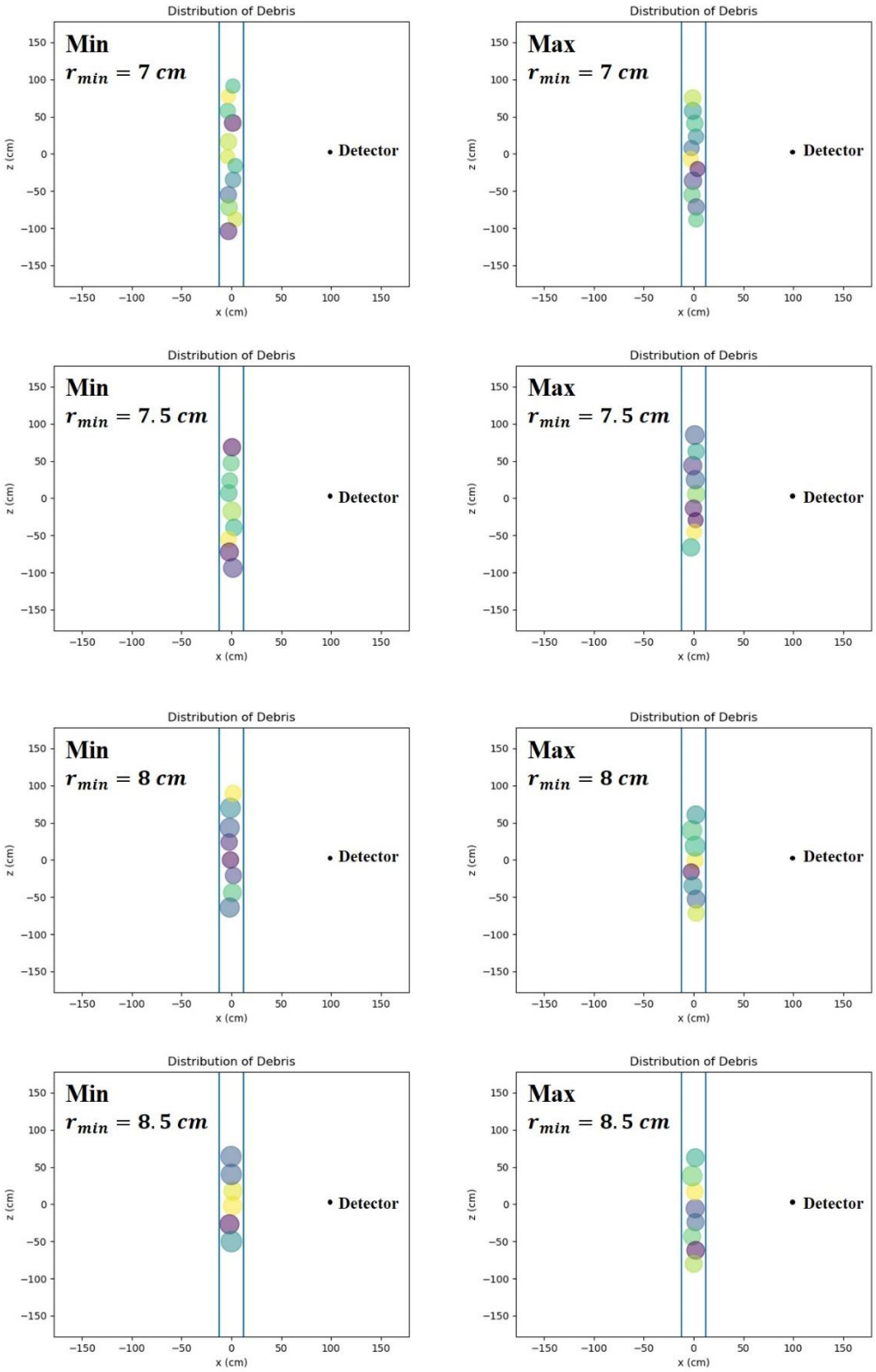


**Figure B. 27 Distribution of the close packed fuel debris in a canister.**

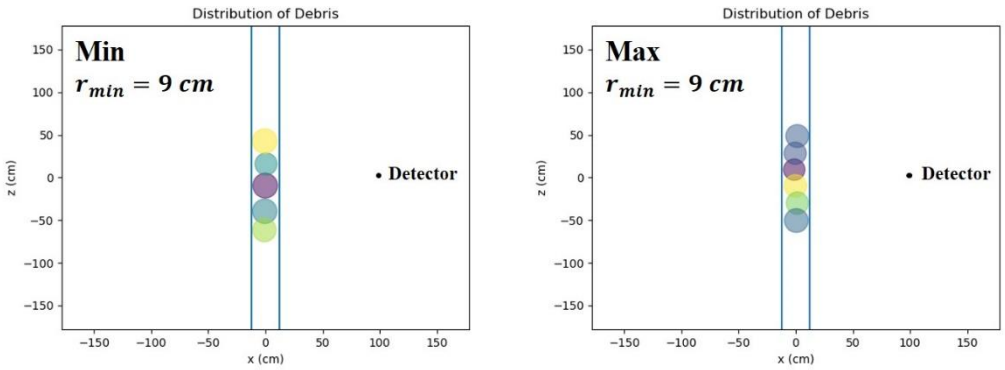


**Figure B. 28 Distribution of the close packed fuel debris in a canister.**

Dose rate estimated at 1m from the center of a canister is affected by the biased distribution of fuel debris when debris are closely packed. More debris are at the lower half of a canister and it affected to the estimated dose rate. At this section, photon dose rate has been estimated 1m from the center of a fuel canister which close packed fuel debris are moved to the center of the canister. The point detector is located at the center of debris pile for all samples by moving the pile of debris to the center of a canister. This assumption is not physical because fuel debris may pile up from the bottom of a canister. However, this is assumed to exclude affect of the biased distribution of fuel debris on the dose rate and focus on other factors.

Photon dose rate of close paced fuel debris decreases by the increase of the minimum radius $r_{min}$ (Figure B. 20). The average dose rate almost linearly decreases from 116.2 rem/hr at 1 cm of $r_{min}$ to 80.04 rem/hr at 6 cm of $r_{min}$, then its gradient decreases for $r_{min}$ larger than 6 cm up to 70.12 at 9 cm of $r_{min}$. Standard deviation of the dose rate has a maximum at 5.5 cm of $r_{min}$ which is 3.16 rem/hr (Figure B. 21). The maximum of standard deviation at 5.5 cm of $r_{min}$ is less than 4 % of the average dose rate. Range of dose rate has several local maximums and minimums.

## B. 4. Neutron dose rate of the loose packed fuel debris in a canister

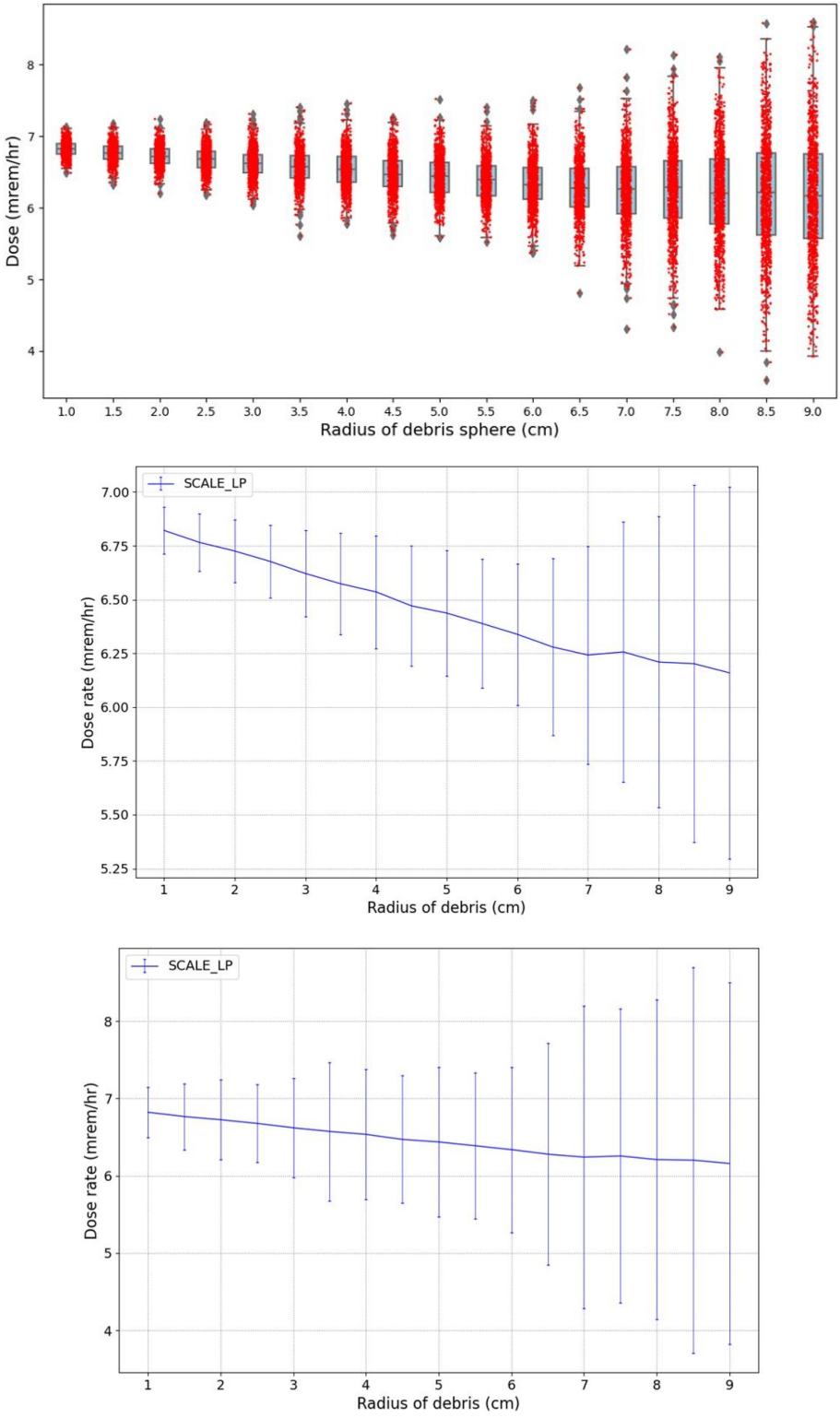


**Figure B. 29 Neutron dose rate of the loose packed fuel debris.** The estimated dose rates (top), the average dose rate with the standard deviation (middle), the average dose rate with the range (bottom)

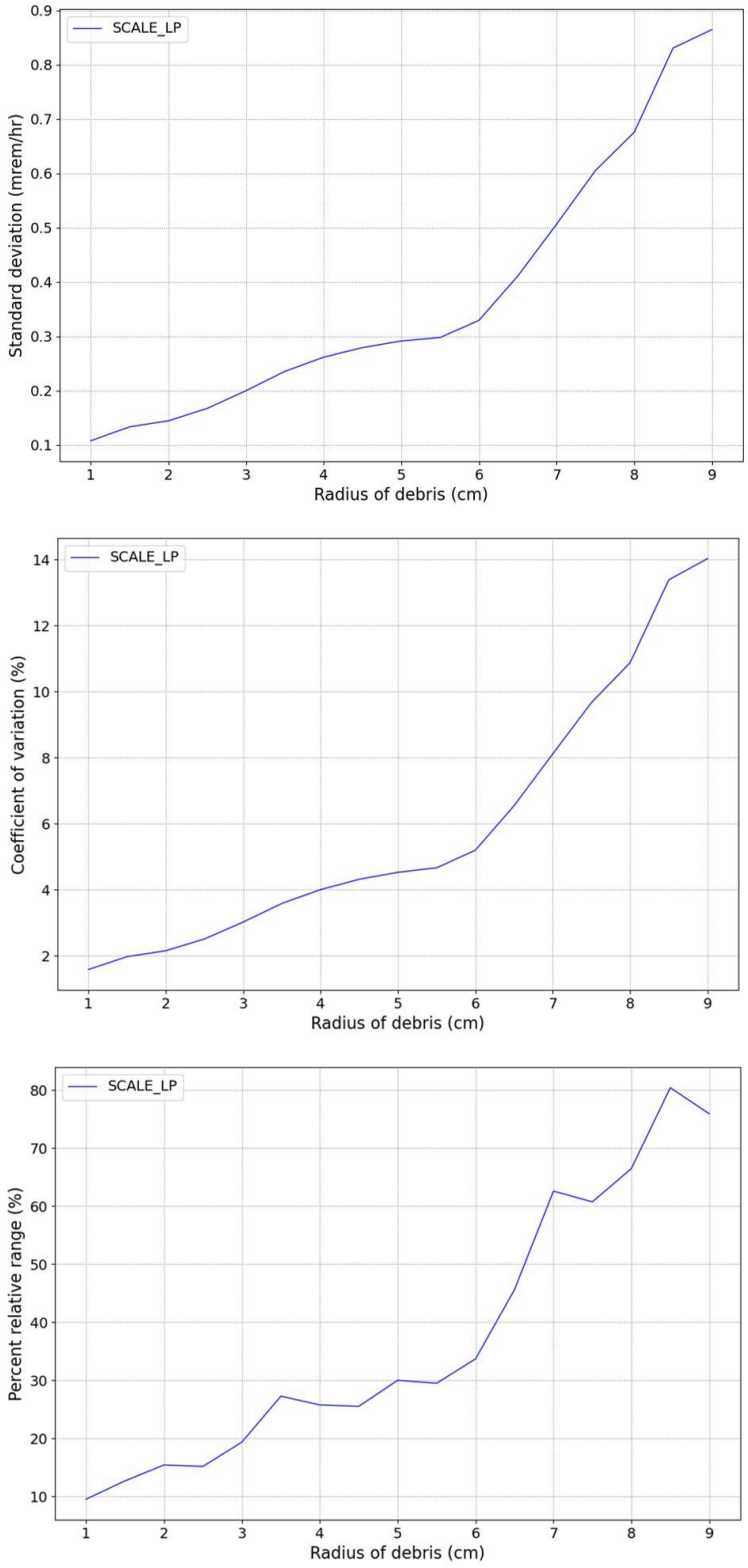


**Figure B. 30 Uncertainty of the loose packed fuel debris.** The standard deviation (top), the coefficient of variation (middle), the percent relative range (bottom)

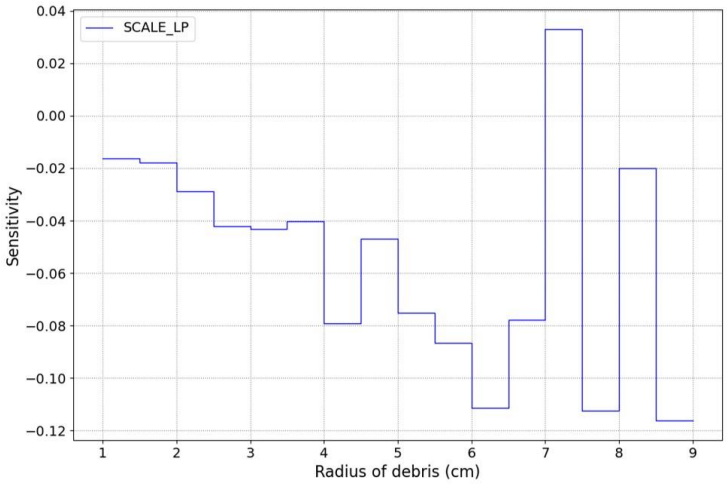


**Figure B. 31 Sensitivity index of the loose packed fuel debris.**

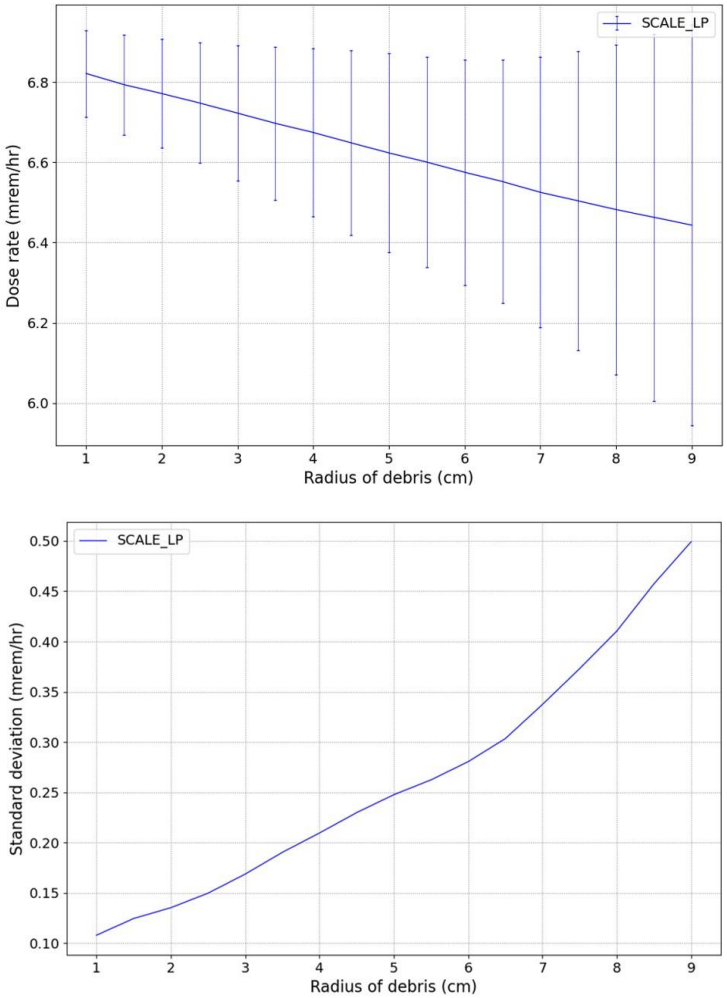


**Figure B. 32 Cumulative graphs.** The average dose rate (top), the standard deviation (bottom)

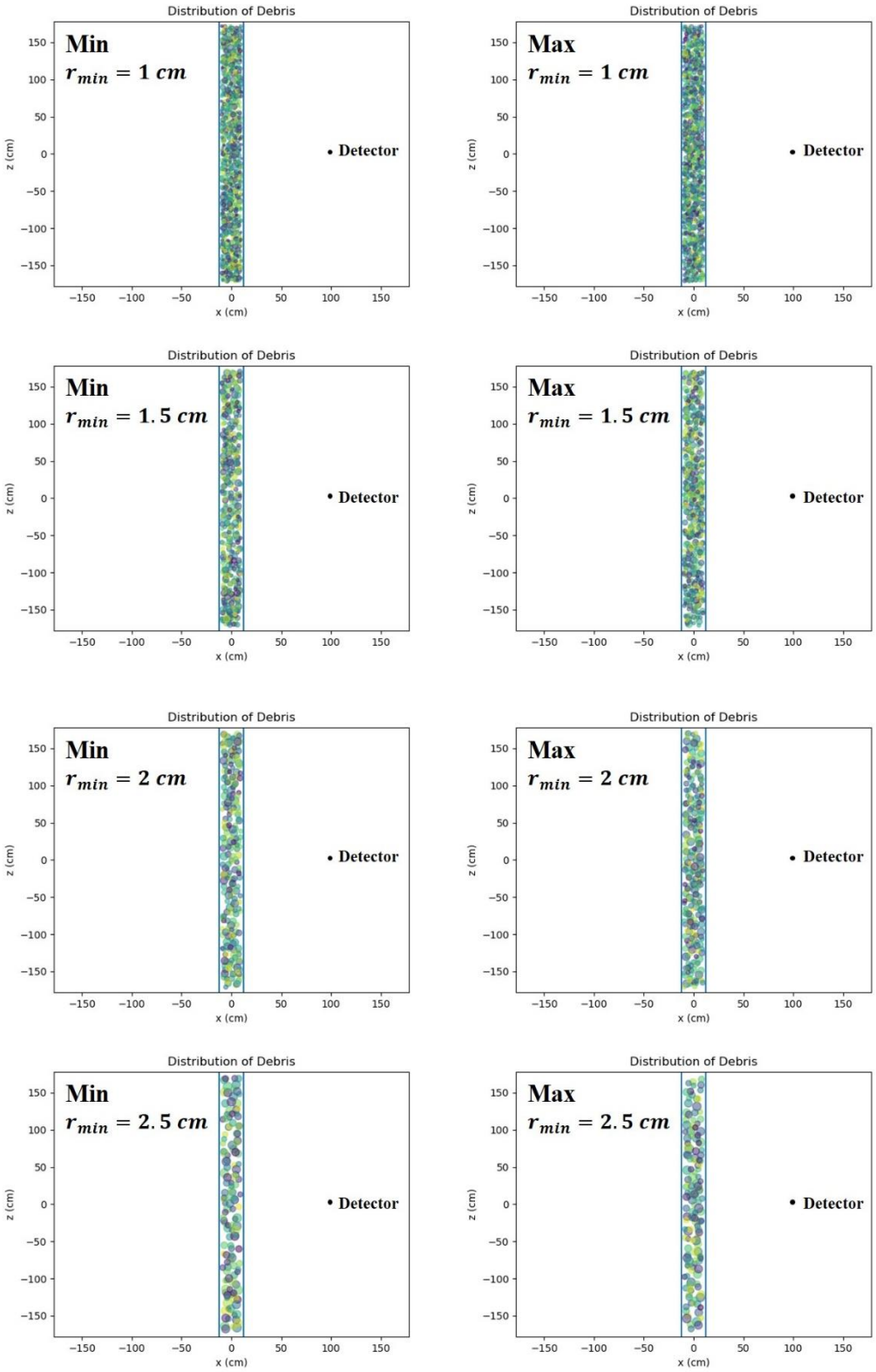


**Figure B. 33 Distribution of the loose packed fuel debris in a canister.**

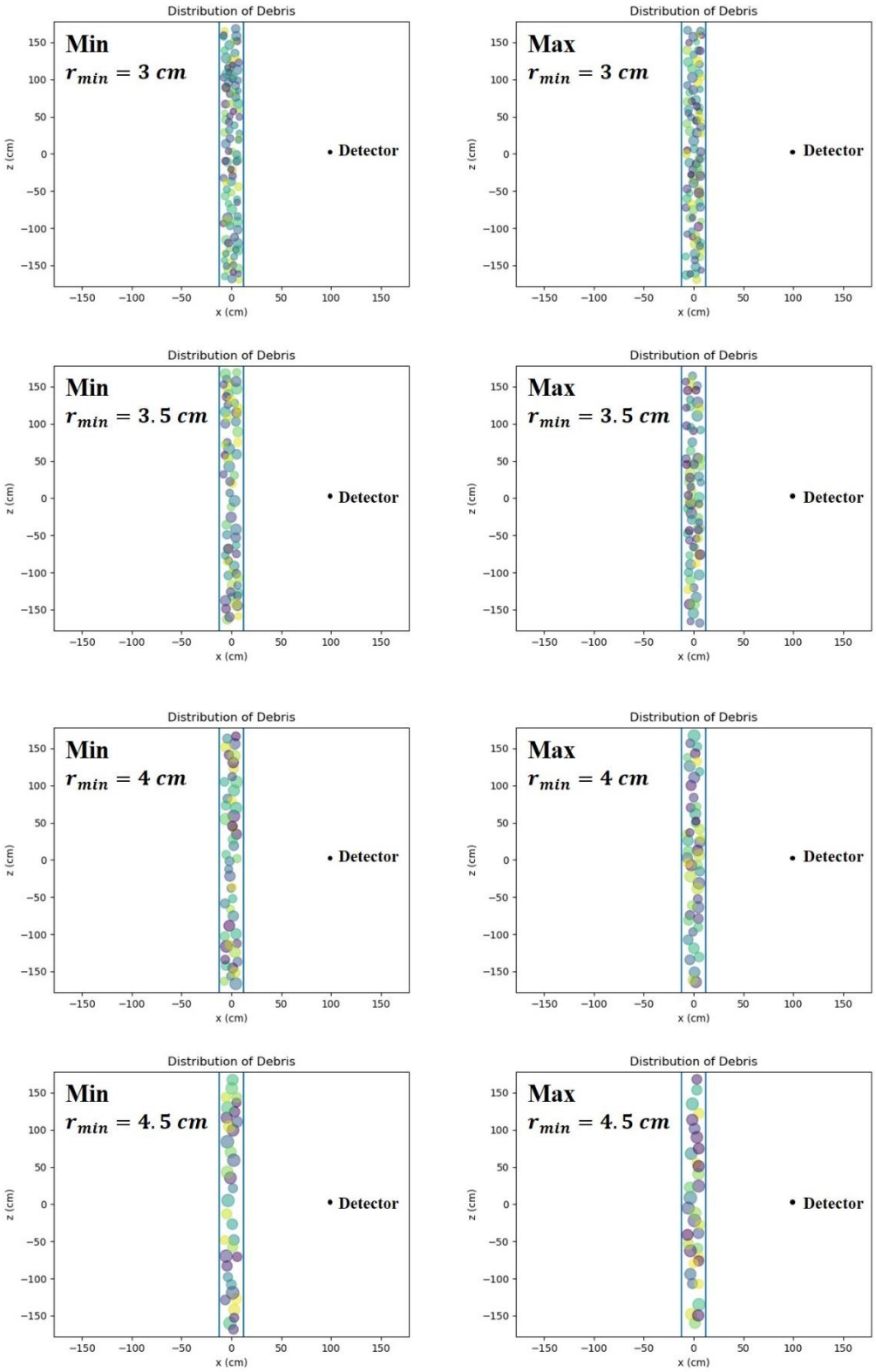


**Figure B. 34 Distribution of the loose packed fuel debris in a canister.**

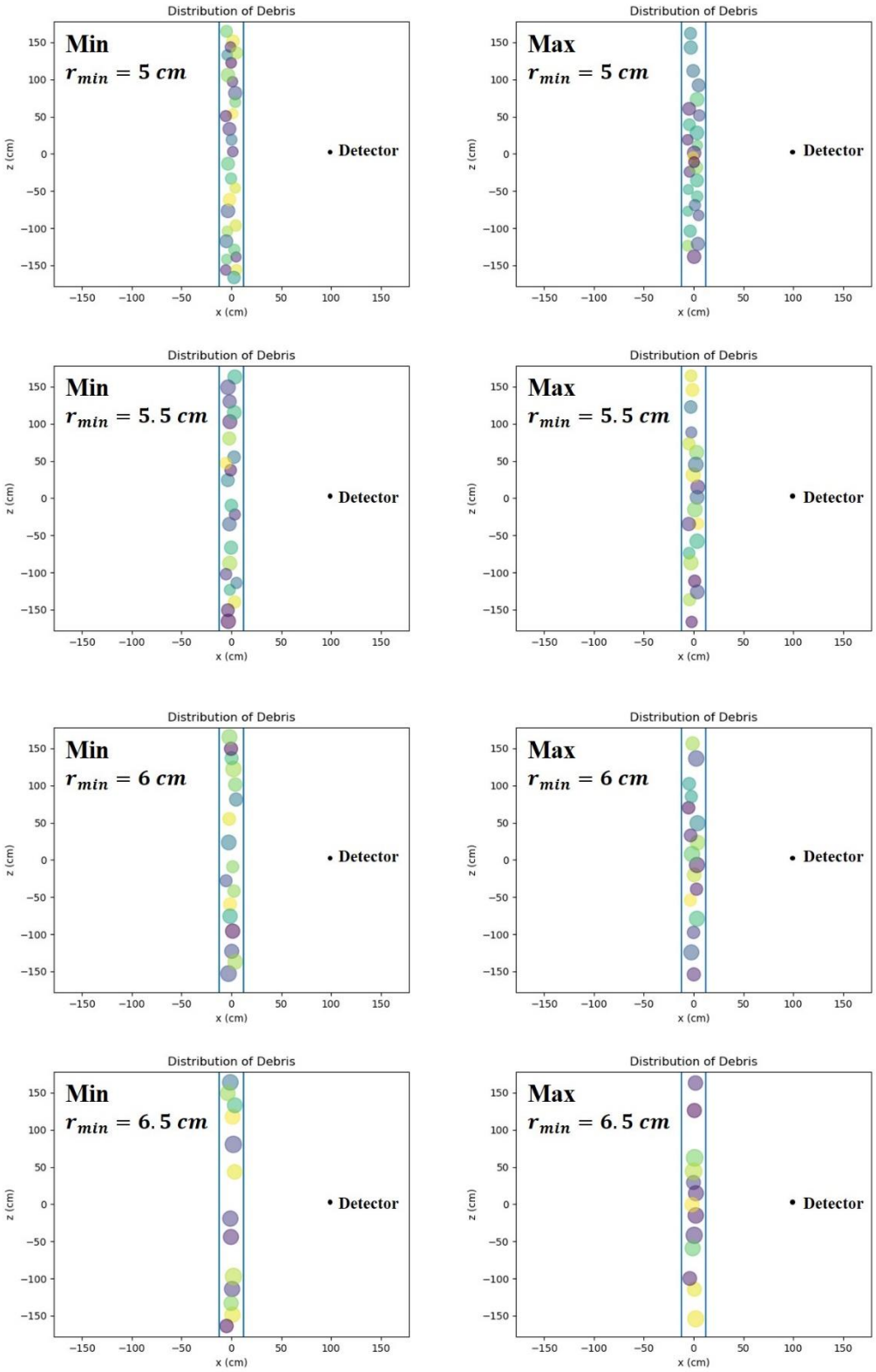


**Figure B. 35 Distribution of the loose packed fuel debris in a canister.**

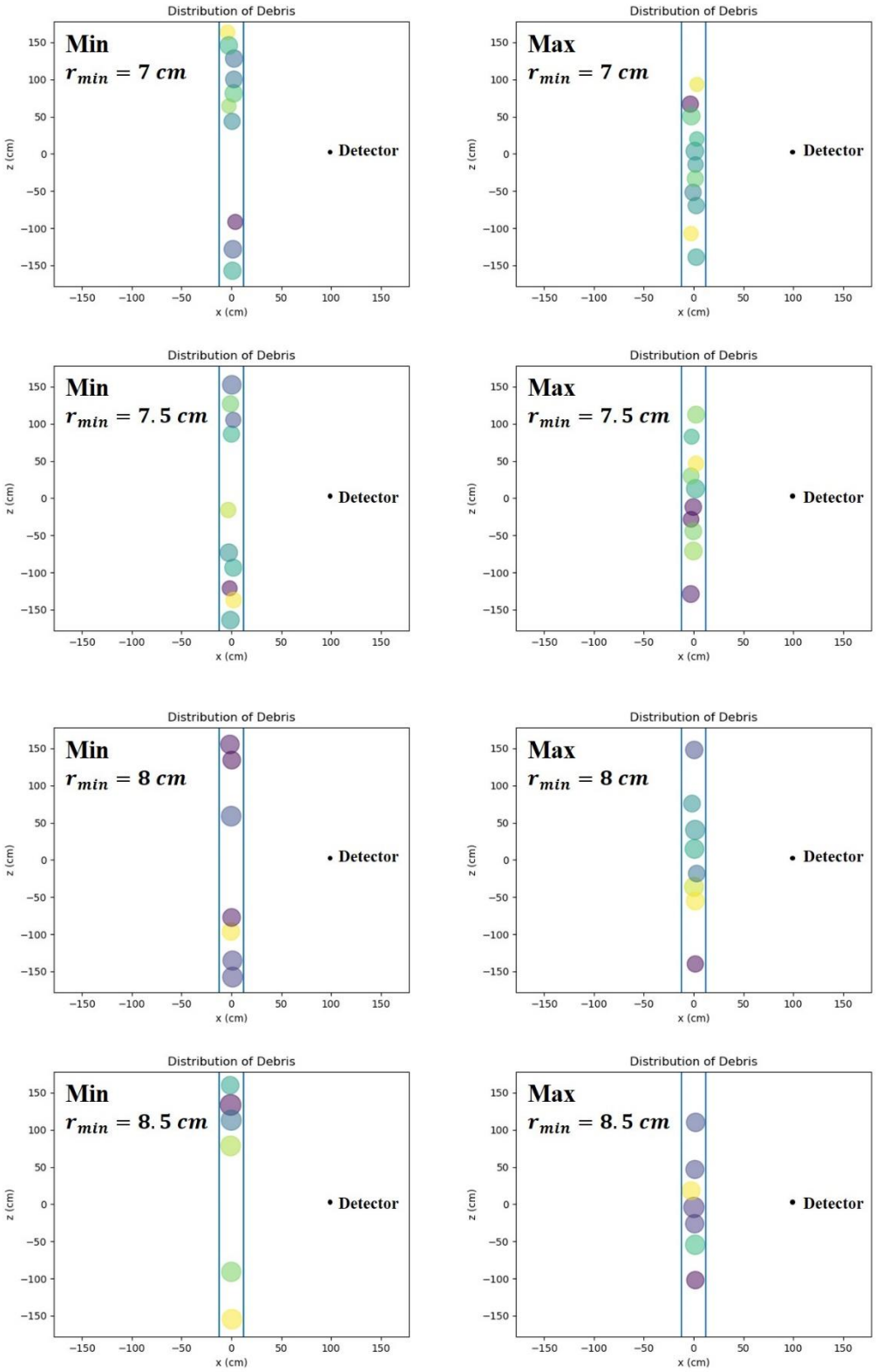


**Figure B. 36 Distribution of the loose packed fuel debris in a canister.**

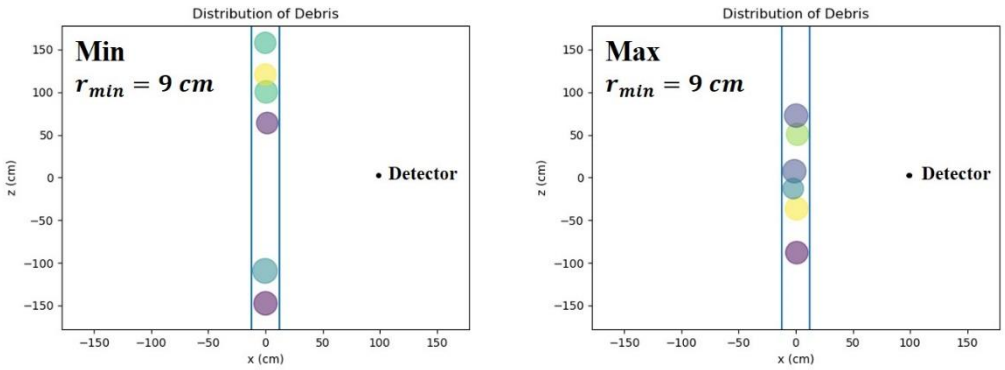


**Figure B. 37 Distribution of the loose packed fuel debris in a canister.**

Neutron dose rate decreases by the decrease of the minimum radius $r_{min}$ of sample group, but its average values does not change a lot by the change of $r_{min}$ (Figure B. 29). Average neutron dose rate of the loose packed fuel debris is 6.82 mrem/hr for 1.0 cm of $r_{min}$ and it is 6.16 mrem/hr for 9.0 cm $r_{min}$. On the other hand, standard deviation of the neutron dose rate increases by the increase of the $r_{min}$ which are 0.11 mrem/hr for 1.0 cm of $r_{min}$ and 0.86 mrem/hr for 9.0 cm of $r_{min}$ (Figure B. 30). The coefficient of variation is 1.6 % of the average dose rate for 1.0 cm of $r_{min}$, and 14 % of the average dose rate for 9.0 cm of $r_{min}$. Range of the neutron dose rate is much larger than the standard deviation. Range of data is 0.65 mrem/hr for 1.0 cm of $r_{min}$ which is 9.53 % of the average dose rate, and the range is 4.67 mrem/hr for 9.0 cm of $r_{min}$ which is 75.8 % of the average dose rate.

The neutron mean free path in fuel debris is longer than the mean free path of high energy photons, and neutron radiation is less attenuated while passing fuel debris than photons do. Therefore, the self-attenuation and the particle self-shielding which depend on the size of fuel debris less affect to the change of neutron dose rate than they do to photon dose rate, and the average dose rate does not decrease a lot by the change of $r_{min}$. Calculated dose rate depends more on the vertical distribution of fuel debris in a canister rather than the size of fuel debris, and each sample group has large deviation of data because of the differences in vertical distribution affected to the total path length from debris to a point detector.

## B. 5. Neutron dose rate of the close packed fuel debris in a canister (moved to center)

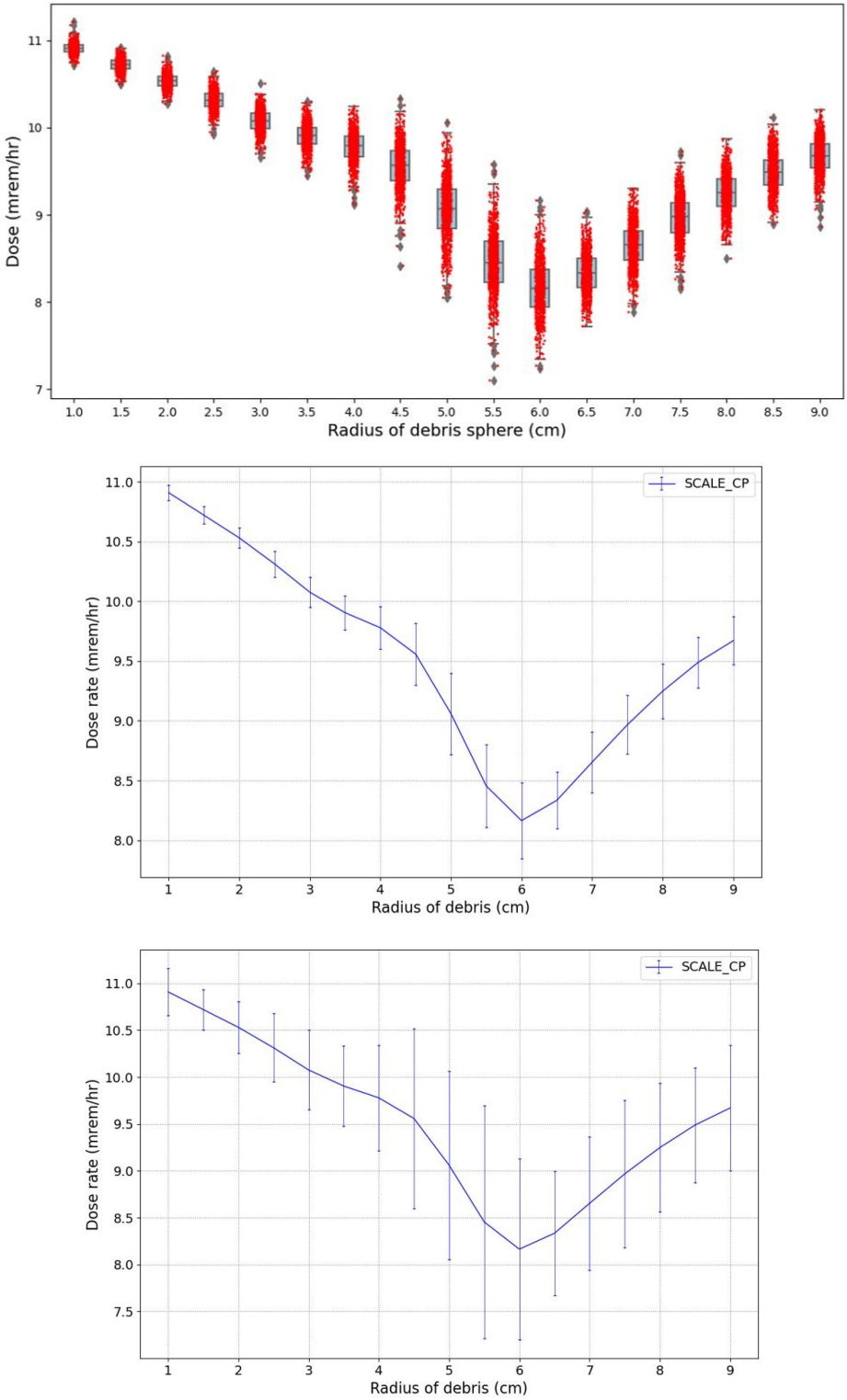


**Figure B. 38 Neutron dose rate of the close packed fuel debris.** The estimated dose rates (top), the average dose rate with the standard deviation (middle), the average dose rate with the range (bottom)

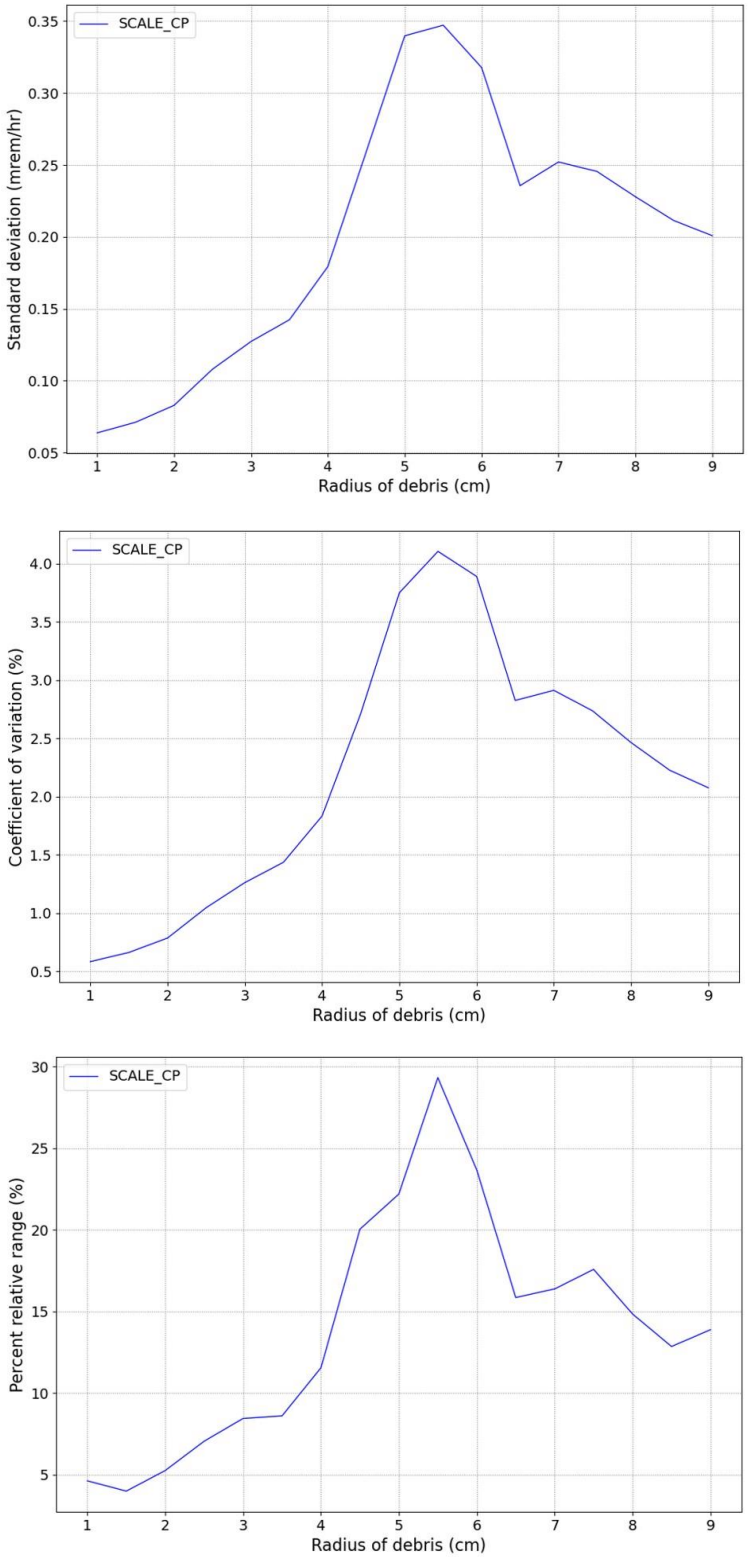


**Figure B. 39 Uncertainty of the close packed fuel debris.** The standard deviation (top), the coefficient of variation (middle), the percent relative range (bottom)

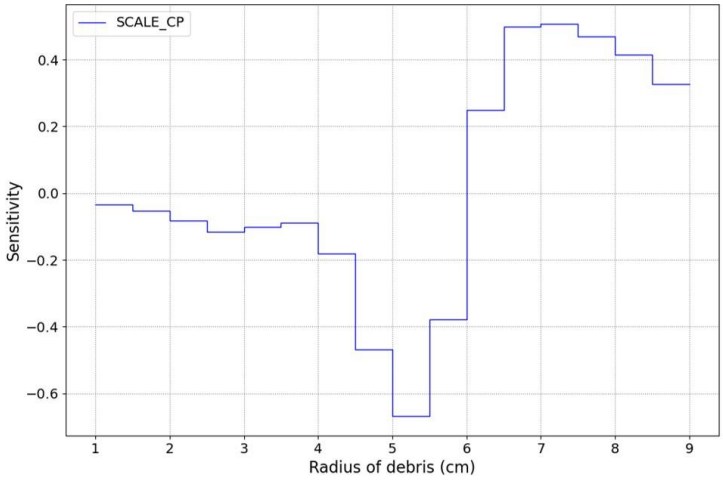


**Figure B. 40 Sensitivity index of the close packed fuel debris.**

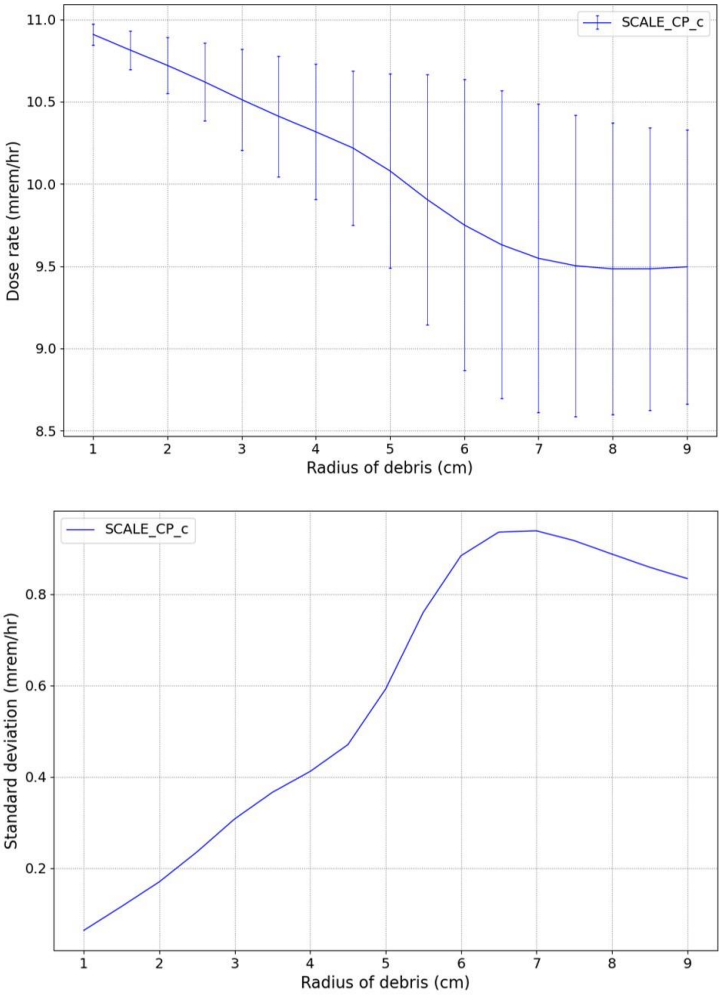


**Figure B. 41 Cumulative graphs.** The average dose rate (top), the standard deviation (bottom)

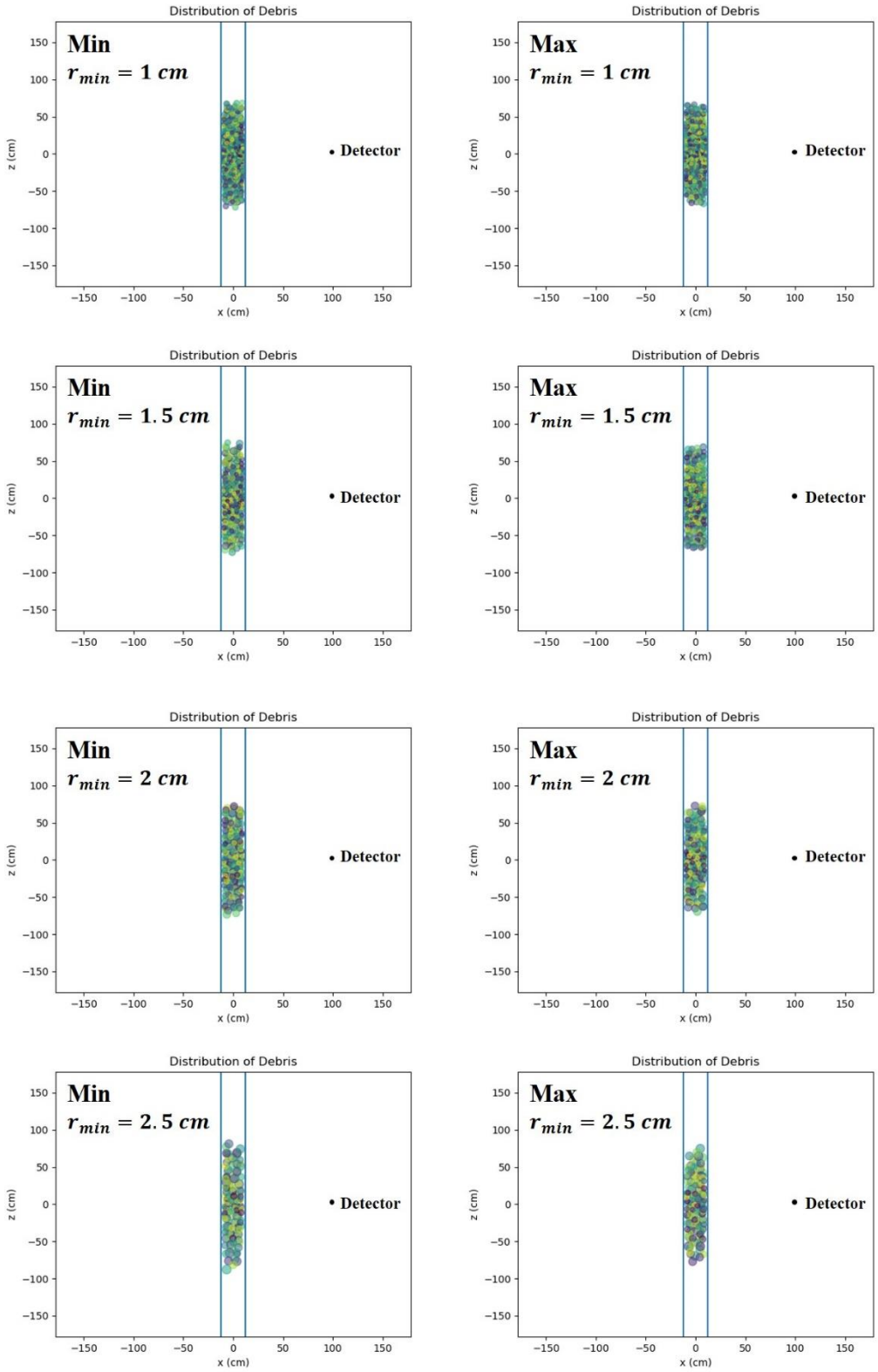


**Figure B. 42 Distribution of the close packed fuel debris in a canister.**

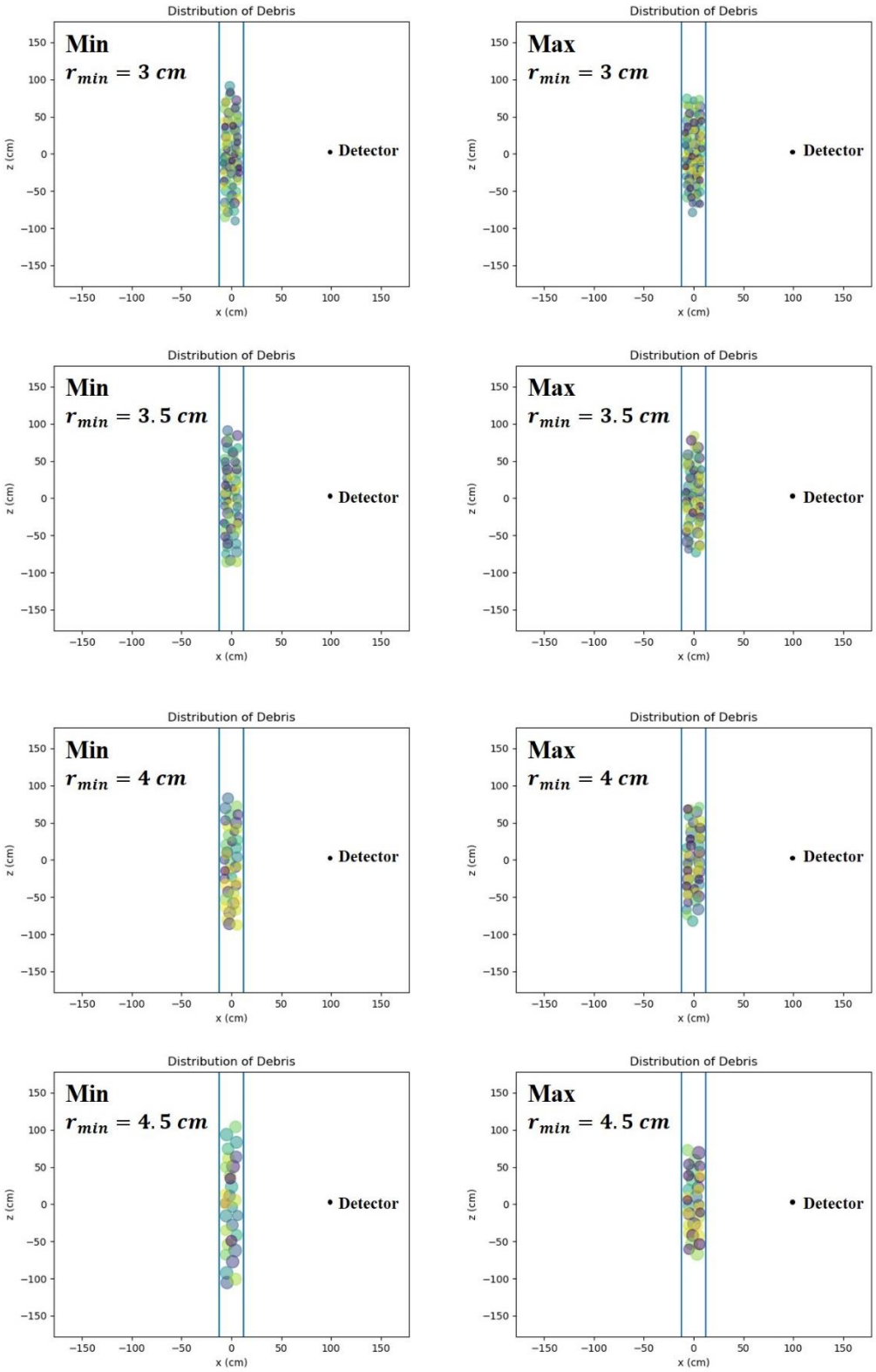


**Figure B. 43 Distribution of the close packed fuel debris in a canister.**

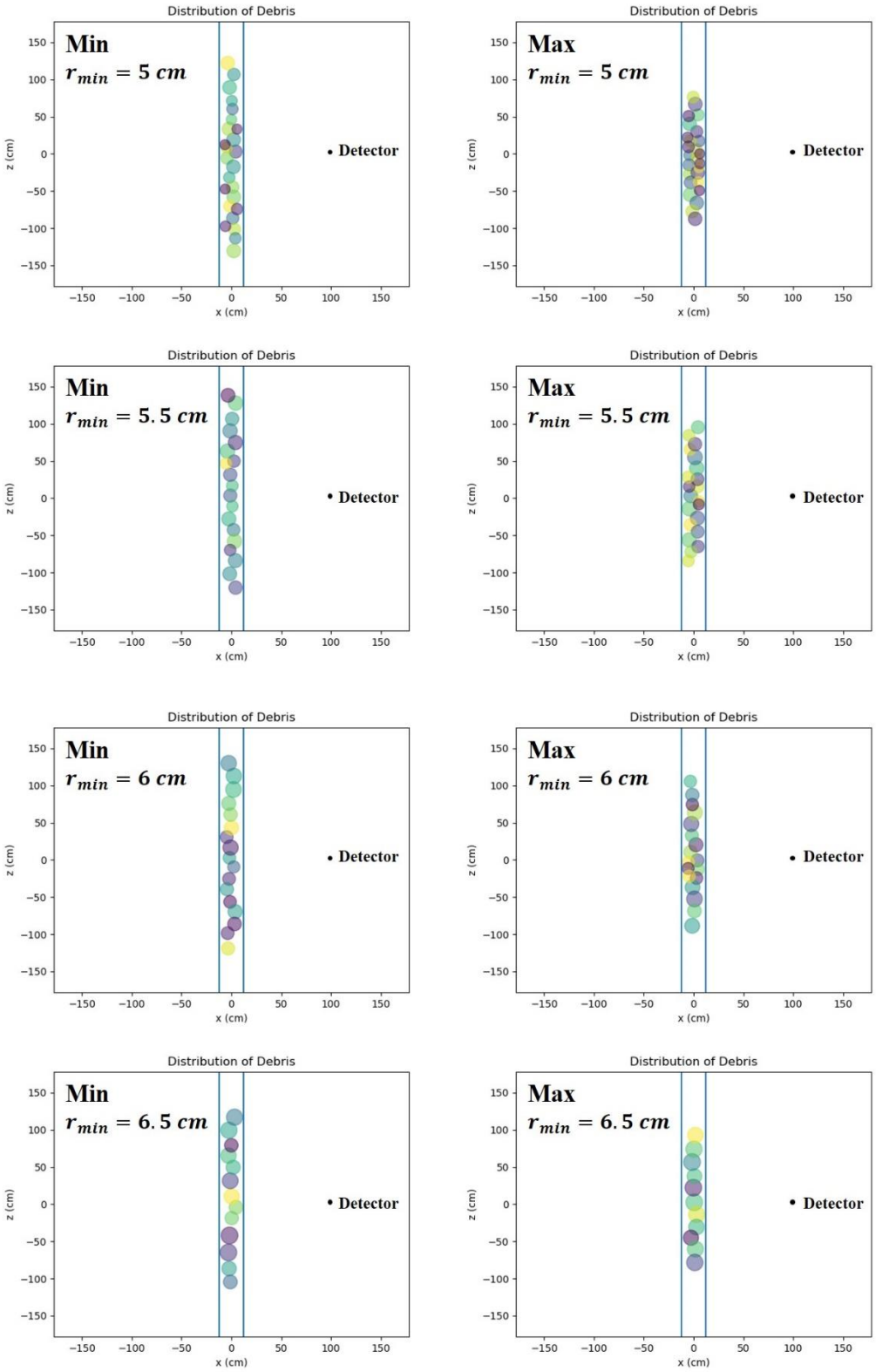


**Figure B. 44 Distribution of the close packed fuel debris in a canister.**

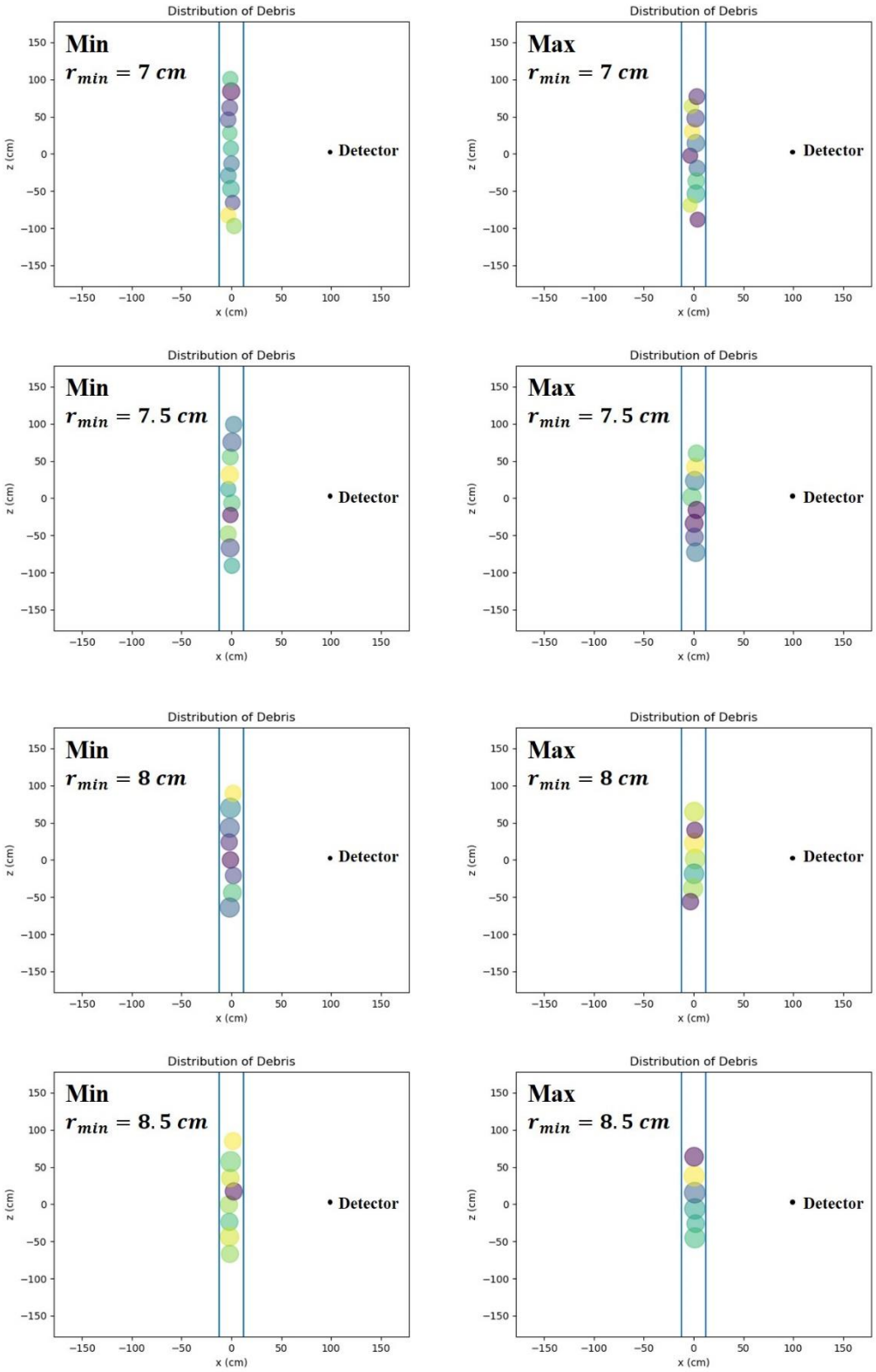


**Figure B. 45 Distribution of the close packed fuel debris in a canister.**

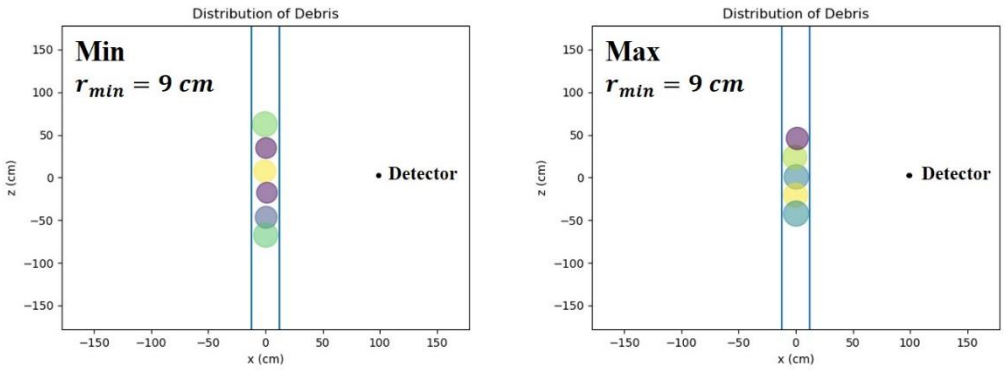


**Figure B. 46 Distribution of the close packed fuel debris in a canister.**

Neutron dose rate of close packed fuel debris decreases by the change of the minimum radius $r_{min}$ when $r_{min}$ is smaller than 6.0 cm. However, the dose rate increases by the increase of $r_{min}$ when $r_{min}$ is larger than 6.0 cm (Figure B.38). The average neutron dose rate is 10.9 mrem/hr for 1.0 cm of $r_{min}$, and the minimum value of the average dose rate is 8.16 mrem/hr for 6.0 cm of $r_{min}$. The average dose rate is 9.67 mrem/hr for 9.0 cm of $r_{min}$. Graph of the standard deviation has a global maximum and a local maximum which are 0.35 mrem/hr and 0.25 mrem/hr at 5.5cm and 7 cm of $r_{min}$ (Figure B. 39). These maximum values of standard deviations are 4.5 % and 2.91 % of dose rates at 5.5 cm and 7 cm of $r_{min}$. Range of data including outliers also has maximum value at 5.5 cm of $r_{min}$ which is 2.4 mre/hr.

Geometrical distribution of fuel debris in a canister for the maximum and minimum neutron dose rate of each sample group is similar with the distribution of photon dose rate. However, it does not exactly match with the geometric distribution of photon dose rate because the variability of neutron dose rate depends more on the vertical distribution of fuel debris rather than the self-attenuation or particle self-shielding. The unique shape of the graphs of neutron dose rate can be explained by the side view of the fuel debris in a canister (Figure B. 42 ~ 46). Neutron dose rate decreases by the increase of $r_{min}$ because of the vertical height of the pile of debris is increases for $r_{min}$ less than 6 cm. Neutron dose rate increases by the increase of $r_{min}$ for larger than 6 cm because the height decreases.

**B. 6. Photon dose rate of the loose packed fuel debris in a canister (same radius)**

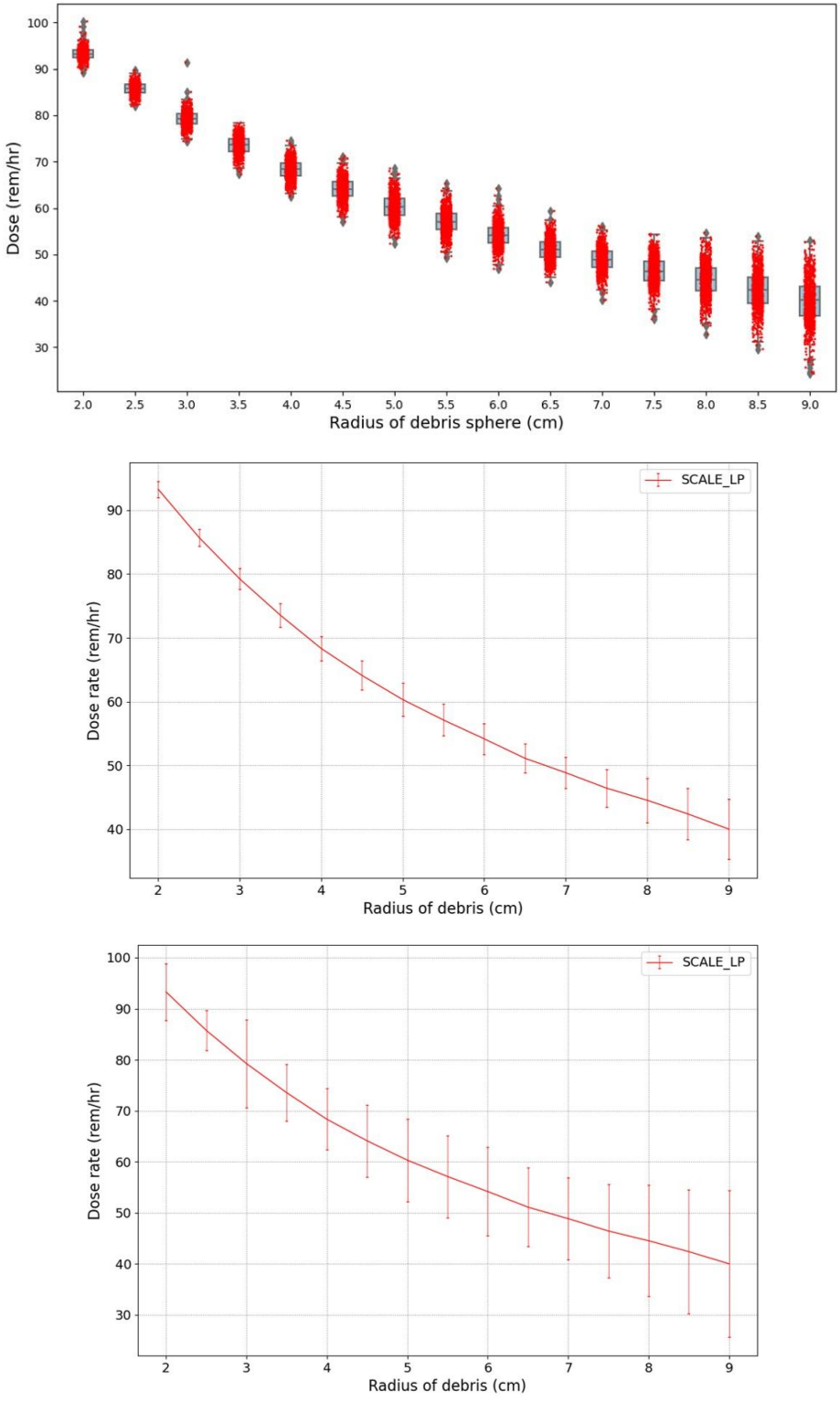


**Figure B. 47 Photon dose rate of the loose packed fuel debris.** The estimated dose rates (top), the average dose rate with the standard deviation (middle), the average dose rate with the range (bottom)

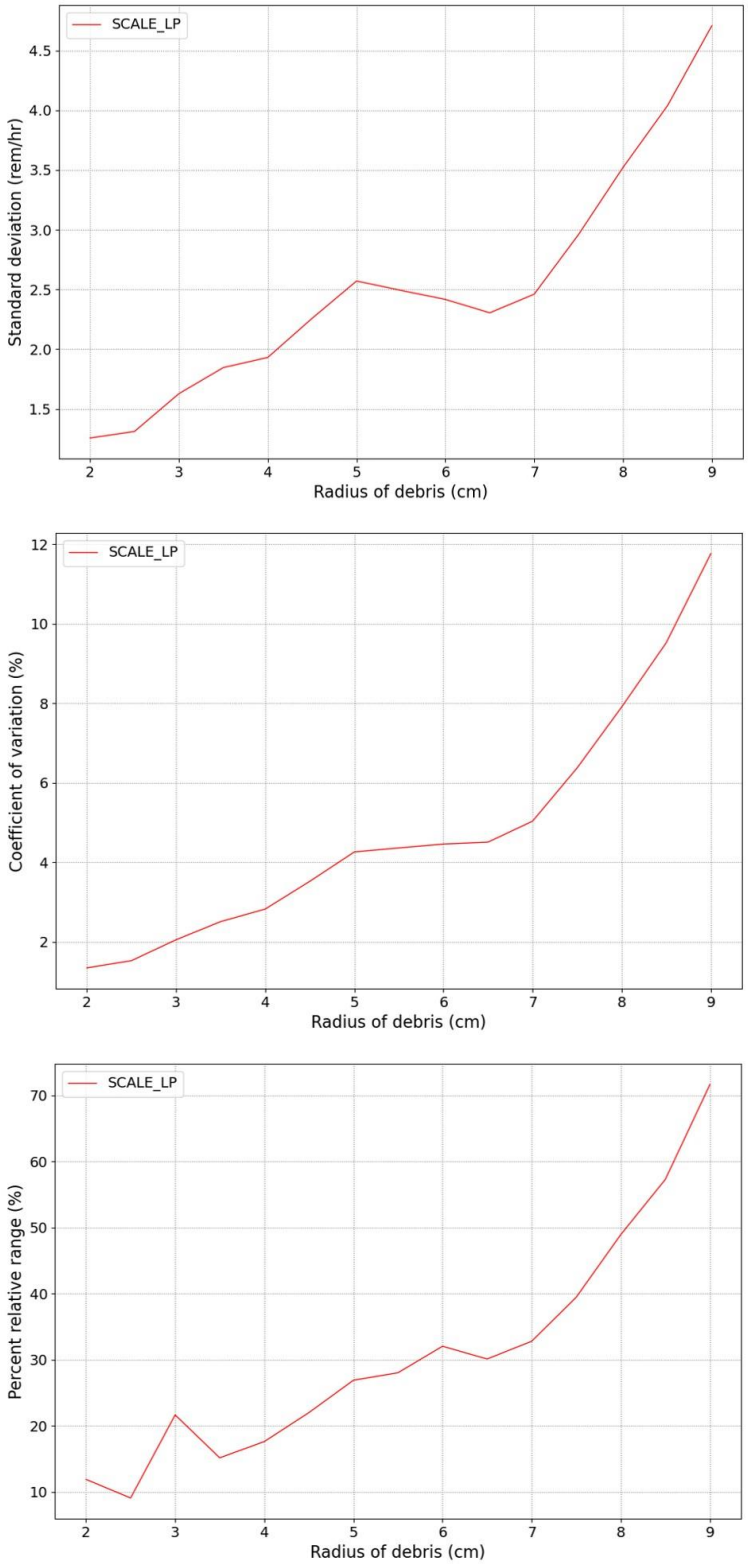


**Figure B. 48 Uncertainty of the loose packed fuel debris.** The standard deviation (top), the coefficient of variation (middle), the percent relative range (bottom)

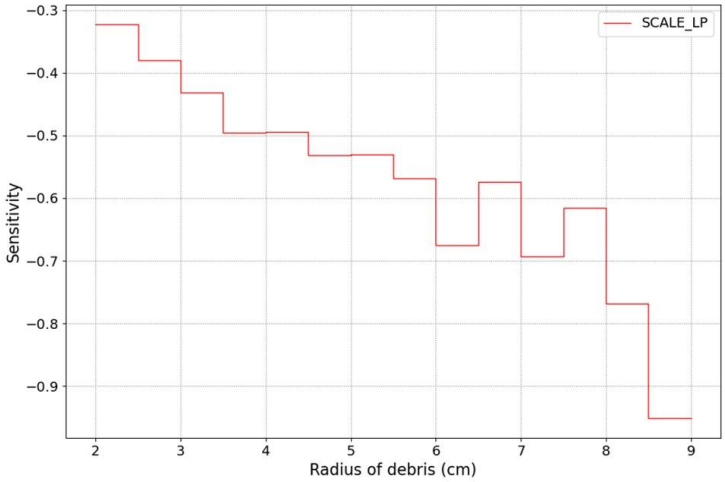


**Figure B. 49 Sensitivity index of the loose packed fuel debris.**

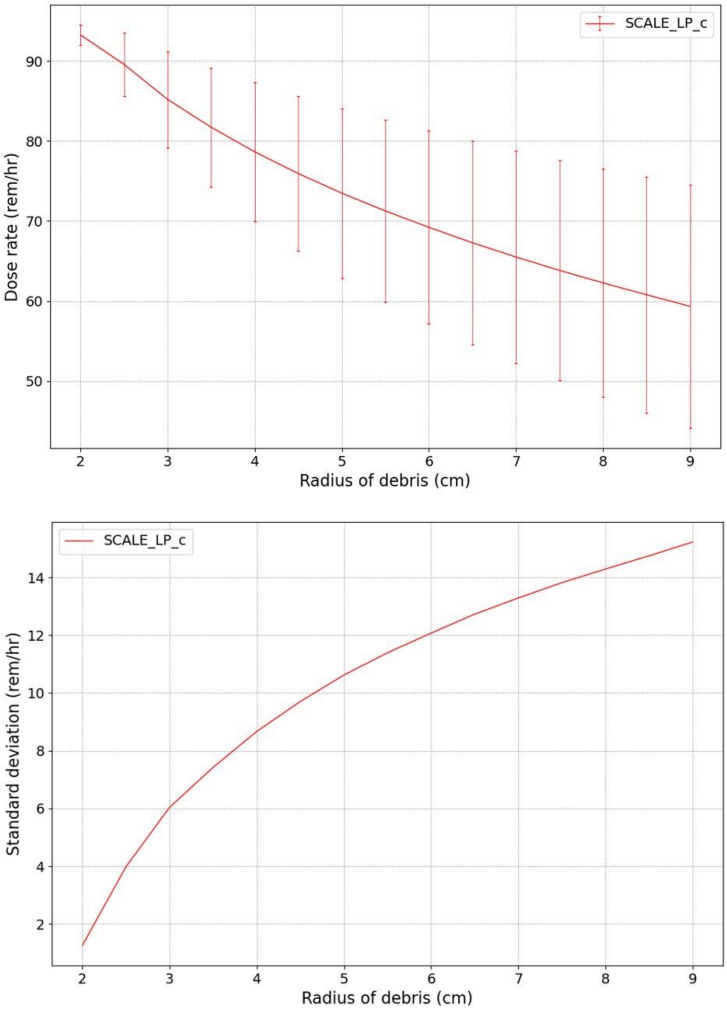


**Figure B. 50 Cumulative graphs.** The average dose rate (top), the standard deviation (bottom)

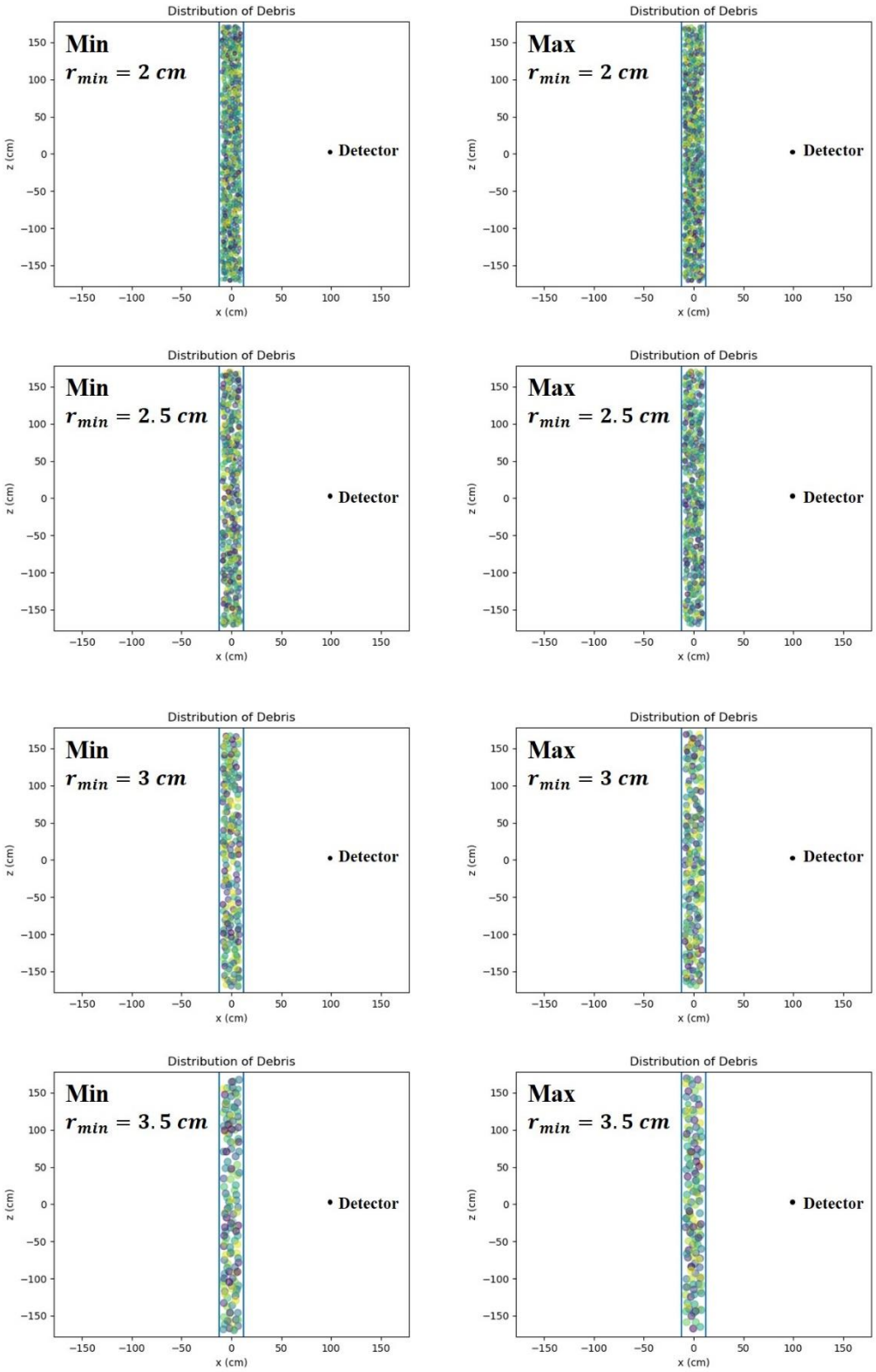


**Figure B. 51 Distribution of the loose packed fuel debris in a canister.**

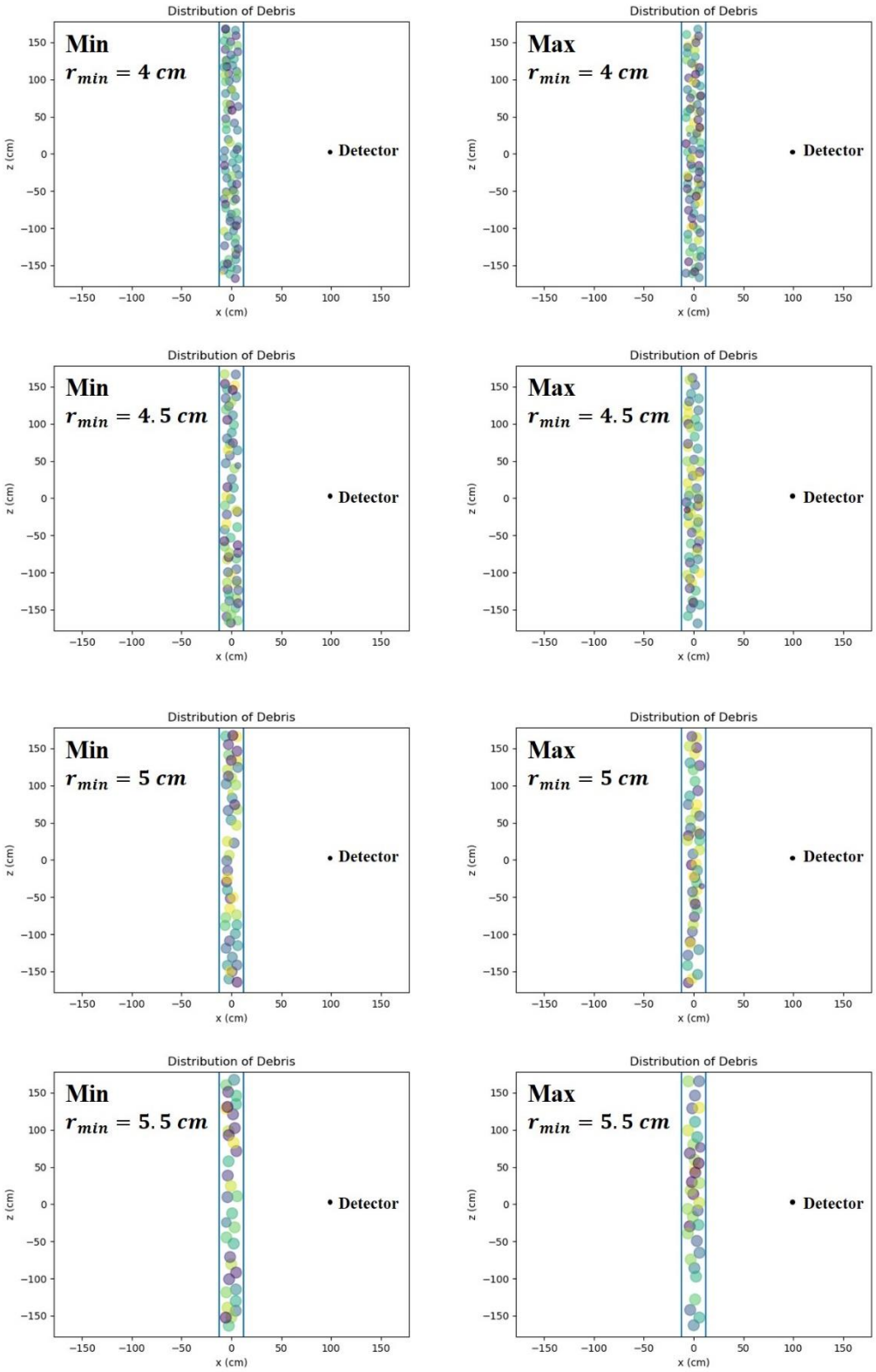


**Figure B. 52 Distribution of the loose packed fuel debris in a canister.**

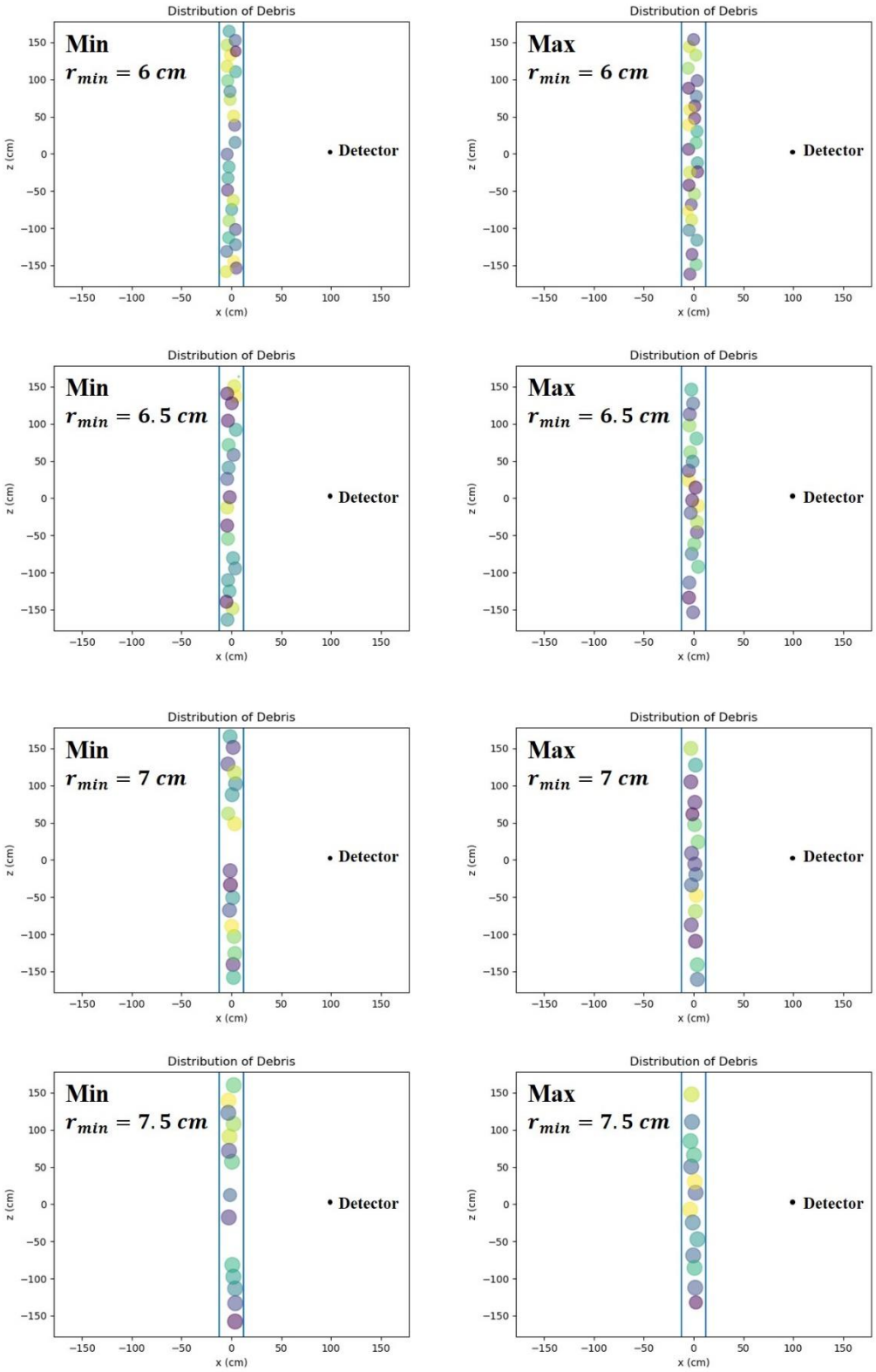


**Figure B. 53 Distribution of the loose packed fuel debris in a canister.**

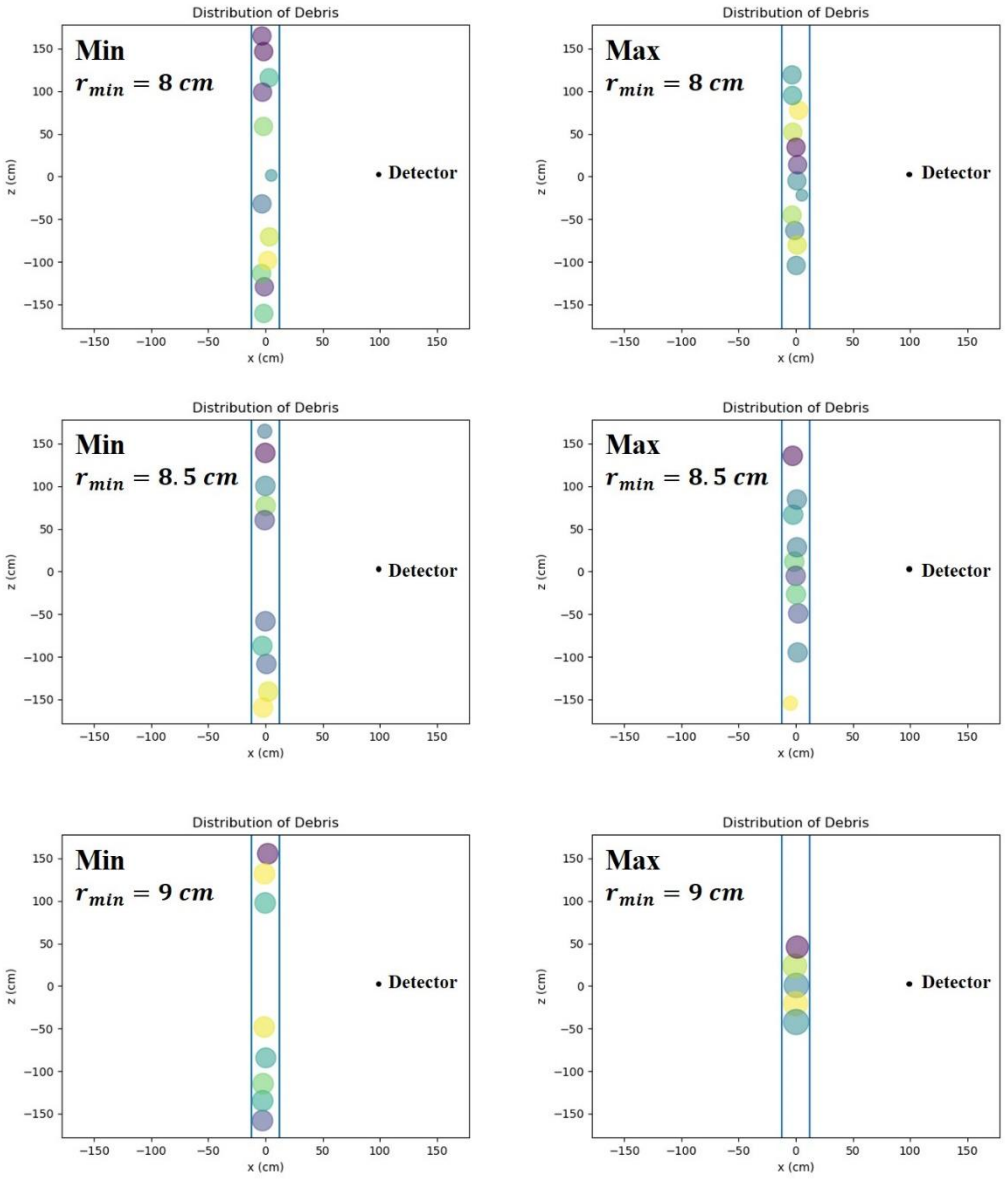


**Figure B. 54 Distribution of the loose packed fuel debris in a canister.**

## B. 7. Neutron dose rate of the loose packed fuel debris in a canister (same radius)

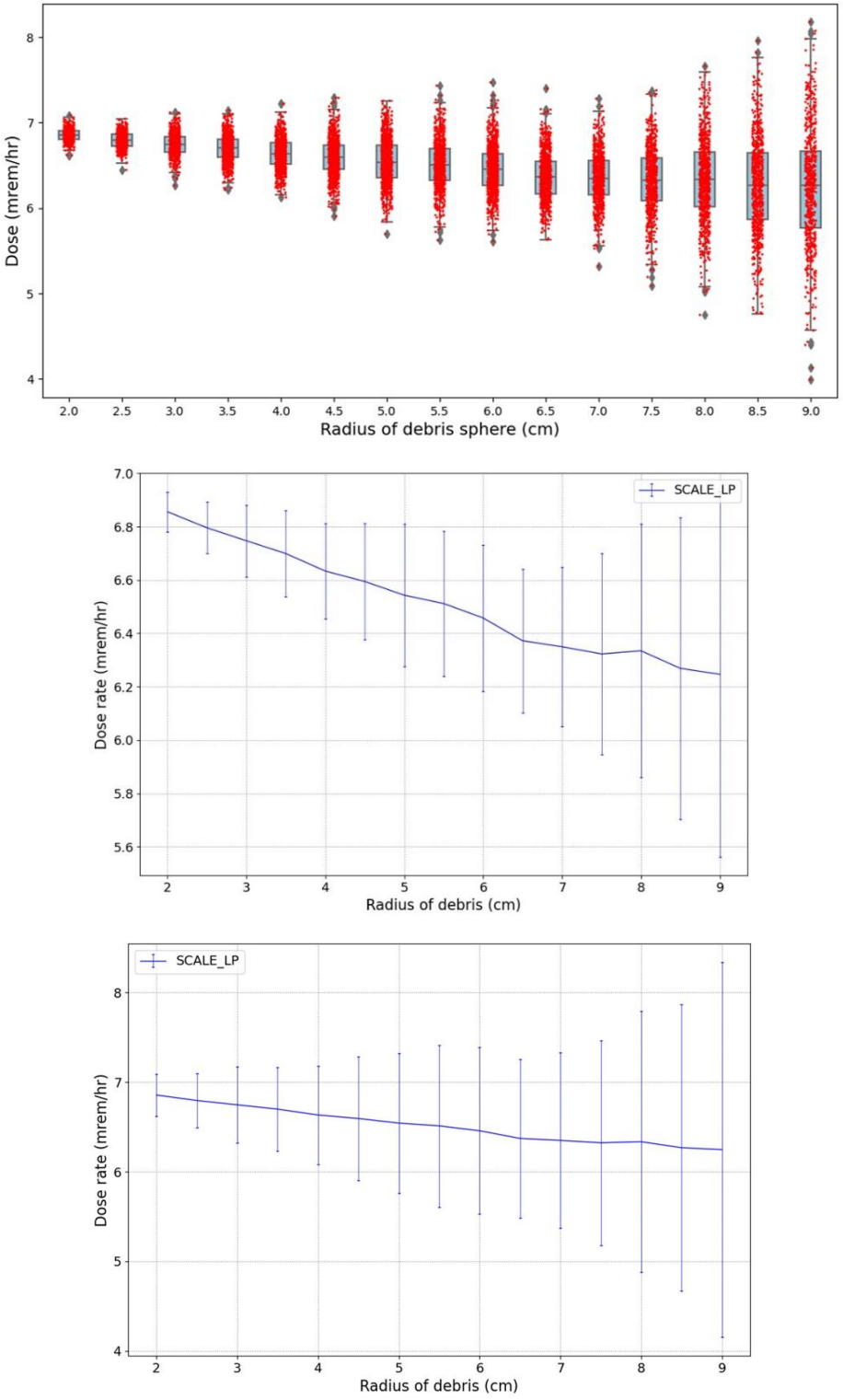


**Figure B. 55 Neutron dose rate of the loose packed fuel debris.** The estimated dose rates (top), the average dose rate with the standard deviation (middle), the average dose rate with the range (bottom)

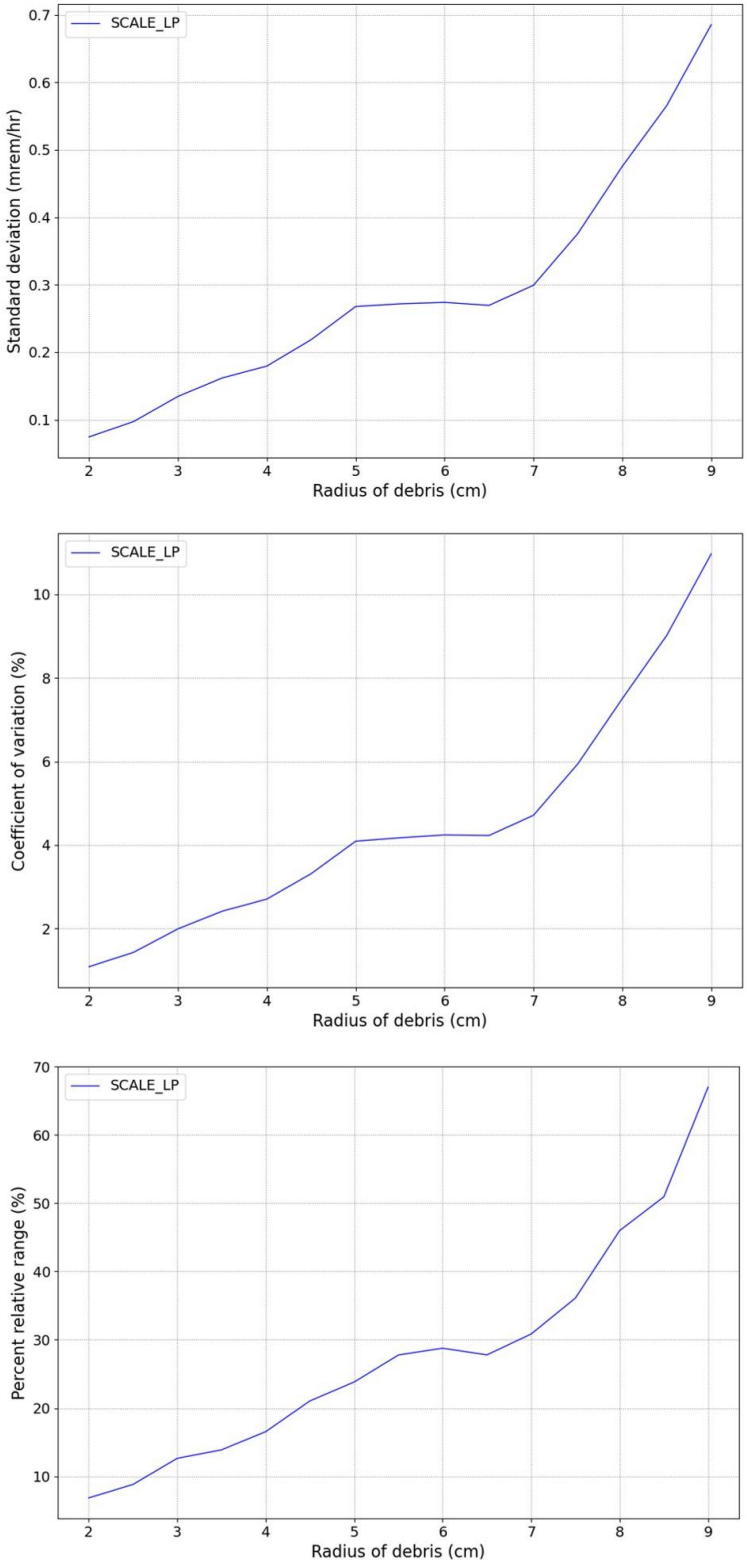


**Figure B. 56 Uncertainty of the loose packed fuel debris.** The standard deviation (top), the coefficient of variation (middle), the percent relative range (bottom)

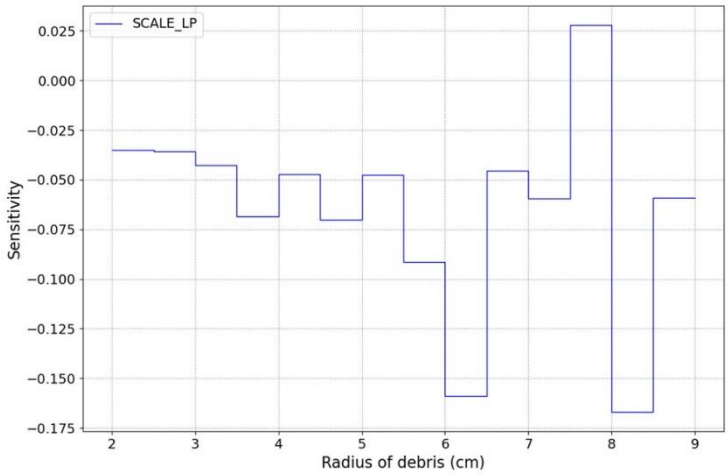


**Figure B. 57 Sensitivity index of the loose packed fuel debris.**

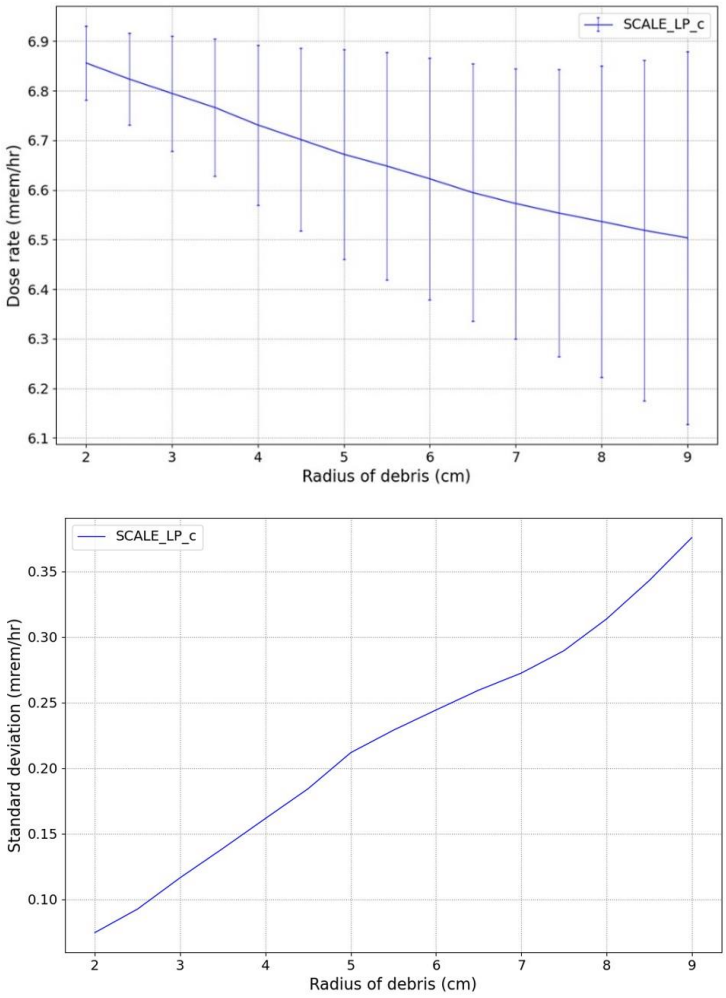


**Figure B. 58 Cumulative graphs.** The average dose rate (top), the standard deviation (bottom)

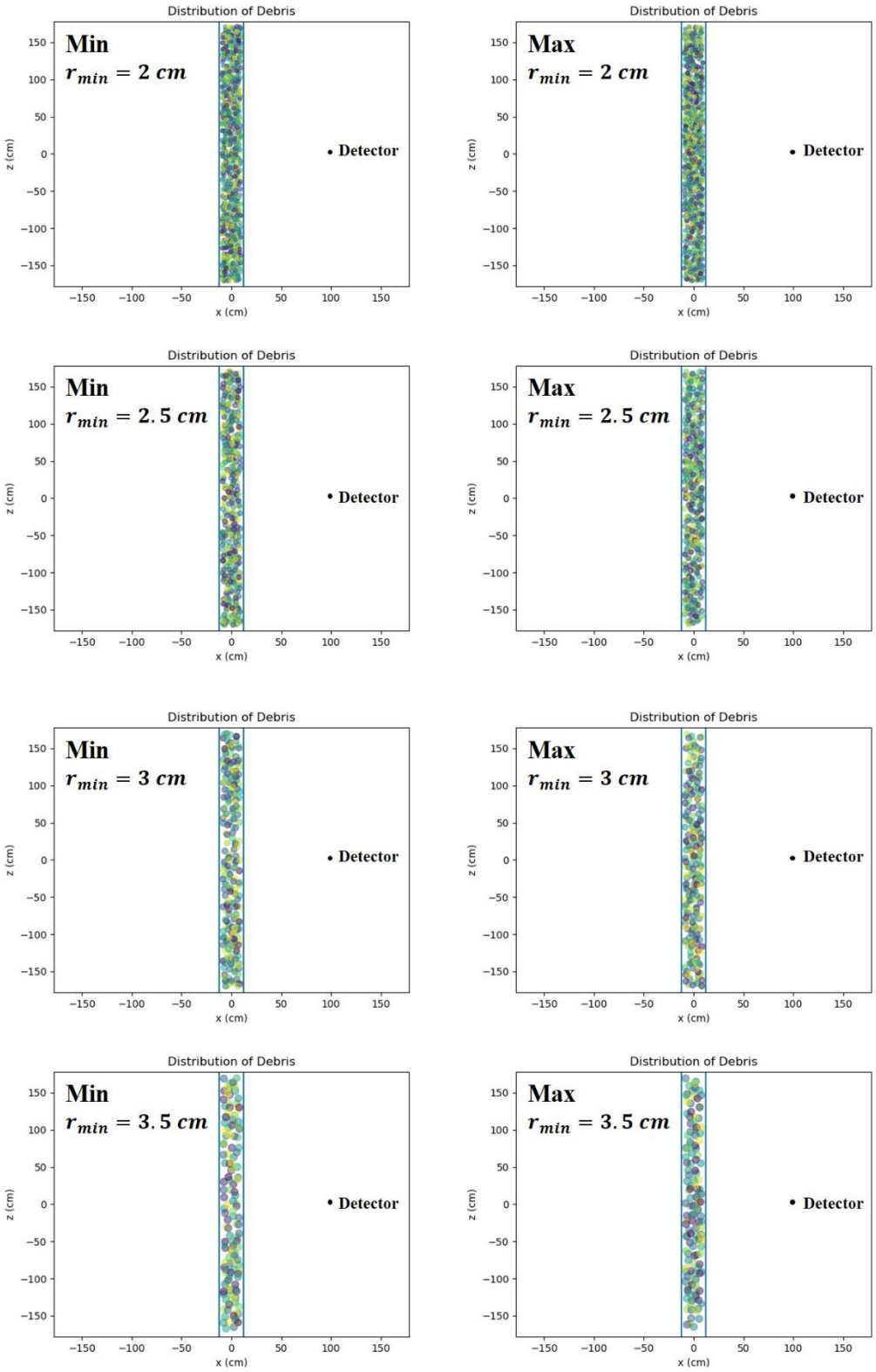


**Figure B. 59 Distribution of the loose packed fuel debris in a canister.**

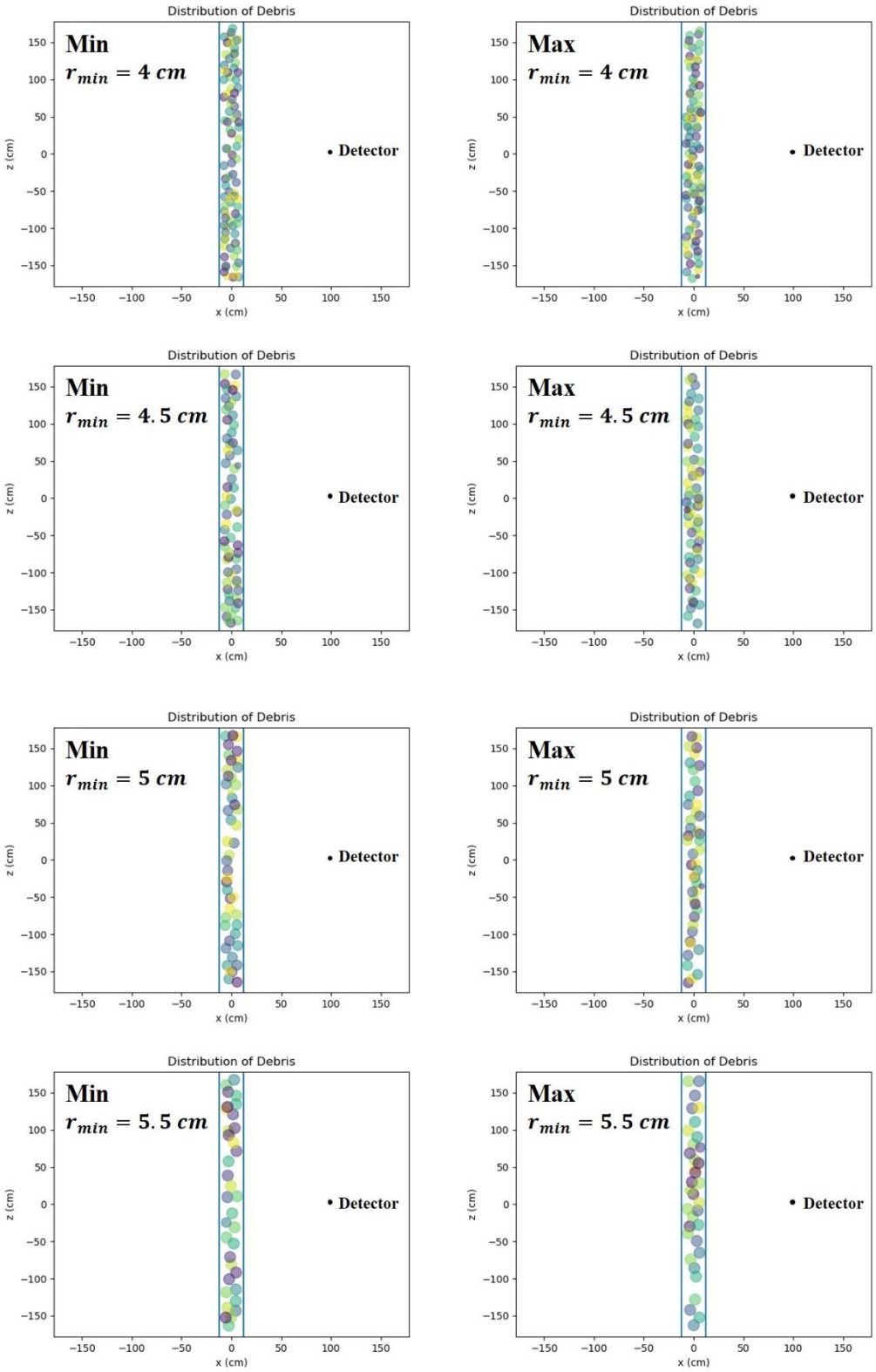


**Figure B. 60 Distribution of the loose packed fuel debris in a canister.**

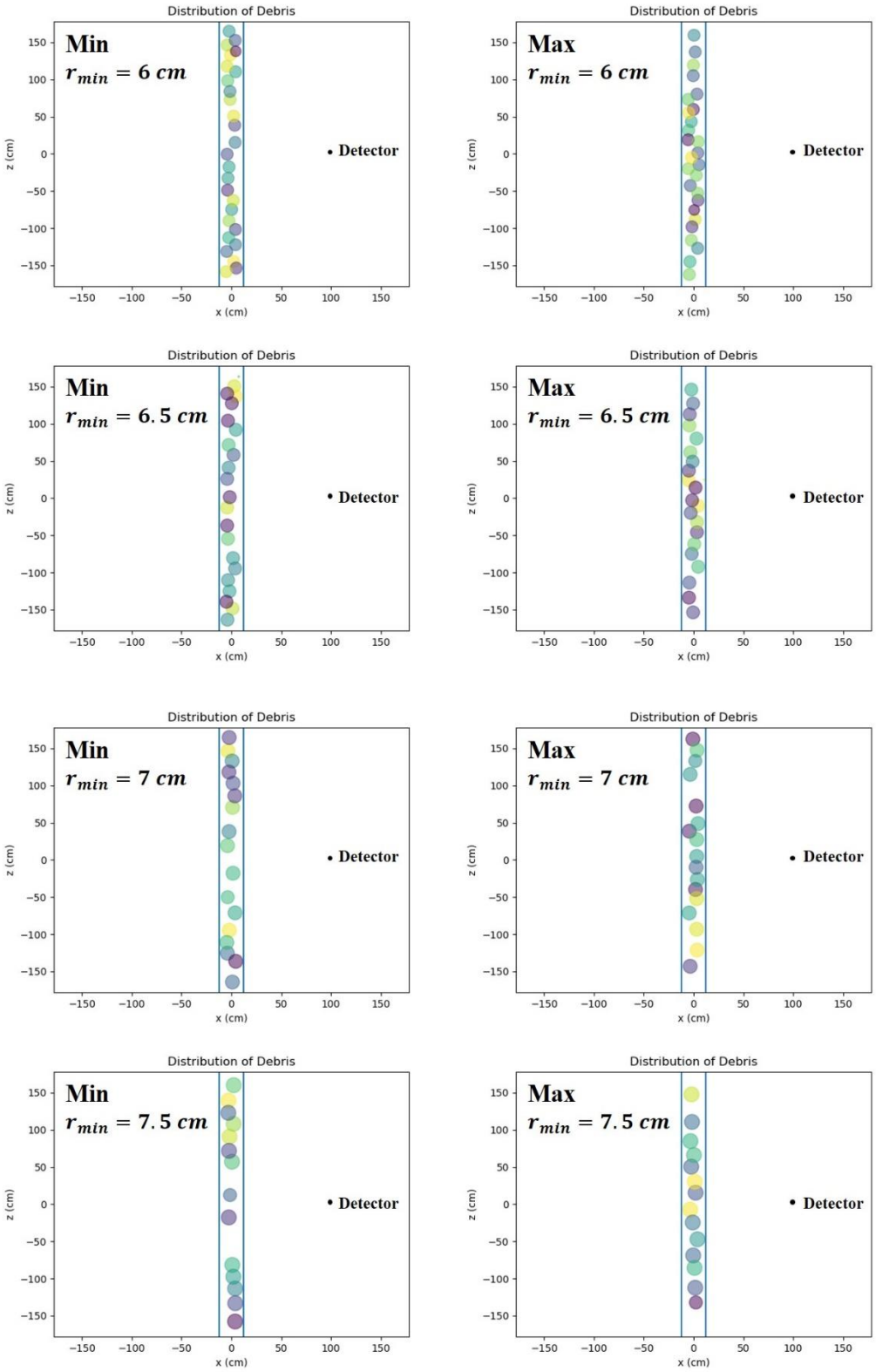


**Figure B. 61 Distribution of the loose packed fuel debris in a canister.**

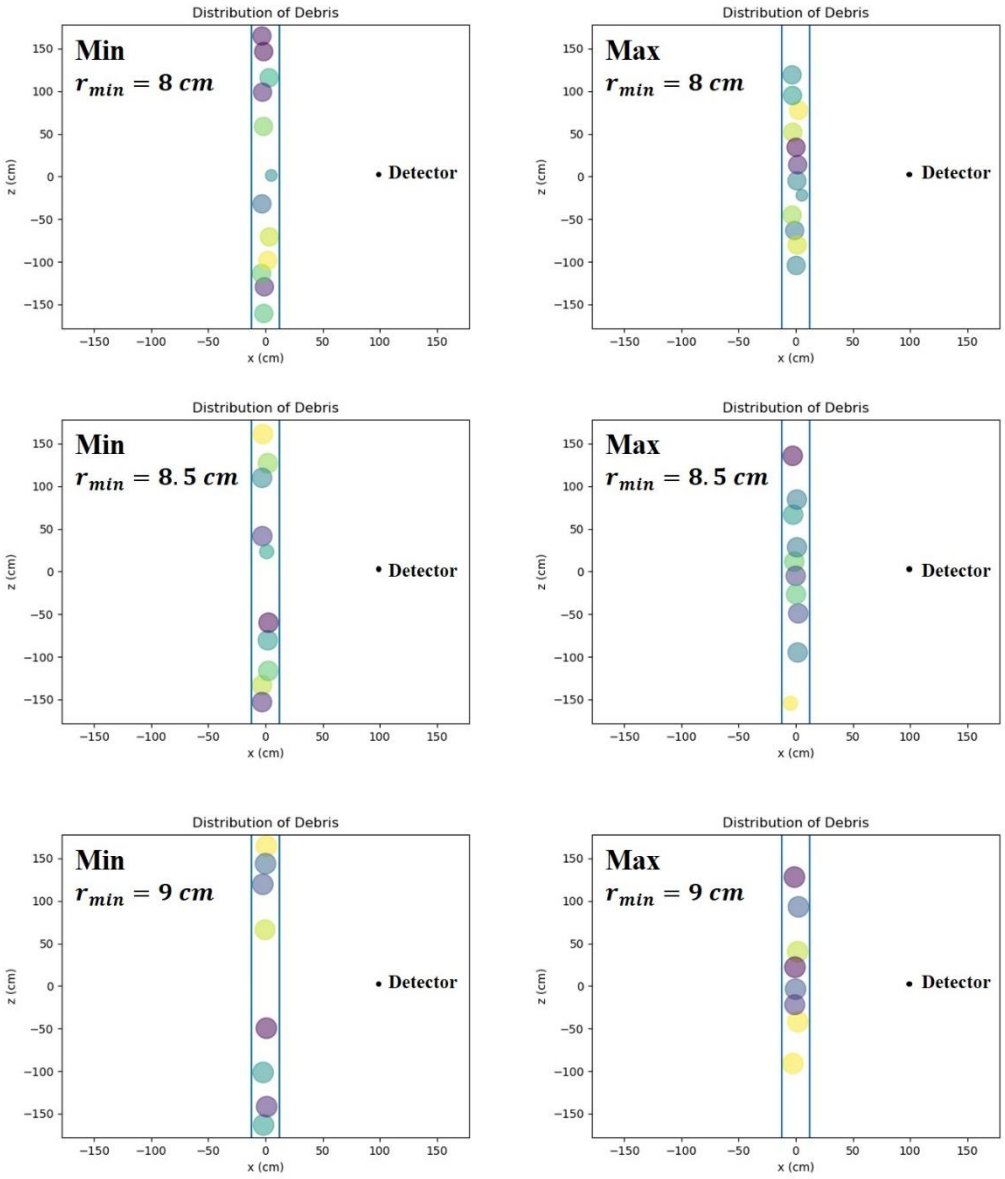


**Figure B. 62 Distribution of the loose packed fuel debris in a canister.**

## B. 8. Photon dose rate of the loose packed fuel debris in three small containers

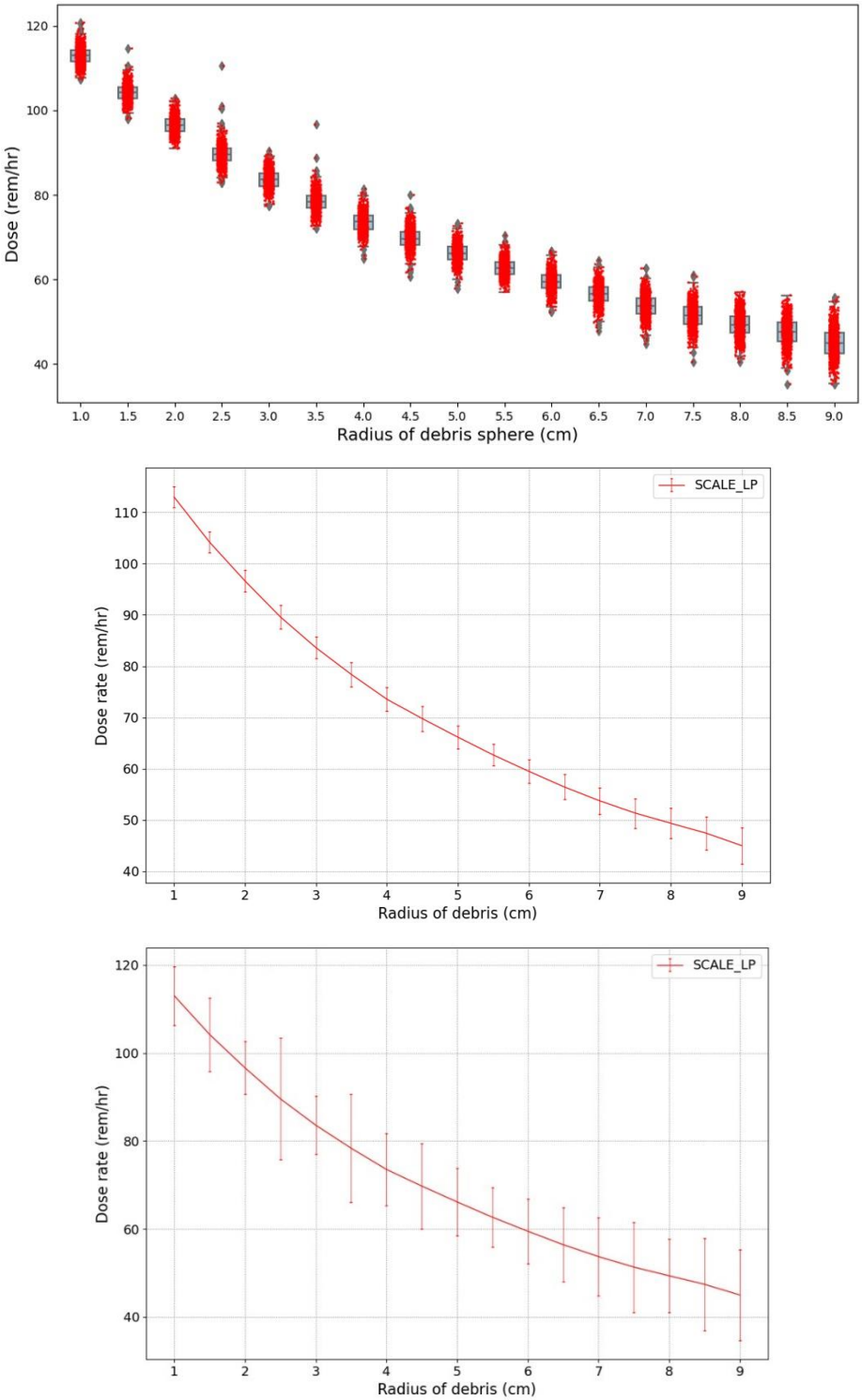


**Figure B. 63 Photon dose rate of the loose packed fuel debris.** The estimated dose rates (top), the average dose rate with the standard deviation (middle), the average dose rate with the range (bottom)

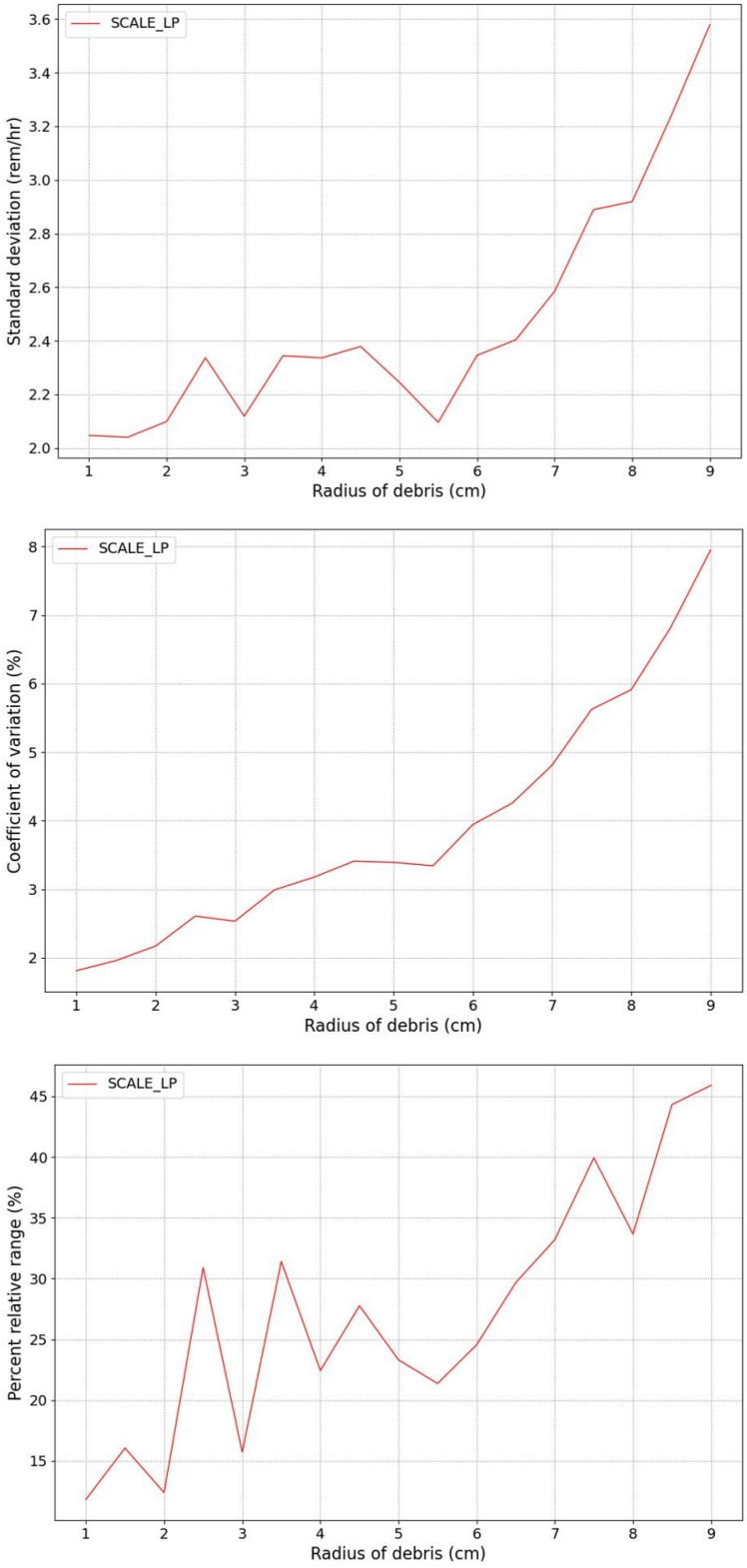


**Figure B. 64 Uncertainty of the loose packed fuel debris.** The standard deviation (top), the coefficient of variation (middle), the percent relative range (bottom)

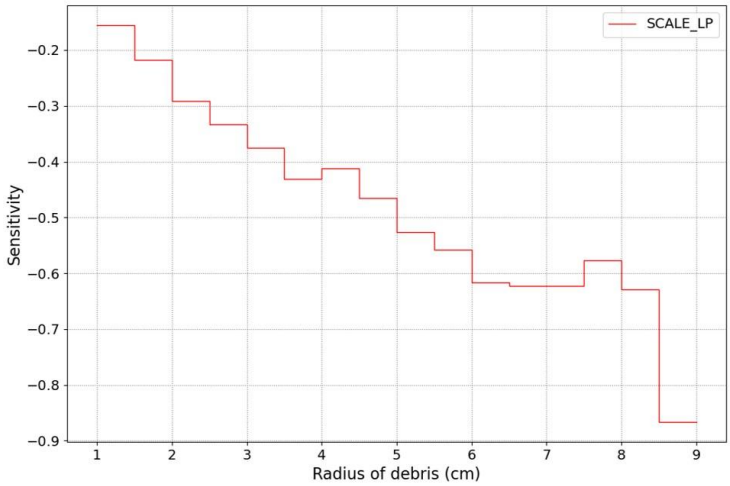


**Figure B. 65 Sensitivity index of the loose packed fuel debris.**

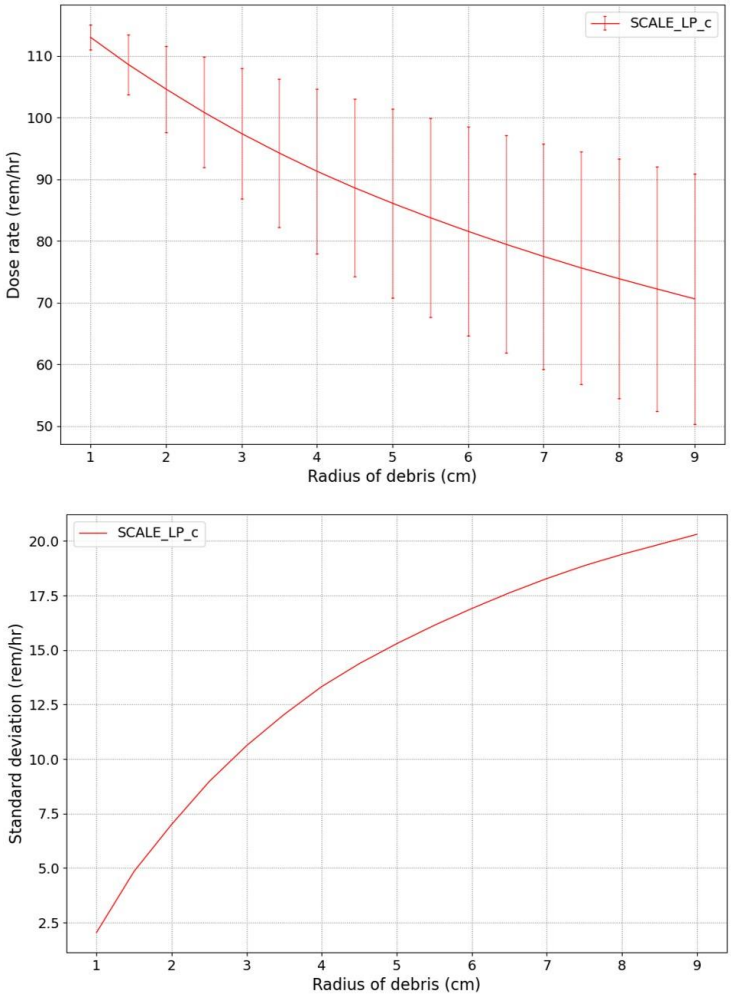


**Figure B. 66 Cumulative graphs.** The average dose rate (top), the standard deviation (bottom)

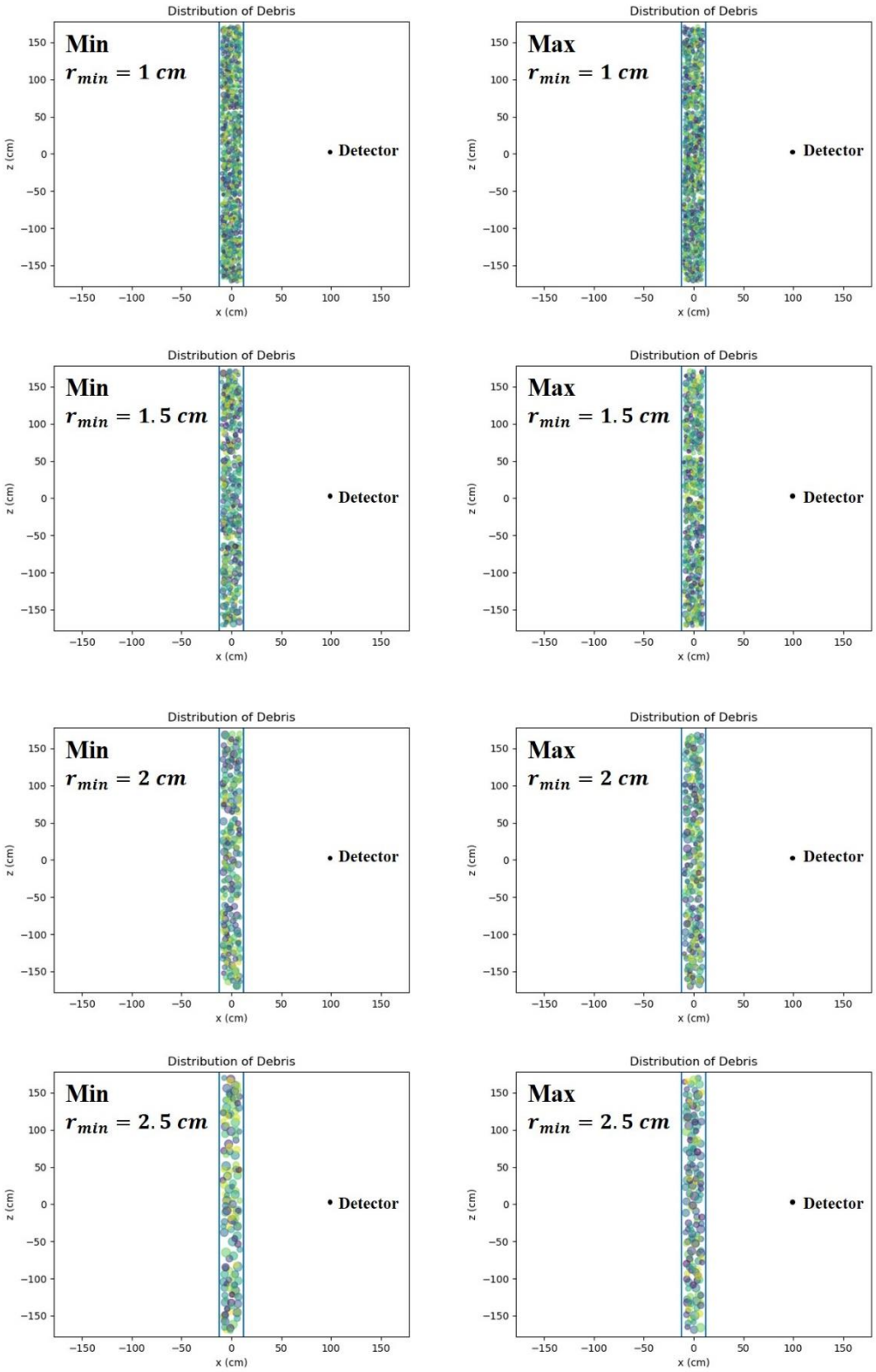


**Figure B. 67 Distribution of the loose packed fuel debris in three small containers.**

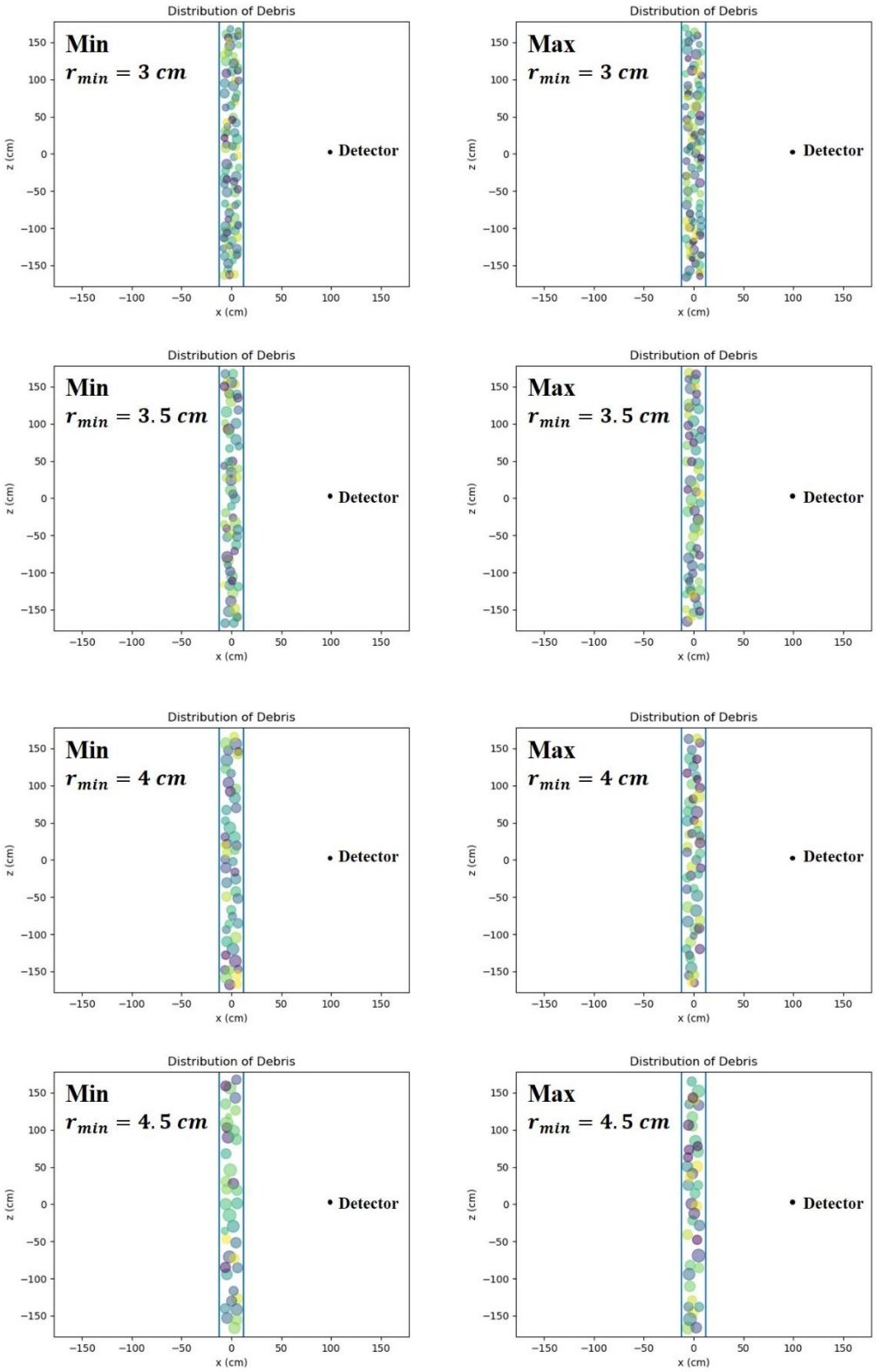


**Figure B. 68 Distribution of the loose packed fuel debris in three small containers.**

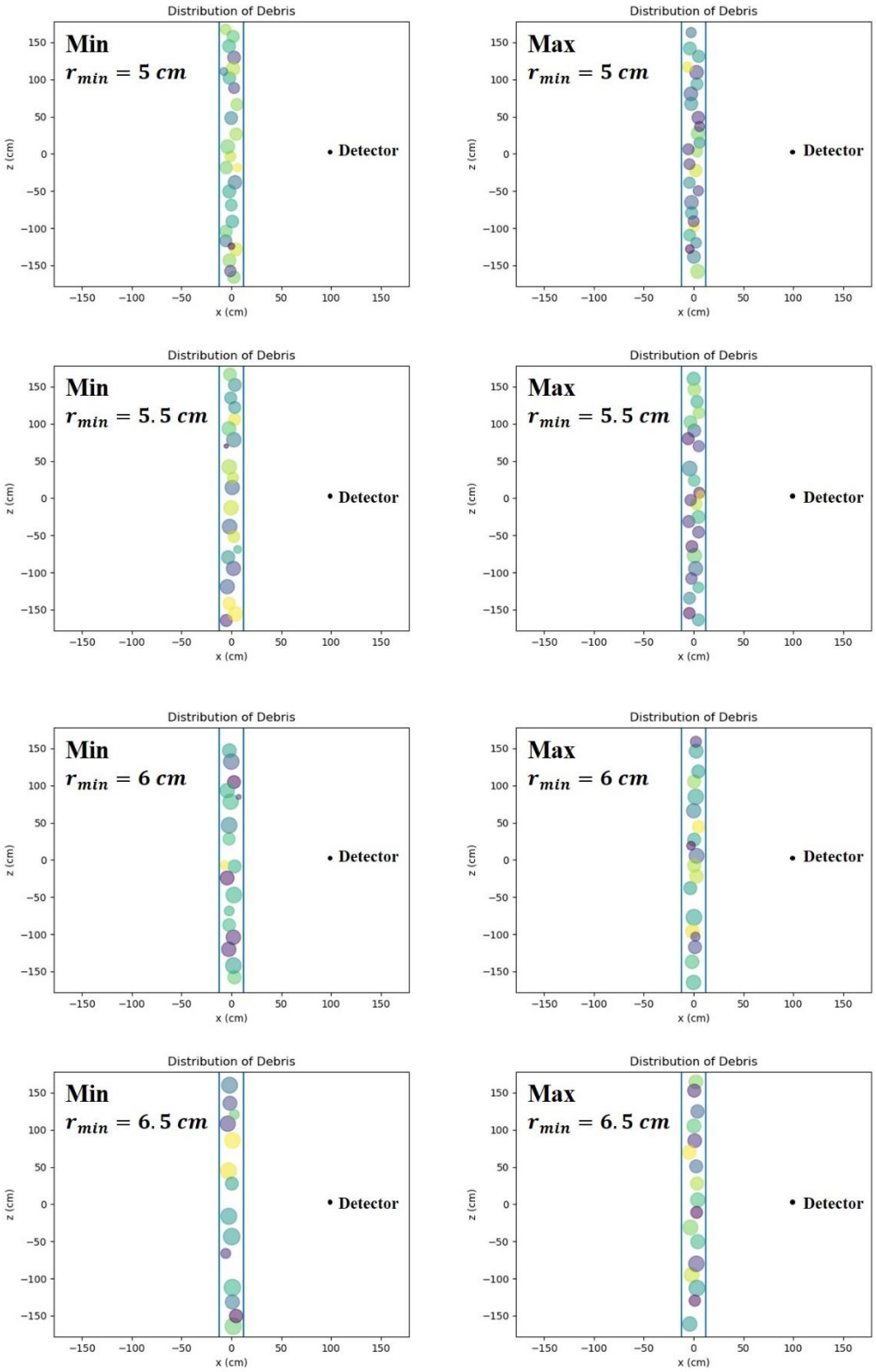


**Figure B. 69 Distribution of the loose packed fuel debris in three small containers.**

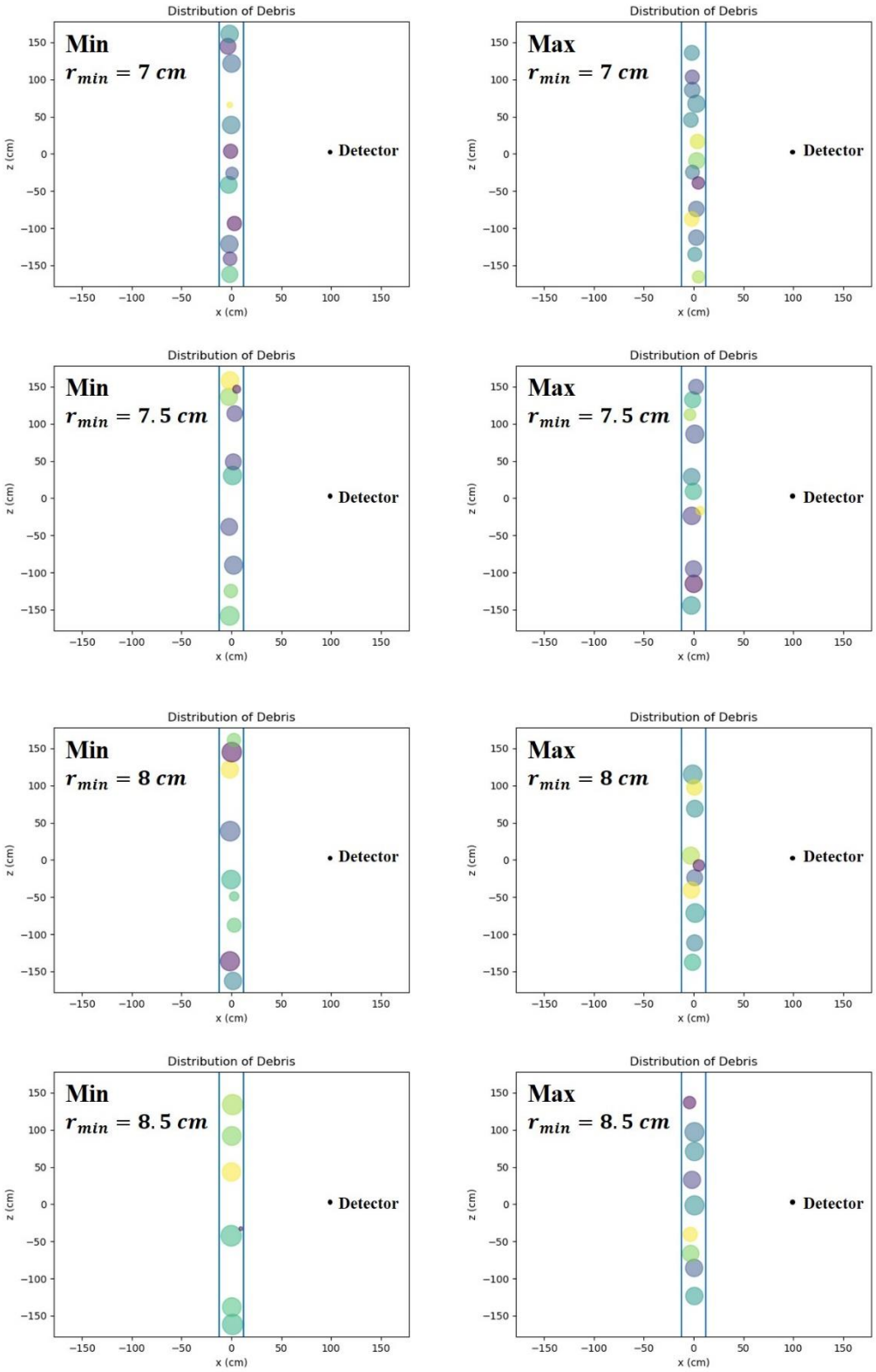


**Figure B. 70 Distribution of the loose packed fuel debris in three small containers.**

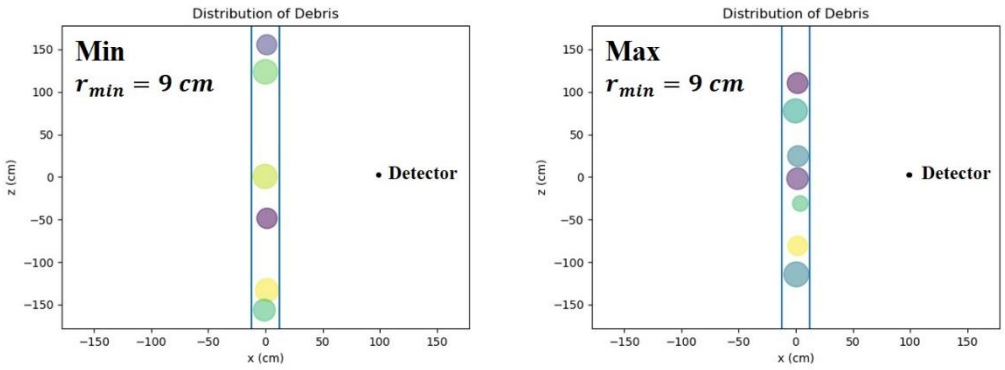


**Figure B. 71 Distribution of the loose packed fuel debris in three small containers.**

TEPCO Japan prepared small containers for the retrieval of fuel debris, and the retrieved fuel debris will be contained in the small container before being placed in a fuel canister. For the analysis on affect of the small container on the radiation dose rate, it is assumed that three small containers are placed in a fuel canister. Dose rate from fuel debris with this assumption can be affected a lot by the material and wall thickness which is used for the small container. Therefore, wall thickness of the small container is ignored for this analysis, and only the space for the spatial distribution of fuel debris in a canister are divided into three to evaluate the changes in dose rate by the spatial divisions in a canister.

Median dose rate of each sample group is very similar with the box plot of the fuel canister without small containers. However, vertical dispersion of data at the graph is smaller than the dispersion of the canister without small containers (Figure B.63). The average dose rate exponentially decreases by the increase of the minimum radius $r_{min}$ like the fuel canister without small containers. The photon dose rate for 1 cm of $r_{min}$ and 9 cm of $r_{min}$ are 112.9 rem/hr and 45.0 rem/hr each. These values are very similar with the dose rate of loose packed debris in a canister without small containers which are 113.3 rem/hr and 44.8 rem/hr. Standard deviation increases by the increase of $r_{min}$ but the gradient of the graph is discontinuous (Figure B. 64). Standard deviation of dose rate is smaller than the estimated values of a canister without small containers. Range of data is from 11.9 rem/hr to 24.6 rem/hr.

## B. 9. Photon dose rate of the close packed fuel debris in three small containers

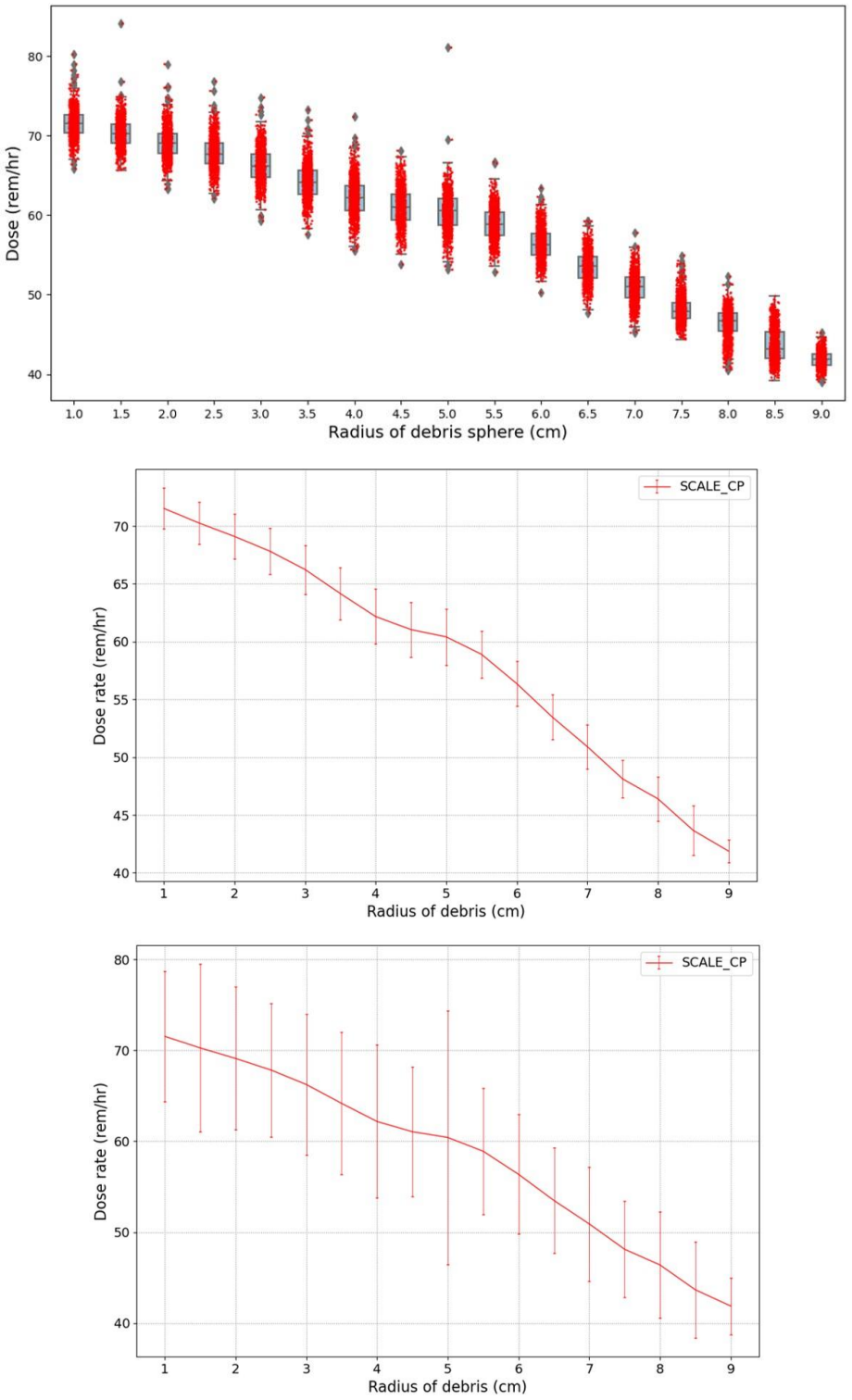


**Figure B. 72 Photon dose rate of the close packed fuel debris.** The estimated dose rates (top), the average dose rate with the standard deviation (middle), the average dose rate with the range (bottom)

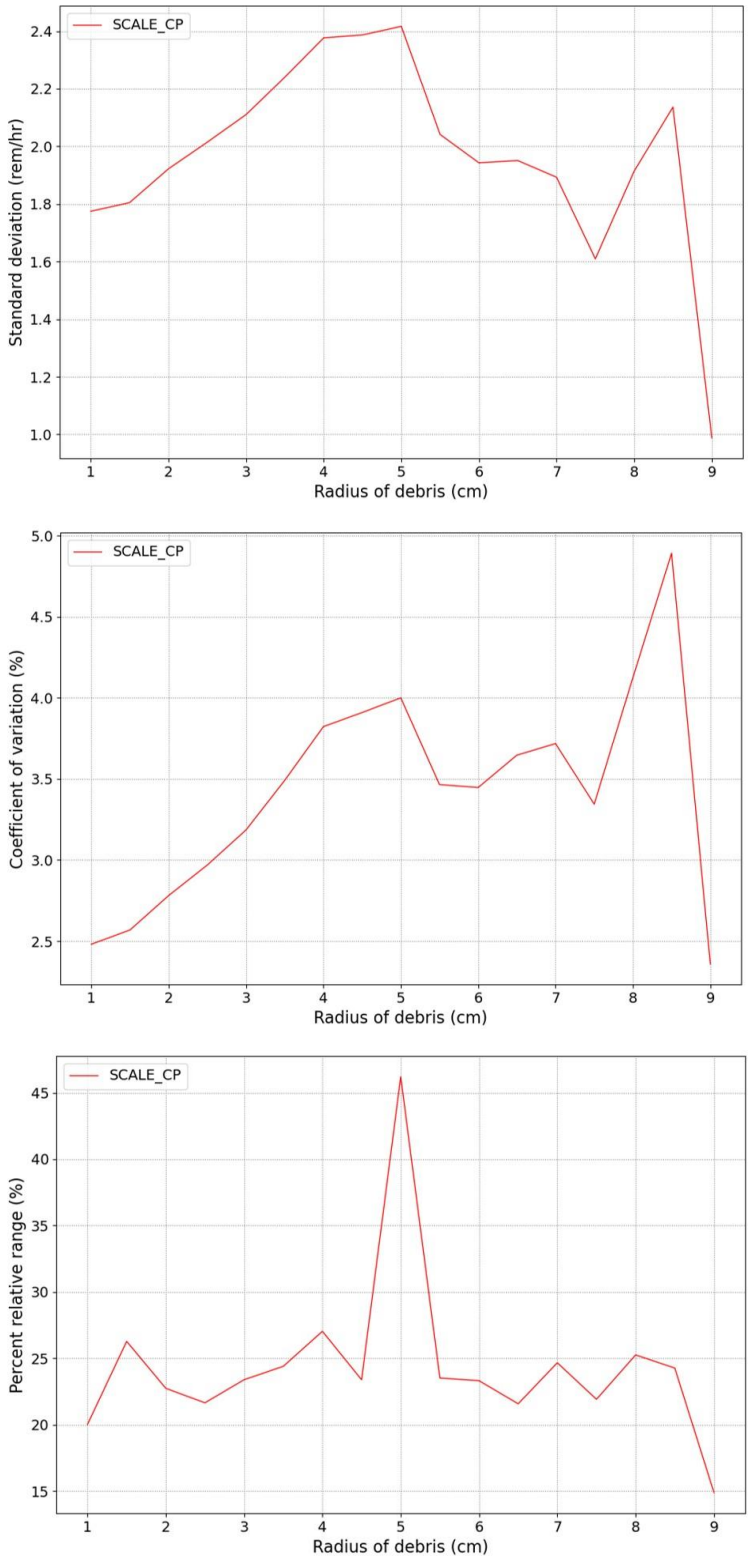


**Figure B. 73 Uncertainty of the close packed fuel debris.** The standard deviation (top), the coefficient of variation (middle), the percent relative range (bottom)

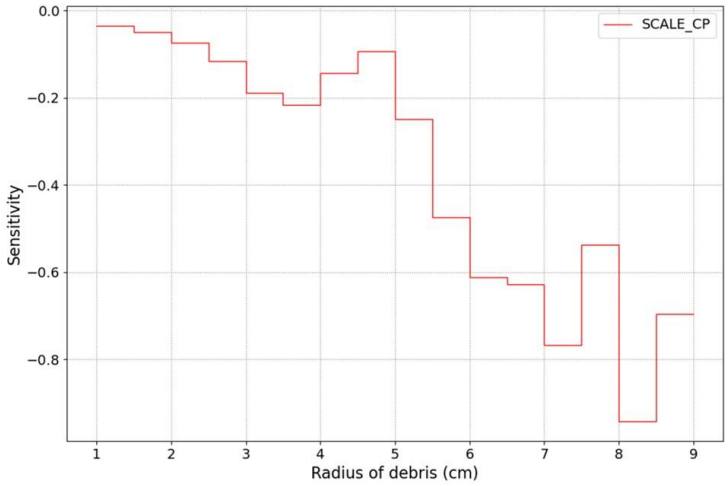


**Figure B. 74 Sensitivity index of the close packed fuel debris.**

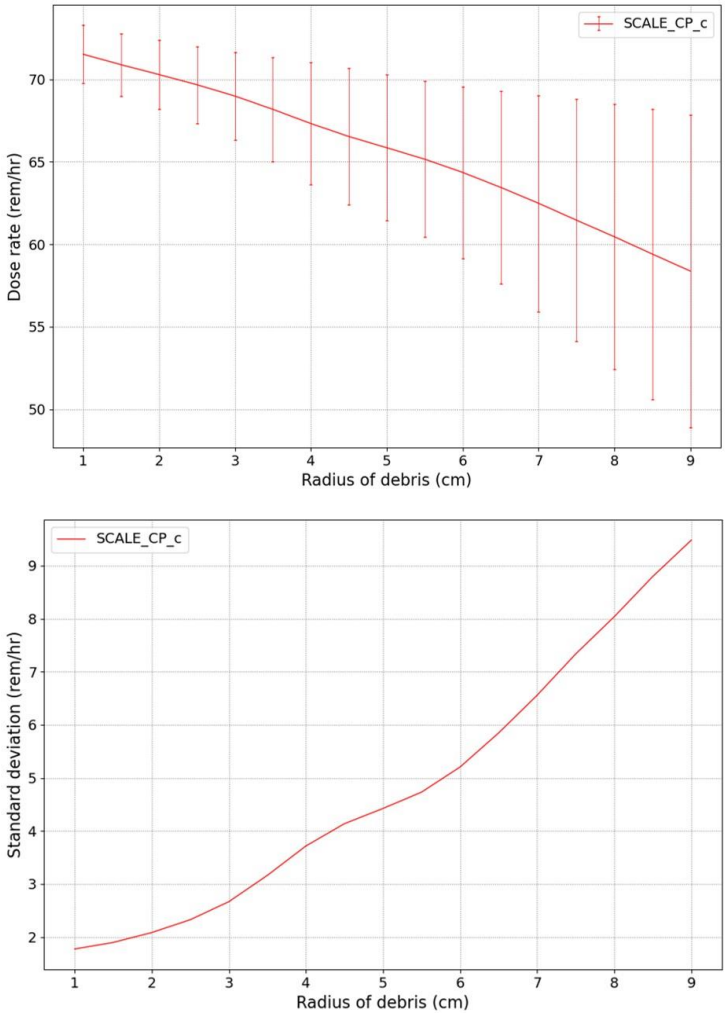


**Figure B. 75 Cumulative graphs.** The average dose rate (top), the standard deviation (bottom)

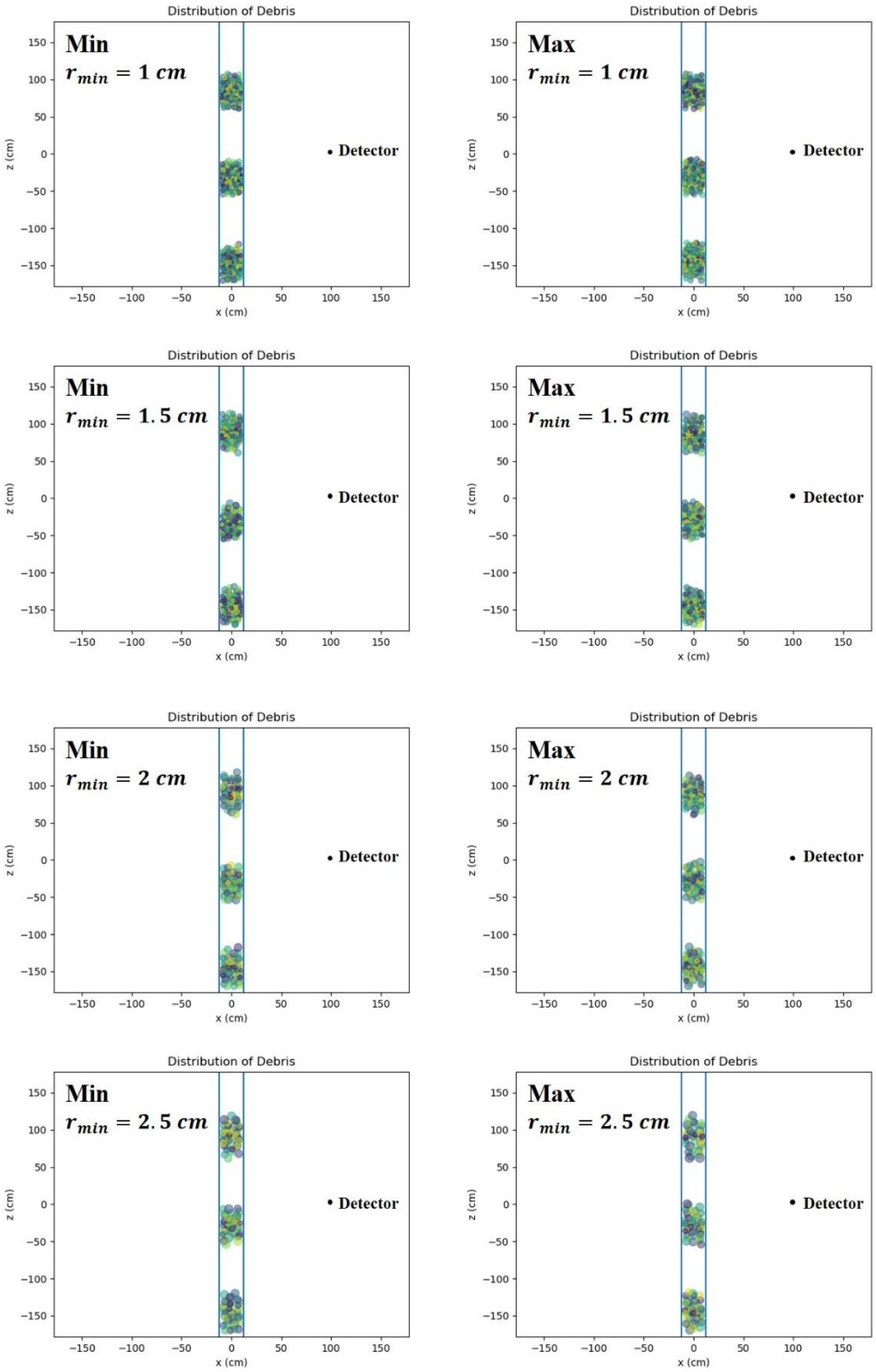


**Figure B. 76 Distribution of the close packed fuel debris in three small containers.**

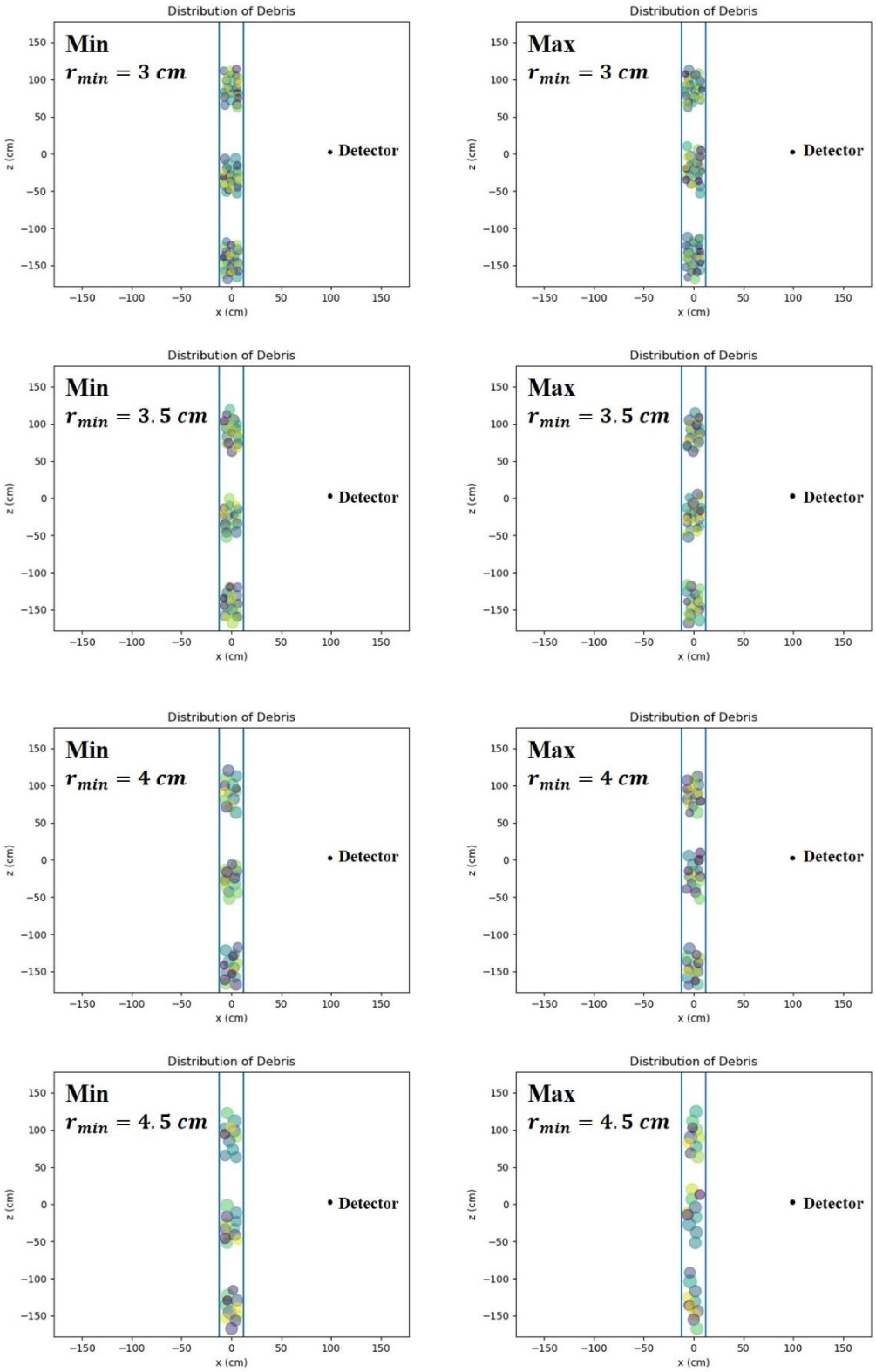


**Figure B. 77 Distribution of the close packed fuel debris in three small containers.**

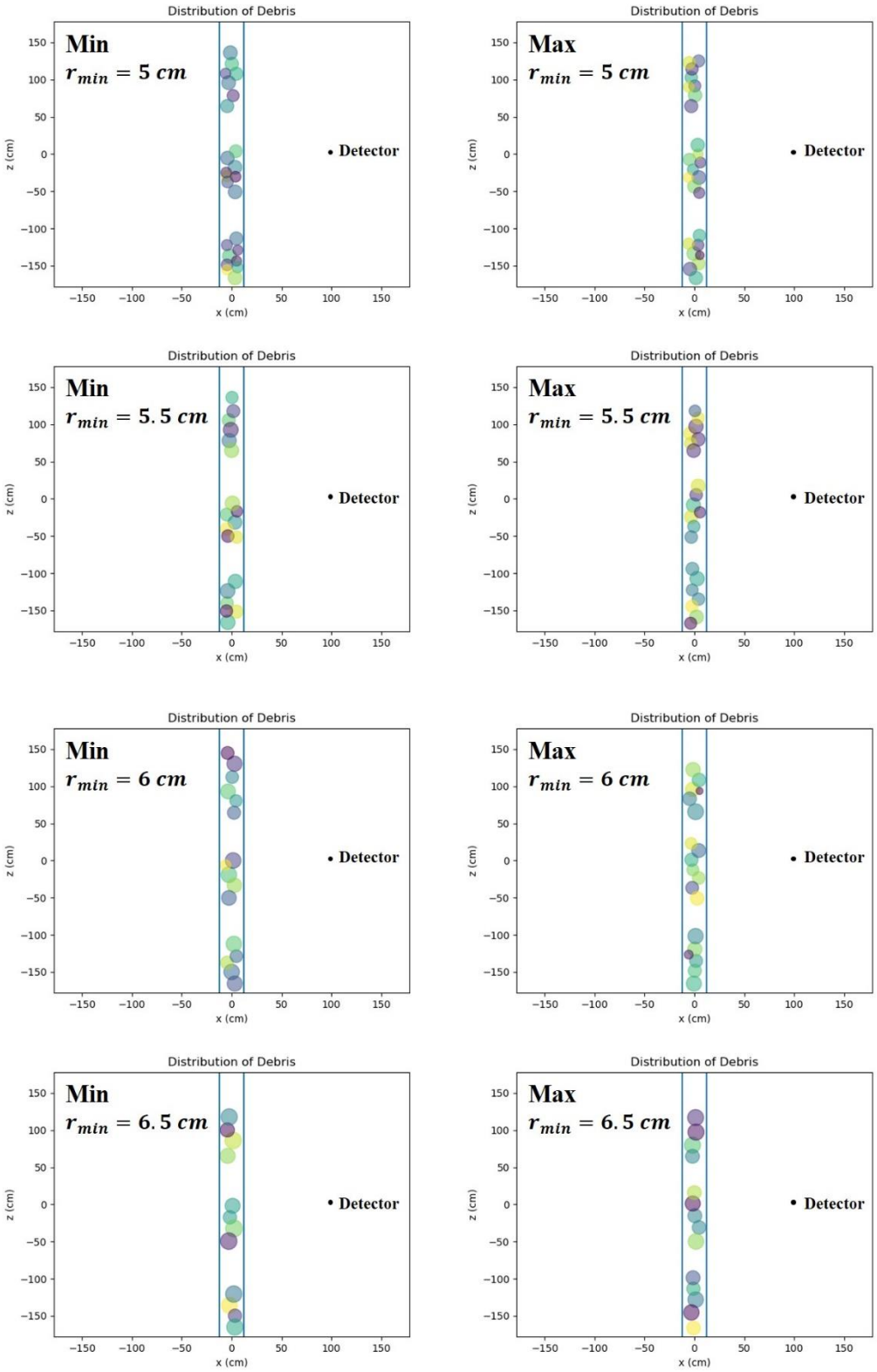


**Figure B. 78 Distribution of the close packed fuel debris in three small containers.**

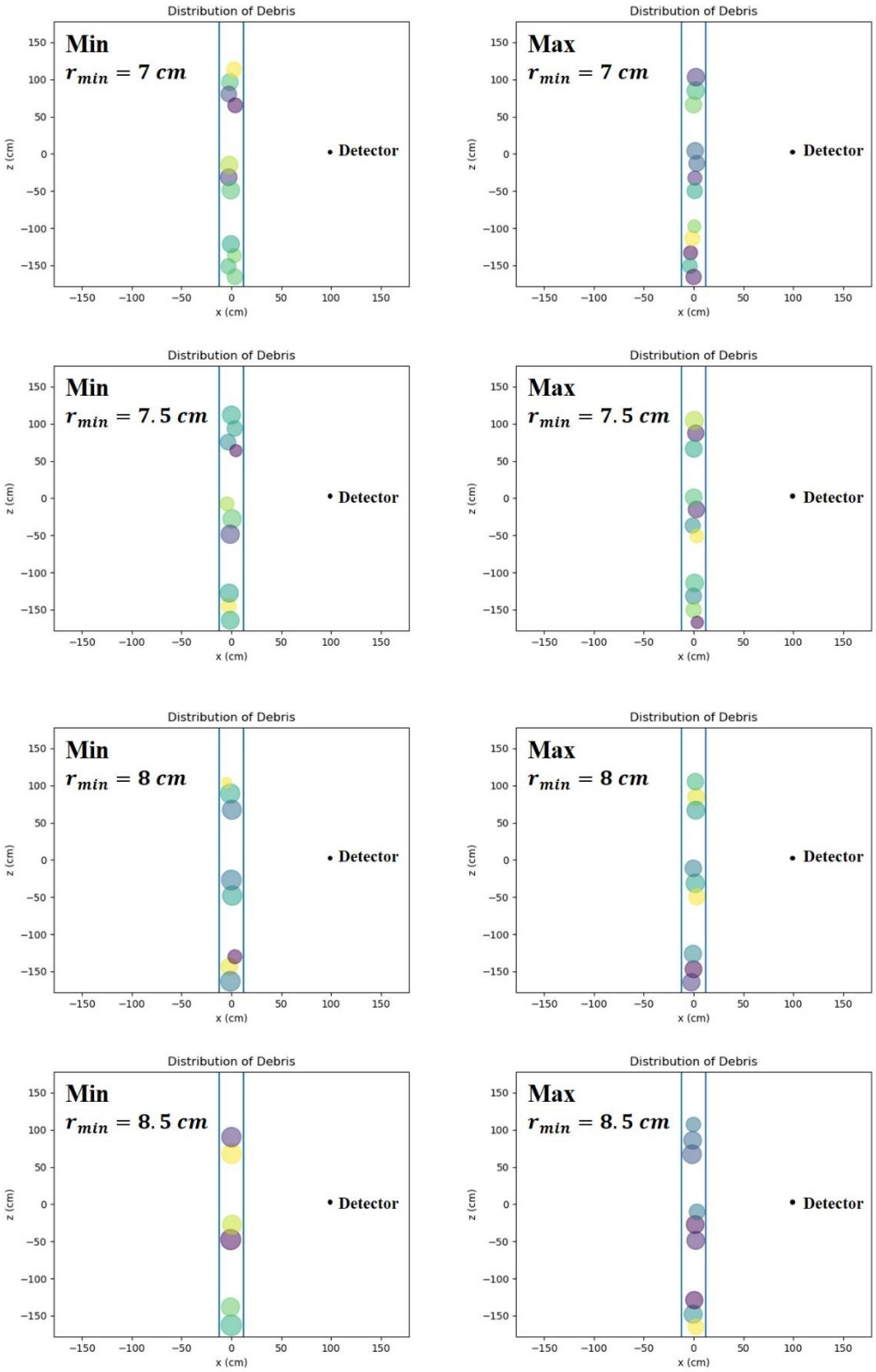


**Figure B. 79 Distribution of the close packed fuel debris in three small containers.**

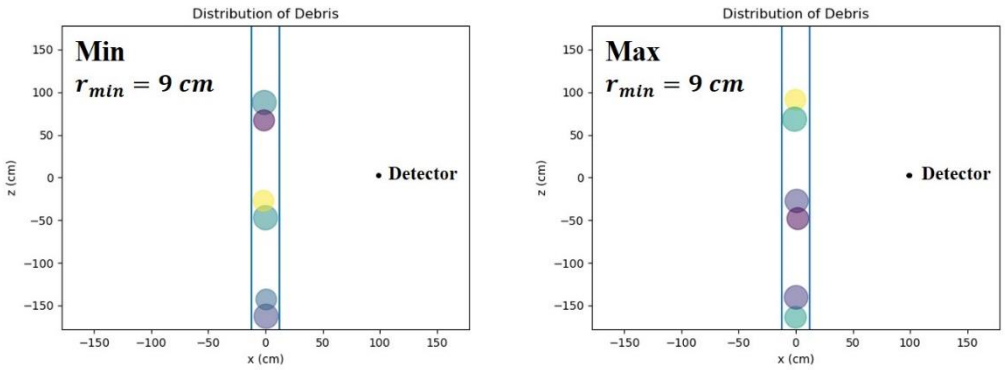


**Figure B. 80 Distribution of the close packed fuel debris in three small containers.**

Photon dose rate from close packed fuel debris in a fuel canister with three small containers decreases by the increase of the minimum radius $r_{min}$ like loose packed fuel debris. However, it does not exponentially decrease unlike the dose rate of loose packed debris (Figure B. 72). Average photon dose rate is 71.5 rem/hr and 41.9 rem/hr for 1 cm of $r_{min}$ and 9 cm of $r_{min}$ each. These values are very different from the photon dose rate of the close packed fuel debris in a canister without small containers. Variability of standard deviation by the change of the $r_{min}$ is also not like the standard deviation of other cases (Figure B. 73). The standard deviation has 2.41 rem/hr of maximum at 5 cm of $r_{min}$, and it has 1.61 rem/hr of local minimum and 2.14 rem/hr of maximum at 7.5 cm and 8.5 cm of $r_{min}$. The coefficient of variation has its maximum at 8.5 cm of $r_{min}$ which is a local maximum of the standard deviation. Range of data decrease by the decrease of $r_{min}$ but its graph is discontinuous. This graph has a spike of range at 5 cm of $r_{min}$ because its range has been calculated by subtracting the minimum from the maximum including outliers of the data.

## Appendix C Regionally averaged photon dose rate

This chapter has graphs which estimate dose rate and uncertainty at a cylindrical region using the SCALE based model developed in Chapter 3. Photon and neutron dose rate are evaluated by assuming a cylindrical shell whose center is the same as the center of the canister (Figure C. 1). The inner wall of the cylindrical shell is 1m from the surface of the canister, and SCALE calculated the photon dose rate from fuel debris at this region by using region tally. Graphs of each section are organized like Appendix B excepting for the graphs on the distribution of fuel debris in a canister.

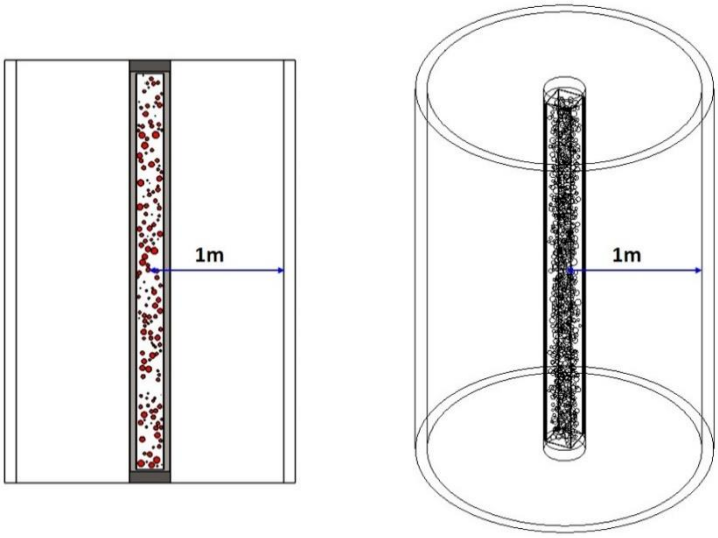


**Figure C. 1 Region for the evaluation of dose rate.** A cylindrical shell is assumed to estimate the regionally averaged photon dose rate in the cylindrical shell. The inner wall of the cylinder is 1m apart from the surface of the canister. Height of the region (cylindrical shell) is the same as the height of the canister, and the thickness of the shell is 10cm.

Average dose rate of the loos packed fuel debris in a canister exponentially decreases by changes in the minimum radius $r_{min}$ (Figure C. 2). The average dose rate is 72.4 rem/hr for 1 cm of $r_{min}$ and 28.9 rem/hr for 9 cm of $r_{min}$. Standard deviation of the photon dose rate increases by the increase of $r_{min}$ from 0.44 rem/hr for 1 cm of $r_{min}$ up to 1.07 rem/hr for 9 cm of $r_{min}$ (Figure C. 3). The coefficient of variation at these two are 0.61 % and 3.7 % of each average dose rate. The coefficient of variation is much smaller than the evaluated values by point tally because dose rates are regionally averaged. Range of the photon dose rate also increases by changes in $r_{min}$. Range is 2.94 rem/hr for 1.0 cm of $r_{min}$ and 7.84 rem/hr for 9.0 cm of $r_{min}$ which are 4.06 % and 31.1 % of the average dose rate of each sample group.

Graph of the regionally averaged photon dose rate of the close packed fuel debris in a canister has local maximums and a minimum but it linearly decreases when the minimum radius $r_{min}$ is larger than 5.5 cm (Figure C. 6). Dispersion of data at the graph of box plots is larger than the dispersion of data for the loose packed debris but it is also smaller than the dispersion of data for point tally because dose rates are regionally averaged at the cylindrical shell. The average dose rates are 39.74 rem/hr and 25.64 rem/hr for 1 cm and 9 cm of $r_{min}$, and the average dose rates at the local maximums are 40.63 rem/hr and 39.12 rem/hr for 2.5 cm and 5 cm of $r_{min}$. Standard deviation of dose rate has local maximums at 4.5 cm and 8.9 cm of $r_{min}$ which is 1.15 rem/hr and 0.99 rem/hr (Figure C. 7). The coefficient of variation at these $r_{min}$ are 2.97 % and 3.9 % each. Range of the photon dose rate has several local maximums and minimums, and the global maximum is 7.3 rem/hr at 4.5 cm of $r_{min}$ which is 18.9 % of the average dose rate.

Regionally averaged photon dose rate of the loose packed fuel debris in a fuel canister with three small containers exponentially decreases by the change of the minimum radius $r_{min}$ like the fuel debris in a canister without small containers does (Figure C. 10). Average photon dose rates are very similar with the dose rate of fuel debris in a canister without small containers, and they are 72.3 rem/hr and 29.7 rem/hr for 1cm and 9 cm of $r_{min}$. Graph of the standard deviation is different from the graph of the debris in canister without small containers, but overall value of it increases by the change of $r_{min}$ like the canister without containers does (Figure C. 11)). Standard deviations are 0.44 rem/hr and 1.09 rem/hr for 1 cm and 9 cm of $r_{min}$. Coefficient of variations are 0.61 % and 3.67 % of the photon dose rate for 1 cm and 9 cm of $r_{min}$. Range of the dose rate has several local maximums and minimums like the canister without small containers does, and it is 3.6 rem/hr and 6.17 rem/hr for 1 cm and 9 cm of $r_{min}$ which are 4.98 % and 20.8 % of the dose rate.

Photon dose rate of the close packed fuel debris in a fuel canister with three small containers decreases by the change of the minimum radius $r_{min}$ (Figure C. 14). It non-linearly decreases for $r_{min}$ smaller than 5.5 cm, and it linearly decreases for $r_{min}$ larger than 5.5 cm. Average photon dose rates are 45.7 rem/hr for 1 cm of $r_{min}$ and 27.7 rem/hr for 9 cm of $r_{min}$. Standard deviations of the photon dose rate are 0.46 rem/hr and 0.24 rem/hr for 1 cm and 9 cm of $r_{min}$ (Figure C. 15). Coefficient of variations are 1 % and 0.87 % of the average dose rate for 1 cm and 9 cm of $r_{min}$. Its maximum is 3.3 % of the average dose rate for 8.5 cm of $r_{min}$. Range of the dose rate has several local maximums and minimums, and the global maximum is 4.92 rem/hr at 7 cm of $r_{min}$ which is 14.6 % of its average photon dose rate.

## C. 1. Photon dose rate of the loose packed fuel debris in a canister

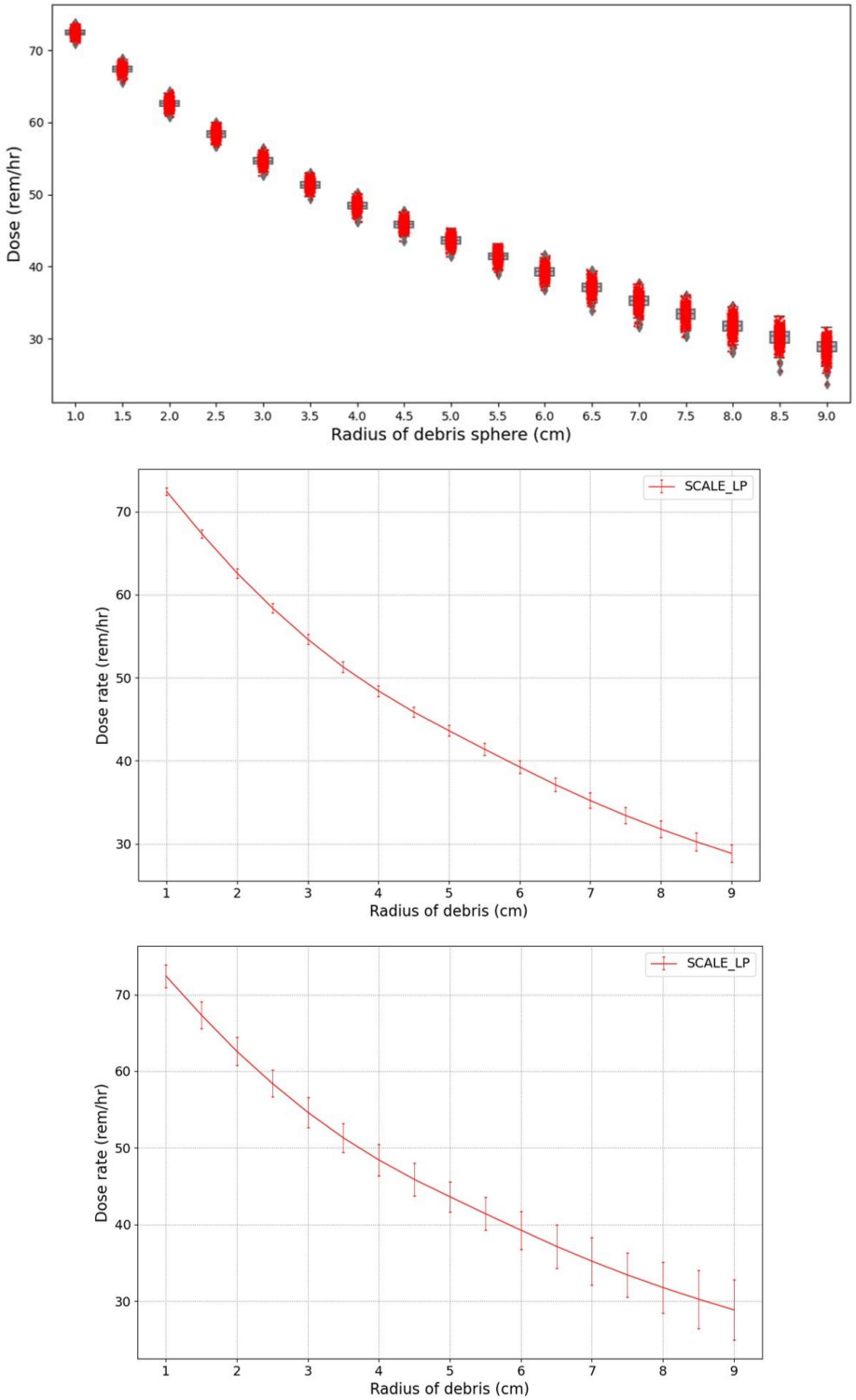


**Figure C. 2 Photon dose rate of the loose packed fuel debris.** The estimated dose rates (top), the average dose rate with the standard deviation (middle), the average dose rate with the range (bottom)

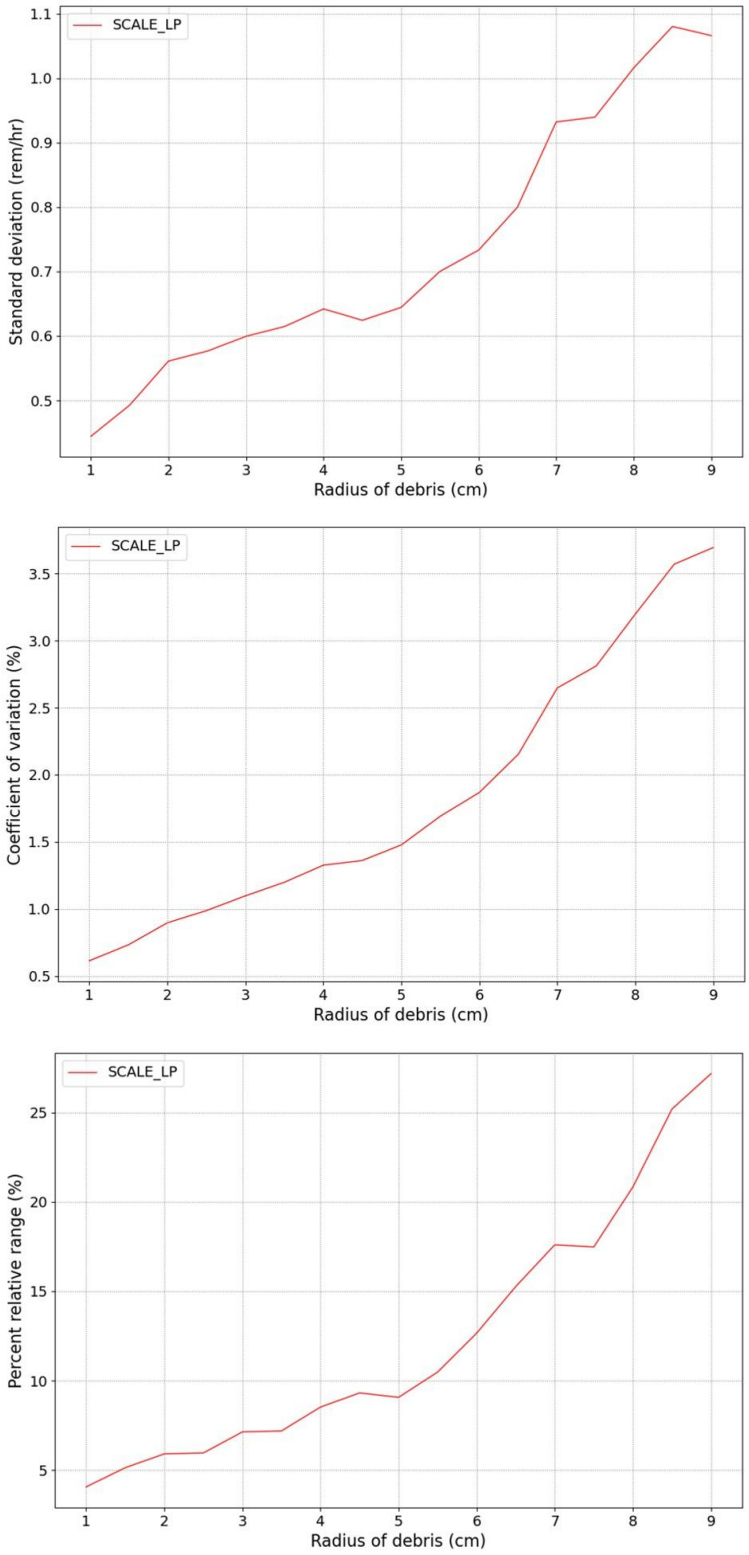


**Figure C. 3 Uncertainty of the loose packed fuel debris.** The standard deviation (top), the coefficient of variation (middle), the percent relative range (bottom)

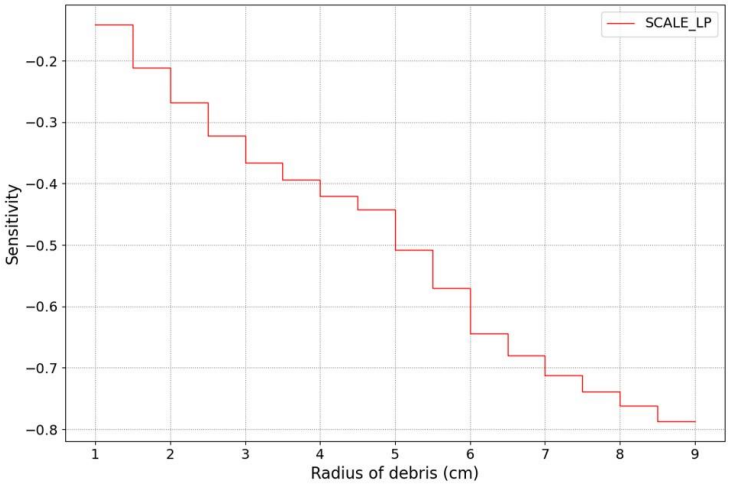


**Figure C. 4 Sensitivity index of the loose packed fuel debris.**

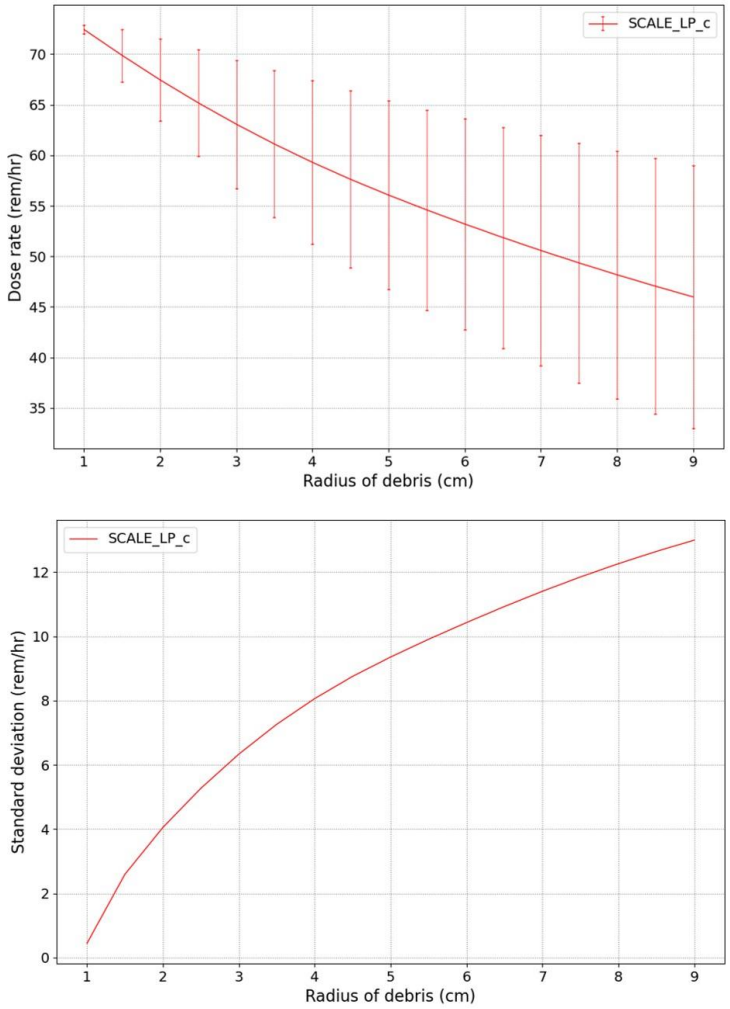


**Figure C. 5 Cumulative graphs.** The average dose rate (top), the standard deviation (bottom)

## C. 2. Photon dose rate of the close packed fuel debris in a canister

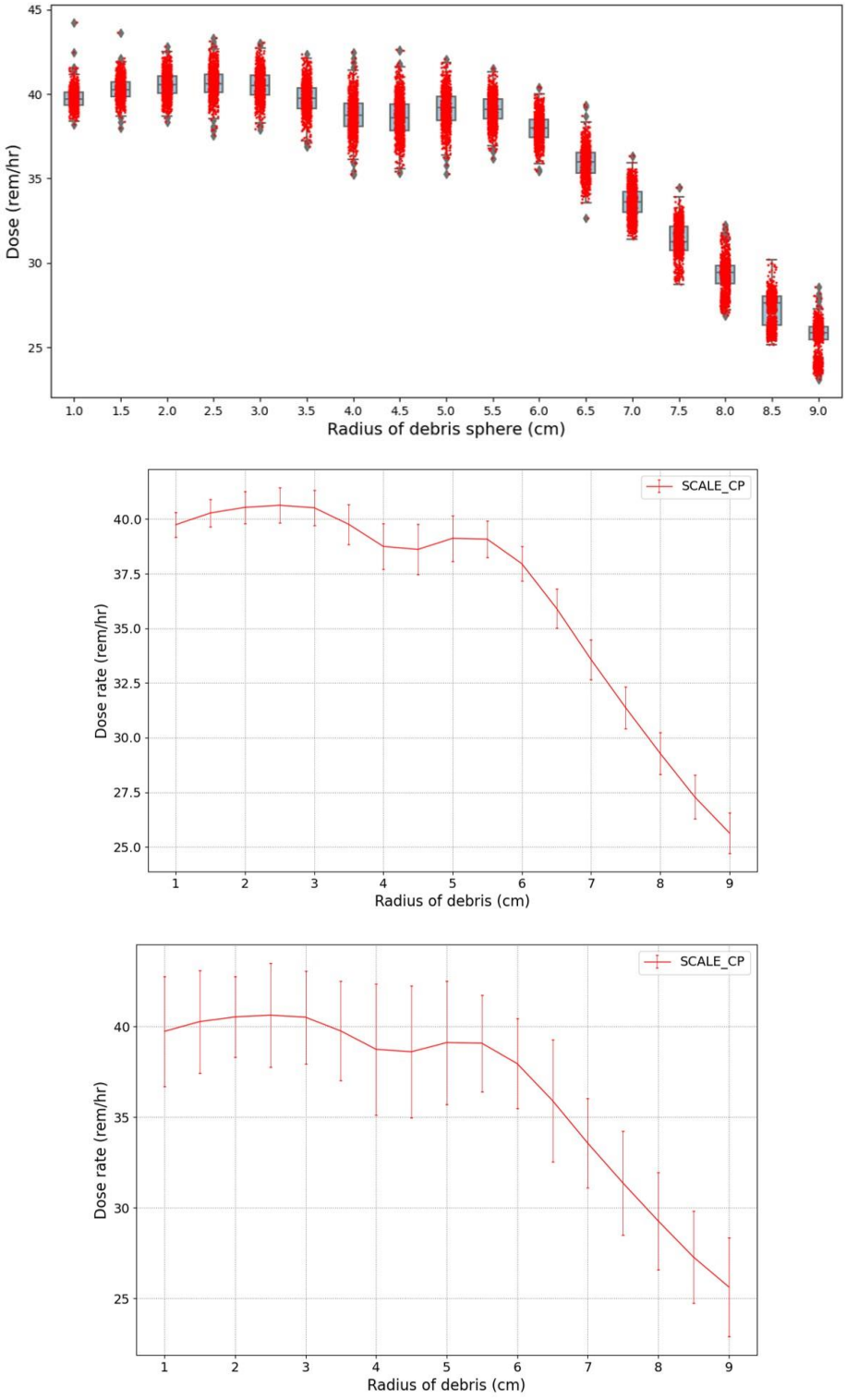


**Figure C. 6 Photon dose rate of the close packed fuel debris.** The estimated dose rates (top), the average dose rate with the standard deviation (middle), the average dose rate with the range (bottom)

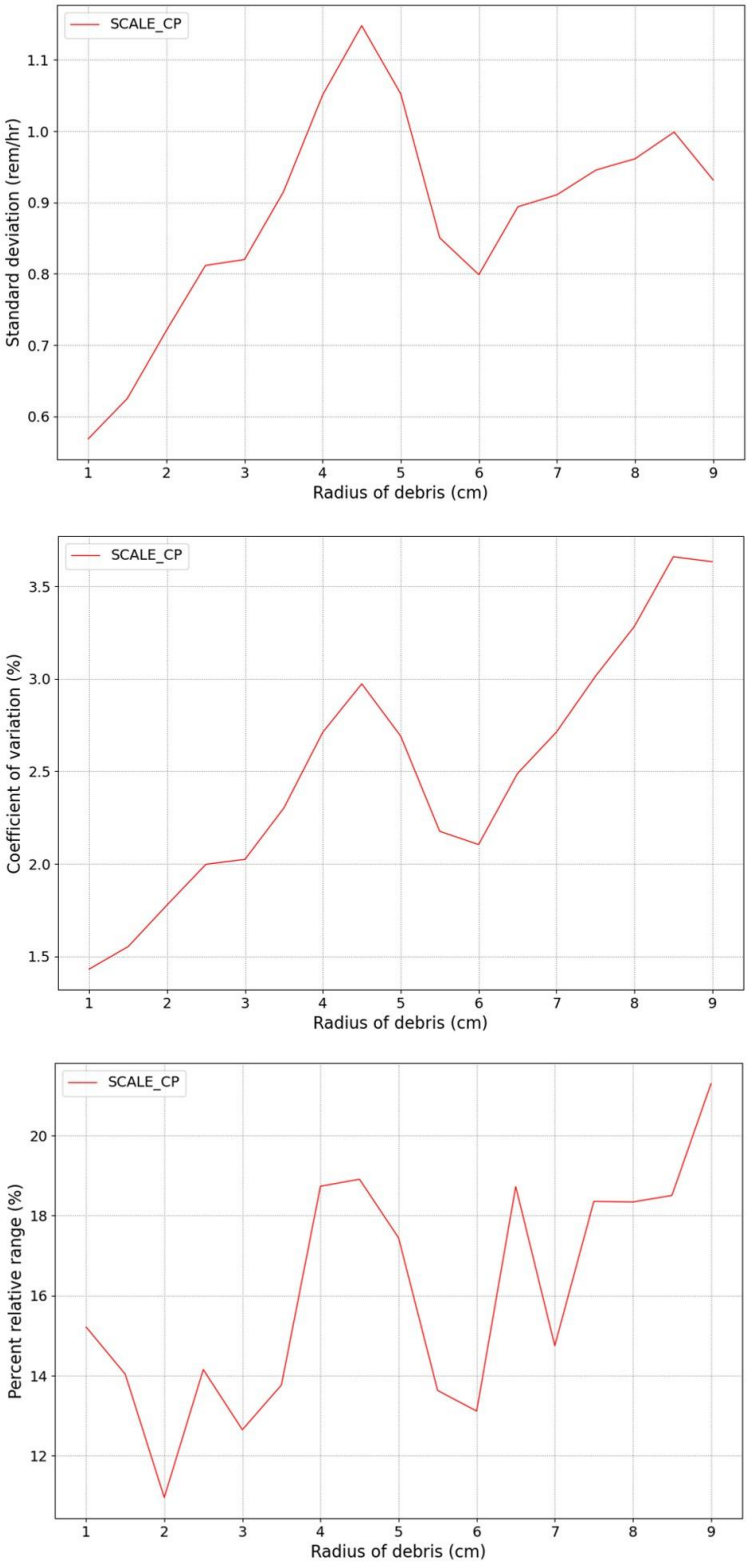


**Figure C. 7 Uncertainty of the close packed fuel debris.** The standard deviation (top), the coefficient of variation (middle), the percent relative range (bottom)

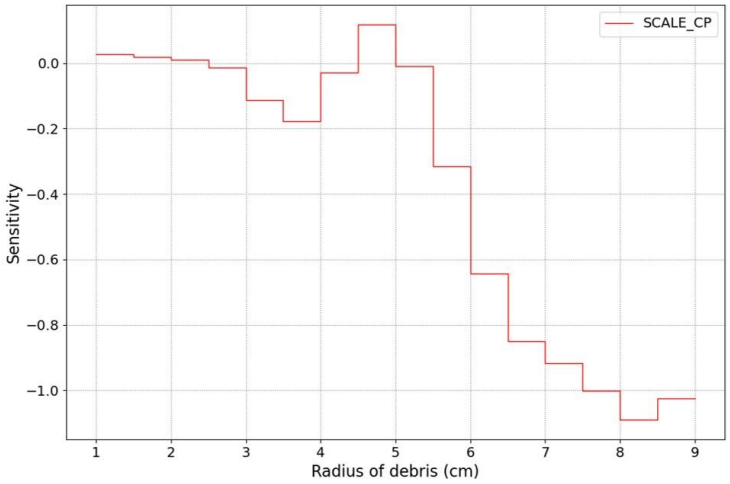


**Figure C. 8 Sensitivity index of the close packed fuel debris.**

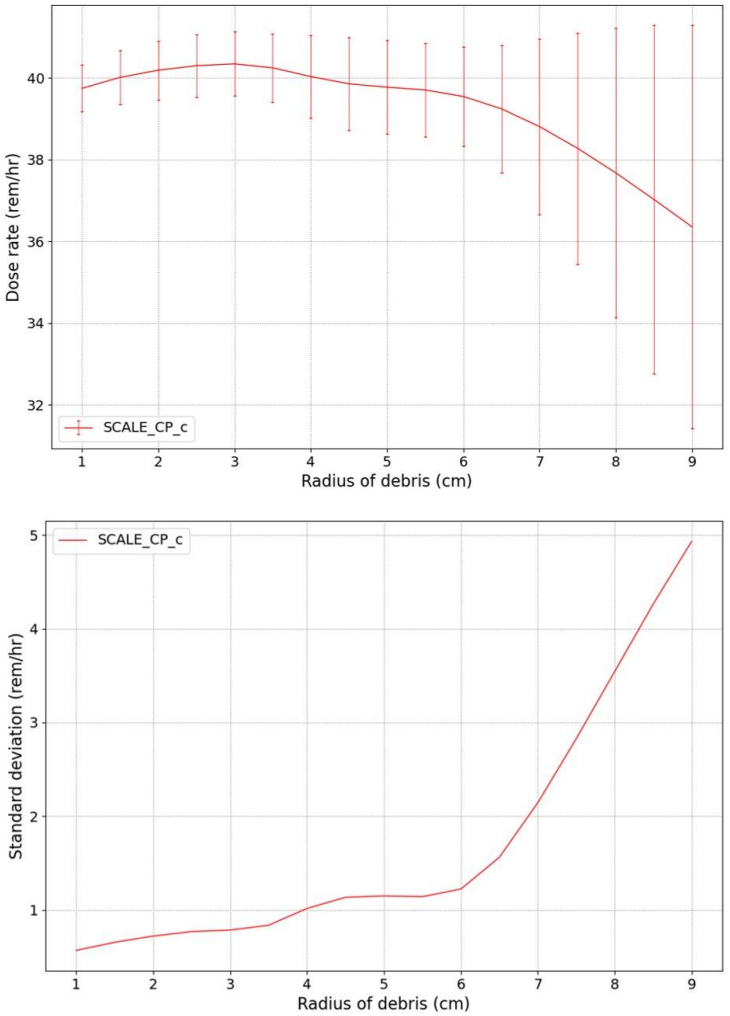


**Figure C. 9 Cumulative graphs.** The average dose rate (top), the standard deviation (bottom)

## C. 3. Photon dose rate of the loose packed fuel debris in three small containers

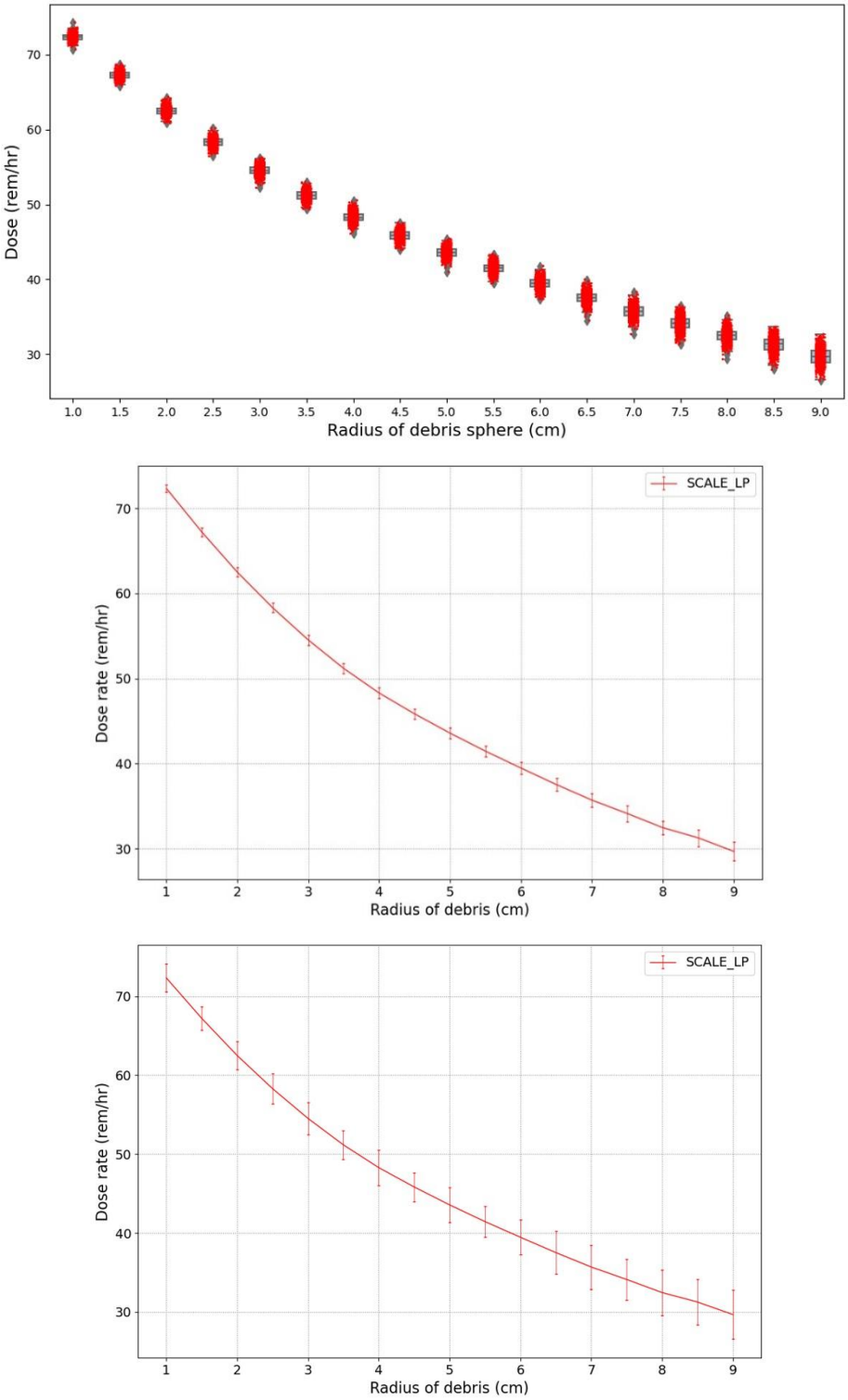


**Figure C. 10 Photon dose rate of the loose packed fuel debris.** The estimated dose rates (top), the average dose rate with the standard deviation (middle), the average dose rate with the range (bottom)

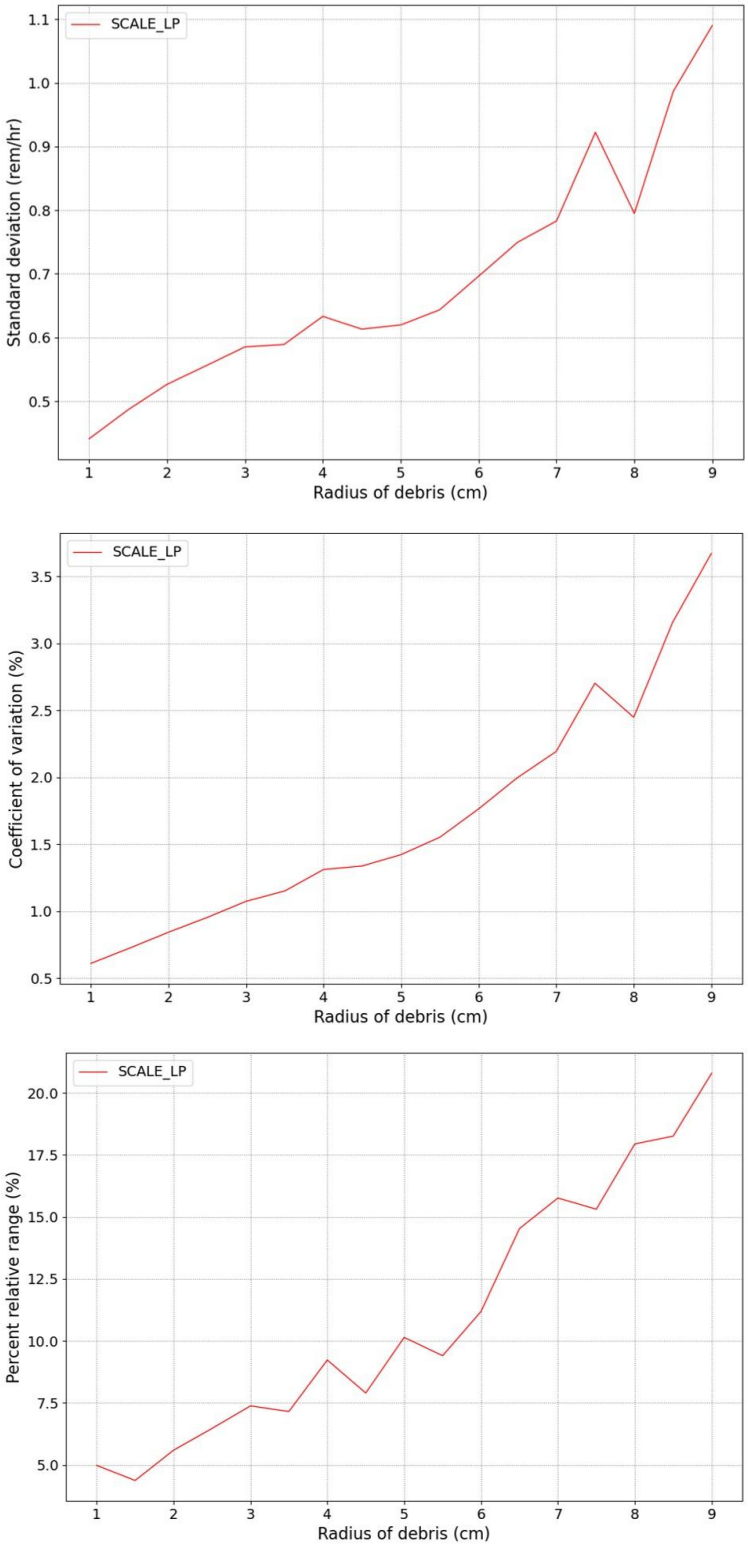


**Figure C. 11 Uncertainty of the loose packed fuel debris.** The standard deviation (top), the coefficient of variation (middle), the percent relative range (bottom)

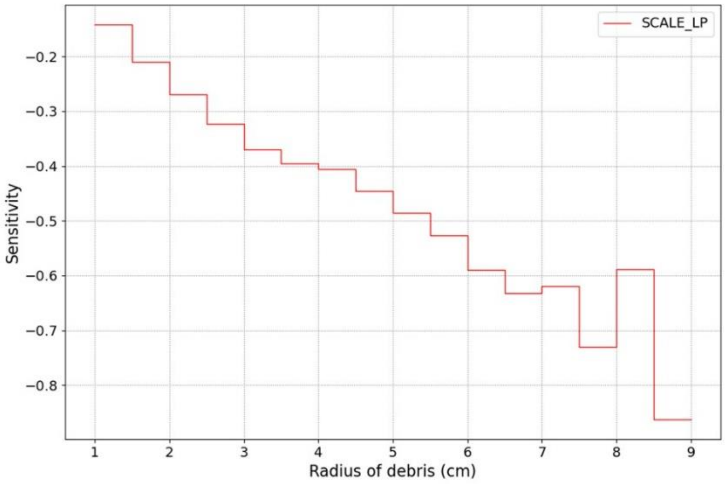


**Figure C. 12 Sensitivity index of the loose packed fuel debris.**

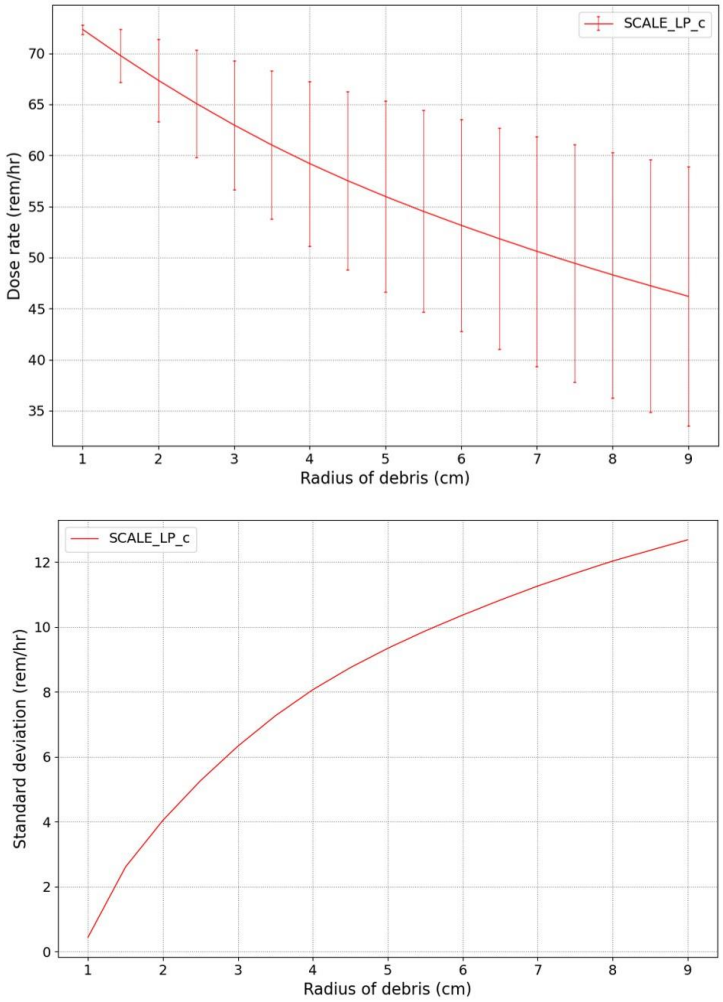


**Figure C. 13 Cumulative graphs.** The average dose rate (top), the standard deviation (bottom)

## C. 4. Photon dose rate of the close packed fuel debris in three small containers

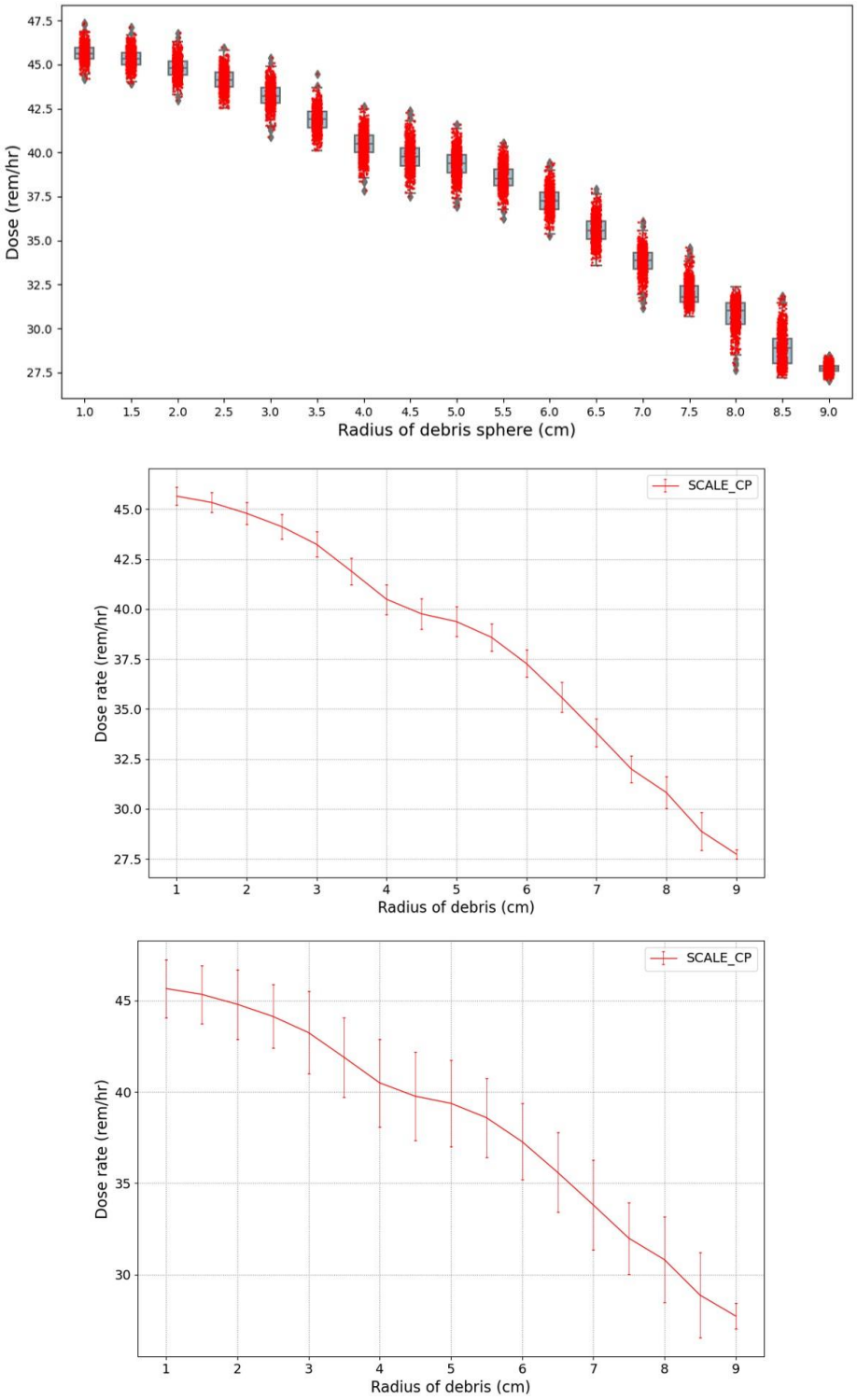


**Figure C. 14 Photon dose rate of the close packed fuel debris.** The estimated dose rates (top), the average dose rate with the standard deviation (middle), the average dose rate with the range (bottom)

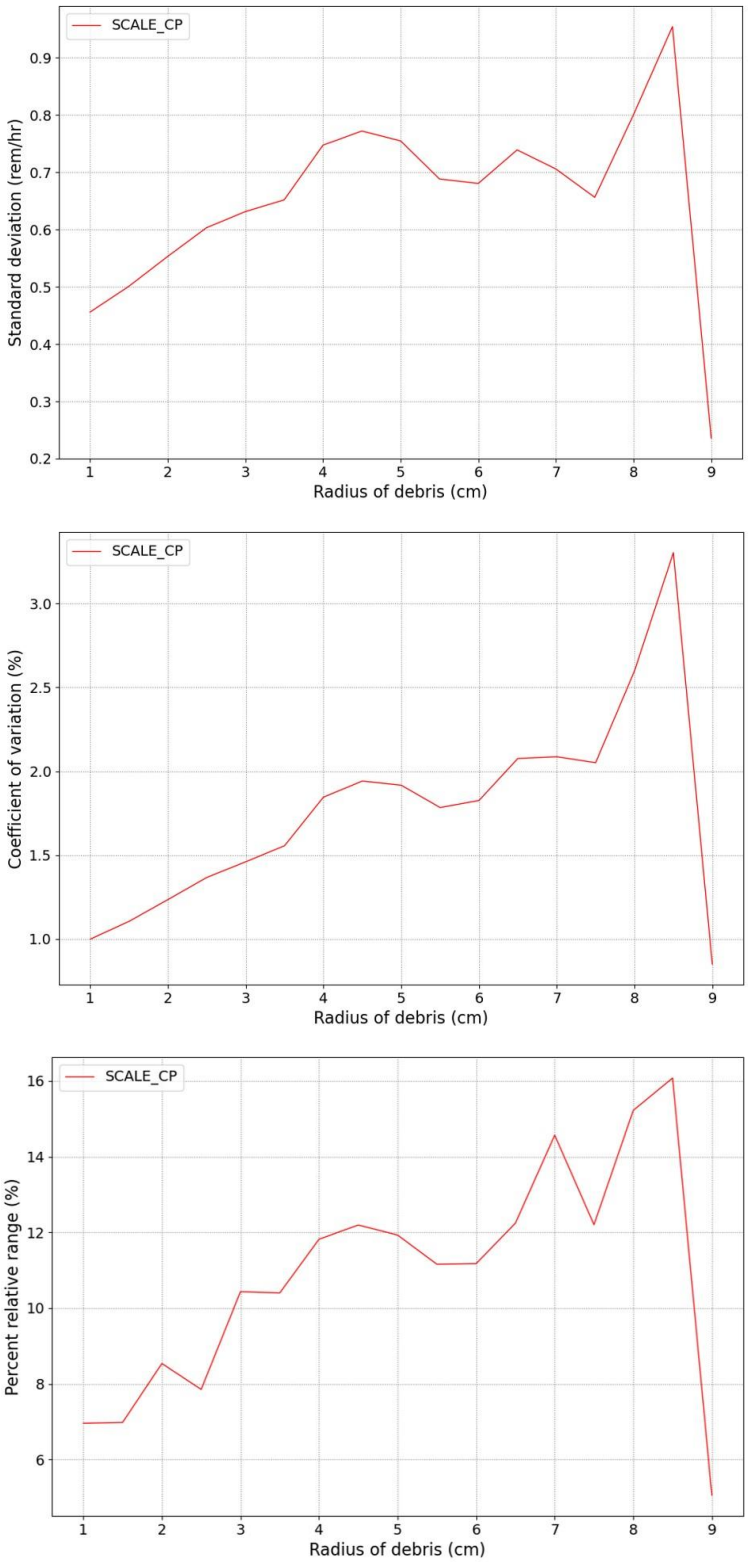


**Figure C. 15 Uncertainty of the close packed fuel debris.** The standard deviation (top), the coefficient of variation (middle), the percent relative range (bottom)

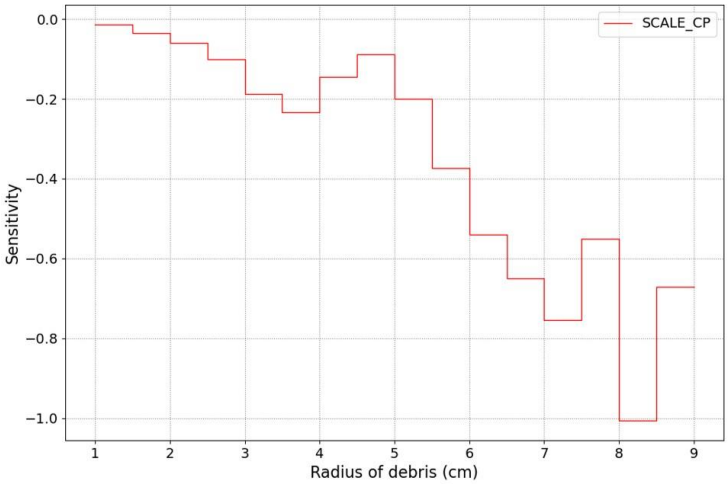


**Figure C. 16 Sensitivity index of the close packed fuel debris.**

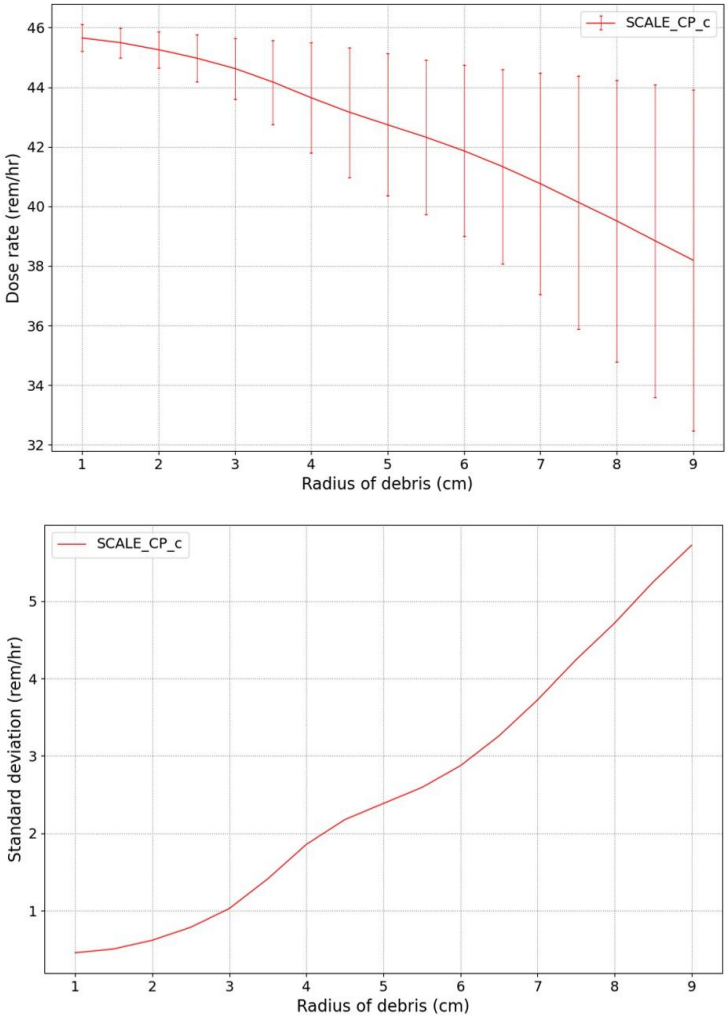


**Figure C. 17 Cumulative graphs.** The average dose rate (top), the standard deviation (bottom)

## Appendix D. Photon and neutron dose rate at vertically divided regions

Radiation dose rate depends on the location of the detectors which is assumed for the estimation, and results of the evaluation at previous chapters were diverse by the location. According to the result, evaluation on the variability of the dose rate by the location of the detector is required for better understanding of the uncertainty of dose rate. Therefore, Dose rate and its uncertainty is evaluated at this chapter by using mesh tally which calculates radiation dose rates for vertically divided regions. A cylindrical region in which its center is the same as the center of a fuel canister is assumed for the evaluation. Its height is 5m, and it is divided into 25 regions by 20cm each. Its inner radius is 1 m larger than the outer radius of the canister, and thickness of the cylindrical region is 10 cm. Therefore, radiation dose rates are evaluated at 1m from the surface of the fuel canister for 25 vertically different regions by assuming these 25 regions (Figure D. 1).

Photon and neutron dose rate at each region is calculated by using SCALE for 17 sample groups which are assorted by the minimum radius from 1 cm to 9 cm. Each sample group has 1,000 samples which are results from 1,000 times of estimations by SCALE. Estimated photon dose rates are plotted in a form of a density plot which visualizes dose rates for 25 regions of each sample group (Figure D. 2). The result of estimation is also plotted by using line plots to visualize more details (Figure D. 3).

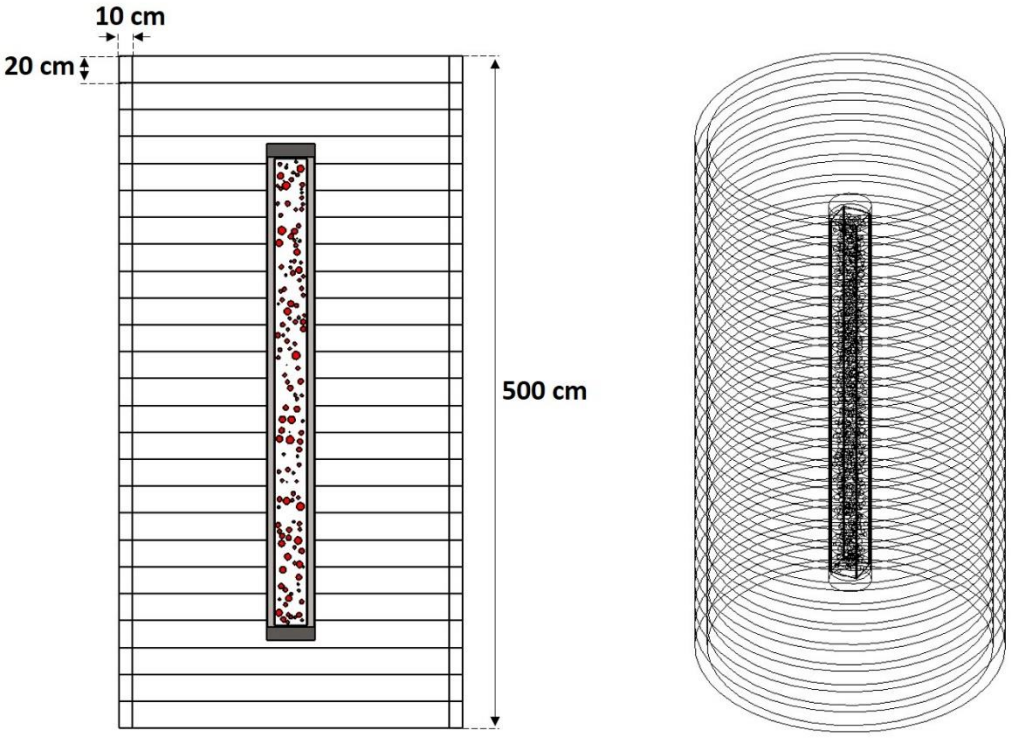


**Figure D. 1 The 25 cylindrical regions for the evaluation of dose rate.**

Photon dose rate of loose packed fuel debris in a fuel canister has its maximum at the medium height of a canister with 1cm of minimum radius $r_{min}$, and then it gradually decreases by the change of $r_{min}$ and the vertical height from the center. Dose rates of sample groups with the medium height decreases by the change of $r_{min}$, and all sample groups have a maximum at the medium height. The maximum dose rate is at the left side of the density plot, and it is displayed in thick red colors (Figure D. 2). Photon dose rate estimated at a point can be 6 times larger than a dose rate at other detector locations depending on regions. Dose rates at the top and bottom are smaller than 10 rem/hr for 9 cm of $r_{min}$ whereas the dose rate of medium height is larger than 60 rem/hr for 1 cm of $r_{min}$. On the other hand, the coefficient of variation has its maximums at the top and bottom region for 9 cm of $r_{min}$ (Figure D. 4). The coefficient of variation increases by the change of the vertical height from the center of a canister, and it also increases by the increase of the size of debris. The coefficient of variation is smaller than 5 % of its average dose rate at the medium height for 1 cm of $r_{min}$ whereas it is larger than 25 % of its average dose rate at the top and bottom region for 9 cm of $r_{min}$.

Density plot of photon dose rate from close packed fuel debris in a fuel canister is biased to regions at the lower region, and vertical heights of maximums are different by sample groups unlike the dose rate of loose packed debris (Figure D. 6). Density plot of the coefficient of variation is also biased, and the maximum dose rate is located near the top regions of the sample group with 5 cm of $r_{min}$ (Figure D. 8). The density map has a global maximum at the region near the top, and a local maximum at the region near the bottom. These two maximums are not at the top (250 cm) and bottom (-250 cm) of the vertical region unlike the loose packed fuel debris. Each sample group has a saddle point between two maximums.

Photon dose rate of loose packed fuel debris in a fuel canister with three small containers are very similar with the loose packed fuel debris in a fuel canister without small containers (Figure D. 10). Its density plot also has a global maximum at the left side of the plot which is located at the medium height of the vertical region (1 cm of $r_{min}$, center of the vertical region). The maximum value of each sample group is at the medium height. On the other hand, the density plot of the coefficient of variation is very different from the density plot of loose packed debris in a canister without small containers (Figure D. 12). This density plot has two global maximums at the top and bottom region for 9 cm of $r_{min}$, and it has two local maximums between these two. Therefore, each sample group has three saddle points between two maximums.

Density plot of photon dose rate from close packed fuel debris in a fuel canister with three small containers is also biased to the lower region but it is less biased than the dose rate of a canister without small containers. Maximum dose rate of each sample group is at the same vertical height, but it is at between the vertical region -20 cm and -40 cm. The density plot of the coefficient of variation is also biased, and it has a global maximum at the top region like the coefficient of variation of the close packed fuel debris in a canister without small containers. However, each sample group has three saddle points between maximums.

## D.1. Plots of photon dose rate (Estimated by SCALE based model)

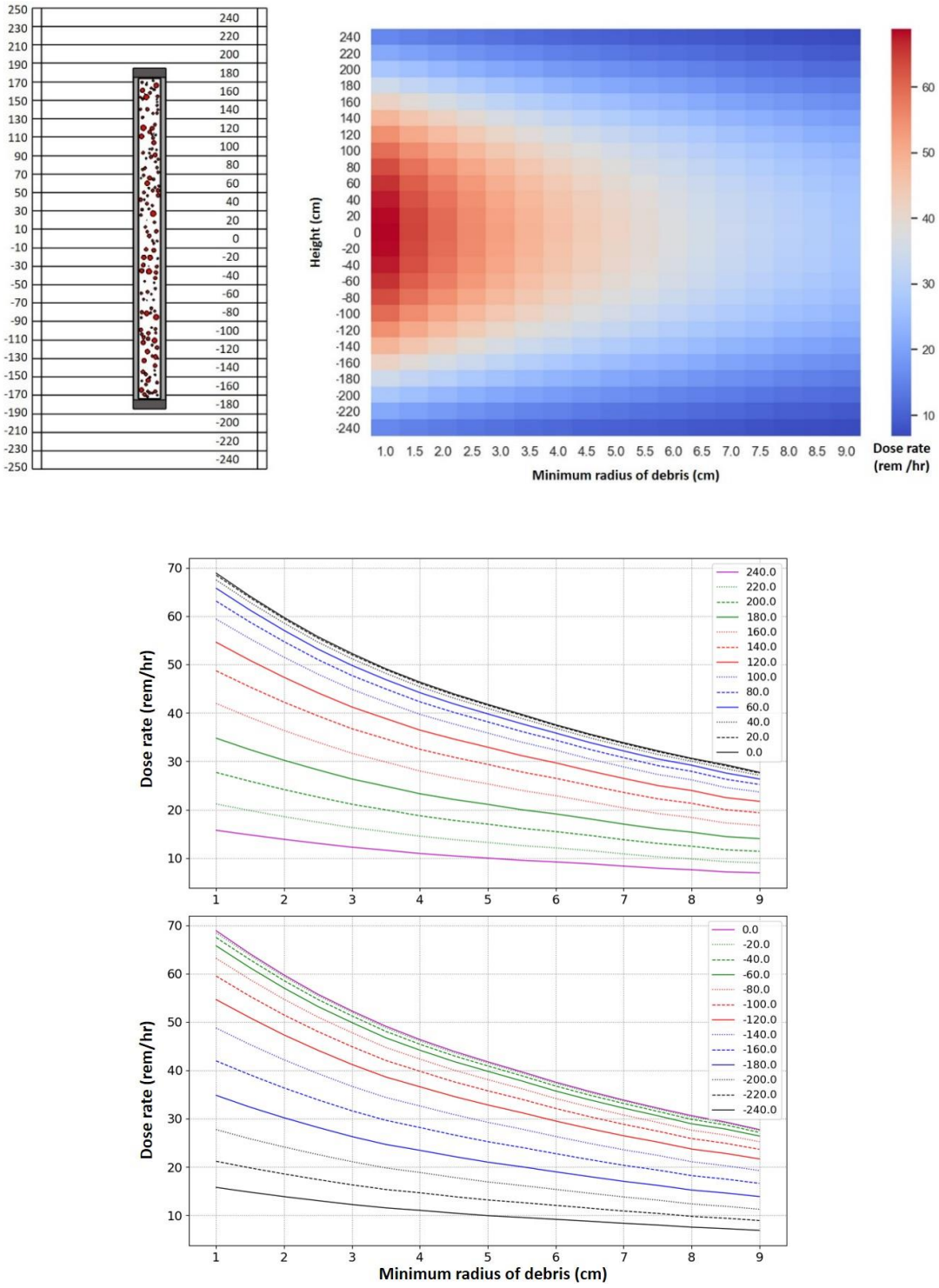


**Figure D. 2 Density plot (top) and line plots of the photon dose rate for the loose packed fuel debris in a canister**

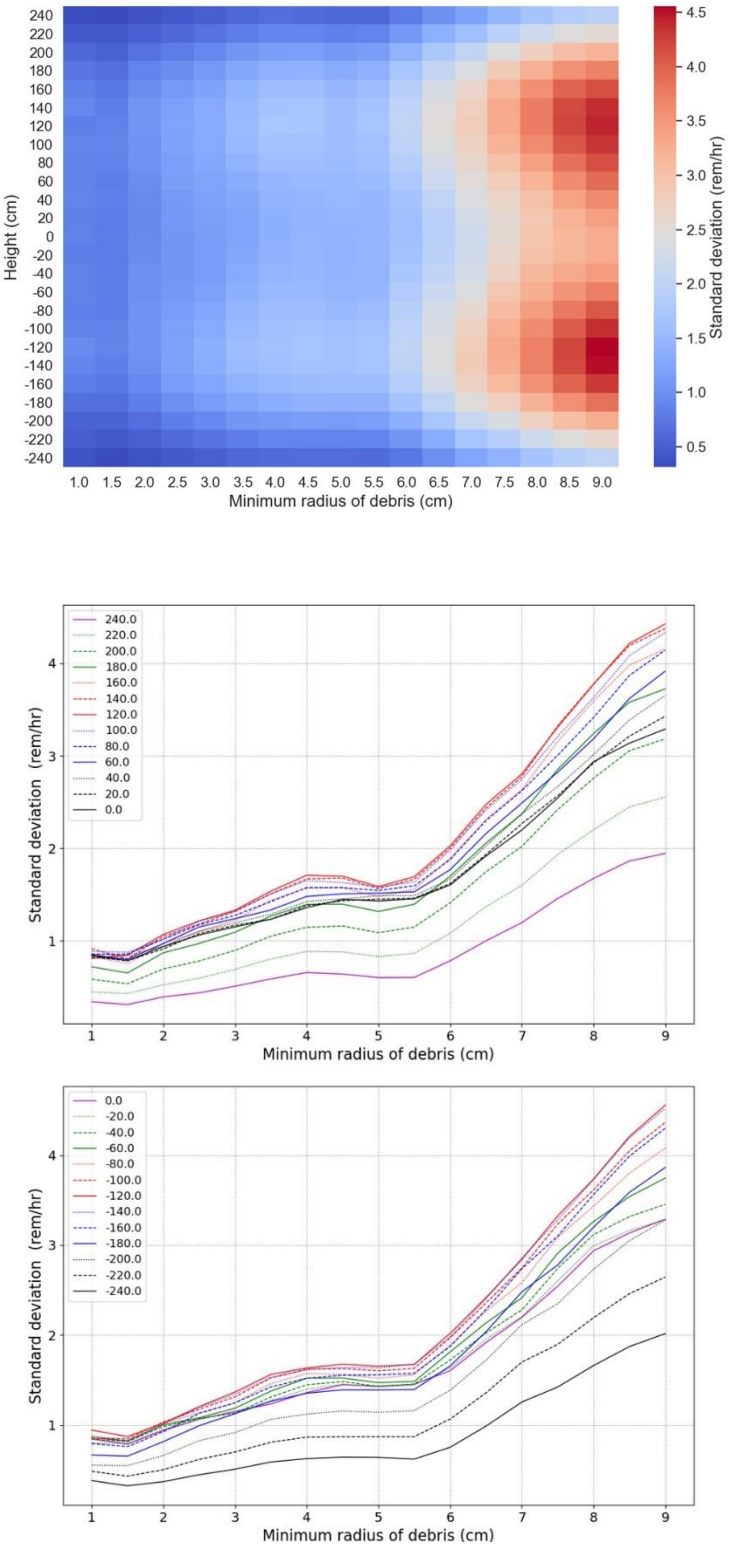


**Figure D. 3 Density plot (top) and line plots of the standard deviation of the photon dose rate of loose packed fuel debris in a canister**

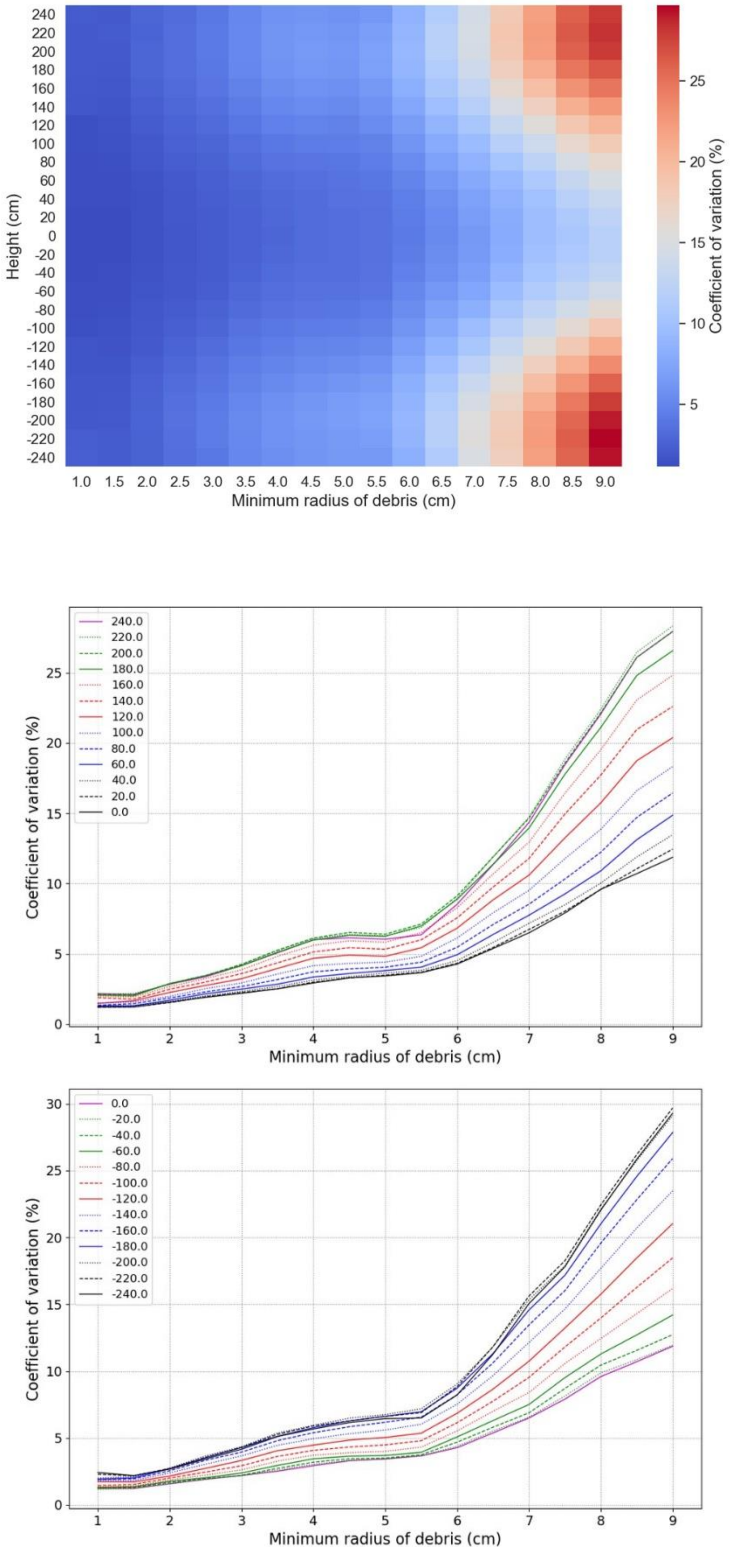


**Figure D. 4 Density plot (top) and line plots of the coefficient of variation of the photon dose rate of loose packed fuel debris in a canister**

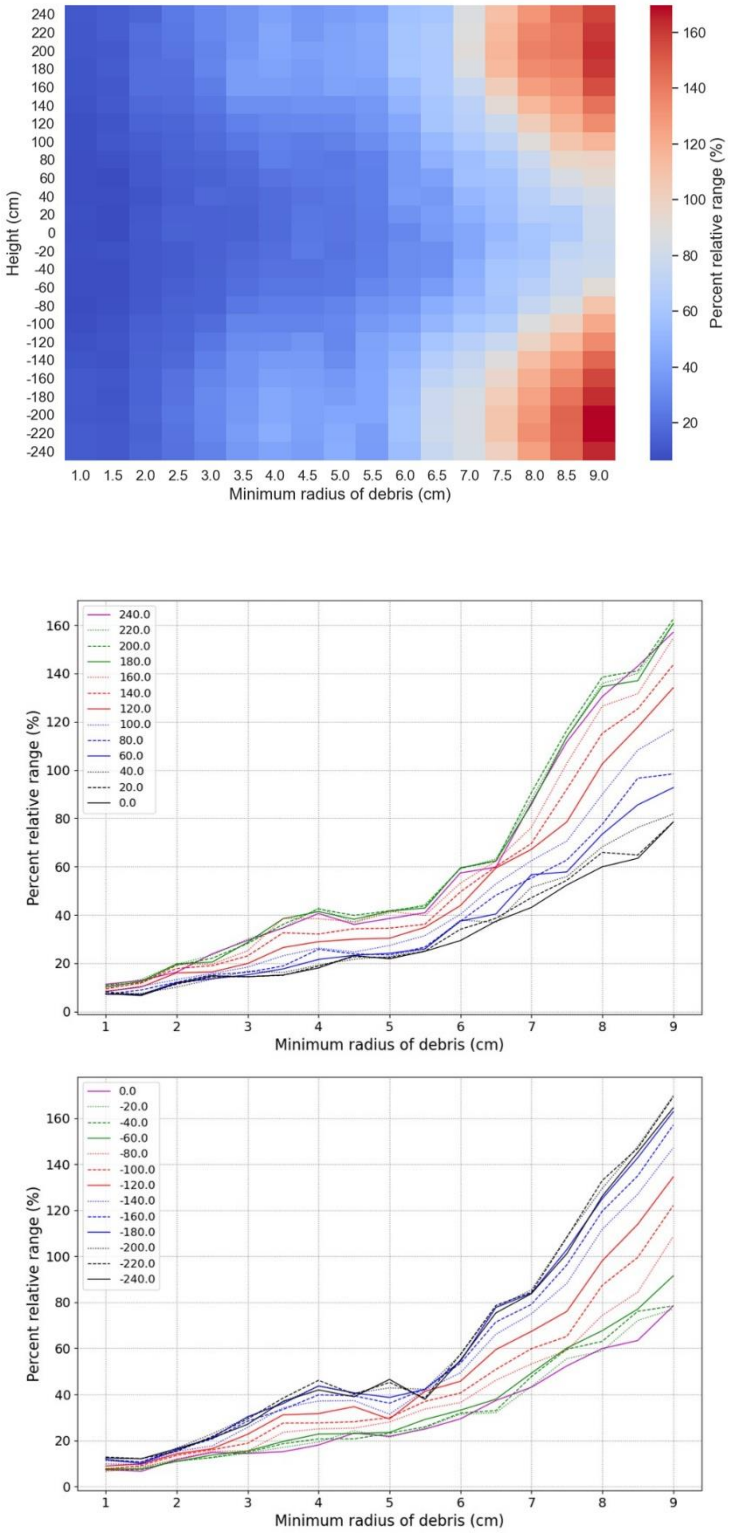


**Figure D. 5 Density plot (top) and line plots of the percent relative range of the photon dose rate of loose packed fuel debris in a canister**

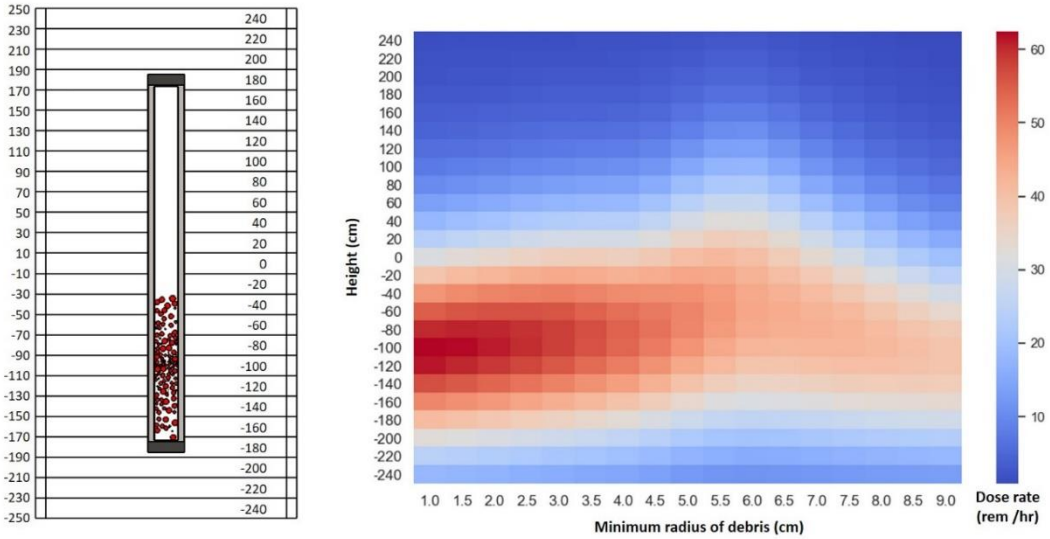


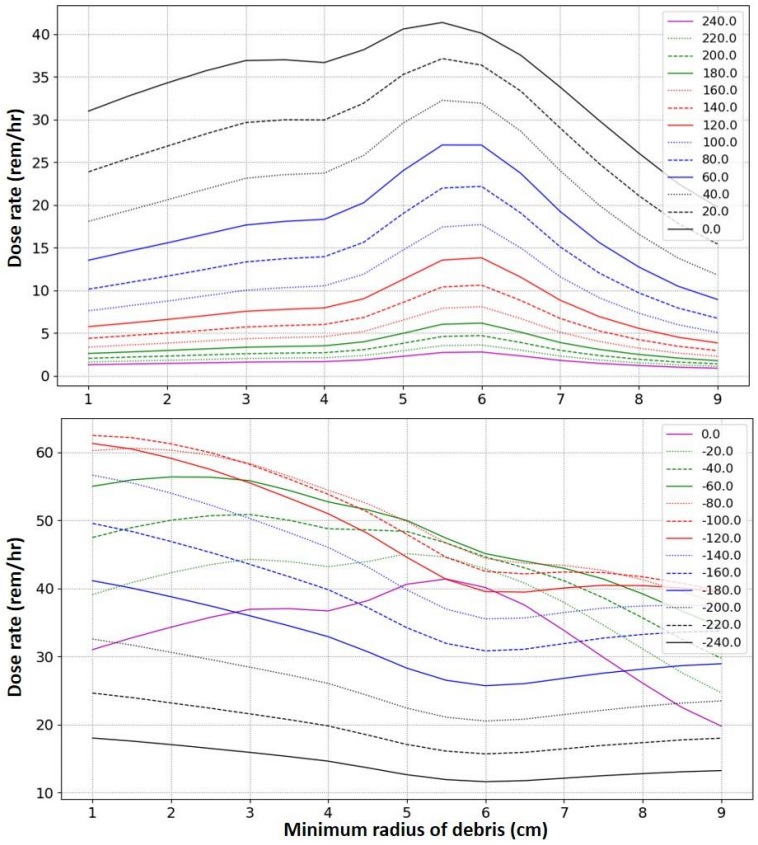


**Figure D. 6 Density plot (top) and line plots of the photon dose rate for the close packed fuel debris in a canister**

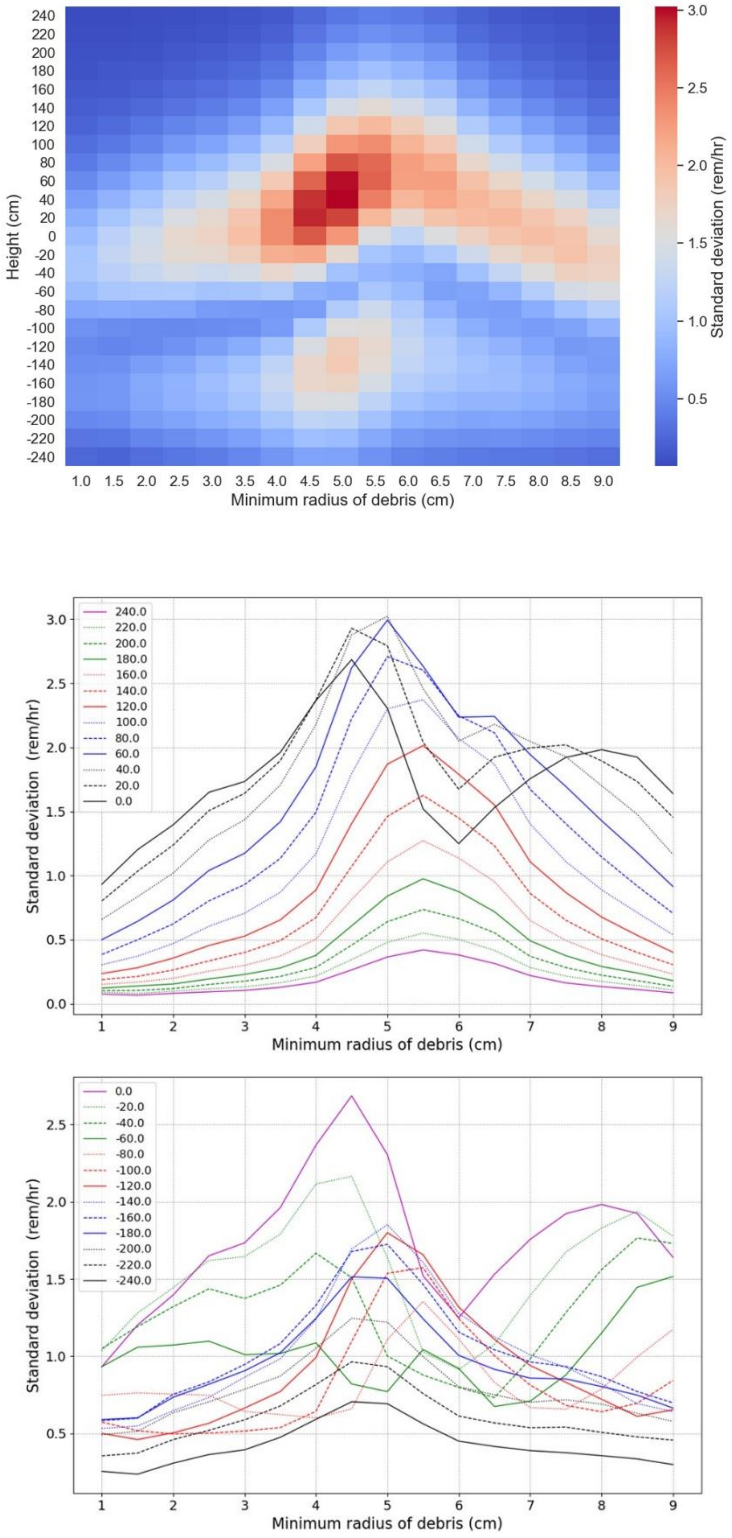


**Figure D. 7 Density plot (top) and line plots of the standard deviation of photon dose rate for close packed fuel debris in a canister**

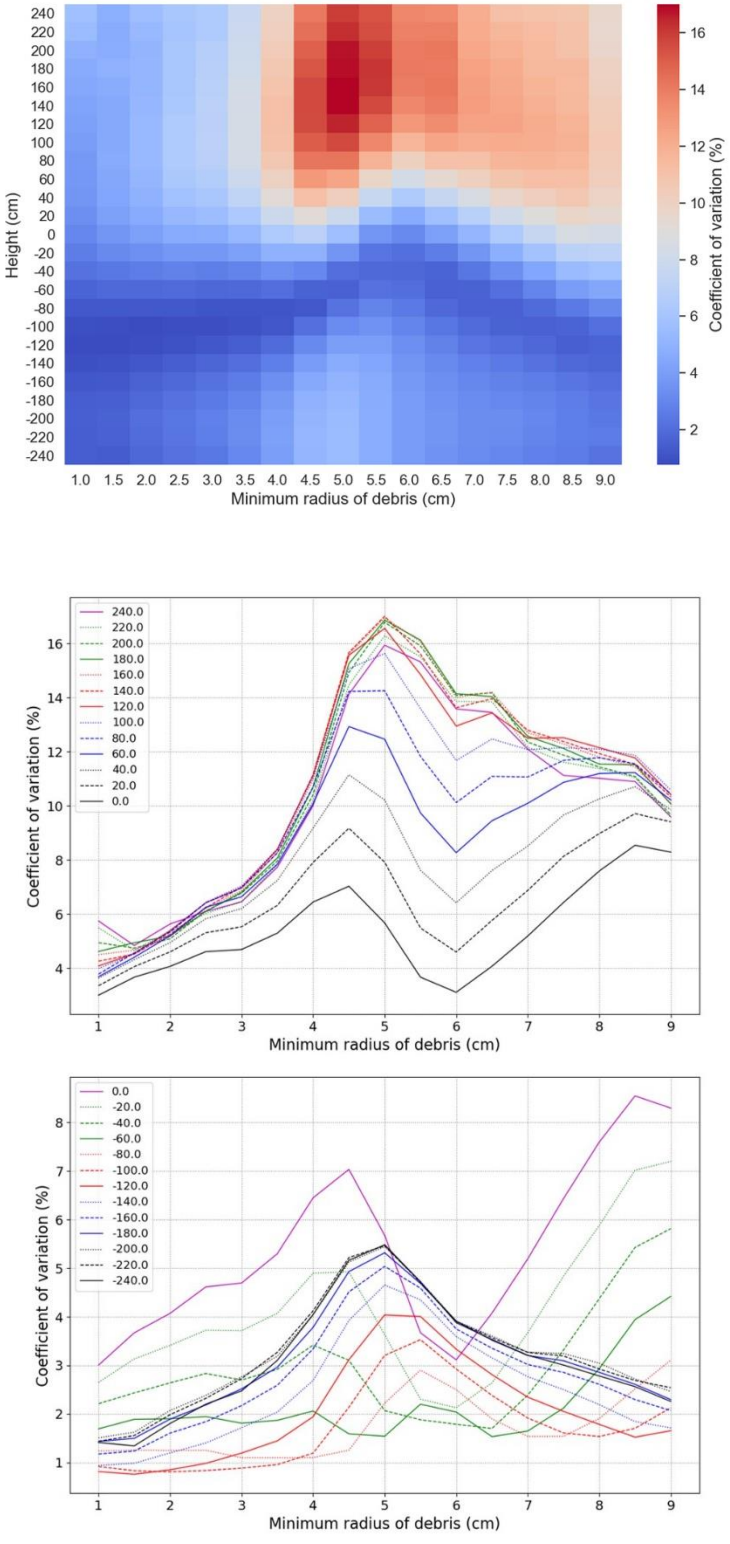


**Figure D. 8 Density plot (top) and line plots of the coefficient of variation of photon dose rate for close packed fuel debris in a canister**

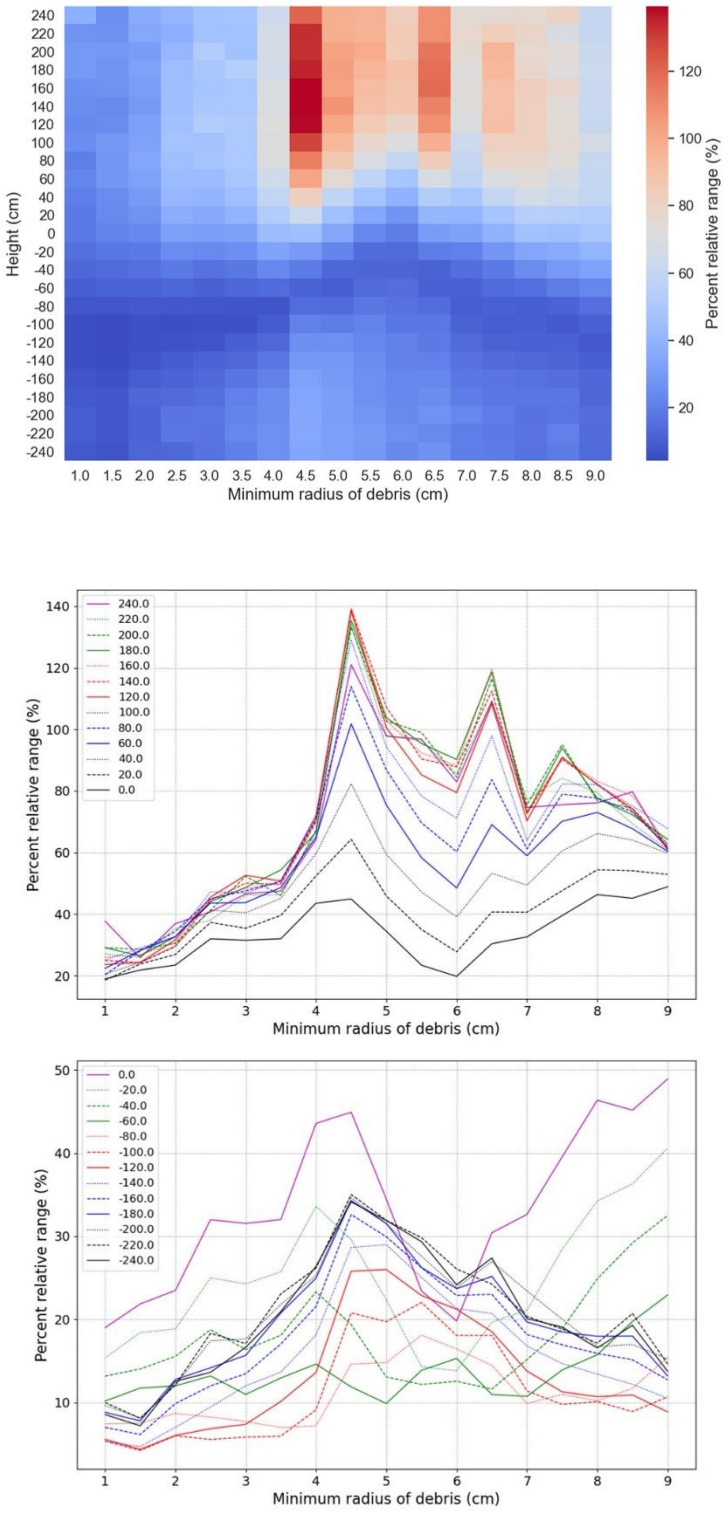


**Figure D. 9 Density plot (top) and line plots of the percent relative range of photon dose rate for close packed fuel debris in a canister**

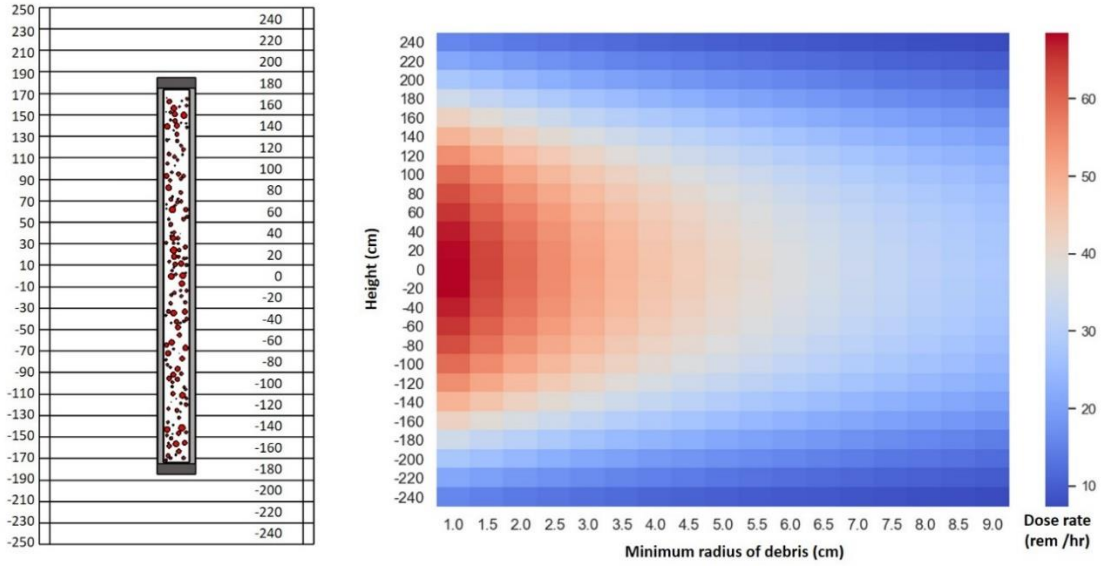


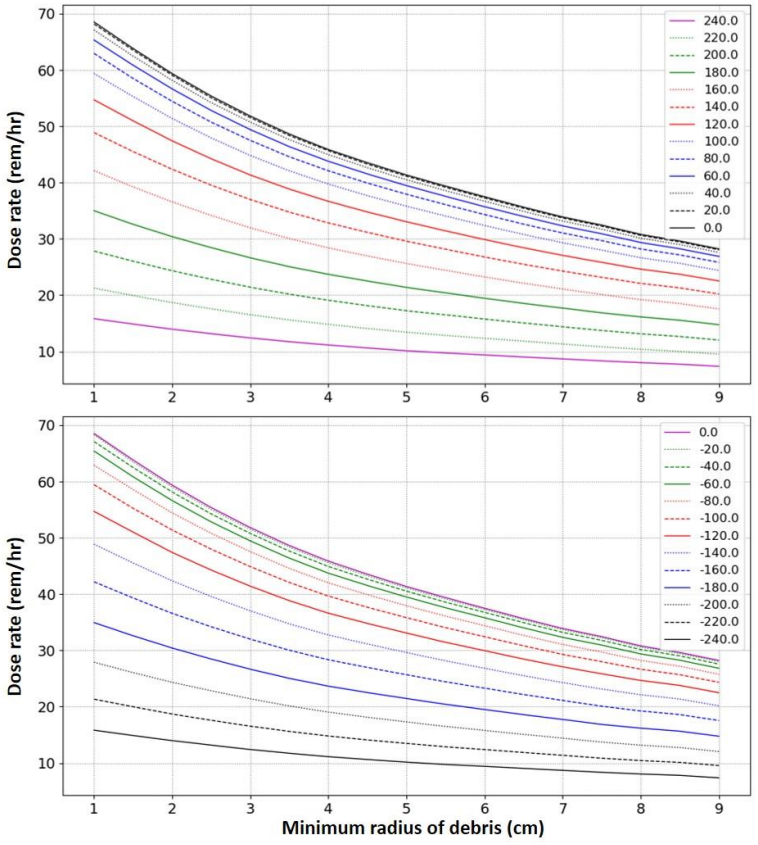


**Figure D. 10 Density plot (top) and line plots of the photon dose rate for the loose packed fuel debris in a canister with three small containers**

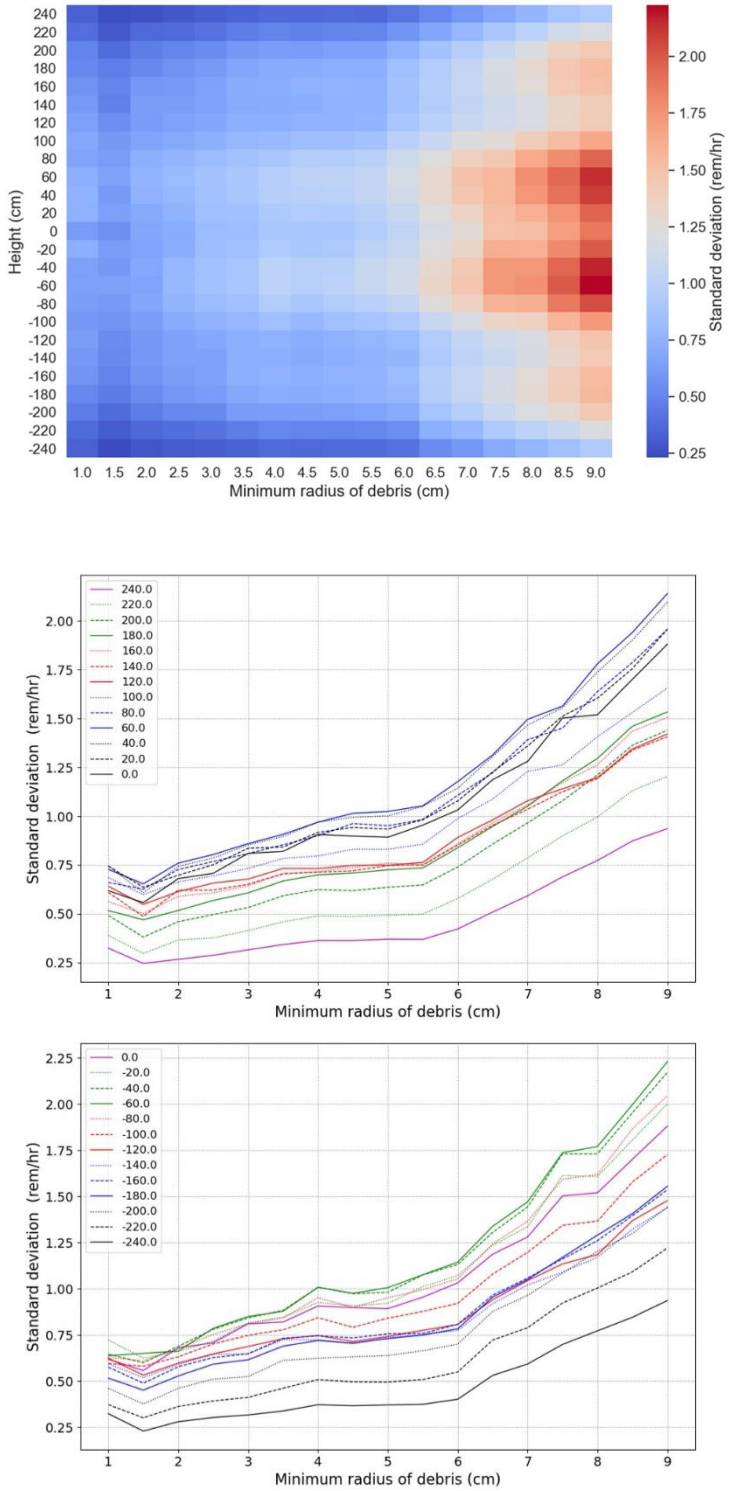


**Figure D. 11 Density plot (top) and line plots of the standard deviation of photon dose rate for the loose packed fuel debris in a canister with three small containers**

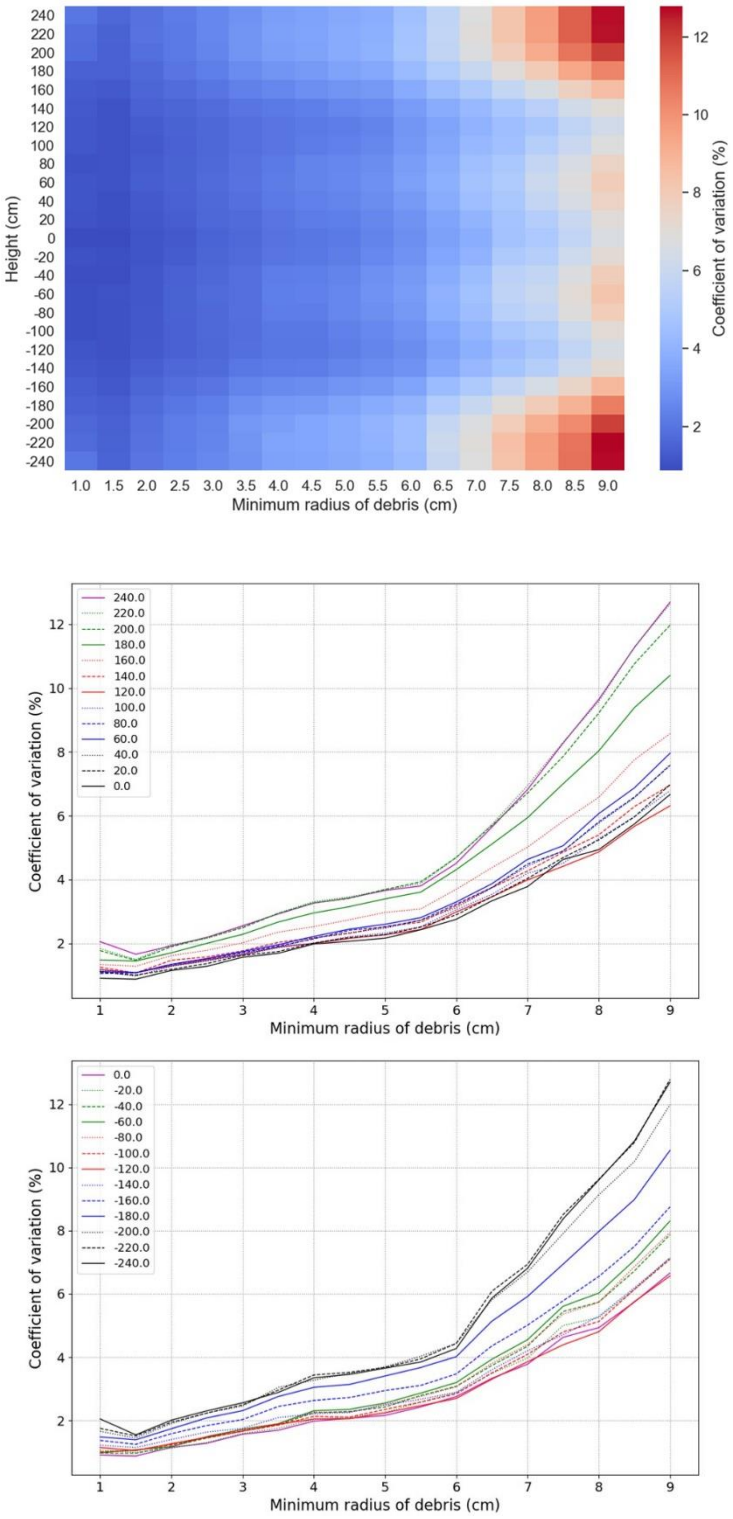


**Figure D. 12 Density plot (top) and line plots of the coefficient of variation of photon dose rate for the loose packed fuel debris in a canister with three small containers**

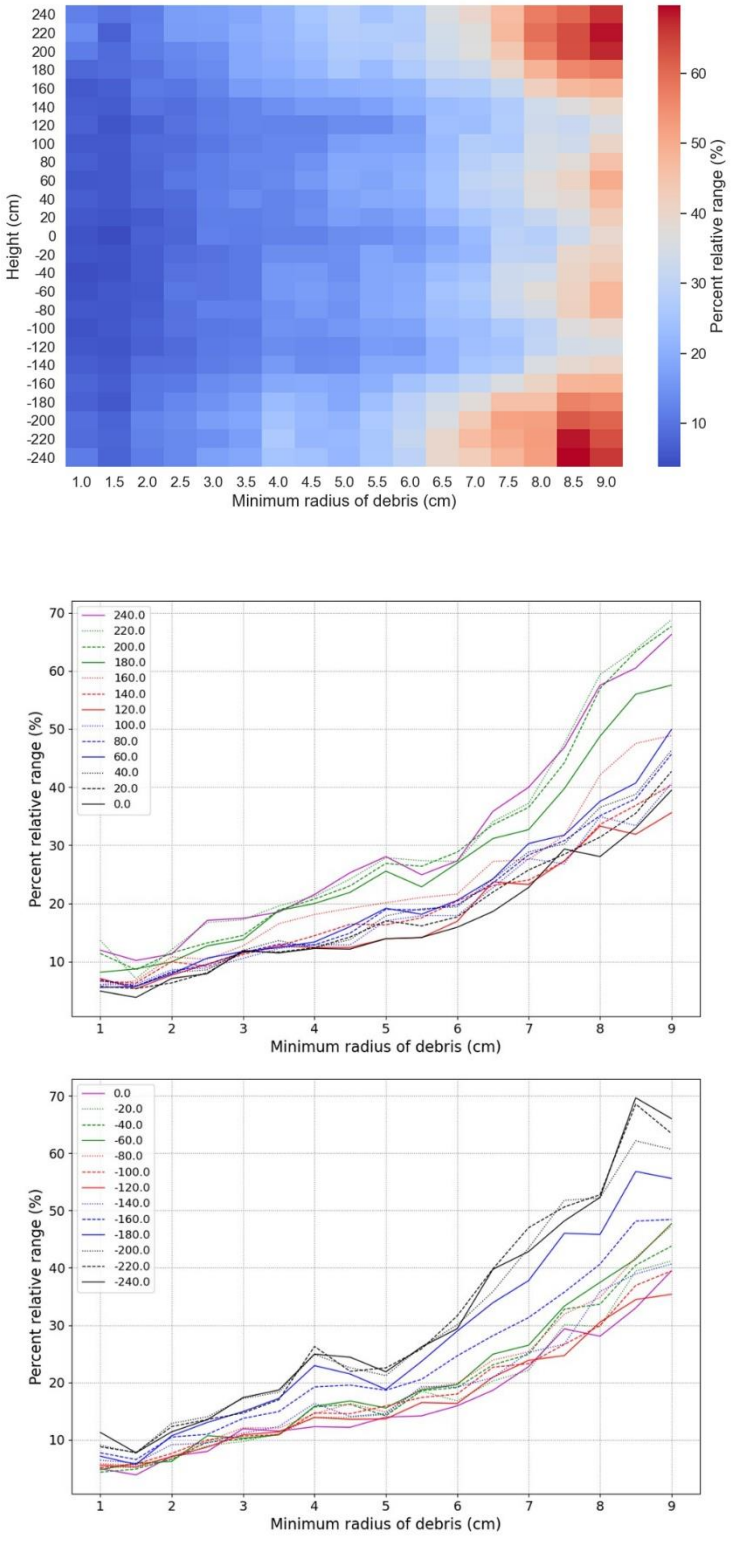


**Figure D. 13 Density plot (top) and line plots of the percent relative range of photon dose rate for the loose packed fuel debris in a canister with three small containers**

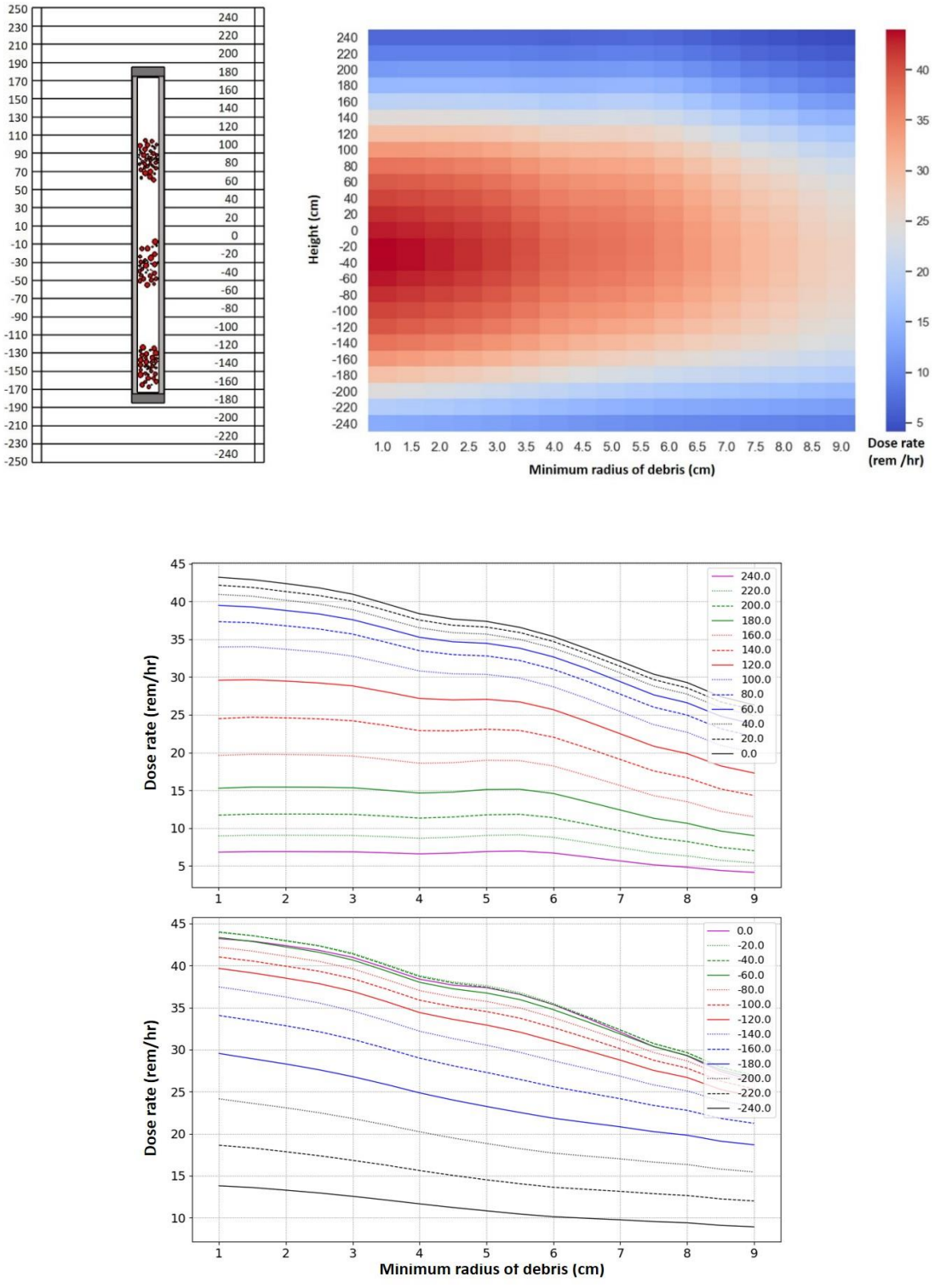


**Figure D. 14 Density plot (top) and line plots of the photon dose rate for the close packed fuel debris in a canister with three small containers**

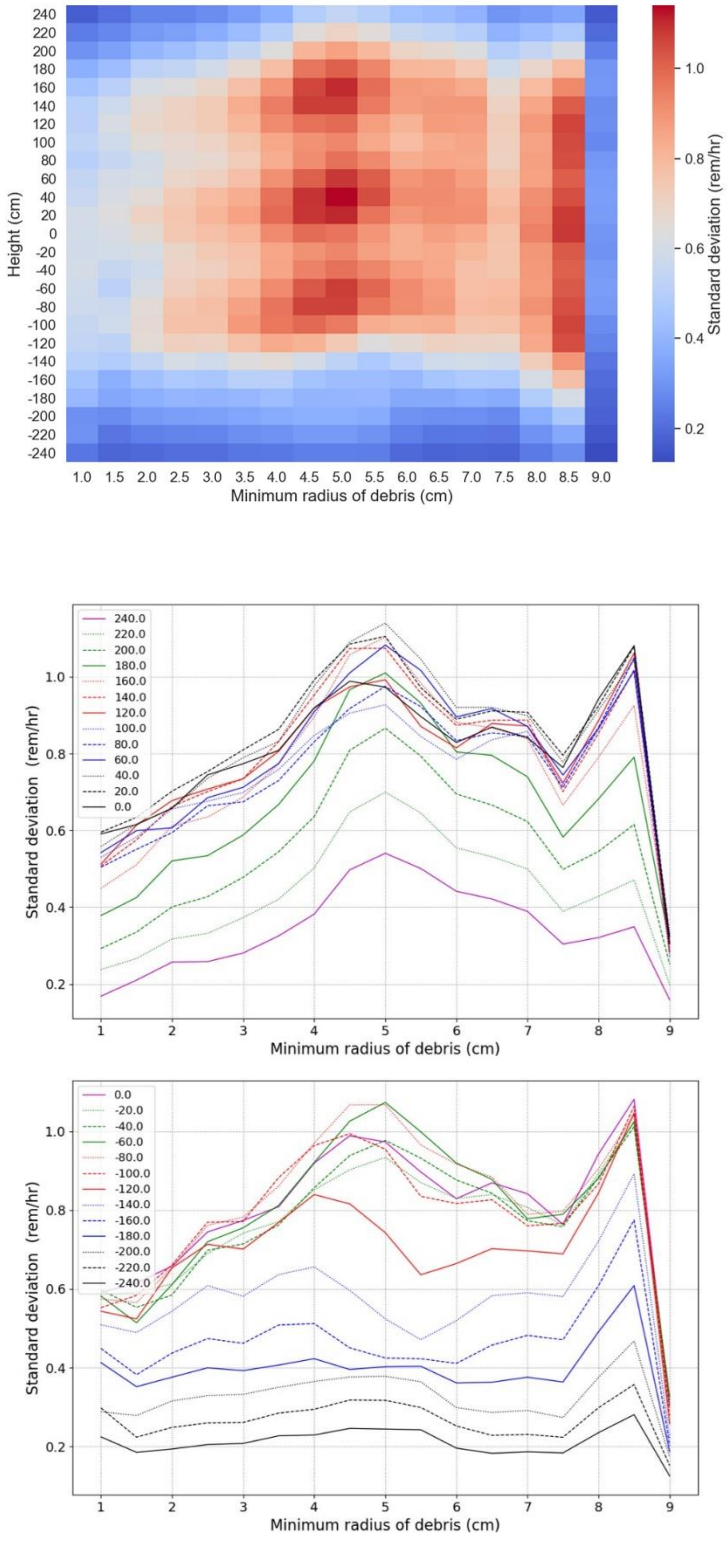


**Figure D. 15 Density plot (top) and line plots of the standard deviation of photon dose rate for the close packed fuel debris in a canister with three small containers**

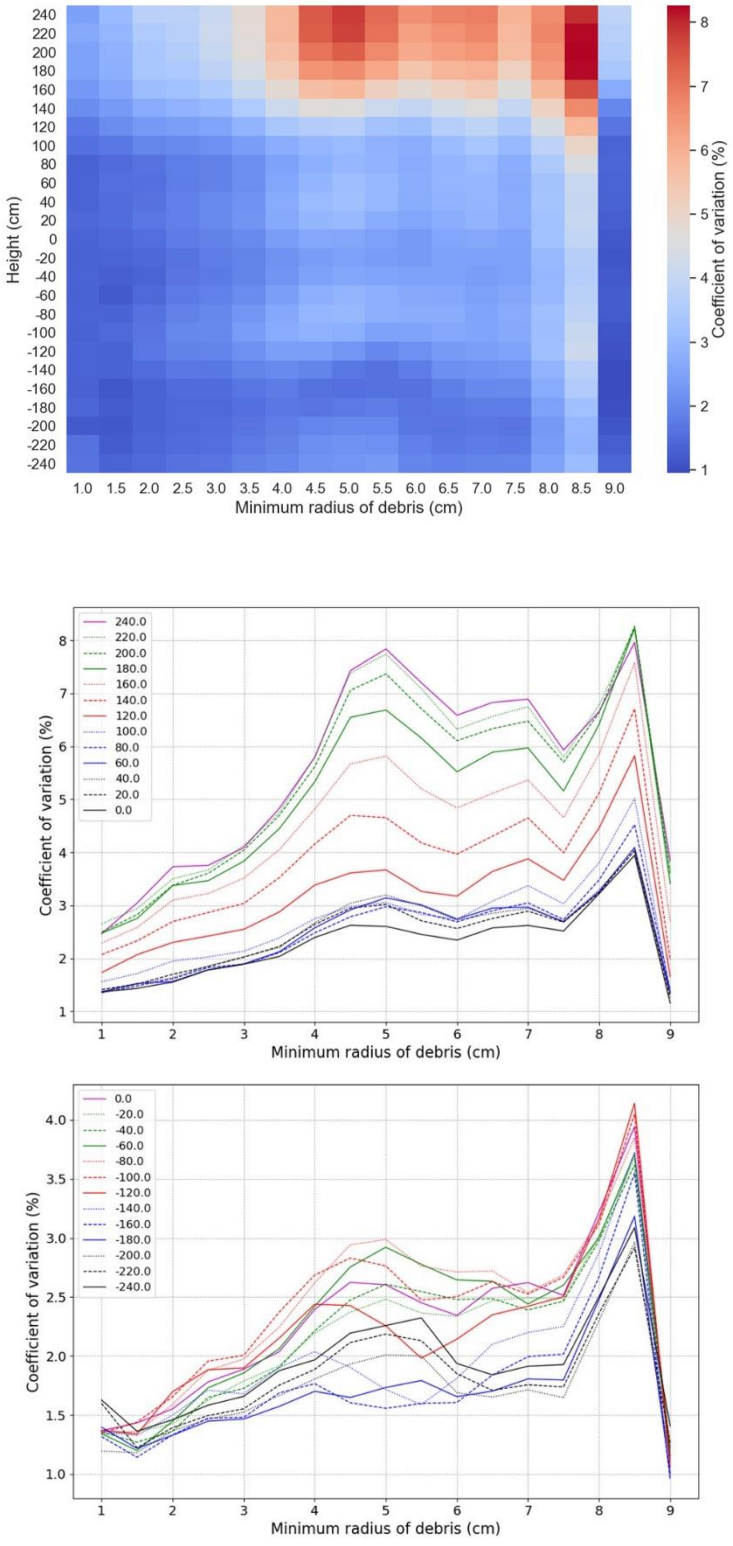


**Figure D. 16 Density plot (top) and line plots of the coefficient of variation of photon dose rate for the close packed fuel debris in a canister with three small containers**

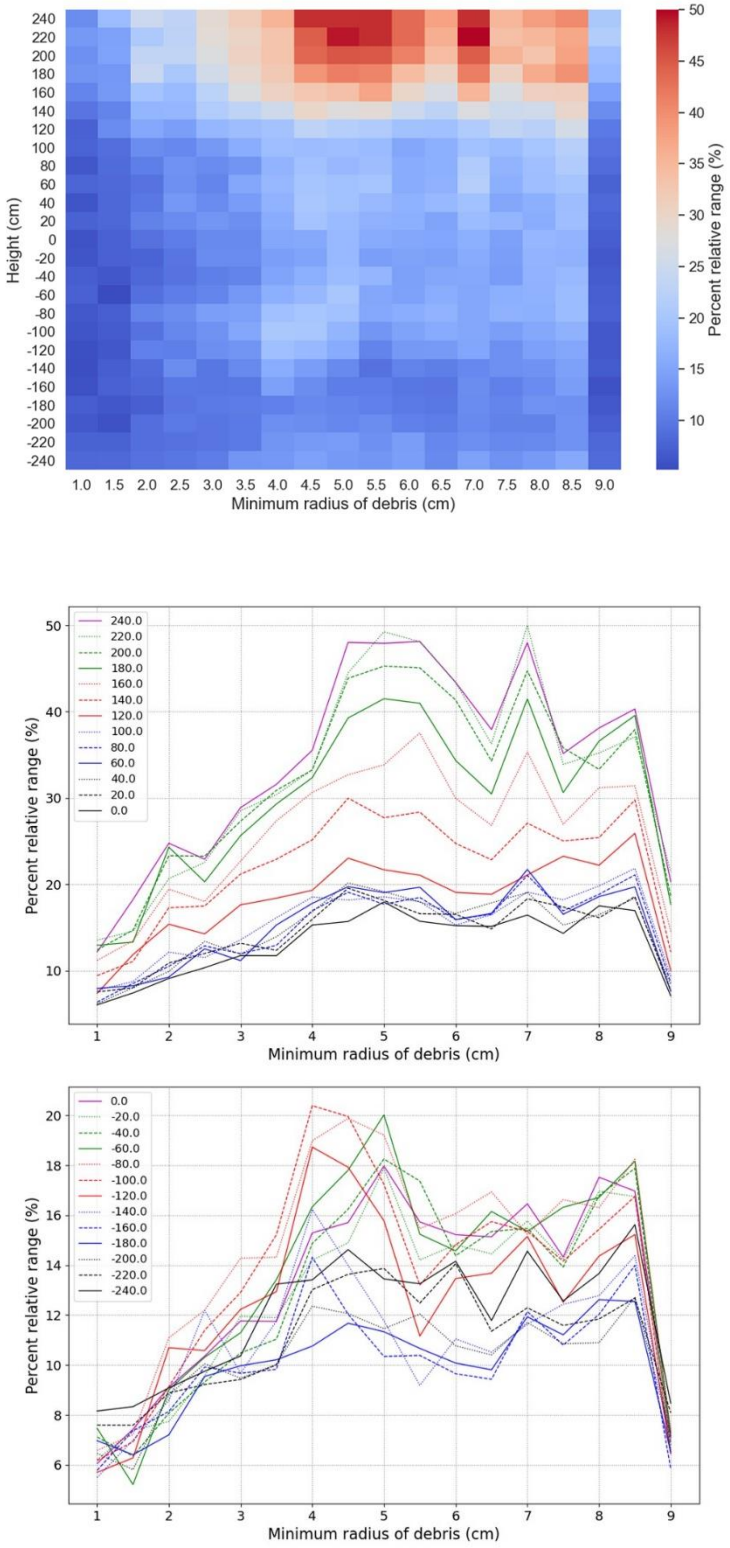


**Figure D. 17 Density plot (top) and line plots of the percent relative range of photon dose rate for the close packed fuel debris in a canister with three small containers**

## D.2. Plots of neutron dose rate (Estimated by SCALE based model)

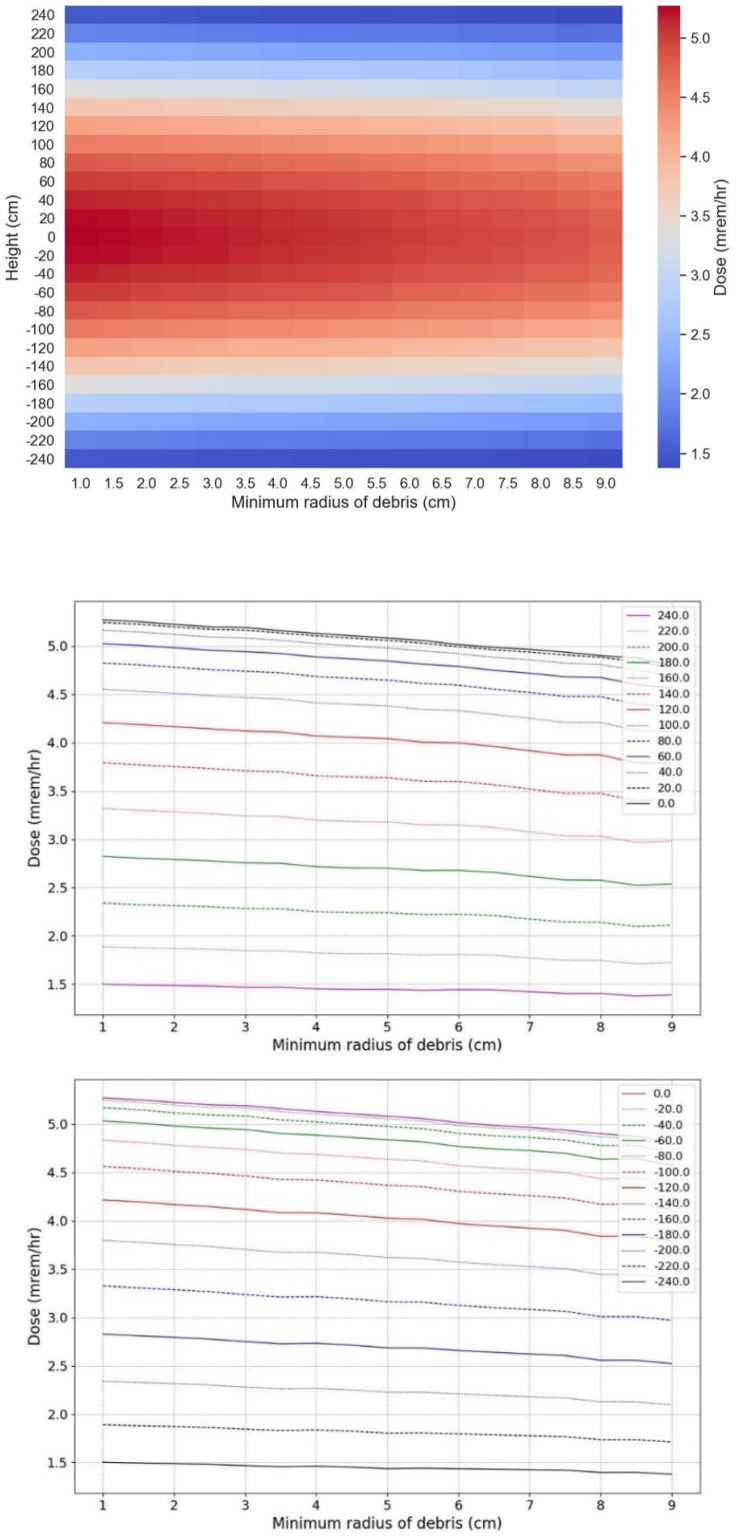


**Figure D. 18 Density plot (top) and line plots of the neutron dose rate for the loose packed fuel debris in a canister**

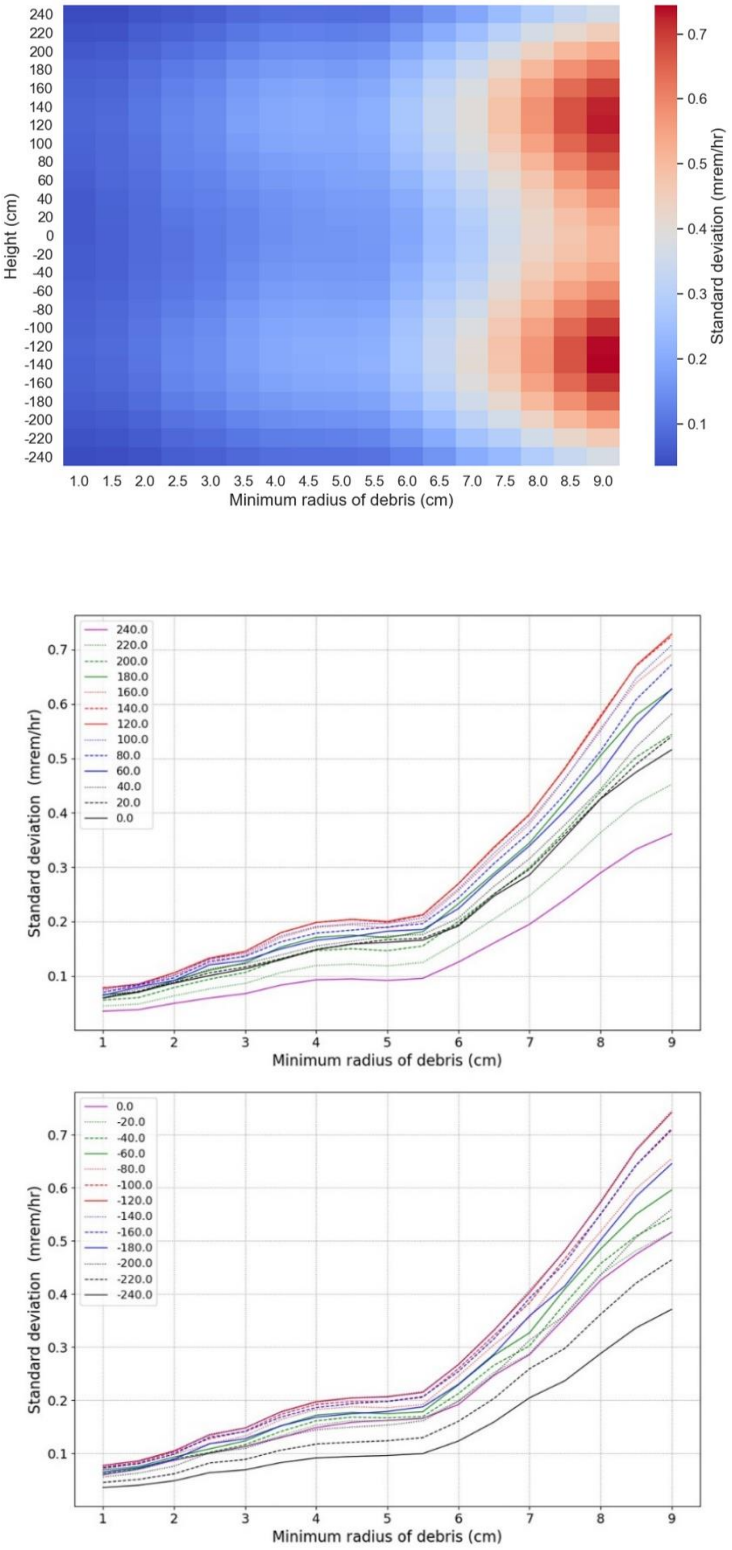


**Figure D. 19 Density plot (top) and line plots of the standard deviation of neutron dose rate for the loose packed fuel debris in a canister**

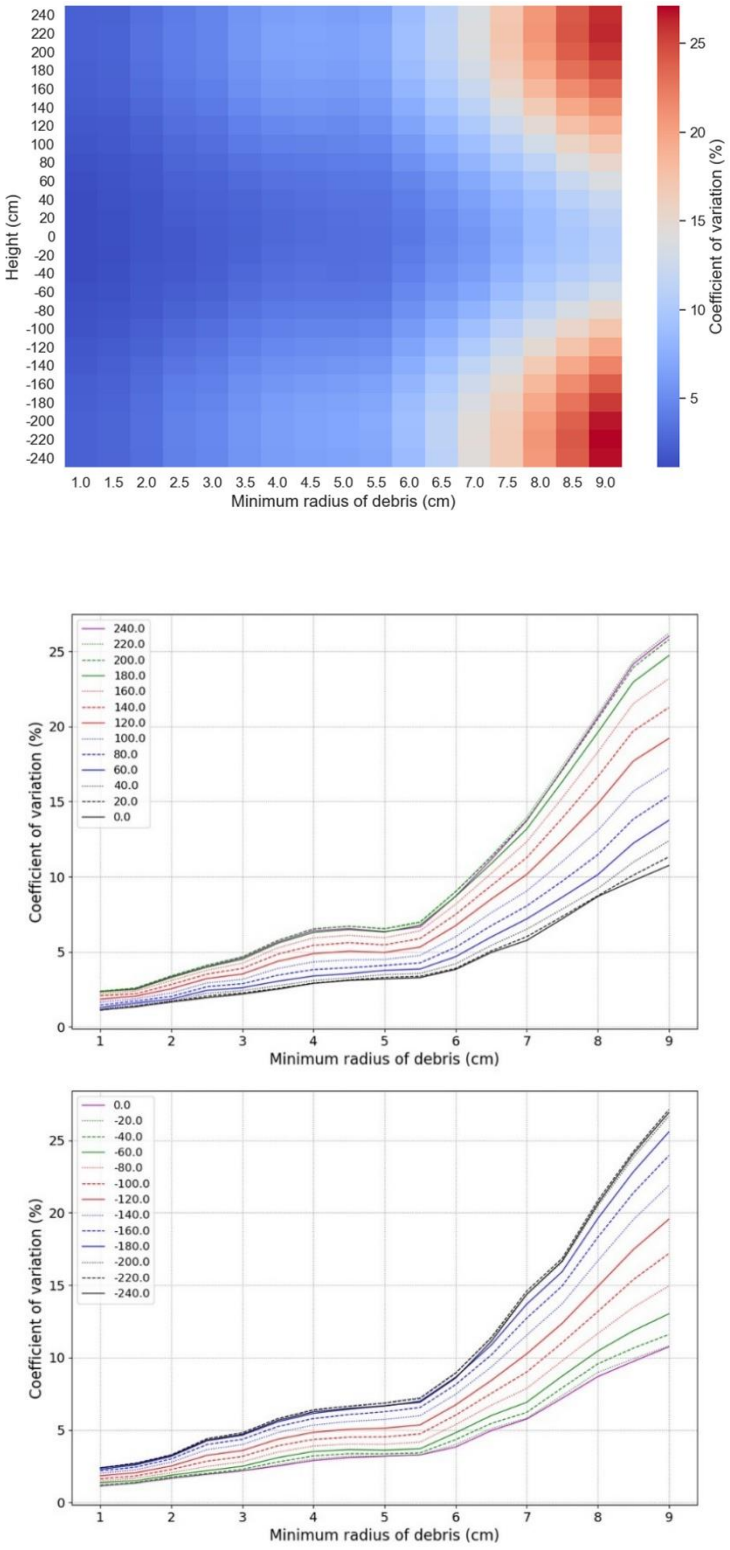


**Figure D. 20 Density plot (top) and line plots of the coefficient of variation of neutron dose rate for the loose packed fuel debris in a canister**

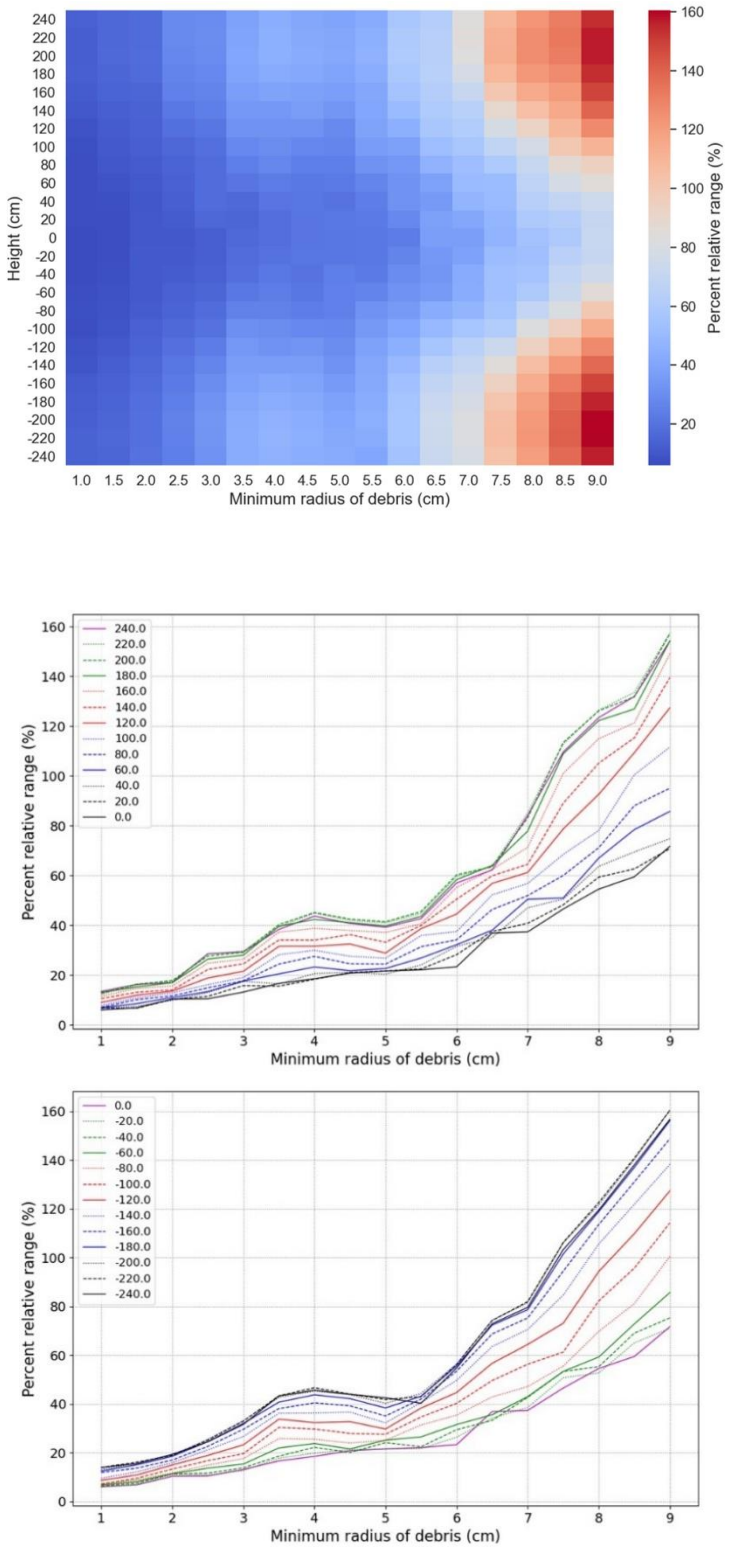


**Figure D. 21 Density plot (top) and line plots of the percent relative range of neutron dose rate for the loose packed fuel debris in a canister**

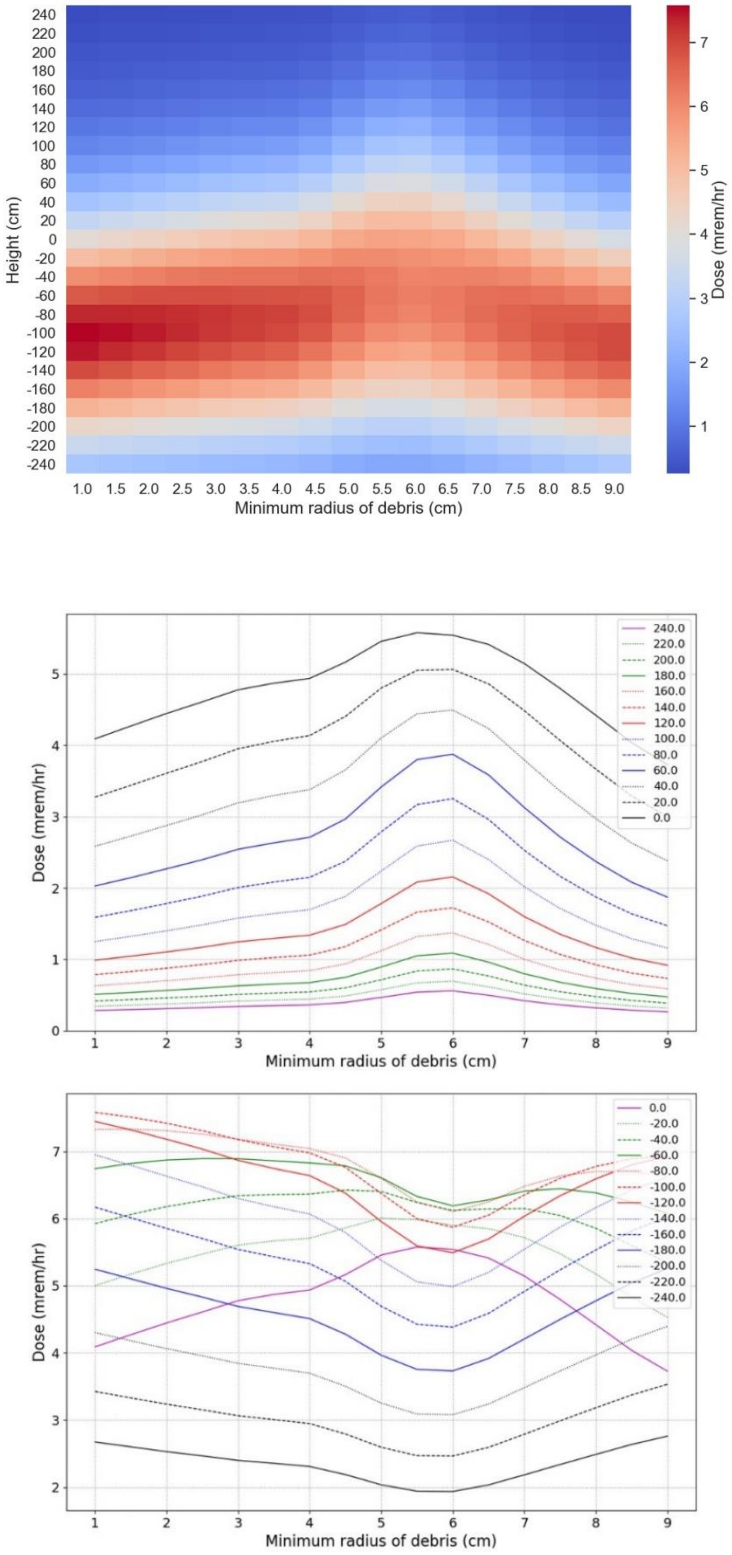


**Figure D. 22 Density plot (top) and line plots of the neutron dose rate for the close packed fuel debris in a canister**

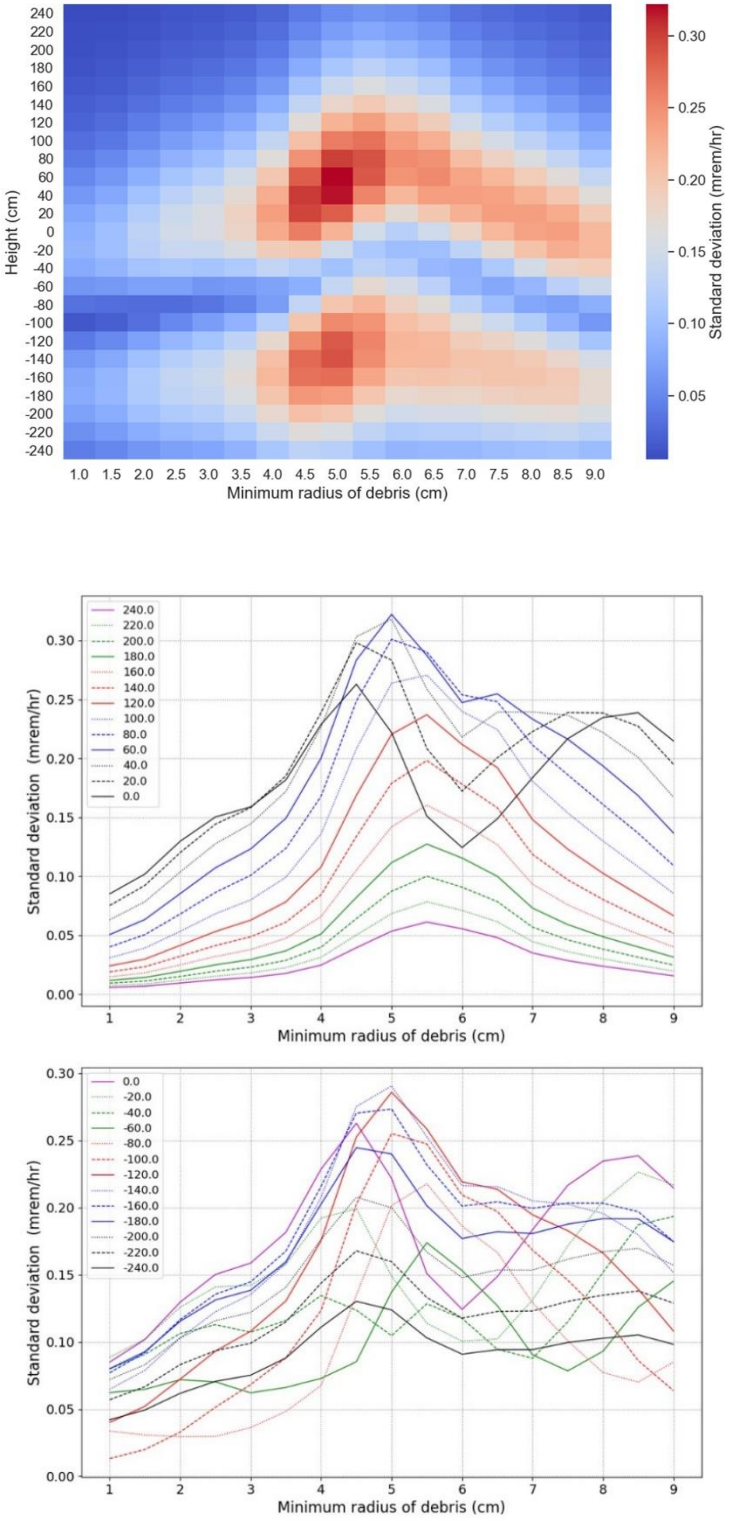


**Figure D. 23 Density plot (top) and line plots of the standard deviation of neutron dose rate for the close packed fuel debris in a canister**

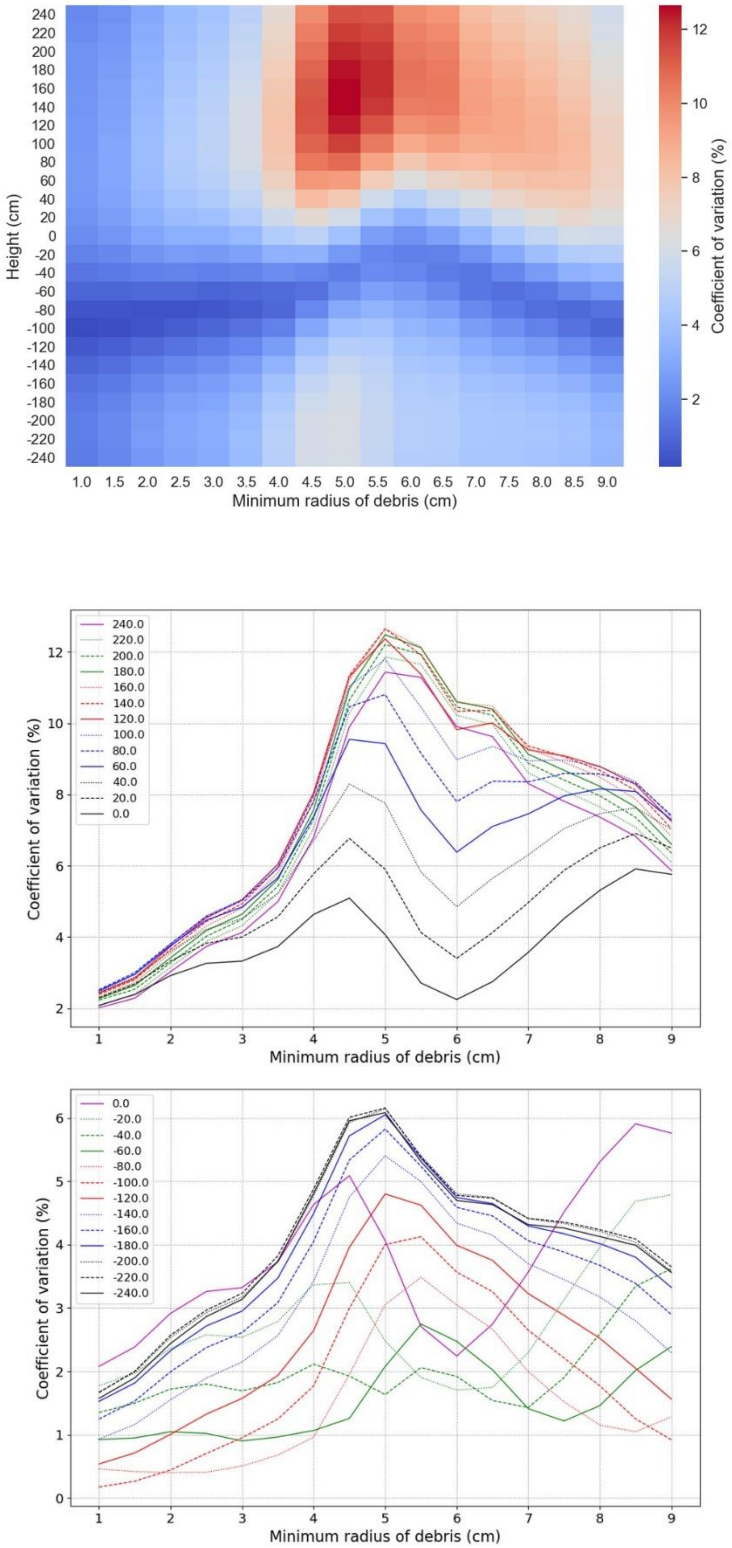


**Figure D. 24 Density plot (top) and line plots of the coefficient of variation of neutron dose rate for the close packed fuel debris in a canister**

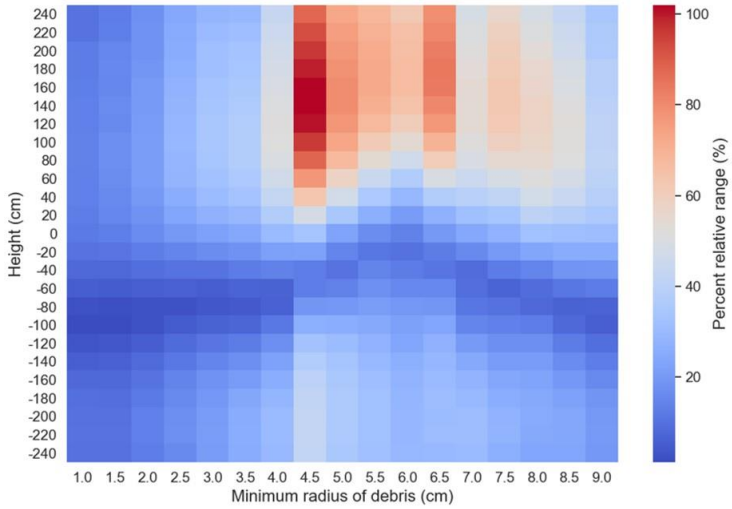


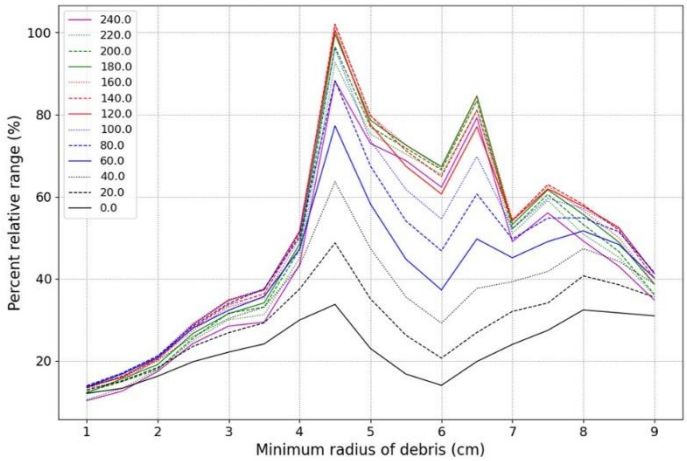


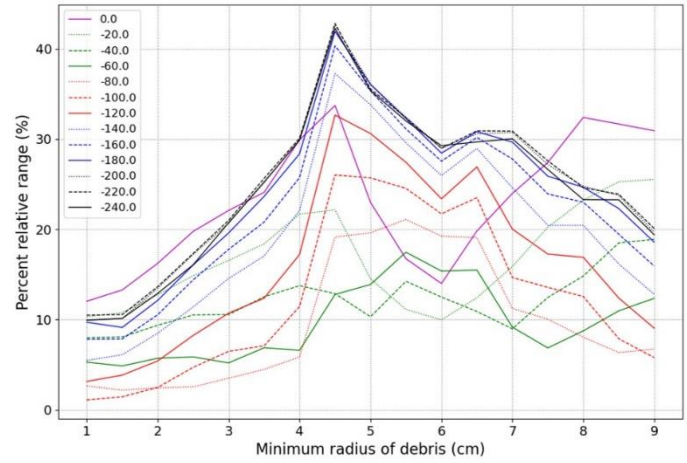


**Figure D. 25 Density plot (top) and line plots of the percent relative range of neutron dose rate for the close packed fuel debris in a canister**

## D.3. Plots of photon flux (Estimated by SCALE based model)

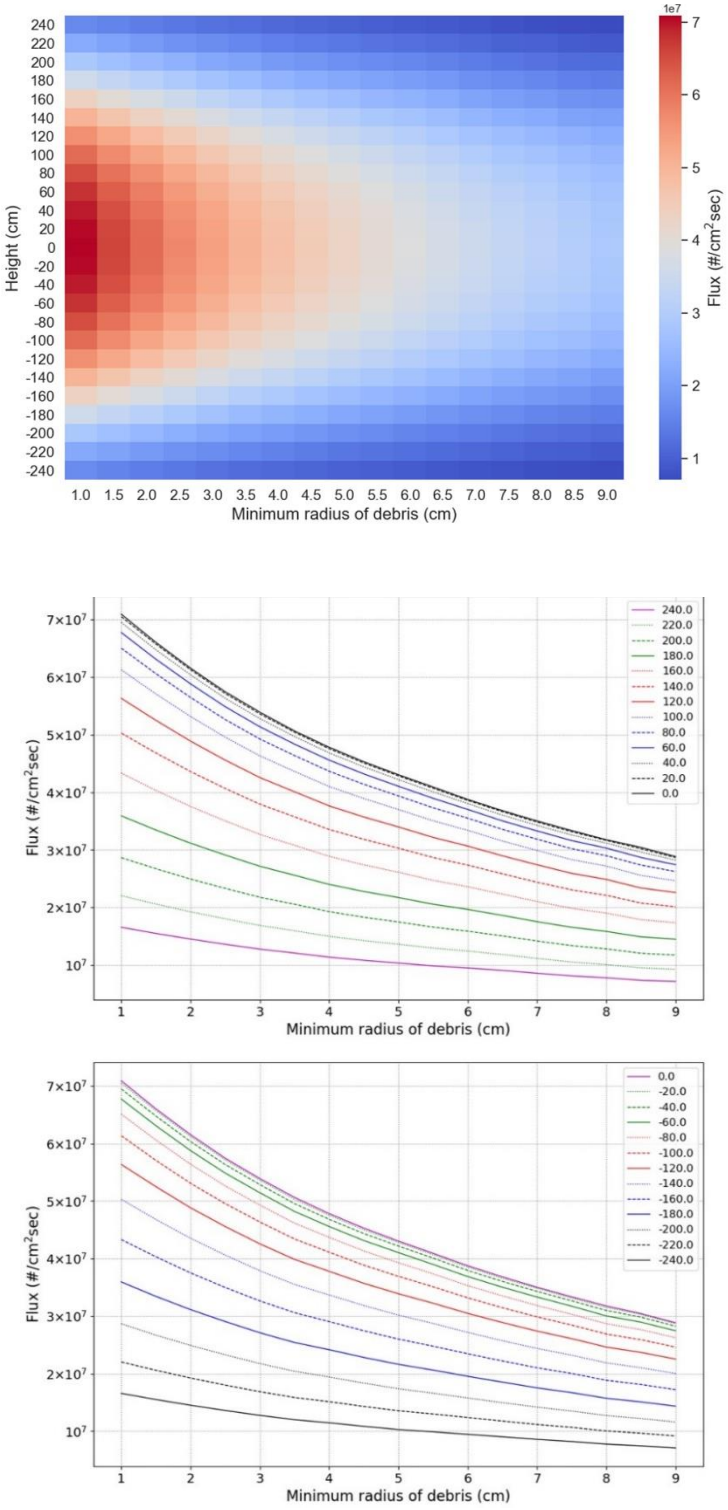


**Figure D. 26 Density plot (top) and line plots of the photon flux for the loose packed fuel debris in a canister**

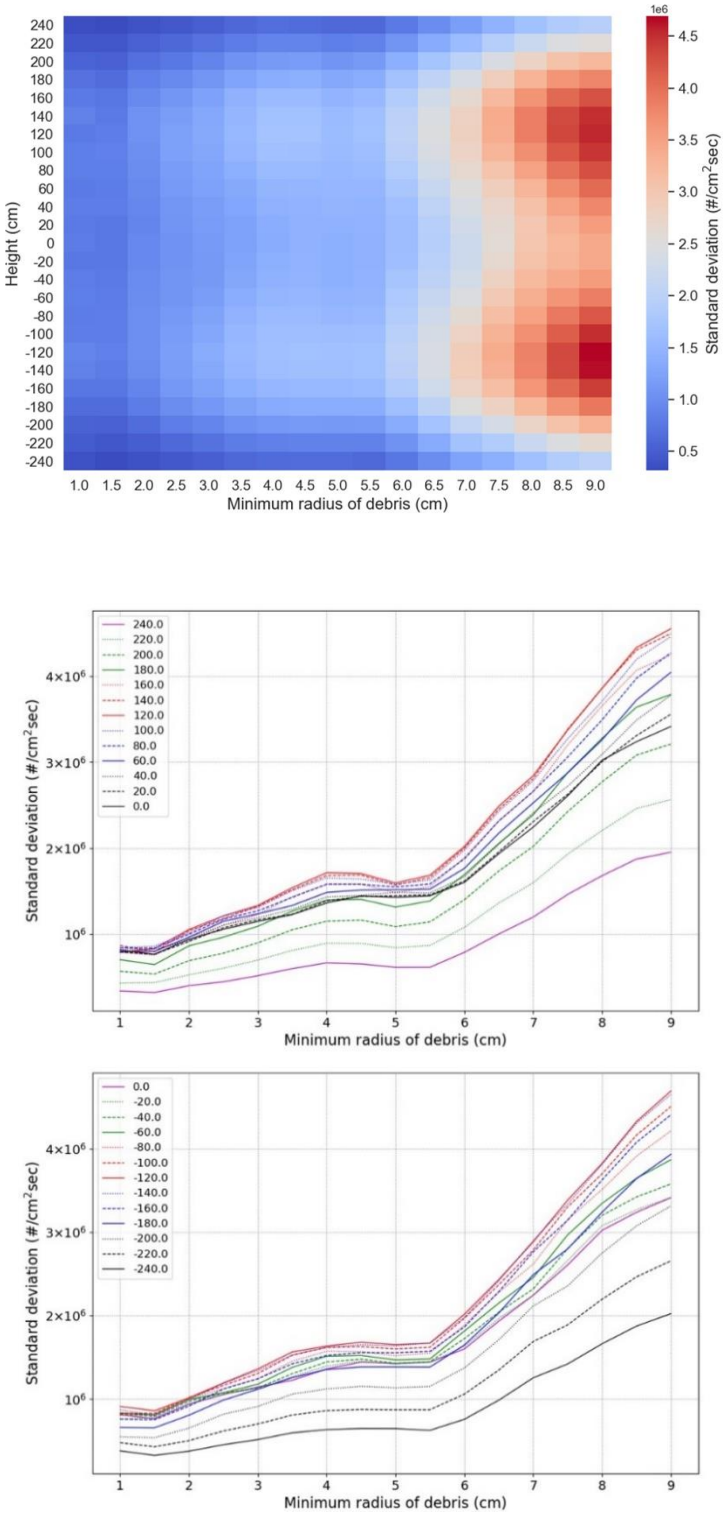


**Figure D. 27 Density plot (top) and line plots of the standard deviation of the photon flux of loose packed fuel debris in a canister**

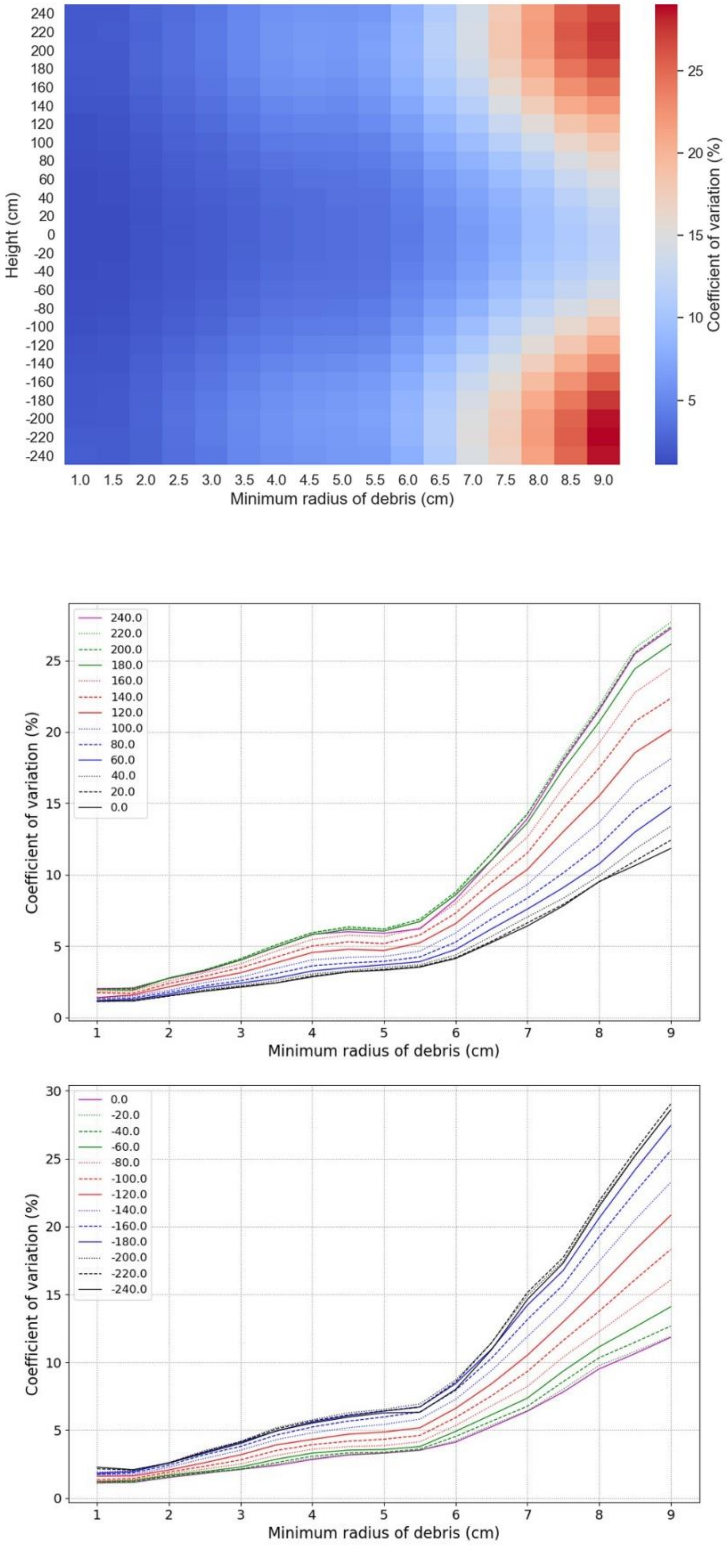


**Figure D. 28 Density plot (top) and line plots of the coefficient of variation of the photon flux of loose packed fuel debris in a canister**

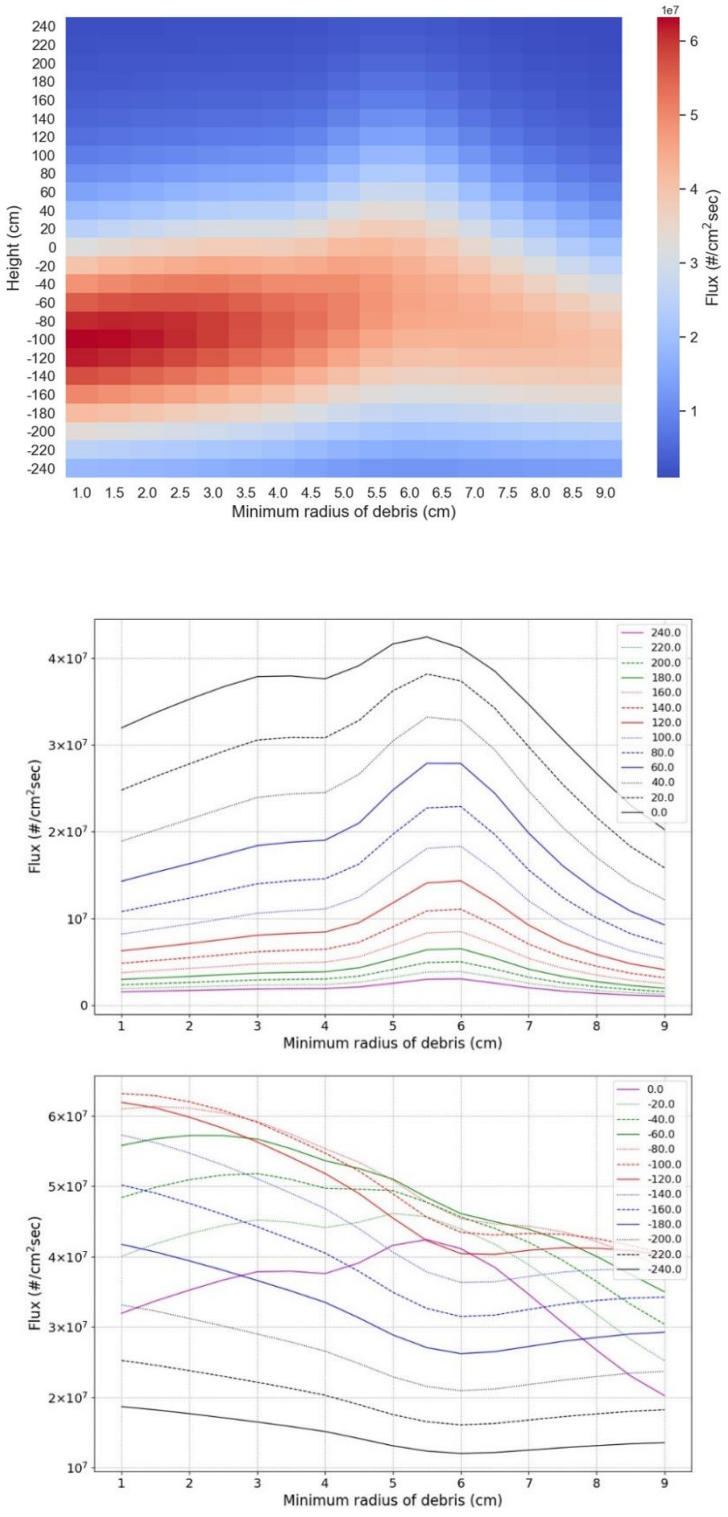


**Figure D. 29 Density plot (top) and line plots of the photon flux for the close packed fuel debris in a canister**

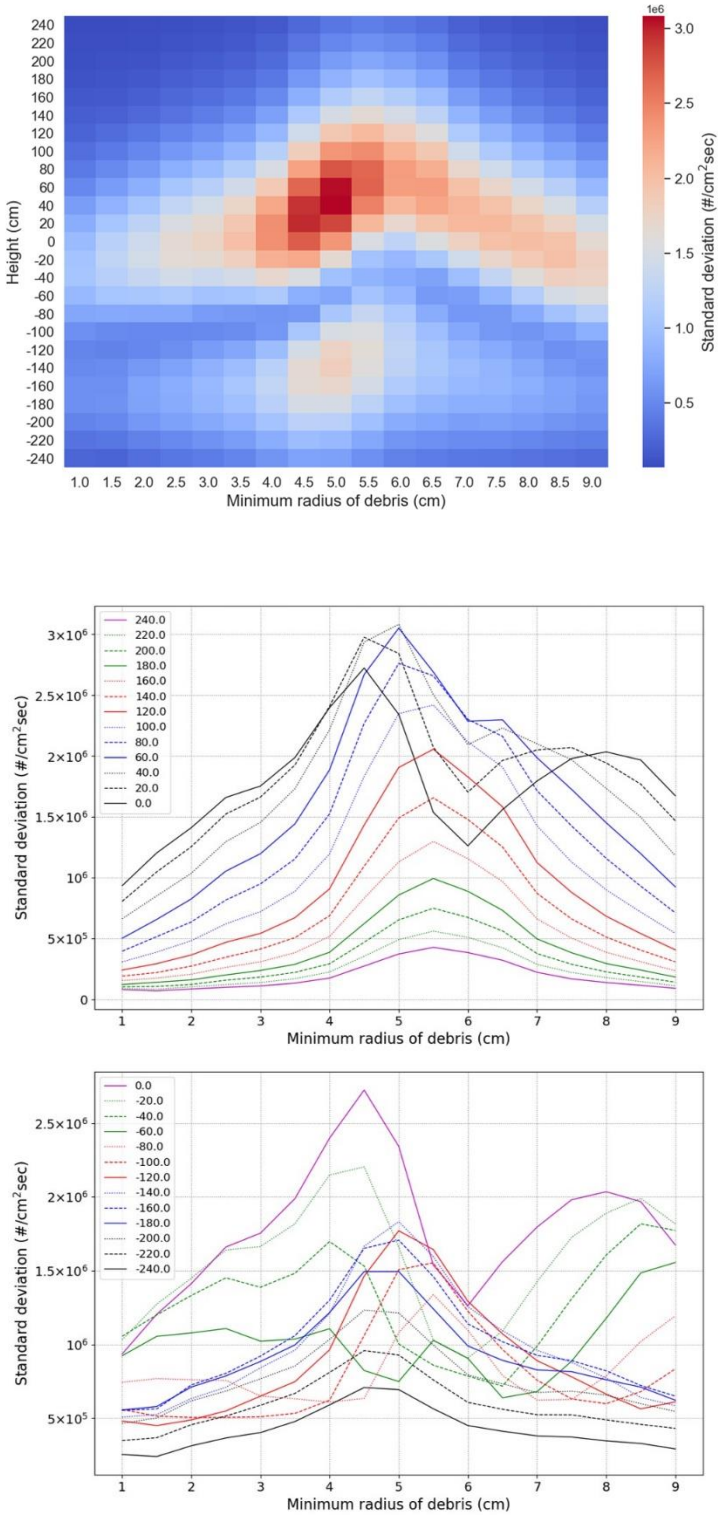


**Figure D. 30 Density plot (top) and line plots of the standard deviation of photon flux for close packed fuel debris in a canister**

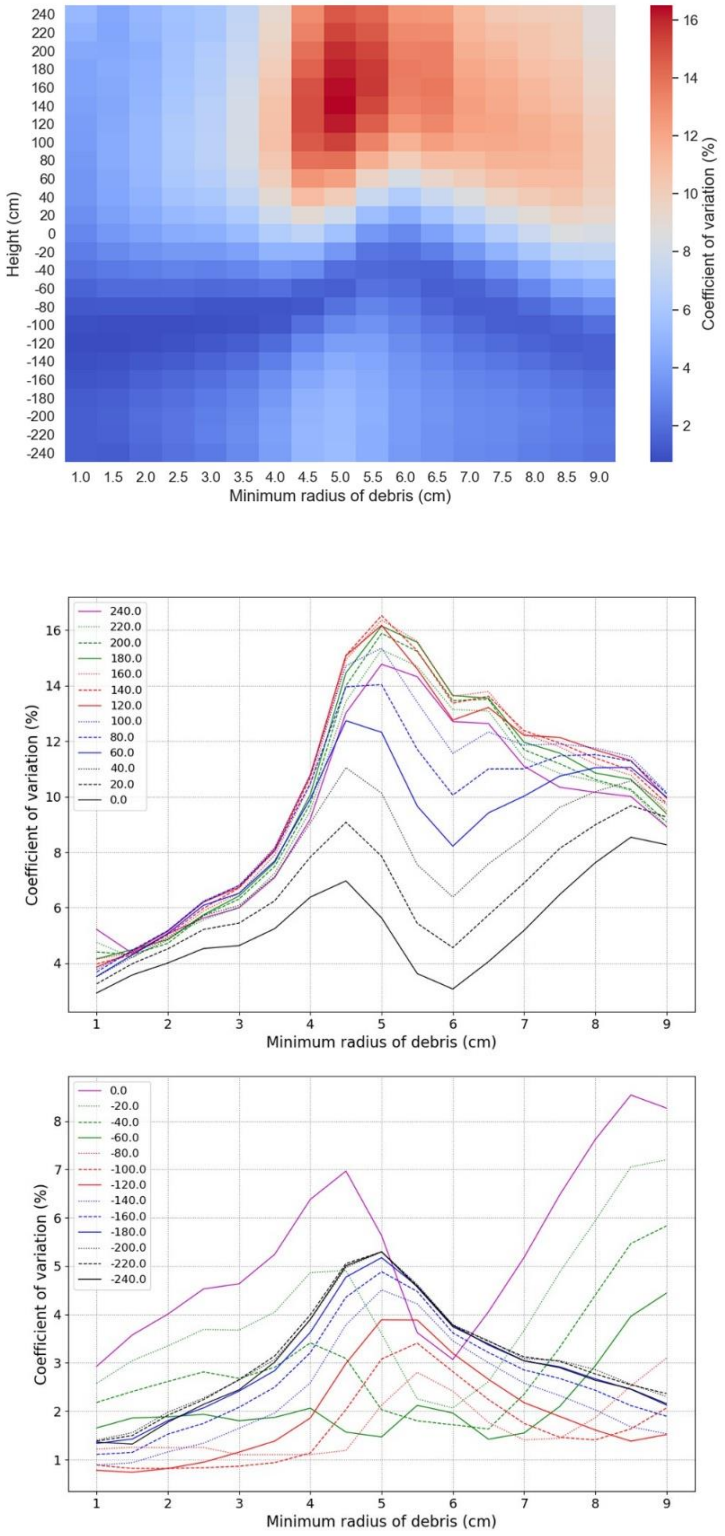


**Figure D. 31 Density plot (top) and line plots of the coefficient of variation of photon flux for close packed fuel debris in a canister**

## D.4 Plots of photon flux (Estimated by Simple model)

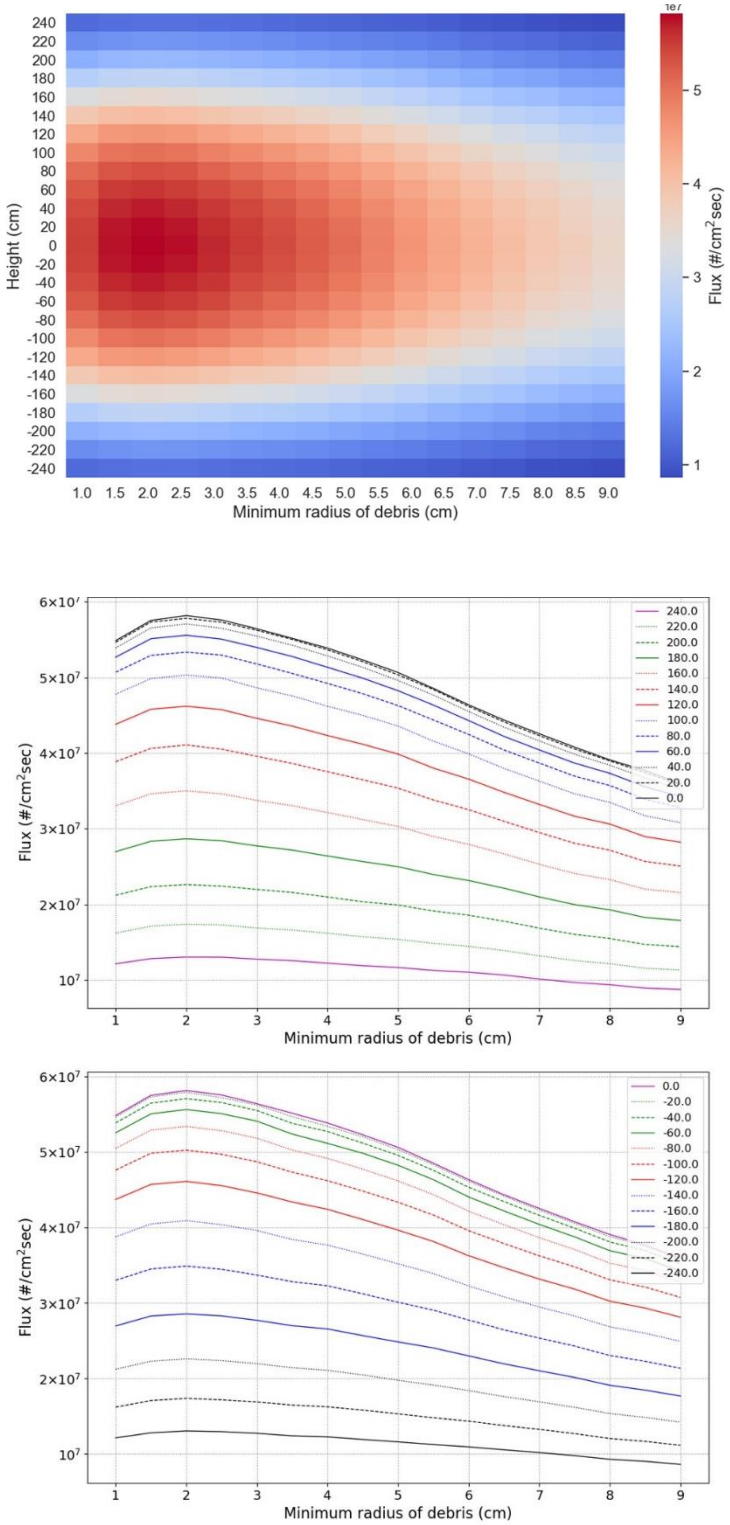


**Figure D. 32 Density plot (top) and line plots of the photon flux for the loose packed fuel debris in a canister**

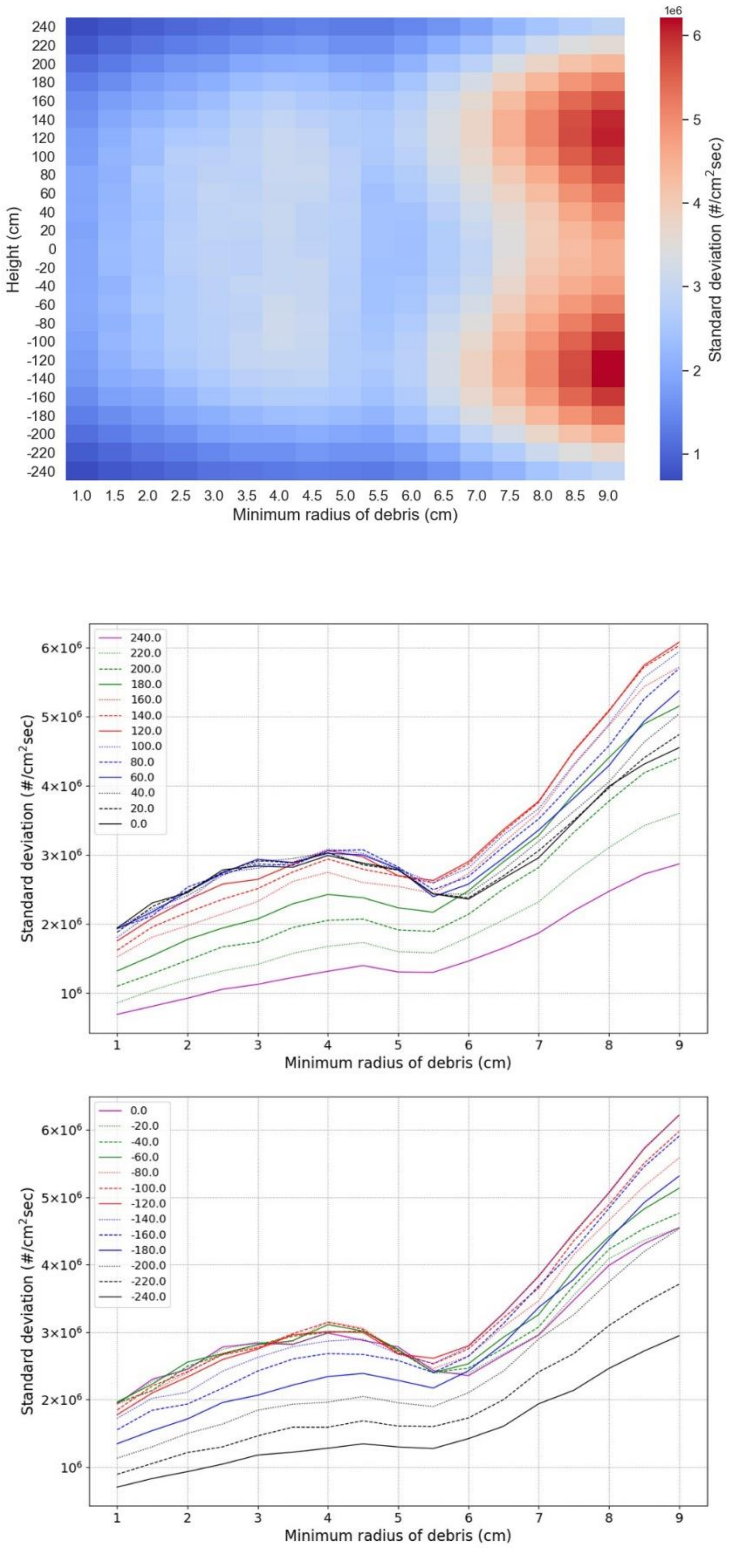


**Figure D. 33 Density plot (top) and line plots of the standard deviation of the photon flux of loose packed fuel debris in a canister**

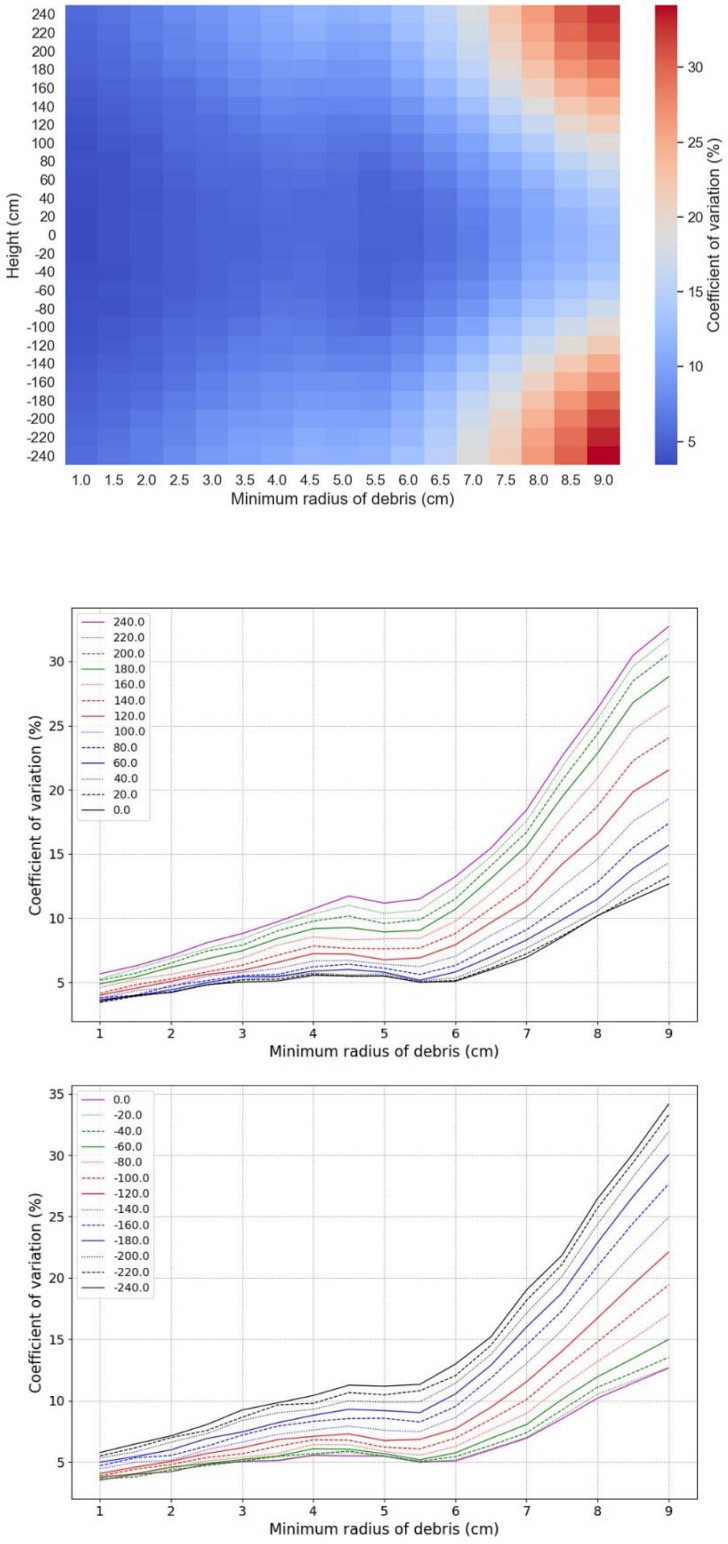


**Figure D. 34 Density plot (top) and line plots of the coefficient of variation of the photon flux of loose packed fuel debris in a canister**

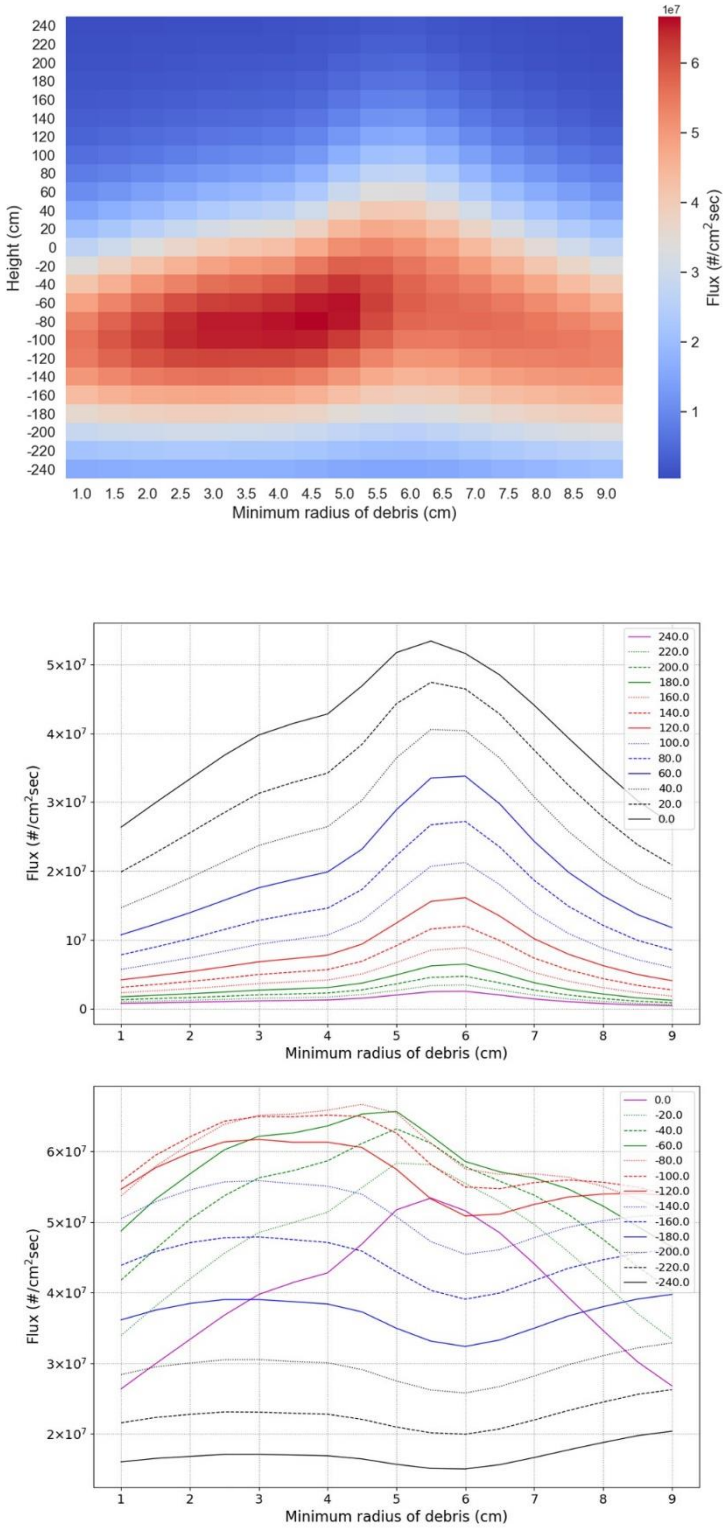


**Figure D. 35 Density plot (top) and line plots of the photon flux for the close packed fuel debris in a canister**

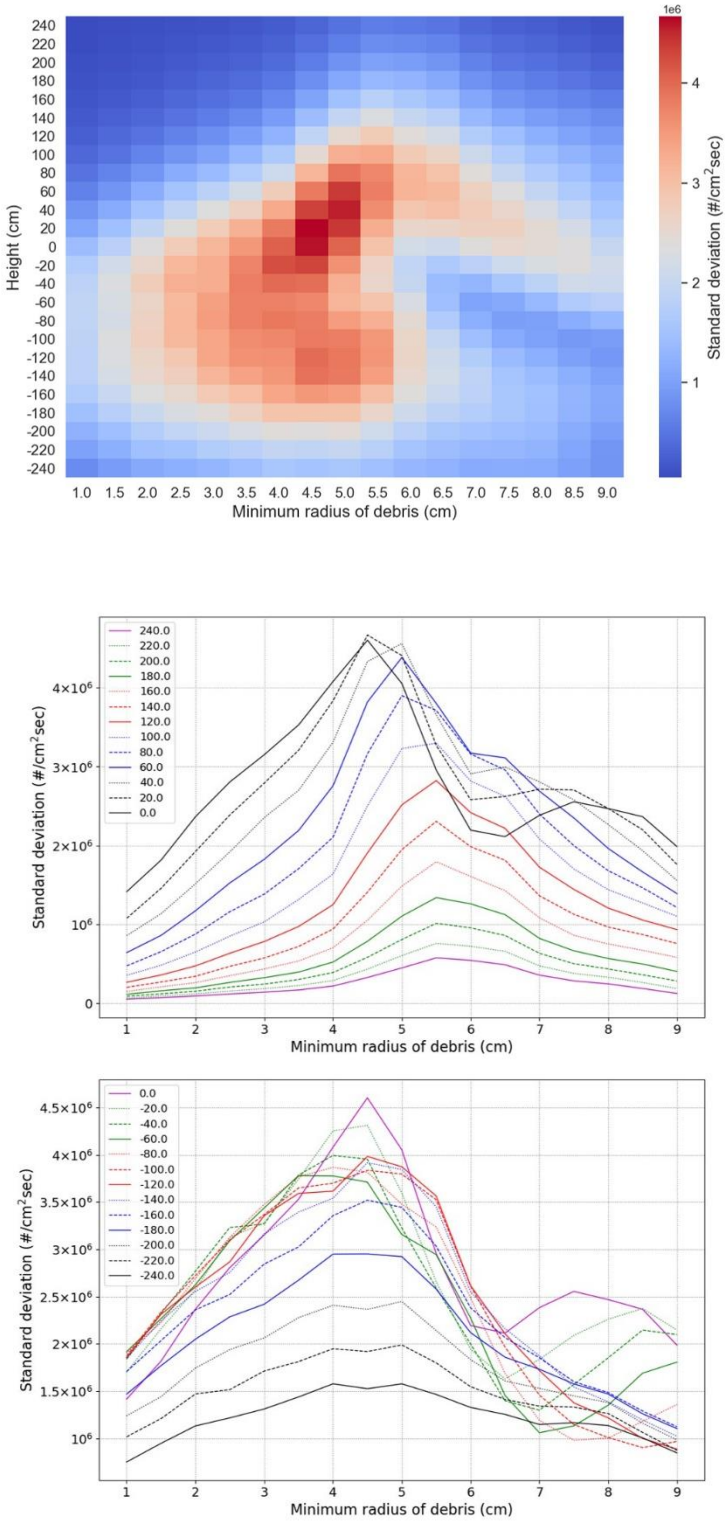


**Figure D. 36 Density plot (top) and line plots of the standard deviation of photon flux for close packed fuel debris in a canister**

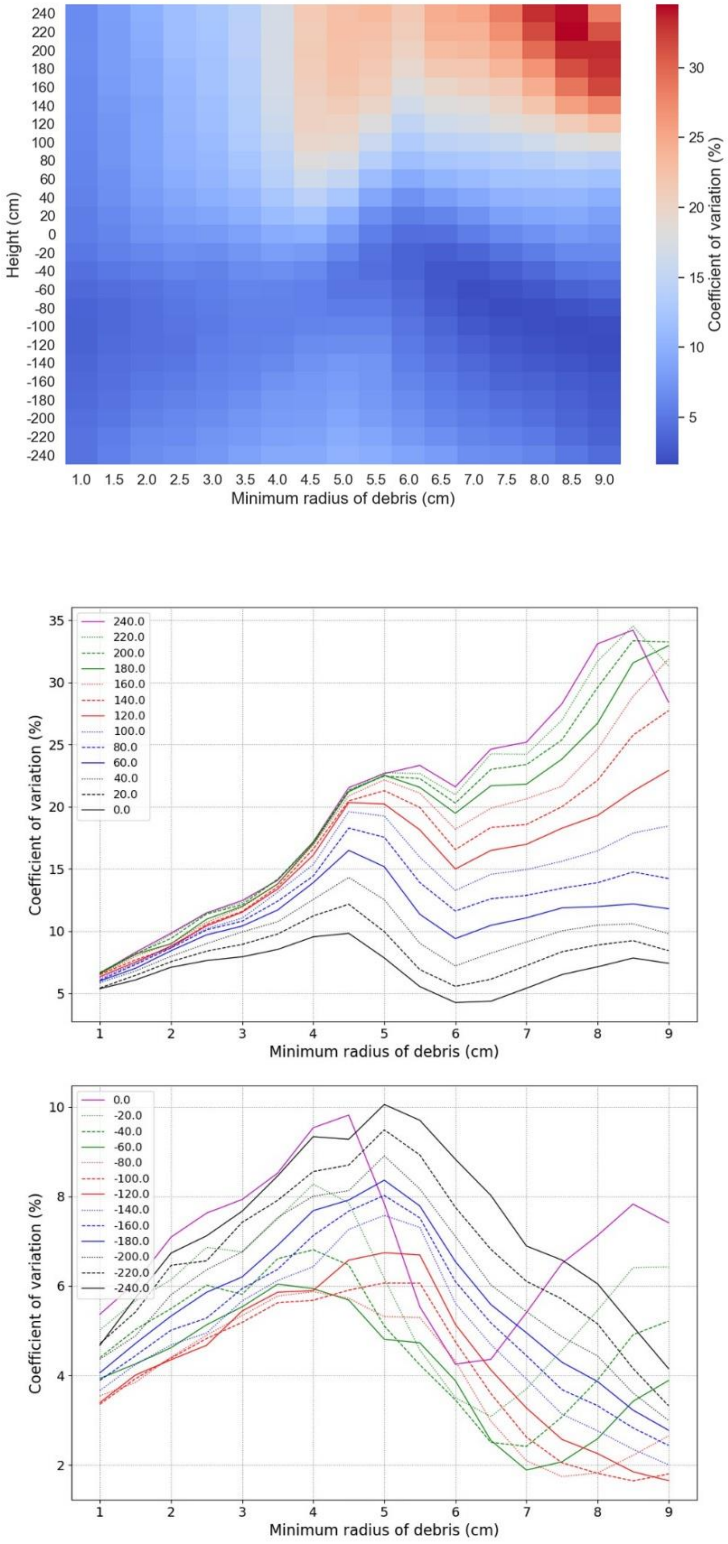


**Figure D. 37 Density plot (top) and line plots of the coefficient of variation of photon flux for close packed fuel debris in a canister**

## D. 5 Plots of photon flux (Estimated by Shmakov model)

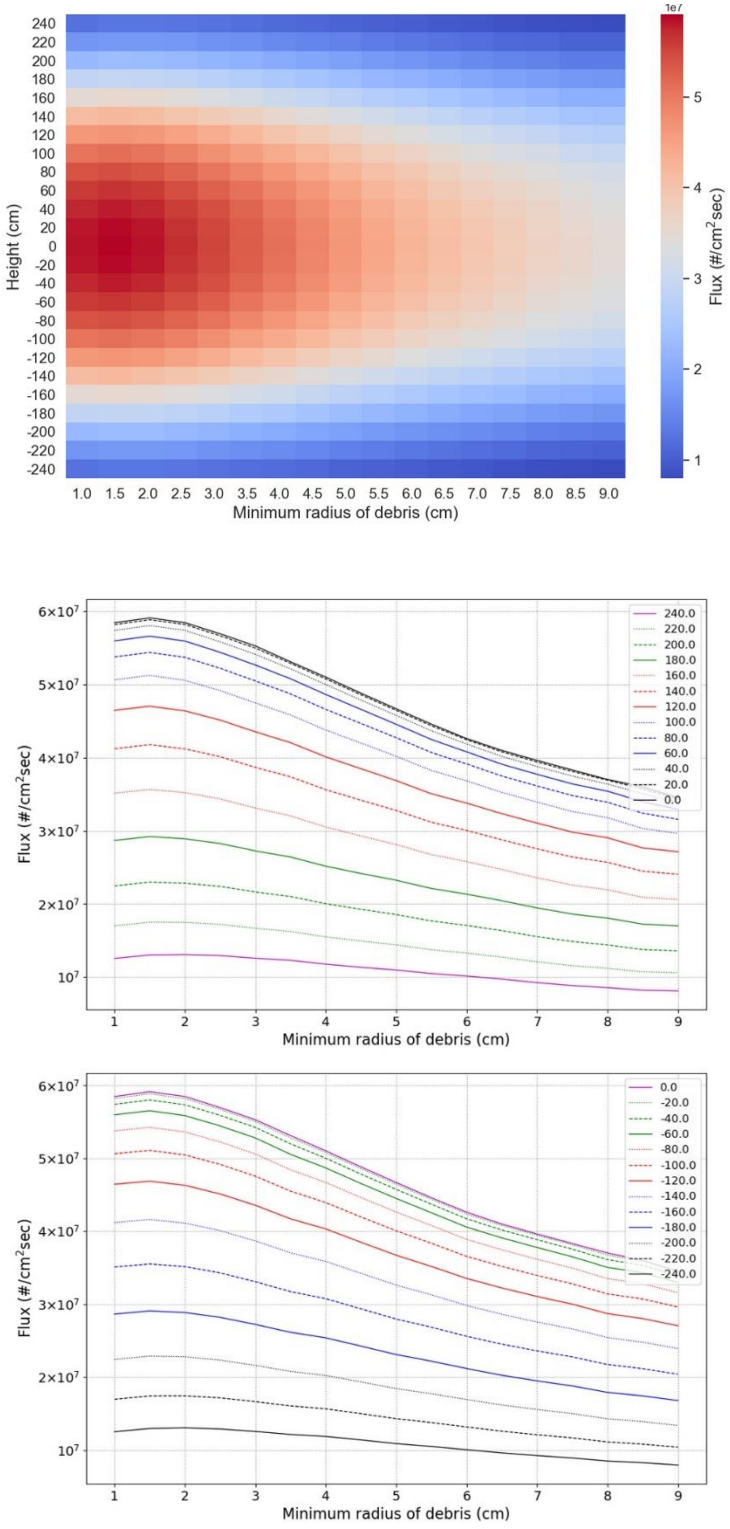


**Figure D. 38 Density plot (top) and line plots of the photon flux for the loose packed fuel debris in a canister**

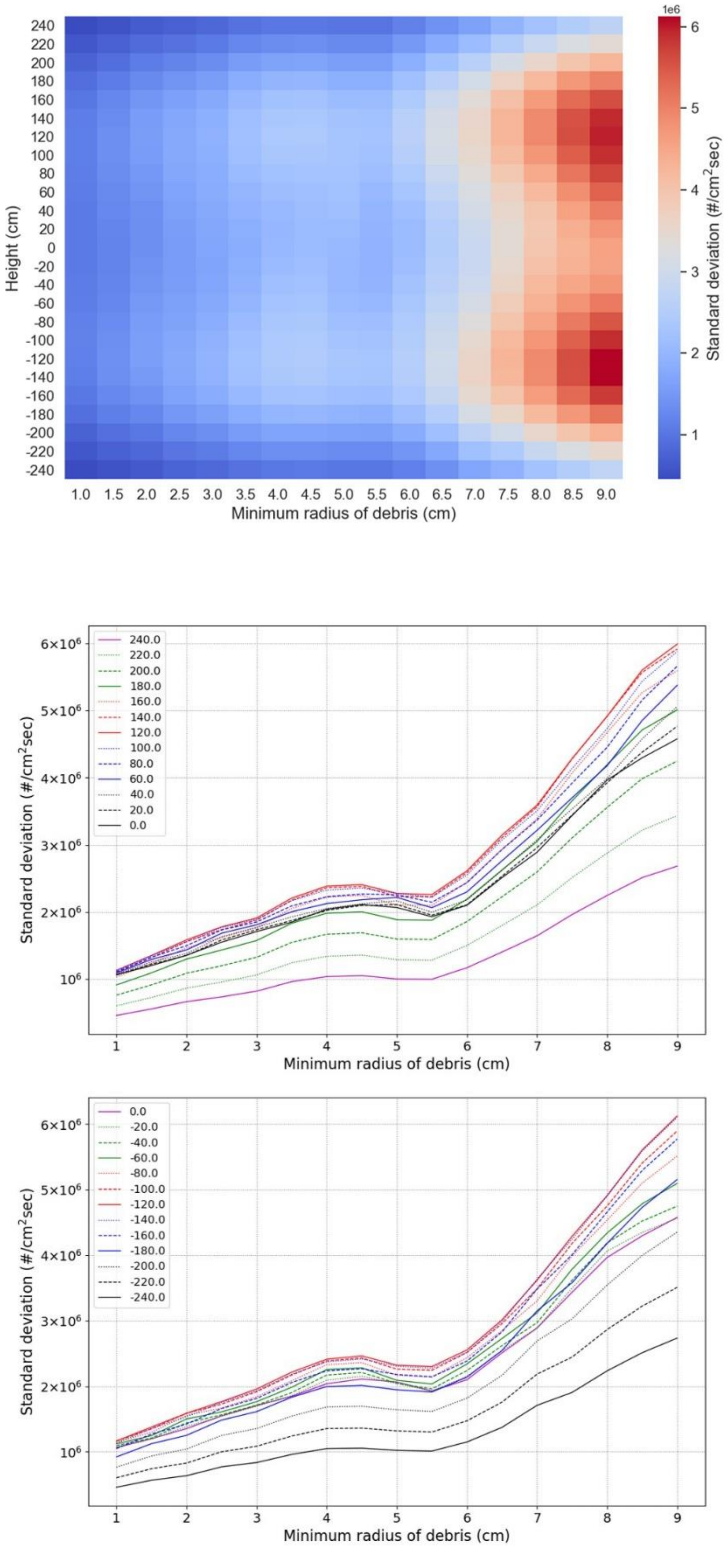


**Figure D. 39 Density plot (top) and line plots of the standard deviation of the photon flux of loose packed fuel debris in a canister**

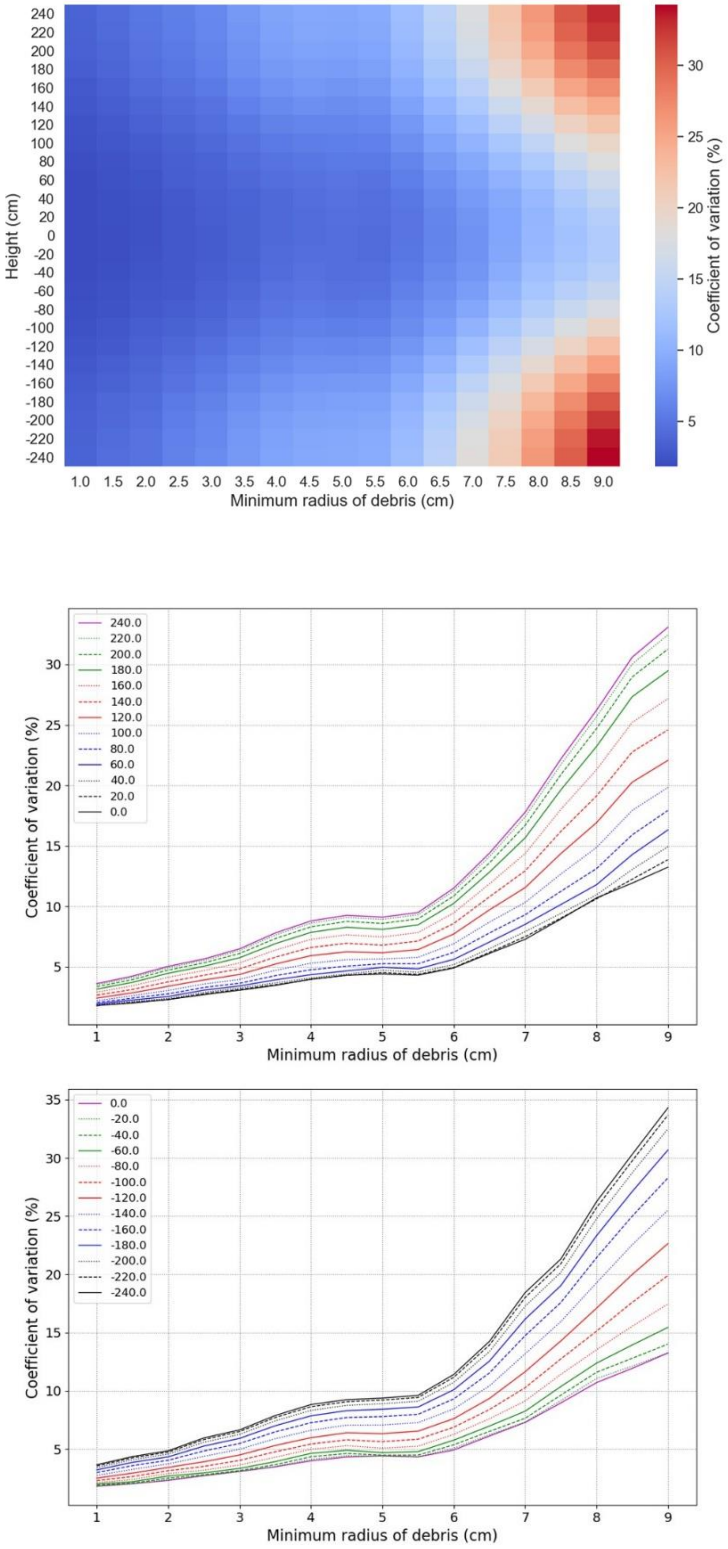


**Figure D. 40 Density plot (top) and line plots of the coefficient of variation of the photon flux of loose packed fuel debris in a canister**

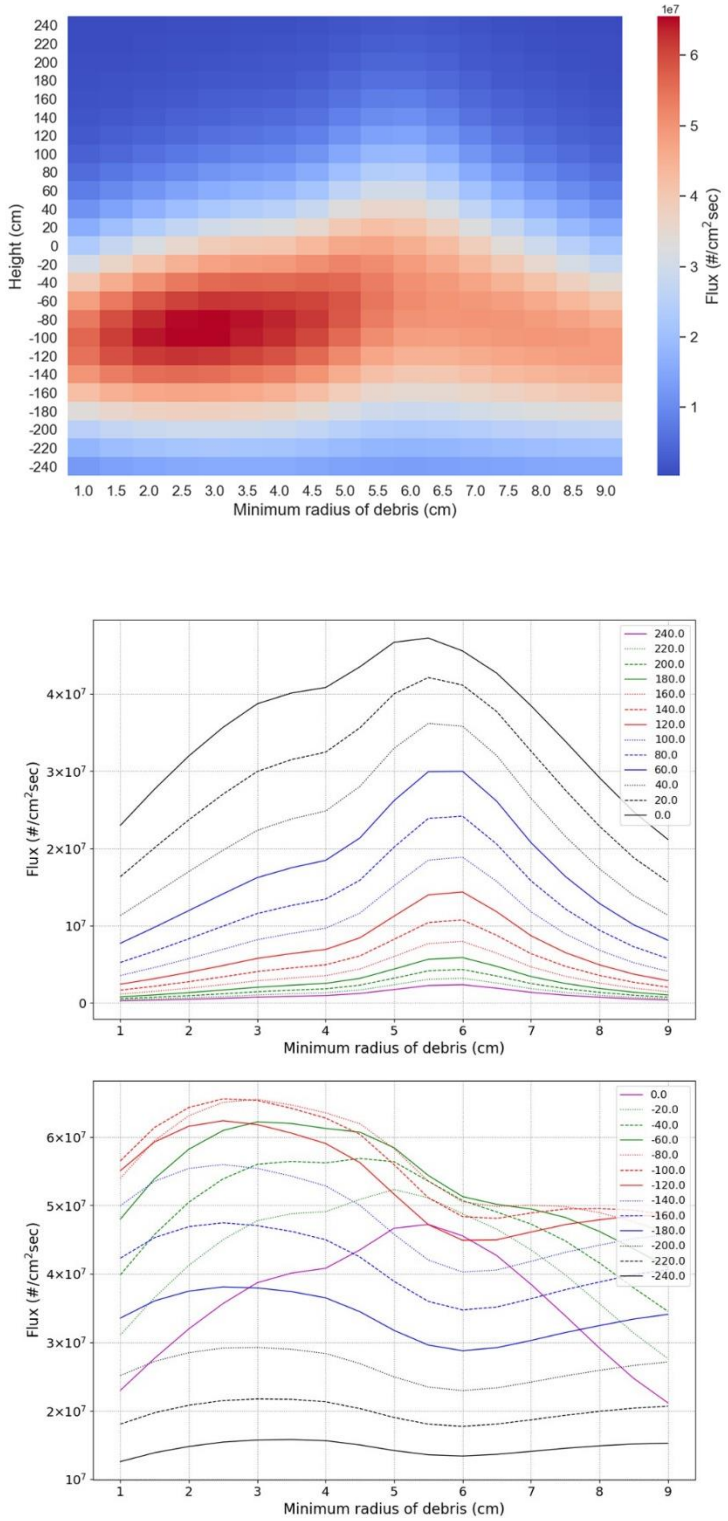


**Figure D. 41 Density plot (top) and line plots of the photon flux for the close packed fuel debris in a canister**

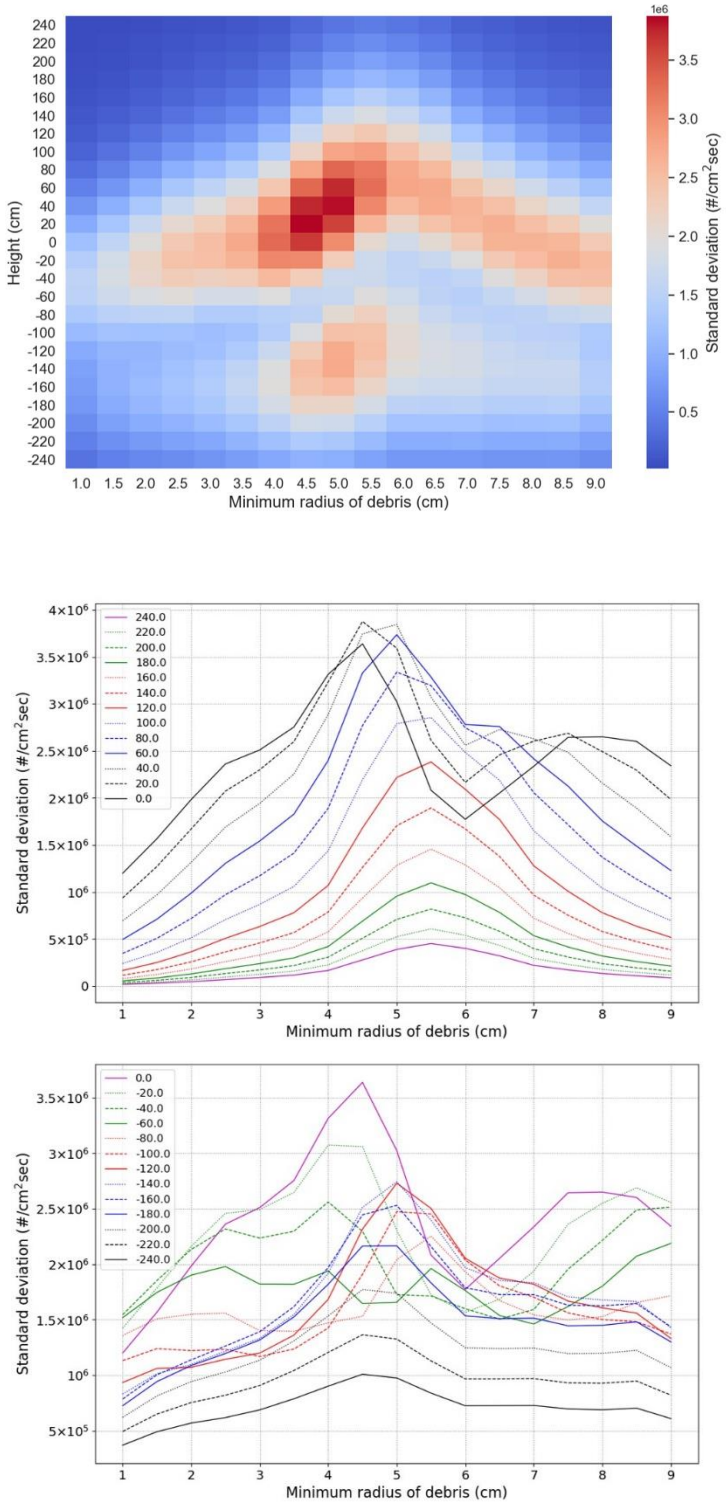


**Figure D. 42 Density plot (top) and line plots of the standard deviation of photon flux for close packed fuel debris in a canister**

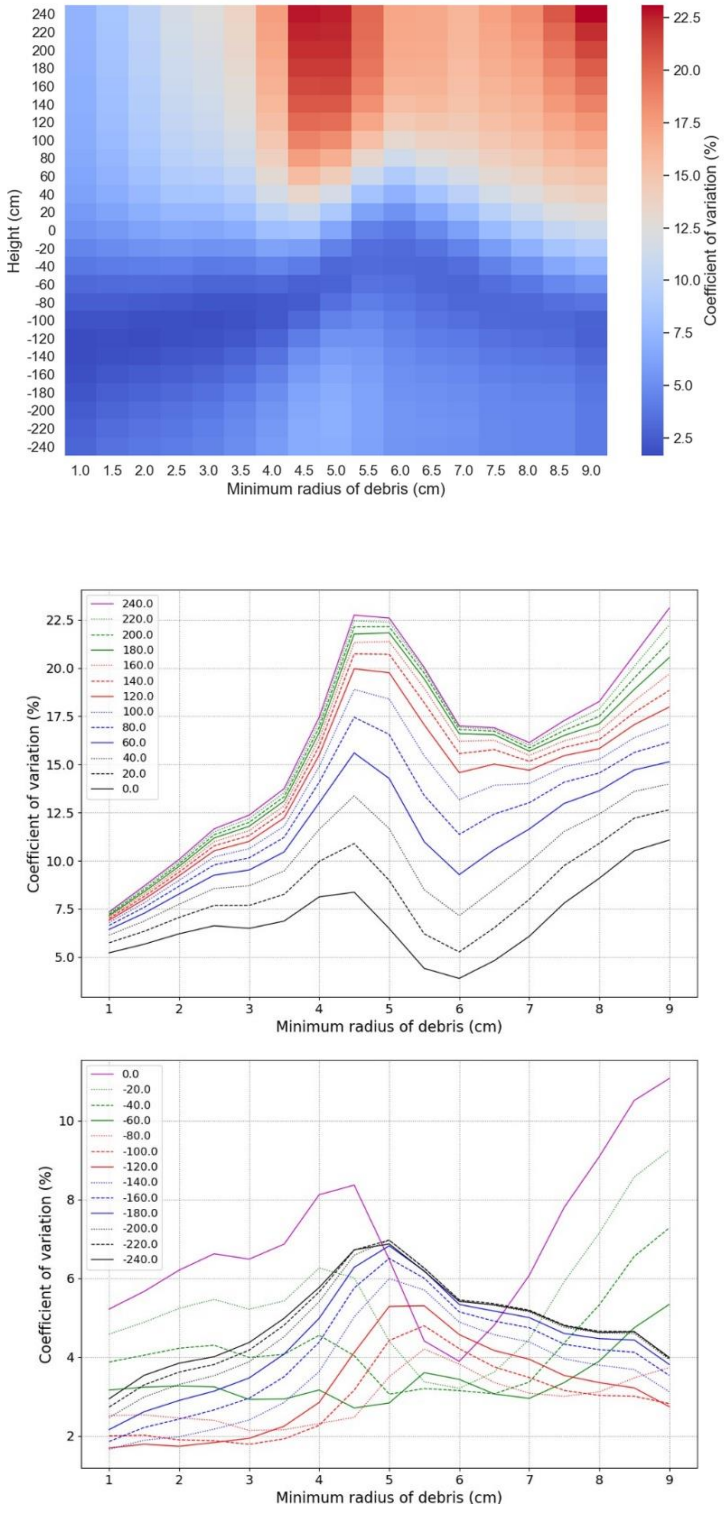


**Figure D. 43 Density plot (top) and line plots of the coefficient of variation of photon flux for close packed fuel debris in a canister**

## D. 6 Plots of photon flux (Estimated by the modified Shmakov model)

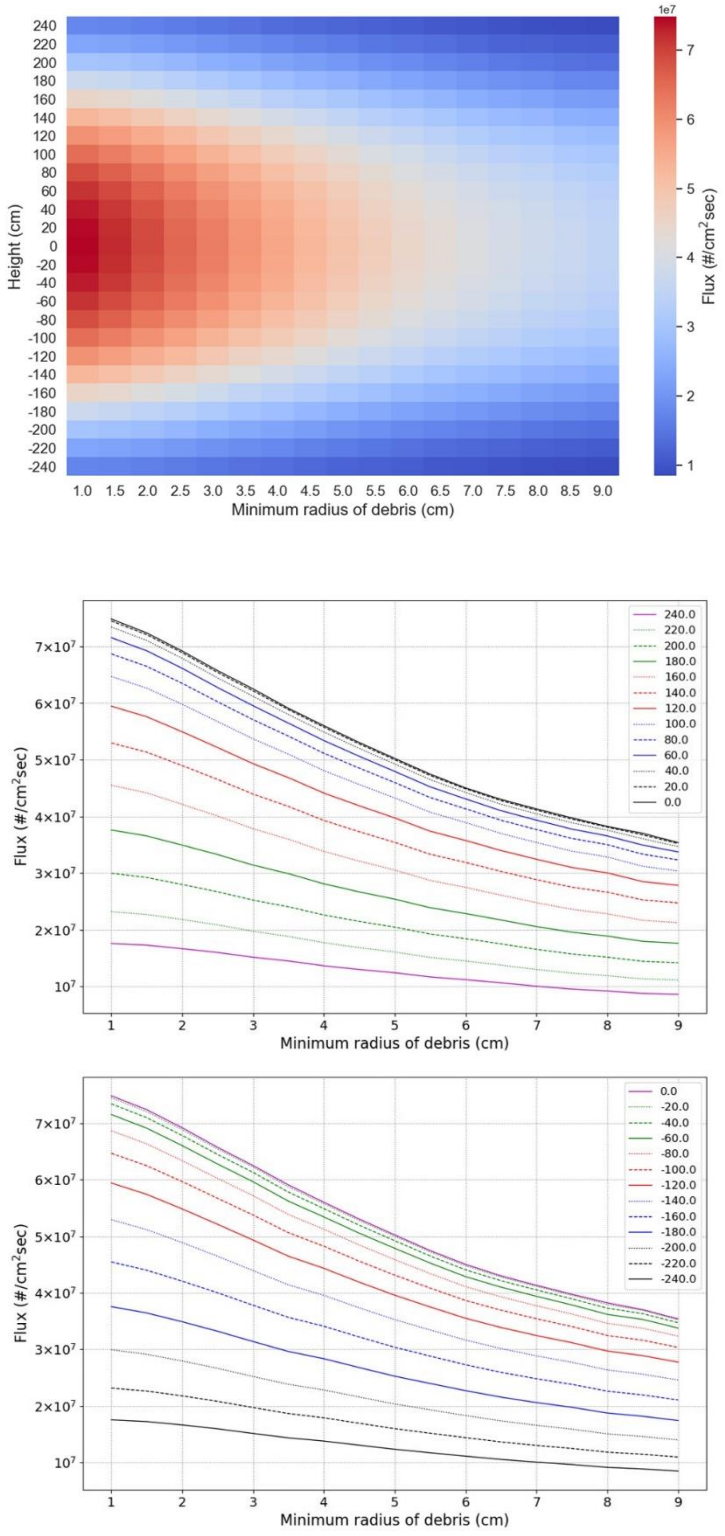


**Figure D. 44 Density plot (top) and line plots of the photon flux for the loose packed fuel debris in a canister**

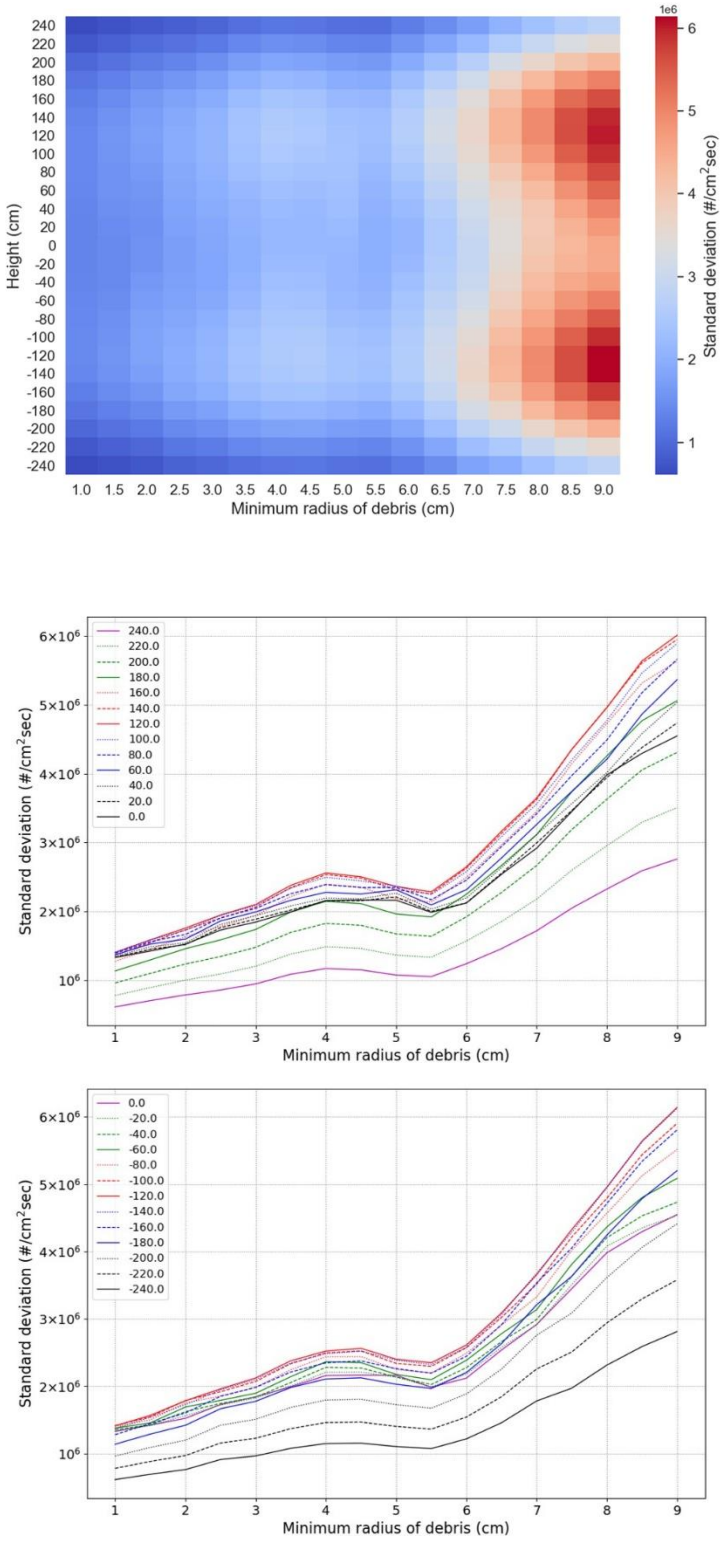


**Figure D. 45 Density plot (top) and line plots of the standard deviation of the photon flux of loose packed fuel debris in a canister**

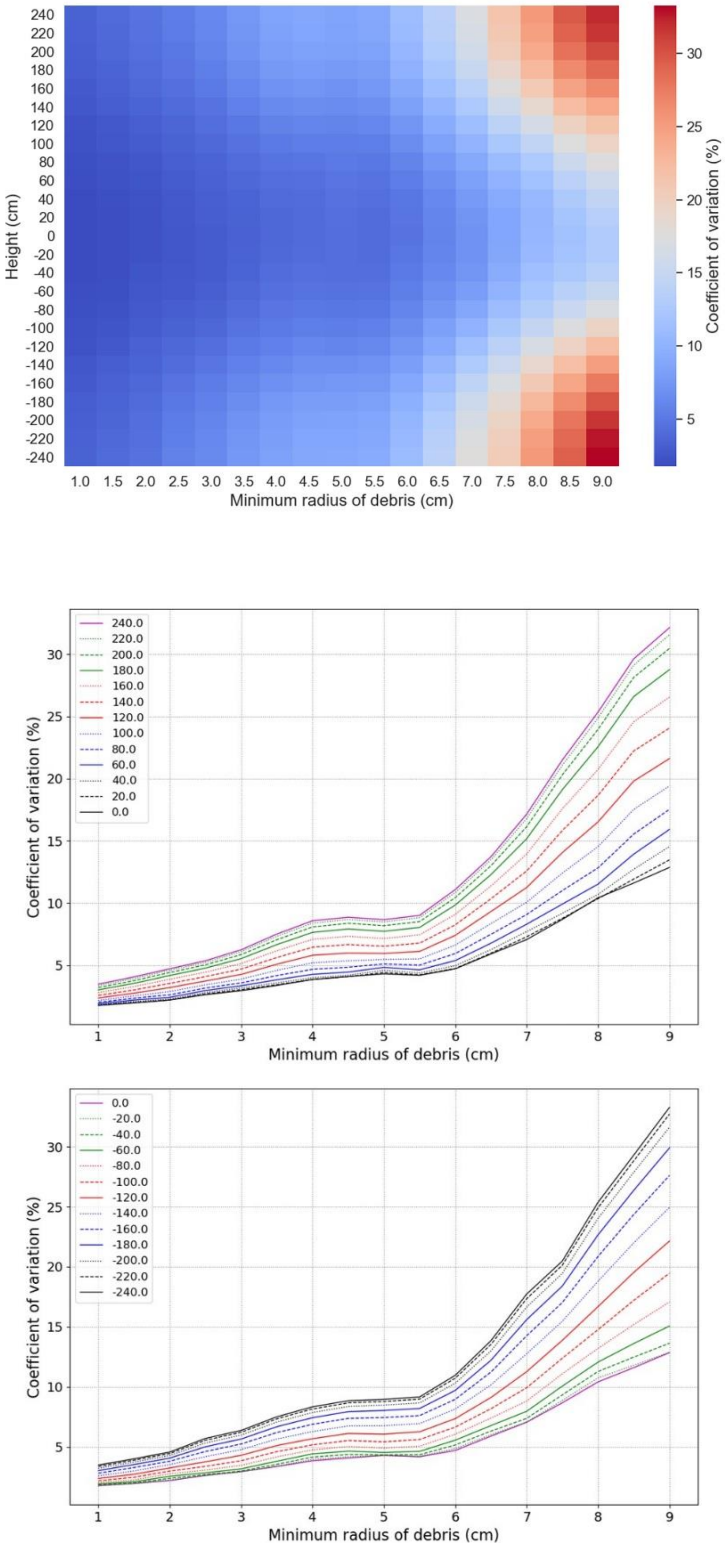


**Figure D. 46 Density plot (top) and line plots of the coefficient of variation of the photon flux of loose packed fuel debris in a canister**

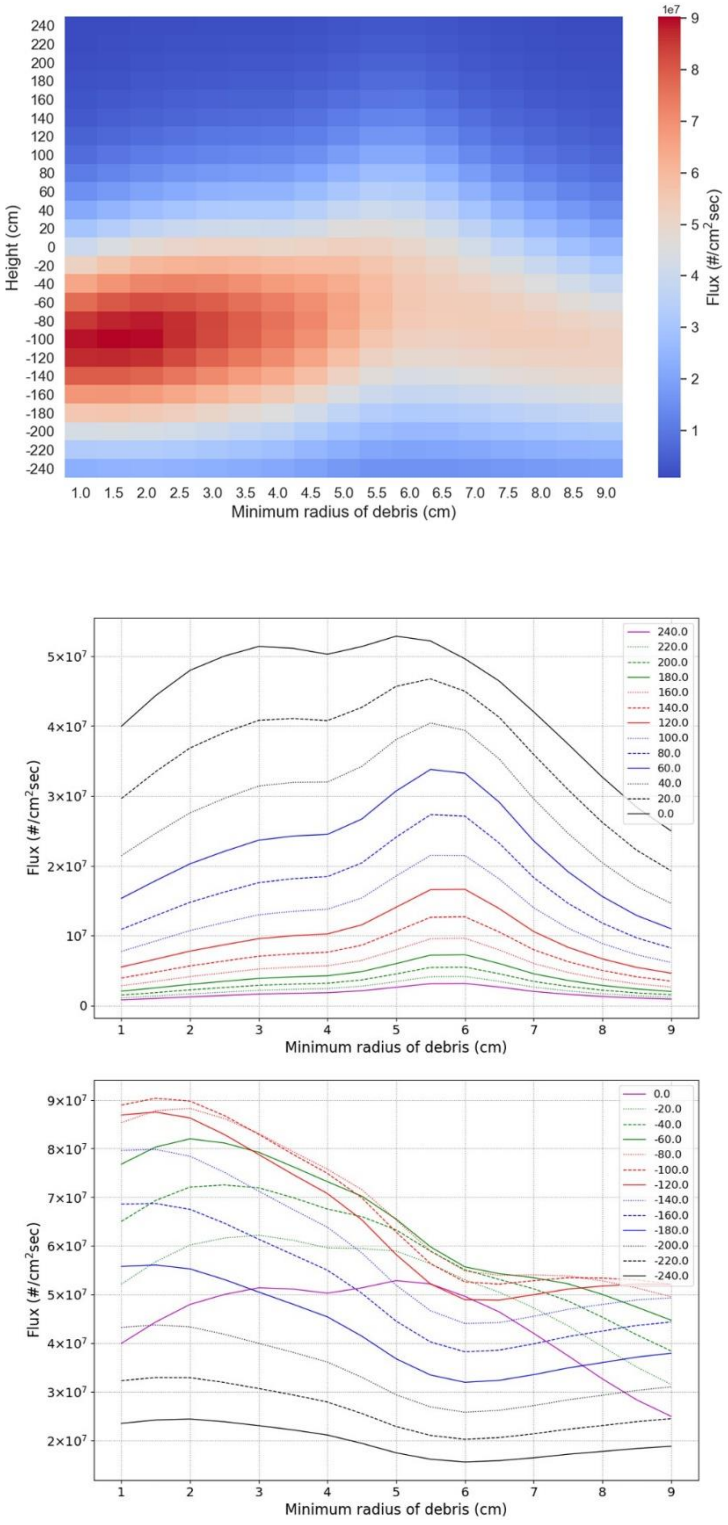


**Figure D. 47 Density plot (top) and line plots of the photon flux for the close packed fuel debris in a canister**

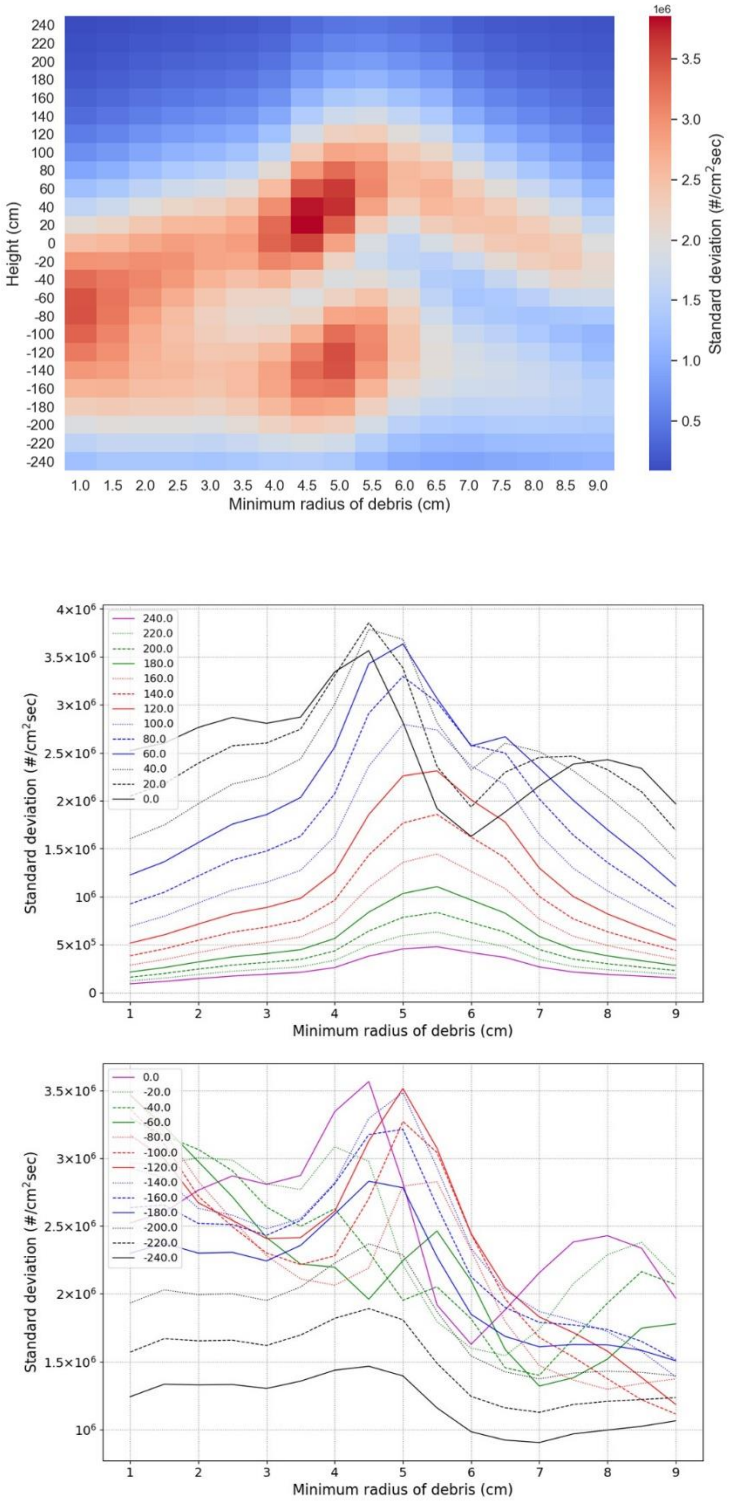


**Figure D. 48 Density plot (top) and line plots of the standard deviation of photon flux for close packed fuel debris in a canister**

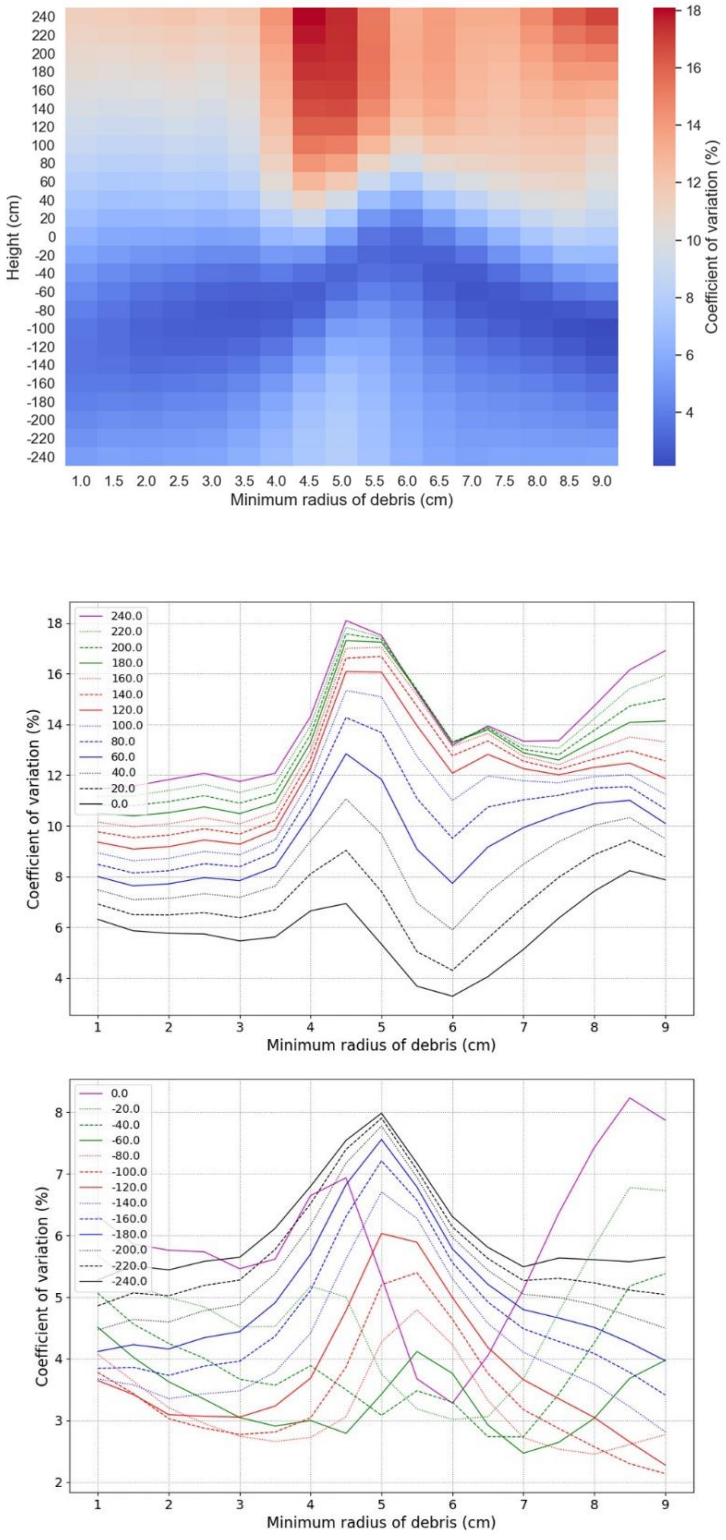


**Figure D. 49 Density plot (top) and line plots of the coefficient of variation of photon flux for close packed fuel debris in a canister**

## D. 7 Plots of photon flux for the canister with three small containers (Estimated by SCALE based model)

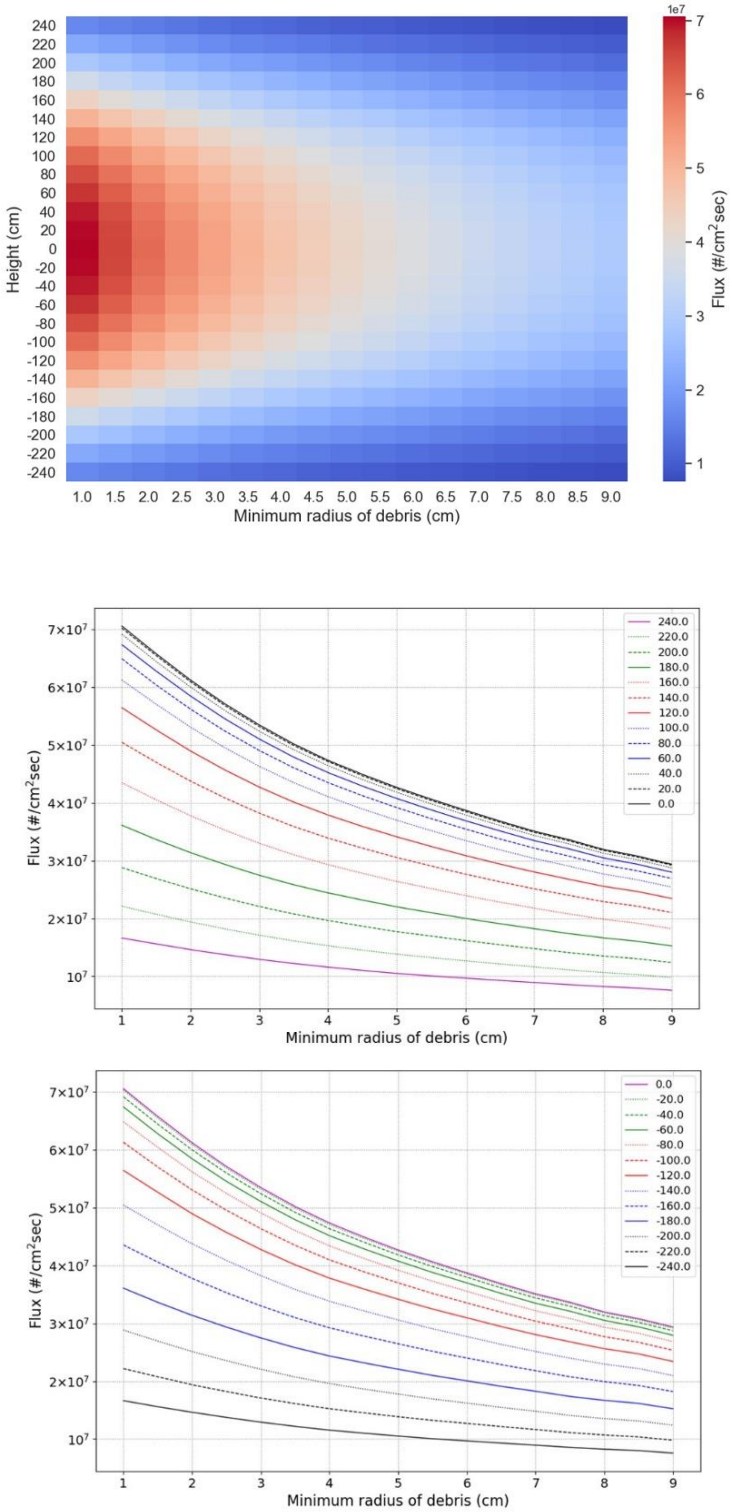


**Figure D. 50 Density plot (top) and line plots of the photon flux for the loose packed fuel debris**

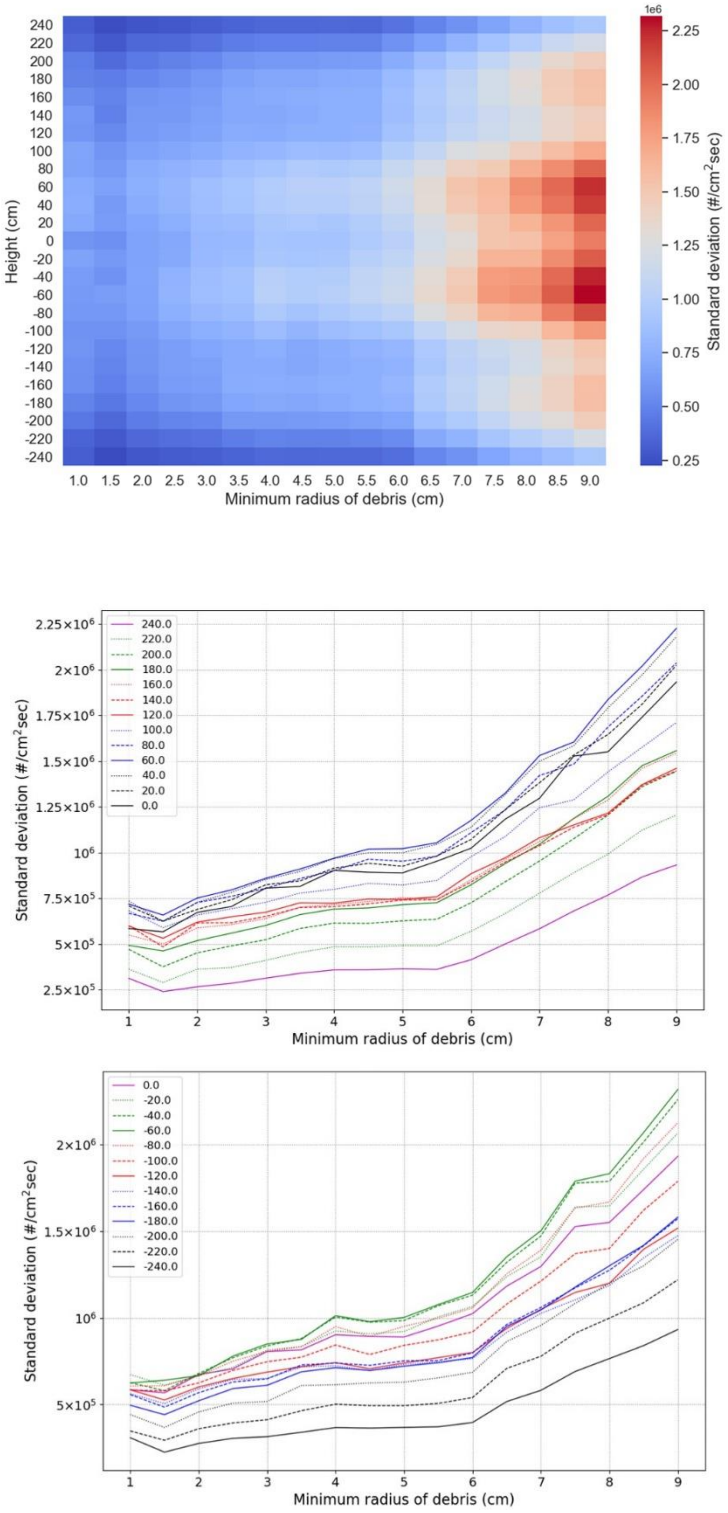


**Figure D. 51 Density plot (top) and line plots of the standard deviation of photon flux for the loose packed fuel debris in a canister with three small containers**

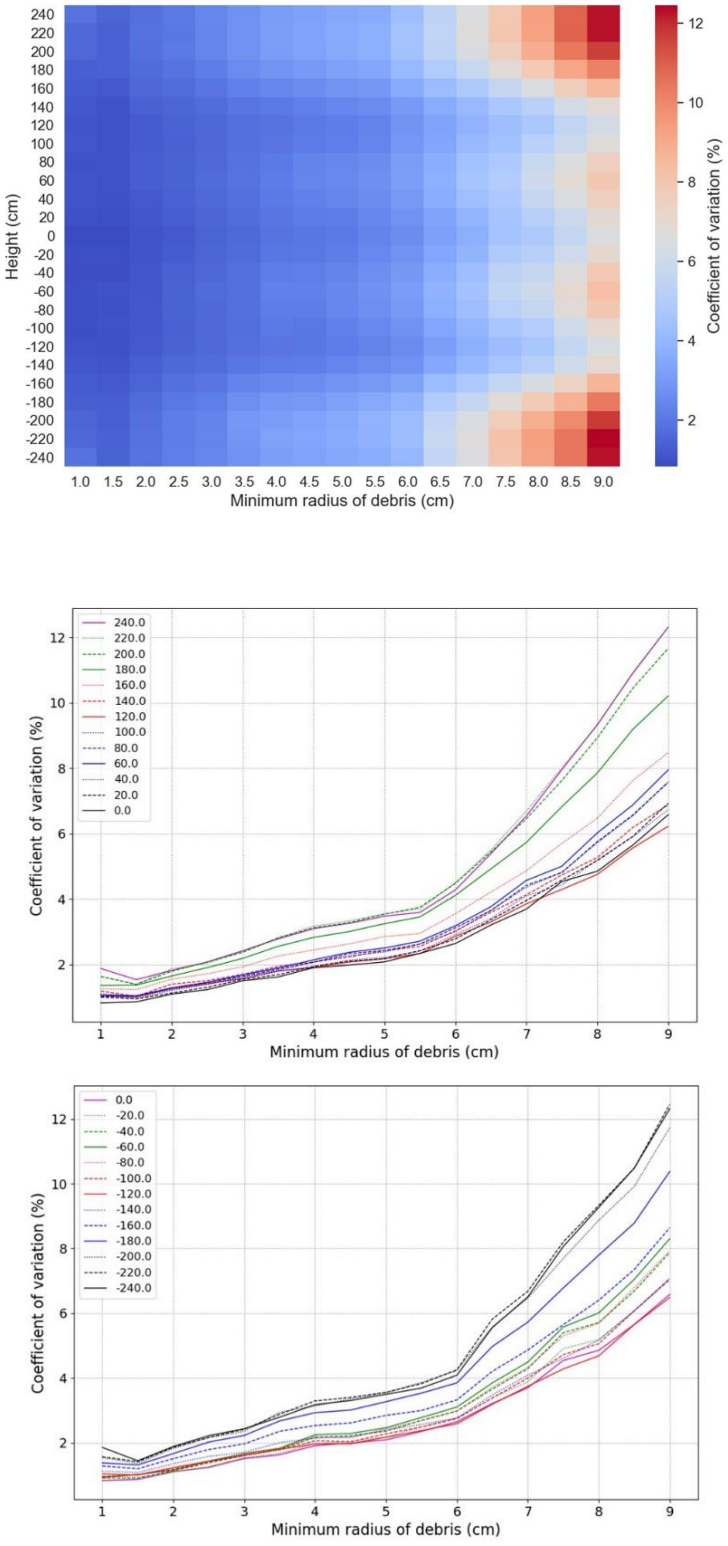


**Figure D. 52 Density plot (top) and line plots of the coefficient of variation of photon flux for the loose packed fuel debris in a canister with small containers**

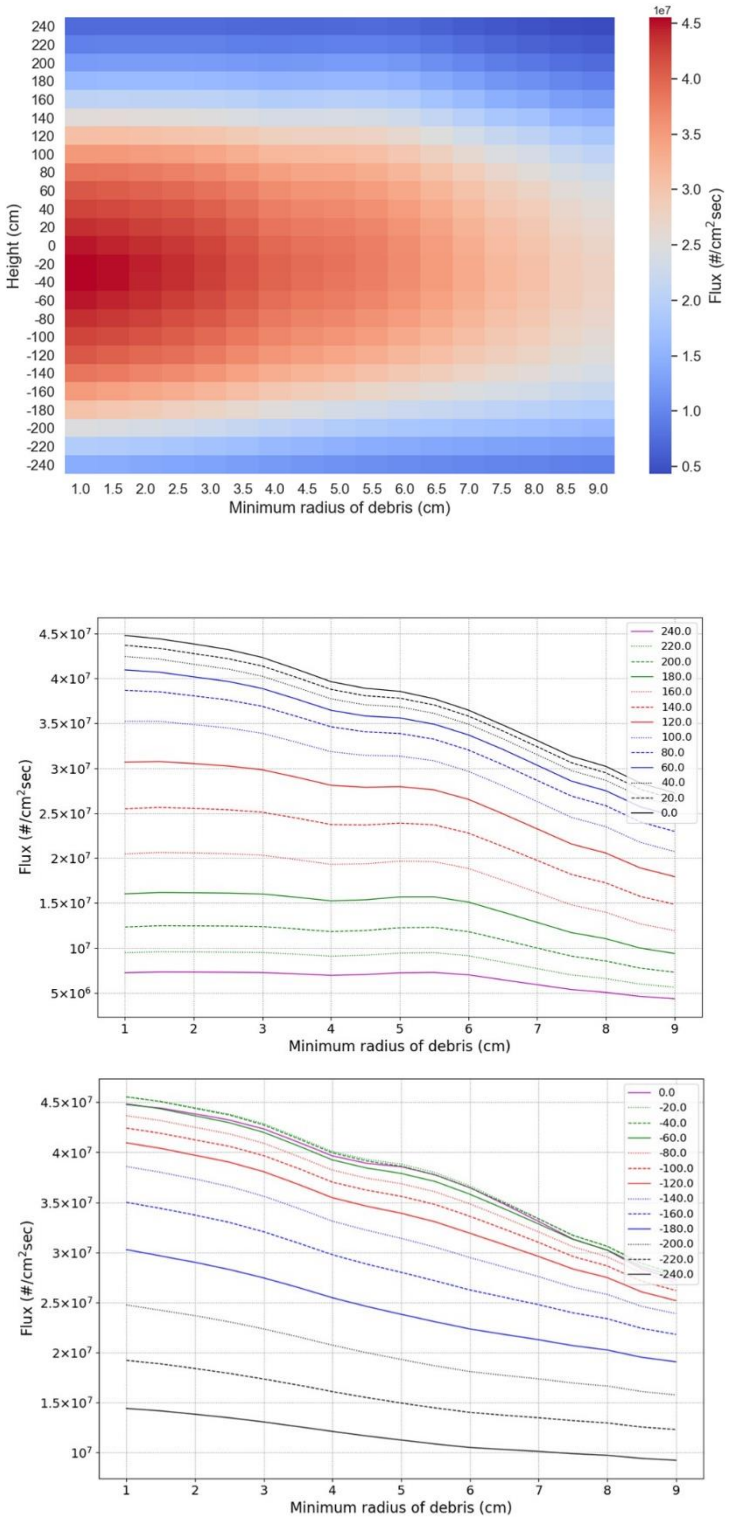


**Figure D. 53 Density plot (top) and line plots of the photon flux for the close packed fuel debris in a canister with three small containers**

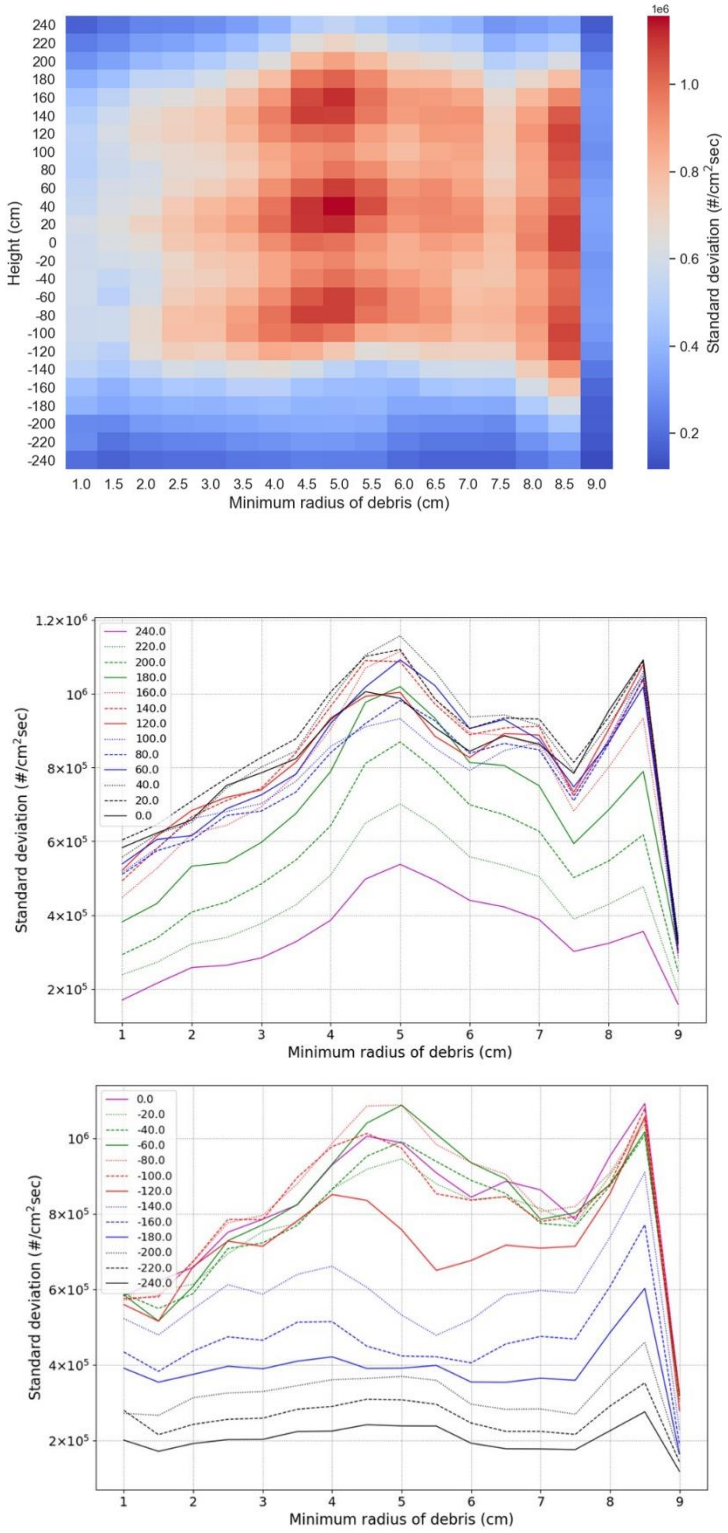


**Figure D. 54 Density plot (top) and line plots of the standard deviation of photon flux for the close packed fuel debris in a canister with small containers**

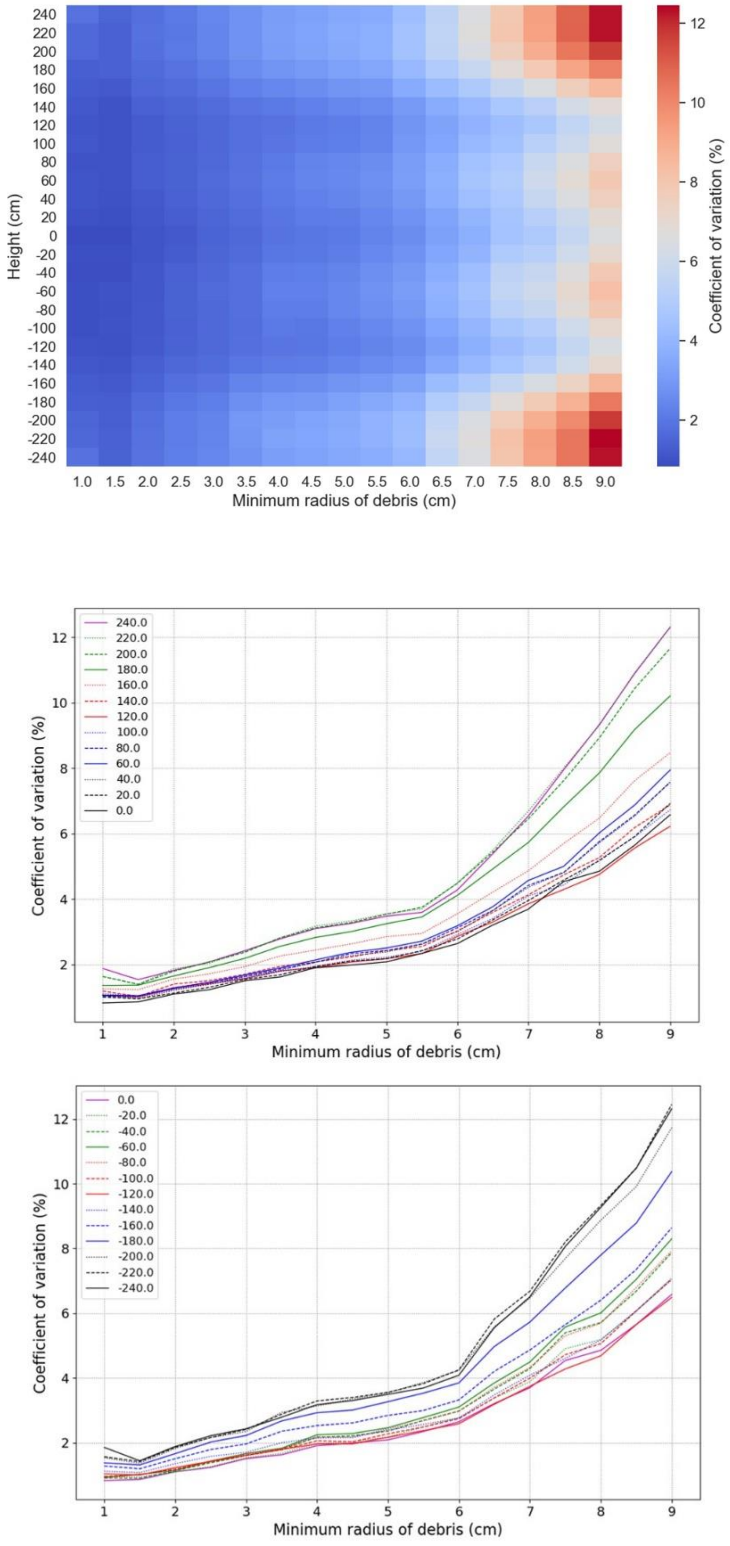


**Figure D. 55 Density plot (top) and line plots of the coefficient of variation of photon flux for the close packed fuel debris in a canister with small containers**

## D. 8 Plots of photon flux for the canister in a transfer cask

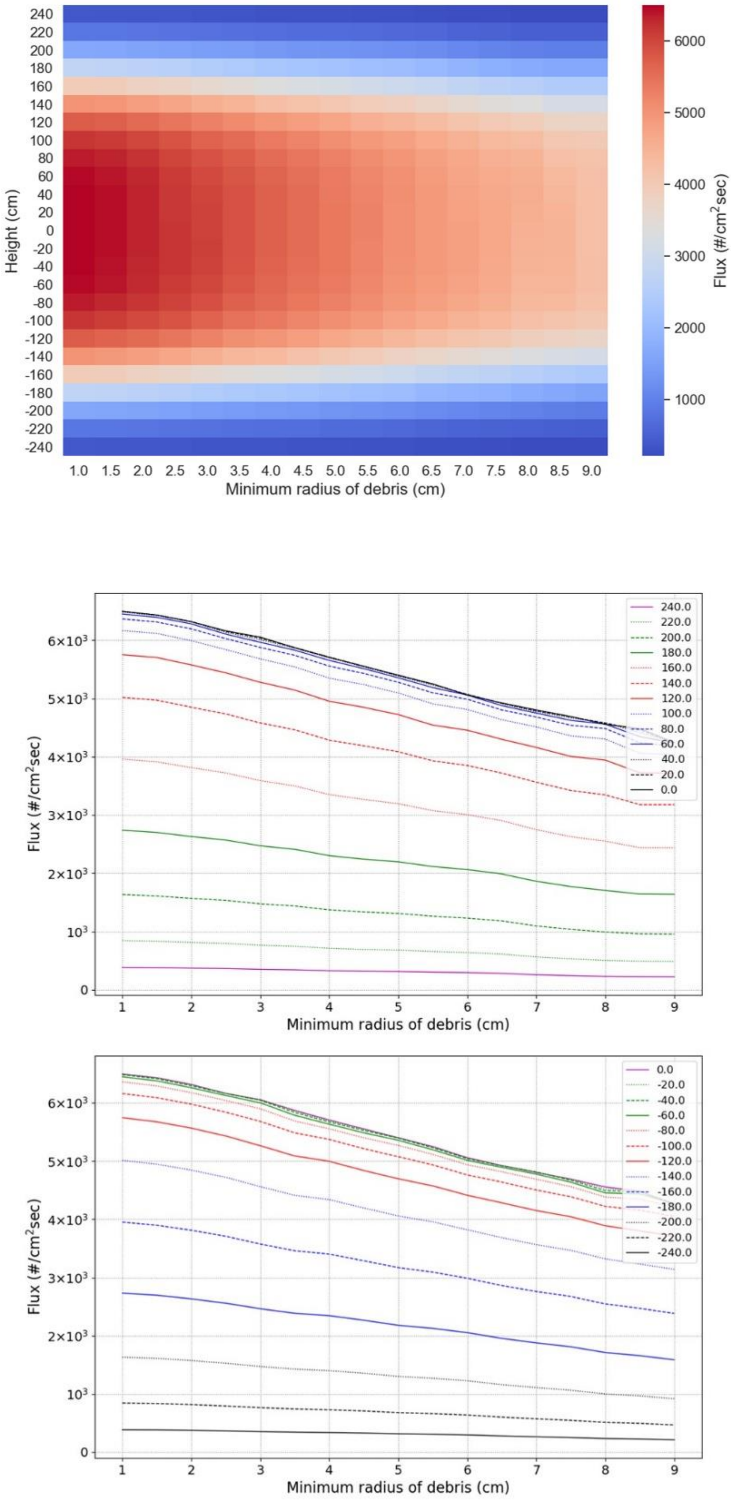


**Figure D. 56 Density plot (top) and line plots of the photon flux for the loose packed fuel debris**

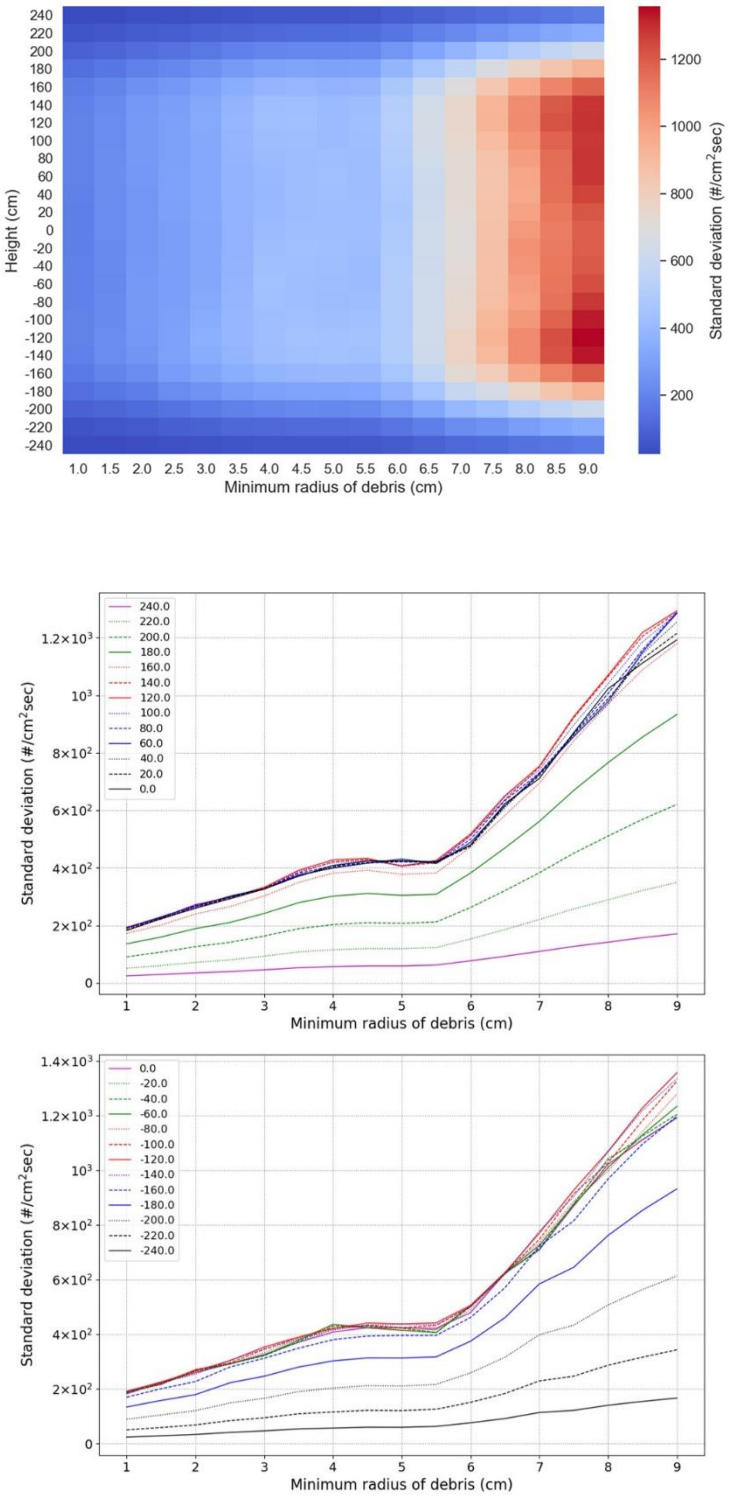


**Figure D. 57 Density plot (top) and line plots of the standard deviation of photon flux for the loose packed fuel debris in a canister in a transfer cask**

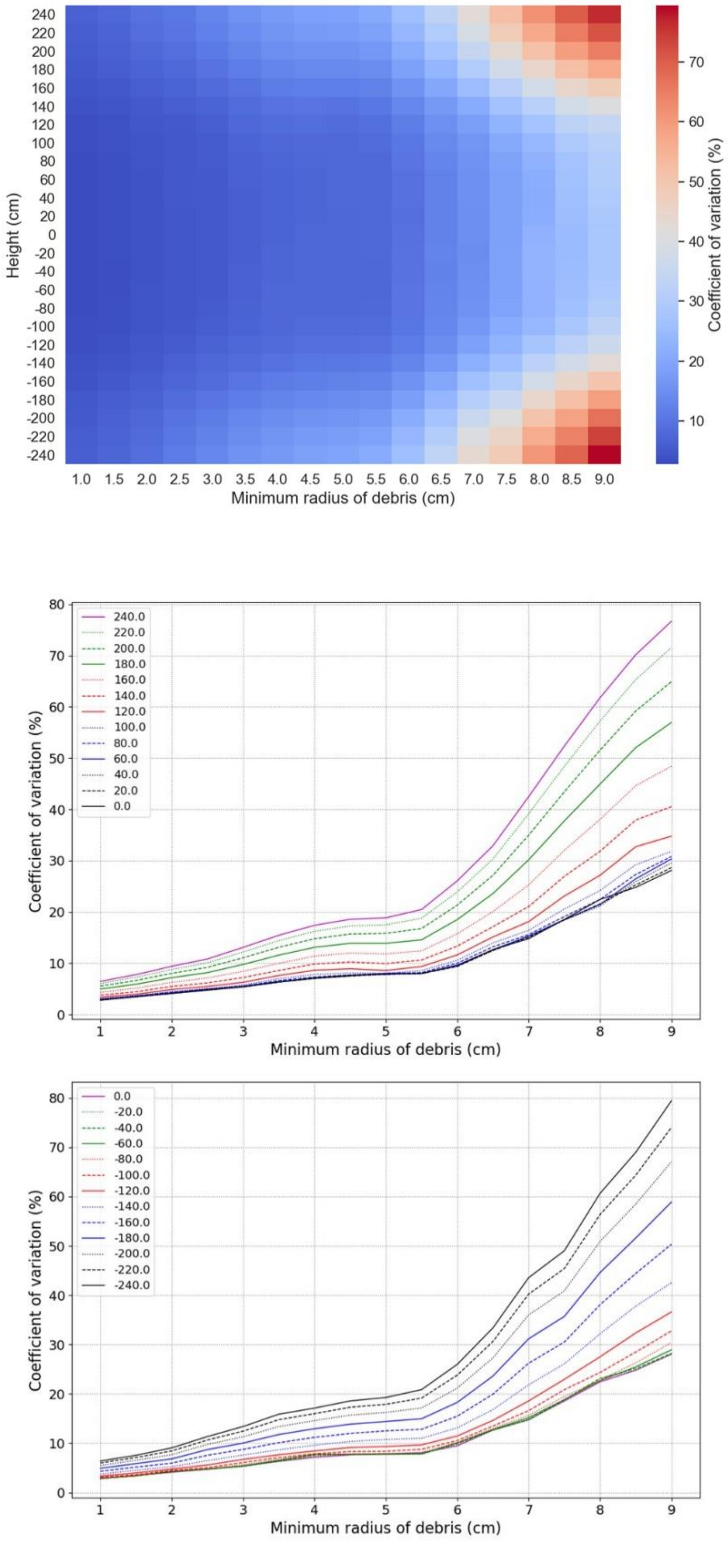


**Figure D. 58 Density plot (top) and line plots of the coefficient of variation of photon flux for the loose packed fuel debris in a canister in a transfer cask**

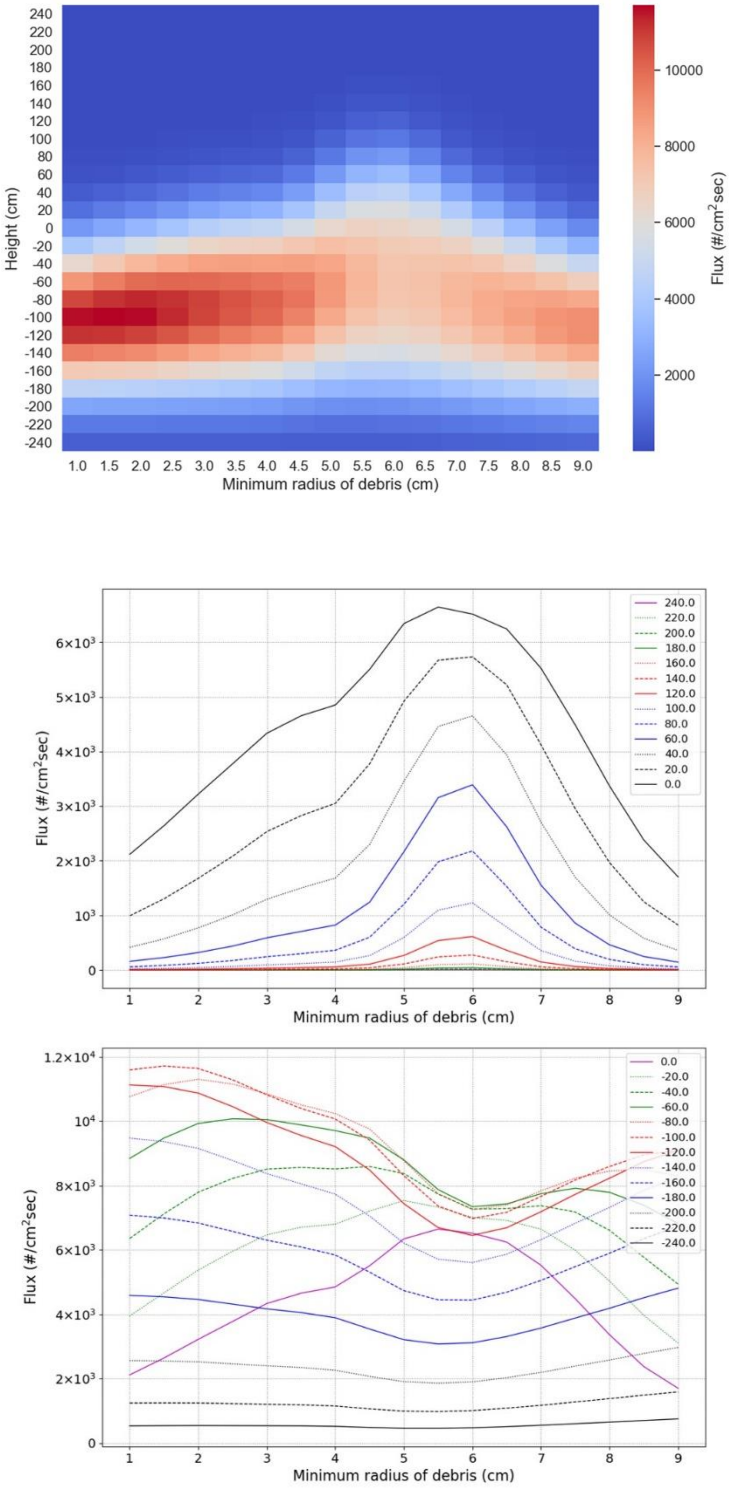


**Figure D. 59 Density plot (top) and line plots of the photon flux for the close packed fuel debris in a canister in a transfer cask**

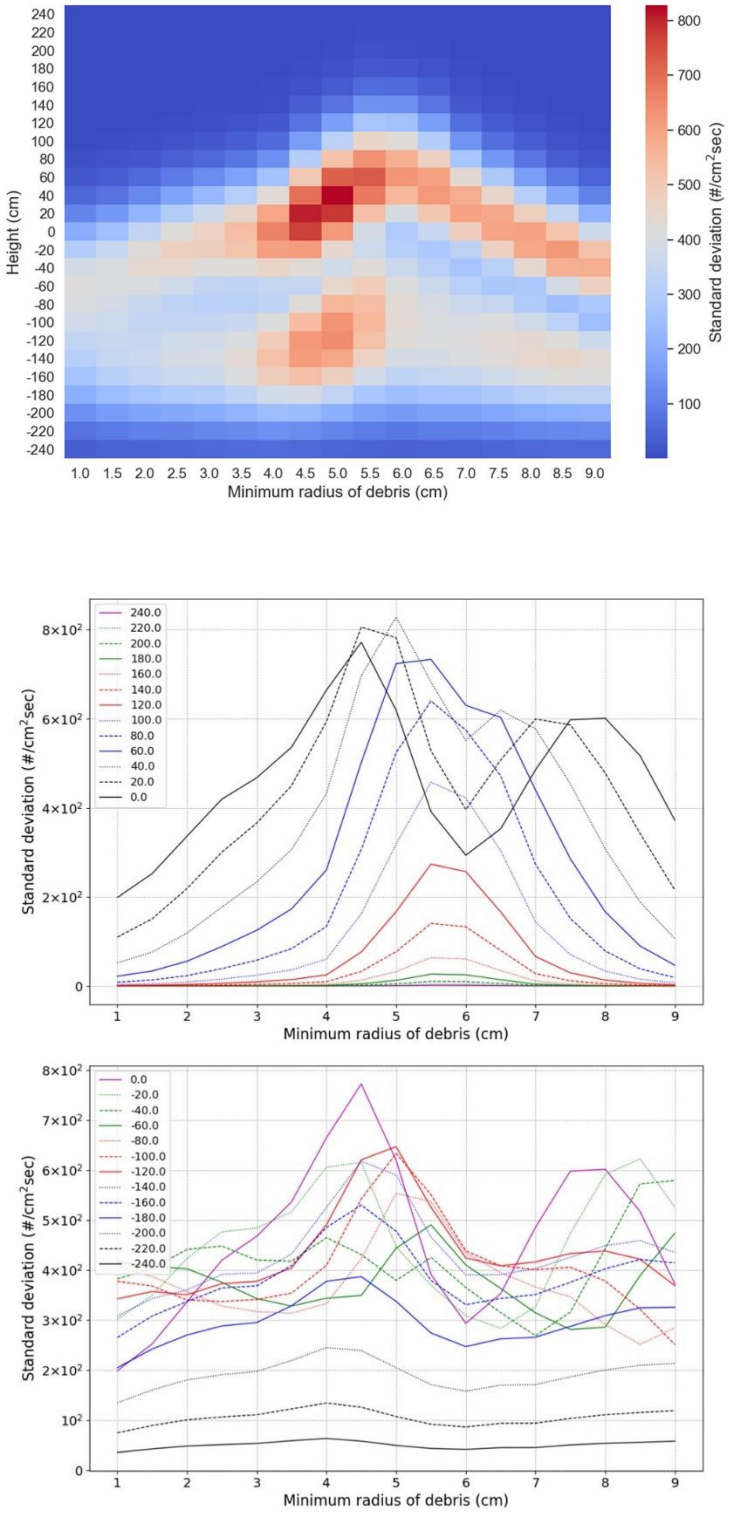


**Figure D. 60 Density plot (top) and line plots of the standard deviation of photon flux for the close packed fuel debris in a canister in a transfer cask**

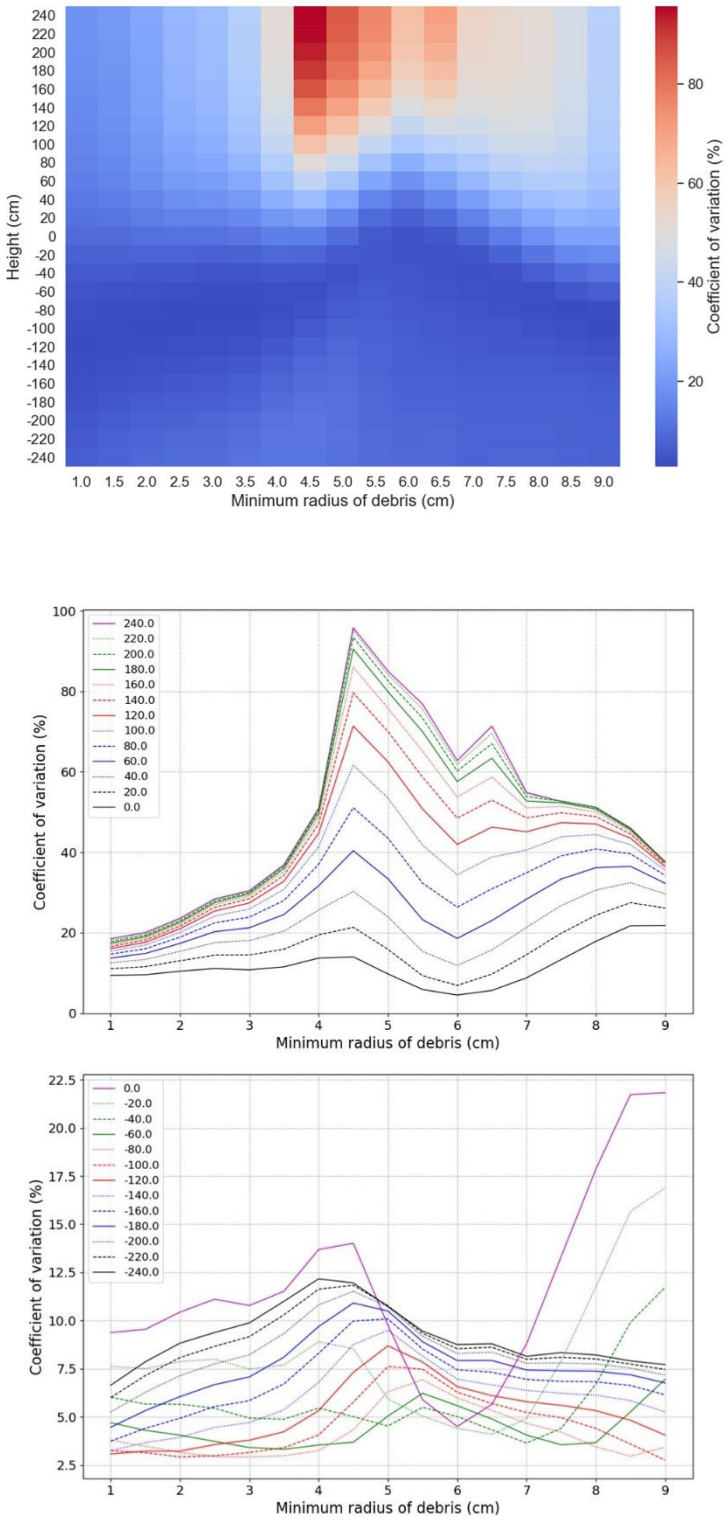


**Figure D. 61 Density plot (top) and line plots of the coefficient of variation of photon flux for the close packed fuel debris in a canister in a transfer cask**

## Appendix E Photon flux of fuel debris in a transport cask

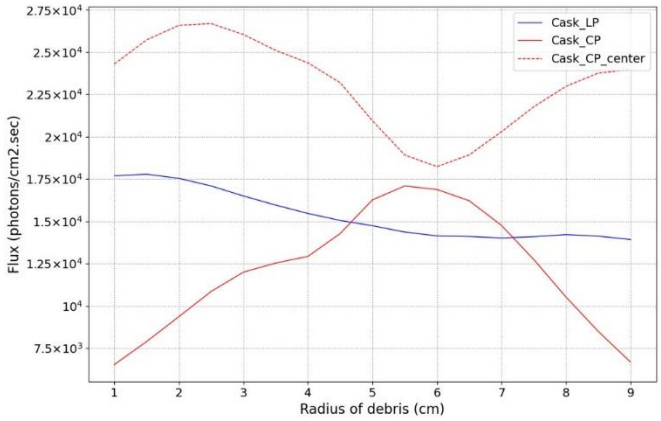


**Figure E. 1 Average photon flux of fuel debris in a transport cask**

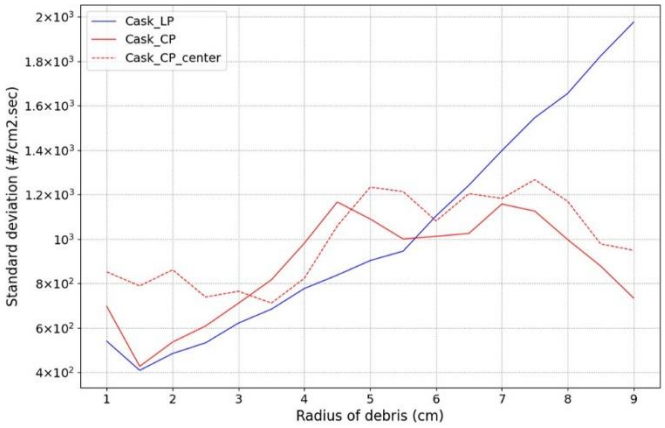


**Figure E. 2 Standard deviation of the photon flux of fuel debris in a transport cask**

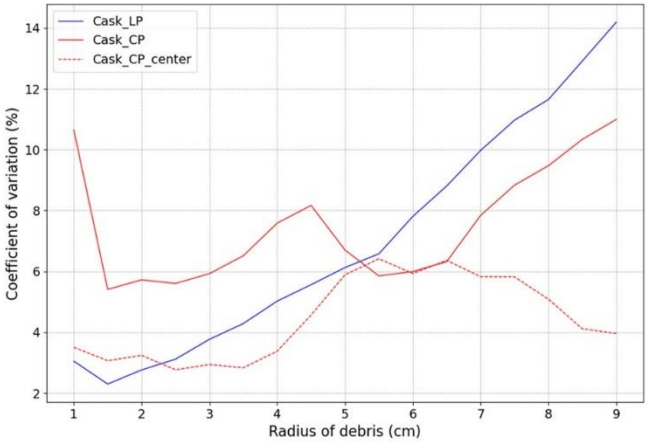


**Figure E. 3 Coefficient of variation of photon flux of fuel debris in a transport cask**

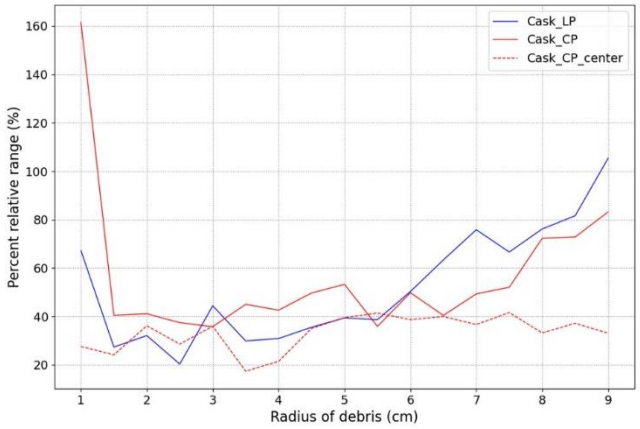


**Figure E. 4 Percent relative range of photon flux of fuel debris in a transport cask**

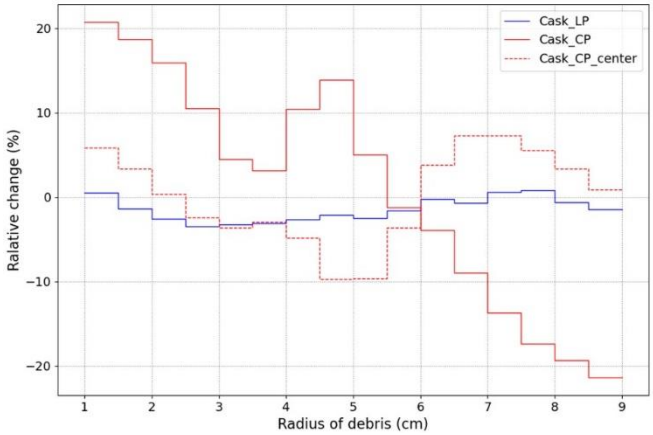


**Figure E. 5 Relative change of photon flux by changes of the minimum radius of fuel debris**

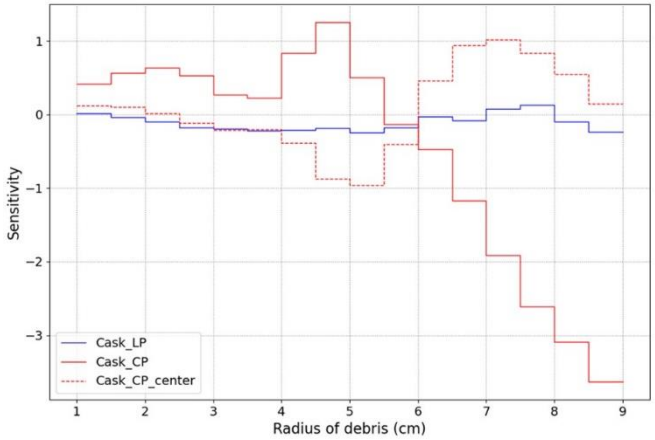


**Figure E. 6 Sensitivity of photon flux for changes of the minimum radius of fuel debris**

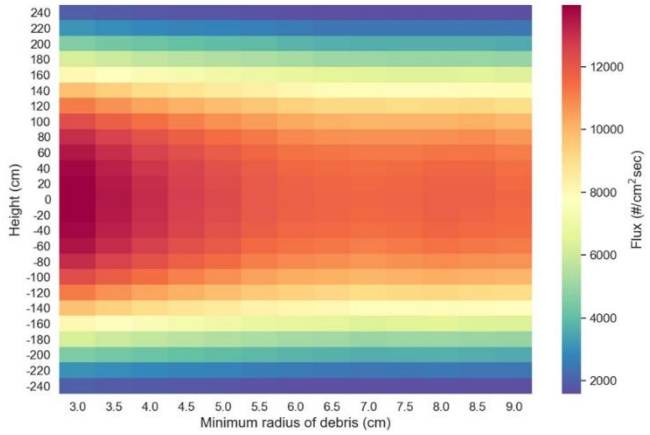


**Figure E. 7 Average photon flux of the loose packed fuel debris in a transport cask**

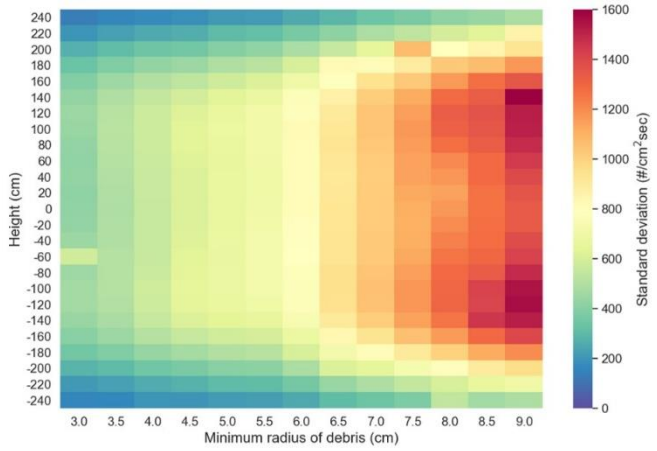


**Figure E. 8 Standard deviation of the loose packed fuel debris in a transport cask**

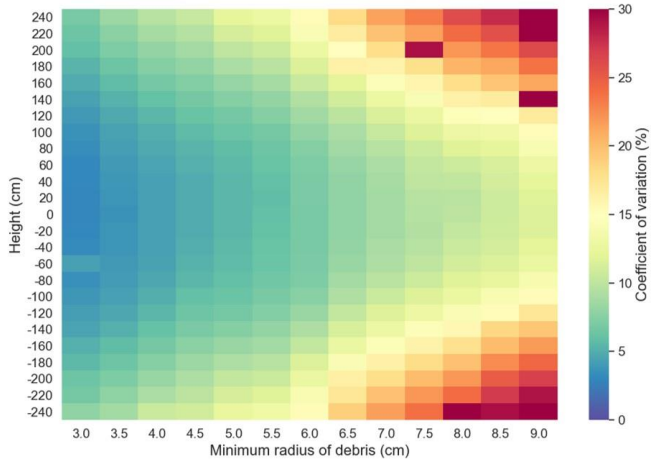


**Figure E. 9 Coefficient of variation of the loose packed fuel debris in a transport cask**

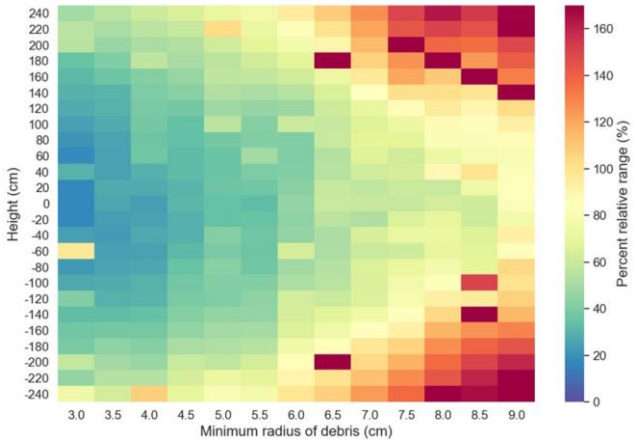


**Figure E. 10 Percent relative range of the loose packed fuel debris in a transport cask**

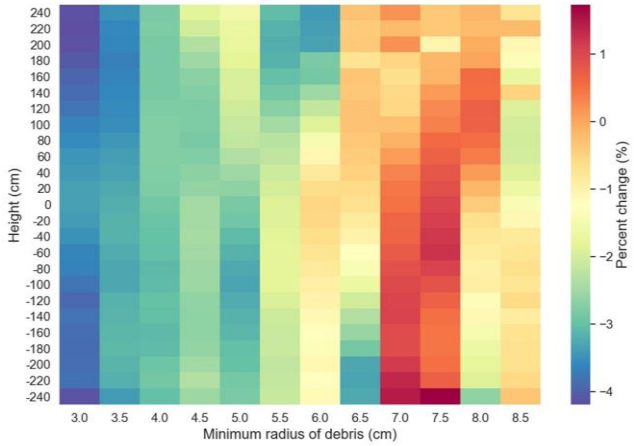


**Figure E. 11 Percent change of the loose packed fuel debris in a transport cask**

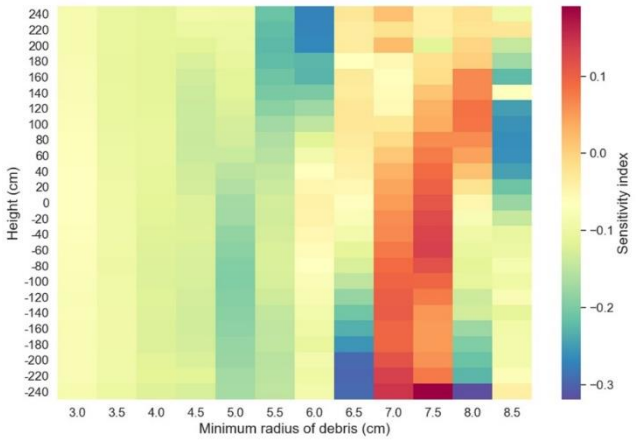


**Figure E. 12 Sensitivity index of the loose packed fuel debris in a transport cask**

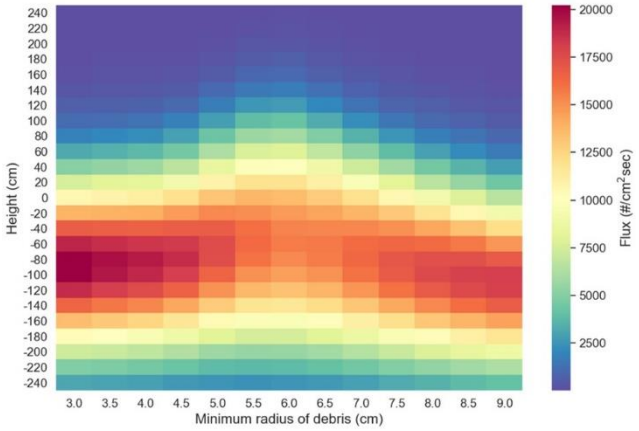


**Figure E. 13 Average photon flux of the close packed fuel debris in a transport cask**

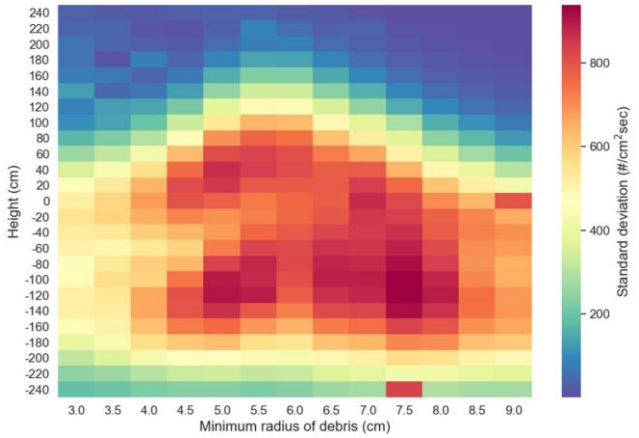


**Figure E. 14 Standard deviation of the close packed fuel debris in a transport cask**

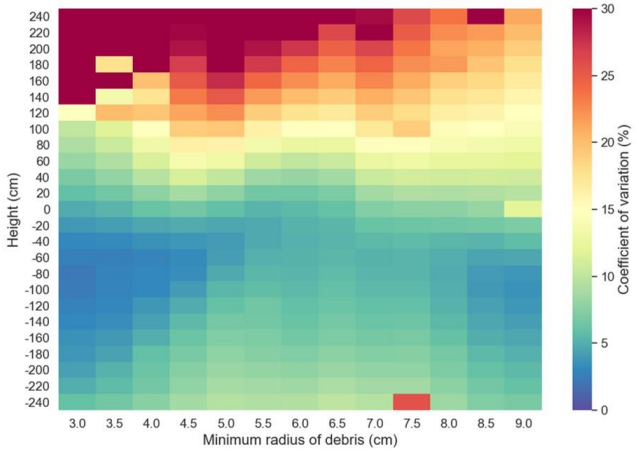


**Figure E. 15 Coefficient of variation of the close packed fuel debris in a transport cask**

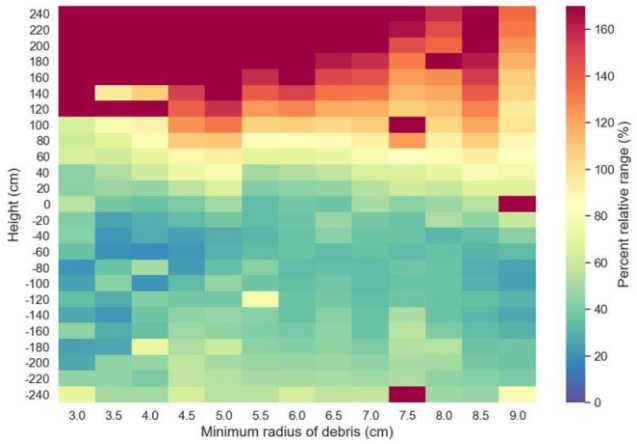


**Figure E. 16 Percent relative range of the close packed fuel debris in a transport cask**

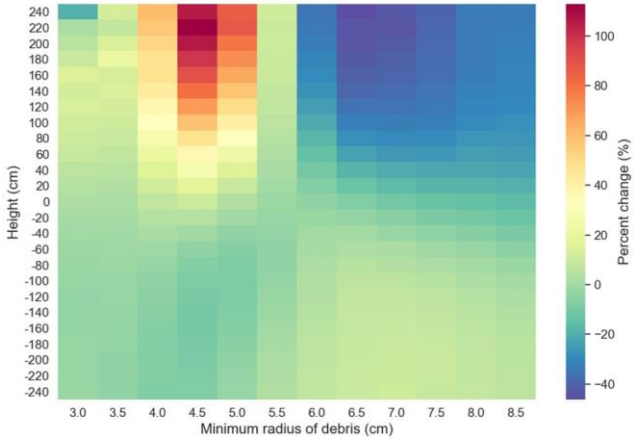


**Figure E. 17 Percent change of the close packed fuel debris in a transport cask**

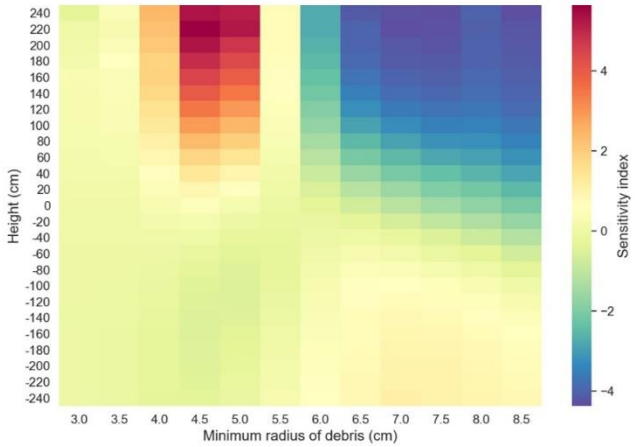


**Figure E. 18 Sensitivity index of the close packed fuel debris in a transport cask**

## Appendix F. Photon flux by changes in the horizontal location of detector

### F. 1. Photon flux of fuel debris for a point detector at locations up to 600 m from the surface of a fuel canister.

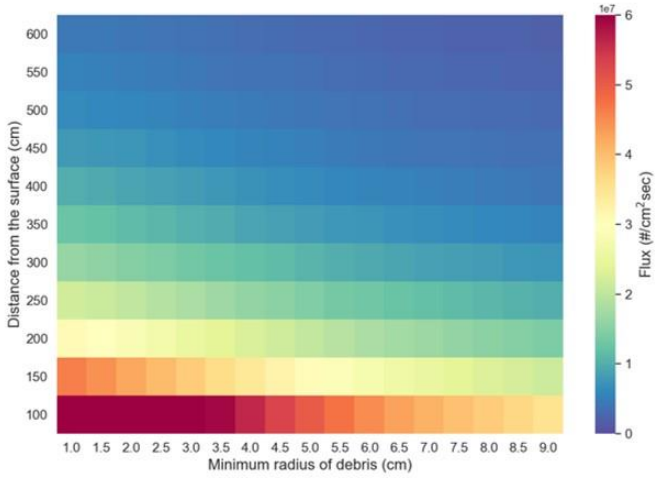


**Figure F. 1 Photon flux of loose packed fuel debris in a fuel canister**

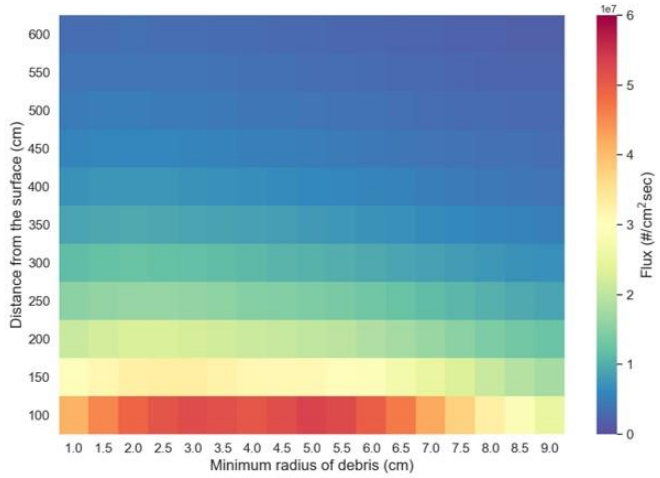


**Figure F. 2 Photon flux of close packed fuel debris in a fuel canister**

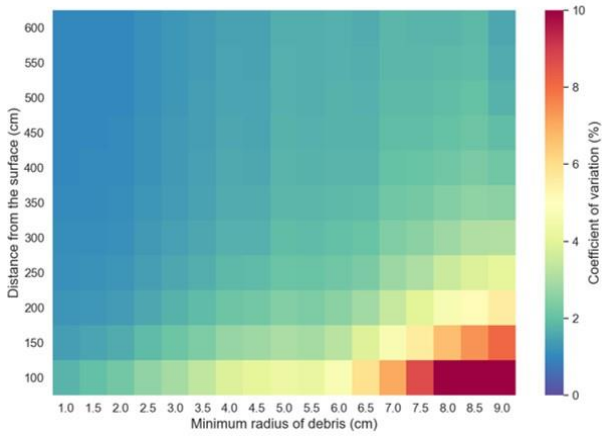


**Figure F. 3 Coefficient of variation of photon flux of loose packed fuel debris in a fuel canister**

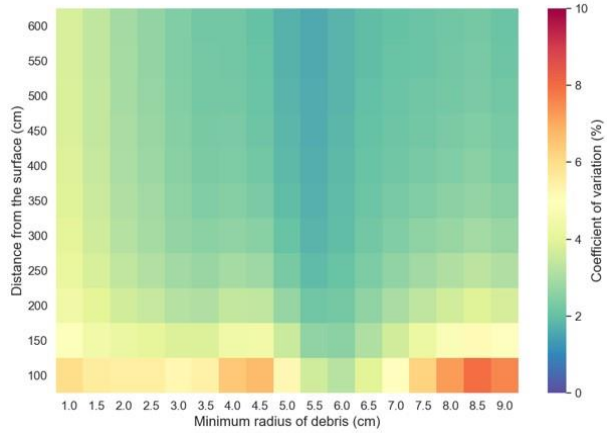


**Figure F. 4 Coefficient of variation of photon flux of close packed fuel debris in a fuel canister**

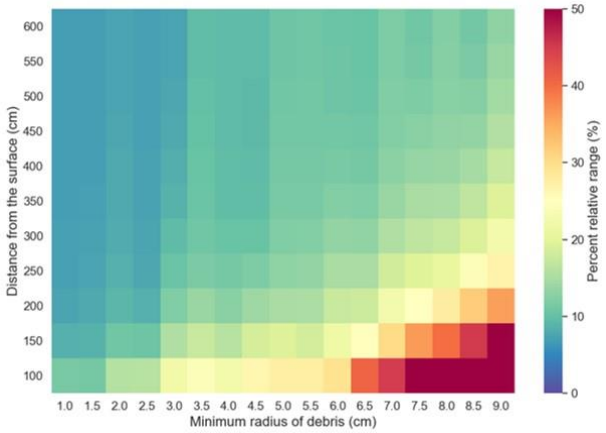


**Figure F. 5 Percent relative range of photon flux of loose packed fuel debris in a fuel canister**

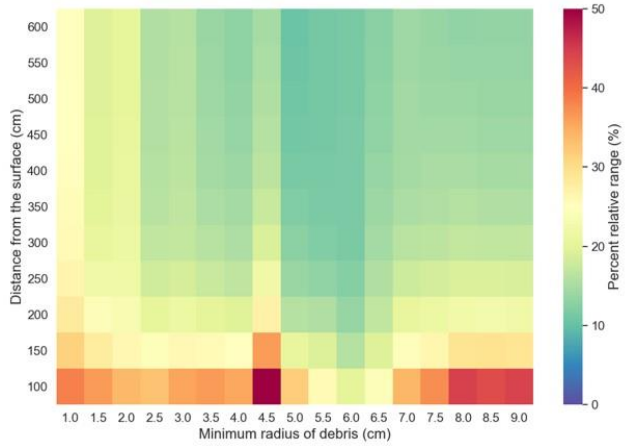


**Figure F. 6 Percent relative range of photon flux of close packed fuel debris in a fuel canister**

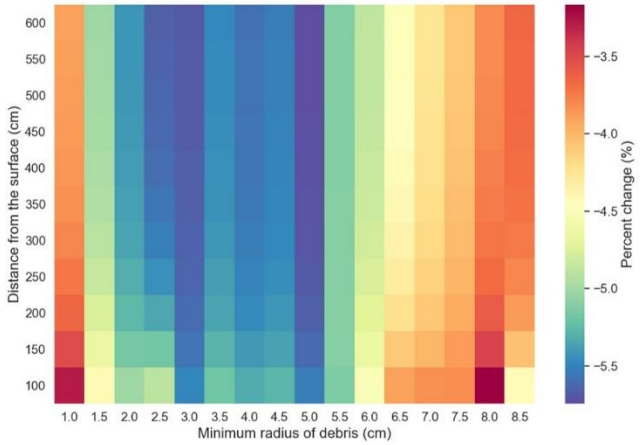


**Figure F. 7 Percent change of photon flux by changes in the minimum radius of fuel debris for the loose packed fuel debris in a fuel canister**

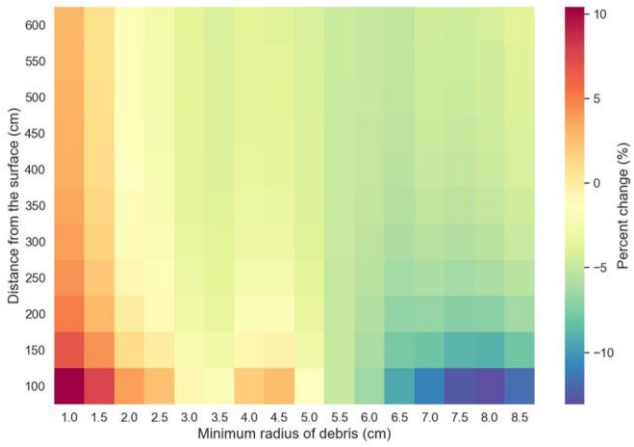


**Figure F. 8 Percent change of photon flux by changes in the minimum radius of fuel debris for the close packed fuel debris in a fuel canister**

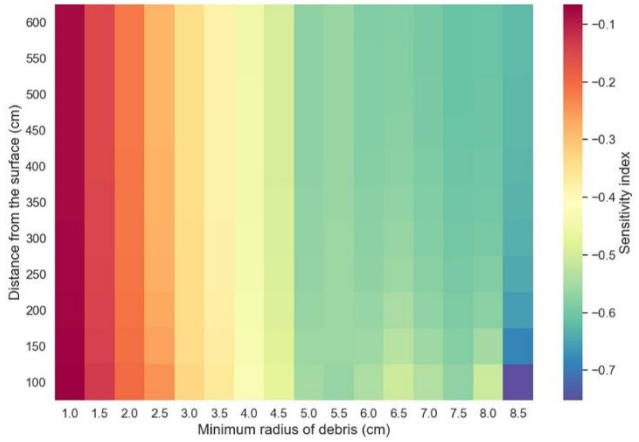


**Figure F. 9 Sensitivity of photon flux by changes in the minimum radius of fuel debris for the loose packed fuel debris in a fuel canister**

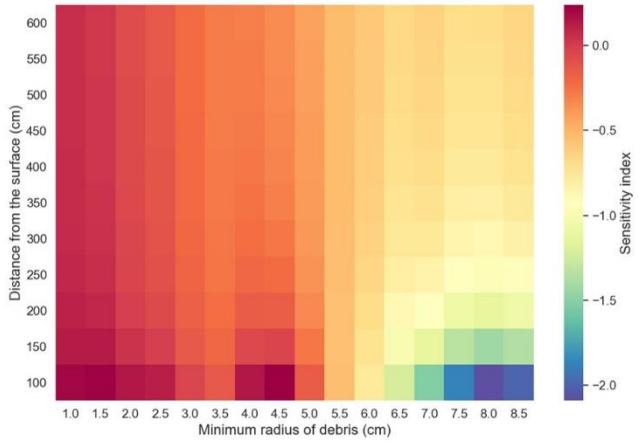


**Figure F. 10 Sensitivity of photon flux by changes in the minimum radius of fuel debris for the close packed fuel debris in a fuel canister**

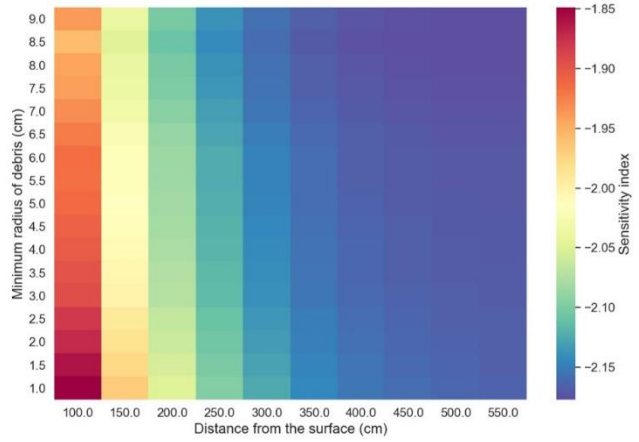


**Figure F. 11 Sensitivity of photon flux by changes in the distance from the surface of canister for the loose packed fuel debris in a fuel canister**

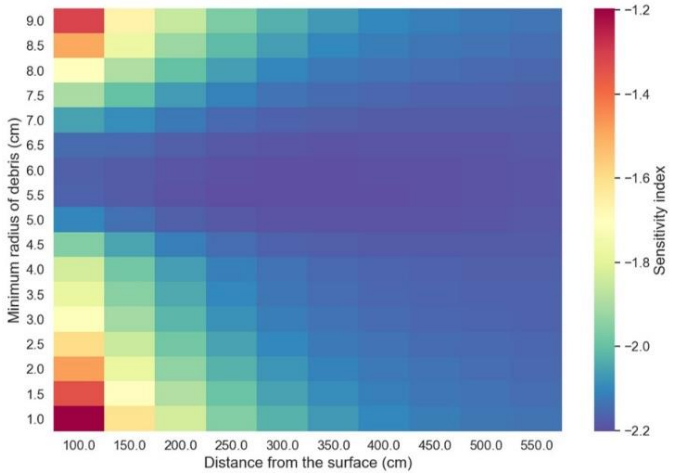


**Figure F. 12 Sensitivity of photon flux by changes in the distance from the surface of canister for the close packed fuel debris in a fuel canister**

**F. 2 Photon flux of fuel debris for a point detector at locations up to 400 m from the surface of a fuel canister.**

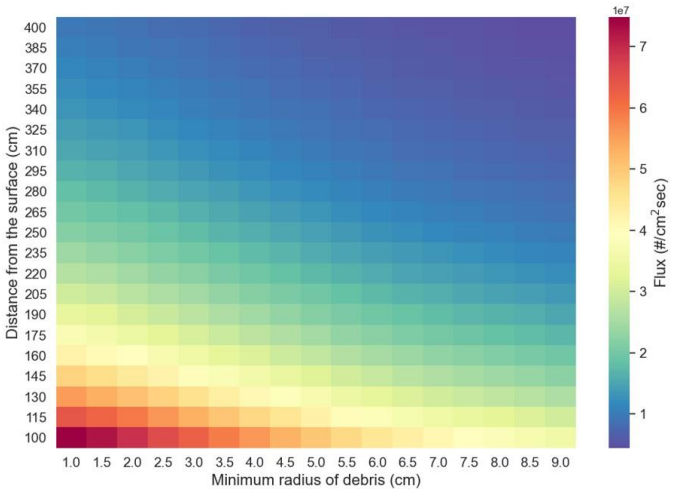


**Figure F. 13 Photon flux of loose packed fuel debris in a fuel canister**

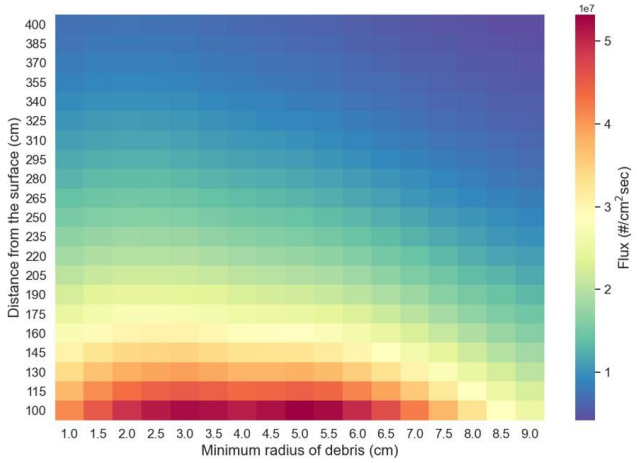


**Figure F. 14 Photon flux of close packed fuel debris in a fuel canister**

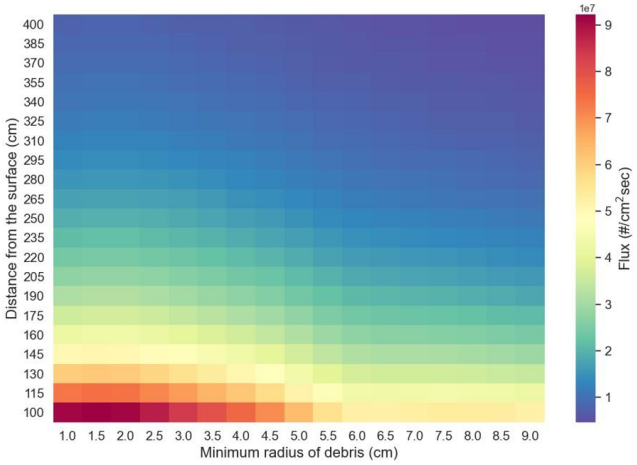


**Figure F. 15 Photon flux of close packed fuel debris in a fuel canister which is estimated -100 cm from the vertical center of the canister**

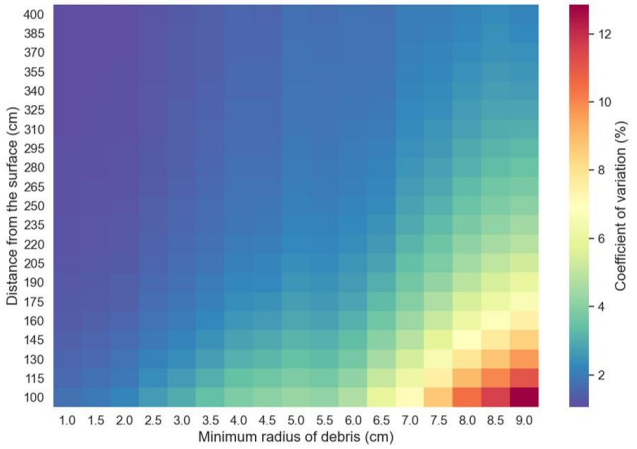


**Figure F. 16 Coefficient of variation of photon flux of loose packed fuel debris in a fuel canister**

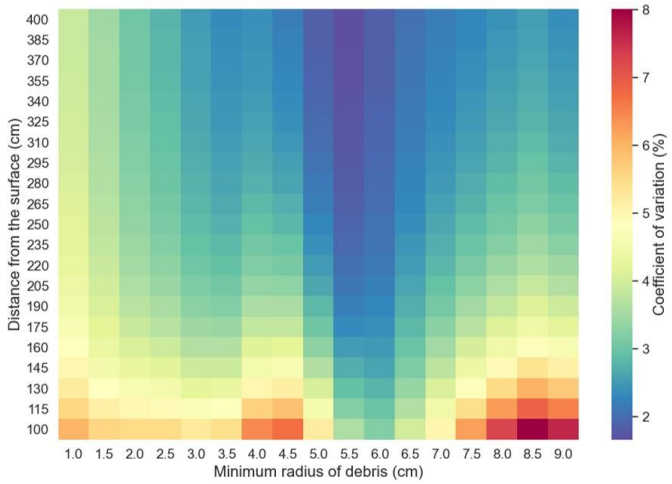


**Figure F. 17 Coefficient of variation of photon flux of close packed fuel debris in a fuel canister**

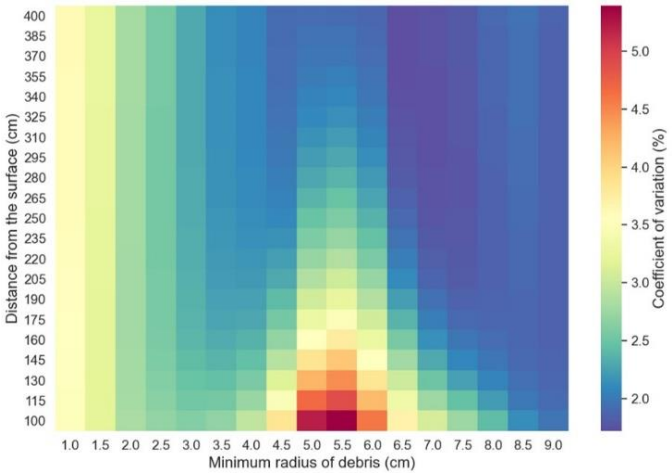


**Figure F. 18 Coefficient of variation of photon flux of close packed fuel debris in a fuel canister which is estimated -100 cm from the vertical center of the canister**

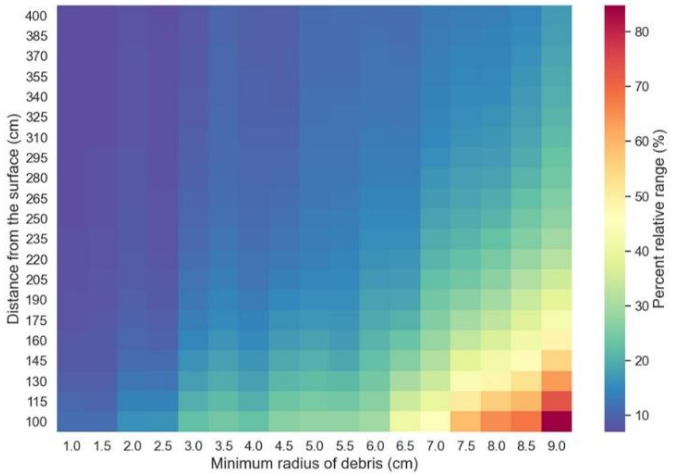


**Figure F. 19 Percent relative range of photon flux of loose packed fuel debris in a fuel canister**

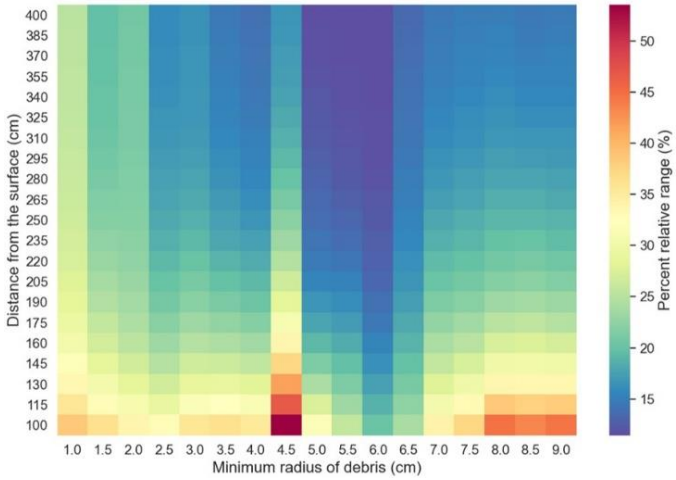


**Figure F. 20 Percent relative range of photon flux of close packed fuel debris in a fuel canister**

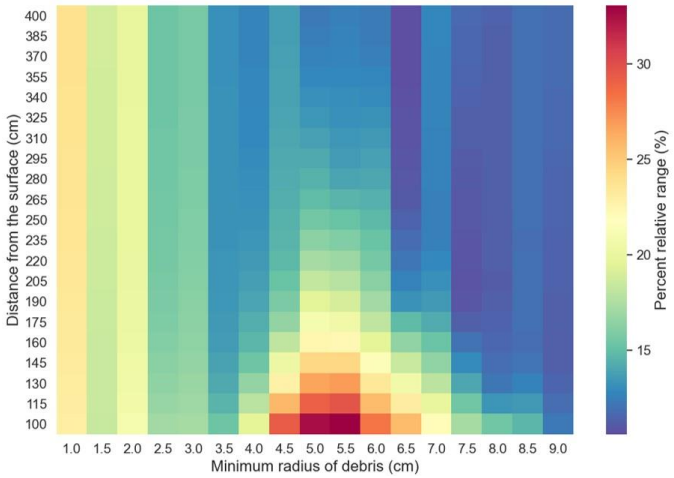


**Figure F. 21 Percent relative range of photon flux of close packed fuel debris in a fuel canister which is estimated -100 cm from the vertical center of the canister**

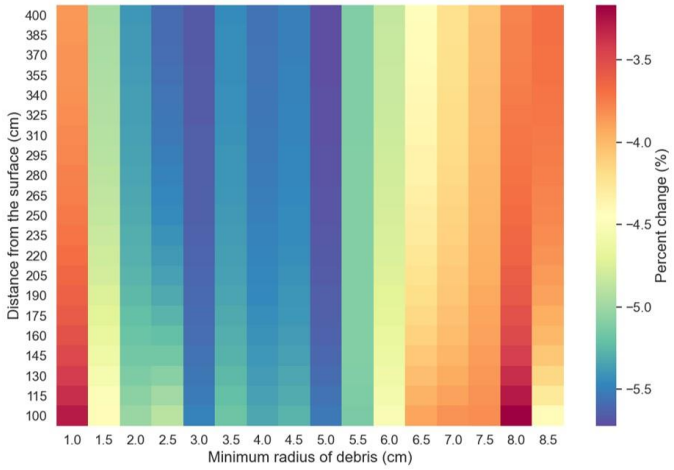


**Figure F. 22 Percent change of photon flux by changes in the minimum radius of fuel debris for the loose packed fuel debris in a fuel canister**

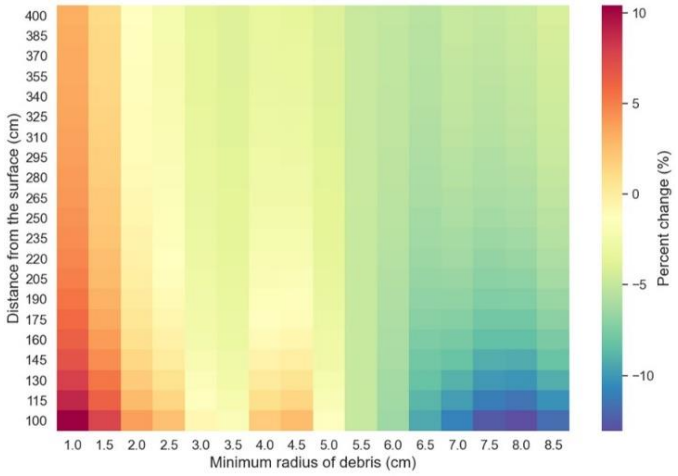


**Figure F. 23 Percent change of photon flux by changes in the minimum radius of fuel debris for the close packed fuel debris in a fuel canister**

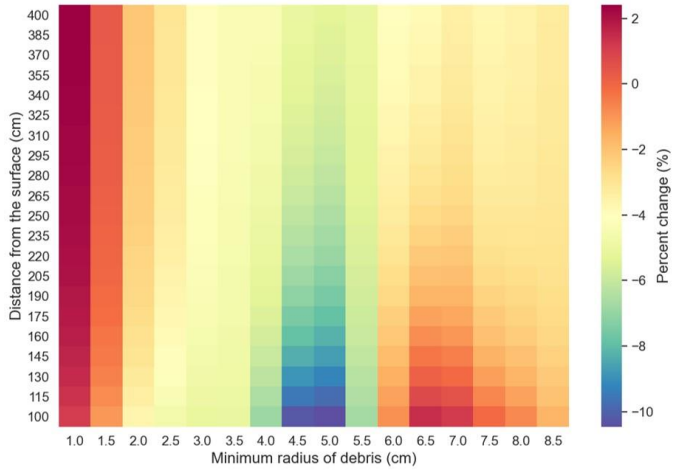


**Figure F. 24 Percent change of photon flux by changes in the minimum radius of fuel debris for the close packed fuel debris in a fuel canister which is estimated -100 cm from the vertical center of the canister**

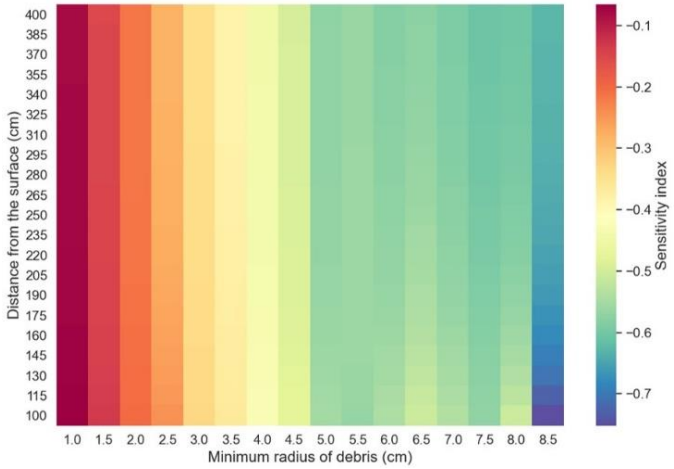


**Figure F. 25 Sensitivity of photon flux by changes in the minimum radius of fuel debris for the loose packed fuel debris in a fuel canister**

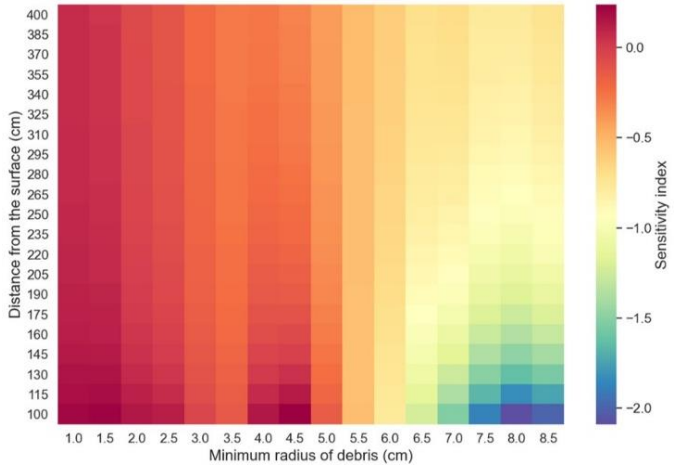


**Figure F. 26 Sensitivity of photon flux by changes in the minimum radius of fuel debris for the close packed fuel debris in a fuel canister**

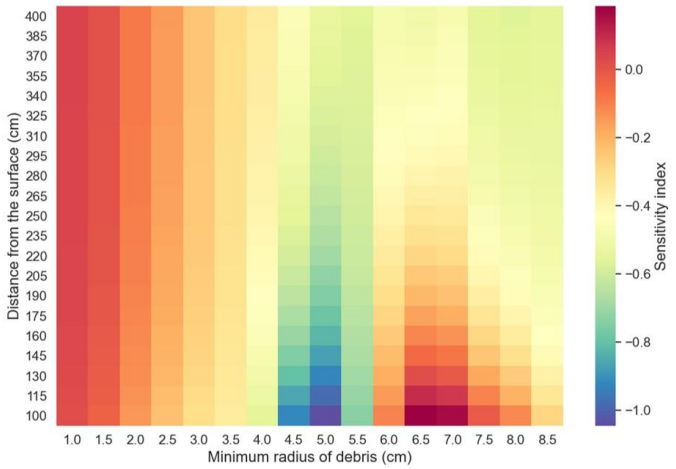


**Figure F. 27 Sensitivity of photon flux by changes in the minimum radius of fuel debris for the close packed fuel debris in a fuel canister which is estimated -100 cm from the vertical center of the canister**

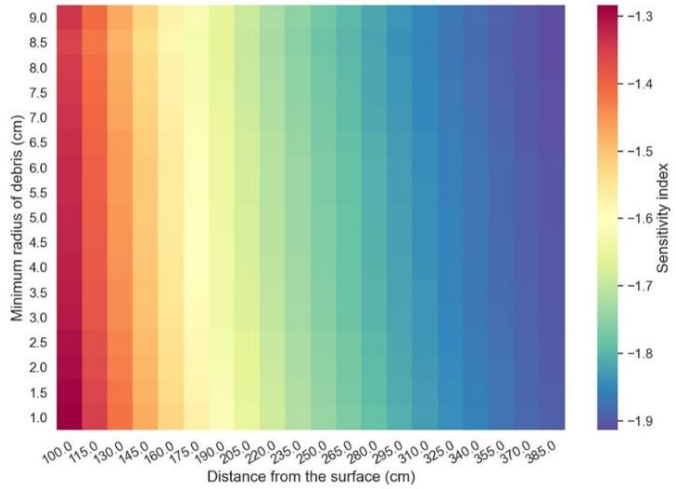


**Figure F. 28 Sensitivity of photon flux by changes in the distance from the surface of canister for the loose packed fuel debris in a fuel canister**

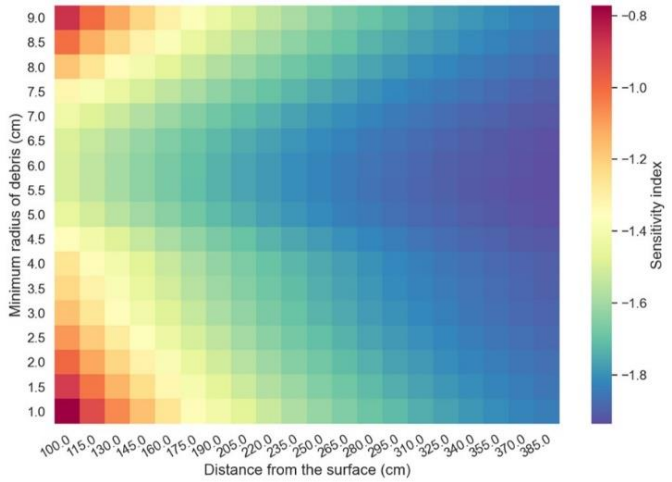


**Figure F. 29 Sensitivity of photon flux by changes in the distance from the surface of canister for the close packed fuel debris in a fuel canister**

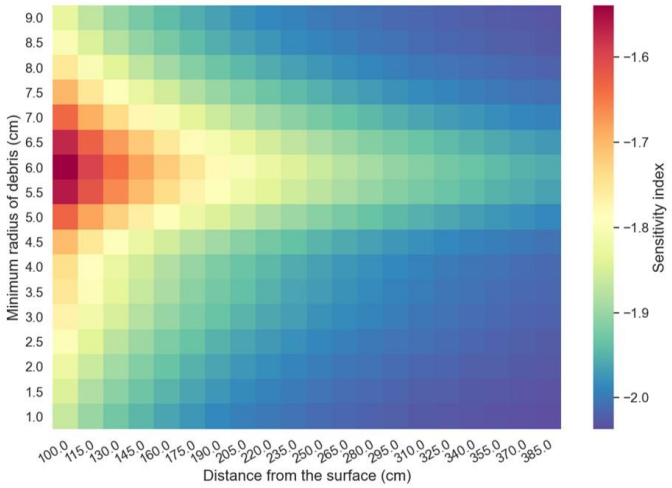


**Figure F. 30 Sensitivity of photon flux by changes in the distance from the surface of canister for the close packed fuel debris in a fuel canister which is estimated -100 cm from the vertical center of the canister**

## Appendix G. Miscellaneous

### G. 1 Method of data fitting and regression analysis

In Chapter 3, data from the model has been analyzed and it has been fitted to formulas which describe dose rate and its standard deviation. Even if some analytical tools such as the statistic module of 'R' can be used to get a formula for the trend line of a graph on the simulation data, these tools have not been used. Instead, a simple idea has been used with the Monte Carlo method. At the beginning of the process for data fitting, formulas which are similar with the graph of data have been chosen, then it has been plotted with the graph of data. After plotting the formula, coefficients of the formulas have been estimated by using Monte Carlo method (Figure G. 1).

At the beginning of the process for data fitting, several spots on the graph of data has been chosen. After choosing spots, distance between two lines (graph of data and the formula) is assumed as an objective of optimization. The formula and its coefficients are assumed as a restriction and variables of optimization. After the preparation for the optimization analysis, variables are randomly sampled, and optimal values of coefficients are estimated.

This method is very simple and easy to make an algorithm to be used with a python code. This simple method finds coefficients in a short time, and well fitted data to the assumed formula. Formulas with the estimated coefficient are matched with data from SCALE, especially it well matched for the photon dose rate and its standard deviation. However, it took a comparatively long time when the assumed formula was inappropriate. Especially, it takes a long time to estimate the coefficient of formulas on the standard deviation of the neutron dose rate because the variability of data is non-linear.

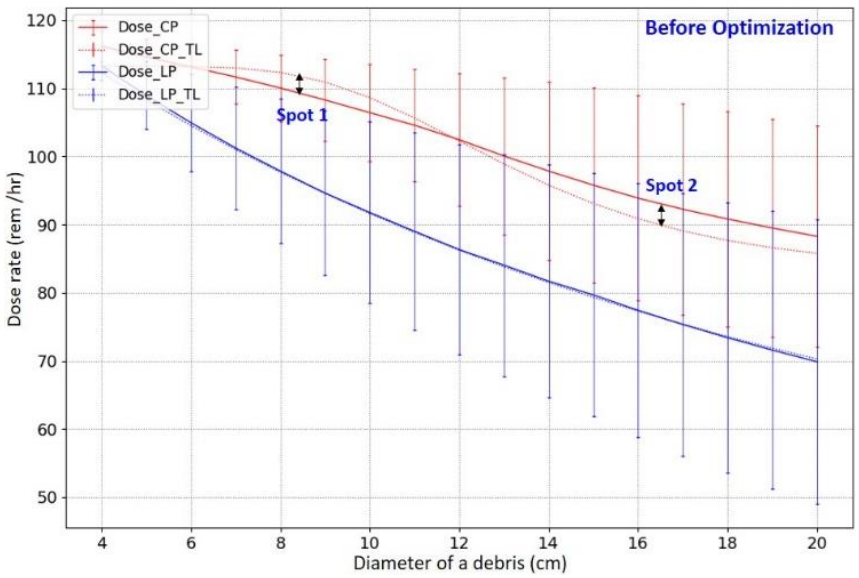


**Figure G. 1 Before fitting line to data**

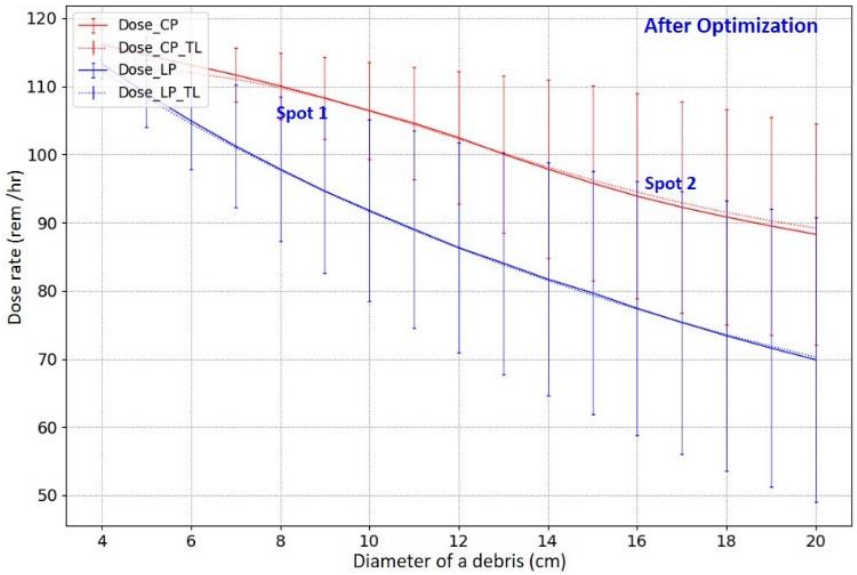


**After fitting line to data**

**Figure G. 2 Estimation of coefficients by using Monte Carlo method.** Red dashed lines at the left graph is the trend line of photon dose rate for close packed fuel debris. The line does not match with the thick red line (graph of dose rate data for close packed fuel debris.) The red dashed line at right graph is well matched with the thick red line after modifying coefficients of formula by using Monte Carlo method.

## Appendix G. 2 Sensitivity analysis on the effective multiplication factor

As a supplementary study, the effective multiplication factor ($K_{eff}$) has been calculated. Fuel debris in a canister does not be a critical state at any diameter of debris and $K_{eff}$ is smaller than 0.7. $K_{eff}$ decreases by the increasing of diameter of debris and standard deviation (STD) of $K_{eff}$ increases by increasing of the diameter (Figure G. 3). $K_{eff}$ of close packed debris is larger than $K_{eff}$ of loose packed debris and $K_{eff}$ of loose packed debris has smaller STD than close packed debris (Figure G. 4).

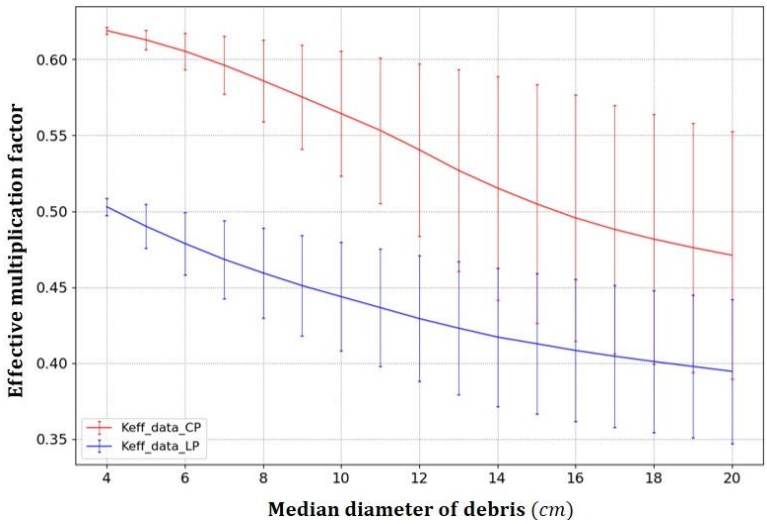


**Figure G. 3 Effective multiplication factor of fuel debris.** Red line is the $K_{eff}$ of close packed debris and the blue line is the $K_{eff}$ of loose packed debris. The vertical lines are standard deviations of $K_{eff}$.

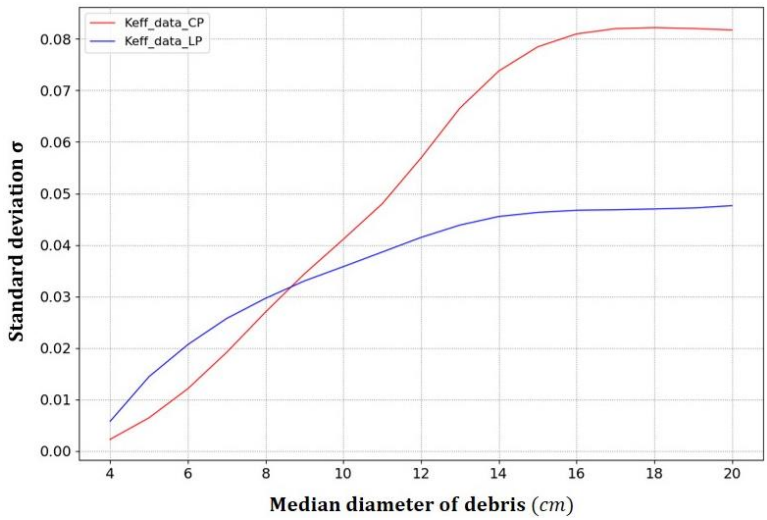


**Figure G. 4 Standard deviation of $K_{eff}$.** Red line is the STD of close packed debris and the blue line is the STD of loose packed debris.